PREDICTING OFFSHORE WIND ENERGY RESOURCES (POWER)

Authors:

G M Watson[1,2], J A Halliday[1], R A Brownsword[1], J P Palutikof[3], T Holt[3], R J Barthelmie[4], J P Coelingh[5], E J van Zuylen[5], J W Cleijne[6]

[1]Energy Research Unit, CLRC Rutherford Appleton Laboratory, Chilton, Didcot, Oxon OX11 0QX, UK

Tel : +44-1235-445559, Fax : +44-1235-446863, e-mail : j.a.halliday@rl.ac.uk

[2]Now at Tyndall Centre for Climate Change Research, University of East Anglia, Norwich, NR4 7TJ, UK

[3]Climatic Research Unit, University of East Anglia, Norwich, NR4 7TJ, UK

[4]Dept of Wind Energy and Atmospheric Physics, Risoe National Laboratory, PO Box 49, DK-4000 Roskilde, Denmark

[5]Ecofys bv, P.O. Box 8408, NL-3503 RK Utrecht, The Netherlands

[6]KEMA Power Generation and Sustainables, P.O. Box 9035, NL-6800 ET Arnhem, The Netherlands

Contract JOR3-CT98-0286

FINAL INTERNAL REPORT

1st August 1998 to 31st July 2001

Research funded in part by

THE EUROPEAN COMMISSION

in the framework of the Non Nuclear Energy Programme **JOULE II**

Table of Contents

		Page
	Abstract	**i**
	Executive Summary	**ii**
Chapter 1:	**Background to POWER project**	**1-1**
1.1	The importance of offshore wind energy in Europe	1-1
1.2	The demand for information on offshore wind energy resources	1-1
1.3	Estimating offshore wind energy resources in European waters	1-2
1.4	POWER project objectives	1-3
1.5	Structure of this report	1-4
Chapter 2:	**Introduction to the POWER project**	**2-1**
2.1	General characteristics of the wind field over the sea	2-1
2.2	Basic POWER methodology	2-2
2.3	Application of the POWER methodology to European waters	2-3
Chapter 3:	**Calculating geostrophic winds from sea level pressure data**	**3-1**
3.1	Introduction	3-1
3.2	Theoretical background	3-1
3.3	Sources of pressure data considered	3-1
3.4	Interpolation of the pressure data	3-2
3.5	Calculating the geostrophic wind	3-11
3.6	Testing the geostrophic wind calculated from interpolated pressure data	3-12
3.7	Using radiosonde data to validate the geostrophic wind	3-21
3.8	Results	3-42
3.9	Conclusions	3-43
3.10	References for Chapter 3	3-43
Chapter 4:	**Transforming geostrophic winds to turbine hub heights using WAsP**	**4-1**
4.1	Introduction	4-1
4.2	The Wind Atlas Analysis and Application Programme (WAsP)	4-1
4.3	WasP 5 versus WasP 6.0	4-1
4.4	Application of WAsP throughout European waters	4-2
4.5	Variable sea surface roughness	4-2
4.6	WAsP results	4-8
4.7	References to Chapter 4	4-12
Chapter 5:	**The coastal discontinuity model**	**5-1**
5.1	Coastal discontinuity – theoretical background	5-1

5.2		CDM modelling and results	5-2
	5.2.1.	Outline of the CDM approach: geostrophic version	5-2
	5.2.2.	Application and assessment of the GEO-CDM	5-7
	5.2.3.	The role of variable surface roughness and tidal range	5-19
	5.2.4.	The impact of stability on offshore flow	5-22
5.3		Integrating the CDM and WAsP for the POWER project	5-24
	5.3.1	Comparison of predictions based on geostrophic wind speeds	5-24
	5.3.2	Applying the CDM to WAsP predicted wind speeds	5-29
5.4		Validation	5-38
	5.4.1	Validation of stability routines	5-38
	5.4.2	CDM modelling of SODAR derived wind speeds	5-39
	5.4.3	Comparison of modelled and measured offshore wind speed profiles	5-53
5.5		Conclusions	5-57
5.6		References for Chapter 5	5-58
Chapter 6:		**SODAR measurements**	**6-1**
6.1		Introduction to SODAR	6-1
6.2		Basic description of SODAR measurement principle	6-1
6.3		Features of SODAR measurements	6-1
6.4		Description of Aerovironment 4000	6-2
6.5		SODAR measurement campaigns	6-2
6.6		SODAR measurements at Measuring Post Noordwijk (MPN)	6-2
	6.6.1	Introduction	6-2
	6.6.2	Data processing and software	6-5
	6.6.3	Data analysis	6-7
	6.6.4	Conclusions	6-17
	6.6.5	Comparison of SODAR data with MPN measuring mast data	6-18
	6.6.6	Summary of results	6-24
	6.6.7	Discussion	6-25
6.7		Analysis of SODAR data collected in the UK	6-26
	6.7.1	The Weybourne site	6-26
	6.7.2	Data processing	6-27
	6.7.3	Analysis of the data	6-29
6.8		References for Chapter 6	6-35
Chapter 7:		**Variability of offshore winds**	**7-1**
7.1		Introduction	7-1
7.2		The long-term characteristics of the wind field over Western Europe	7-1
	7.2.1	Introduction	7-1
	7.2.2	Data and methodology	7-1
	7.2.3	Principal Components Analysis of the geostrophic wind data	7-2

	7.2.4	Patterns of Factor Loading	7-3
	7.2.5	Summary	7-7
	7.2.6	Testing the stability of the factor loadings	7-8
	7.2.7	Factor scores	7-8
	7.2.8	Wind speed time series	7-9
	7.2.9	Summary and conclusions	7-15
7.3		The diurnal cycle of the coastal wind field of the UK	7-16
	7.3.1	Introduction	7-16
	7.3.2	Data	7-16
	7.3.3	Method	7-16
	7.3.4	Results	7-17
	7.3.5	Conclusions	7-26
7.4		Analysis of wind gusts	7-26
	7.4.1	Introduction	7-26
	7.4.2	Extreme value analysis of maximum daily gust speed	7-29
	7.4.3	Conclusions	7-32
7.5		Reference for Chapter 7	7-32
Chapter 8:		**Wind and wave loading**	**8-1**
8.1		Introduction	8-1
	8.1.1	Environmental conditions for offshore wind turbines	8-1
	8.1.2	Design criteria	8-4
	8.1.3	The UKMO-data set	8-4
	8.1.4	Wind and wave climate analysis	8-5
	8.1.5	Relevant conclusions	8-9
	8.1.6	References	8-9
	8.1.7	Annex 1: Footprint data for 14 locations	8-10
Chapter 9:		**Confidence limits for mean monthly wind speeds**	**9-1**
9.1		Introduction	9-1
9.2		Data	9-1
9.3		Methodology	9-2
9.4		Results	9-3
9.5		Comments	9-4
		Confidence limits for Region 1 Coasts of Northern Europe	9-5
		Confidence limits for Region 2 Coasts of Western Mediterranean	9-6
		Confidence limits for Region 3 Coasts of Southern UK to Northern Iberia	9-7
		Confidence limits for Region 4 Coasts of Iceland to Scotland	9-9
		Confidence limits for Region 5 Coasts of Northwest Africa and Southern Iberia	9-10
		Confidence limits for Region 6 Coasts of Eastern Mediterranean	9-11
9.6		References for Chapter 9	9-13

Chapter 10:		**Comparisons with measured data**	**10-1**
10.1		Introduction	10-1
10.2		The Netherlands	10-1
	10.2.1	Introduction	10-1
	10.2.2	Data sources	10-1
	10.2.3	Measuring Networks ZEGE	10-3
	10.2.4	Measuring Network North Sea (MNZ)	10-10
	10.2.5	Conclusions	10-17
	10.2.6	Comparison with POWER results	10-18
	10.2.7	Overall conclusions	10-19
10.3		Denmark	10-20
	10.3.1	Data source	10-20
	10.3.2	Wind speeds	10-20
	10.3.3	Variation in wind speeds through the year	10-22
	10.3.4	Variation with direction	10-23
	10.3.5	Wind speed distributions	10-24
	10.3.6	Conclusions	10-25
10.4		The Mediterranean	10-26
		1. Introduction	10-26
		2. Data and climatology	10-27
		3. Results	10-28
		4. Final remarks	10-29
		5. Bibliography	10-30
10.5		Comparison with a previous EU study	10-31
10.6		References for Chapter 10	10-31
Chapter 11		**The POWER TOOL Software**	**11.1**
11.1		The Power Tool	11.1
	11.1.1	The Wind Details Box	11.1
	11.1.2	The Wind Map Box	11.1
	11.1.3	The Wave Map Box	11.2
	11.1.4	The Wave Details Box	11.2
11.2		Installation of POWER Tool	11.3
11.3		Technical Appendix – The Weibull distribution	11.5
11.4		Technical Appendix – Calculation of wind turbine power	11.5
11.5		Technical Appendix – Defining a power curve	11.5
11.6		Technical Appendix – Definition of terms	11.5
APPENDIX 1		**PUBLICATIONS**	**A-1**
1		Conference Presentations	A-1

2	Papers	A2
3	Book Chapter	A-2
4	Other	A-2
5	Internal Project Reports	A-2
6	Reports submitted to the European Commission	A-2

Abstract

In the coming years, exploitation of offshore wind energy is set to play a central role in Europe's overall energy strategy by assisting EU member state governments to achieve their national greenhouse gas emission reduction targets (both now and in the future), whilst continuing to meet the demand for energy. However, development and integration of offshore wind energy is currently handicapped by significant knowledge gaps, including a scarcity of good quality information on the extent, characteristics and distribution of the offshore wind energy resource.

The objective of the Predicting Offshore Wind Energy Resources (POWER) project was to improve the understanding of the nature and distribution of Europe's offshore wind resource. In particular the project team set out to improve upon previous estimates of the European offshore wind energy resource, to consider a number of additional factors that could affect its exploitation on a commercial basis and to present the information in a straightforward, yet useful format.

Within POWER, a novel wind resource assessment methodology was developed which can produce long-term and spatially detailed estimates of the wind conditions at offshore sites covering a wide area. Furthermore, the team applied this methodology to the region 30ºN to 70ºN and 15ºW to 30ºE on a grid of 0.5º resolution, an area which covers the major sea areas bordering EU countries – the North Sea, the Baltic, the Mediterranean and the eastern North Atlantic.

The POWER project has produced state-of-the-art estimates of the extent and distribution of Europe's offshore wind energy resources not only in the coastal zone – the current focus of the offshore wind industry's attention – but also throughout the region's far offshore areas, where there is potential for wind energy to be exploited in the longer-term.

On a local scale, POWER provides detailed first estimates of the long-term environmental conditions at specific offshore locations. This information is useful to the offshore wind energy industry since this is the exact type of data required for initial scoping and feasibility studies for new offshore wind energy developments. It may be possible to base preliminary assessments of the turbine power output as well as other key parameters such as initial values of the design parameters for turbine support structures from the POWER results.

The data on wind and wave parameters for European waters produced by the POWER project has been compiled as a set of Microsoft Excel work books. The data can be accessed using the "POWER tool" - a simple graphical user interface (GUI) that allows the user to display, in both numerical and graphical form, data from the database of wind and wave parameters

The POWER project's techniques should enable the wind energy industry to exploit the offshore wind energy resource with greater confidence, and hence facilitate a future expansion of the wind turbine manufacturing and installation industry – with the consequent employment opportunities.

Executive Summary

1 Partnership

The POWER consortium was made up of the following organisations : Co-ordinator : Energy Research Unit, CLRC Rutherford Appleton Laboratory, Chilton, Didcot, Oxon OX11 0QX, UK (contact person : Dr Jim Halliday, Tel : +44-1235-445559, Fax : +44-1235-446863, e-mail : j.a.halliday@rl.ac.uk); Climatic Research Unit, University of East Anglia, Norwich, NR4 7TJ, UK (Contact person : Dr Jean Palutikof, Tel : +44 1603 593647, Fax : +44 1063 507784, e-mail : j.palutikof@uea.ac.uk); Dept of Wind Energy and Atmospheric Physics, Risoe National Laboratory, PO Box 49, DK-4000 Roskilde, Denmark (Contact person : Dr Rebecca Barthelmie, Tel : +45 46 77 5020, Fax : +45 46 77 5970, e-mail : r.barthelmie@risoe.dk); Ecofys bv, P.O. Box 8408, NL-3503 RK Utrecht, The Netherlands (Contact person : Dr Jan Coelingh, Tel +31 30 2808 395, Fax : +31 30 2808 301, e-mail : j.coelingh@ecofys.nl); KEMA Power Generation and Sustainables, P.O. Box 9035, NL-6800 ET Arnhem, The Netherlands (Contact person : Hans Cleijne, Tel : +31 26 3566 393, Fax : +31 26 4458 279, e-mail : j.w.cleijne@kema.nl)

2 Objectives of POWER

In the coming years, offshore wind energy is set to play a central role in Europe's overall energy strategy by assisting EU member state governments to achieve their national greenhouse gas emission reduction targets (both now and in the future), whilst continuing to meet the demand for energy. However, development of offshore wind energy is currently handicapped by significant knowledge gaps, especially good quality information on the extent, characteristics and distribution of the offshore wind energy resource. The Predicting Offshore Wind Energy Resources (POWER) project was an ambitious attempt to improve the understanding of the nature and distribution of this resource.

3 Introduction

Perhaps the most significant obstacle to the assessment of offshore wind resources to date has been the lack of measured offshore wind data on which to base the estimates. Happily, the POWER project methodology does not rely directly on observed anemometer data to predict wind conditions offshore. Instead, the estimates are based on grids of atmospheric pressure data at mean sea level covering the area of interest. The methodology consists of three basic steps:

1. The mean sea level pressure gradient is used to calculate the geostrophic wind.

2. The geostrophic wind is transformed to the sea surface layer by applying the Wind Atlas Analysis and Application Program (WAsP).

3. In nearshore areas, a coastal discontinuity model (CDM) has been used to investigate the effects of atmospheric stability on wind predictions in the land/sea transition zone.

The stability routines in the CDM existed as a local (km) scale model. The model was significantly expanded for POWER to a) allow use of geostrophic wind speed , b) to allow land based profiles as input (for comparison with the SODAR data) and c) finally to utilise WAsP input (to attempt to make stability corrections). Within the POWER project, the CDM was "fine-tuned" using both existing offshore mast data and coastal SODAR (SOund Detection And Ranging) data. In addition, the estimates of wind resource were supplemented by assessments of short-term variability and information on regions of extreme environmental loading. Since historical atmospheric pressure data dates back to 1880 and beyond, the methodology allowed the long-term (decade to decade) variability of the offshore wind resource also to be investigated.

A schematic flow diagram of the POWER methodology is shown in Figure 1.

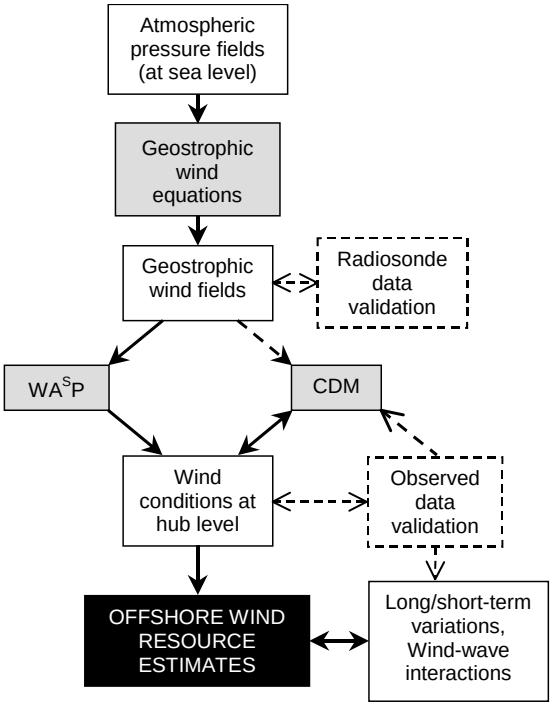

Figure 1 Flow schematic illustrating POWER methodology

4 Calculating geostrophic winds from sea level pressure data

Geostrophic winds are theoretical winds which flow parallel to isobars (contours of equal surface pressure) and which are a good approximation to the actual wind in the free atmosphere. Within the context of the POWER project, geostrophic winds are of particular interest because they can be calculated from surface pressure data. This is significant because while measured wind data at offshore locations are spatially and temporally sparse and often of variable quality, there are several good quality data sets of atmospheric pressure available that cover offshore areas. This means the atmospheric pressure data can be used to construct geostrophic wind conditions, which can then in turn be manipulated using well-established wind resource assessment techniques.

Atmospheric pressure data at mean sea level were obtained from the US National Centers for Environmental Prediction (NCEP) for the period 1985-97, at 6-hourly intervals and on a 2.5º latitude by 2.5º longitude grid. These data were interpolated onto a 0.5º latitude by 0.5º longitude grid using bicubic spline interpolation.

The interpolated atmospheric pressure data were then used to calculate the sea level pressure gradients in the westerly and southerly directions at each point in the 0.5º by 0.5º latitude/longitude grid. Finally, The pressure gradient at each grid point was then used to calculate the geostrophic wind speed and direction for each grid point and time step using equations 1 and 2:

$$U_g = -\frac{1}{f_c \rho}\frac{\partial p}{\partial y} \qquad 1$$

$$V_g = -\frac{1}{f_c \rho}\frac{\partial p}{\partial x} \qquad 2$$

where:

U_g and V_g are the westerly and southerly components of the geostrophic wind speed respectively
f_c is the local Coriolis force for the given latitude
ρ is the density of air
$\partial p/\partial y$ is the component of atmospheric pressure gradient from west to east
$\partial p/\partial x$ is the component of atmospheric pressure gradient from south to north

Figure 2 shows the distribution of the mean annual geostrophic winds calculated from the NCEP pressure data in the period 1985 to 1997.

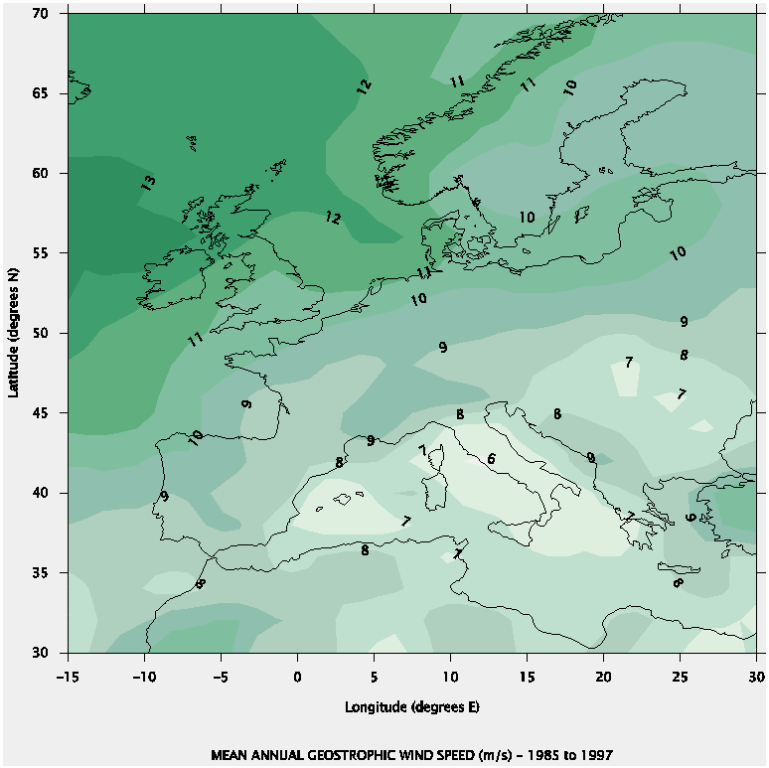

Figure 2 Calculated mean annual geostrophic wind speeds (m s^{-1}) – 1985 to 1997

Radiosonde data were obtained from the British Atmospheric Data Centre (BADC) for the period 1990 to mid-1998 from an extensive network of European stations. Observations from the radiosonde ascents at selected sites were used to compare the observed wind speeds and directions above the friction layer with the calculated geostrophic winds. There was an overall good agreement between the data sets.

The calculation of geostrophic winds, and their validation, are discussed in full in [1, Chapter 3].

5 Transforming geostrophic winds to turbine hub heights using WAsP

The Wind Atlas Analysis and Application Programme (WAsP) [2] is a linear flow model that can be used to transform geostrophic winds to the surface layer. WAsP is well-established and commonly used throughout the wind energy community to perform wind resource assessments. The model's calculations are based on the geostrophic drag law combined with models of stability and development of internal boundary layers (IBL). Coastal effects are modelled assuming differences in mean onshore and offshore stability and using internal boundary layer theory to modify wind speed profiles over the width of the coastal zone.

Mean wind conditions for the period 1985-97 were estimated using WAsP at eight hub heights at each POWER grid point over the sea. The hub height levels (10m, 30m, 50m, 70m, 90m, 110m, 130m and 150m above mean sea level respectively) were chosen to cover the range of expected hub heights of wind turbines that are likely to be sited offshore in the coming years. In addition, the monthly and inter-annual variability of the wind conditions in European waters were also investigated by performing WAsP model runs estimating the mean monthly and mean yearly wind conditions at all offshore grid points. Finally, some additional WAsP runs were performed to obtain offshore wind predictions at specific locations and heights, which could be compared directly against observed data for validation purposes (see section 10).

An example of the results from the WAsP runs performed are presented in Figure 3 – a plot showing the distribution of mean wind speeds for the period 1985-1997 at 50m above mean sea level throughout the POWER project area.

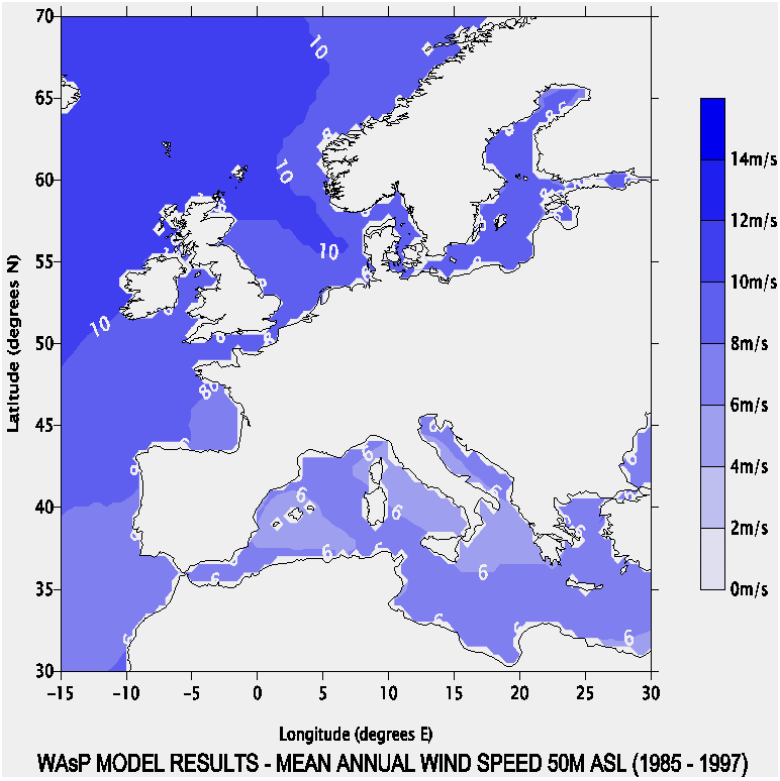

Figure 3 Plot showing the distribution of mean annual wind speeds at 50m a.s.l. throughout EU waters

The results indicate that the highest wind speeds are found in along the Atlantic margin, the North Sea and Baltic regions with mean annual wind speeds at 50m above sea level in excess of 8.0ms^{-1} throughout these areas. The highest wind speeds are experienced north and west of Scotland, where mean annual wind speeds greater than 10.5 ms^{-1} are expected. An interesting feature is evident in the North Sea, where a finger of relatively high wind speeds extends into the basin from the north. By contrast, the most of Mediterranean basin is less windy, with extensive regions experiencing mean annual wind speeds of less than 6ms^{-1}. However, good wind speeds are to be found in parts of the Aegean.

Although there are some slight discrepancies present, overall these results broadly compare with earlier offshore wind resource estimates [6] and [7]. {The discrepancies in the WAsP results mentioned mainly arise from the use of different input data (e.g. Moore [6] used 900 mb data and the European Wind Atlas [7] used surface data).}

WAsP uses a simple approach to modelling aerodynamic roughness, assuming a constant sea surface roughness length z_0=2x10^{-4}m for all sea areas, wind conditions and sea states. However, whereas the roughness of land features can be thought of as essentially constant, the sea surface geometry and roughness alter continuously with varying wind speed.

One of the project's objectives was to assess the effect of variable sea surface roughness on offshore wind speed predictions. The project team investigated this using a new parameterisation for z_0 [3] to calculate aerodynamic roughness values in European waters over the period January 1987 to December 1996. The results suggest that that for the bulk of the time, z_0 values are very small indicating the sea surface is aerodynamically very smooth. However, there are relatively short periods, mostly corresponding to the high wind events, when the sea surface roughness increases significantly with predicted values of z_0 in excess of 4x10^{-3}m. In order to get an indication of the distribution and overall variability of the sea surface roughness, the mean value of z_0, as well as its standard deviation, was calculated. An example of the results obtained are illustrated in Figures 4a and 4b.

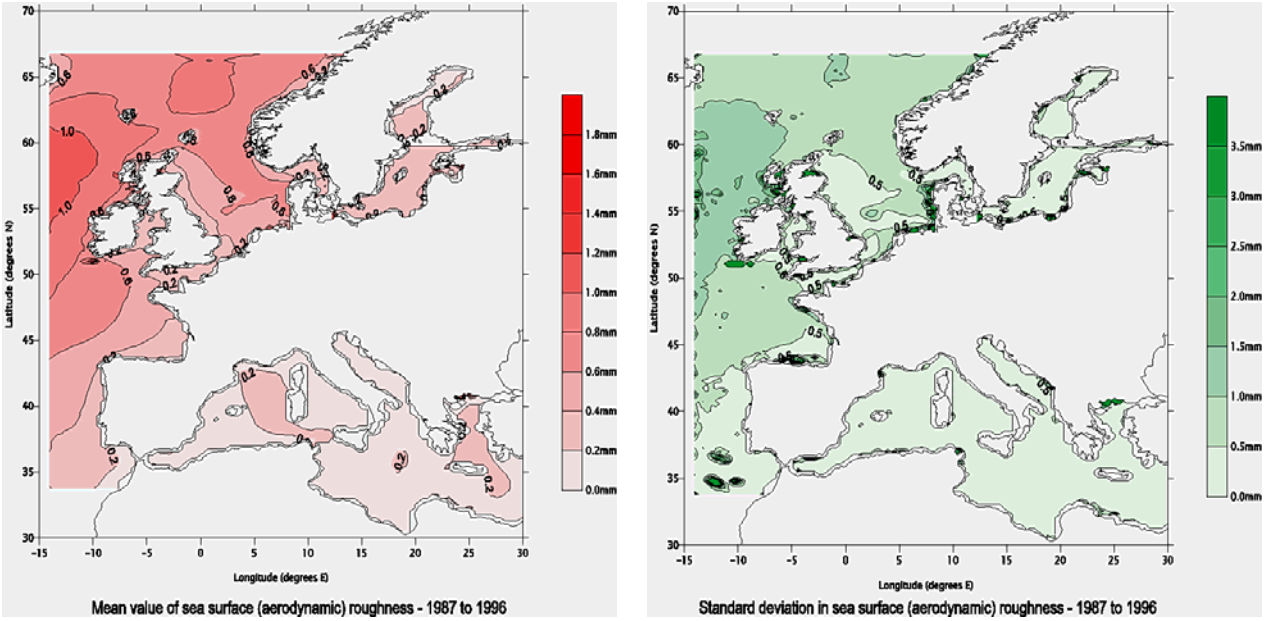

(a) **(b)**

Figure 4 Distributions of mean value of sea surface roughness, z_0, and its standard deviation – 1987 to 1996

During the course of the project, the project team became aware of the results of other modelling studies [4] [5] [1, Chapter 5] which indicate that the variability in the z_0 values predicted here would result in only small differences (less than 0.5%) in predicted wind speeds compared to the existing WAsP predictions. Furthermore, [4] suggests that thermal stratification/stability issues have a much greater impact on offshore wind resources than changes in sea surface roughness. However, as discussed below, it proved impossible to assess whether stability-corrected results were an improvement on the close-to-neutral predictions made with WasP. Finally, the tidal range at a site may also impact on the wind speed predictions, particularly as in some areas large expanses of rough foreshore may be exposed at low water. It should be remembered that some parts of the POWER project area are subject to large (>4m) tidal ranges and so this could be a significant effect at these locations. However, for the majority of the POWER assessment area the tidal range is much less than 4m for this effect will not be significant.

Therefore, although it is clear that variable sea surface roughness will modify wind speed predictions slightly, the impact of other contributory factors are expected to dominate and therefore no attempt was made to correct the POWER WAsP results for variations in sea surface roughness.

The WAsP modelling performed within the project, and other related investigations, are discussed in full in [1, Chapter 4].

6 Modelling the coastal discontinuity

In coastal sea areas the wind regime is influenced by the adjoining land surfaces resulting in some complex interactions. In stable atmospheric conditions in particular, the influence of upwind land surfaces on the offshore wind speed profiles can be determined over long distances [8] (up to 50km and potentially beyond in highly stable conditions).

The CDM [9 and 10] is a combined stability and internal boundary layer (IBL) model which was significantly exhanced during the POWER project and based on similar principles to WAsP - the major difference being that on- and off-shore stabilities are calculated in each time step and used to modify individual offshore wind speed profiles from the logarithmic while accounting for the differential growth of the IBL in varying stability conditions. The CDM determines its stability corrections from data of air and sea temperature data.

During its development, the performance of the stability component of the model was evaluated by comparing the Monin-Obukhov length stability parameter values predicted with observed values measured at a number of sites in Danish waters. In addition, preliminary CDM results were compared

with the results of detailed analyses of data from meteorological masts in Danish waters. Further refinement and validation of the CDM was achieved using various data observed at coastal and offshore sites. Some of these data come from existing masts and platforms, however within the POWER project additional data were collected for this purpose using a mini-SODAR device (see Section 6).

Two versions of the CDM were applied to European waters within the POWER project:

1. GEOCDM - configured to take time series of geostrophic wind conditions as input
2. WASPCDM- configured to accept WAsP predicted wind speed distributions for each direction sector as input.

Development of the CDM has so far focused on accounting for roughness and stability changes between land and sea. As such, the representation of some of the other wind transformation processes in the CDM are not as advanced as found in the WAsP model. This means that the predictions made using the GEOCDM are based on a simplified transformation model and on this basis have not been used for the final POWER results.

The advantage of WASPCDM approach is that WAsP can give more accurate predictions of wind speed corrected for local orography, shelter and roughness. However, since the WAsP output is in the form of mean wind speed profile predictions the CDM stability correction must also be a mean value for each sector. Unfortunately, it was found that this does not necessarily improve the average wind speed profile predictions. The reason for this is that individual time series corrections of wind speed profiles for stability can either be positive or negative - hence calculating the average of the corrected wind speed profiles does not give the same result as calculating an average of the stability corrections and then using this to correct the mean wind speed profile.

A further problem highlighted is the spatial resolution of the stability correction. The initial data sets are supplied on 0.5 by 0.5 ° grid whereas it is known that mean offshore wind speeds vary on scales of about 0.5 km in coastal regions. CDM and WAsP applied at the 0.5 by 0.5 ° grid scale are unable to resolve complex coastlines, however, applying the same techniques with an improved coastline resolution would improve the predictions. However, at the time of the project, such data were not readily available.

In addition the use of air temperatures from mixed land/sea grid cells may not provide an accurate determination of stability, particularly when combined with a sea surface temperature data base from different sources. Errors in the source databases are of the same order as the temperature difference which is used to calculate the stability parameter. However to improve the stability correction is more difficult since a) currently sea surface and air temperatures are not available at better than 0.5 by 0.5° grid resolution and b) a more precise estimate of stability requires either direct flux measurements or a measured temperature difference.

Thus overall, it was found that applying the CDM, in its current form at least, to WASP predicted wind speeds does not improve the predictions. Therefore, although it is clear that coastal effects are expected to modify wind speed predictions, no additional CDM corrections have been included in POWER's final output, as at the present time the input data of stability and coastline resolution were not available in the resolution needed. It is suggested that when such data do become available, the effect of applying the CDM corrections should be re-examined.

Development and validation of the CDM and its application to European Union waters is discussed in more depth in [1, Chapter 5].

7 Wind speed profiles using SODAR

SODAR (SOund Detection And Ranging) is a remote sensing technique for making wind speed and direction measurements at various heights. The technique is based on the reflection of sound pulses from turbulence in the atmosphere. The time taken for a reflection to be detected is used to determine the range (height) and the Doppler shift in the reflected signal is used to determine the wind speed and direction at particular heights. These data can then be used to build vertical profiles of the wind speed and direction at heights well above conventional meteorological masts.

Within the POWER project three sets of SODAR measurements were performed:

1. SODAR trials at Petten (The Netherlands): October 1998 - May 1999

Equipment trials were carried out by staff from Ecofys in collaboration with ECN and gave the project staff valuable experience in setting up the SODAR system and performing the mesurements as well as enabling them to set up quality control and analysis systems for the observations.

2. *Measuring Post Noordwijk (9km off the coast of The Netherlands): January –June 2000*
   In total 4 months of good quality observed data were obtained while the SODAR system was installed at the Measuring Post Noordwijk (MPN) research platform owned and operated by the Public Works Department (Rijkwaterstaat), Directie Noordzee. These measurements were used to help validate the Coastal Discontinuity Model.

3. *Weybourne (UK)*
   SODAR data were measured at a coastal site in eastern England by staff from the UEA.

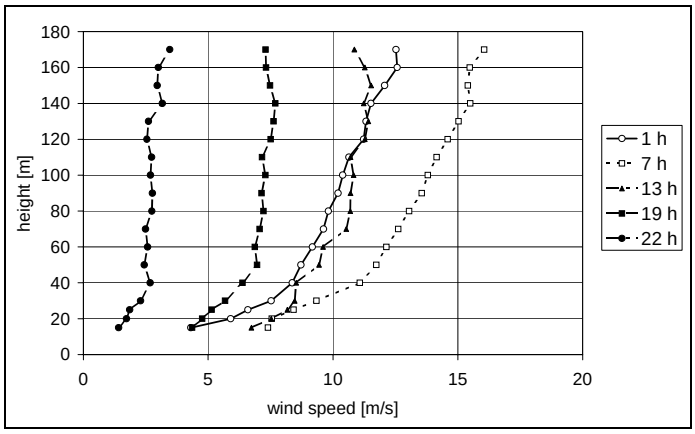

Figure 5 Example of wind speed profiles at MPN as measured with a SODAR on one day. The profiles shown are hourly averages

The SODAR has proved to be a very useful device to measure wind speed profiles and can help to describe boundary layer phenomena. However, it was found that the quality of SODAR measurements tends to be adversely affected by rain and background noise (e.g. from waves, wind whistling through superstructures, diesel generators etc.). Furthermore, SODAR height performance is affected by the stability conditions; the more unstable the atmosphere, the better the height performance.

A more detailed account of the SODAR equipment and a description and analysis of the data obtained can be found in [1, Chapter 6].

8 Time-dependent variability

Offshore wind speeds are known to vary over a wide range of time scales:

long-term – inter-annual, decadal and other long-term trends such as climate change
medium-term - seasonal and diurnal cycles
short-term – e.g. gusts

The scale of these variations is sufficient to have economic implications for both onshore and offshore wind farms. Given this importance, within POWER, the project team sought to extend the current understanding of three types of variability in the offshore wind regime, namely, long-term trends, the diurnal cycle and gusts. The analyses and results are described more fully in [1, Chapter 7].

Long-term trends

Historical records of sea level pressure in Europe extend back to the 1870s. Happily, this means that the POWER methodology can be used to investigate the long-term (decade to decade) variability of the offshore (and onshore) wind resource.

Monthly mean geostrophic wind speeds were calculated using the technique outlined in Section 3 and based on UK Meteorological Office's daily records of mean sea level pressure dataset throughout Europe for the period 1900 to 1997. The monthly mean geostrophic wind speeds were then organised in space using Principal Components Analysis (PCA) to identify the dominant regional wind regimes over Europe. PCA is a statistical technique which performs two important functions;

1. Reduction of the data set to a new set of components (or modes of variability), representing only major patterns of variance that may be of interest.
2. Objective identification of important modes of variability which are orthogonal, that is, they have no common variations (they are uncorrelated).

Here, the PCA identified seven important components, each associated with a spatial pattern of windiness and which together explain over 83% of the total variance in the original data. One of the components (designated here as number 3) was found to influence north Africa only, and so was not considered further.

The spatial patterns of the components have regions where the influence of the component is particularly strong. As an example, Figure 6a shows the pattern of loadings associated with the first component of the PCA. This has strong influence over the Baltic and southern Scandinavia. Inspection of the spatial patterns for each component showed that a set of grid squares in the original dataset of geostrophic winds could be identified as being most strongly associated with each component.

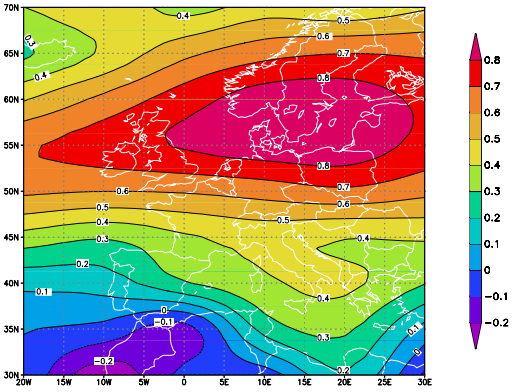

(a)

Example of factor loading pattern – Factor 1, explaining 26.37% of the variance

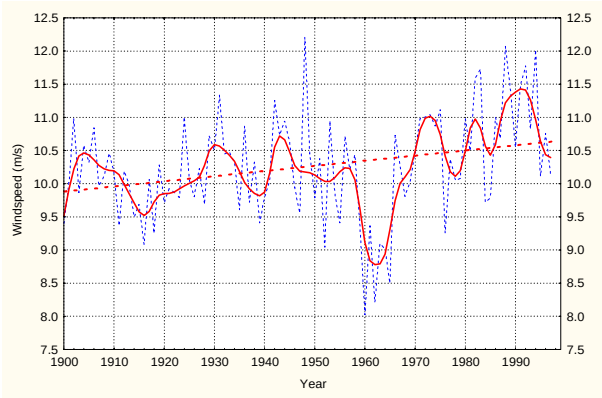

(b)

Example of wind speed trend - Winter (Oct. to Feb.) wind speeds associated with Factor 1

Figure 6 Examples of long-term trend analysis plots

Therefore, for each component, the wind speeds for the associated grid squares were averaged to produce a composite seasonal time series of wind speeds. Only grid squares over the sea were considered in this process. The resulting seasonal time series were examined for trend and periodic behaviour. Figure 6b shows the example time series for the first component, which is strongly associated with a set of grid squares over the Baltic, the North Sea, and the coastal waters of Scandinavia, the UK and Ireland. In Figure 6b we show the wind speed time series together with a smoothed line, to reveal the overall time series features of the data, and the linear trend line over the whole period of record. This particular example shows that winter wind speeds over north western Europe have a long-term rising trend that is largely a function of increasing wind speeds since the 1960s. Prior to this, the record shows no trend. There is no evidence of regular periodicity in these data.

Although there is no indication in the data of any significant periodic activity, there is considerable evidence of stable long-term trends associated with particular factors. This is important since a background of rising trend, for example, in the more northern high wind speed regions, may mean more downtime as turbines cut-out more frequently. Conversely, rising trend in relatively low wind speed regions may mean that a currently inadequate resource may eventually become economically viable.

In terms of assessing offshore wind potential, the regions affected by trends can be determined from Table 1. The final column gives the percentage change in wind speed over the period of trend described in the previous two columns. For example, if we were interested in exploiting the offshore wind resources of Greece we can see from Table 1 that Greece is experiencing a very small falling trend associated with Factor 2. However, the wind field associated with Factor 7 has rising trend over southern Greece with an increase in wind speeds of 30% over 60 years in summer and of 10% over

100 years in winter. Given that wind speeds off Greece are relatively low, the rising trend is encouraging for the development of offshore wind energy, assuming that it persists.

Basin	Country	Factors	Season	Trend	Duration (yrs)	Amount (%)
Atlantic	Belgium	1, 4	winter	rising	40	+15
	Denmark	1	winter	rising	40	+15
	France	1, 4	winter	rising	40	+15
		2	winter	falling	100	Very small
	Germany	1	winter	rising	40	+15
	Holland	1, 4	winter	rising	40	+15
	Ireland	1, 4	winter	rising	40	+15
	Portugal	2	winter	falling	100	Very small
		4	winter	rising	40	+15
		6	summer/winter	none/falling	0/100	0/-8
	Spain	2	winter	falling	100	Very small
		4	winter	rising	40	+15
		6	summer/winter	none/falling	0/100	0/-8
	United Kingdom	1, 5, 4	winter	rising	40, 80, 40	+15, +20, +15
Baltic	Denmark	1	winter	rising	40	+15
	Finland	1, 5	winter	rising	40, 80	+15, +20
	Germany	1	winter	rising	40	+15
	Sweden	1, 5	winter	rising	40, 80	+15, +20
Mediterranean	France	2	winter	falling	100	Very small
	Greece	2	winter	falling	100	Very small
		7	summer/winter	rising	60/100	+30/ Very small
	Italy	2	winter	falling	100	Very small
	Spain	2	winter	falling	100	Very small
		6	summer/winter	none/falling	0/100	0/-8

Table 1 *Countries affected by trend in seasonal wind speeds*

Medium-term variability: the diurnal cycle

Wind speed variations related to the diurnal cycle have implications for the sustained productive capacity of a wind farm. The diurnal cycle of coastal wind was examined using example stations around the United Kingdom. Ten coastal stations were selected on the basis of geographical coverage, suitable site exposure, and length of record.

Analysis of these data demonstrate that consideration of the diurnal cycle of wind speed is essential in any assessment of offshore wind potential, especially for the near offshore where early wind farm developments are most likely to be located. For winds with a land fetch (i.e. approaching the anemometer from over a land surface) there is a pronounced diurnal cycle, peaking in the early afternoon, in spring, summer, and autumn. The peak of the cycle can give higher mean hourly wind speeds in summer than in winter. No diurnal cycle, or a weak cycle peaking in the early hours of the morning, is associated with winds having a sea fetch (i.e. approaching the anemometer from over a sea surface). In winter, wind speeds have no diurnal cycle irrespective of fetch. The diurnal cycle appears not to have any relation to the direction of the wind, being purely a function of land fetch. Moreover, any relation with the geographical location of the recording station appears to be weak.

Figure 7 shows an example of these data for one of the selected coastal stations. In this case the plots are based on data recorded at Gorleston on the east coast of England between 1987 and 1993.

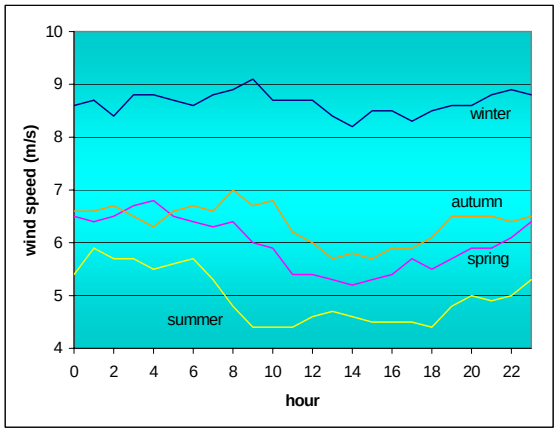

(a)

Gorleston: sea fetch diurnal cycle by season

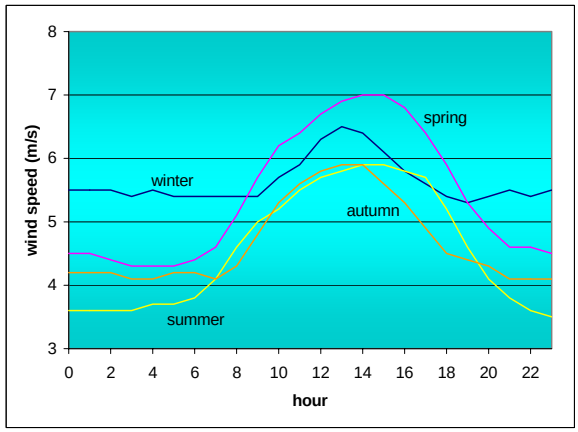

(b)

Gorleston: land fetch diurnal cycle by season

Figure 7 Examples of diurnal cycle analysis plots

Overall, the suggestion is that the results should apply equally to other European coasts at similar latitudes, including the whole of the North Sea, the Baltic Sea, central and southern Norway, western France and, probably, the Atlantic coasts of Spain and Portugal. The Mediterranean behaves essentially as an inland sea, with little mixing between warm surface water and cool water advected from polar latitudes. Thus, it is likely that the surface waters have more of a diurnal cycle of temperature than the open ocean and that the difference in wind speeds between land and sea fetches is less pronounced than on the coasts of the North Atlantic. Station data from the Mediterranean would be required to test this hypothesis.

Short-term variability: Gusts

Due to difficulties in obtaining gust data from offshore sites, it was decided to concentrate on exploring techniques for obtaining information on extreme events. The UK coastal station datasets used in the analysis of the diurnal cycle of wind speed also contain information on the maximum gust speed in each hour. In order to best represent patterns of gust behaviour over the open sea, only the four stations with no land fetch were considered. Of these, the most complete record was for Tiree, a small island off the west coast of Scotland, where 15 years of gust data were available (1983-1997).

A simple but elegant method of examining the long-term behaviour of maxima involves fitting the Generalised Extreme Value (GEV) Distribution to the data. If a reasonable fit is obtained, various statistics about the return period of maximum gusts over many years can be deduced. Three methods of fitting the GEV to the annual maximum gust were tested:

- maximum likelihood,
- method of moments, and
- probability weighted moments (PWM)

Figure 8a shows the time series of the 15 annual maxima for Tiree. Figure 8b shows the cumulative density functions (CDF) derived empirically from this maximum gust time series together with the

CDF from the GEV, calculated using PWM, that best fits this time series. The match appears to be very good.

Overall, the results indicated that extreme value analysis offers a valuable technique for the evaluation of damaging high wind occurrence at offshore wind speed sites. From a relatively short run of data, here 15 years, it is possible to explore the behaviour of severe winds over 50 years.

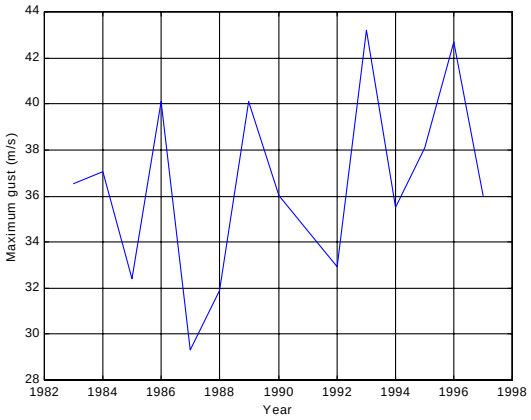

(a)

Annual gust maxima for Tiree

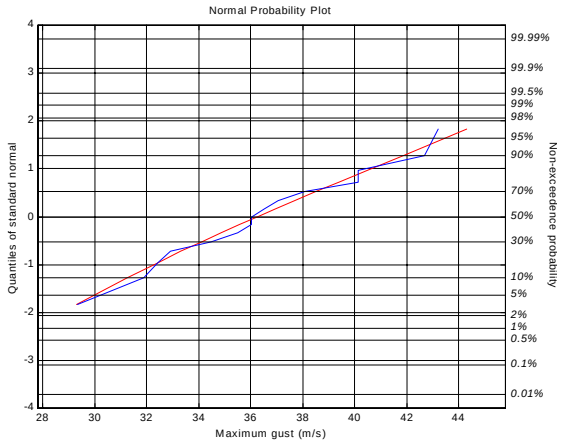

(b)

Normal probability plot of empirical (blue line) and GEV (red straight line) functions for Tiree annual maximum gust speeds

Figure 8 Example results from analysis of extreme gusts

9 Waves

Offshore wind turbines are designed to withstand the fatigue loading and extreme loads that are encountered at sea locations. To this end it is important to characterise both the wind loads, the wave loads and the correlations between them. Modern design codes use the wave state as input to generate the corresponding loads. The wave state is characterised by the significant wave height, the wave direction, the wave period and the corresponding wave conditions.

Previous studies (e.g. Opti-OWECS) have shown that the loads that offshore wind turbines have to withstand are generated by wind sea. The time period of these waves corresponds to the dynamic response periods of the structure, whereas swell waves have much longer wave periods and thus are less of a problem to the structure.

The POWER study has concentrated on mapping these parameters for the European seas. In addition, for selected areas more detailed “footprint” data have been compiled. The footprint-data give more insight in the wind and wave pattern, i.e. the annual variations, monthly variations, extreme conditions, and frequency distributions. Moreover, the footprints contain correlations between wind and wave conditions, such as scatter diagrams which can be used for design purposes.

These data have been retrieved from the UK Meteorological Office’s European wave model archive covering the area 30.5°N to 66.75°N and 14.0°W to 35.5°E. This comprises the Baltic Sea, the North Sea, the Atlantic, the Mediterranean Sea and the Black Sea.

Generally, the significant wave height with a 50 year return period is the determining wave load for offshore constructions. Figure 9 depicts the distribution of this load for the European seas. We can conclude that the most severe wave conditions appear in the Atlantic Ocean (Norway, Ireland, France and Spain). The Baltic sea is sheltered for extreme wave conditions. Surprisingly in parts of the Mediterranean quite severe wave conditions might occur.

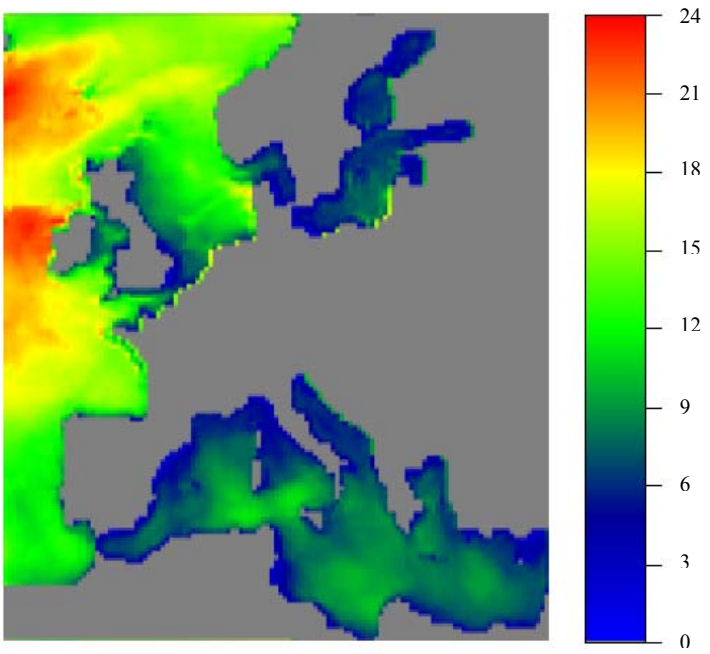

Figure 9 Extreme wave height (m) for a 50 year return period

More details of the analysis of wave data can be found in [1, Chapter 8].

10 Confidence limits

A bootstrapping estimation method was used to gauge the reliability of the final POWER wind speed estimates by calculating 95% confidence limits in the calculated mean monthly wind speeds.

Essentially, bootstrapping uses the available data to create a large number of extra data sets using resampling with replacement. Using the Weibull parameters for each directional bin estimated by WAsP (see Section 4), twelve sets of simulated wind speeds were created, one for each directional bin, with 100 simulated wind speeds per bin. The creation of simulated data fitting a known distribution (in this case the Weibull distribution) is fairly straightforward and the facility is available in many commercial statistics packages including MatLab. The simulated data were then used to calculate the monthly mean wind speed for that grid square for each direction bin. To arrive at an overall mean, the bin means were weighted according to the frequency of wind speeds associated with each direction, and then summed. The 95% confidence limits for the overall mean were derived by applying the frequency weighting procedure to the confidence limits for each directional bin.

Clearly, the method is complex, and the project team found it impractical to perform the analysis for each height and grid point. Therefore, effort was concentrated on six grid squares, each chosen to represent one of the regions identified as important in the analysis of the long-term wind field patterns (see Section 7). Furthermore, 95% confidence limits were produced for a single height (90m a.s.l.) selected to be a typical hub height for offshore wind turbines. Note, however, that the methodology can be readily applied to data for any height at any location.

The use of Monte Carlo simulation to calculate confidence limits was also investigated. The confidence limits were similar to those from bootstrapping but the analysis took 100 times longer, making the use of this method prohibitively slow.

The methodology and results of the analysis of confidence limits are described more fully in [1, Chapter 9].

11 Comparisons with measured data

POWER's WAsP model results were compared with measured data from sites off the coasts of The Netherlands (Measuring Network Zeeland (ZEGE) and Measuring Network North Sea (MNZ)), Denmark (meteorological masts at Horns Rev and Læsø Syd) and the Mediterranean. In some cases, the source data had been subjected to inconsistent processing techniques which meant that a significant amount of effort was required to reconstruct the observation data to make them consistent and thus suitable for the comparison.

The comparison results presented here merely provide an overview of the comparisons performed. Full details are given in [1, Chapter 10].

Dutch waters

Figure 10 and Table 2 both compare observed and calculated values of mean annual wind speeds for six stations in Dutch waters - three of the Measuring Network North Sea (K13, Euro platform (EPF) and Measuring Post Noordwijk (MPN)) and three of the ZEGE network (Oosterschelde 4 (OS4), Brouwershavensche gat 2 (BG2) and Vlakte van de Raan (VR)).

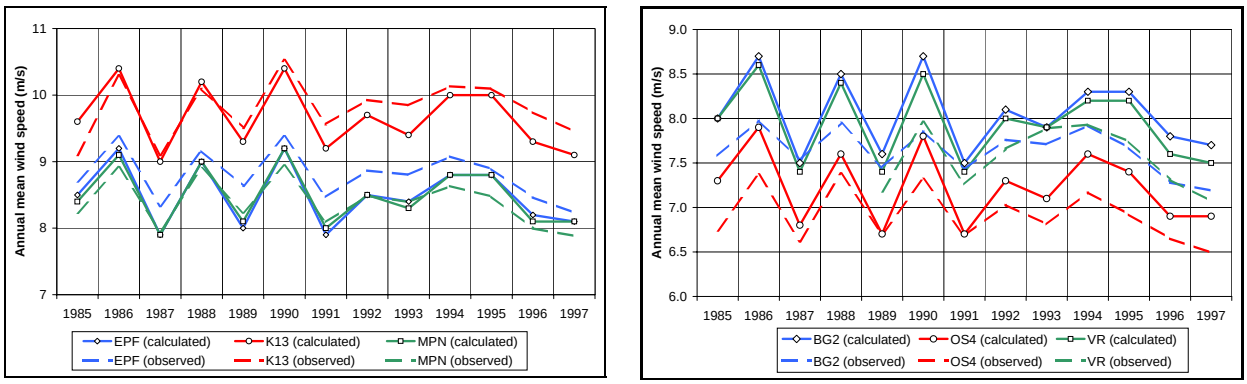

(a) *Measuring Network North Sea*

(b) *ZEGE*

Figure 10 Comparison of observed and calculated annual mean wind speeds in Dutch waters

The dashed lines are the results of the averages of the (reconstructed) observations, the solid lines are the POWER WAsP calculations

Table 2: Overview of observed versus calculated mean wind speeds.

Location	EPF	K13	MPN	BG2	OS4	VR
observed mean wind speed (m/s)	8.80	9.80	8.40	7.64	6.91	7.56
calculated mean wind speed (m/s)	8.50	9.66	8.48	8.05	7.23	7.86
observed/calculated	104%	101%	99%	95%	96%	96%

The results of these comparisons suggest the POWER results show good agreement with the observed data in Dutch waters.

Danish waters

The POWER WasP results were also compared against high quality wind speed profile data collected by ELSAM on purpose-built meteorological masts at two prospective offshore wind farms sites for in Danish waters – Horns Rev and Læsø Syd. These data were gathered over the 12 month period between June 1999 and May 2000.

Figures 11a and 11b compare POWER WAsP model mean annual wind speed estimates with wind speeds observed at Horns Rev and Læsø Syd respectively.

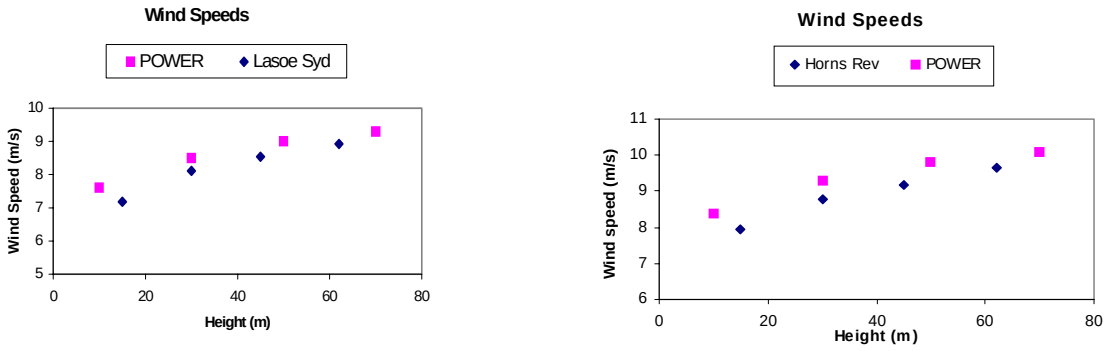

(a) (b)

Horns Rev *Læsø Syd*

Figure 11 Observed and calculated mean vertical wind speed profile in Danish waters

At first sight, these results suggest POWER has overestimated the mean wind speeds at these site by the order of 0.5m/s. However, it must be remembered that the ELSAM Horns Rev/ Læsø Syd observations represent the wind conditions that occurred at these locations during a single 12 month period (June 1999-May 2000), whereas the POWER results represent mean wind speeds over 13 year period (1985-1997). Figure 12 and 13 show POWER estimates of the inter-annual variation in mean wind speed over this 1985-1997 period at Horns Rev and Læsø Syd respectively. It is clear that from year to year there is significant variation in the mean wind speeds at the sites. Furthermore, the ELSAM Horns Rev/ Læsø Syd observed wind speed values lie within the overall range of mean wind speed values estimated for the sites.

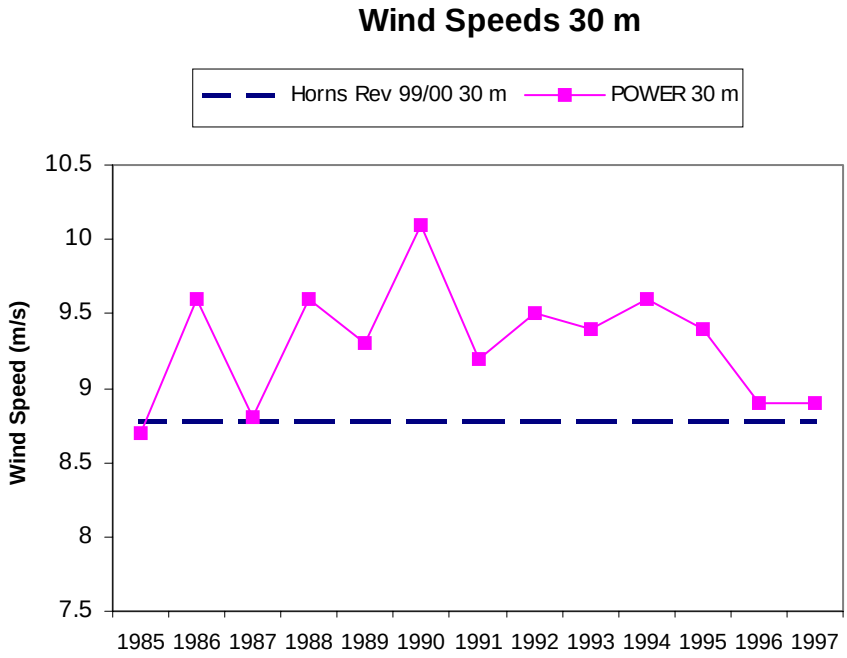

Figure 12 – Predicted variation in mean yearly wind speed at 30 m ASL for Horns Rev 1985-97

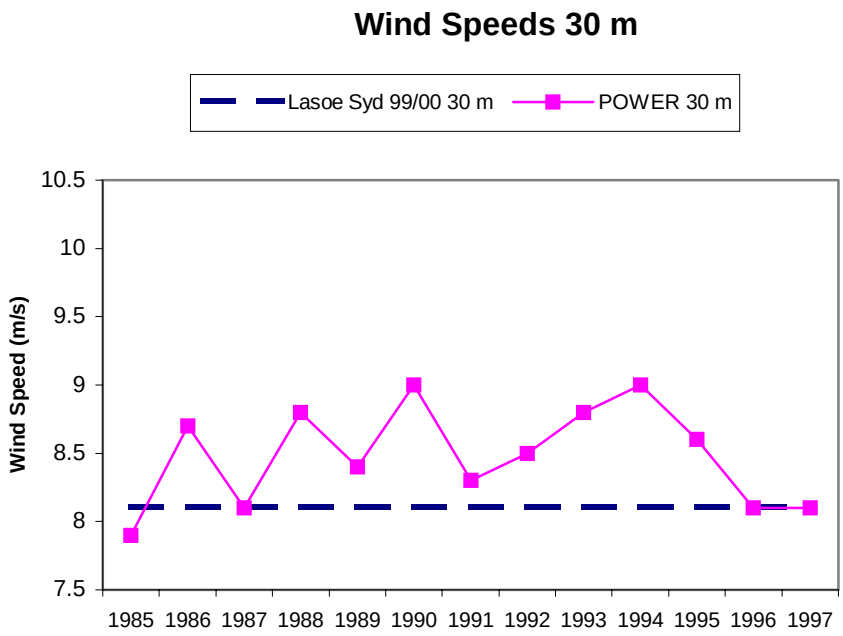

Figure 13 – Predicted variation in mean yearly wind speed at 30 m ASL for Læsø Syd 1985-97

Figures 14 and 15 compare the observed variation in mean monthly wind speed (for June 1999 to May 2000) with the POWER model estimates for Horns Rev and Læsø Syd. The correlation between the observed and calculated values is good.

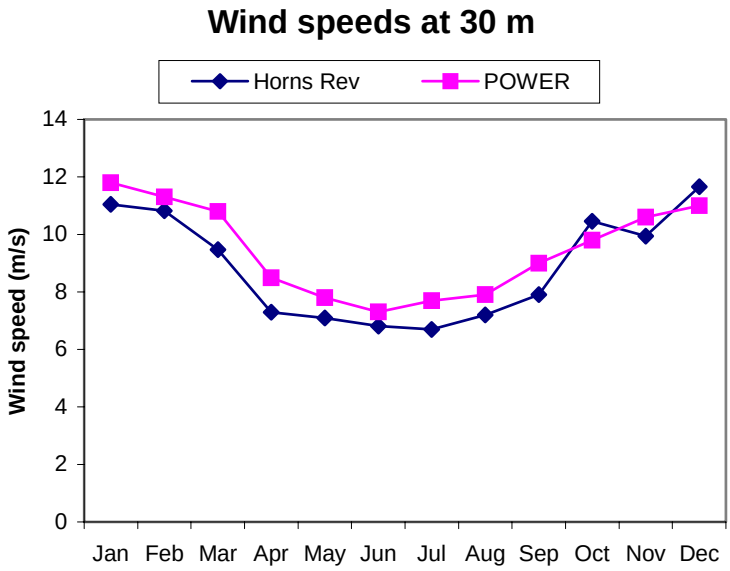

Figure 14 – Comparison of observed and calculated monthly variations in wind speed at Horns Rev

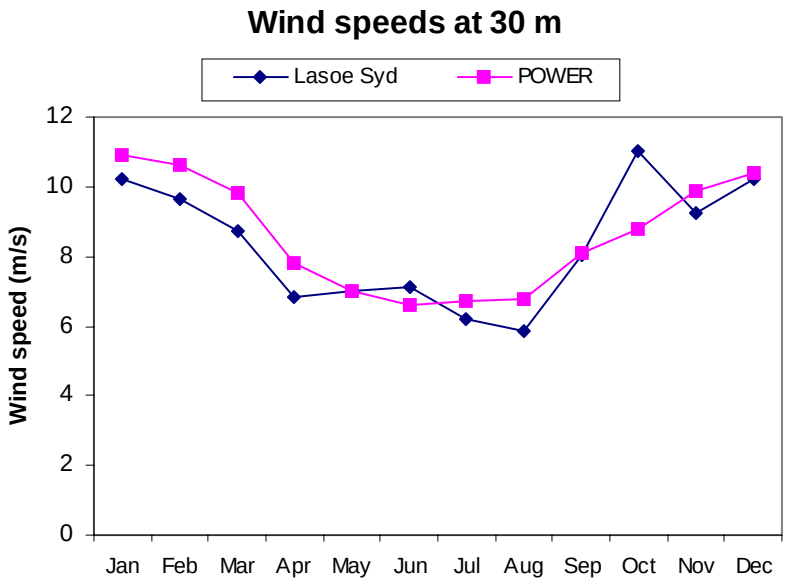

Figure 15 – Comparison of observed and calculated monthly variations in wind speed at Læsø Syd

Figures 16 and 17 show the observed and calculated wind rose at Horns Rev and Læsø Syd respectively.

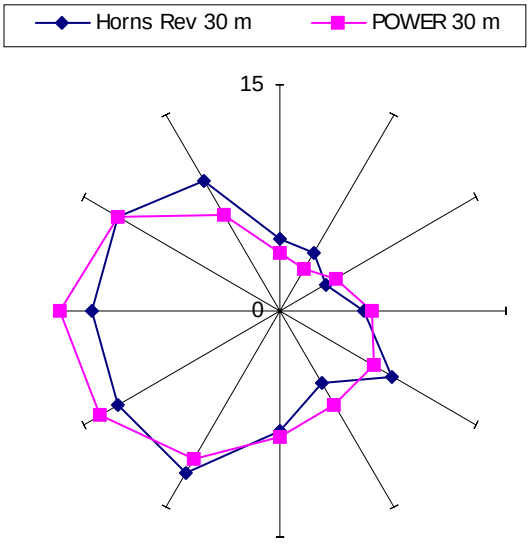

Figure 16 – Comparison of observed and calculated wind rose at Horns Rev

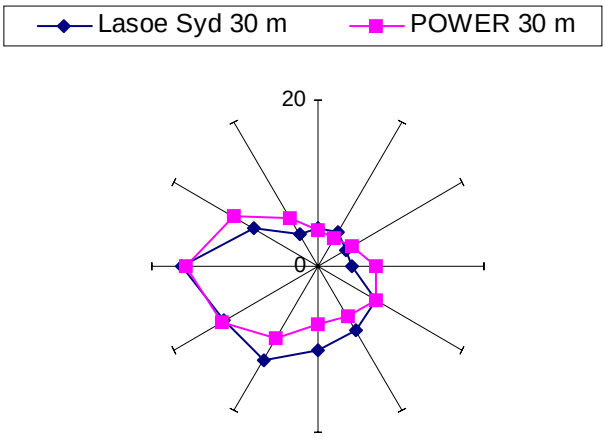

Figure 17 – Comparison of observed and calculated wind rose at Læsø Syd Figure

Finally, Figures 18 and 19 show the observed and calculated wind speed distributions at Horns Rev and Læsø Syd respectively. In both cases, the POWER results seem to have under-estimated the frequency of medium- to low wind speeds, but over-estimated the frequency of high wind speeds

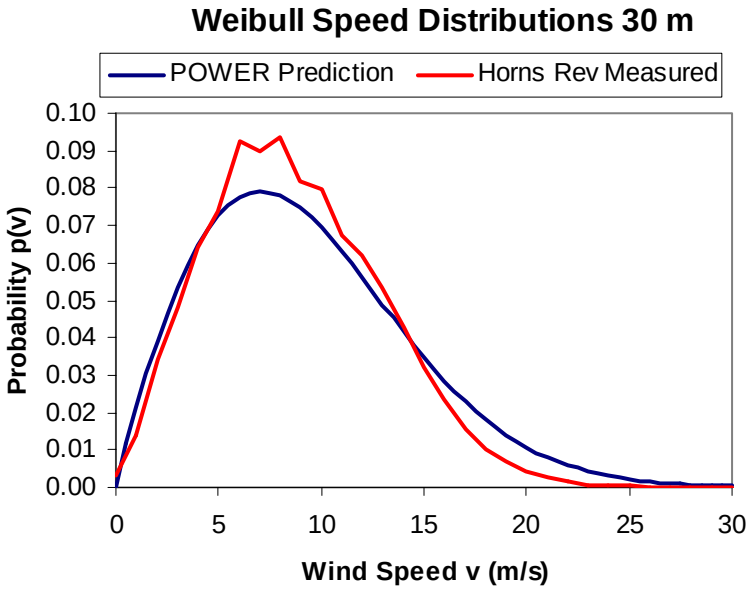

Figure 18– Comparison of observed and calculated wind speed distribution at Horns Rev

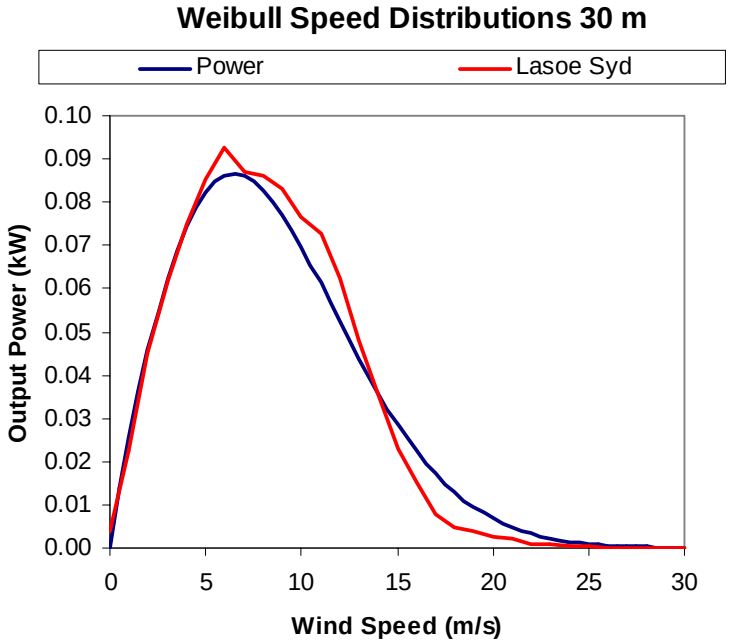

Figure 19 – Comparison of observed and calculated wind speed distribution at Læsø Syd

Overall, comparison of observed and calculated wind conditions at both of these proposed Danish offshore wind farm sites indicate that the POWER results are a good representation of the typical wind regime for these sites.

12 Conclusions

On a regional and national scale, POWER has produced state-of-the-art estimates of the extent and distribution of Europe's offshore wind energy resources not only in the coastal zone – the current focus of the offshore wind industry's attention – but also throughout the region's far offshore areas, where there is potential for wind energy to be exploited in the longer-term by turbines mounted on floating structures. Hence, this information will enable the most appropriate and economically attractive areas for offshore wind energy development to be identified, both now and in future.

On a local scale, POWER provides detailed first estimates of the long-term environmental conditions at specific offshore locations. This information is useful to the offshore wind energy industry since this is the exactly the type of data required for initial scoping and feasibility studies for new offshore wind energy developments. It may be possible to base preliminary assessments of the turbine power output as well as other key parameters such as initial values of the design parameters for turbine support structures etc. on the POWER results. This enables the broad technical and economic feasibility of an offshore wind farm at a particular site to be established without the need to initiate costly and time-consuming an offshore meteorological data gathering campaign. If the site is suitable, more detailed (and short-term) wind and wave monitoring studies can then be performed at the site, which refine the initial POWER estimates for detailed design purposes.

13 The POWER tool

The data on wind and wave parameters for European waters produced by the POWER project has been compiled as a set of Microsoft Excel work books. The data can be accessed using the "POWER tool" - a simple graphical user interface (GUI) that allows the user to display, in both numerical and graphical form, data from the database of wind and wave parameters.

14 Acknowledgements

The authors would like to acknowledge the support of the Directorate General XII of the European Commission who are providing part funding for this project under JOULE programme contract JOR3-CT98-0286 – POWER (Predicting Offshore Wind Energy Resources).

15 References

1. G M Watson, J A Halliday, J P Palutikof, T Holt, R J Barthelmie, J P Coelingh, E J van Zuylen, J W Cleijne (2002). Predicting Offshore Wind Energy Resources – Final report of EC Contract JOR3-CT98-0286 – restricted circulation report.
2. N G Mortensen, L Landberg, I Troen and E L Petersen (1993) 'Wind Atlas Analysis and Application Program (WAsP) Vol 1: Getting Started'. Risø National Laboratory user guide: Risø-I-666(EN)(v.1).
3. Taylor P K and Yelland M J (2000), The Dependence of Sea Surface Roughness on the Height and Steepness of the Waves, accepted in final form by Journal of Physical Oceanography in May 2000
4. Frank H P, Larsen S E and Højstrup J (2000), Simulated Wind Power Offshore Using Different Parameterizations for the Sea Surface Roughness, Wind Energy; 3
5. Lange B and Høstrup J (2000), The influence of waves on the offshore wind resource, Proceedings of the European Seminar on Offshore Wind Energy in Mediterranean and other European Seas (OWEMES 2000), Siracusa, April 2000
6. Moore D (1982), '10 to 100m winds calculated from 900mb wind data', Proceedings of the 4th British Wind Energy Association Conference, Cranfield, BHRA
7. Risø National Laboratory (1989) Isovent map on URL http://130.226.52.108/oceanmap.htm, accessed 17/01/00.
8. S C Pryor and R J Barthelmie (2002), Statistical analysis of flow characteristics in the coastal zone, *Journal of Wind Engineering and Industrial Aerodynamics*, **90**, 201-221
9. R J Barthelmie (1999) 'Developing a coastal discontinuity model for the POWER project', Proceedings of the 1999 Twenty First BWEA Wind Energy Conference, Cambridge 1-3 September 1999, Professional Engineering Publishing.
10. R J Barthelmie (2000), 'Measurements and modelling of coastal meteorology', Proceedings of the OWEMES 2000 Conference, Siracuse, Sicily 13-15 April 2000, ENEA.

CHAPTER 1 : Background to the POWER project

Chapter authors:
G M Watson and J A Halliday (CLRC Rutherford Appleton Laboratory)

1.1 The importance of offshore wind energy in Europe

The countries of the European Union (EU) are faced with the challenge of meeting the energy needs of Europe's industries and of its population in general. At the same time the global community is becoming increasingly aware of the need to consider the strain that human activities are placing on the planet. In particular, there is widespread concern that modern societies' broad reliance on carbon-based energy sources within a so-called "carbon economy" is leading to significant changes in the composition of the atmosphere, which in turn is believed will be responsible for large scale and long-term changes to global climate. The international response has been to draw up the UN Framework Convention on Climate Change (UNFCCC) – an international agreement which sets out the overall policy framework for addressing the climate change issue. The Kyoto Protocol to UNFCCC set out for the first time a binding commitment for developed nations – including the member states of the EU - to achieve reductions in emissions of carbon dioxide and other greenhouse gases. Furthermore, climate scientists point out that the Kyoto reductions should be seen as only the first step in a longer-term effort to reduce greenhouse gas emissions by the 60% or more that will be required to restore and sustain the balance within the planet's atmosphere.

In this setting, renewable energy technologies are set to play a central role in assisting EU member state governments achieve their national carbon dioxide reduction targets (both now and in the future), whilst continuing to meet the demand for energy.

Compared to other regions, Europe is blessed with an extensive wind energy resource which has the potential to provide for a significant component of the its future energy needs. By the mid-1990s land-based wind energy developments were firmly established on a commercial basis in several EU countries. However, increasing pressure on land use has led to a move to develop wind power offshore; Denmark, Sweden, the Netherlands, the UK, Eire and France have either already started to develop offshore wind energy installations, or have plans to do so in the near future and other EU member states, such as Belgium, are currently considering developments of this kind.

It has become apparent that rapid exploitation of the offshore wind energy is an important part of Europe's overall energy strategy. Development is currently handicapped by significant knowledge gaps, including a scarcity of good quality information on the extent, characteristics and distribution of the offshore wind energy resource. Clearly these issues must be addressed before Europe's offshore wind energy resource can be exploited fully.

1.2 The demand for information on offshore wind energy resources

Information on offshore wind energy resources is sought by several end user groups ranging from policy-makers and planners at regional (e.g. EU), national (e.g. EU member state) and local (e.g. local government/district authority or equivalent) scales to the fledgling offshore wind industry who are seeking to develop offshore wind energy on a commercial basis. Knowledge of the overall extent and distribution of the offshore wind resource is required to:

- Identify the most appropriate and economically attractive regions/areas for offshore wind energy development.
- Develop regional/national/local energy strategies that are in accordance with current and future regulation and other initiatives such as the Kyoto Protocol, Agenda 21 etc..
- Plan investment in new technologies, suitable infrastructure etc. in areas where offshore wind energy developments are expected to go ahead.
- Provide underpinning knowledge when developing any future trading scheme of "green" electricity, carbon credits, investment in technology transfer projects etc.

In addition, offshore wind farm developers have a series of specific data needs and require accurate, detailed and long-term characteristics of the local wind regime and wave conditions to:

- Select the most favourable site(s) for an offshore wind farm within the broadly attractive regions already identified.
- Assess and/or infer many of the fundamental environmental design parameters for the wind turbines and support structures at the chosen site.
- Provide evidence of the technical and commercial viability of a proposed project (required when seeking support (e.g. financing, planning permission etc.) for a new development. The local wind regime not only controls the amount of energy that is harvested at the site, but also influences directly the operation and maintenance regime of the turbine(s). Together, these factors largely determine the initial capital and maintenance costs of the development as well as its revenue potential.
- Predict suitable windows of opportunity for construction, installation, maintenance and repair operations.
- Identify the optimum operation, maintenance and repair regime for the offshore wind development.

It is clear that various categories of end user need an accurate knowledge of the offshore wind regime. Furthermore these user groups need this information at a range of levels of detail and geographical scale.

1.3 Estimating offshore wind energy resources in European waters

After years of study, meteorologists now have a relatively good understanding of the wind regime over the land, as well as a toolbox of wind models and data manipulation techniques that can be used to estimate the wind resource in particular sites. There have also been numerous studies to assess onshore wind energy resources ranging from specific data gathering campaigns followed by detailed analysis of the local wind regime at sites selected for wind energy developments to broad-brush assessments of the extent and distribution of the onshore wind energy resource throughout Europe and, at a higher resolution, in several EU member states.

By contrast, the phenomena that influence offshore winds are not well understood at the present time and measured wind data at offshore locations are spatially and temporally sparse and of variable quality. This scarcity of information means there is little on which to base offshore wind models and, unfortunately, it is believed that many of the data manipulation techniques used onshore cannot be extended to offshore sites. There have, however, already been a few basic assessments of the offshore wind resources in EU waters, which have demonstrated that the offshore wind resource is very large, particularly in the waters of northern Europe. However, without detailed knowledge of the characteristics and distribution of the resource the offshore wind industry is unable to answer questions on the economics of offshore wind energy because of the uncertainties that still exist.

Together these limitations represent a severe handicap to commercial exploitation of the resource. To illustrate the difficulties currently faced by offshore wind energy developers it is, perhaps, useful to compare methods currently available to assess the detailed wind energy resource onshore and offshore sites.

At onshore locations it is common practice to first consult a wind atlas to get an initial indication of the resource in the locality. It is then straightforward and inexpensive to erect one or more meteorological masts at the selected site, and to gather numerous data parameters for a period of several months, if not years. Typically these masts (and their foundations) have a standard design and are relatively cheap to install. Furthermore at onshore there are few difficulties in supplying the power demands of the instruments and it is easy to visit the site frequently to recover the data gathered (which therefore does not need to be stored for long periods) and for maintenance and repair purposes.

To produce a long-term estimate of the wind speeds for the onshore site, the short-term measurements from the mast are correlated with those from a nearby meteorological station where reliable long-term

data is available. Fortunately there is an extensive system of well-established meteorological stations throughout Europe where long-term and historical data suitable for this purpose is available.

By contrast, very few offshore wind atlases have been produced to date and even these are largely based on extrapolation and interpolation of onshore data. In addition, offshore meteorological masts are expensive and difficult to install and very costly also to operate – particularly for prolonged periods. The offshore environment is notoriously harsh and in these areas structures such as meteorological masts and their instruments are subject to severe loading and high rates of corrosion. Typically each offshore meteorological mast and its foundation must be specifically designed to cope with the wind, wave, ice, current and seabed ground conditions at the site. Furthermore, in these conditions it is not straightforward to ensure an adequate power supply at the mast or to make regular visits to maintain and repair the instruments mounted on them and to retrieve the data gathered. Consequently, offshore meteorological masts have been erected in only a very small number of locations and the data gathered have an extremely high commercial value and as such are not always in general circulation.

Finally, in the almost total absence of reliable long-term measured offshore wind data developers are forced to correlate short-term offshore mast measurements with long-term data from a nearby onshore site. These sites are often a considerable distance apart and, in any case, the correlation may not be appropriate due to the differing on-and offshore climatologies.

It is easy to see why there is considerable interest in establishing an accurate knowledge of the wind regime in offshore waters.

1.4 POWER project objectives

The Predicting Offshore Wind Energy Resources (POWER) project was an ambitious attempt to improve the understanding of the nature and distribution of Europe's offshore wind resource. In particular the project team set out to improve upon previous estimates of the European offshore wind energy resource, to consider a number of additional factors that could affect its exploitation on a commercial basis and to present the information in straightforward, yet useful format.

The project had the following specific objectives:

1. To develop and document a combined three-model methodology for the estimate of wind power offshore applied to EU waters which gives more accurate estimates of the offshore resource (where suitable observed data exists) than current estimates, in particular, the European Wind Atlas, the Germanischer Lloyd/Garrad Hassan study (JOUR 0072) and Young and Holland's Atlas of the Oceans: Wind and Wave Climate.

2. To produce two detailed data sets of SODAR measurements of on-to-off- and off-to-on-shore winds on the east coast of England and on the Dutch coast.

3. To produce a data product that will allow an end user:

    a) To find out the long term wind power resource at a given offshore location in European Union waters.

    b) To assess the expected inter-annual and seasonal variability at that site.

    c) To deduce the expected wind speed distribution at the location of interest.

    d) To investigate whether the area of interest is unsuitable for offshore wind farm siting due to excessive wind/wave loading and extreme gust events.

4. To make and document a case-study at prospective offshore wind farms site(s) in order to validate the data product at site(s) where observed data exists.

The project was organised into a set of 12 discrete work packages, each tackling a specific task within the overall work programme. However, during the course of the project it became increasingly apparent that the work packages were not arranged in the most logical manner for reporting purposes. Therefore in this report the POWER project team's work and findings are not presented within a framework of work packages, but instead have been regrouped and reordered to guide the reader

through the project more logically.

1.5 Structure of this report

The reports starts (in Chapter 2) by describing the basic POWER methodology; it then describes (in Chapter 3) how the geostrophic winds were calculated using pressure data using an interpolation method, and the checks carried out to test the accuracy of the resulting wind fields; Chapter 4 describes the use of the WaSP package to transform the geostrophic winds to a range of turbine hub heights; Chapter 5 introduces the Coastal Discontinuity Model (CDM) and its application, before comparing the WaSP and CDM wind fields, and the modelled and measured offshore wind profiles; Chapter 6 describes the SODAR measurements made in the Netherlands and in the UK, reviews the usefulness of the SODAR instrument , and then compares the on-shore and off-shore winds; Chapter 7 examines the variability of offshore winds : long-term trends, diurnal cycles and gusts; Chapter 8 describes wind/wave modelling carried out and the results obtained; Chapter 9 reports on the confidence limits calculated for monthly mean offshore wind speeds – these were calculated on a regional basis; Chapter 10 describes the comparison of the POWER wind field with measured data in the Netherlands, in Denmark, in the Mediterranean, and with those obtained by an earlier EU study. Finally, Chapter 11 describes the POWER Tool, a simple graphical user interface, which allows the user to display in graphical and tabular form the POWER results for a specified grid point.

Appendix 1 of the report lists the publications issued during the study.

CHAPTER 2 : Introduction to the POWER project

Chapter author: G M Watson (CLRC Rutherford Appleton Laboratory)

2.1 General characteristics of the wind field over the sea

In offshore areas it is generally thought that wind speeds will be higher and there will be a smaller vertical wind gradient and less turbulence than at onshore sites. This means that it should be possible for offshore wind turbines to have higher energy outputs and suffer less fatigue loading and thereby to have a longer active life compared to those on land.

However, in coastal sea areas the wind regime is influenced by the adjoining land surfaces resulting in some complex interactions. There is evidence that in some circumstances this zone of coastal influence extends a large distance from the shore - perhaps as far as a couple of hundred km from the nearest land. This coastal zone is the region of immediate interest since, for the foreseeable future at least, technical and logistics limitations associated with water depth and distance to shore mean that offshore wind developments are likely to be restricted to seabed-mounted wind turbines in nearshore areas. Within this “coastal discontinuity zone”, there are various phenomena that may affect wind conditions, driven by differences between the land and sea such as changes in surface roughness, temperature and atmospheric stability including:

Internal Boundary Layer (IBL) development

Sea breeze circulation

Low level jets

Internal boundary layers (IBL) form downwind of a significant step change in surface roughness such as a coastline. In off-shore wind conditions, airflow in the lowest layer is in equilibrium with the sea surface, but there will be an upper layer which retains equilibrium with the air over the land. There will also be an adjustment or blending layer where the two air masses meet but the mixed wind profile can extend downstream for a significant distance.

IBL growth varies under different stability conditions. In stable conditions offshore the IBL grows slowly and can remain below 100m for considerable distances inhibiting momentum exchange and impacting on the wind speed profile. Conversely, in unstable conditions the IBL grows quickly and rapidly attains equilibrium. It is interesting to note that in very stable atmospheric conditions (with low mixing rates), it is possible for the hub of a coastal offshore wind turbine to be above the lower layer and operate in the upper airflow. Indeed, in this scenario, the turbine rotor will experience conditions characteristic of the wind over land rather than the sea and no benefit will have been gained by constructing the turbine in the sea.

Sea breezes are driven by convection. As the land heats up during the day, the overlying air warms and rises. Cooler sea air is drawn inland to replace it and a convection cell develops. The resulting on-shore winds may mask a weak weather pattern and produce very different wind conditions to those forecast by synoptic models. The convection system may reverse during the night resulting in an off-shore land breeze.

Low level jets are characterised by an increase in mean wind speed accompanied by high wind shear, which can in turn spawn high levels of turbulence. There are many postulated causes of low-level jets, one of which is advective acceleration as a mass of air is blown off-shore. They occur as low as 50 m height and up to 600m height and may increase in intensity over time (6 – 8 hours) as the air mass travels over the sea. In areas where jets appear, offshore wind turbines will experience higher wind speeds, but will also encounter more severe loading and fatigue.

The wind also interacts with the sea. As the wind passes over the water, energy is transferred from the air to form wind-generated waves. This continues until the sea state is fully developed. When the wind drops the sea state also declines, but usually at a slower rate. In most conditions, the transfer of momentum between the sea and the air mass almost cancels out, however at low wind speeds a momentum feedback loop may develop that transfers energy from swell back to the wind.

Offshore wind speeds are also known to vary over a wide range of time scales:

Diurnal cycles

Seasonal cycles

Decadal cycles - unforced/internal variations e.g. the North Atlantic Oscillation (NAO)

Long-term variations – forced/external variations e.g. greenhouse warming

The scale of these variations is sufficient to have economic implications for onshore and offshore wind farms, and given that an offshore wind farm is likely to have a design life of 30 years or more, it is important to put any period of observation/measurement into the context of the long-term cycles of variability when assessing offshore wind resources.

Finally, there are a couple of other features of the offshore wind regime which may be of particular pertinence to offshore wind farm developments:

- The spatial variability of the wind resource within an offshore wind farm may be less compared to an onshore development. This is because on land a 10-15% variation can be expected due to topographical effects that are not an issue offshore (except in near-coastal areas). However, it is possible that the issue of wakes will add a similar degree of uncertainty to the resource of an offshore wind farm – particularly in large wind farms.

- It is also worth noting that due to lower offshore turbulence the wake effects generated by each turbine in the wind farm will likely propagate over larger distances than onshore, and that the effects of stability on wake propagation are expected to be larger. The implication is that wind farm design/spacing between turbines needs to be carefully considered. [*Aside: This topic is currently the subject of an EU supported research project Ref: ERK6-1999- 00001 ENDOW (Efficient Development of Offshore Windfarms).*]

2.2 Basic POWER methodology

Perhaps the most significant obstacle to the assessment of offshore wind resources to date has been the lack of measured offshore wind data on which to base the estimates. The POWER project team has now developed a novel methodology which can, nonetheless, produce long-term and spatially detailed estimates of the wind conditions at offshore sites covering a wide area.

The POWER methodology does not rely directly on observed wind data to predict wind conditions offshore. Instead, the estimates are based on grids of atmospheric pressure data at mean sea level covering the area of interest. This means that the POWER methodology may be used to produce spatially detailed estimates of wind conditions at offshore sites covering a large area.

The methodology is built up of three basic steps:

1. The pressure gradient at mean sea level is used to calculate the geostrophic wind.

2. The geostrophic wind is transformed to the sea surface layer by applying the Wind Atlas Analysis and Application Program (WAsP).

3. In nearshore areas, a coastal discontinuity model (CDM) is used to predict wind conditions taking account of effects atmospheric stability experienced in the land/sea transition zone.

Within the POWER project, the CDM is “fine-tuned” using both existing offshore mast data and coastal SODAR (SOund Detection And Ranging) data. In addition, the estimates of wind resource are supplemented by assessments of short-term variability and information on regions of extreme environmental loading. Since historical atmospheric pressure data dates back to 1880 and beyond, the methodology allows the long-term (decade to decade) variability of the offshore wind resource also to be investigated.

A schematic flow diagram of the POWER methodology is shown in Figure 2.1.

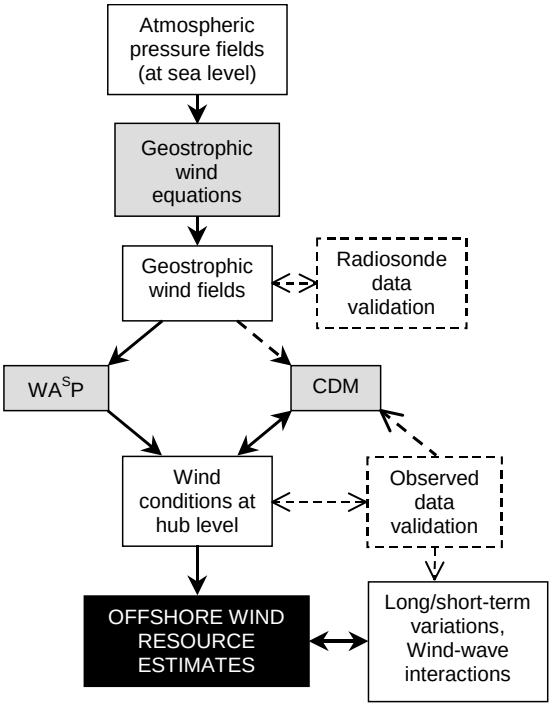

Figure 2.1 Flow schematic of POWER methodology

Note that within the POWER project, no attempt was made to model low-level jets

2.3 Application of the POWER methodology to European waters

The project team have applied this POWER methodology to the region 30ºN to 70ºN and 15ºW to 30ºE on a grid with the 0.5º x 0.5º latitude/longitude resolution. As Figure 2.2 shows, this area covers the major sea areas bordering European Union countries – the North Sea, the Baltic, the Mediterranean and the eastern North Atlantic.

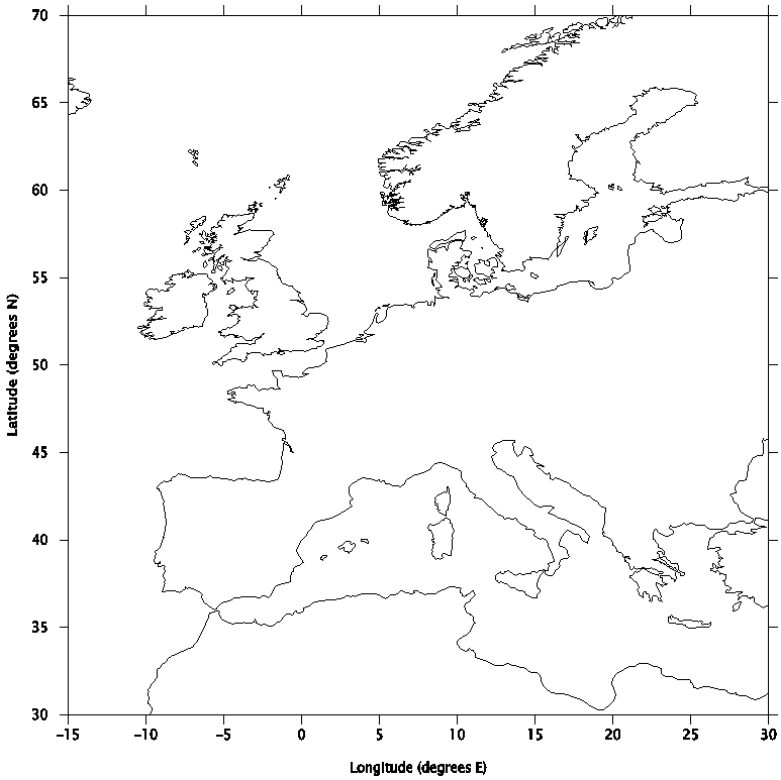

Figure 2.2 Map showing the European sea area where the POWER methodology was applied

On a regional and national scale, POWER has produced state-of-the-art estimates of the extent and distribution of Europe's offshore wind energy resources not only in the coastal zone – the current focus of the offshore wind industry's attention – but also throughout the region's far offshore areas, where there is potential for wind energy to be exploited in the longer-term by turbines mounted on floating structures. Hence, this information will enable the most appropriate and economically attractive areas for offshore wind energy development to be identified, both now and in future.

On a local scale, POWER provides detailed first estimates of the long-term environmental conditions at specific offshore locations. This information is useful to the offshore wind energy industry since this is the exactly the type of data required for initial scoping and feasibility studies for new offshore wind energy developments. It may be possible to base preliminary assessments of the turbine power output as well as other key parameters such as initial values of the design parameters for turbine support structures etc. on the POWER results. This enables the broad technical and economic feasibility of an offshore wind farm at a particular site to be established without the need to initiate costly and time-consuming an offshore meteorological data gathering campaign. If the site is suitable, more detailed (and short-term) wind and wave monitoring studies can then be performed at the site, which refine the initial POWER estimates for detailed design purposes.

CHAPTER 3 : Calculating geostrophic winds from sea level pressure data

Chapter authors:
G M Watson and Dr J A Halliday (CLRC Rutherford Appleton Laboratory) & Dr T Holt and Dr J P Palutikof (University of East Anglia)

3.1 Introduction

This Chapter describes in detail the first step in the POWER methodology (see Section 2.2) whereby mean sea level atmospheric pressure gradients are used to calculate geostrophic winds throughout an area of interest. It also reports on the application, testing and validation of this procedure in EU waters within the POWER project.

3.2 Theoretical background

The geostrophic wind is a theoretical wind calculated from surface pressure data. A balance is assumed between the flow of air from high to low pressure regions and the effects of the rotation of the Earth as manifested in the "Coriolis Effect". The geostrophic wind flows parallel to the isobars (contours of equal surface pressure), and a good approximation to the actual wind in the free atmosphere. A more detailed explanation of the geostrophic wind can be found in standard meteorological texts, for example, James (1994)

The geostrophic wind is the horizontal equilibrium wind (V_G), blowing parallel to the isobars, which represents the exact balance between the horizontal pressure gradient force:

$$-\left(1/\rho\right)\nabla_H p \qquad 3.1$$

and the horizontal component of the Coriolis Force:

$$fV_G \qquad 3.2$$

where $\nabla_H p$ is the horizontal pressure gradient, ρ is the air density, and f is the Coriolis parameter, which is a function of the Earth's angular momentum (Ω) and latitude (φ):

$$f = 2\Omega \sin\varphi . \qquad 3.3$$

The magnitude of V_G is given by:

$$V_G = \left|\left(1/f\rho\right)\nabla_H p\right| \qquad 3.4$$

Low pressure is to the left of the wind vector in the northern hemisphere, and to the right in the southern hemisphere.

From Equation 3.4, the geostrophic wind speed is a function of latitude, pressure gradient and air density. A reasonable assumption for air density is 1.2 kgm^{-3}. Making this assumption, and knowing latitude, only information on the pressure gradient is required to permit calculation of the geostrophic wind speed.

3.3 Sources of pressure data considered

Initially, three potential sources of atmospheric pressure data were identified for use in the POWER project:

1. The European Centre for Medium Range Weather Forecasting (ECMWF) – output from an on-going reanalysis of atmospheric data.
2. National Center for Atmospheric Research (NCAR) – 12-hourly data, gridded at a resolution of 5º latitude by 5º longitude. 1899 - present.

3. UK Meteorological Office – daily/monthly mean sea level pressure data for the Northern Hemisphere, gridded from synoptic charts at a resolution of 5º latitude by 10º longitude between 15ºN and 65ºN, and a lower resolution at higher latitudes. 1880 to present.

Of these data sources, the NCAR data set was considered to be the best long-term record of atmospheric pressure available.

However, by the time work on the POWER project commenced (in August 1998), the availability of suitable data had changed. In the intervening period, the National Centers for Environmental Prediction (NCEP) model had been used to reanalyse its source data based on a process of physical interpolation. This has generated readily available, 6-hourly atmospheric pressure data on a 2.5º latitude by 2.5º longitude grid. Moreover, the NCEP data dates back to 1948 and the historical data set is being continuously extended.

Unfortunately ECMWF were unable to supply data in a useable format immediately and consequently this potential source of data was not pursued further. In addition, it was decided that interpolation of the coarse resolution (5º x 10º) UK Met. Office data onto a fine (0.5º) grid would be inappropriate.

As a result, only two sets of atmospheric pressure source data – the NCAR and NCEP data sets - were selected as for detailed consideration as source data. UEA worked with the NCEP data (6 hourly on a 2.5º x 2.5º grid) while CLRC-RAL worked in parallel on the NCAR data set (12 hourly on a 5º x 5º grid). Test geostrophic wind speed vector and stream function plots calculated from the NCEP and NCAR data sets were compared for three sample days in 1990 (for details of the methodology used see sections 3.4 and 3.5). The dates selected represent a severe storm and typical winter and summer days and in each case the plots compared well, both with each other and with some independent validation data.

On this basis it was judged that both the NCEP and NCAR atmospheric pressure data sets would be suitable source data. However, given that the NCEP atmospheric pressure has a finer spatial (2.5º x 2.5º) and temporal (6-hourly) resolution it was considered superior to the NCAR data set. Furthermore, the NCAR data had numerous temporal gaps which made manipulation of the data in FORTRAN programs laborious. In view of this, the NCEP atmospheric data covering a 13 year period (1985 to 1997 inclusive) was selected as the primary source data for the POWER geostrophic wind calculations.

3.4 Interpolation of the pressure data

The NCEP atmospheric pressure data are available on a 2.5º x 2.5º latitude/longitude grid. The geostrophic wind was required on a 0.5º x 0.5º latitude/longitude grid. Therefore, the pressure data had to be interpolated onto the finer grid before performing the geostrophic wind computations. Since pressure is a relatively smoothly varying field at mid-latitudes, interpolation techniques were used that give smoothly varying estimates that are accurate at the original grid nodes. Two methods of interpolation were tested, bi-cubic and bi-cubic spline interpolation.

Since the most testing conditions for interpolation are during severe storms, when pressure gradients are greatest, four storms were used to examine the performance of the interpolation routines against each other and against an independent data set. The independent data used for testing were the surface pressure charts from the European Meteorological Bulletin (EMB). These are contoured by hand from station measurements and provide a rigorous, independent test of the interpolated data.

3.4.1 Bi-cubic interpolation

The main weakness of bi-cubic interpolation is that the user is required to specify derivative information at each grid point (Press et al., 1992). This is usually estimated using numerical methods. The method can give apparently reasonable interpolations that are inaccurate because of the approximate nature of the numerical technique used to specify the derivatives. However, the revised Akima algorithm used in this study provides reliable derivatives.

3.4.2 Bi-cubic spline interpolation

Essentially a variant of bi-cubic interpolation, bi-cubic spline interpolation uses one-dimensional splines to provide the derivative information. The bi-cubic spline provides the smoothest curve possible through the data, in the sense of minimising the mean squared sum of second derivatives (Watson, 1992). A problem with the method is that in regions of high gradient and sharp changes in

direction of the raw data, the interpolation can "overshoot" giving rise to anomalies such as negative rainfall! Mid-latitude gridded pressure data are not normally prone to sharp changes in direction so bi-cubic splines are a particularly useful way of interpolating pressure data. To overcome the problem of overshooting, a spline routine with the facility for introducing "tension" to the spline was used. This gives the technique known as "rubber-sheeting", where the interpolated data fit the original grid accurately and the interpolated points are located on a notional elastic sheet between them that can be pulled to any required level of tautness. To maximise the derivative information in the data, and allow realistic interpolation of low pressure centres between grid nodes, we start with minimal tension and search for evidence of overshooting.

3.4.3 Method of comparison

In a storm situation there are many closely packed isobars thus providing a challenging case study in which to evaluate interpolation techniques. Four storms were chosen, for each the meteorological chart for a time nearest to the time of maximum storm intensity was used. The test domain is 15º W to 15º E, and 45º N to 70º N. Three plots are presented; an isobar plot of the storm at the current time based on the spline-interpolated data, and latitudinal and longitudinal cross-sections of the test (EMB chart) and interpolated data near the centre of the storm. For copyright reasons it is not possible to present a digitized version of the EMB charts. Differences between the test charts and the interpolated data will be described where relevant. However, a general point is worth noting at this stage. The EMB charts have a 5º x 5º latitude/longitude grid. To digitize the cross-sections, we interpolated visually at increments of 2.5 degrees. This means that the cross-sections are not always through the centre of the storm, and that the location of the lowest pressure from the test data may suffer from apparent drift due to the relatively coarse resolution of these data. Finally, although hand contouring introduces a level of skill not available to computer generated contours, it is still prone to error where the data are sparse. Thus, although the EMB charts are expected to be more reliable than any gridded data, and are hence a suitable source of validation data, they may also contain problems in this analysis where pressure gradients are extremely high.

3.4.4 Results of the comparison

Storm of 16 October, 1987

This was the "hurricane" that devastated much of south-eastern England. Figure 3.1 shows the storm before it made landfall, as contoured by GrADS from the 0.5º x 0.5º spline-interpolated pressures. The distribution of pressure about the centre is very asymmetrical, with the region of strong winds being confined to the south-eastern quarter (this makes it something of a textbook storm). This interpolation is a very good representation of the overall pressure pattern observed for this storm. The location of the region of lowest central pressure is virtually identical to that found in the EMB chart. However, even though the 972 mb contour in Figure 3.1 is in roughly the same position as on the EMB chart, the observed gradient within that contour is much greater than indicated by the interpolations in Figure 3.1. This is discussed more fully in the description of the latitudinal and longitudinal cross-sections.

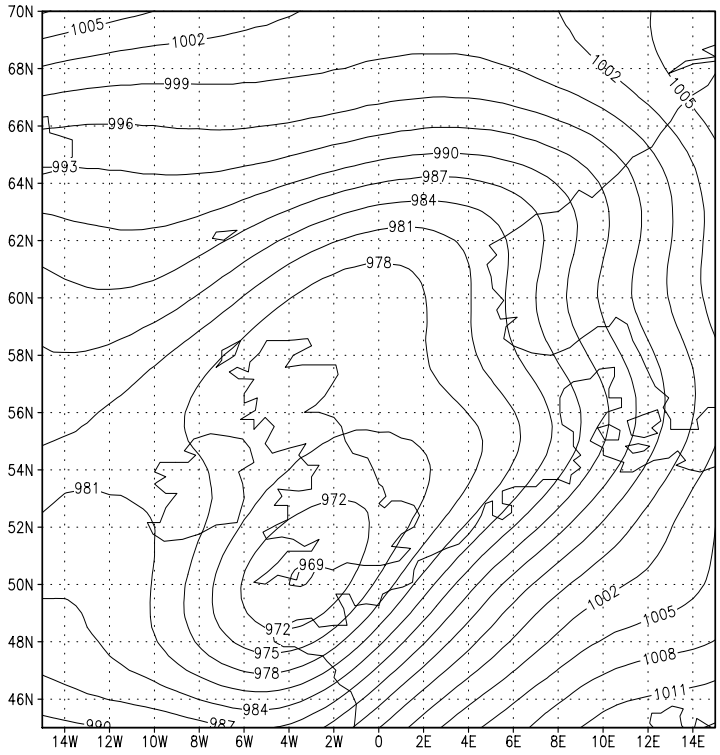

Figure 3.1 00 hrs 16/10/87

Figure 3.2 shows a cross section along 5º W, extracted from the EMB chart at 2.5º intervals (solid line) together with the curves from the interpolated NCEP data (dashed lines). There is very little difference between the results from the two interpolation methods, but both overestimate the minimum pressure by about 15 mb. Other than this the interpolated pressures are in good agreement with the observed data. The reason for the underestimated central pressure is that this storm was a very unusual event with an extremely high pressure gradient over two degrees of latitude/longitude. This is sub-gridscale to our original pressure grid (2.5 x 2.5 degrees). Therefore, the interpolation routines had little information on gradients close to the storm centre. This problem is compounded by the asymmetrical nature of this storm, with virtually all the high wind speeds in the south-eastern quadrant. Fortunately, storms like this are extremely rare. The event is included to demonstrate the errors likely to occur where the original data has insufficient information to perform a reliable interpolation.

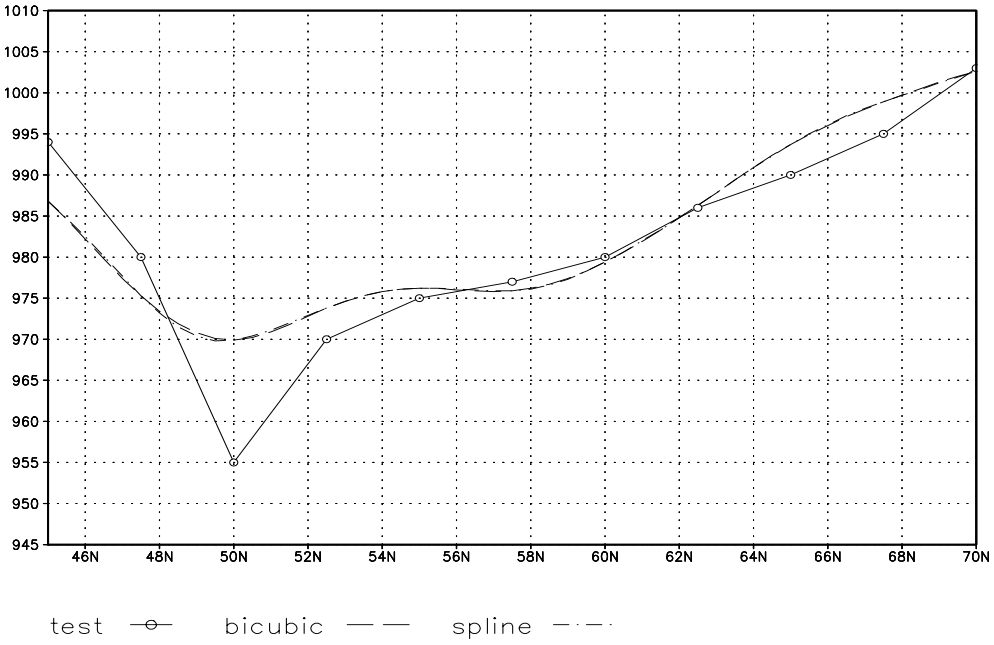

Figure 3.2 00 hrs 16/10/87, cross-section along 5ºW

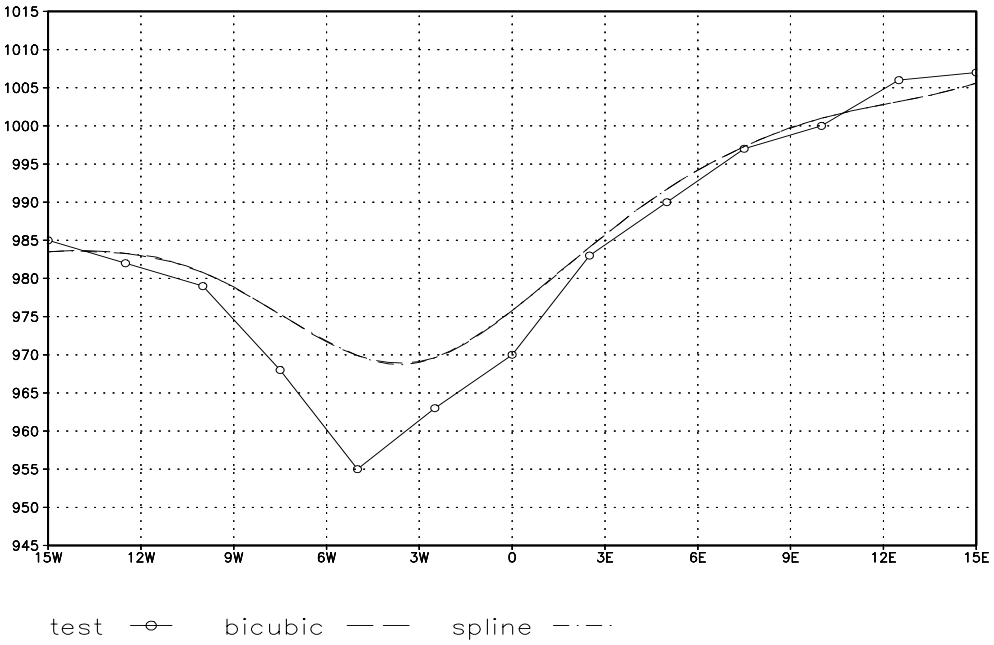

Figure 3.3 00 hrs 16/10/87, cross-section along 50ºN

Figure 3.3 shows a longitudinal cross-section at 50º N of the storm in Figure 3.1. Again, the results from the two interpolation methods are virtually identical and the interpolated data overestimate the central pressure by about 15 mb. The apparent drift in the location of the minimum pressure is an artefact due to sampling the EMB chart at 2.5º intervals.

Storm of 26 January, 1990

This storm caused a severe surge off the Netherlands when centred over Norway for several hours. To give a better cross-section, we show its location 6 hours earlier (Figure 3.4). Again, this is an accurate representation of the EMB chart. The latitudinal cross-section along 2.5º E (Figure 3.5) shows an excellent match between the interpolated and test data, although there is a suggestion that the data sets are not precisely in phase. This is manifested much more strongly in the longitudinal cross-section at 57.5º N (Figure 3.6), and is because the test data are not aligned precisely through the centre of the storm and suffer from the effects of relatively low resolution. Generally, the interpolated data provides an excellent match with the observed, and the central pressure of the storm is within 1 mb of the observed central pressure.

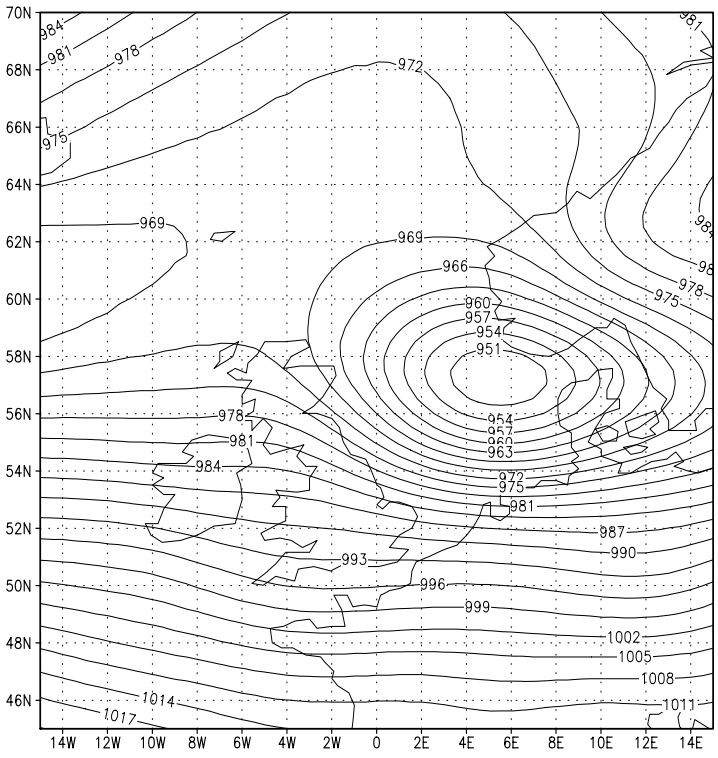

Figure 3.4 00 hrs 26/1/90

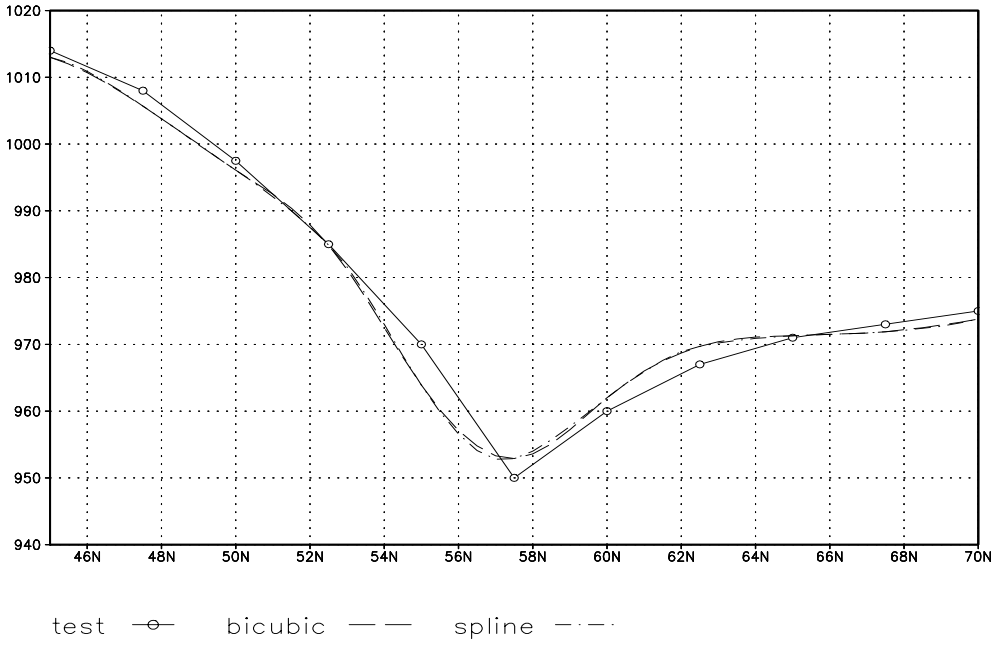

Figure 3.5 00 hrs 26/1/90 cross-section along 2.5ºE

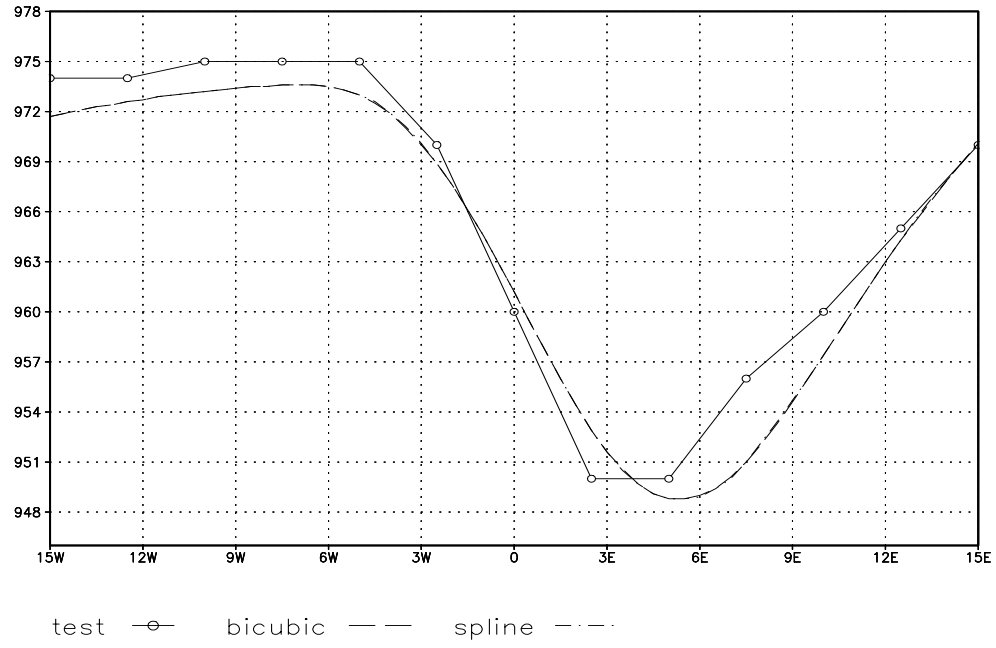

Figure 3.6 00 hrs 26/1/90 cross-section along 57.5º N

Storm of 12 December, 1990

This storm was not particularly severe, but was chosen for test purposes because it had a double storm centre that might not be picked up by the interpolation routine. Unfortunately, the centre associated with the parent low is beyond the northern limits of the test map, but it can be inferred from the way the isobars open in the top right corner of the map, indicating a centre at about 72º N and 16º E. This is an accurate representation of the observed chart, with the location of the centre shown in Figure 3.7

closely matching the observed location and the alignment of the axis between the two centres, along the coast of Norway, matching the observed axis perfectly.

Although the test data in the cross sections (Figures 3.8 and 3.9) suffer from apparent drift, there is a good match between the observed and interpolated data. The interpolated minimum pressure is within 3 mb of the observed minimum.

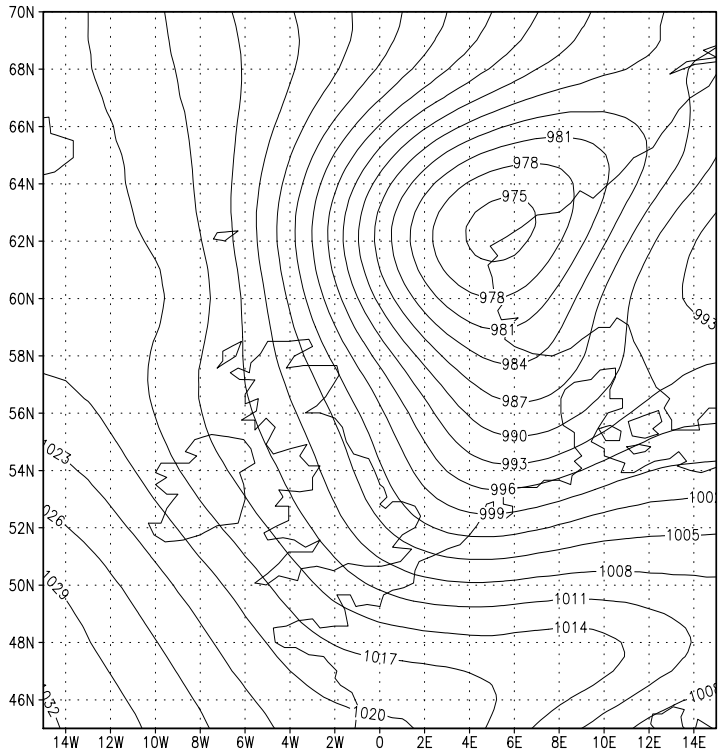

Figure 3.7 00 hrs 12/12/90

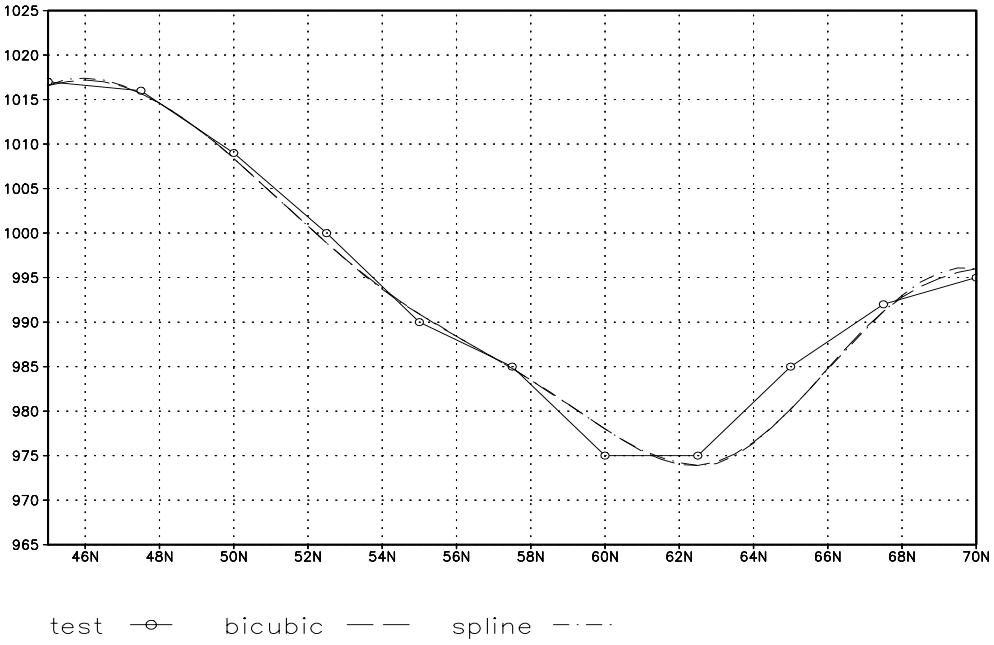

Figure 3.8 00 hrs 12/12/90 cross-section along 5º E

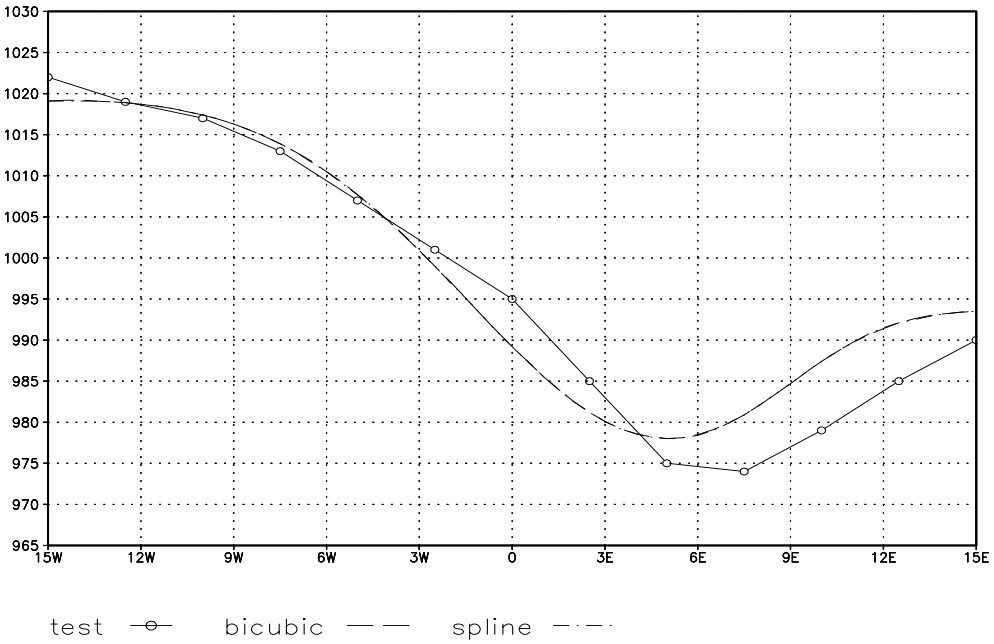

Figure 3.9 00 hrs 12/12/90 cross-section along 60º N

Storm of 5 January, 1991

This storm caused severe surges in the Irish Sea. There is good agreement between the observed pressure field and the interpolated field shown in Figure 3.10. The cross-sections (Figures 3.11 and 3.12) indicate that, although the interpolations give a good representation of the pressure field, they underestimate the central pressure of the depression by about 6 mb (Figure 3.12).

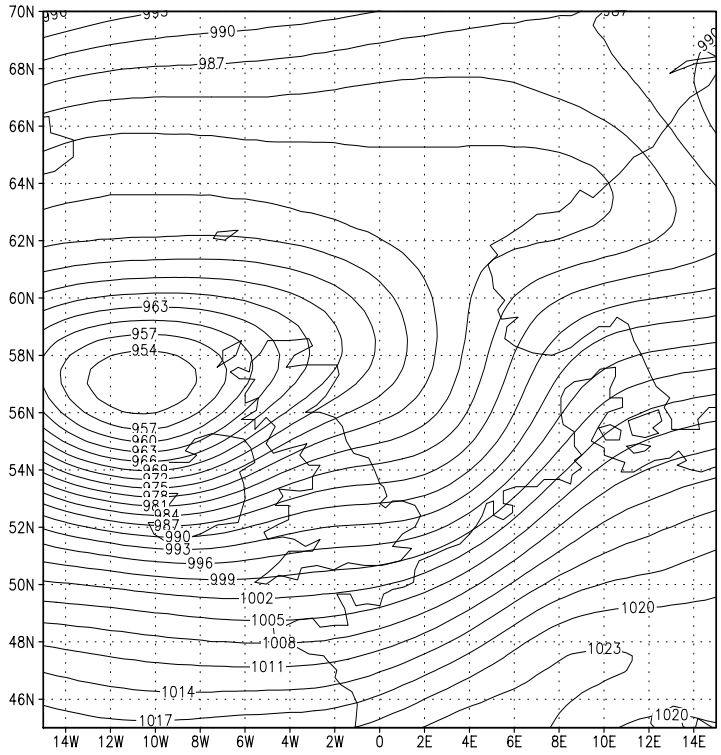

Figure 3.10 12 hrs 5/1/91

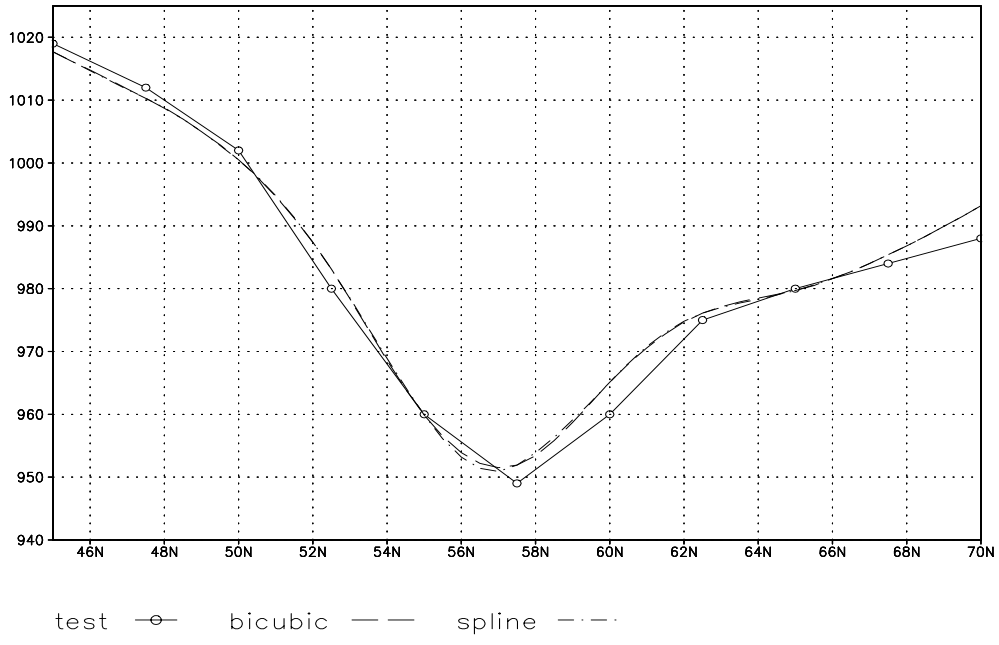

Figure 3.11 12 hrs 5/1/91 cross-section along 10º W

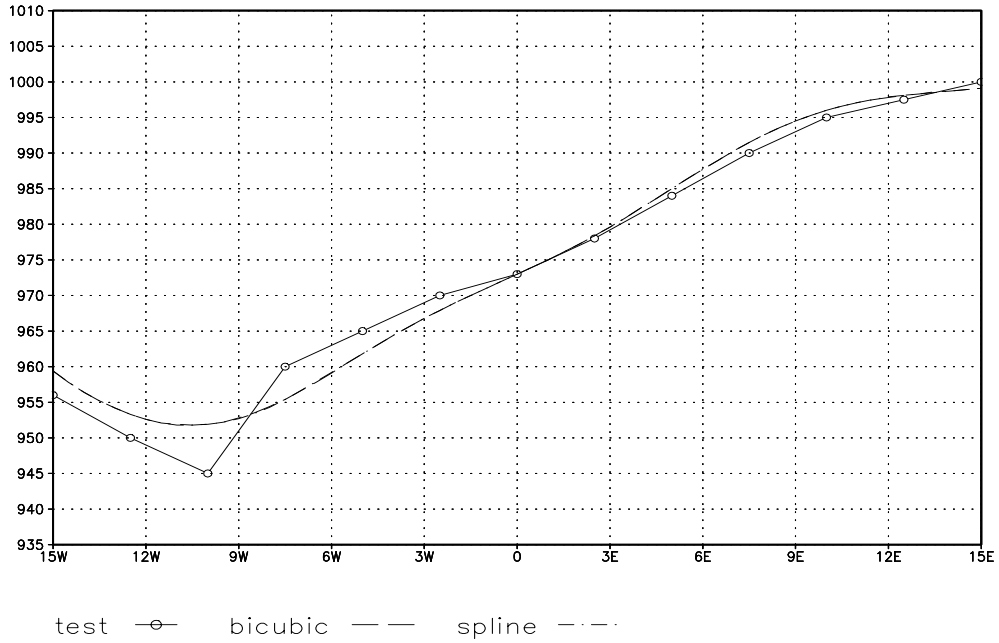

Figure 3.12 12 hrs 5/1/91 cross-section along 57.5º N

3.4.5 Conclusions regarding choice of interpolation scheme

The interpolation methods used in this study are in very close agreement in all the severe storm case studies, indicating that either method would be suitable for interpolating the NCEP pressure data onto a 0.5º x 0.5º latitude/longitude grid. The test data indicates that the interpolated data gives an accurate representation of mid-latitude storms. The only exception to this is for storms with gradients that are sub-gridscale to the original gridded pressure data. However, one should consider that the test data themselves are also the product of some interpolation. Although we consider them a good representation of the pressure field, they are only exact when the contour coincides with a meteorological station. There are some instances where it is impossible to say which data set is in error when the match is less than perfect. For example, the occasions when the test and interpolated datasets seem out of phase near the storm centre are due to the relatively coarse resolution of the digitised EMB test data.

We decided to use the bi-cubic spline method of interpolation for the remainder of this study since, with pressure data, it gives essentially the same results as Akima's bi-cubic interpolation and is faster to compute. There is no indication that the spline interpolation overshoots in conditions of very severe gradient.

3.5 Calculating the geostrophic wind

The 6-hourly interpolated atmospheric pressure data for the period 1985-97 was used to calculate the sea level pressure gradients in the westerly and southerly directions at each point in the 0.5º by 0.5º latitude/longitude grid. These components of pressure gradient were then converted to components of geostrophic wind using equations 3.5 and 3.6:

$$U_g = -\frac{1}{f_c \rho}\frac{\partial p}{\partial y} \qquad 3.5$$

$$V_g = -\frac{1}{f_c \rho}\frac{\partial p}{\partial x} \qquad 3.6$$

where:

U_g and V_g are the westerly and southerly components of the geostrophic wind speed respectively
f_c is the local Coriolis force for the given latitude
ρ is the density of air
$\partial p/\partial y$ is the component of atmospheric pressure gradient from west to east
$\partial p/\partial x$ is the component of atmospheric pressure gradient from south to north

3.6 Testing the geostrophic wind calculated from interpolated pressure data

3.6.1 Introduction

Here, we test the success of the procedure for calculating the geostrophic winds (see sections 3.4 and 3.5) by comparing the results with the surface wind field calculated by NCEP and output as part of the reanalysis data on a 2.5º x 2.5º latitude/longitude grid. Although the wind fields should not be identical, since the NCEP winds will have slightly different directions and speeds because of the effects of surface friction, there should be sufficient similarity to identify any errors (particularly systematic errors) in the computation of the geostrophic wind.

For testing. we selected three dates from a sample year, to include a severe storm, a winter day and a summer day with relatively light winds. The test data are presented in three formats for each of the three dates: maps of resultant wind vectors, maps of stream function (directional contours of the flow of air), and a table of comparative summary statistics.

3.6.2 The nature of the “Geostrophic Wind"

A more detailed explanation of the geostrophic wind can be found in standard meteorological texts, for example, James (1994). Here we concentrate on testing the data produced for POWER by comparing these to the surface wind calculated by NCEP. The geostrophic wind is a theoretical wind calculated from surface pressure data. A balance is assumed between the flow of air from high to low pressure regions and the effects of the rotation of the Earth as manifested in the “Coriolis Effect”. The geostrophic wind flows parallel to the isobars (contours of equal surface pressure), and reflects the flow of air in frictionless conditions. This can be taken to be above 500-1000 m, but varies greatly depending on factors such as the nature of the underlying surface, in terms of topography and roughness, and on the stability of the overlying air. Because of surface friction, the wind at 10 m will be different from the geostrophic wind in speed and direction. The relationship is complex, depending on the square of the wind speed, the surface roughness, the effects of funnelling due to surface topography, and the stability of the atmosphere.

In very simplistic terms, we can describe the main effects of friction to be:

- Slowing due to frictional retardation caused by the roughness of the surface. One would expect wind speeds at 10 m to be roughly 30% of the geostrophic wind speeds over land and roughly 60% of geostrophic wind speeds over the sea. The different amount of slowing is due entirely to the difference in surface roughness between the land and the sea. The slowing increases with wind speed.

- Turning of the wind to the left around low pressure centres in the Northern Hemisphere. The amount of turning is a function of height and normally approximates the simple spiral defined by Ekman. The change in direction of the 10 m wind relative to the geostrophic wind could be of the order of 15 to 20 degrees.

In this study, we are calculating the geostrophic wind from pressure data at 0.5º x 0.5º latitude/longitude nodes. The calculations are performed using pressure gradients over a particular pressure node from 1º north and south of the node (that is, gradients over 2º of latitude), and 2º east and west of the node (gradients over 4º of longitude). The doubling of the distance for longitude gradients roughly counters the effect of convergence of longitude lines as one approaches the Pole. This gives an approximately square box for the pressure gradient calculations of about 230 km (varying with latitude).

Storm of 26 January, 1990

Before discussing the particular features of this test it is important to note adjustments to the data that are made for pragmatic reasons. To display the wind vectors of the calculated geostrophic wind at their true resolution (0.5º x 0.5º) would result in a meaningless forest of lines. Therefore, we skipped all vectors other than those at 2.5º x 2.5º intervals, giving vectors at the same points for the test and geostrophic data. Since the stream function plots are contours, all available data can be used. This means that the stream function of the geostrophic data can display small circulations that are missing from the test plots since they are sub-grid scale to those data. This occurs over Spain, for example, when comparing Figures 3.19 and 3.20.

The wind vectors shown in Figures 3.13 and 3.14 indicate that the calculated geostrophic wind (Figure 3.14) compares superficially well with the surface wind field from NCEP (Figure 3.13). However, the scaling (indicated beneath each vector plot) shows that a vector for geostrophic wind speeds represents twice the wind speed of a vector the same size on the surface wind speed map. This is partly because of the effects of surface friction reducing the wind speeds at the surface and partly because of differences in the spatial resolution of the raw data. The geostrophic winds are computed from pressure data that is at a spatial resolution 5 times higher than that of the surface winds. Around the storm centre, where pressure gradients and wind speeds are highest, the better spatial resolution allows the computation of geostrophic wind speeds that are sub-grid scale to the surface wind data. Effectively, in this crucial region, the test data are smoothed in space and cannot reflect the rapid changes in wind speed over a small area that are encountered around a very severe storm.

The plots of streamfunction (Figures 3.15 and 3.16) appear to be different in the region of the storm centre (off western Denmark). In fact, both stream function plots are correct. In figure 3.16, the wind is frictionless and runs parallel to the isobars, so the stream function plot is essentially the same as a contour plot of surface pressure. In Figure 3.15, we see the effects of surface friction turning the direction of the wind towards the centre of the storm (to the left in the Northern Hemisphere), so that the concentric contours around the storm centre have more of the appearance of a vortex.

The statistics in Table 3.1 are calculated across all grid points and indicate that the standard deviation and range of the u and v components of the geostrophic wind field are much higher than those of the test data. This is to be expected given the differences in scaling already noted in the discussion of Figures 3.13 and 3.14.

Table 3.1 Wind speed statistics from the test and interpolated data for 00 hrs 26/01/90

Wind component	**Minimum**	**Maximum**	**Standard deviation (n-1)**
Test u (m/s)	-19.2	33.9	8.91
Interpolated u (m/s)	-36.1	62.0	14.42
Test v (m/s)	-18.6	21.1	5.73
Interpolated v (m/s)	-39.4	31.2	10.21

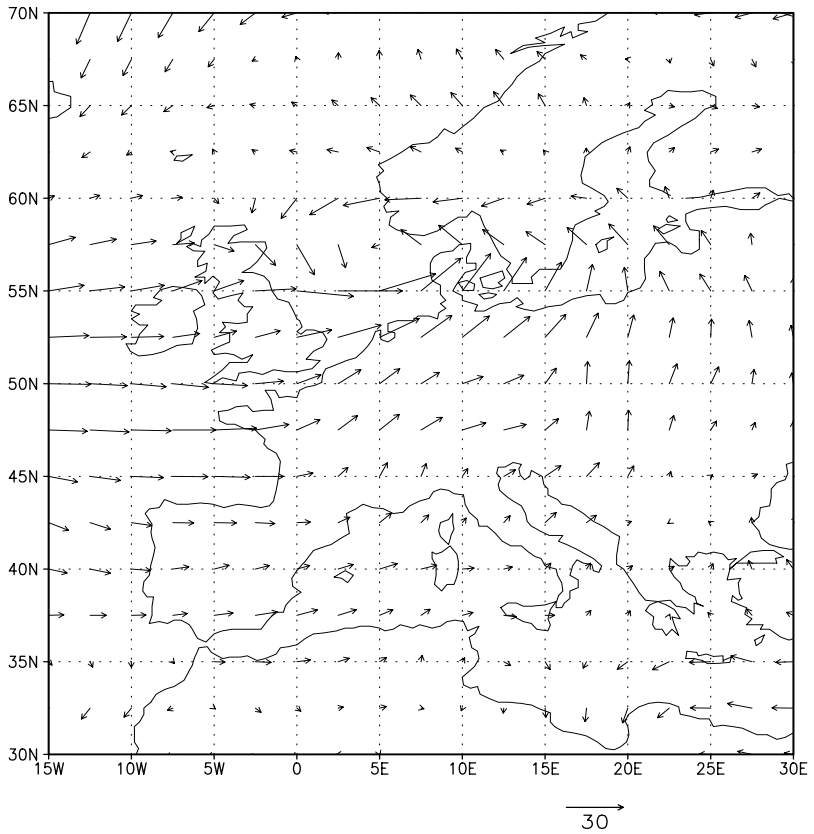

Figure 3.13 Wind vectors from test data for 00 hrs, 26/01/1990

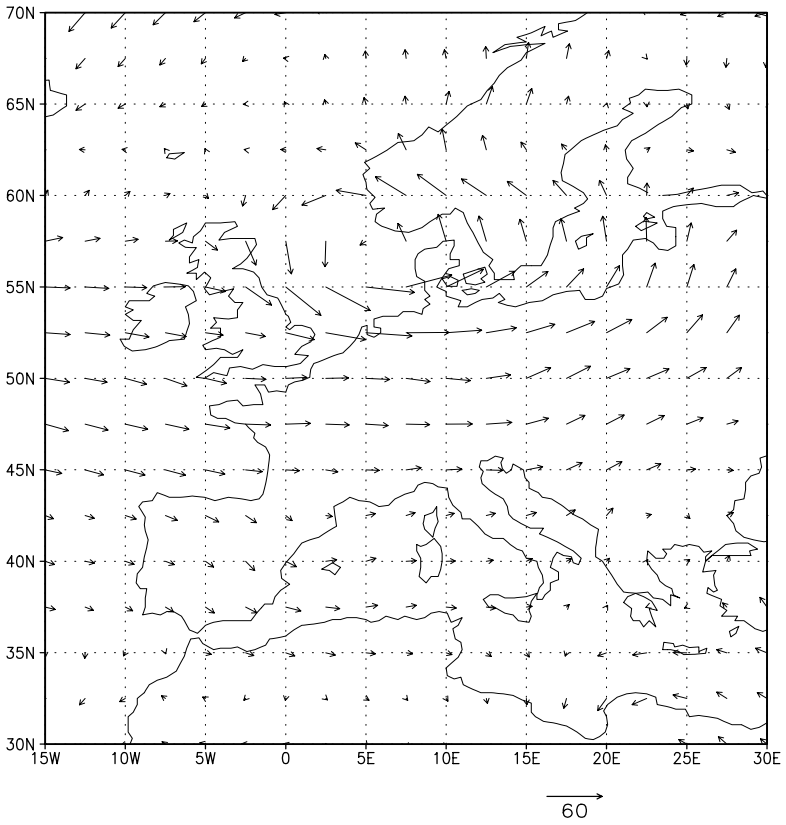

Figure 3.14 Wind vectors from interpolated pressure data for 00 hrs, 26/01/1990

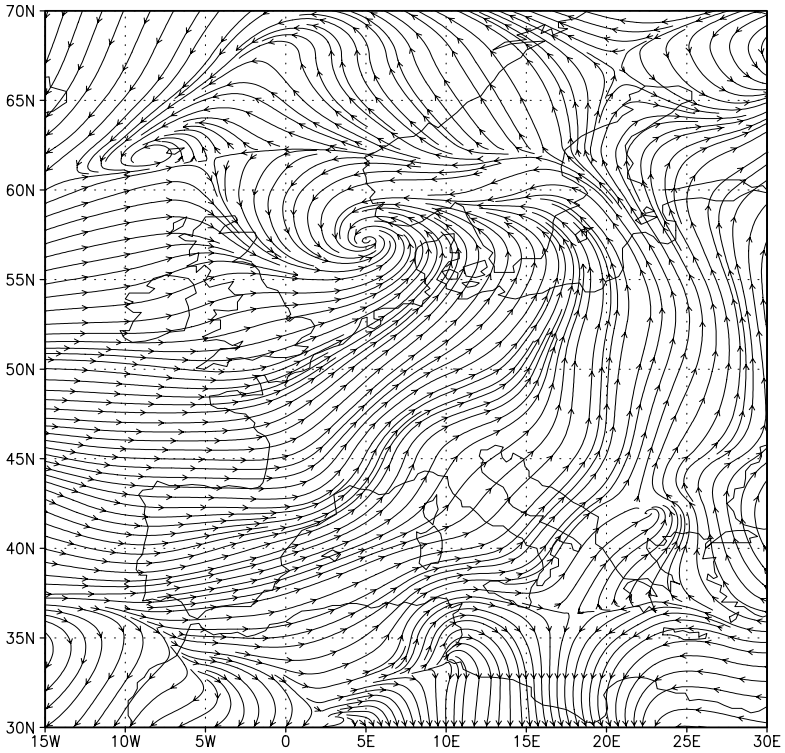

Figure 3.15 Stream function from test data for 00 hrs, 26/01/1990

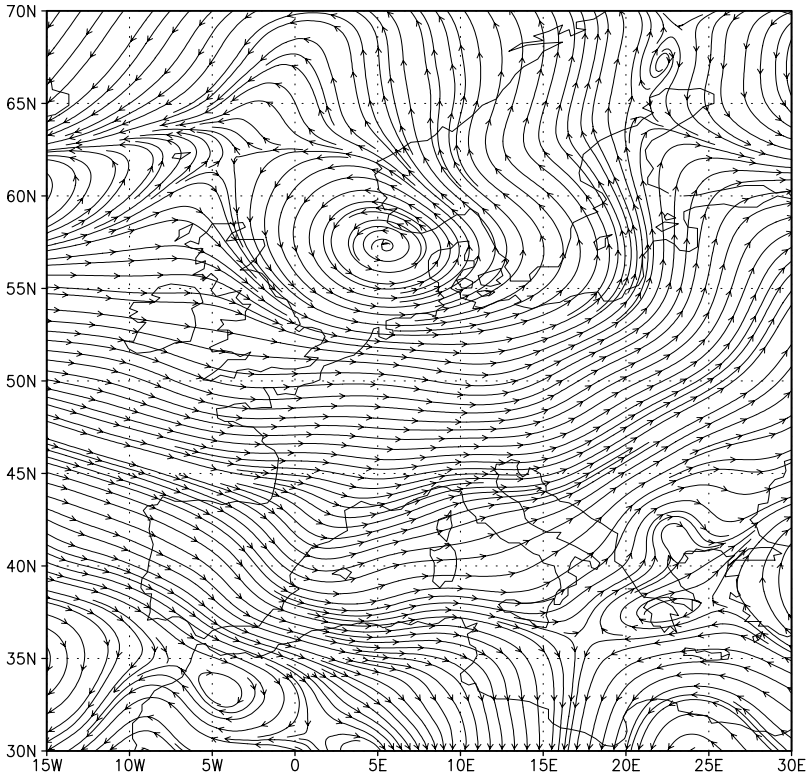

Figure 3.16 Stream function from interpolated pressure data for 00 hrs, 26/01/1990

Winter day, 1 January, 1990

The wind speeds for a "normal" winter day compare much better than in the extreme case of the severe storm used in the previous example. Figures 3.17 and 3.18 show good agreement between the patterns and scaling of wind vectors. The plots of stream function for the test and interpolated data (Figures 3.19 and 3.20, respectively) indicate comparable fields with the effect of cross-isobar flow evident at every pressure centre shown in the test data chart (Figure 3.19).

Although the statistics of the u components of the wind compare well between the test and interpolated fields (Table 3.2), there is a large discrepancy between the v components. Since the geostrophic wind has to have higher *resultant* wind speeds than the surface wind, the way this is reflected in the u and v components varies with the configuration of surface pressure at a particular time. Thus, there is no significance in the fact that on this occasion the v component shows the discrepancy.

Table 3.2 Wind speed statistics from the test and interpolated data for 00 hrs 01/01/90

Wind component	**Minimum**	**Maximum**	**Standard deviation (n-1)**
Test u (m/s)	-16.8	16.2	5.46
Interpolated u (m/s)	-17.6	17.4	6.45
Test v (m/s)	-8.2	13.5	4.68
Interpolated v (m/s)	-17.5	22.6	7.93

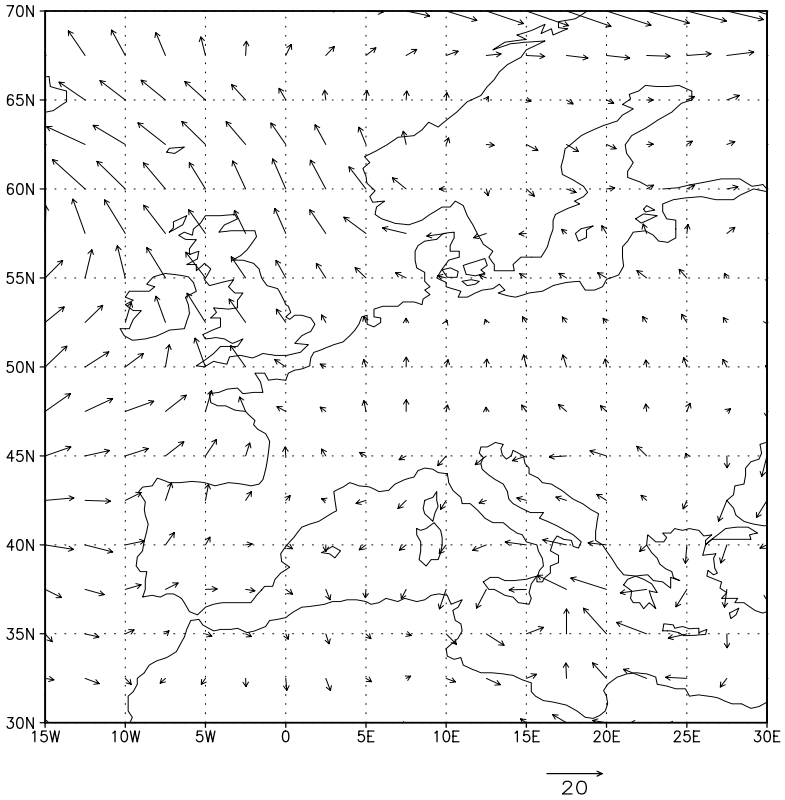

Figure 3.17 Wind vectors from test data for 00 hrs, 01/01/1990

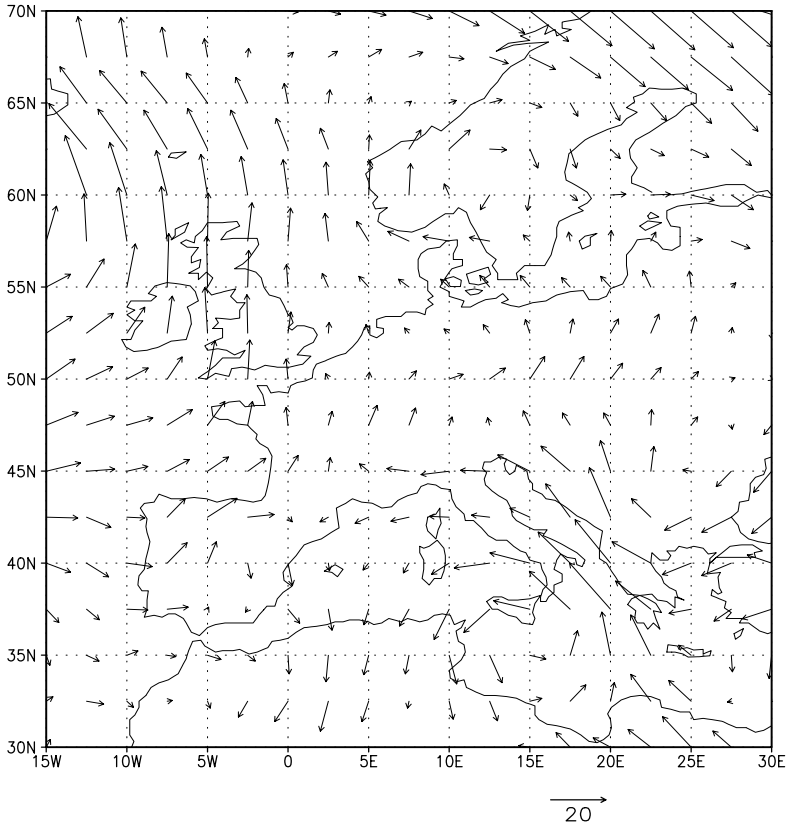

Figure 3.18 Wind vectors from interpolated pressure data for 00 hrs, 01/01/1990

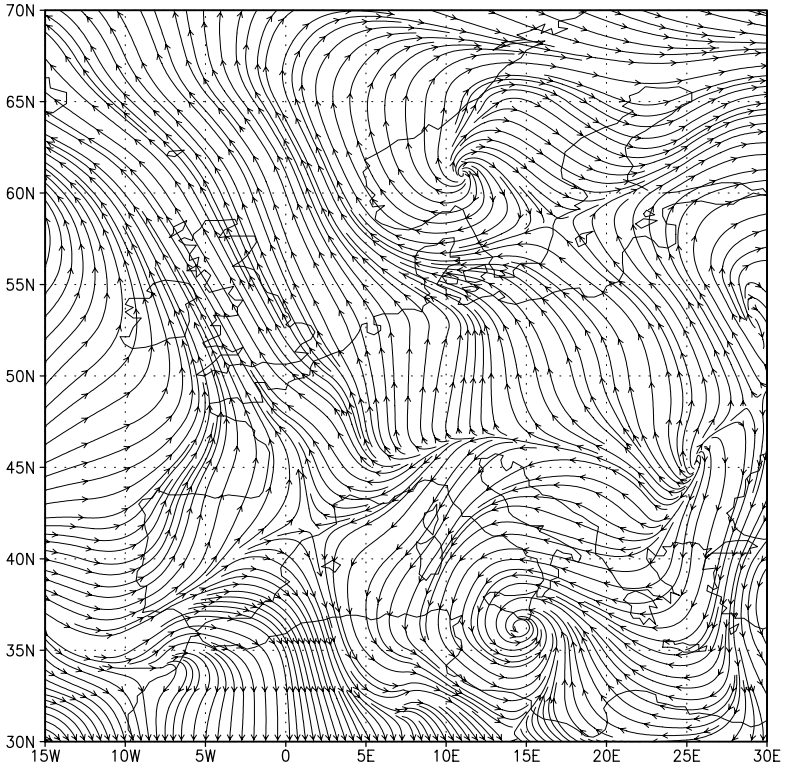

Figure 3.19 Stream function from test data for 00 hrs, 01/01/1990

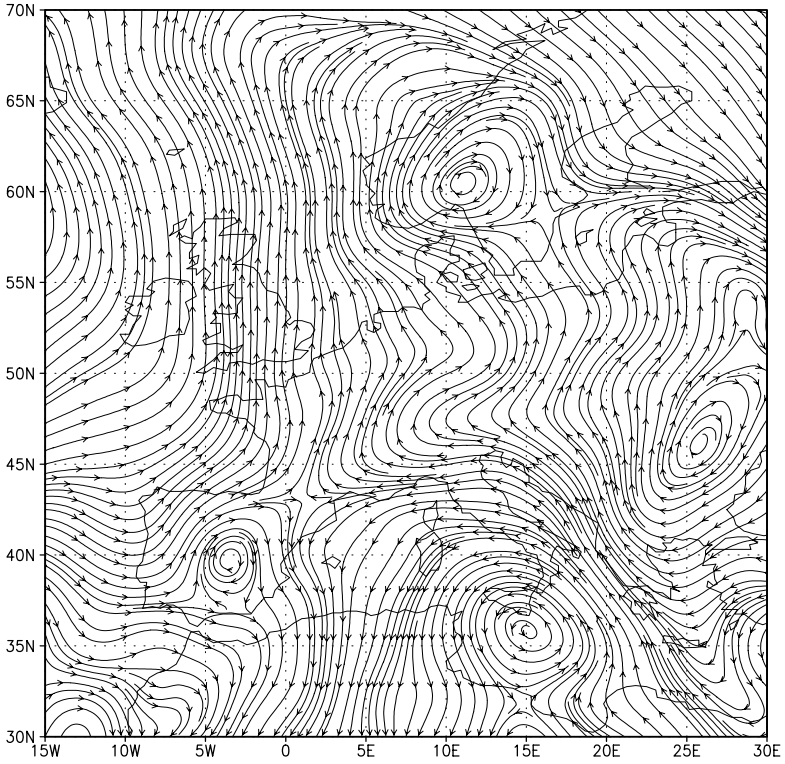

Figure 3.20 Stream function from interpolated pressure data for 00 hrs, 01/01/1990

Summer day, 24 June, 1990

In many ways, the example of a summer day is the most severe test of the geostrophic winds since the hemispheric circulation is at its weakest.

Figures 3.21 to 3.24 indicate that the geostrophic wind calculated from the interpolated pressure data is correct. The scaling for the geostrophic and test wind vectors (Figures 3.21 and 3.22) is different, but this simply reflects the higher speeds of the frictionless flow. The statistics in Table 3.3 show that the interpolated u and v components of the geostrophic wind have higher variability than the test u and v components.

Table 3.3 Wind speed statistics from the test and interpolated data for 00 hrs 24/06/90

Wind component	Minimum	Maximum	Standard deviation (n-1)
Test u (m/s)	-10.8	13.9	4.10
Interpolated u (m/s)	-18.0	22.0	6.18
Test v (m/s)	-12.8	12.6	4.61
Interpolated v (m/s)	-14.5	18.4	5.79

3.6.3 Conclusions regarding comparison of POWER geostrophic winds with NCEP surface winds

The examples shown in this section indicate that the geostrophic wind calculated for POWER has consistent variability with the surface wind and is, therefore, a good basis for the development of the models to predict near-surface winds in the far offshore and near-shore zone.

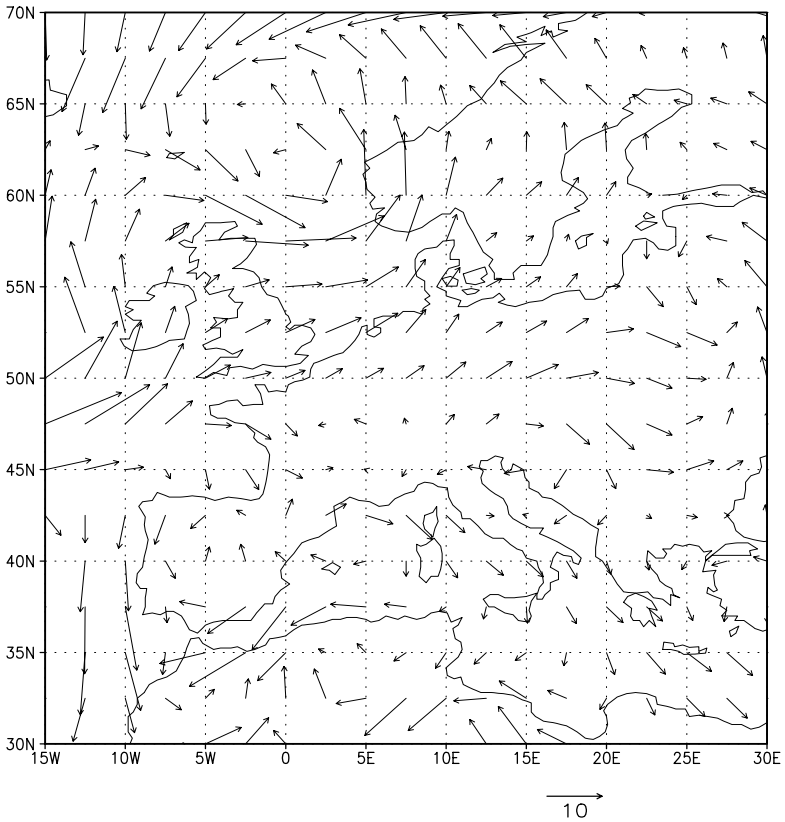

Figure 3.21 Wind vectors from test data for 00 hrs, 24/06/1990

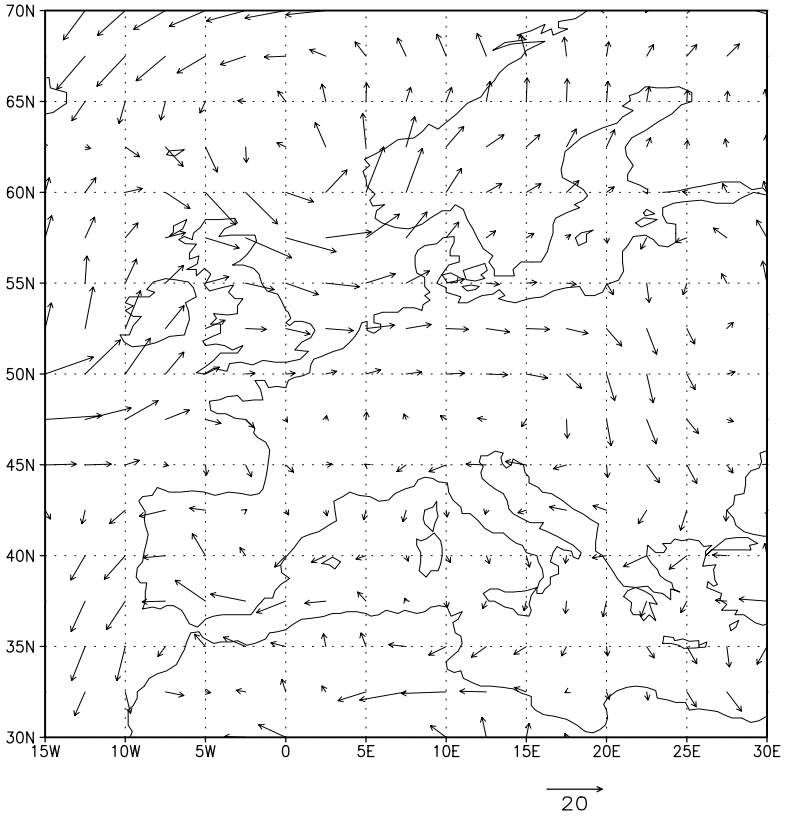

Figure 3.22 Wind vectors from interpolated pressure data for 00 hrs, 24/06/1990

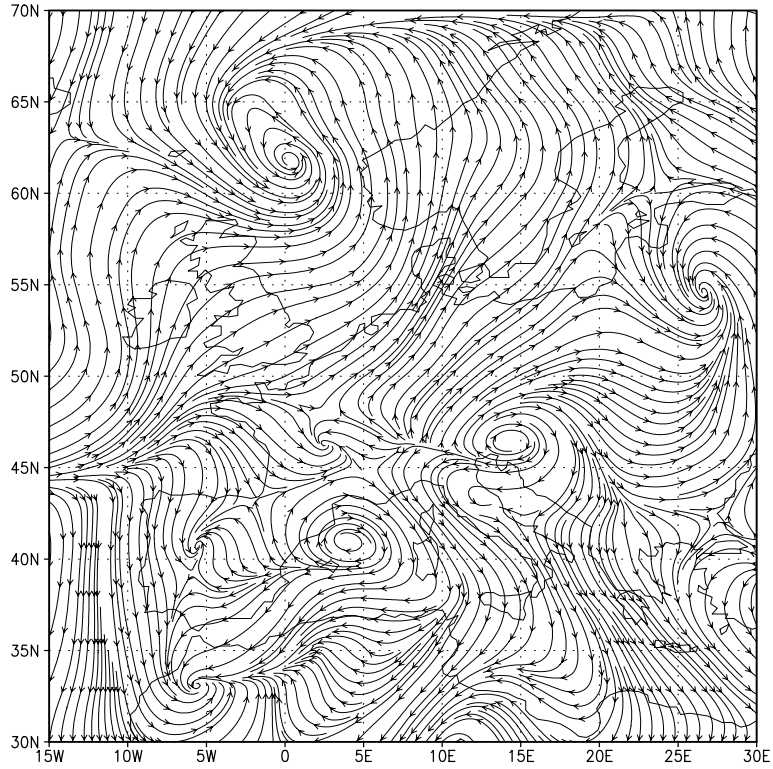

Figure 3.23 Stream function from test data for 00 hrs, 24/06/1990

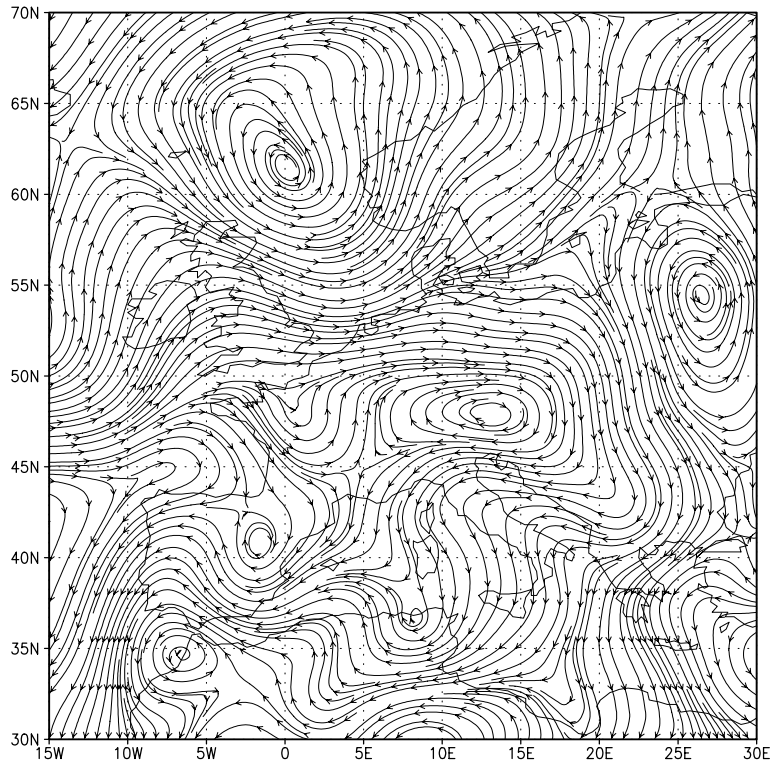

Figure 3.24 Stream function from interpolated pressure data for 00 hrs, 24/06/1990

3.7 Using radiosonde data to validate the geostrophic wind

3.7.1 Introduction

In Section 3.6, we tested the geostrophic winds computed from pressure data interpolated onto a 0.5º x 0.5º latitude/ longitude grid by comparing with the surface wind field calculated by NCEP (Kalnay et al., 1996) on a 2.5º x 2.5º latitude/longitude grid. Although this approach would identify any errors in the calculation, it can only be used as a very general test of the validity of the calculated wind field, since the geostrophic wind is a frictionless wind, representing flow 500 to 1000 m above the surface. Furthermore, the surface wind field used for testing is only partly based on observations, much of it is derived from theoretical computations performed using a numerical model. Here we use observations from radiosonde ascents to compare the observed frictionless flow with the theoretical wind derived from the assumptions of geostrophic theory.

For our initial analysis, we take the three dates from 1990 used in Section 3.6. These include a severe storm, a winter day and a summer day with relatively light winds. For each date we present charts of the geostrophic wind speed and direction, superimposed with the appropriate radiosonde observations, for three successive 12-hourly time steps. Similar plots are then presented for a date in 1997, to ensure that the initial findings are consistent and to provide a preliminary assessment of changes in the radiosonde network.

Although the charts provide a detailed overview of the relationship between the geostrophic wind and the observed frictionless wind, it is only possible to consider a small number of timesteps in this way. To examine long term relationships, we provide comparative summary statistics of the geostrophic wind speeds and radiosonde observations for the whole of 1990 and 1997. We conclude that the geostrophic wind is an excellent representation of frictionless flow over the POWER study area.

3.7.2 The Radiosonde Data

Radiosonde data were obtained from the British Atmospheric Data Centre (BADC) for the period 1990 to mid-1998 from an extensive network of European stations. The observation interval ranges from 3 to 12 hours and measurements are often recorded at different heights at different stations. This does not matter for our purposes, since we can use test observations from a wide band of heights to represent frictionless flow. There can be large numbers of missing values, particularly during storm conditions.

As we are primarily interested in the near-shore and far offshore wind fields, and it is desirable to use radiosonde data free from the effects of local topography, we selected coastal radiosonde stations lying below 100 m above msl. This subset of stations was further reduced by a requirement that they have a recording programme covering the period 1990 to mid-1998 and observations at 00 hrs and 12 hrs for each day. Although this report does not use data over the whole of this period, a continuous programme of measurements indicates that the stations are permanent and available for more extensive study if needed. The locations of the 37 radiosonde stations fulfilling these conditions are shown in Figure 3.25. The numbers and division into sub-basins are supplied for reference in later sections.

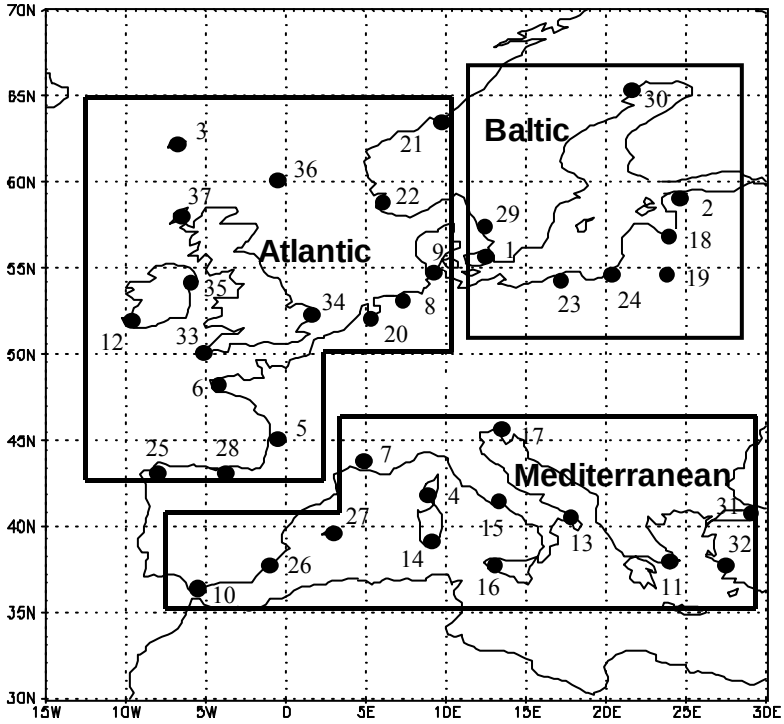

Figure 3.25 Locations of the radiosonde stations used in this report

To accommodate the need to select radiosonde wind speeds and direction from above the friction layer, we extracted these variables for the first occurrence of data at a height between 600 and 900 m. This range of heights was selected empirically as covering a large enough range to minimise missing values and retaining the characteristics of frictionless flow. It is important to note that the "correct" height for measuring frictionless flow varies a great deal depending on factors such as local atmospheric stability, surface topography, and circulations aloft. The latter point partly explains why we need an upper limit to our range even though all winds above a certain level will be frictionless. There are different regimes of horizontal flow at various levels in the atmosphere. Therefore, we need to try to ensure that our frictionless flow is representative of flow at the surface with friction removed, and not influenced by flow at a greater height. The problem is illustrated using the radiosonde observations shown in Table 3.4.

For one example time step, Table 3.4 illustrates the increase in wind speeds and change in direction with height. Between the surface and 813 m, these changes are in accordance with Ekman theory. Between 813 m and 980 m the linkage with the effects of surface friction is ended as wind speeds start to decline with height and the wind direction starts to change in the opposite direction. It is interesting to note that the difference in wind direction between 40 m and 813 m is 30 degrees. McIlveen (1992) states that the maximum value of the change in wind direction between the surface and the gradient (frictionless) layer "seldom exceeds 30 degrees". Therefore, the optimum frictionless wind speed and direction from the data in Table 3.4 are at 813 m. This is also the only value on this time step that falls within our search range of 600 to 900 m height. It should be noted that these data were chosen to illustrate the point. Generally, the patterns are not so clear cut, although the appropriate height for frictionless flow is usually evident.

We now compare the geostrophic wind with the radiosonde observations for each of our sample dates. Although a detailed examination of the wind field on particular time steps is likely to reveal occasional incorrect readings from the radiosondes, we will ignore these and concentrate on the overall match with the geostrophic wind. Where radiosonde information appears to be consistently incorrect, however, we will point this out.

Table 3.4 Sample radiosonde data

Pressure (mb)	Height (m)	Wind direction	Wind speed (knots)
746	2580	115	12
800	2010	130	15
850	1510	135	18
899	1050	145	19
906	980	145	20
925	813	150	20
977	360	145	17
1000	172	140	11
1016	40	120	6

Storm of 26 January, 1990

A few general comments about the way the data in the validation exercises are presented are appropriate here. Although contour maps are not the method normally used to display wind speeds, they are chosen here since they facilitate comparison with the station observations. Radiosonde wind speeds are plotted in a large bold font to distinguish them from the contour labels for the geostrophic data. Although there are potentially 37 radiosonde sites to include in the plots, in all the examples there are several sites with no readings at any given time. Missing values were omitted from the plots, so the locations of radiosonde data can apparently differ between plots depending on the availability of data.

With wind direction, contouring is not practicable because of the discontinuity at 360/0 degrees. Therefore, we present wind direction by plotting the value at each radiosonde site. The adjacent value in brackets is the geostrophic wind direction at the nearest 0.5 degree grid point. So, for example, in Figure 3.27, the frictionless wind direction from the radiosonde in the region of London is 210 degrees, and the corresponding geostrophic wind direction is 234 degrees.

Figures 3.26 to 3.31 show the comparative wind speed and direction for 12 hours preceding the storm, the time of the storm, and 12 hours after the storm. Three time steps are included to compensate for missing values in the radiosonde data. There tend to be more missing values when wind speeds are high.

12 hrs, 25/1/1990

Figure 3.26 shows that for this timestep, in the region of highest geostrophic wind speeds (50-55 m/s over the south of England), wind speeds are underestimated at the nearest radiosonde station by about 20 m/s. This is not surprising when one considers that this was one of the most severe storms to strike the UK and that virtually all radiosondes in the region display missing values for this time step. At most other locations, where the wind speeds are lower, there is good agreement between the wind speeds from the radiosonde data and the geostrophic wind speeds.

There is generally good agreement between the observed and calculated wind direction shown in Figure 3.27.

00 hrs, 26/1/1990

Twelve hours later, the storm centre has shifted over the North Sea (Figures 3.28 and 3.29). There are still large numbers of missing values in the region of the storm centre and the radiosonde wind speeds near the centre (Figure 3.28) appear to be underestimated by about 20 m/s). Away from the storm centre, however, there is generally good agreement between the geostrophic wind speeds and those from the radiosonde ascents.

Again, there is generally good agreement between the observed and calculated wind direction shown in Figure 3.29.

12 hrs, 26/1/1990

As the storm weakens and moves over Scandinavia, there is a marked reduction in the number of missing values (over the UK, for example, see Figures 3.30 and 3.31), which is a clear indication that high wind speed conditions have a damaging influence on the collection of radiosonde data. A preliminary assessment suggests that the cutoff for reliable radiosonde wind speeds is in the region of 30 m/s.

The pattern of agreement between geostrophic wind speed and direction and the corresponding radiosonde data is the same as for the previous time steps. In the region of the storm centre, radiosonde wind speeds appear to be underestimated by about 10 m/s.

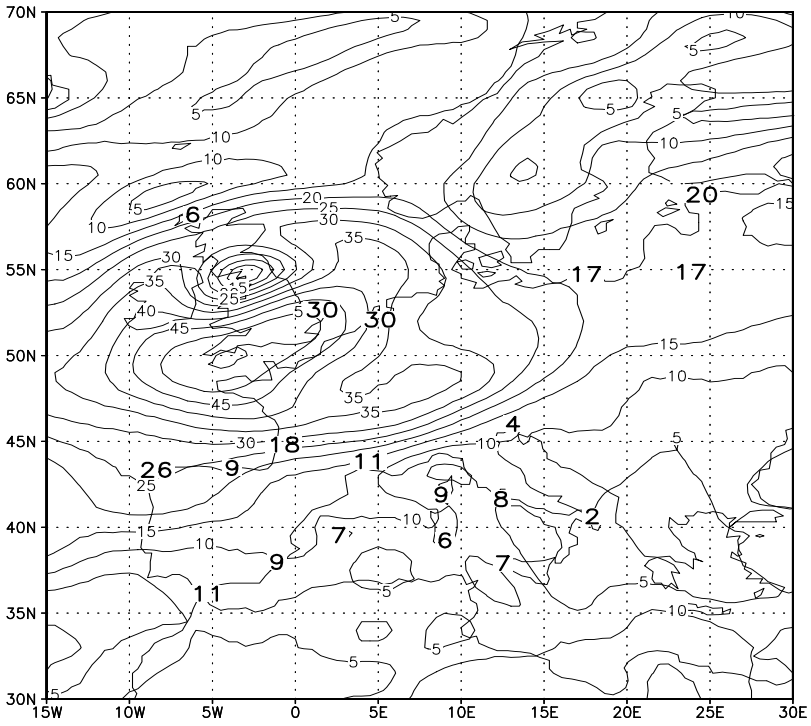

Figure 3.26 Wind speed (m/s) for 12 hrs, 25/01/90

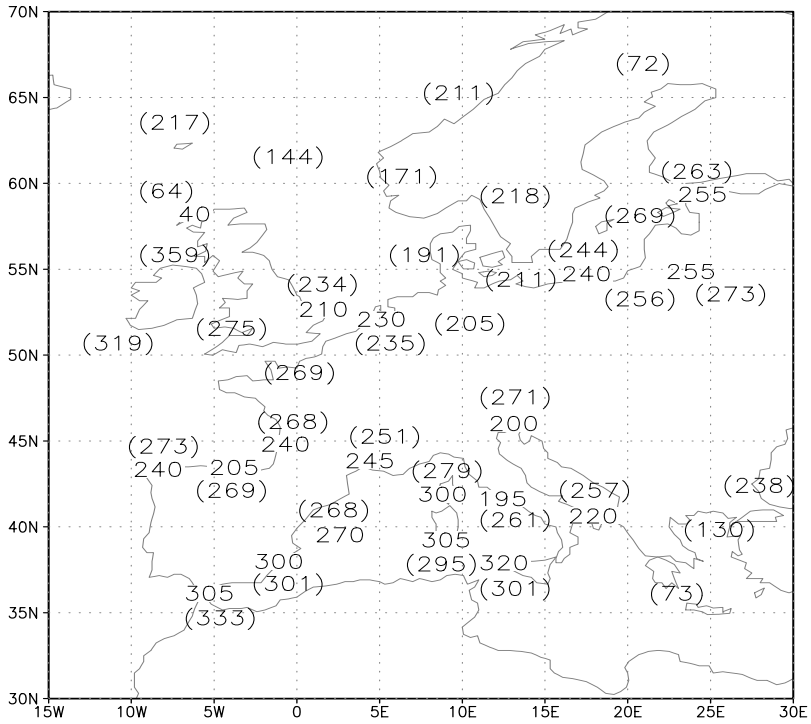

Figure 3.27 Wind direction for 12 hrs, 25/01/90

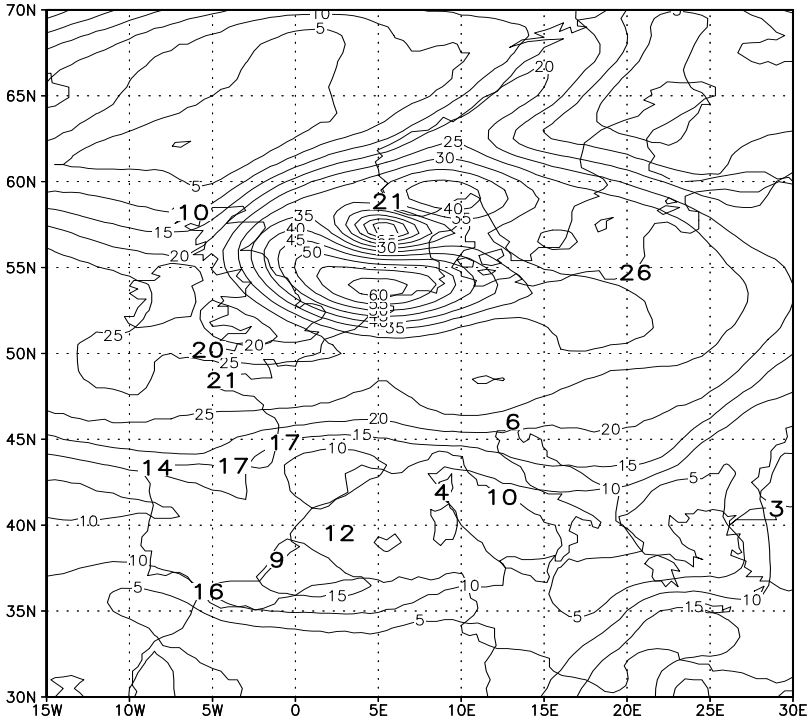

Figure 3.28 Wind speed (m/s) for 00 hrs, 26/01/90

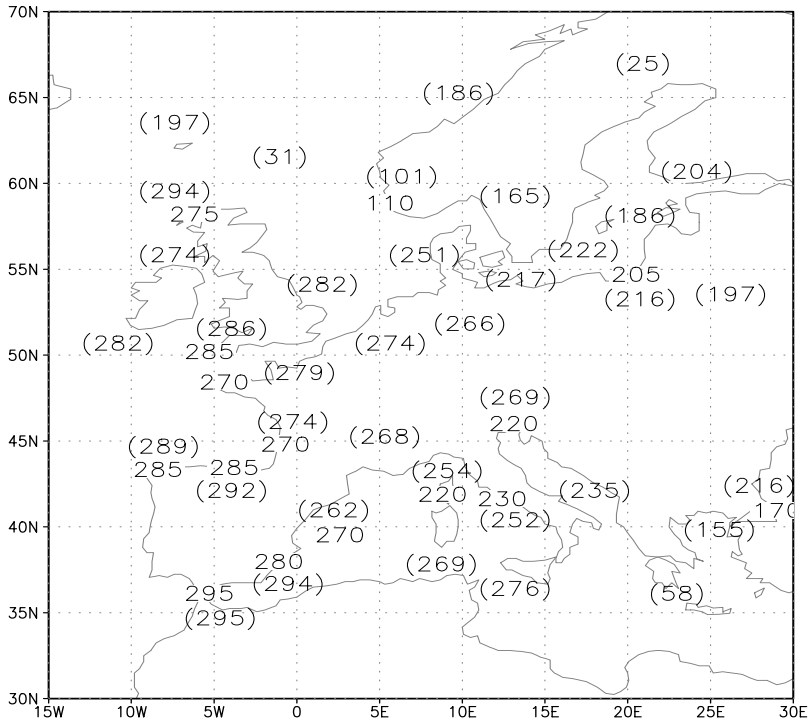

Figure 3.29 Wind direction for 00 hrs, 26/01/90

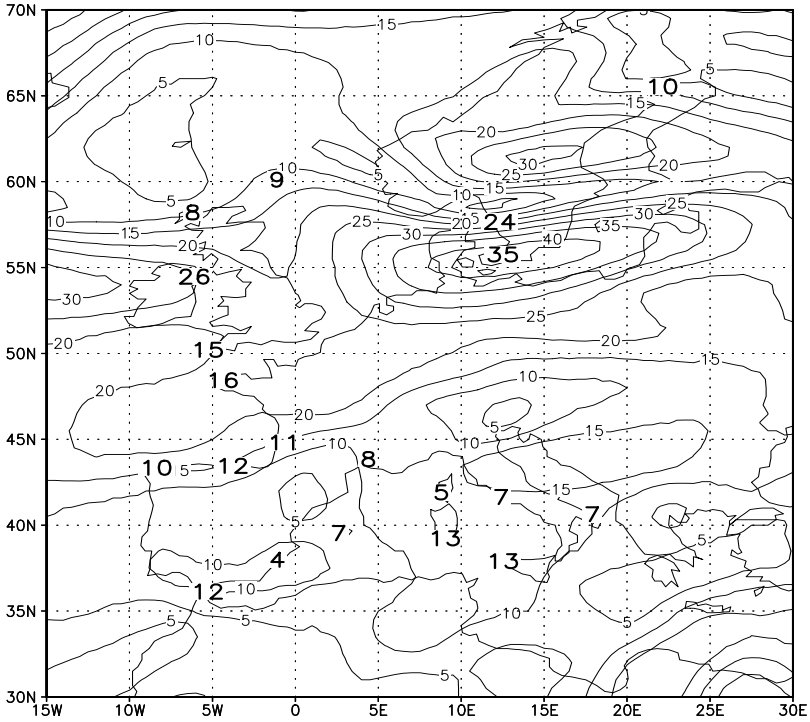

Figure 3.30 Wind speed (m/s) for 12 hrs, 26/01/90

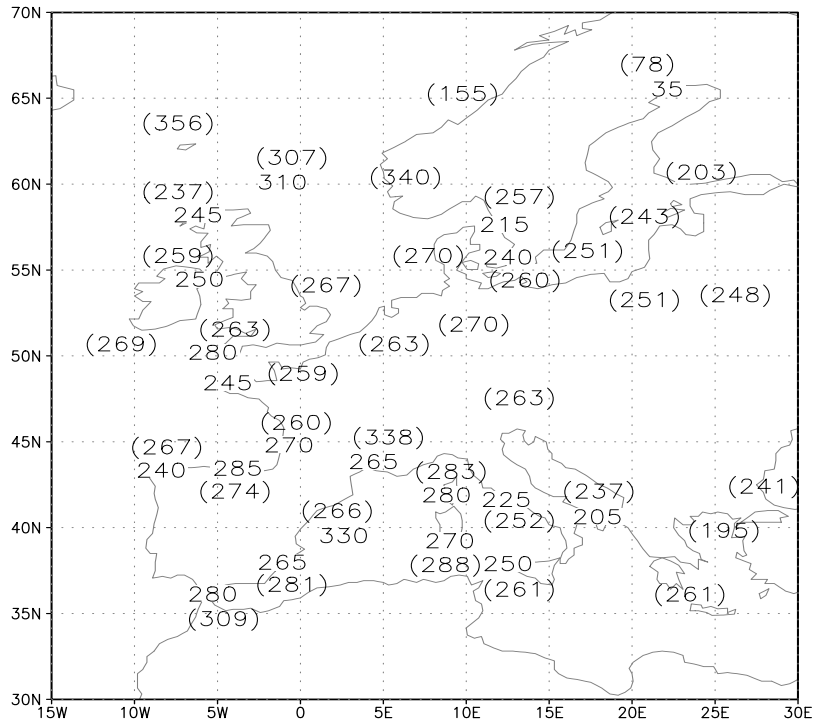

Figure 3.31 Wind direction for 12 hrs, 26/01/90

Winter day, 1 January, 1990

We have noted in the previous example that the radiosonde data appears to suffer from underestimated wind speed and large numbers of missing values in the region of severe storms. We now examine the relationship between the calculated geostrophic wind speed and direction, and the equivalent radiosonde data, during more "normal" conditions in winter and summer. Our first example is a "typical" winter scenario reflecting the relatively calm conditions associated with the establishment of a continental anticyclone, taking three successive 12-hourly time steps beginning at 00 hrs, 1 January, 1990.

00 hrs, 1/1/1990

Figures 3.32 and 3.33 indicate that the geostrophic and radiosonde wind speed and direction compare much more favourably during the low wind speed regime associated with anticyclonic weather. A notable exeception is Italy, which appears to have inaccurate wind speed and direction from the radiosonde data.

12 hrs, 1/1/1990

Comparisons remain good twelve hours later, although the radiosonde data for southern Italy still appears to have problems (Figures 3.34 and 3.35).

00 hrs, 2/1/1990

Again, the overall comparison is good, but parts of Italy still have problematic radiosonde data (Figures 3.36 and 3.37).

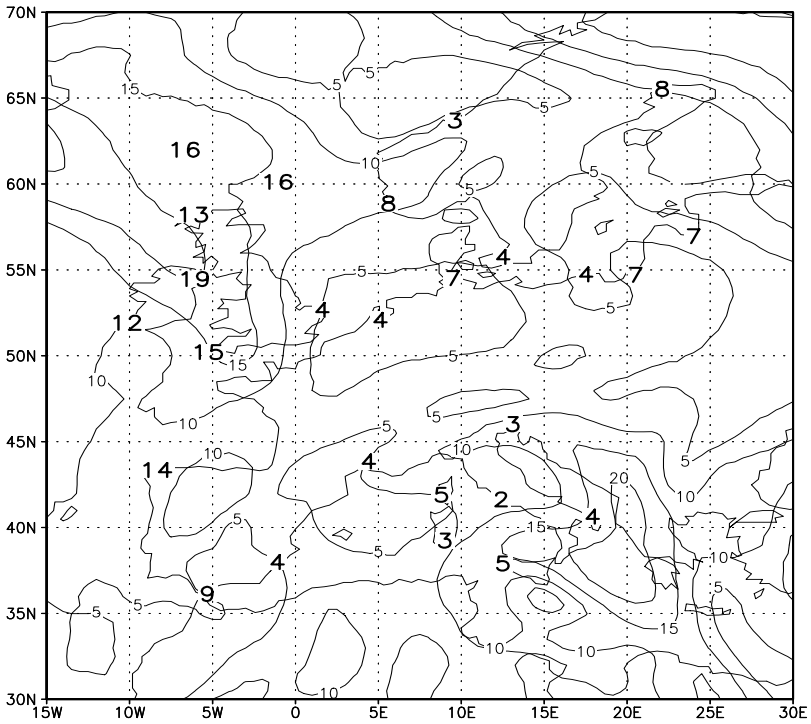

Figure 3.32 Wind speed (m/s) for 00 hrs, 01/01/90

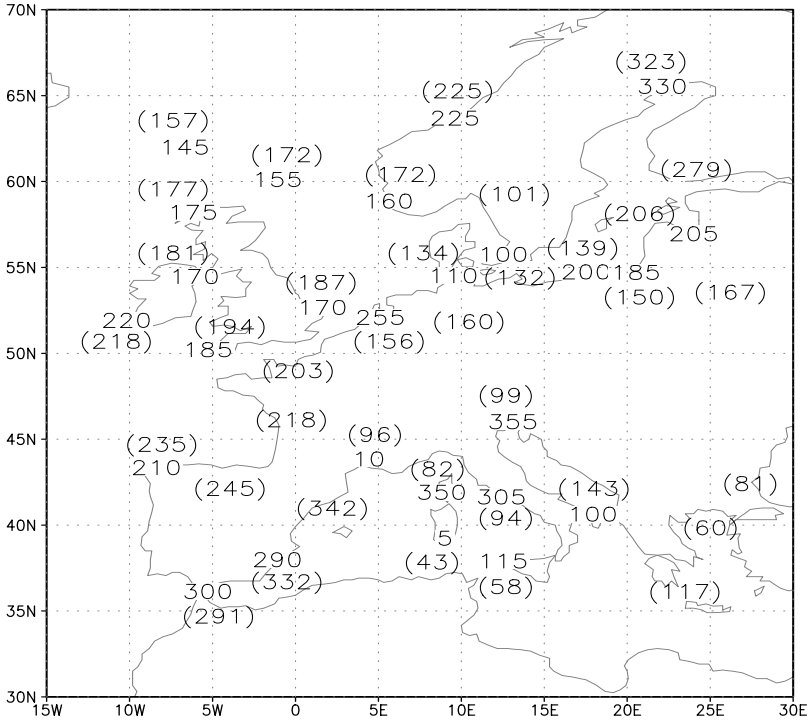

Figure 3.33 Wind direction for 00 hrs, 01/01/90

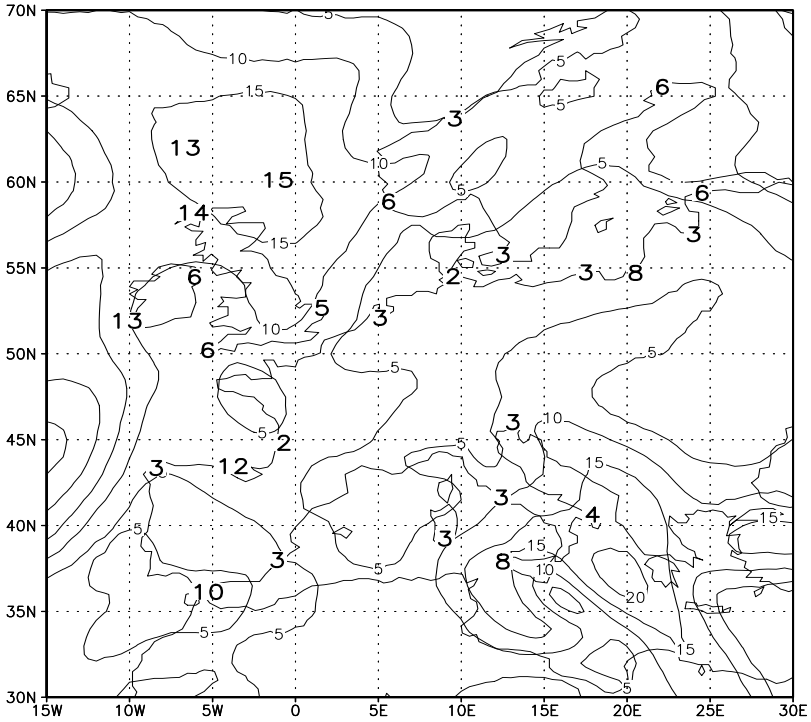

Figure 3.34 Wind speed (m/s) for 12 hrs, 01/01/90

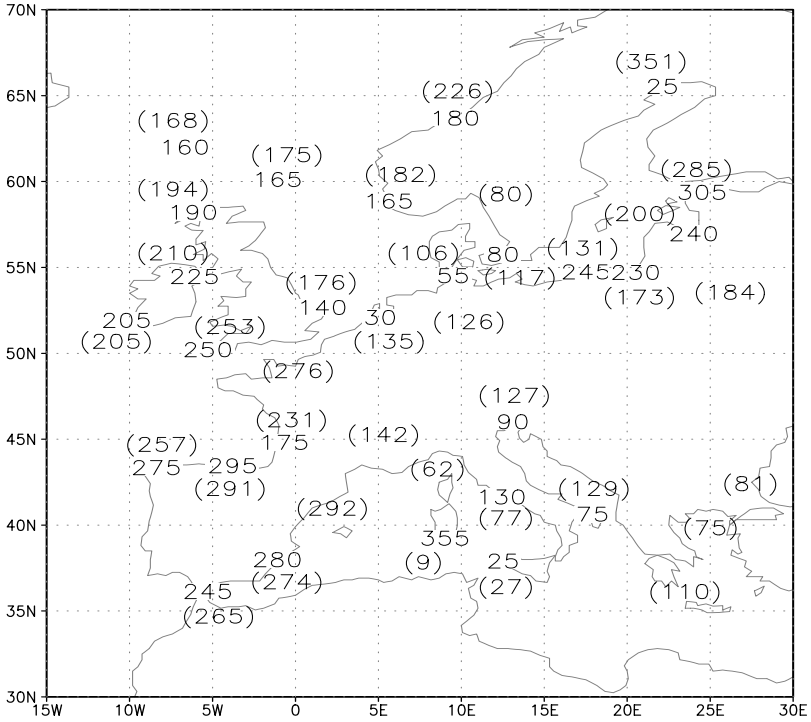

Figure 3.35 Wind direction for 12 hrs, 01/01/90

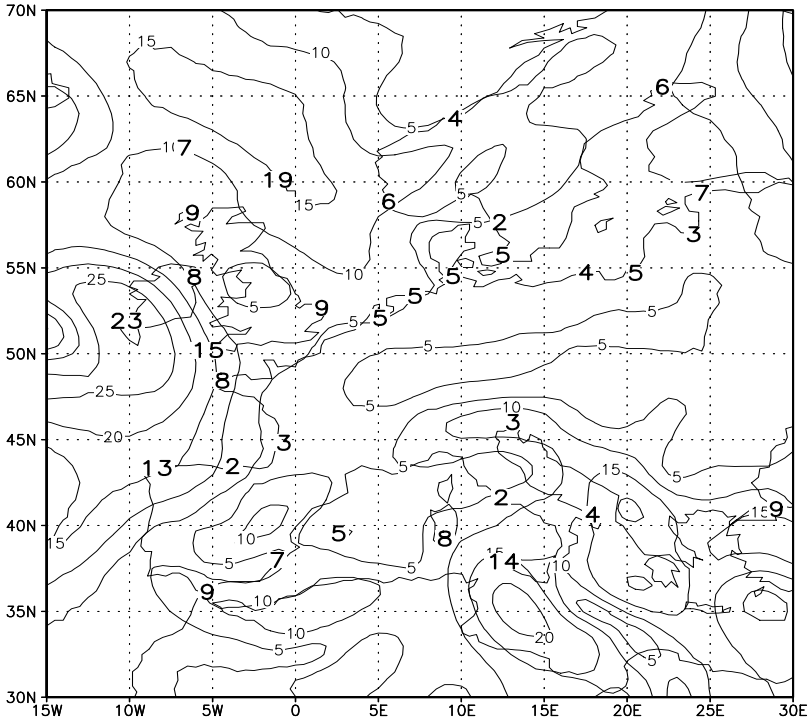

Figure 3.36 Wind speed (m/s) for 00 hrs, 02/01/90

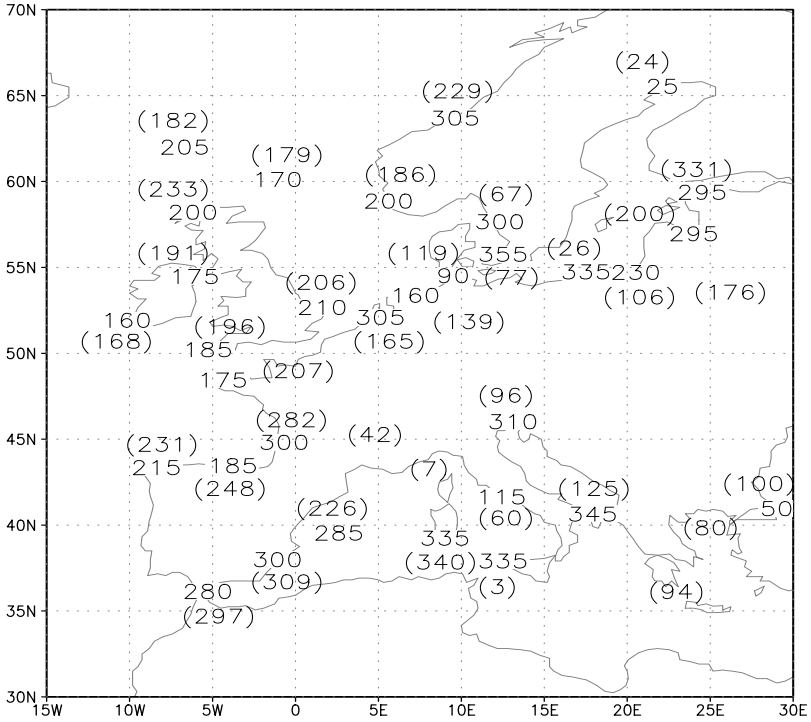

Figure 3.37 Wind direction for 00 hrs, 02/01/90

Summer day, 24 June, 1990

This example shows typically slack summer circulation over Europe.

As might be expected under conditions of low windiness, there is generally good agreement between the geostrophic and observed wind speed and direction throughout the region over all three timesteps (Figures 3.38 to 3.43). Again, southern Italy appears to have incorrect estimates of wind direction from the radiosonde.

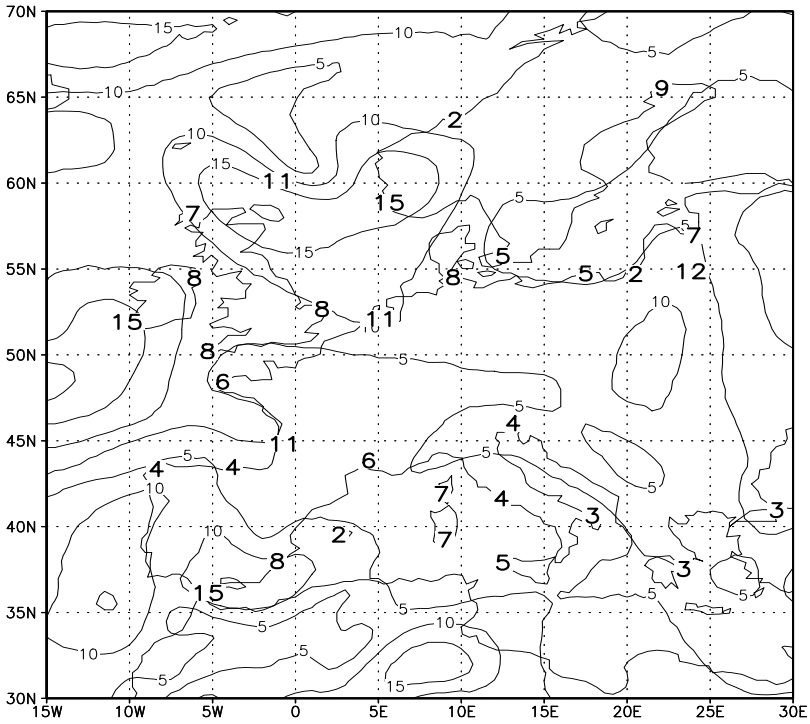

Figure 3.38 Wind speed (m/s) for 00 hrs, 24/06/90

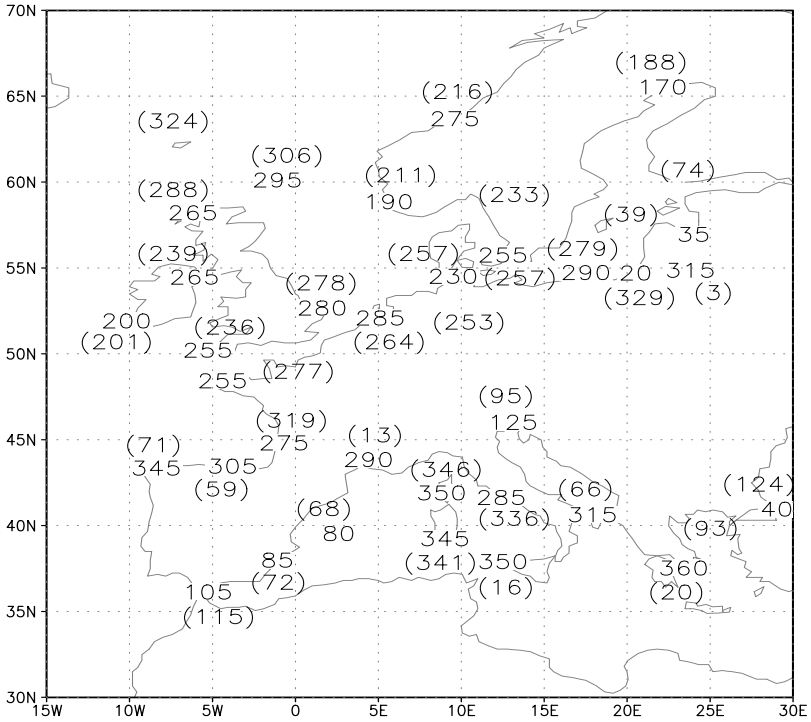

Figure 3.39 Wind direction for 00 hrs, 24/06/90

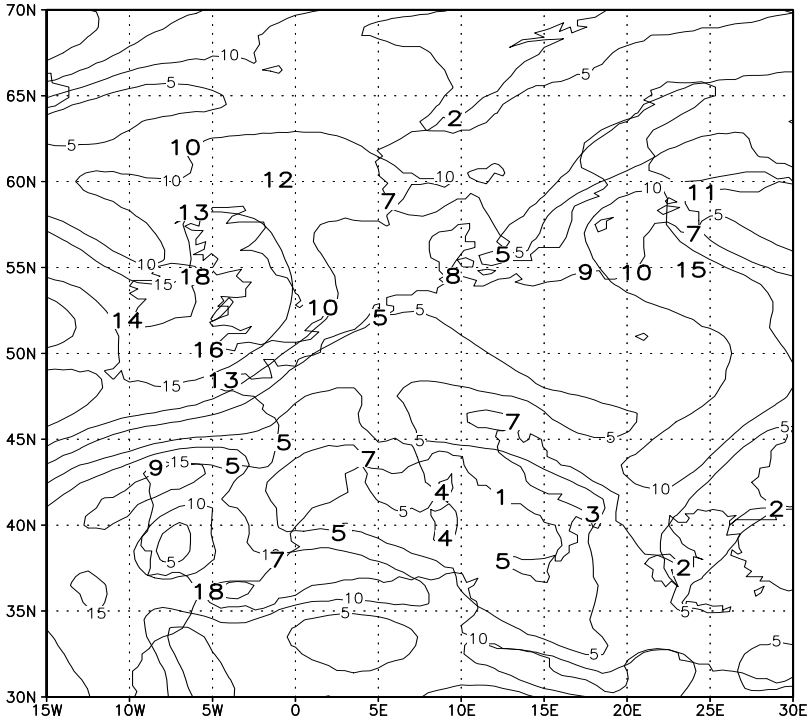

Figure 3.40 Wind speed (m/s) for 12 hrs, 24/06/90

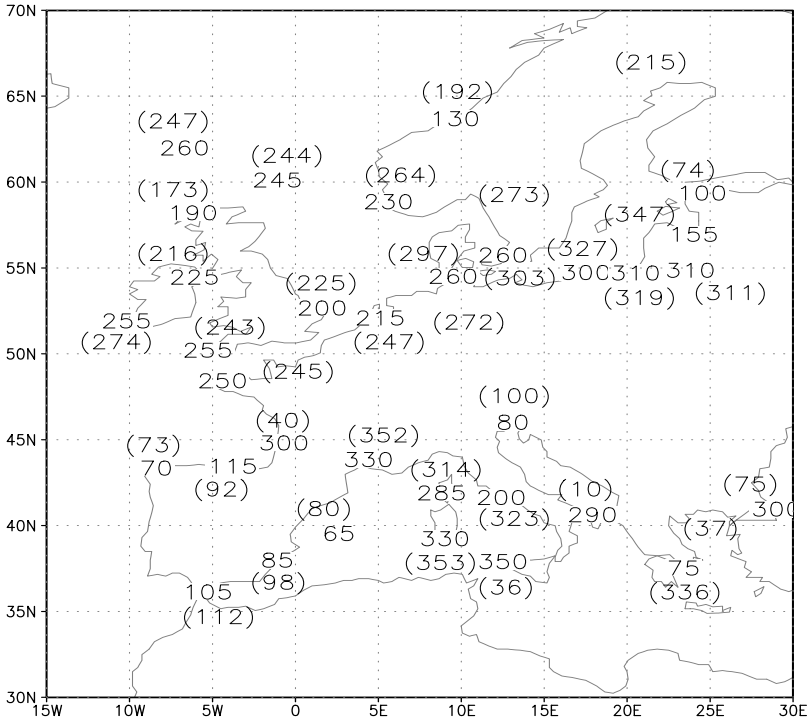

Figure 3.41 Wind direction for 12 hrs, 24/06/90

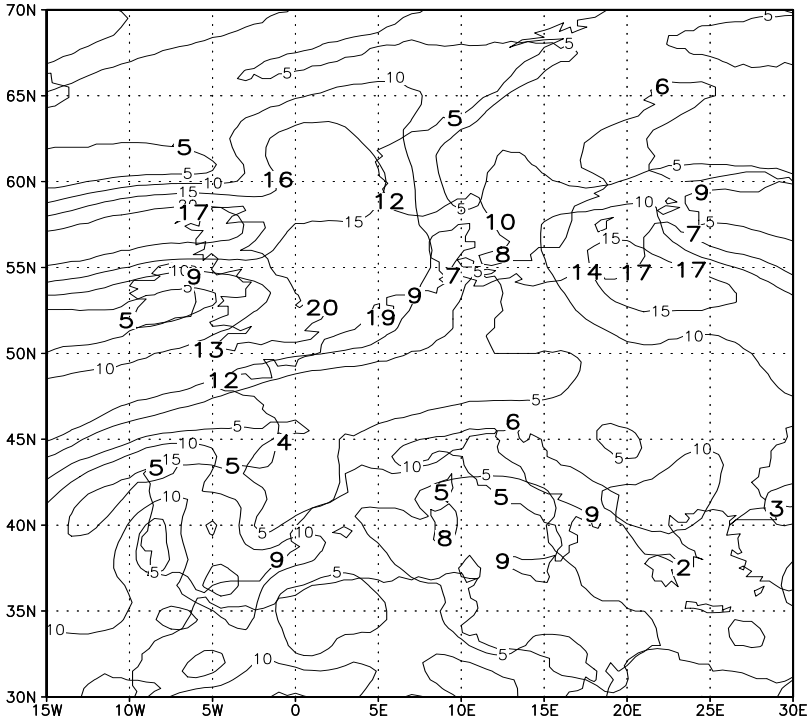

Figure 3.42 Wind speed (m/s) for 00 hrs, 25/06/90

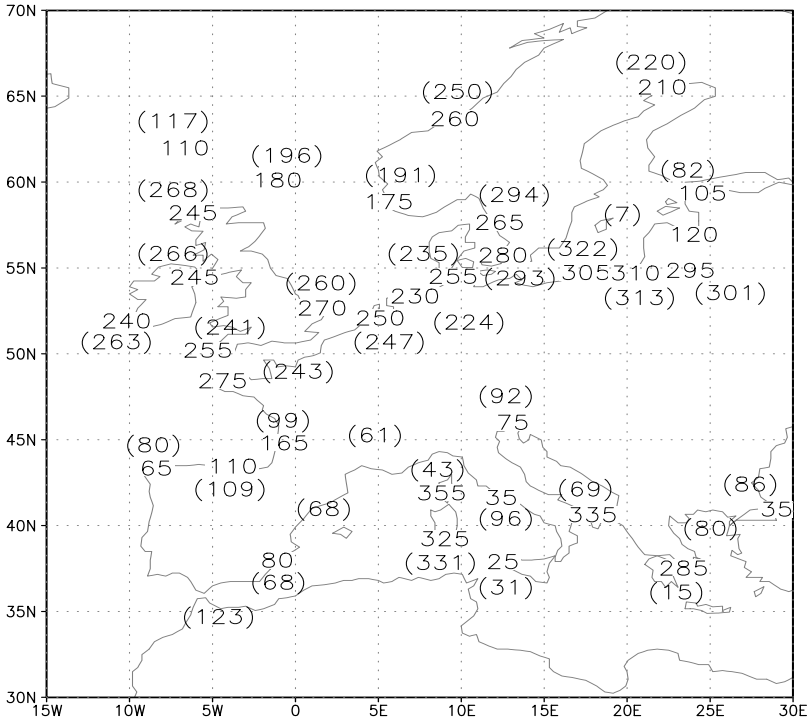

Figure 3.43 Wind direction for 00 hrs, 25/06/90

Winter day, 1 January 1997

We take a final example for a "normal" winter day from 1997. This is because there are fewer missing values in the later years of radiosonde ascents and it gives a more complete picture of the performance of the geostrophic approximation over the Mediterranean.

The overall correspondence between the observed wind speed and direction and the geostrophic values in Figures 3.44 to 3.49 is good. There are very few inconsistencies. The maps demonstrate that the calculated geostrophic wind field is valid for the Mediterranean.

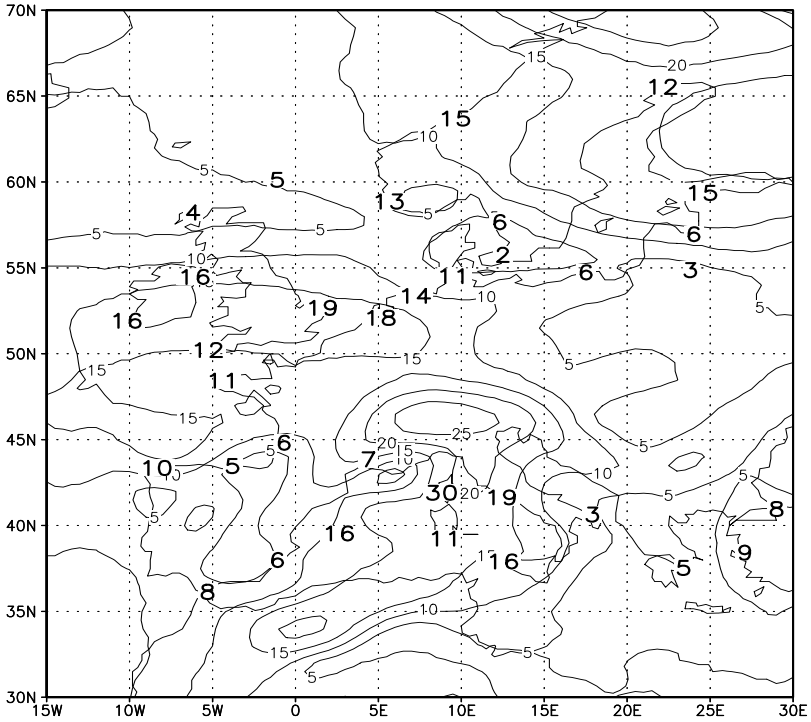

Figure 3.44 Wind speed (m/s) for 00 hrs, 01/01/97

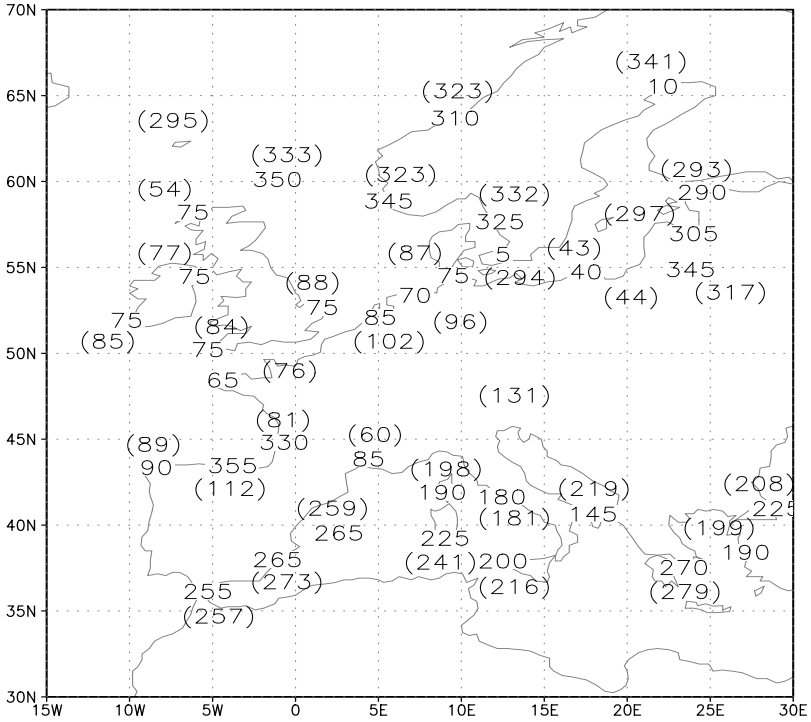

Figure 3.45 Wind direction for 00 hrs, 01/01/97

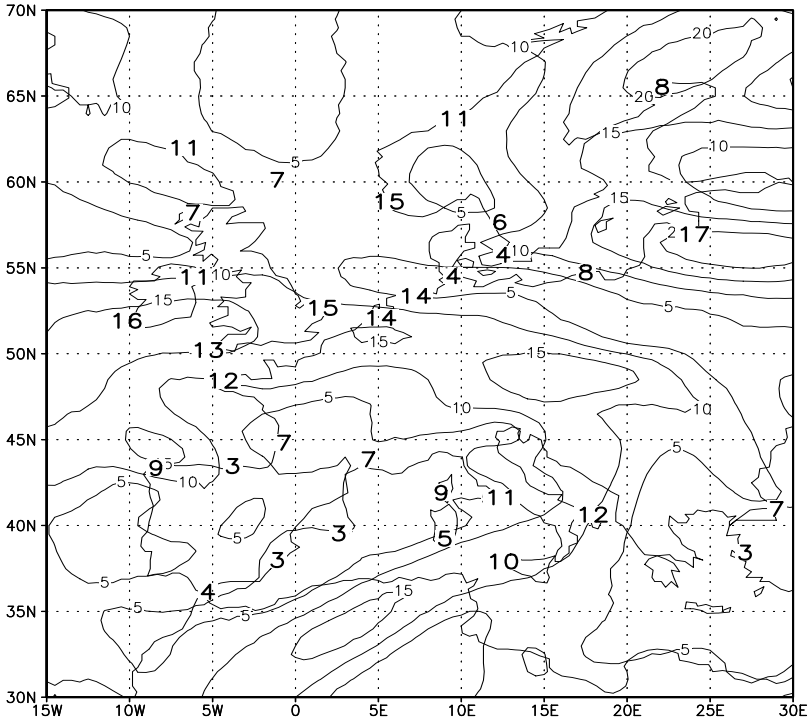

Figure 3.46 Wind speed (m/s) for 12 hrs, 01/01/97

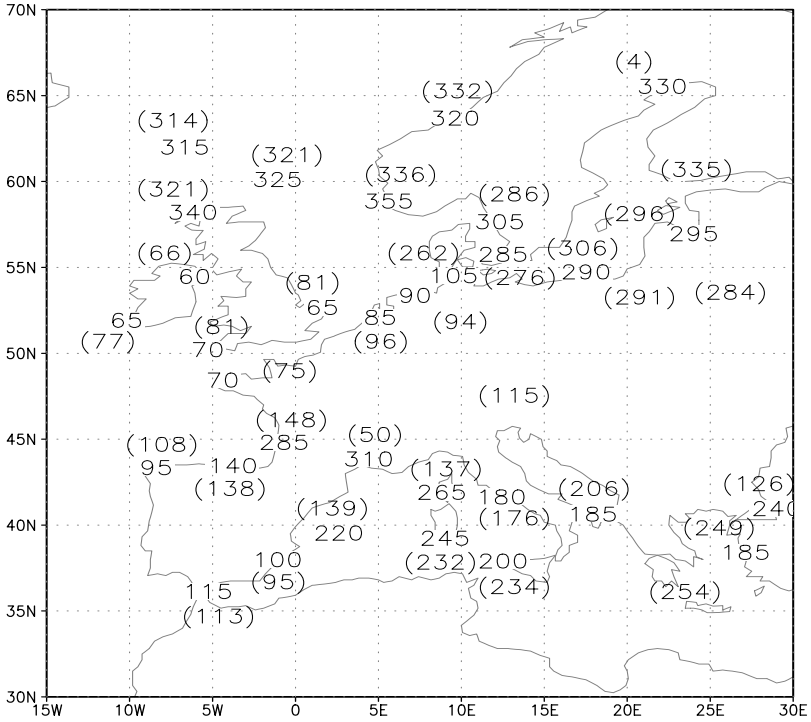

Figure 3.47 Wind direction for 12 hrs, 01/01/97

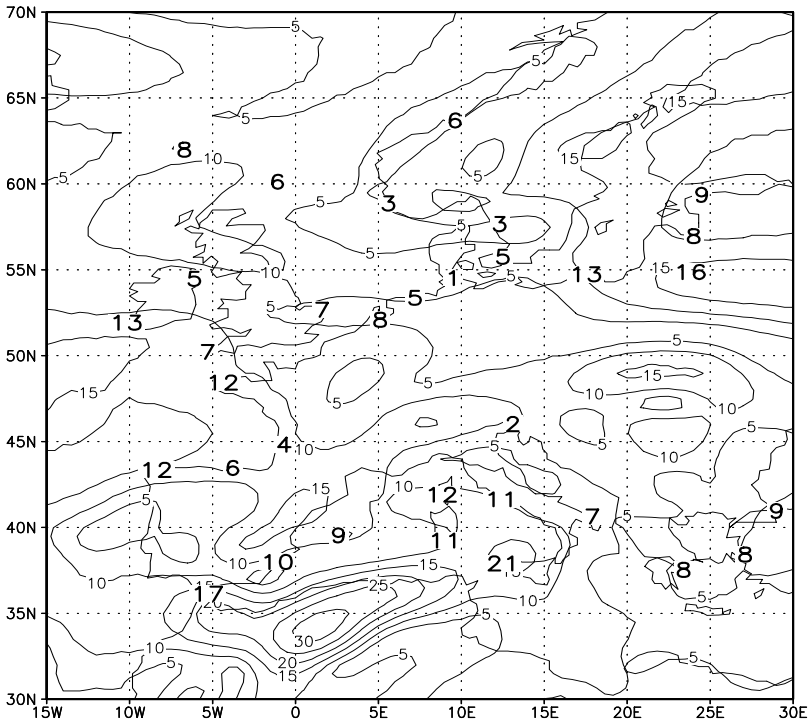

Figure 3.48 Wind speed (m/s) for 00 hrs, 02/01/97

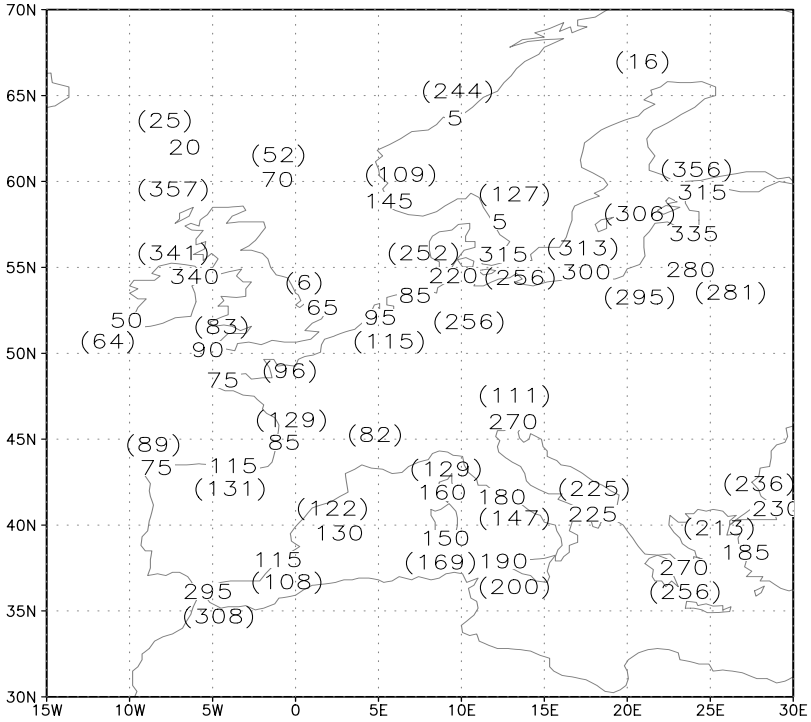

Figure 3.49 Wind direction for 00 hrs, 02/01/97

3.7.3 Comparison of statistics from radiosonde and geostrophic wind data for 1990 and 1997

The examples shown above illustrate qualitatively a fairly good agreement between the geostrophic wind and observations from radiosondes at the first atmospheric levels where friction has little effect on flow. We now extend the study by performing a quantitative comparison. Because of the numerical difficulties in comparing wind directions oscillating between 350 to 10 degrees, we restrict the analysis to wind speeds. We present summary results for all radiosonde ascents from 37 stations during the years 1990 and 1997. The time interval is 12-hourly to accommodate those stations not taking measurements at 6-hourly intervals.

Table 3.5 shows the analysis for the 1990 data. The column headings are:

- id a station identification number related to the numbers in Figure 3.25. The number is preceded by A (Atlantic), B (Baltic), or M (Mediterranean) depending on the sub-basin in which the station is located.
- r the correlation coefficient between the radiosonde and geostrophic wind speeds
- rmse root mean square error
- miss % percentage of missing values in the radiosonde data
- rng ra the range of the radiosonde data (absolute vale of maximum – minimum)
- rng ge the range of the geostrophic wind speeds
- std ra the standard deviation of the radiosonde data
- std ge the standard deviation of the geostrophic wind speeds
- ave ra the mean of the radiosonde data
- ave ge the mean of the geostrophic wind speeds.

Station 32 had no observations in 1990. The shaded rows in Table 3.5 indicate that these radiosonde stations are giving suspect observations. This is evidenced by one or more of the following:

- anomalously low correlation with geostrophic wind speeds,
- anomalously high rmse,
- anomalously large range,
- anomalies in the mean and/or standard deviation.

Only rows where it is evident that the radiosonde data are in error have been highlighted. For example, for Station 2, the range of 451.7 m/s is clearly in error. There are other rows where there may be problems but the cause is less clear cut. Generally, the summary statistics for 1990 indicate a good relationship between the geostrophic wind and the observed wind from the radiosonde. The last row in Table 3.5 gives the average of the various parameters (excluding the suspect rows). The rows in Table 3.5 are organised by sub-basin to facilitate examination of spatially systematic errors in the data. There are no obviously suspect radiosonde stations in the Atlantic region, four in the Mediterranean, and four (half the stations) in the Baltic.

The equivalent data for 1997 are shown in Table 3.6. The Atlantic has acquired one suspect radiosonde station, and the Baltic has none, an impressive improvement on the 1990 tally. The Mediterranean, on the other hand, still has four suspect rediosonde stations, three of which were present in the 1990 tally (the remaining one had no data in 1990). This apparently persistent failure in instrumentation for 25% of the Mediterranean radiosonde stations requires further detailed examination and possibly remedial

measures such as a training programme sponsored by the WMO.

There is little difference between the summary data for 1990 and 1997, other than that the percentage of missing values has fallen with time.

Although the validation works well, a somewhat surprising result is that the variance and means are slightly higher in both years for the geostrophic wind speeds compared with the radiosonde data. This is the opposite of what would be expected, since the calculation of the geostrophic wind involves an element of spatial smoothing generally assumed to provide less variable and lower estimates of wind speed than would be obtained from measurements in situ. The results also provide independent confirmation of the validity of the interpolation of the pressure data.

Table 3.5 Comparative wind speed statistics for 1990

id	r	rmse	miss %	rng ra	rng ge	std ra	std ge	ave ra	ave ge
A3	0.85	3.1	29	35.5	34.4	5.9	6.4	10.6	11.5
A5	0.76	3.1	21.5	27.3	29.1	4.8	5.4	7.6	8.2
A6	0.79	3.1	42.5	26.8	38.4	5	6.2	9.2	10.4
A8	0.87	2.7	66.7	27.3	35	5.7	6.9	9.8	10.5
A9	0.89	3	9.6	31.9	33.1	6.6	6.9	11.6	11.9
A12	0.92	2.5	11	34.5	39.8	6.5	6.9	11.5	12.1
A20	0.9	2.7	9	32.4	39.2	6.2	7	10.3	11
A21	0.73	4.4	22.2	37	33.3	6.4	6.6	9.8	11
A22	0.84	3.2	24.4	31.9	41.6	5.8	7.2	10.3	12.3
A25	0.8	3.3	15.1	31.9	38.7	5.6	6.7	8.8	11
A28	0.69	3.6	29.9	31.4	35.3	4.9	6	6.9	8.9
A33	0.9	2.7	8.6	36.5	44.8	6.2	6.8	11.6	11.6
A34	0.89	2.7	11	37.6	46.2	6.1	7	10.8	11.4
A35	0.91	2.9	10.7	35.5	38.1	7	8	12.3	13.2
A36	0.89	3	16.8	32.4	37.2	6.4	6.9	11.5	12.3
A37	0.9	3	15.2	38.1	46.8	6.9	7.5	12.3	12.9
Aave	**0.85**	**3.1**	**21.5**	**33.0**	**38.2**	**6.0**	**6.8**	**10.3**	**11.3**
B1	0.87	3	12.2	46.8	41.5	6.1	6.6	10.3	11
B2	0.19	18.6	18.1	451.7	30.9	19	5.7	10.5	9.9
B18	0.87	2.8	10	31.9	36.7	5.7	6.1	10.2	10.6
B19	0.31	13.1	18.4	300.9	33.4	13.8	5.8	10.5	10.3
B23	0.89	2.8	18.8	30.9	32.9	6.2	6.5	11.3	11.1
B24	0.58	6.8	34.9	106	33.5	8.4	6.5	11.1	10.8
B29	0.8	3.7	56.7	35	32.4	6.3	6.4	10.9	10.5
B30	0.55	5.7	31	108	30	6.8	5.2	8.5	9
Bave	**0.86**	**3.1**	**24.4**	**36.2**	**35.9**	**6.1**	**6.4**	**10.7**	**10.8**
M4	0.39	2.2	34	13.4	32.3	2.4	4.4	4.3	5.5
M7	0.71	3.6	28.8	26.2	29.8	5.2	5.8	8.6	8.9
M10	0.74	3.3	5.9	24.7	28.4	4.9	4.8	9.1	8.5
M11	0.7	2.8	29	23.7	21.7	3.9	4.1	6.2	7.1
M13	0.46	5.2	21.1	100.3	32.9	5.9	4.8	6.9	6.6
M14	0.76	2.9	21.4	29.3	30.7	4.5	5.1	6.8	7.2
M15	0.52	3.1	21.4	25.2	28.4	3.6	4.5	5	5.8
M16	0.72	3.4	26	29.8	38.5	4.8	5.2	7	7.3
M17	0.26	3.6	18.9	54.5	33	3.7	5.4	3.8	8
M26	0.69	2.5	9	19	27.9	3.5	4.5	5.2	6.7
M27	0.71	2.7	12.7	20.6	26.6	3.9	3.6	5.6	5.6
M31	0.24	8.9	54	158.4	25.7	9.2	5.8	6.8	10
M32									
Mave	**0.69**	**3.0**	**19.3**	**24.8**	**29.0**	**4.3**	**4.7**	**6.7**	**7.1**

Table 3.6 Comparative wind speed statistics for 1997

id	r	rmse	miss %	rng ra	rng ge	std ra	std ge	ave ra	ave ge
A3	0.86	3.1	16.8	35	36.2	6.1	6.7	11.2	11.9
A5	0.74	3.1	11.1	25.2	27.9	4.6	5.2	7.7	8.2
A6	0.5	8.8	12.3	216.6	36.1	10.2	6.6	10.3	10.6
A8	0.82	3.3	10.5	35	32.8	5.8	6.2	9.8	10.4
A9	0.86	3.1	10.1	30.4	34.4	6.1	6.4	10.5	10.9
A12	0.9	2.7	11.4	34	32.6	6	6.6	11	11.5
A20	0.87	2.8	7.1	29.8	32.7	5.6	6.1	9.5	10.2
A21	0.72	4.6	19.3	37	41.1	6.6	7	9.6	10.9
A22	0.84	3.1	14.1	29.8	40.1	5.9	6.9	10	11.3
A25	0.81	3.4	33.8	31.9	31.5	5.8	6.9	8.6	11.2
A28	0.62	3.8	22.9	32.9	33.1	4.8	5.8	6.5	8.7
A33	0.89	2.8	2.7	36.5	41.6	6.2	6.6	10.9	10.7
A34	0.88	2.7	4.9	32.4	45.6	5.8	6.5	10	10.2
A35	0.89	2.9	2.5	34	41.3	6.4	7.5	10.8	11.9
A36	0.91	2.8	5.3	33.4	42.7	6.7	7.1	12.1	12.3
A37	0.88	3.1	4.4	37.6	40.5	6.7	7.3	11.4	11.9
Aave	**0.83**	**3.2**	**11.8**	**33.0**	**36.9**	**5.9**	**6.6**	**10.0**	**10.8**
B1	0.85	2.9	7.4	27.8	40.1	5.6	6.1	9.7	9.9
B2	0.76	3.4	16.4	29.8	44.3	5.2	5.8	8.9	10
B18	0.82	3.1	50.5	26.8	34.6	5.4	6.2	10	10.8
B19	0.85	2.9	53.2	25.7	27.1	5.5	5.9	9.8	10
B23	0.88	2.7	16	36	35.1	5.7	6	10	10.3
B24	0.8	4.3	89.3	30.9	31.3	7.2	7	12.9	13.6
B29	0.8	3.2	21.1	30.9	36.1	5.3	6.1	9.6	9.3
B30	0.76	3.5	26.4	25.7	27.5	5.4	5.8	9.3	9.7
Bave	**0.82**	**3.3**	**35.0**	**29.2**	**34.5**	**5.7**	**6.1**	**10.0**	**10.5**
M4	0.29	4.8	10.5	58.1	30.2	5	4.5	5.6	6.1
M7	0.74	3.8	11.2	44.2	33.5	5.7	6.5	8.6	9.3
M10	0.71	3.1	5.3	25.7	28	4.4	4.6	9.2	7.9
M11	0.7	2.7	35.1	19	24.7	3.8	4.3	6.1	7
M13	0.67	3.5	9.3	28.8	32	4.7	5.5	8.1	7.5
M14	0.76	2.9	17.9	26.2	28.1	4.4	5.2	7.3	7.3
M15	0.54	3.2	9.2	22.6	33.4	3.9	4.8	5.9	6.2
M16	0.73	3.1	17	25.2	26.3	4.5	4.9	7.3	7.5
M17	0.44	2.8	12.9	21.6	34.3	3.1	5.9	3.9	9
M26	0.6	2.8	20	20.6	27.4	3.5	4.6	5.9	6.7
M27	0.66	3.4	20.1	26.8	30.8	4.5	4.6	6.8	6.2
M31	0.49	4.1	2.6	75.6	28.8	4.7	6	6.1	9.7
M32	0.33	3.3	1.4	22.1	30.4	3.5	6	5.5	9.9
Mave	**0.68**	**3.2**	**16.1**	**26.6**	**29.4**	**4.4**	**5.0**	**7.2**	**7.3**

3.7.4 Comparison of seasonal cycles of radiosonde and geostrophic speeds

Figure 3.50 shows the 1990 seasonal pattern of wind speed, from the geostrophic approximation and the radiosonde ascents, for the Atlantic, Baltic, and Mediterranean basins respectively. Monthly averages for each are presented, calculated by averaging for all points within each basin over time and space for the year 1990.

For the Atlantic (Figure 3.50a) there is a good match between the mean monthly wind speeds with the largest discrepancies occurring in the months when the wind speeds are highest. This is either because radiosonde data are inherently unreliable during periods of very high wind speeds, or because the most reliable radiosonde sites are those most affected by missing values during North Atlantic storms, thus biasing the monthly means towards less reliable sites. The Baltic (Figure 3.50b) provides a near-perfect match between the monthly mean wind speeds. The discrepancies noted in the Mediterranean chart (Figure 3.50c) simply reflect the persistent unreliability already noted at certain sites in the

region. At such low mean wind speeds the match should be much closer.

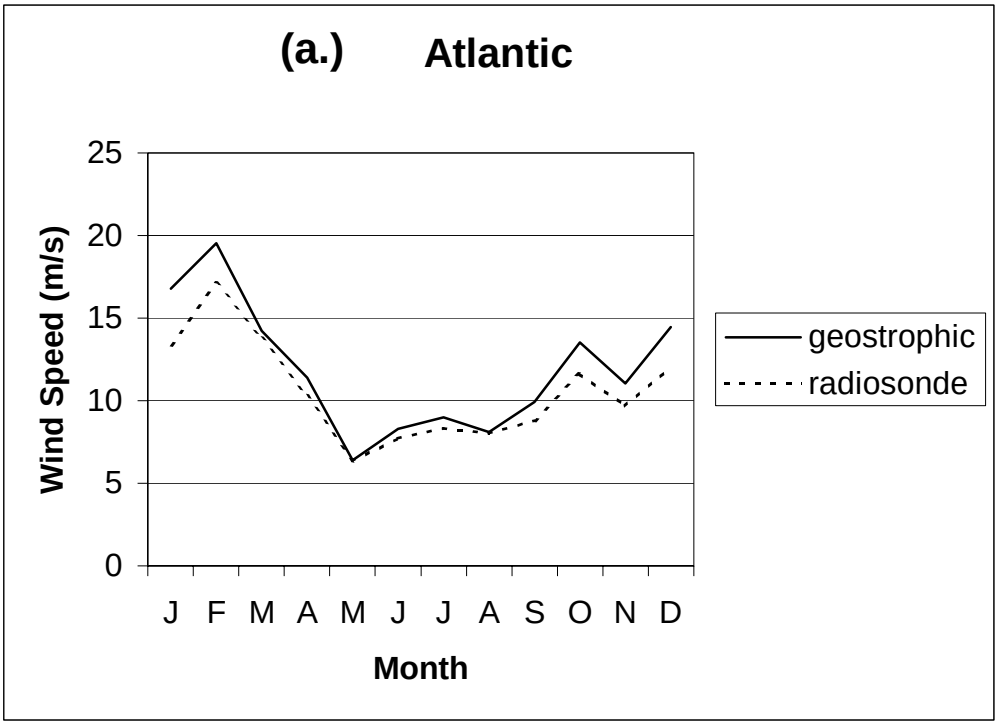

Figure 3.50 Seasonal cycles of wind speed from the Atlantic, Baltic and Mediterranean basins

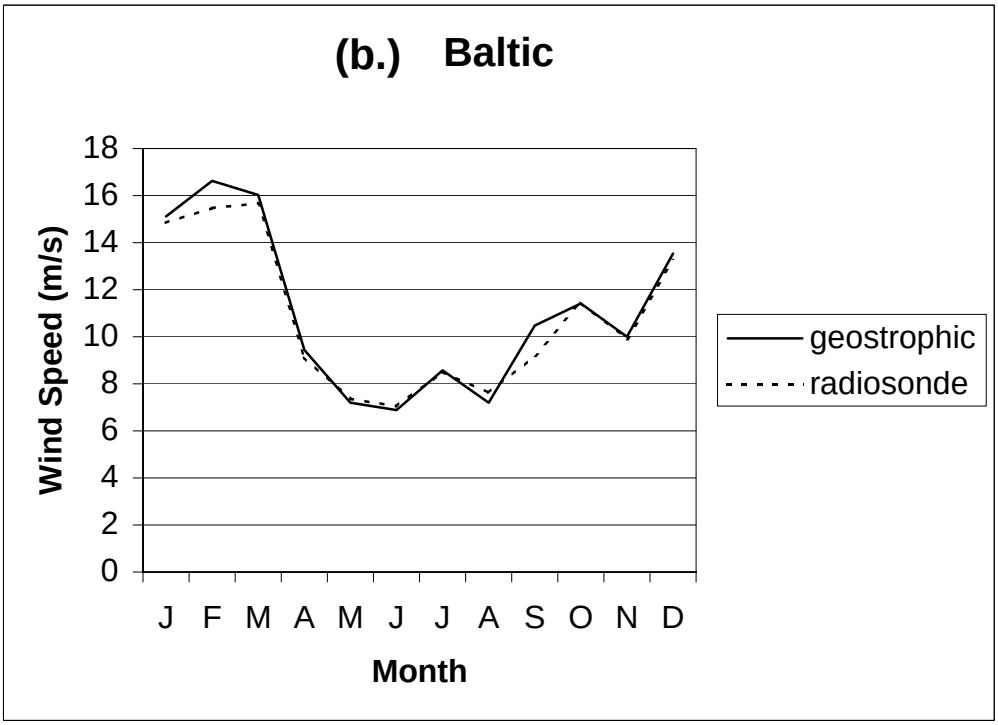

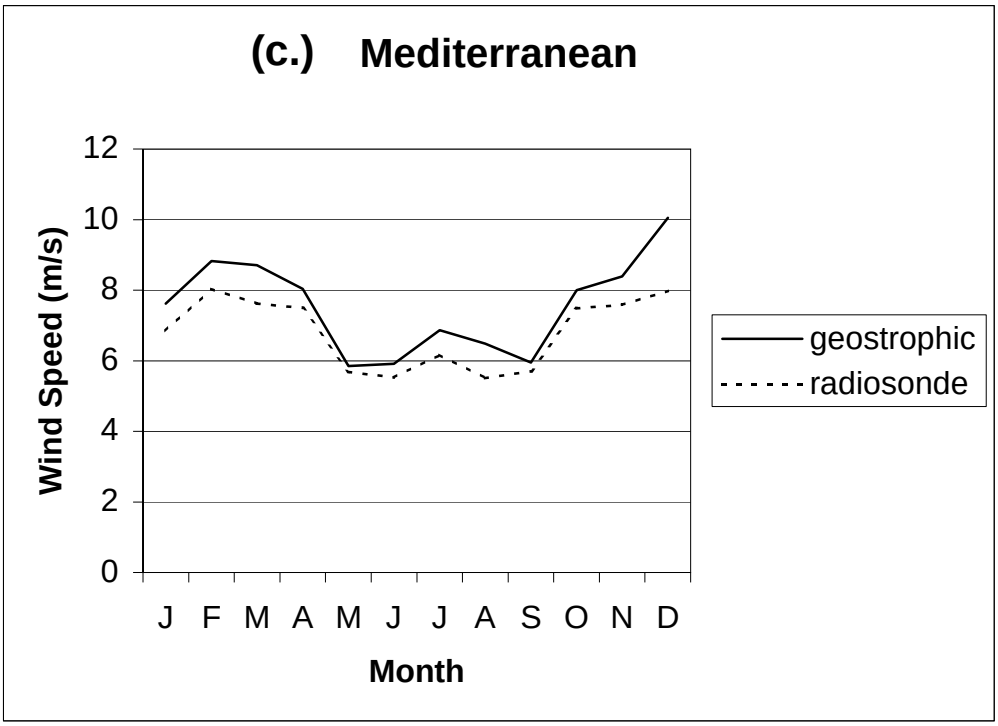

Figure 3.51 Seasonal cycles of wind speed from the Atlantic, Mediterranean and Baltic basins (continued)

3.7.5 Conclusions regarding comparison of POWER geostrophic winds with radiosonde data

Examination of the radiosonde wind data used in POWER reveals many inconsistencies that would make them extremely difficult to use on their own. The Mediterranean appears to be particularly prone to suspect radiosonde data, whereas the Atlantic, and latterly the Baltic, appears to give reliable information. Used to validate geostrophic flow, however, these data are extremely valuable. It is reasonable to assume that, even if they contain systematic errors, the geostrophic data are spatially consistent. This enables us to readily identify suspect radiosonde data, such as the Italian observations for 1 January 1990, and use the remainder for validation.

Given that the radiosonde data are point information, and the geostrophic winds are derived from gridded data with an element of spatial averaging, the results of the validation are remarkably good. The maps and tables provided in this report indicate that the geostrophic wind and direction calculated from the interpolated pressure data are an excellent representation of frictionless flow between 600 and 900 m over the ocean and immediate coastal regions of Europe, including the Mediterranean and the Baltic Sea.

3.8 Results

Figure 3.52 presents a plot of the distribution of mean annual geostrophic wind speeds calculated from the NCEP atmospheric pressure data in the period 1985 - 1997.

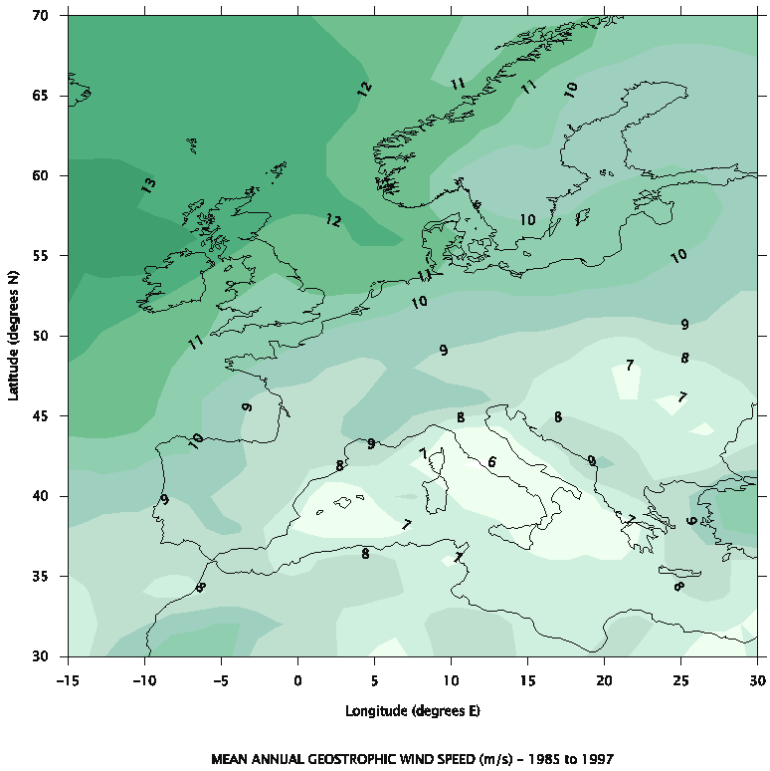

Figure 3.52 Calculated mean annual geostrophic wind speeds (m s^{-1}) – 1985 to 1997

3.9 Conclusions

This chapter has demonstrated that geostrophic winds are an accurate representation of friction-free wind over the ocean and coastal areas:

- The geostrophic wind speed and direction are consistent with frictionless flow from radiosonde observations at coastal stations,
- Where radiosonde data are unreliable, the geostrophic wind speed and direction data provide a spatially consistent alternative,
- Patterns of geostrophic flow are consistent with the surface wind field.

Therefore, the geostrophic wind is suitable for used in the POWER project as the basis for calculating the surface wind using WAsP. This procedure is described in Chapter 4.

3.10 References for Chapter 3

James, I.N. (1994): Introduction to Circulating Atmospheres. Cambridge University Press, Cambridge.

Kalnay, E. et al. (1996): The NCEP/NCAR 40-year reanalysis project. Bull. Amer. Meteor. Soc. 77, 437-471.

McIlveen, R. (1992): Fundamentals of Weather and Climate. Chapman & Hall, London. 497 pp.

Press, W.H. (1992) Numerical Recipes in FORTRAN: The Art of Scientific Computing. Second Edition. Cambridge. 963 pp.

Watson, D.F. (1992) Contouring. A Guide to The Analysis and Display of Spatial Data. Pergamon. 321 pp

CHAPTER 4 : Transforming geostrophic winds to turbine hub heights using WAsP

Chapter author: G M Watson (CLRC Rutherford Appleton Laboratory)

4.1 Introduction

The second step of the POWER methodology (see Section 2.2) is to transform geostrophic winds to the sea surface layer by applying the Wind Atlas Analysis and Application Program (WAsP).

4.2 The Wind Atlas Analysis and Application Programme (WAsP)

WAsP [Mortensen *et al*., 1993] is a linear flow model that can be used to transform geostrophic winds to the surface layer. The model is well-established and commonly used throughout the wind energy community to perform wind resource assessments.

The WAsP model calculations are based on the geostrophic drag law combined with models of stability and development of an internal boundary layer (IBL). The standard version of the software allows coastal effects to be modelled assuming differences in mean onshore and offshore stability and using internal boundary layer theory to modify wind speed profiles over the width of the coastal zone. Within the model adjustments to the wind speed profile offshore are based on the assumption that the wind speed profile in the surface layer (up to approximately 100m) is slightly stable.

WAsP takes as input wind data from one site and estimates the wind regime at another nearby site. Simply put, the model operates in two steps:

step 1) The input wind data is used to calculate the corresponding "high level" geostrophic wind conditions for that time and location. In doing so, the model "subtracts" local effects such as zones of shelter from local obstructions (e.g. buildings or trees), acceleration or deceleration of air flow due to the shape and form of the surrounding landscape (e.g. if the site is on the brow of a hill, air flow from some directions could be accelerated compared to a flat open location) and the characteristics of the local vertical wind speed profile formed by a combination of internal boundary layers, each spawned by boundaries between zones with different surface roughness e.g. lakes, open grassland, crops, forests, urban areas etc..

step 2) The geostrophic wind conditions are transformed down to the second site. This time the model "adds" the local effects associated with the new location. Thus in estimating the wind regime at the second site WAsP takes account of differences in orography, surface roughness, obstructions, height above ground etc. between the two site.

In most cases, the wind data used as input to model will have been measured by instruments mounted on a meteorological mast installed at the site of a proposed wind farm, or at a nearby meteorological monitoring station. However, within POWER the input data is the geostrophic wind speed and direction data calculated from the sea level pressure data (see Chapter 3) and so, in effect, only step 2 of the WAsP model operations is being used. This method is also sometimes referred to in this report as GEOWAsP.

4.3 WAsP 5 versus WAsP 6.0

Plans to use an upgraded version of WAsP software (WAsP version 6.0, first released in March 1999) for POWER were abandoned because:

1. Use of upper air (geostrophic wind) data as input to the model has not been implemented entirely.

2. The ability to run the model remotely, in batch mode, is not supported in this release. This feature is essential for its application in the POWER project as there are a very large number of model runs to perform.

Therefore it was decided that the most recent release of WAsP 5 (version compiled in February 1999) would be used for the POWER project instead. This version of the WAsP model supports both features highlighted above.

4.4 Application of WAsP throughout European waters

The WAsP model was used to transform the calculated geostrophic winds (see Chapter 3) to the surface layer, at each point in the 0.5º x 0.5º latitude/longitude grid that lies over the sea. In practice this means that WAsP analyses were performed at over 3700 grid locations.

Coastline data was extracted from the *Digital Chart of the World* CD-ROM (distributed by PhD Associates Inc.). The *Digital Chart of the World* data contains over 164,000 latitude/longitude coordinate pairs that describe the position of the coast in the area of interest. Where a grid point was situated far offshore (>10km), a constant surface roughness value of 0.0002m was assumed. Alternatively, where a grid point was close to the coast (<10km) a roughness value of 0.0002m was assumed over the sea area and 0.03m over the land.

Mean wind conditions for the period 1985-1997 have been estimated at eight hub heights at each grid point over the sea. The hub height levels (10m, 30m, 50m, 70m, 90m, 110m, 130m and 150m above mean sea level respectively) were chosen to cover the range of expected hub heights of wind turbines that are likely to be sited offshore in the coming years.

In addition, the monthly and inter-annual variability of the wind conditions in European waters were also investigated by performing WAsP model runs estimating the mean monthly and mean yearly wind conditions at all offshore grid points

Finally, some additional WAsP runs were performed to obtain offshore wind predictions at specific locations and heights, which could be compared directly against observed data for validation purposes. (see Chapter 10 for more details).

4.5 Variable sea surface roughnesses

The components of the surface terrain (such as built-up areas, forests, hedges and crops) disturb the air flow close to the ground and generally act to slow down the wind at ground level. This in turn influences the vertical wind speed profile. This aerodynamic "drag" characteristic of a terrain is referred to as its surface roughness and is commonly parameterised by an aerodynamic roughness length, z_0. It is important to understand that "aerodynamic roughness" can be very different to the perception of roughness of a particular surface obtained by sight or touch. Values of z_0, for a selection of terrain types are given in the scientific literature (including [*Troen et al*, 1989]).

In general, the surface of the sea is aerodynamically very "smooth", with correspondingly small z_0 values (typically of the order of 10^{-4} to 10^{-3} m). However, whereas the roughness of land features can be thought of as essentially constant, the sea surface geometry and roughness alter continuously with varying wind speed. Unfortunately, despite decades of work on wind-wave interactions, a conclusive parameterisation of z_0 in terms of wind speed and/or sea state has not yet been identified [*Taylor (ed.),* 2000].

The distribution and variability of estimates of sea surface roughness throughout the POWER project area was investigated using a new parameterisation for z_0 suggested recently by researchers from the Southampton Oceanographic Centre [*Taylor and Yelland,* 2000]. It is proposed that sea surface roughness, z_0, can be predicted from the height and steepness of the waves at the site:

$$\frac{z_0}{H_s} = A\left(\frac{H_s}{L_p}\right)^B \tag{4.1}$$

where H_s and L_p are the significant wave height and peak wavelength for the combined wind sea and swell (resultant) spectrum, and the best estimates for the coefficients are A=1200, B=4.5. This approach has the advantage that it takes into account the effects of not only locally generated wind waves, but also swell waves that have travelled into the area from more remote sites. In addition, it models changes in roughness due to wave shoaling in shallow water and fetch dependency is

automatically accounted for within the wave input data. The formulation has been shown to explain the characteristics of a wide range of data sets, however Taylor and Yelland also point to certain weaknesses in the definition of the coefficients and some potential difficulties with its application. Nevertheless, it was decided that this was the most appropriate parameterisation of z_0 available for the task.

Values of z_0 were calculated using Equation 4.1 based on data from the UK Meteorological Office (UKMO) European Wave Model. The values of H_s were taken directly from the UKMO data, however values of peak wavelength, L_p, were determined from the dispersion relationship:

$$\frac{\omega^2}{g} = k \tanh(kh) \tag{4.2}$$

where ω is the angular wave frequency ($2\pi/T_p$), g is the acceleration due to gravity, k is the wave number ($2\pi/L_p$) and h is the water depth. Figure 4.1 illustrates the water depths throughout the European Wave Model area used in these calculations.

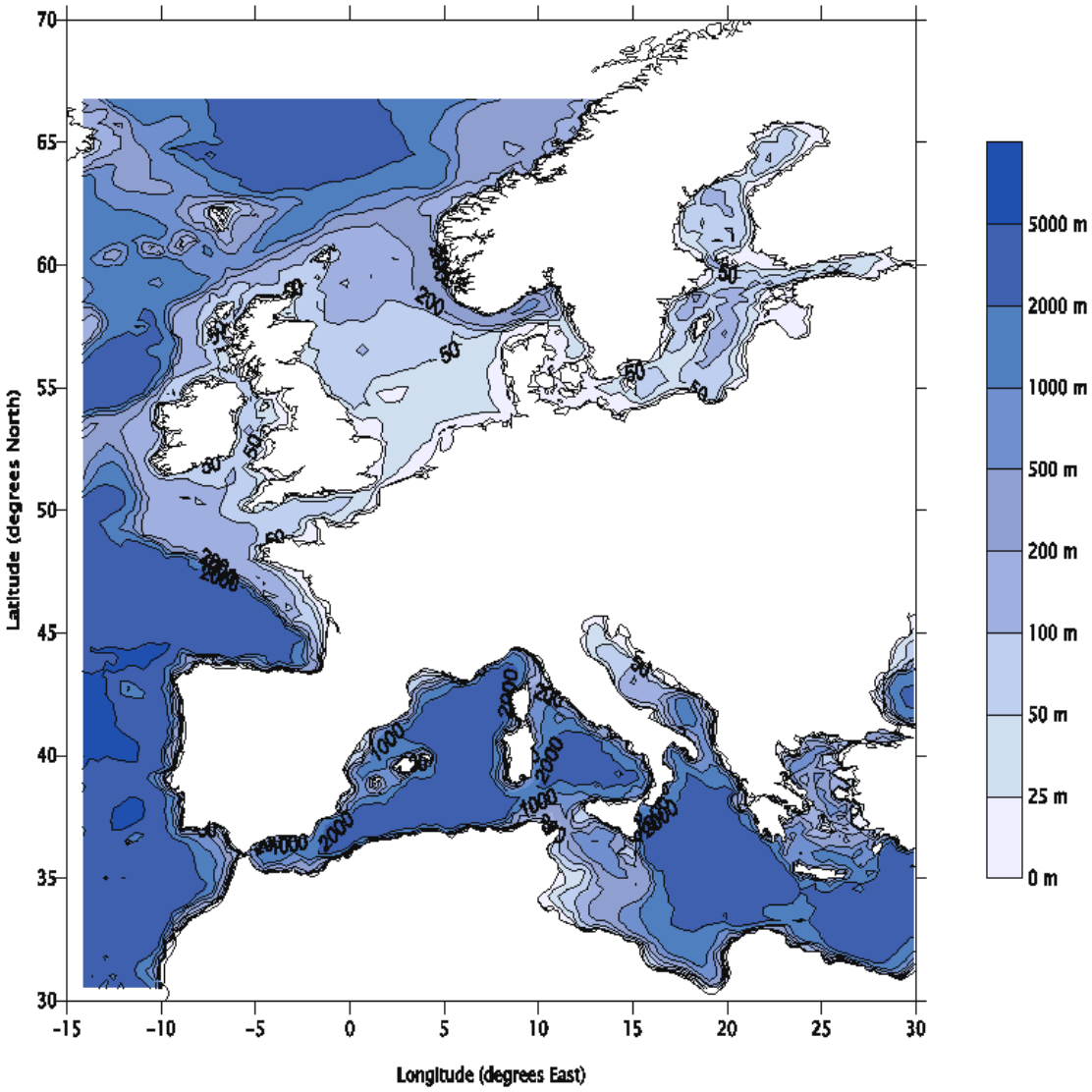

Figure 4.1 Bathymetry in European waters (as used in UKMO European Wave Model)

An example of some typical results are presented in Figure 4.2. These plots show simultaneous time series of wind speed (at a nominal height of 19.5m a.s.l.), wave height, wave period and z_0 for a North Sea location at 3-hourly intervals over a typical winter month. The results suggest that that for the bulk of the time, z_0 values are very small indicating the sea surface is aerodynamically very smooth.

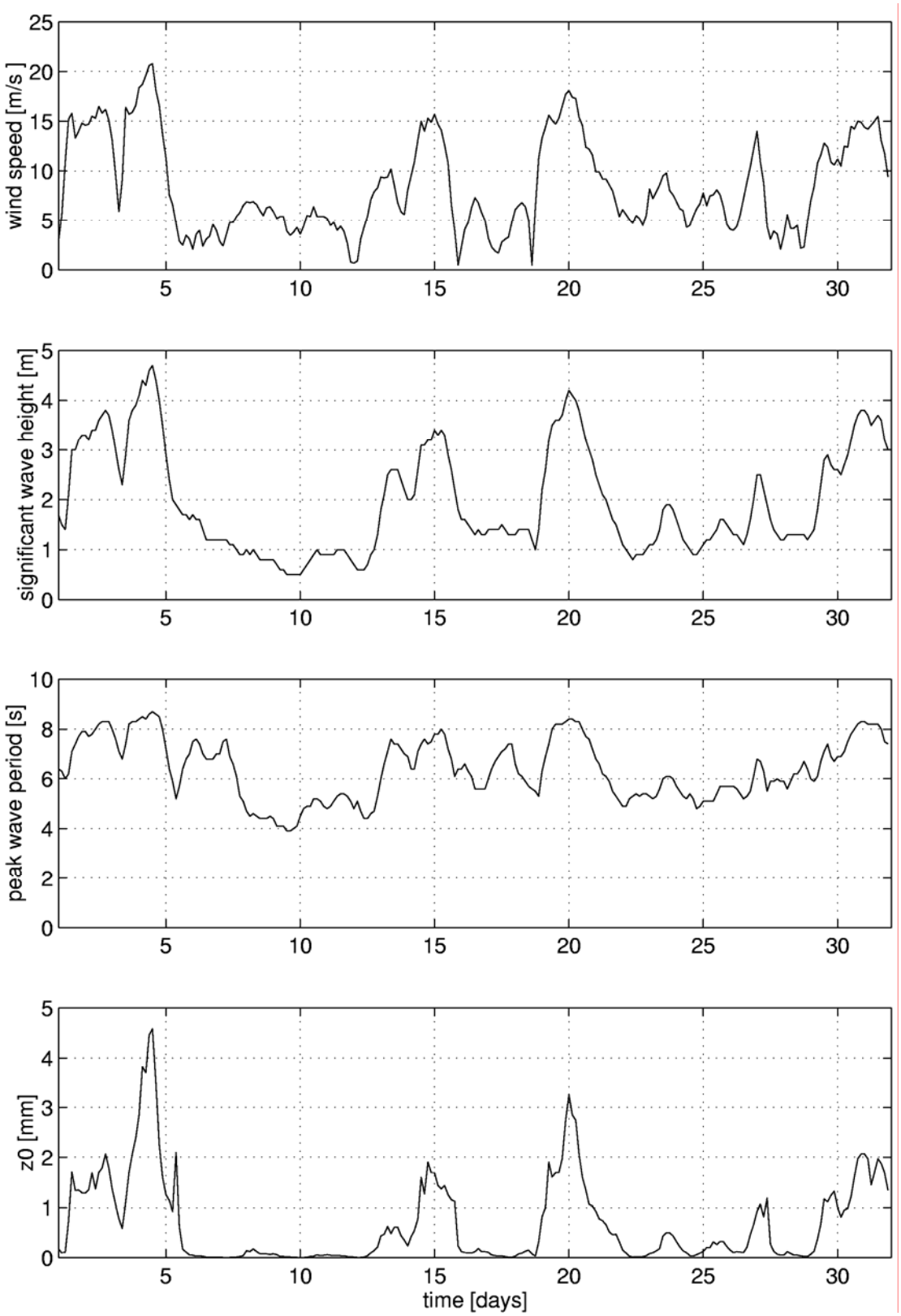

However, there are relatively short periods, mostly corresponding to the high wind events, when the sea surface roughness increases significantly, in this case reaching a maximum value of $z_0 \approx 4.6$mm.

Figure 4.2 Plots showing simultaneous values of wind speed, wave height, wave period and z_0 at a North Sea location during a typical winter month

In order to get an indication of the distribution and overall variability of the sea surface roughness in European waters, the mean value of z_0, as well as its standard deviation, was calculated for each point in the UKMO grid over the period January 1987 to December 1996. The results are illustrated in Figures 4.3a and 4.3b. The overall pattern suggests that relatively high values of sea surface roughness (as well as variability) can be expected along the Atlantic Margin and into the North Sea, with relatively low (and less variable) values of sea surface roughness in the Baltic and Mediterranean Seas. There are also some indications that the values and variability of sea surface roughness are elevated in shallow waters, such as the Dogger Bank (off eastern England) and the shoal waters along the Dutch, German and Danish North Sea coasts. From this, it can be implied that the variability in sea surface roughness is likely to be more of an issue in these areas than elsewhere.

The annual variation in sea surface roughness was investigated by calculating the mean value and standard deviation of z_0 during each quarter of the year over the period 1987 to 1996. The results are presented in Figures 4.4 and 4.5.

The final component of this task was to assess the impact of variable sea surface roughness on the POWER offshore wind resource predictions. In POWER, offshore wind resource predictions have been performed using the WAsP model. The version of WAsP applied uses a very simple approach to roughness modelling, assuming a constant sea surface roughness of z_0=0.2mm for all sea areas, wind conditions and sea states. Recent modelling studies at Risø and NEG Micon A/S [*Frank et al*., 2000] [*Lange et al*., 2000] indicate that these roughness models result in relatively small differences in predicted wind speeds (less than 0.5%). In addition, Barthelmie [2002] has investigated the effect of varying roughness by predicting a range of wind speeds at 50m height, based on 10m wind speeds and using logarithmic wind speed profiles and a range of different roughness between z_0=0.02mm and z_0=30mm (for more details see Chapter 5, Section 5.2.3). Her results indicate a maximum of only 2.8% difference in log-predicted wind speed at 50m from a 25ms^{-1} wind speed at 10m height. This implies that the z_0 values predicted here would result in only small differences in predicted mean wind speeds compared to the existing WAsP predictions. Furthermore, [*Frank et al*., 2000] suggests that thermal stratification/stability issues have a much greater impact on offshore wind resources than changes in sea surface roughness. Finally, the tidal range at a site may also impact on the wind speed predictions, particularly as in some areas large expanses of rough foreshore may be exposed at low water. It should be remembered that some parts of the POWER project area are subject to large tidal ranges and so this could be a significant effect. Although a preliminary attempt at quantifying the impact of varying water levels on turbine hub level wind speeds has been made, more work is needed on this issue. This is beyond the scope of this project.

Therefore, although it is clear that variable sea surface roughness will modify wind speed predictions slightly, the impact of other contributory factors are expected to dominate. In view of all these findings (and the amount of additional time and effort it would entail for very little improvement in accuracy), it was decided that it is *not* appropriate to apply correction factors to the WAsP model estimates to take account of variations in sea surface roughness.

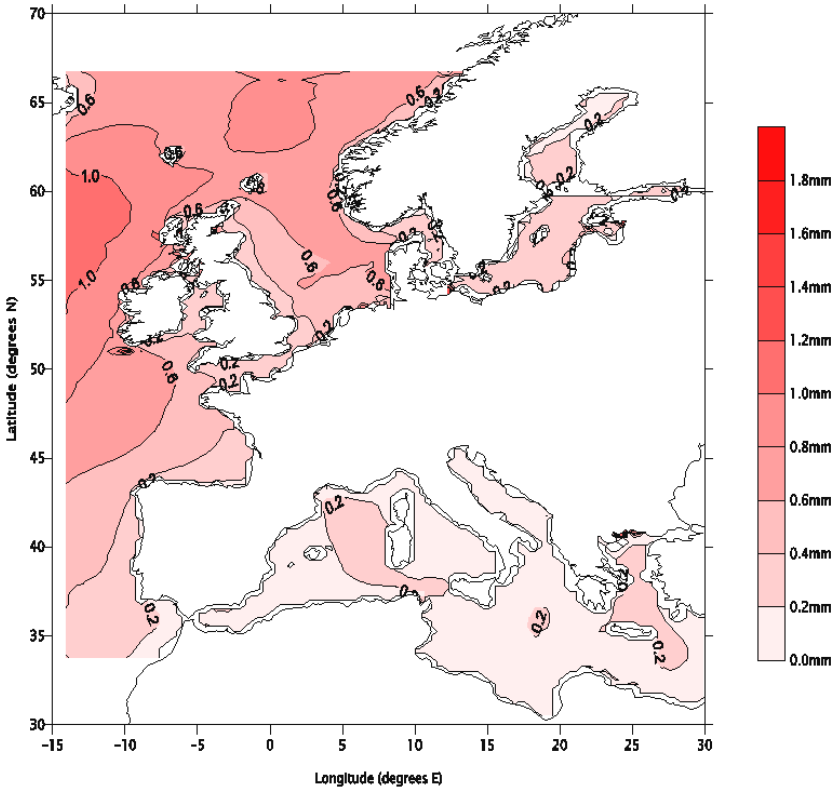

Mean value of sea surface (aerodynamic) roughness - 1987 to 1996

(a)

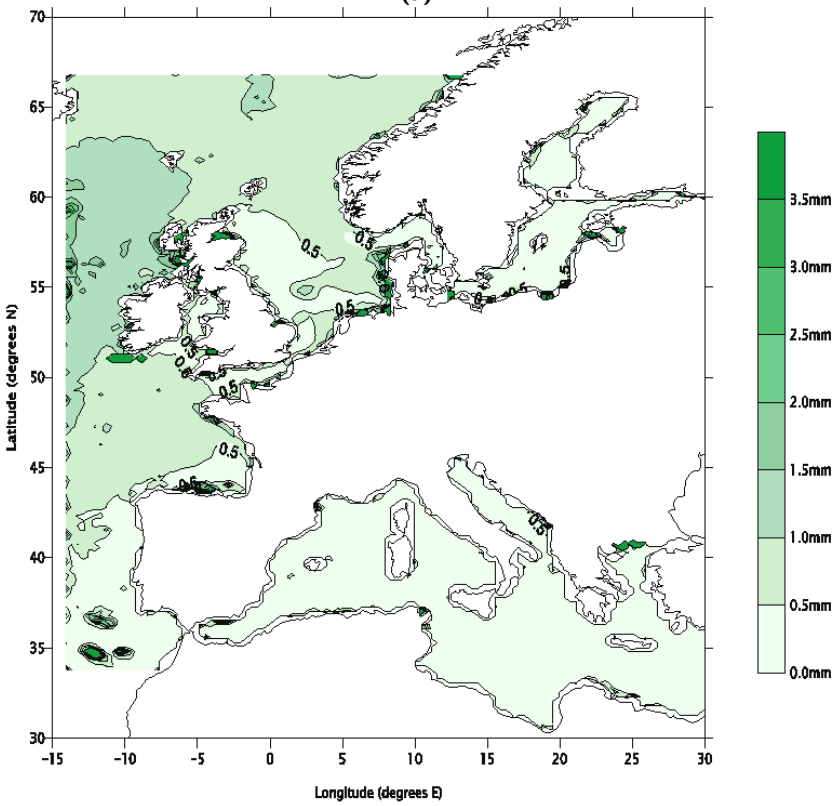

Standard deviation in sea surface (aerodynamic) roughness - 1987 to 1996

(b)

Figure 4.4 Distributions of mean value of sea surface roughness, z_0, and its standard deviation – 1987 to 1996

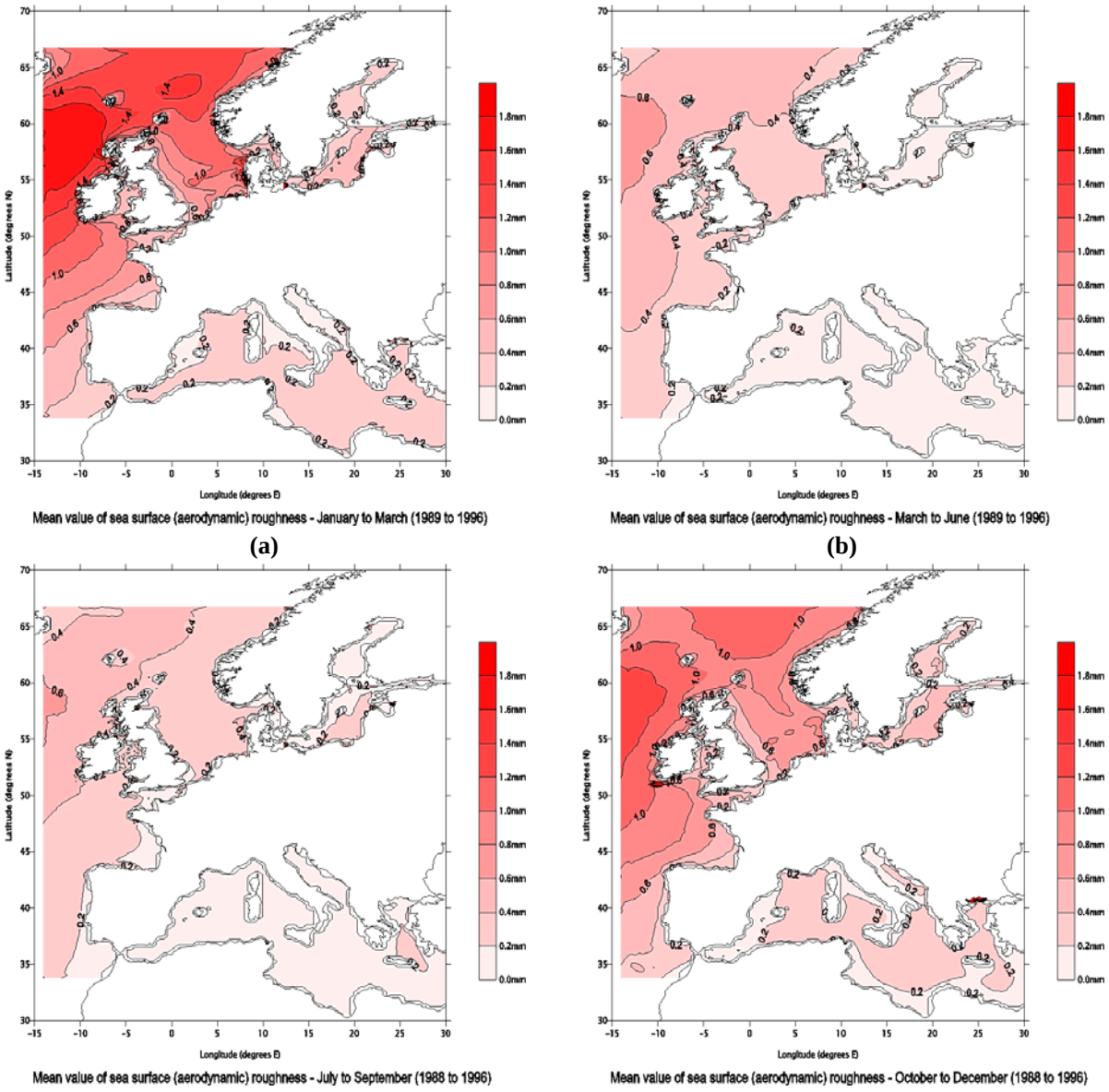

Figure 4.4 **Quarterly distributions of mean value of sea surface roughness, z_0, – 1988 to 1996**

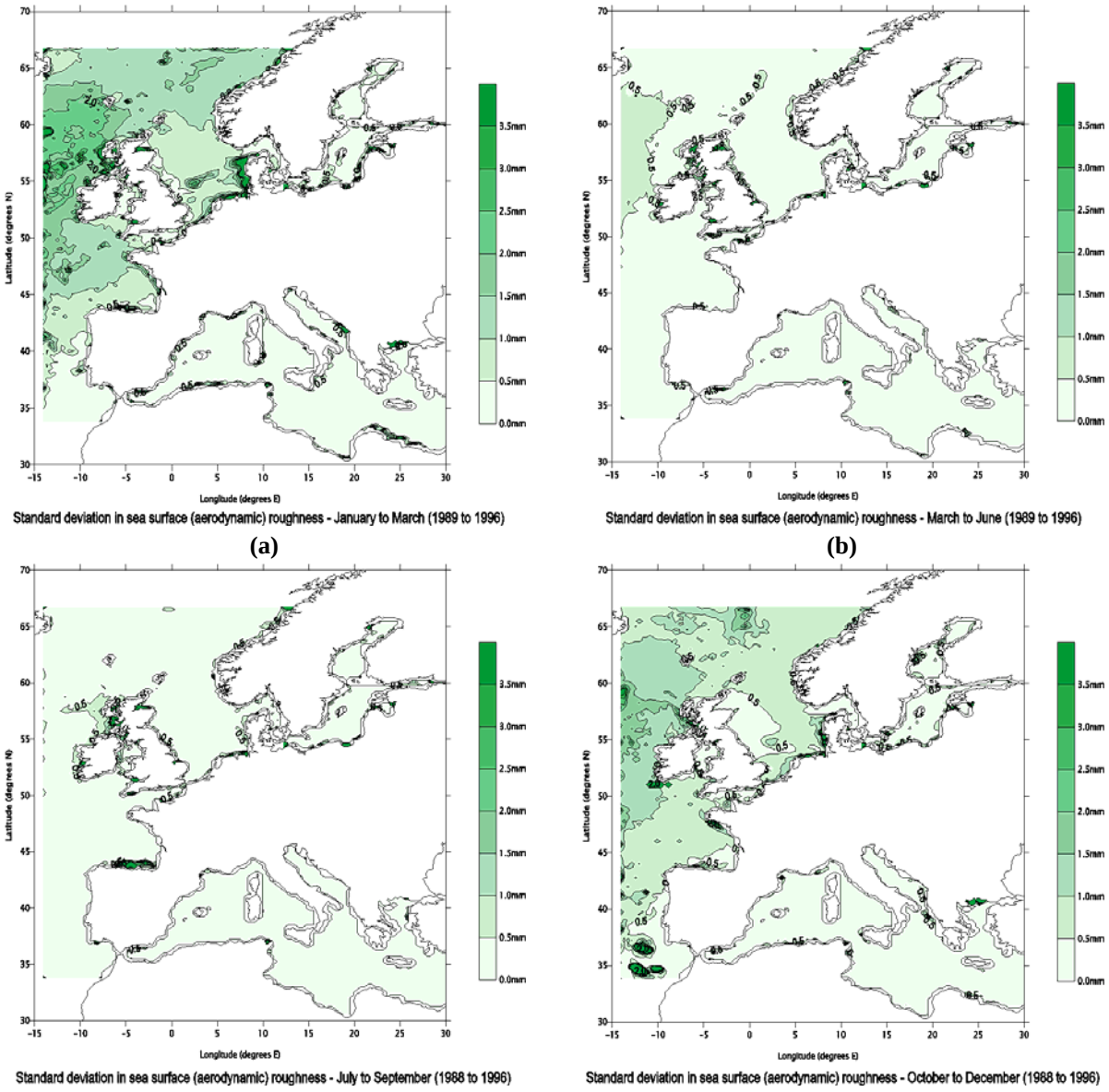

Figure 4.5 **Quarterly distributions of standard deviation of sea surface roughness, z_0, – 1988 to 1996**

4.6 WAsP results

A small selection of the results from the WAsP runs performed are presented here to give an overview of the findings of this section of the project. Full results are presented in the POWERtool (see Chapter 12), although it should be noted that some WAsP output parameters were included since the project team did not consider certain operations within WAsP to be statistically valid for small input data sample sizes involved.

Figure 4.6 presents a map showing the distribution of mean wind speeds for the period 1985-1997 at 50m above mean sea level throughout the POWER project area. The results indicate that the highest wind speeds are found in along the Atlantic margin, the North Sea and Baltic regions with mean annual wind speeds at 50m above sea level in excess of 8.0ms-1 throughout these areas. The highest wind speeds are experienced north and west of Scotland, where mean annual wind speeds greater than 10.5 ms^{-1} are expected. An interesting feature is evident in the North Sea, where a finger of relatively high wind speeds extends into the basin from the north. By contrast, the most of Mediterranean basin is less

windy, with extensive regions experiencing mean annual wind speeds of less than 6ms^{-1}. However, good wind speeds are to be found in parts of the Aegean.

Although there are some slight discrepancies present, overall these results broadly compare with earlier offshore wind resource estimates [Moore, 1982] and [Risø National Laboratory, 1989].

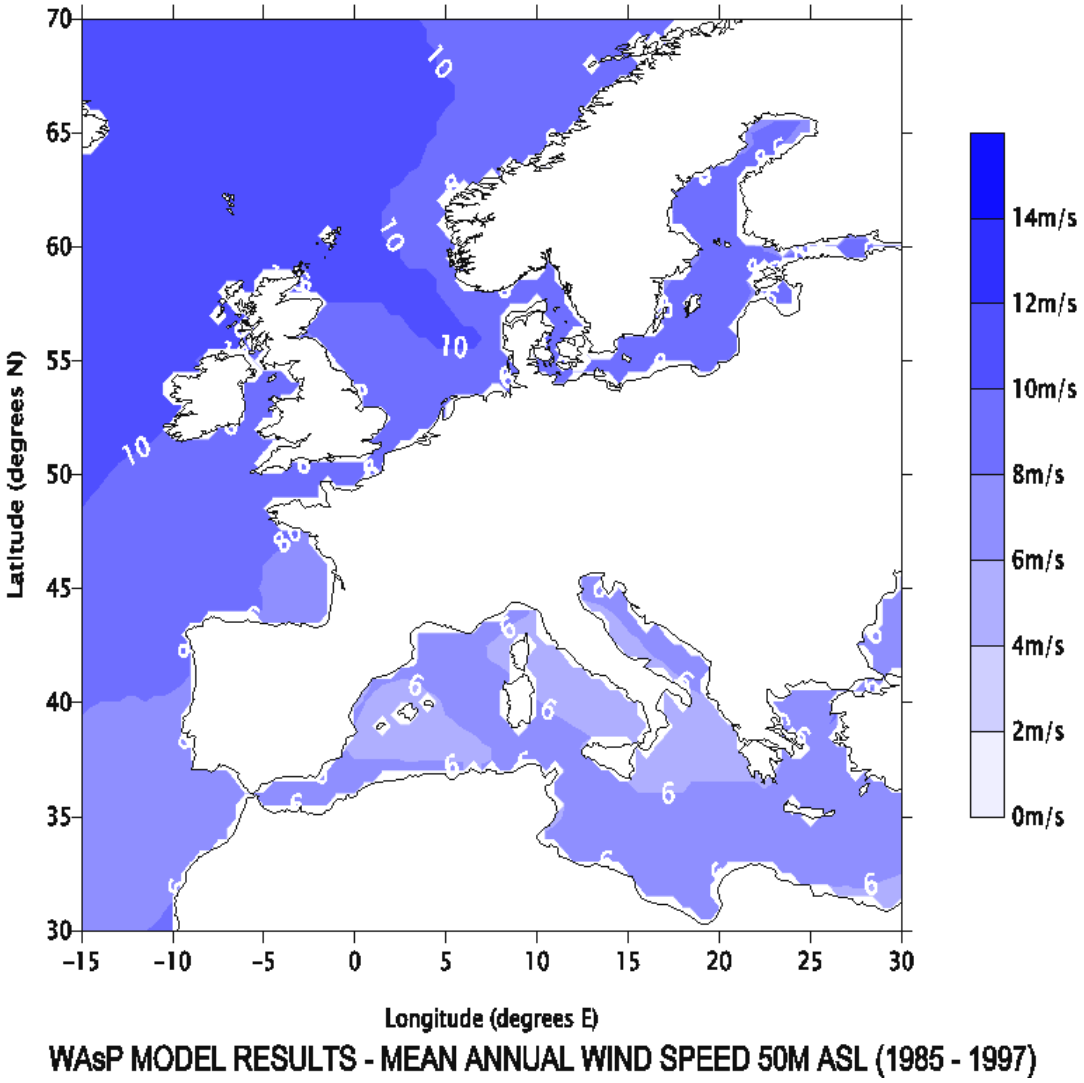

Figure 4.6 Plot showing the distribution of mean annual wind speeds at 50m a.s.l. throughout EU waters

Figures 4.7 to 4.18 illustrate WAsP results showing mean monthly wind speeds at 50m above sea level through the year. The result demonstrate the degree of variability in the offshore wind resource through the year, with significant variations of up to ±25% in mean monthly wind speeds compared to the mean annual values in some areas.

In northern Europe, the windiest month is predicted to be January, with mean wind speeds of over 14ms^{-1} shown west of Scotland and wind speeds in excess of 12ms^{-1} predicted throughout the North Sea basin. The WAsP results indicate that the least windy month in northern Europe is likely to be July with mean monthly wind speeds of no more than 8ms^{-1} predicted in all but a few areas. On this basis, offshore wind farms are likely to generate the largest amounts of power during the windy winter months, but their power output will probably drop in the relatively calm summer months. Happily, this pattern mirrors closely the demand for power by end users in northern Europe.

By contrast, the mean monthly wind distribution patterns in southern Europe are more complex. The WAsP results show parts of the eastern Mediterranean and the Aegean indicate experience relatively high wind speeds in excess of 8ms^{-1} in mid-summer.

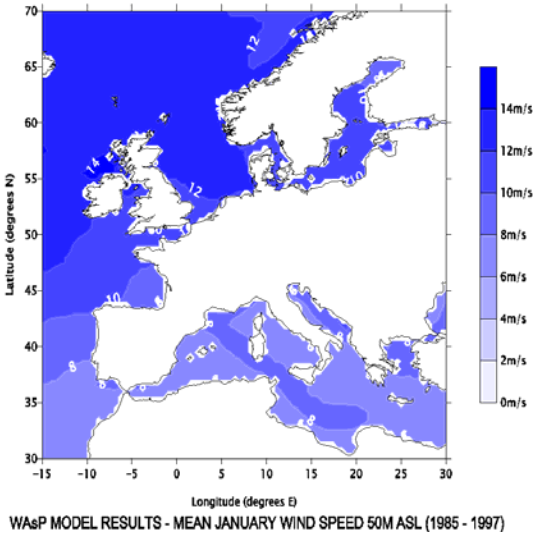

Figure 4.7 Mean January wind speeds at 50m a.s.l.

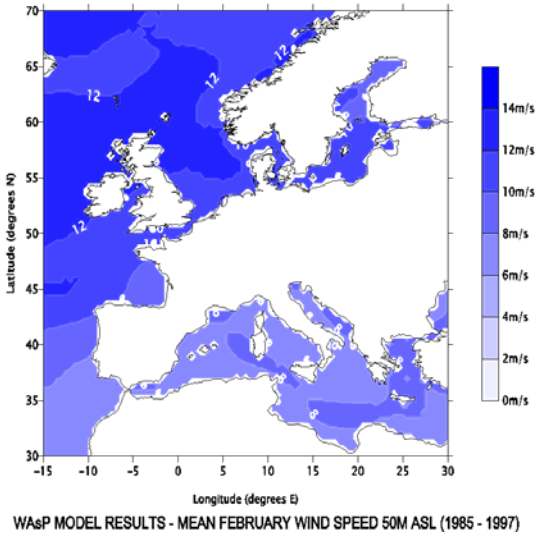

Figure 4.8 Mean February wind speeds at 50m

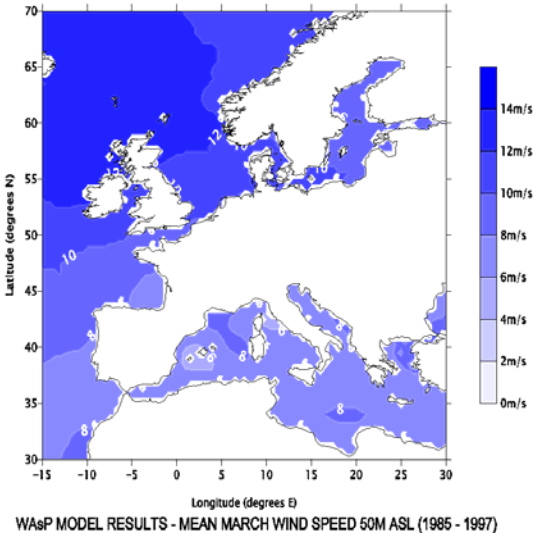

Figure 4.9 Mean March wind speeds at 50m a.s.l.

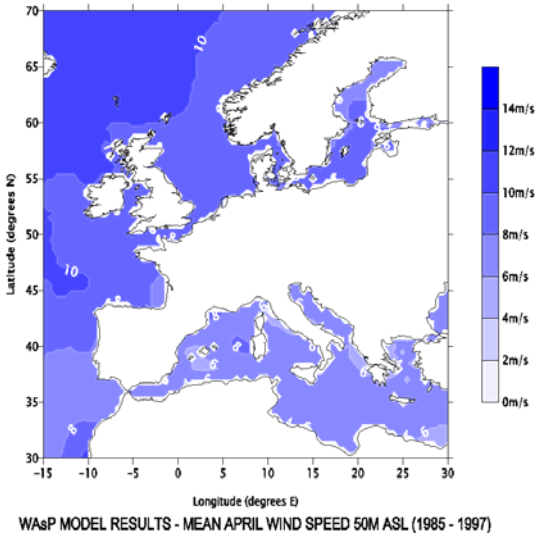

Figure 4.10 Mean April wind speeds at 50m a.s.l.

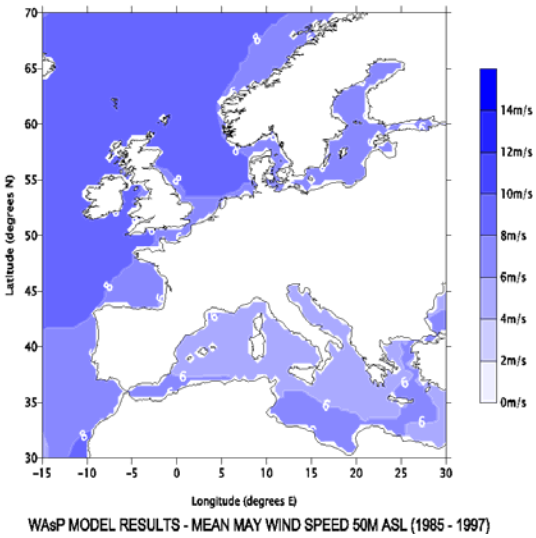

Figure 4.11 Mean May wind speeds at 50m a.s.l.

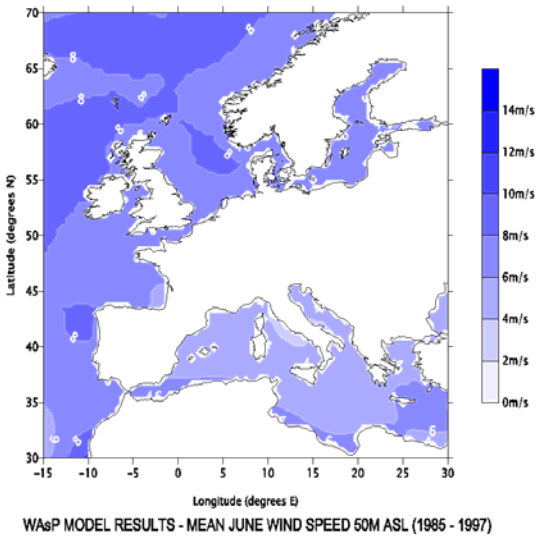

Figure 4.12 Mean June wind speeds at 50m a.s.l.

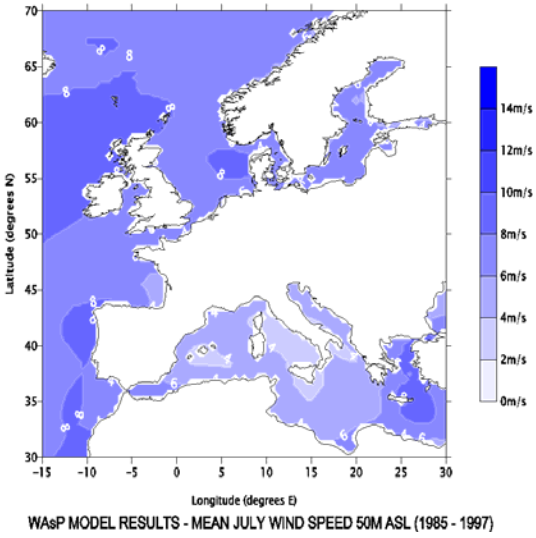

Figure 4.13 Mean July wind speeds at 50m a.s.l.

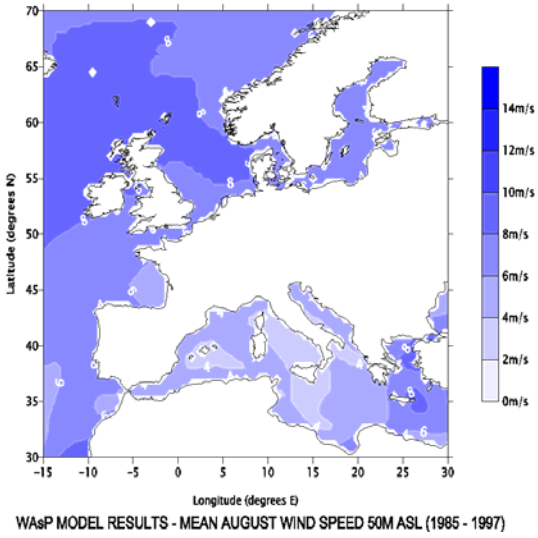

Figure 4.14 Mean August wind speeds at 50m a.s.l.

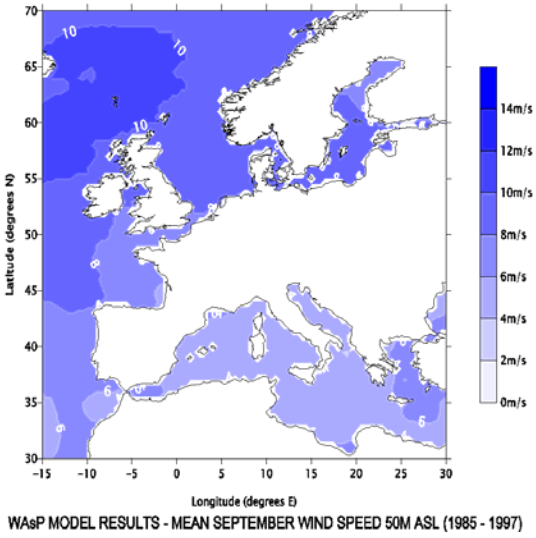

Figure 4.15 Mean September wind speeds at 50m a.s.l.

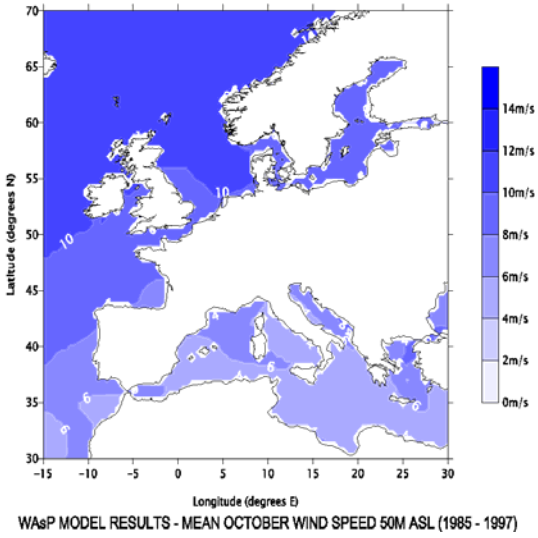

Figure 4.16 Mean October wind speeds at 50m a.s.l

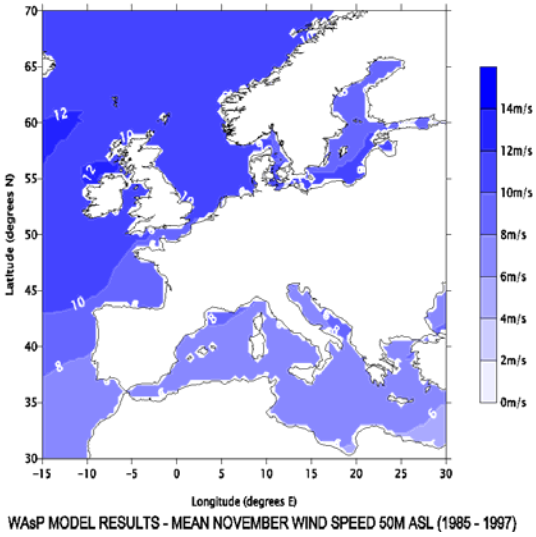

Figure 4.17 Mean November wind speeds at 50m a.s.l.

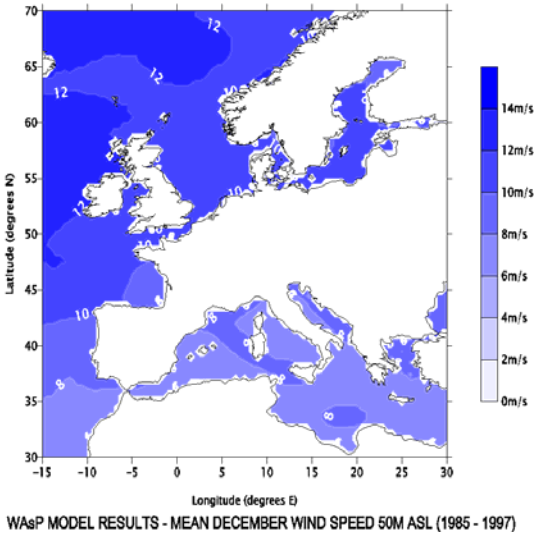

Figure 4.18 Mean December wind speeds at 50m a.s.l.

4.7 References for Chapter 4

Barthelmie, R.J. 2002: Evaluating the impact of wind induced roughness change and tidal range on extrapolation of offshore vertical wind speed profiles. *Wind Energy* (in press).

Frank H P, Larsen S E and Højstrup J (2000), *Simulated Wind Power Offshore Using Different Parameterizations for the Sea Surface Roughness*, Wind Energy; 3, 67-79.

Lange B and Høstrup J (2000), *The influence of waves on the offshore wind resource*, Proceedings of the European Seminar on Offshore Wind Energy in Mediterranean and other European Seas (OWEMES 2000), Siracusa, April 2000

Moore D (1982), '10 to 100m winds calculated from 900mb wind data', Proceedings of the 4th British Wind Energy Association Conference, Cranfield, BHRA.

Mortensen, N.G., L. Landberg, I. Troen, and E.L. Petersen, Wind Analysis and Application Program (WASP), Risø National Laboratory, Roskilde, Denmark, 1993.

Risø National Laboratory (1989) Isovent map on URL http://130.226.52.108/oceanmap.htm, accessed 17/01/00.

Taylor P K (ed.) (2000), Final report of the Joint WCRP/SCOR Working Group on Air-Sea Fluxes (SCOR Working Group 110), *Intercomparison and validation of ocean-atmosphere energy flux fields*, document available online at http://www.soc.soton.ac.uk/JRD/MET/WGASF/index.html

Taylor P K and Yelland M J (2000), *The Dependence of Sea Surface Roughness on the Height and Steepness of the Waves*, accepted in final form by Journal of Physical Oceanography in May 2000

Troen I and Petersen E L (1989), European Wind Atlas, published for the Commission of the European Communities Directorate-General for Science, Research and Development by Risø National Laboratory

CHAPTER 5 : The Coastal Discontinuity Model

Chapter authors: Dr R J Barthelmie (Risø National Laboratory) & Drs. J.P. Coelingh and Dr. L. Folkerts (Ecofys)

5.1 Coastal Discontinuity - theoretical background

The initial focus of this part of the project was to develop and evaluate a coastal model which uses standard meteorological measurements (wind speed, temperature profiles, sea temperature) to estimate stability parameters for use in predicting wind speed profiles. The importance of stability that is addressed within the Coastal Discontinuity Model (CDM) is that:

1) In non-neutral conditions wind speed profiles are distorted from logarithmic. WAsP assumes a slightly stable profile on average which is reasonable for land areas but has not been fully evaluated for all offshore areas. Most of the sites for which full analysis has been conducted in the Baltic and Denmark have been shown to be more frequently stable than unstable (Barthelmie *et al.*, 1999). However off the coast of the Netherlands sites were found to be slightly unstable on average (Coelingh *et al.*, 1998), (Coelingh *et al.*, 1996). Stability has been shown to significant impact the wind speed distribution as flow moves offshore (Pryor and Barthelmie, 1998).

   To calculate the Monin-Obukhov length, heat and momentum fluxes should be measured using a sonic anemometer. Since these data are not available for most offshore sites, fluxes offshore are estimated here using temperature profiles calculated from the difference between air and sea temperature. The routines used were developed at the Royal Netherlands Meteorological Institute (Beljaars *et al.*, 1989). This methodology has the potential to create a large temperature difference since different instruments and techniques were used to determine air and sea temperatures. A comparison of fluxes estimated using the (Beljaars *et al.*, 1989)'s routines and calculated from measured fluxes is given in Section 5.4. The routines have been shown to give good agreement with measured fluxes based on a measured temperature difference. However, the measured temperature difference is a precise measurement while the temperature difference calculated from measured air and sea temperatures is not, unless the two temperature sensors are calibrated together. Errors in temperature measurements are of the same order as the temperature difference. If the temperature datasets are derived from different sources then the errors arising from calculating the temperature difference can be substantial.

2) Internal Boundary Layer (IBL) growth varies under different stability conditions. In stable conditions offshore the IBL grows slowly and can remain below 100 m for considerable distances inhibiting momentum exchange and impacting the wind speed profile (Garratt and Ryan, 1989), (Smedman *et al.*, 1997), (Van Wijk *et al.*, 1990a). Conversely in unstable conditions the IBL grows quickly rapidly attaining equilibrium. To calculate the IBL height the formula presented by (Bergstrom *et al.*, 1988) is used which shows good agreement (Barthelmie and Palutikof, 1996) with that developed by (Van Wijk *et al.*, 1990a). The three layer model used by Risø is based on the same principles as those used in (Van Wijk *et al.*, 1990b), (Van Wijk *et al.*, 1990a), (Bergstrom *et al.*, 1988) focused on prediction on wind speed profiles moving offshore. The three-layer concept involves a lower layer that is in equilibrium with the sea surface, an upper layer which is in equilibrium with the overlying air and an adjustment or blending layer where the two air masses meet.

Stability corrections can be calculated based on Monin-Obukhov similarity theory (see e.g. (Van Wijk *et al.*, 1990b) where the Monin-Obukhov length, L, is given by:

$$L = -\frac{u_*^3}{k(g/\theta)\overline{w'\theta'}} \tag{5.1}$$

where θ is the potential temperature,
k is the von Karman constant,
g is acceleration due to gravity,
u_* is the friction velocity, and
w is the vertical velocity.

Incorporating a stability correction into the logarithmic wind speed profile, the wind speed, U at height, z is calculated by:

$$U = \frac{u_*}{k}\left(\ln\left(\frac{z}{z_o}\right) - \Psi\left(\frac{z}{L}\right) \right) \quad (5.2)$$

where z is the height,
z_0 is the roughness length, and
Ψ is the stability correction to the wind speed and is given by:

$$\Psi = -5\left(\frac{z}{L}\right) \text{ for stable conditions (L>0)} \quad (5.3)$$

and

$$\Psi = 2\ln\left(\frac{1+x}{2}\right) + \ln\left(\frac{1+x^2}{2}\right) - 2\tan^{-1}x + \frac{\Pi}{2} \text{ for unstable conditions (L<0)} \quad (5.4)$$

where:

$$x = \left(1 - 16\left(\frac{z}{L}\right)\right)^{\frac{1}{4}} \quad (5.5)$$

Thus, the magnitude of stability correction to a near-neutral wind speed profile ($\Psi(z/L)$) depends on whether conditions are stable or unstable (the absolute value of the stability correction is larger if conditions are stable) and by how much conditions deviate from near-neutral (as defined by the Monin-Obukhov length). As conditions approach neutral, the Monin-Obukhov length increases, conversely as conditions become more unstable or more stable the Monin-Obukhov length tends towards zero. Note that corrections are subtracted from the near-neutral wind speed, hence the net impact is that corrections are negative in unstable conditions and positive in stable conditions. The wind speed also depends on the ratio u_*/k and u_* is typically lower when conditions are non-neutral.

5.2 CDM Modelling and results

5.2.1 Outline of the CDM approach: geostrophic version

The intention of this part of the project was to modify WAsP derived wind speed profiles to take account of stability effects calculated from air and sea temperature databases. Since WAsP derived wind speeds were not initially available, the first version of the Coastal Discontinuity Model was developed and applied using geostrophic wind speeds as input (Figure 5-1). This is referred to in the following as the GEO-CDM. The following steps were required:

1. Grid points for geostrophic wind speeds were initially latitude and longitude but since fetch (distance to the coast) is required for calculating the height of the internal boundary layer (IBL), the co-ordinates were transformed to Universal Transverse Mercator (UTM). Since the area of offshore wind speeds required crosses several UTM zones, the area has been divided into seven distinct regions as shown in Figure 5-2 to reduce errors associated with the projection. Although no difficulties are anticipated with the reintegration of these areas, small overlaps have been introduced for checking purposes.
2. Coastline data for each area were transformed to UTM co-ordinates.
3. A program was written to calculate the minimum fetch distance for each geostrophic data point offshore. Each pair of geostrophic co-ordinates is given a minimum fetch distance in one of 12 directional bins.
4. To input geostrophic wind data, a linking file was developed to provide latitude, longitude, UTM co-ordinates and filenames for all the geostrophic wind data.
5. The CDM reads in the geostrophic wind speed and data for each grid point. The program searches the fetch file to ensure the co-ordinates are present and determines the minimum fetch distance for each direction.
6. For each geostrophic wind speed value the program determines whether the wind direction is from land, sea or has a mixed fetch over which an internal boundary layer will develop. If the fetch is uniform (either land or sea) friction velocity is used to generate a neutral wind speed profile and the ageostrophic angle is calculated which is used to correct the near surface wind directions. The friction velocity is calculated for a range of geostrophic wind speeds between 3 and 40 m/s. Offshore variable roughness is calculated based on the Charnock equation (Charnock, 1955). This means that the friction velocity offshore is under-estimated in low wind speeds (below about 4 m/s). The constant used in the Charnock equation is 0.018 which is suitable for coastal areas.
7. If an IBL is present Bergström's formula (Bergström *et al.*, 1988) is used to determine the neutral IBL height at the geostrophic grid location. This formulation for the IBL height has been compared with that of (Van Wijk *et al.*, 1990) and is found to produce similar predictions for the IBL height (Barthelmie and Palutikof, 1996). Beneath this height the equilibrium neutral sea profile is used, above this height the equilibrium land wind speed profile is used. Here we use a three layer IBL formulation (Figure 5-3) where the height of the adjustment layer is 20% of the IBL. The effect of varying the depth of this layer is shown in Figure 5-4. Finally

for each offshore grid point a wind speed profile is calculated which depends only on the geostrophic wind speed distribution and the distance of the point to the coastline in each direction.

8. The CDM can be used to either give near-neutral predictions if no air/sea temperatures or temperature profiles are available or the Monin-Obukhov length (stability parameter) is determined according to the sea surface temperature, an air temperature and the wind speed and direction. The CDM has been applied in each area and gives results which should be directly comparable with those of the WAsP model (Mortensen *et al.*, 1993). WAsP and the CDM are based on similar principles. Major differences between WAsP and the version of the CDM which has been applied offshore are:
    - WAsP makes adjustments to the wind speed profile offshore based on the assumption that the wind speed profile in the surface layer (up to approximately first 100m) is slightly stable.
    - CDM has variable roughness offshore which is dependent on the wind speed.
    - WAsP calculates a mean stability correction to the wind speed profile depending whether the location is on- or offshore. The CDM uses the time series data to calculate the stability parameter and correct the wind speed profile for each observation which is then averaged. These two approaches do not give identical results since a mean stability correction is smaller than the average correction as calculated from individual wind speed profiles.

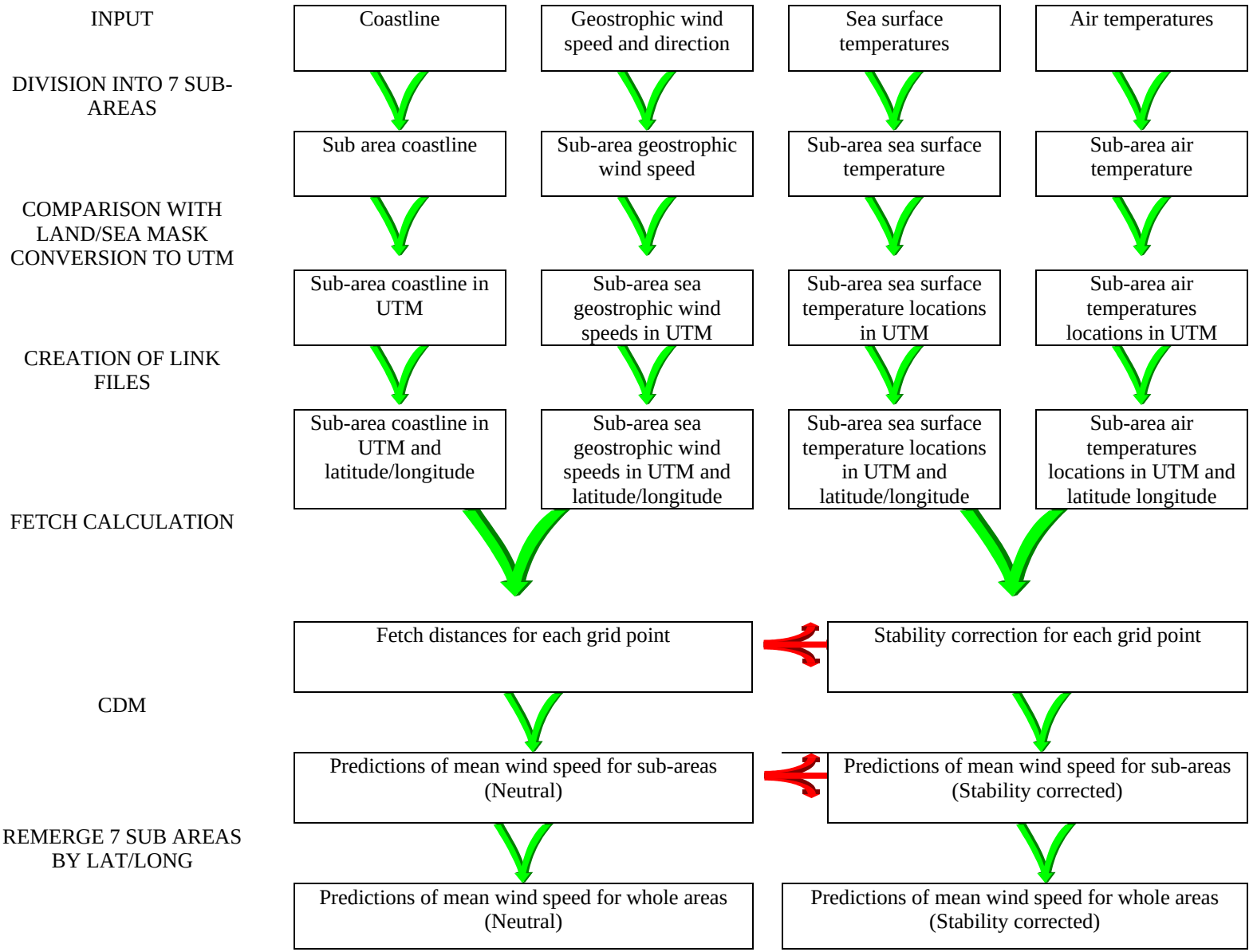

Figure 5-1. Sketch of CDM - geostrophic methodology

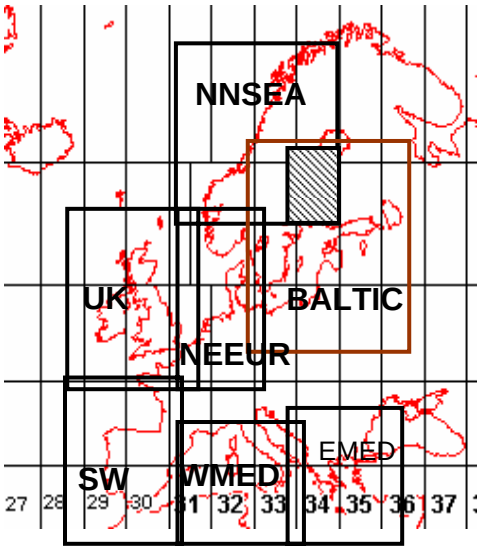

1. BALTIC: Baltic
2. NNSEA: Northern North Sea
3. UK: UK
4. NEEUR: Northeast Europe (as zone 32)
5. SWEUR: Southwest Europe
6. WMED: Western Mediterranean
7. EMED: Eastern Mediterranean

Figure 5-2. Subdivision into seven areas for application of the CDM

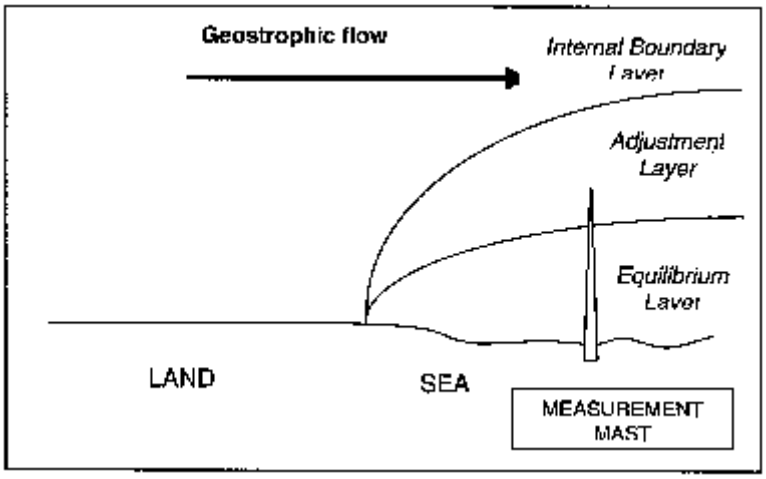

Figure 5-3. Concept of the three-layer IBL

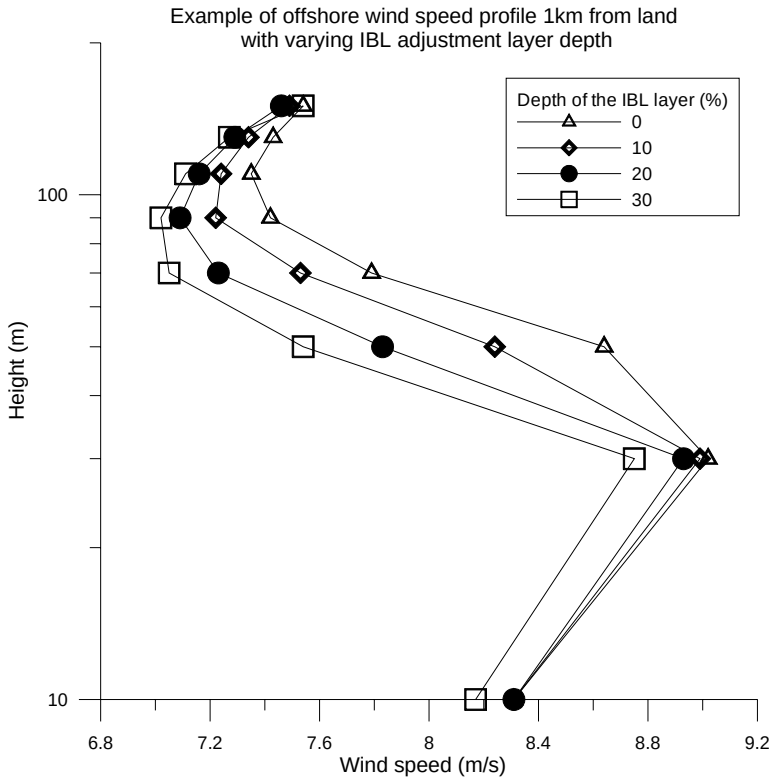

Figure 5-4. Effect of the depth of the adjustment zone (shown as a percentage of the IBL depth) on interpolation on predicted wind speed profiles

5.2.2 Application and assessment of the GEO-CDM

Figure 5-5a shows 1997 geostrophic wind speeds for the European region. These follow the general pattern expected since for this area on average. Highest geostrophic wind speeds occur in the northwest decreasing towards the southeast (Troen and Petersen, 1989). In 1997 highest geostrophic wind speeds exceeding 12 m/s occurred in the northwest and lowest geostrophic wind speeds occurred in the Mediterranean.

Simulations with the GEO-CDM (neutral formulation) appear to give reliable and consistent results for near-surface wind speed profiles (Figure 5-5b) since near-surface wind speeds follow the general pattern given by geostrophic wind speeds. Wind speeds in areas which are strongly affected by thermal flows such as the Baltic show lower wind speeds than anticipated.

Figure 5-6 shows geostrophic and predicted near-surface wind speeds (heights from 10m to 150 m) from the neutral GEO-CDM formulation. One feature that appears consistently in the model results is high near-surface wind speed along the coast of the former Yugoslavia. This results from high geostrophic wind speeds in this area and strong coupling to near-surface winds. As has been noted previously this coupling between geostrophic and near-surface wind speeds is not realistic in Mediterranean areas.

Figure 5-7 shows predicted near-surface wind speeds (heights from 10m to 150 m) with stability correction. In the Baltic the dominance of stable conditions leads to positive corrections to near-surface winds speeds (Barthelmie, 1999b). In addition in these offshore regions are subject to low-level jets at heights below 200 m which are expected to significantly impact the wind resource (Smedman *et al.*, 1996). In the Mediterranean local wind speeds are expected to be impacted by local and regional thermal flows which can only be captured by mesoscale models.

The effect of stability on wind speed profiles is shown in Figures 5-8 and 5-9. The magnitude of the correction to the profile is large when the Monin-Obukhov is small and rapidly decreases as conditions tend toward neutral (i.e. the Monin-Obukhov length exceeds $\pm$1000 m). The mean Monin-Obukhov length for most of European offshore areas (Figure 5-9) is close to neutral. This is expected since stable and unstable conditions tend to balance out over the course of the year. The CDM uses time series data to calculate the stability correction to each wind speed profile and does not use the stability parameter to calculate a mean correction to the profile. Note that some areas are unstable on average (northeast North Sea and parts of the Mediterranean) while some (central Baltic) are stable.
In the following sections two additional parameterisation of the CDM were considered, the first is the role of variable roughness offshore and the second is the width of the coastal zone.

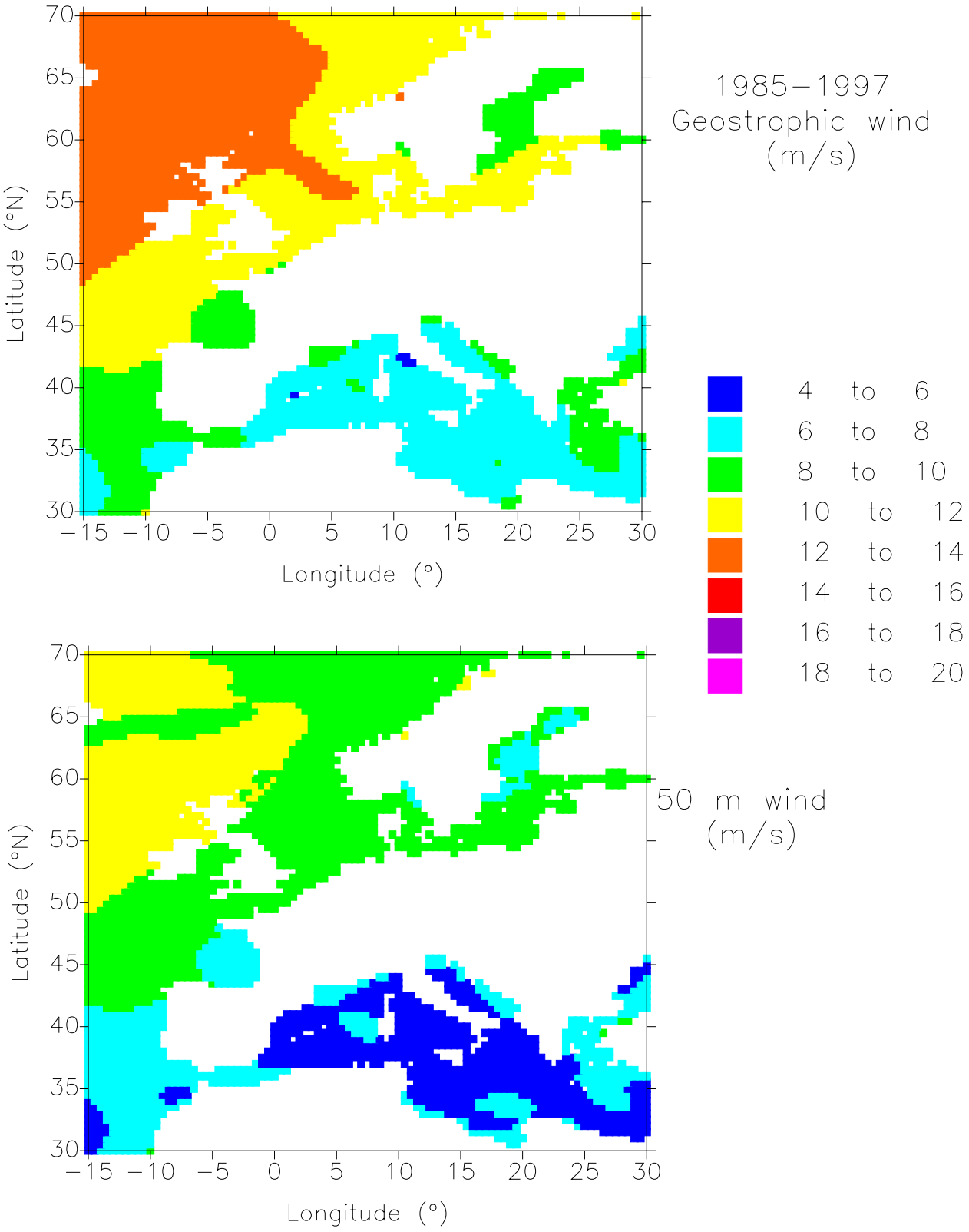

Figure 5-5. a) Mean geostrophic wind speed (1985-1997) and b) GEO-CDM predictions of 50 m wind speeds (neutral formulation).

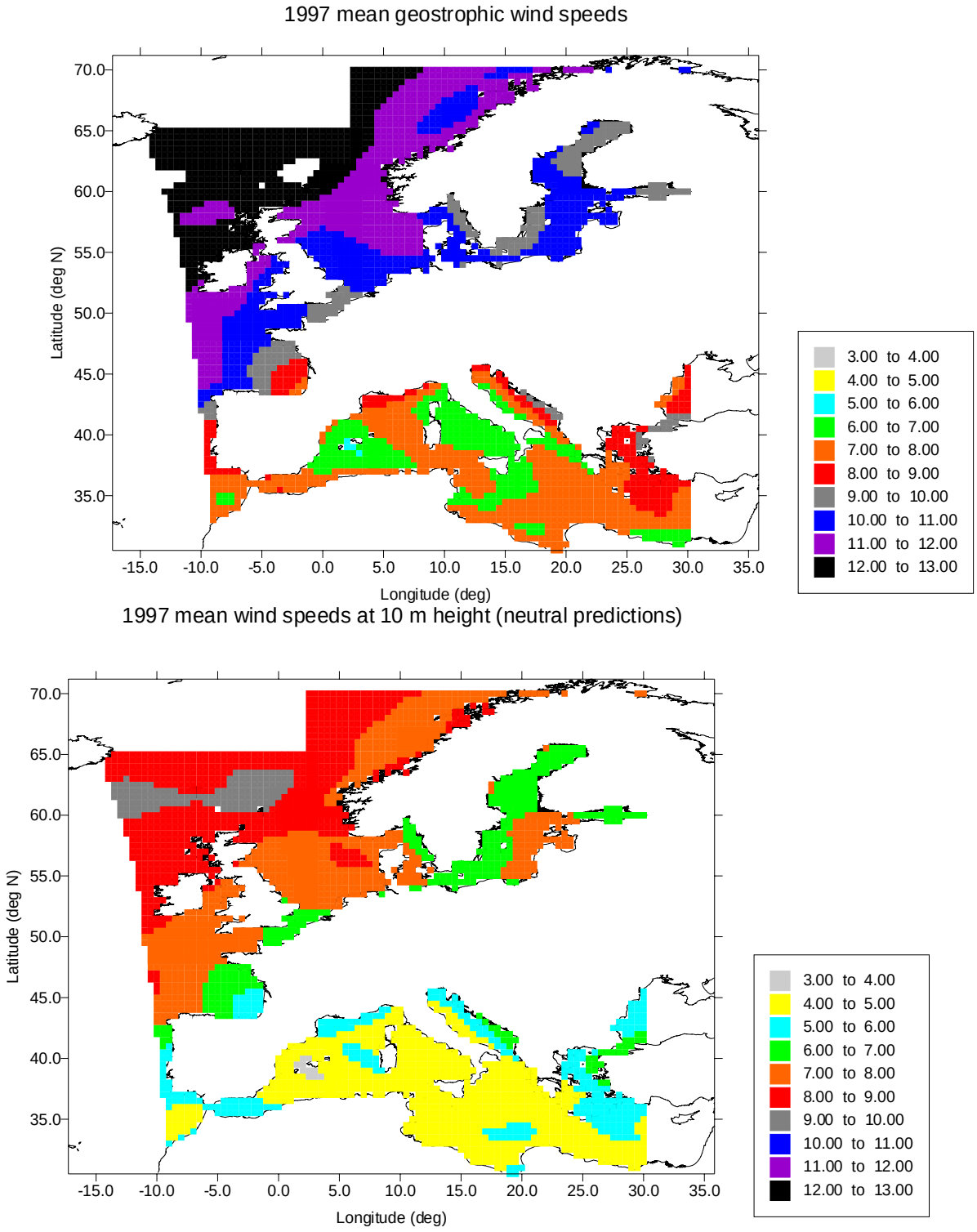

Figure 5-6. Geostrophic wind speeds in 1997 and neutral predictions of wind speed from 10m to 150m above the surface.

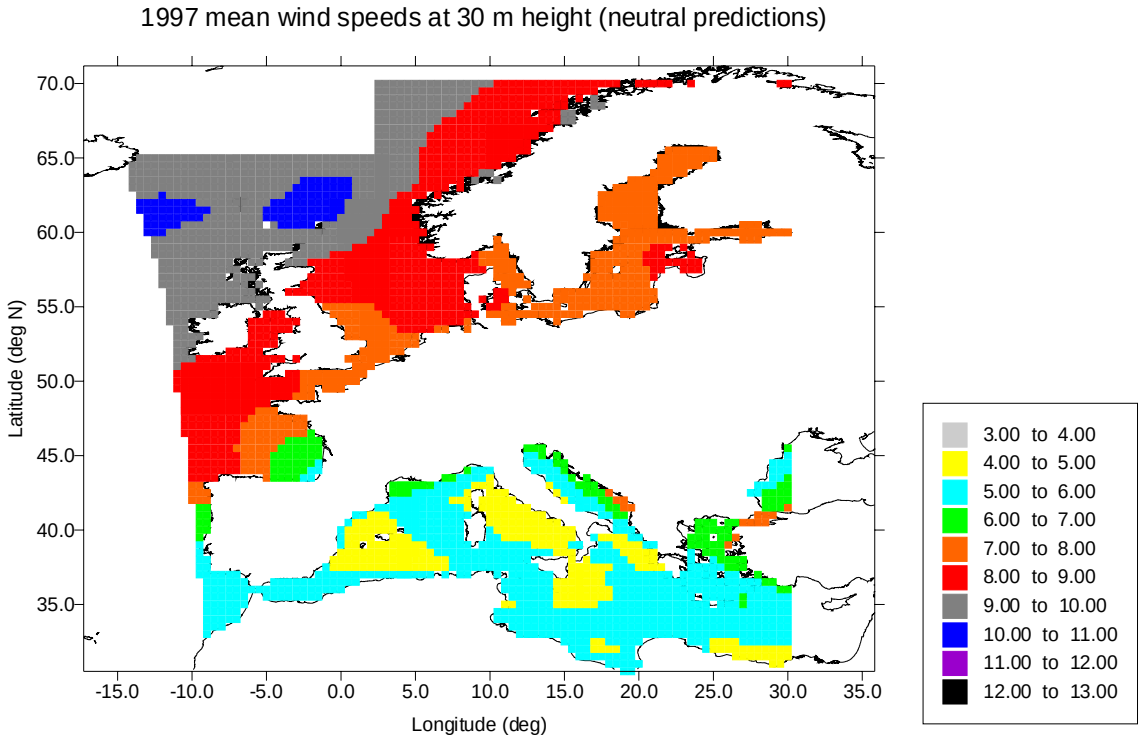

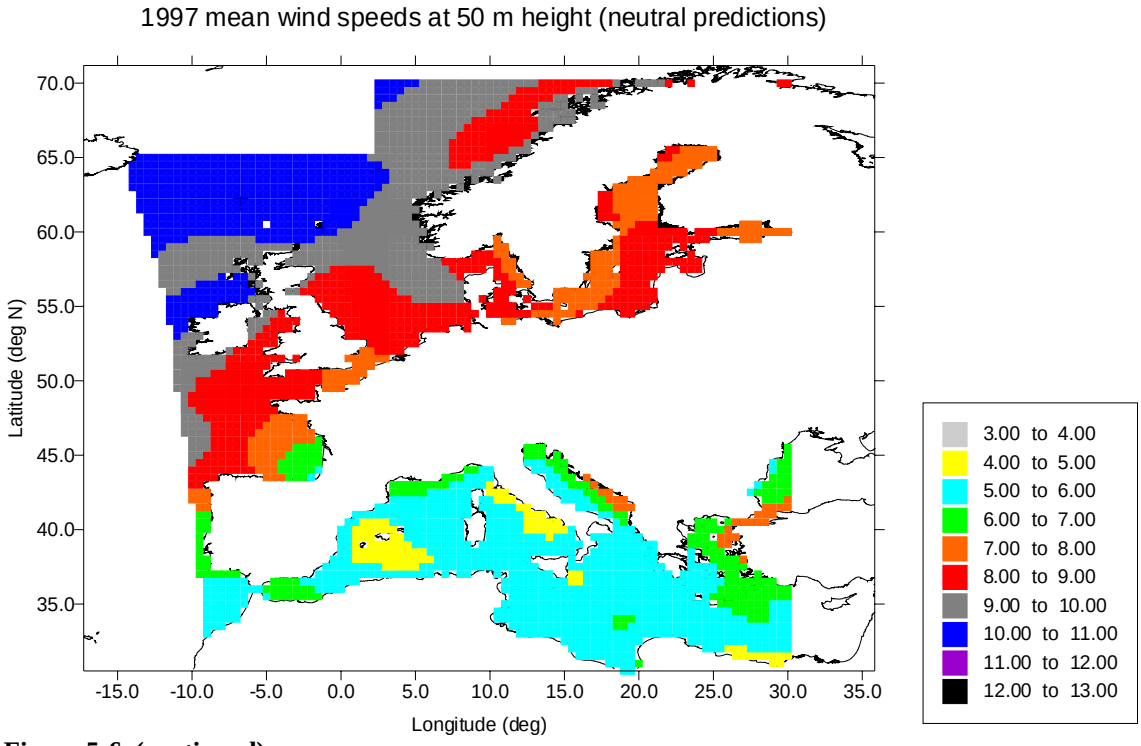

Figure 5-6. (continued).

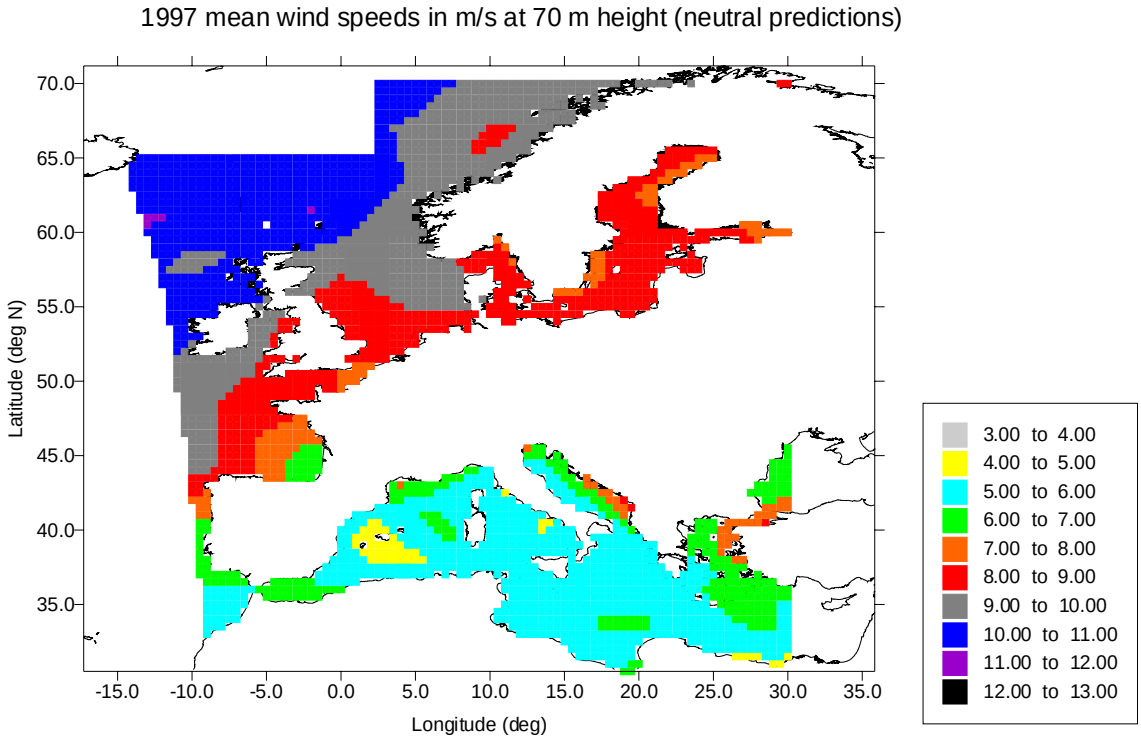

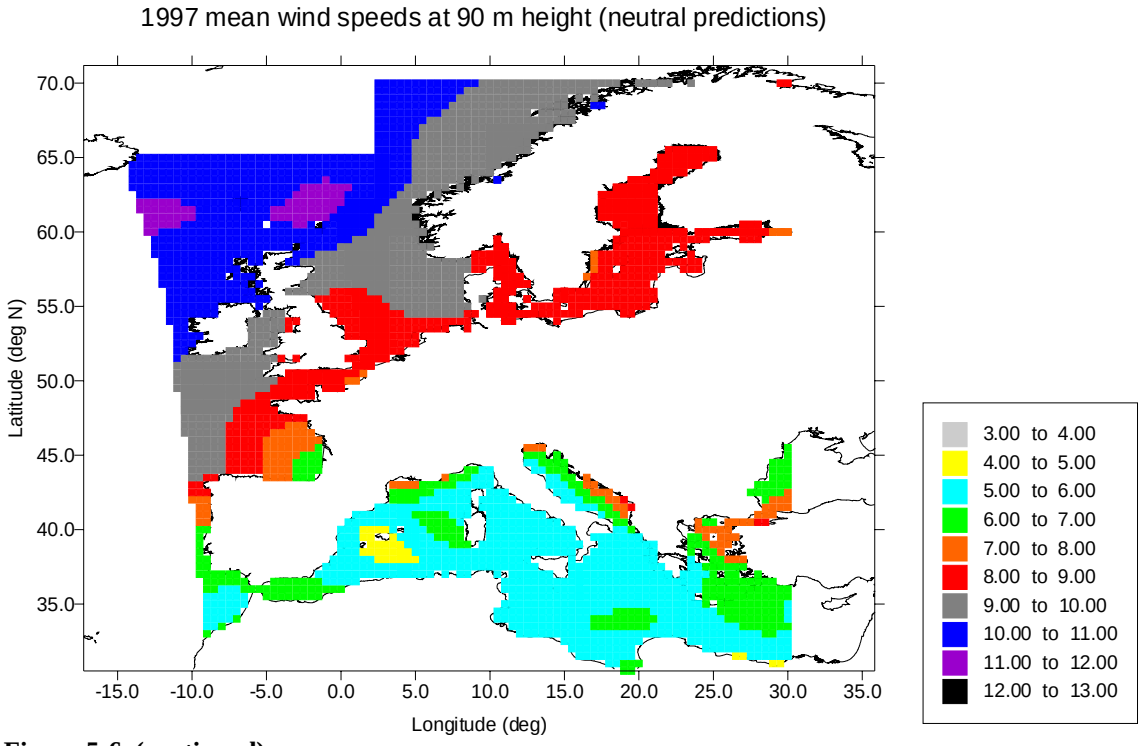

Figure 5-6. (continued).

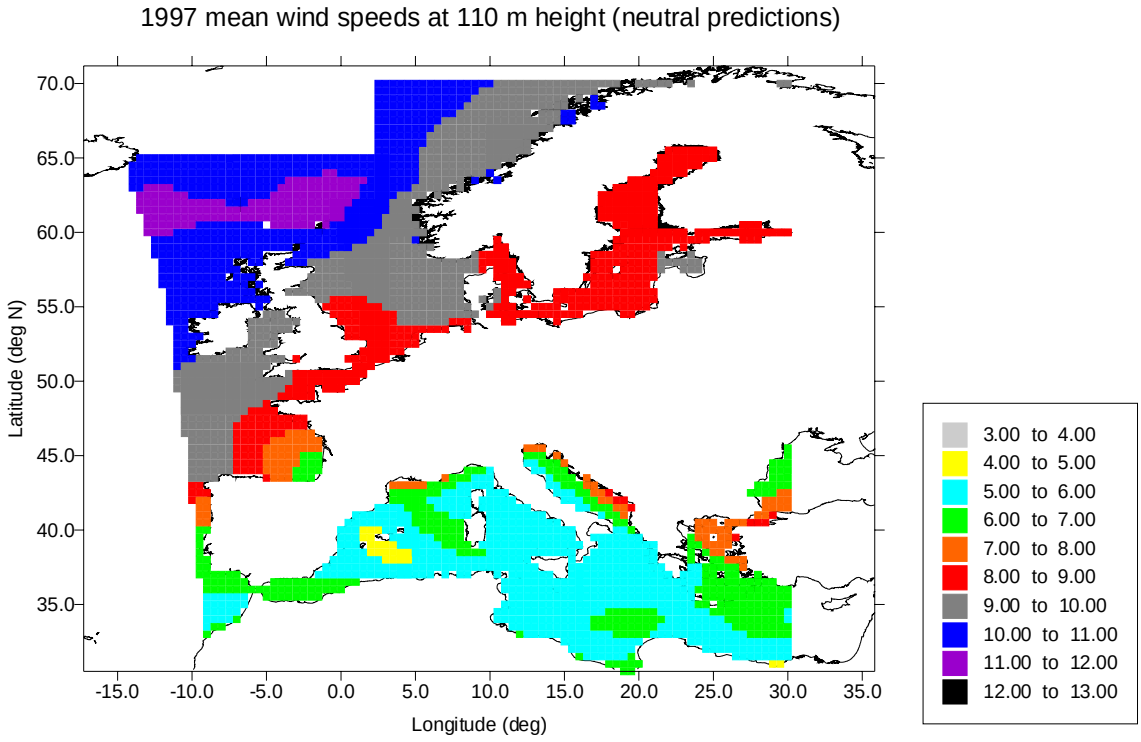

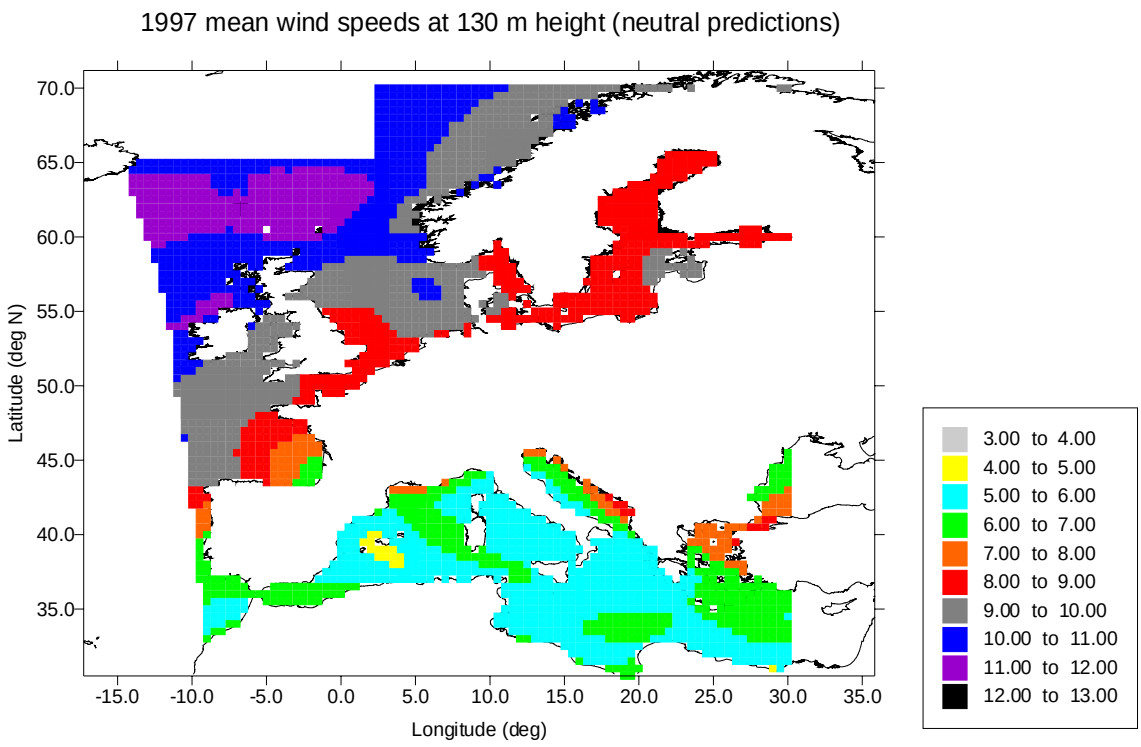

Figure 5-6. (continued).

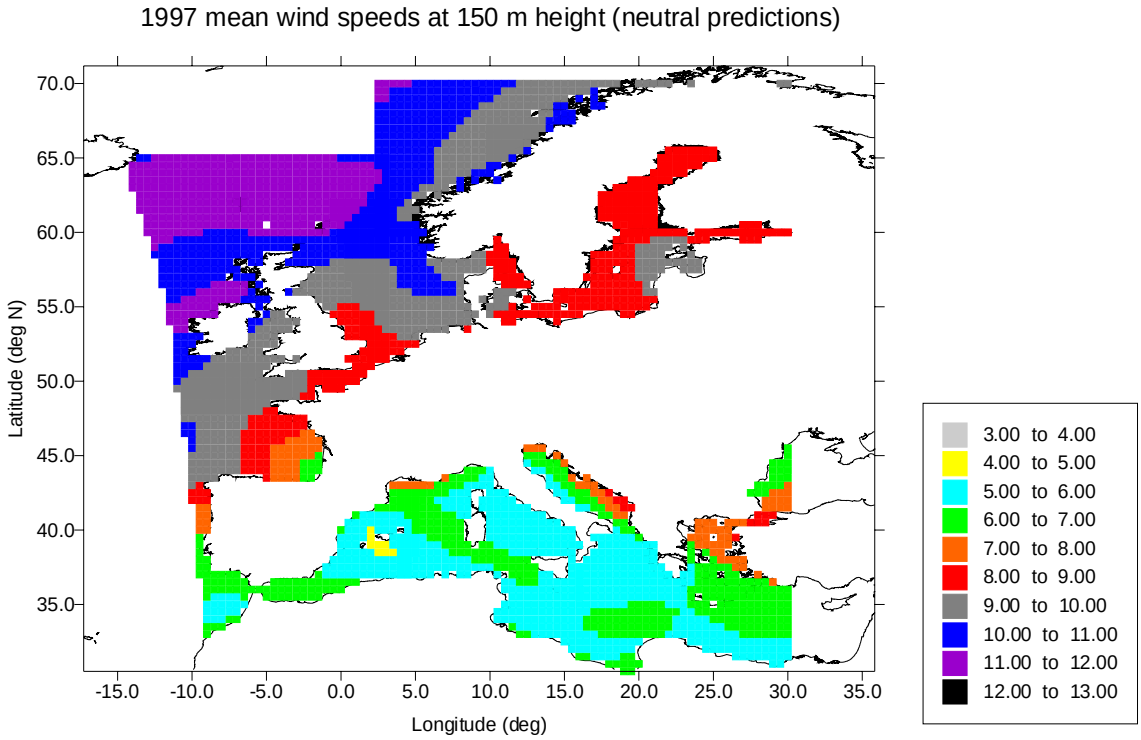

Figure 5-6. (continued).

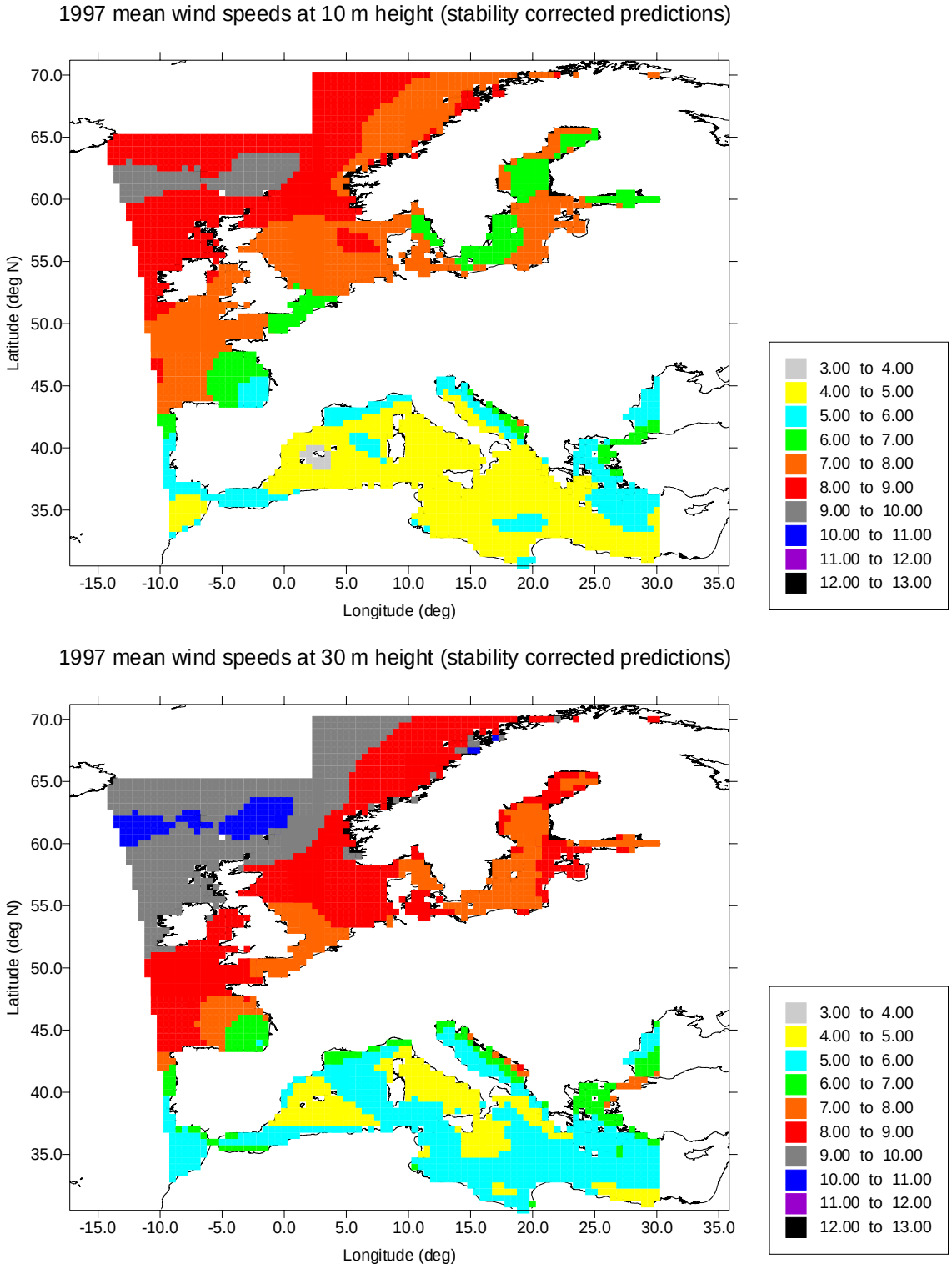

Figure 5-7. Stability corrected near-surface wind speeds from the GEO-CDM (m/s).

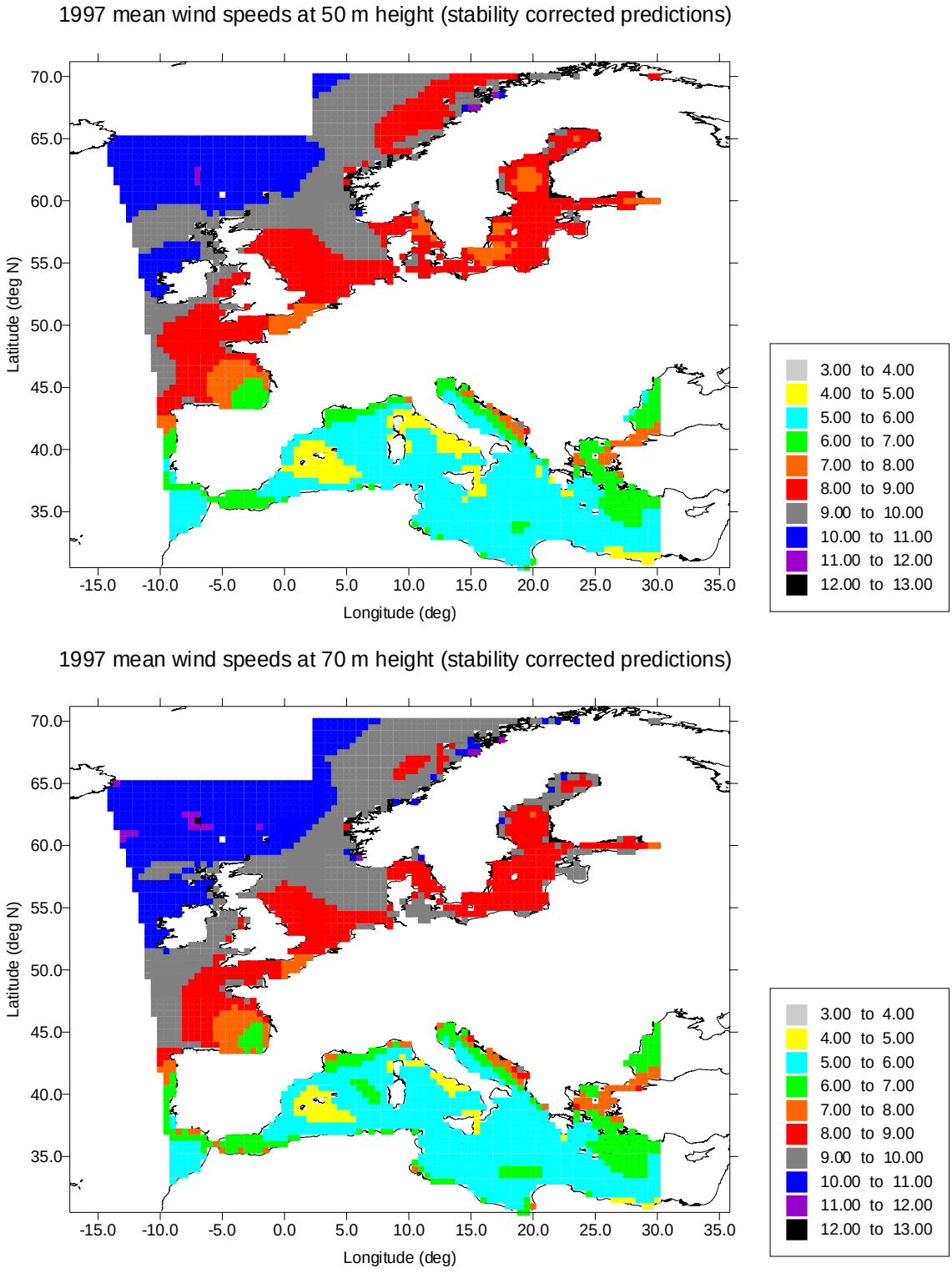

Figure 5-7. (continued).

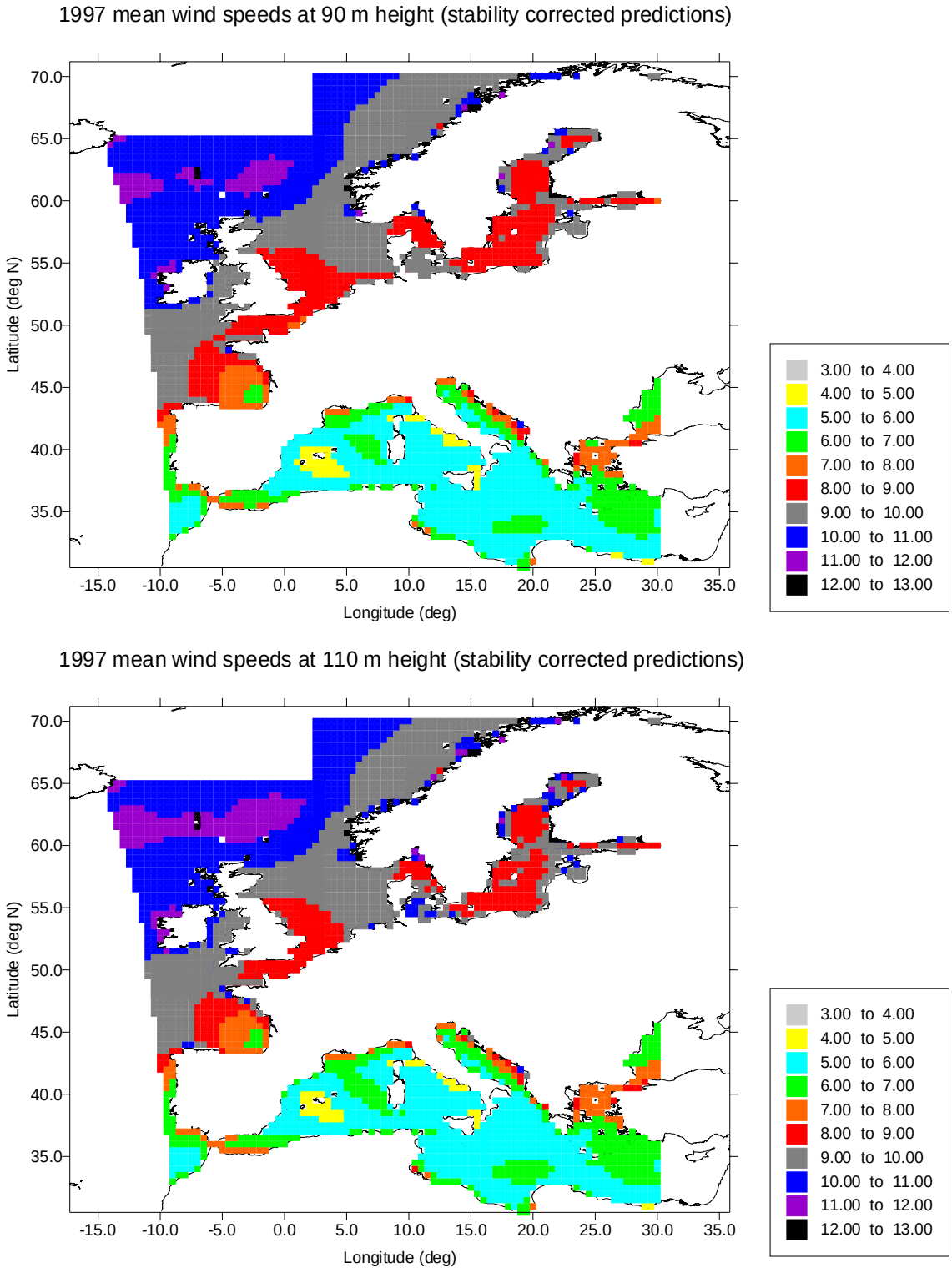

Figure 5-7. (continued).

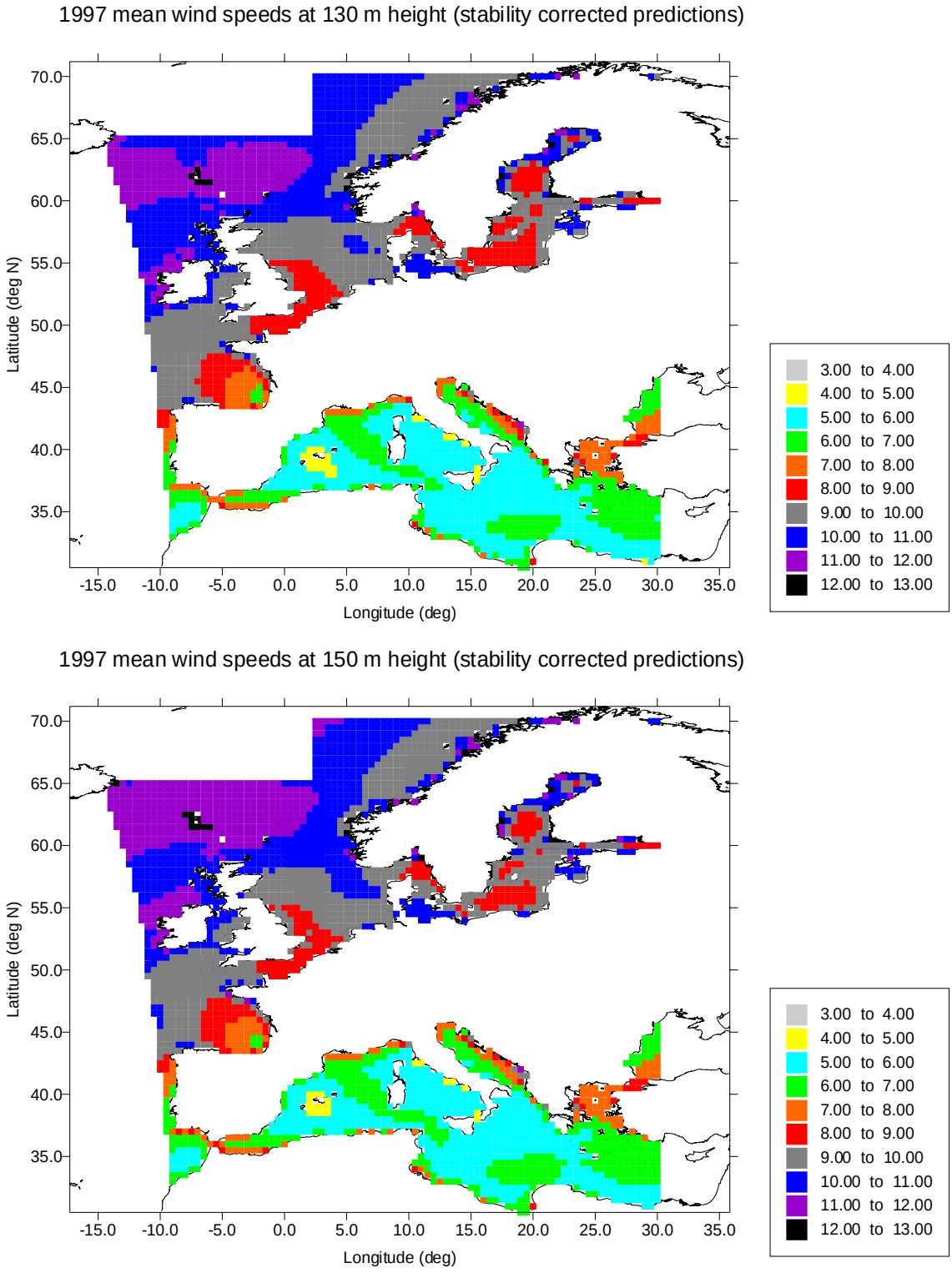

Figure 5-7. (continued).

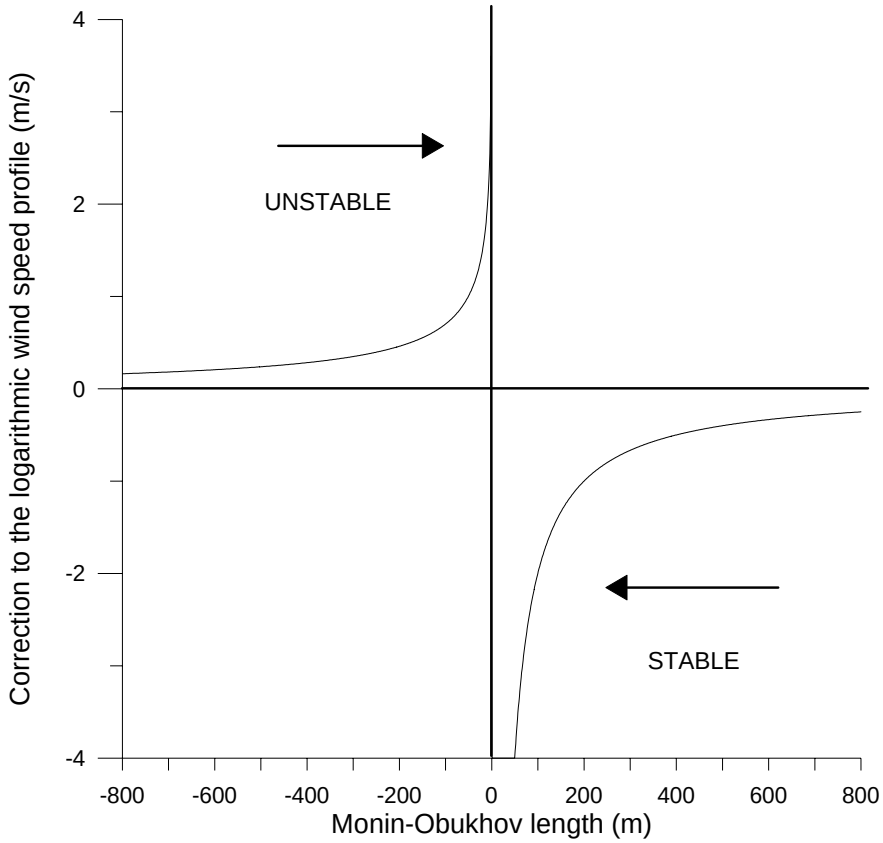

Figure 5-8. Corrections to the wind profile at 40 m based on the Monin-Obukhov length.

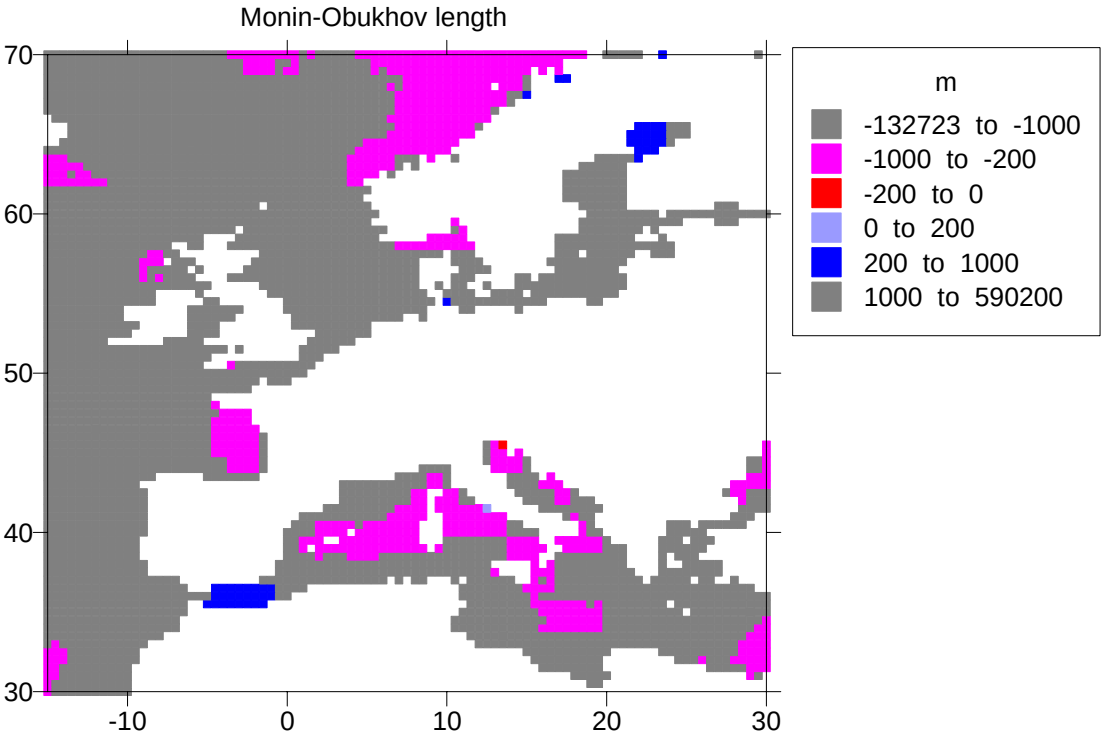

Figure 5-9. CDM calculations of the mean Monin-Obukhov length.

5.2.3 The role of variable surface roughness and tidal range

Variable roughness offshore impacts air-sea exchange and has been extensively studied. If a constant value for roughness of 0.001 to 0.0002 m is not used, the most commonly utilised is the Charnock formula (Charnock, 1955) which estimates roughness based on the friction velocity:

$$z_0 = a\frac{u_*^2}{g} \tag{5.6}$$

where g is acceleration due to gravity and
a is a constant.

As described in (Donelan *et al.*, 1993) the value of a is not constant but has been found to vary from about 0.011 (Smith, 1988) in well-developed seas to 0.018 in coastal areas (Garratt, 1977). Observations and modelling studies (e.g. (Kitaigorodsky and Zislavsky, 1974), (Geernaert *et al.*, 1986), (Nordeng, 1991)) have suggested that a is fetch-wind speed dependent (where fetch is defined as the upwind distance to the coastline), and various formulations for the fetch or wave height dependence of roughness have been proposed e.g. (Johnson *et al.*, 1997).

Discussions of the impact of roughness length on offshore wind resources have mainly focussed on two points:

1) the roughness dependence on wind speed impacts wind speed profiles at higher wind speeds
2) these effects are most important at relatively short fetches

Results of a modelling study by Frank et al. (2000) suggest that using the simplest approach (constant roughness of 0.2 mm as used in WAsP) compared with either Charnock (wind speed dependent roughness) or a fetch dependent roughness gave a relatively small difference in the predicted wind speed (less than 0.5%) even at short fetch distances of 5 km. Frank et al. (2000) suggested that thermal stratification has a much greater impact on offshore wind resources than changes in roughness.

This point can be illustrated by the following. If stability is close to neutral and conditions are in equilibrium then a logarithmic profile is assumed to fit the observed wind speed profile. If wind speed at 10 m height is known then the variation in the effect of roughness can be determined by using the logarithmic wind speed profile. Wind speeds are assumed to lie in the range 5-25 m/s (normal operating range of a wind turbine).

The following observations can be made based on results in Frank et al. (2000):

1. For fetches between 15 and 60 km differences in roughness length are only predicted at wind speeds higher than 12 m/s. In the range of wind speeds 12-25 m/s the maximum difference in roughness between 15 and 60 km fetch is 0.01 m at 15 km and 0.003 m at 60 km. As shown in Table 5-1, this gives a maximum difference of 2.8% in the log-predicted wind speed at 50 m from a 25 m/s wind speed at 10 m height. At more moderate wind speeds (e.g. 15 m/s) the difference in roughness length is 0.0009 m at 60 km fetch to 0.001 m at 15 km. This gives a difference of less than 0.2% in predicted wind speed at 50 m height.
2. Differences in roughness length are larger between open sea (here 60 km fetch) and coastal areas (2 km fetch). At 25 m/s the roughness lengths at 2 km fetch and 60 km fetch are 0.03m and 0.003m. This gives the maximum possible difference in predicted wind speed at 50 m height of 8%. At more moderate wind speeds of 15 m/s the difference in roughness length is 0.0009 m at 60 km fetch to 0.005 m at 2 km fetch. This gives a difference of 3.2% in predicted wind speed at 50 m height.
3. At lower wind speeds the difference in roughness length and hence in predicted wind speed are smaller.

A further point should be made which has not yet been addressed in great detail – the impact of swell or tidal range on predicted wind speed. The reason that tidal range is important is that wind speed extrapolation with height is typically made to a fixed reference height. If the increase in wind speed between the reference height (e.g. 10 m) and a greater height (e.g. 50 m) is based on the logarithmic profile, then the wind speed factor used varies if the distance to the surface varies. The natural logarithm of the reference height is more strongly impacted by the change height of the surface.

Figure 5-10 illustrates this principle for a tidal range of 2 m for three different wind speed scenarios; fixed, typical ‘diurnal’ profile and a ‘cosine’ profile. Note that each has a mean wind speed of 7m/s. While the predicted wind speed varies for the tidal range shown by hour, the differences in the average wind speed over this period is less than 0.1 m/s. As the tidal range increases, the impact of the changing height increase to about 0.2 m/s for a tidal range of 4 m but remains less than 0.3 m/s for wind speeds up to 25 m/s. Thus if the wind profile is close to logarithmic and the tidal range less than 4m, the impact on the predicted wind speed profile up to 50 m height is

expected to be negligible. However, if the height used to predict the wind speed profile is below 10 m from mean sea level the impact will be larger.

Given the relatively small impact of roughness changes on mean wind speed profiles in comparison with other error sources and the difficulty of developing an algorithm combined with obtaining data on wave height and wave age, the Charnock formula is used within the CDM. A constant roughness of 0.0002 m is used in WAsP but the use of two different algorithms is not expected to cause very large differences in the predicted wind speed profiles.

Table 5-1. Predicted wind speed using logarithmic wind speed profile and different roughnesses

		Roughness length (m)									
Wind speed (m/s)	Height (m)	0.03	0.02	0.01	0.005	0.003	0.002	0.001	0.0009	0.0002	0.00002
5	10	5.00	5.00	5.00	5.00	5.00	5.00	5.00	5.00	5.00	5.00
	50	6.39	6.29	6.16	6.06	5.99	5.94	5.87	5.86	5.74	5.61
	100	6.98	6.85	6.67	6.51	6.42	6.35	6.25	6.24	6.06	5.88
7	10	7.00	7.00	7.00	7.00	7.00	7.00	7.00	7.00	7.00	7.00
	50	8.94	8.81	8.63	8.48	8.39	8.32	8.22	8.21	8.04	7.86
	100	9.77	9.59	9.33	9.12	8.99	8.89	8.75	8.73	8.49	8.23
9	10	9.00	9.00	9.00	9.00	9.00	9.00	9.00	9.00	9.00	9.00
	50	11.49	11.33	11.10	10.91	10.79	10.70	10.57	10.55	10.34	10.10
	100	12.57	12.33	12.00	11.73	11.55	11.43	11.25	11.22	10.92	10.58
11	10	11.00	11.00	11.00	11.00	11.00	11.00	11.00	11.00	11.00	11.00
	50	14.05	13.85	13.56	13.33	13.18	13.08	12.92	12.90	12.64	12.35
	100	15.36	15.08	14.67	14.33	14.12	13.97	13.75	13.72	13.34	12.93
13	10	13.00	13.00	13.00	13.00	13.00	13.00	13.00	13.00	13.00	13.00
	50	16.60	16.37	16.03	15.75	15.58	15.46	15.27	15.25	14.93	14.59
	100	18.15	17.82	17.33	16.94	16.69	16.51	16.25	16.21	15.77	15.28
15	10	15.00	15.00	15.00	15.00	15.00	15.00	15.00	15.00	15.00	15.00
	50	19.16	18.88	18.49	18.18	17.98	17.83	17.62	17.59	17.23	16.84
	100	20.95	20.56	20.00	19.54	19.26	19.06	18.75	18.71	18.19	17.63
17	10	17.00	17.00	17.00	17.00	17.00	17.00	17.00	17.00	17.00	17.00
	50	21.71	21.40	20.96	20.60	20.37	20.21	19.97	19.94	19.53	19.09
	100	23.74	23.30	22.67	22.15	21.83	21.60	21.25	21.20	20.62	19.98
19	10	19.00	19.00	19.00	19.00	19.00	19.00	19.00	19.00	19.00	19.00
	50	24.26	23.92	23.43	23.02	22.77	22.59	22.32	22.28	21.83	21.33
	100	26.53	26.04	25.33	24.76	24.39	24.14	23.75	23.70	23.04	22.33
25	10	25.00	25.00	25.00	25.00	25.00	25.00	25.00	25.00	25.00	25.00
	50	31.93	31.47	30.82	30.29	29.96	29.72	29.37	29.32	28.72	28.07
	100	34.91	34.26	33.33	32.57	32.10	31.76	31.25	31.18	30.32	29.39

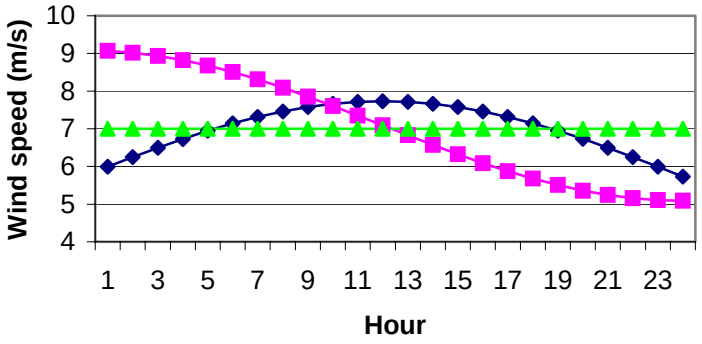

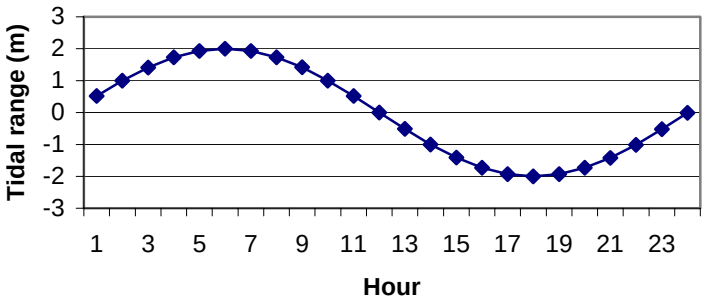

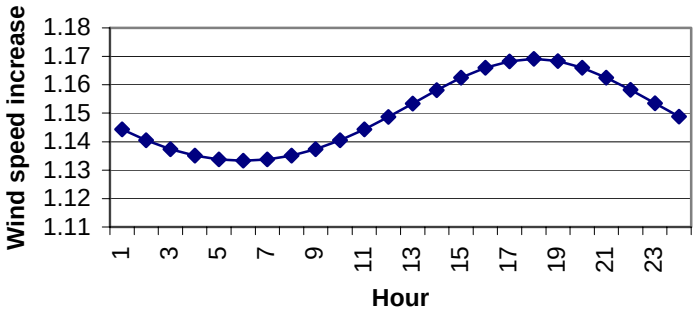

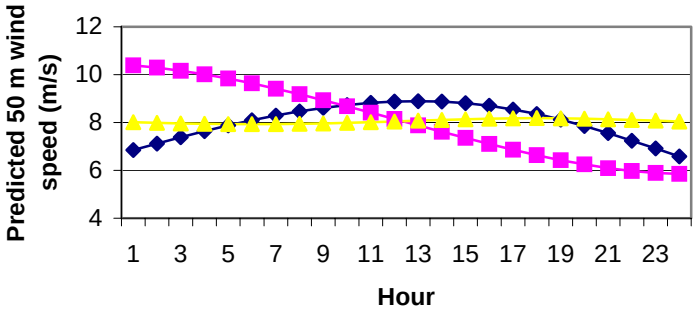

Figure 5-10: Impact of tidal range on predicted wind speed. Top: Wind speed scenario Next: Tidal range. Next: Wind speed increase between 10 m and 50 m height Bottom: Predicted wind speed at 50 m height. (from Barthelmie, 2000).

5.2.4 The impact of stability on offshore flow

Modification of the flow in the coastal zone as a result of the discontinuity in stability and roughness has profound implications for the wind speed distribution and hence for offshore wind energy production. [*Pryor and Barthelmie, 1998*] found that with offshore flow at 1.2-1.7 km from the coast the flow to the new surface conditions had propagated vertically to at least 20 m height. However, the form of the wind speed distributions above 20 m height were not statistically different at the sea masts indicating that flow at this height had not significantly changed as a result of the modified surface conditions. [*Pryor and Barthelmie, 1999*] extend this analysis further to examine fetch dependence of flow modification using data from Gedser land mast (located on the tip of a north-south oriented island) and the Rødsand mast (located approximately 11 km offshore to the west). Using conditional sampling the data from Rødsand and Gedser were classified based on stability (as determined from application of the [*Beljaars et al., 1989*] routines) and fetch characteristics (i.e. distance to the coast-line along the prevailing wind direction). Figure 5-11 shows the wind speed distributions from the two masts at 10 and 50 m height sampled by fetch and stability class (for over land flow to the Gedser mast, and over sea flow to the Rødsand mast). As shown, acceleration of the flow due to the lower roughness of the sea surface is most marked at 10 m height under all stability conditions and is much less pronounced at 50 m.

These distributions have been quantitatively compared using two standard statistical tests:

- The Wilcoxon matched-pairs signed ranks test (which tests the equality of the magnitude of observations in two series)
- The Kolmogorov-Smirnov equality of distributions test (which tests whether the form of two distributions is similar).

As expected, wind speed distributions at all heights and in all stability classes indicated higher wind speeds at the sea mast (i.e. significant Wilcoxon matched pair results). The results also indicate that except at the 50 m height the wind speed distributions exhibit a different form at the Gedser and Rødsand masts. It is hypothesised that this is due to a change in momentum exchange with the surface which causes a modification of the wind speed profile. At 50 m height, however, the adjustment to the modified surface fluxes has not significantly altered the form of the wind speed distribution even after a fetch of over 20 km. This suggests that at this height the flow characteristics are still heavily influenced by the land surface over which the wind had previously blown. The exception to this result is found under stable conditions with short fetch. This anomaly is the subject of further analysis and can not currently be explained. Both sets of analysis suggest that the width of the coastal zone (the offshore area which is affected by the presence of land) is strongly dependent on the height examined and the prevailing stability conditions. Hence the CDM utilises a coastal band of 50 km. If the grid point is less than 50 km from the coast the CDM calculates equilibrium on- and offshore wind speed profiles and the IBL height according to stability conditions and then predicts the wind speed profile at the given distance.

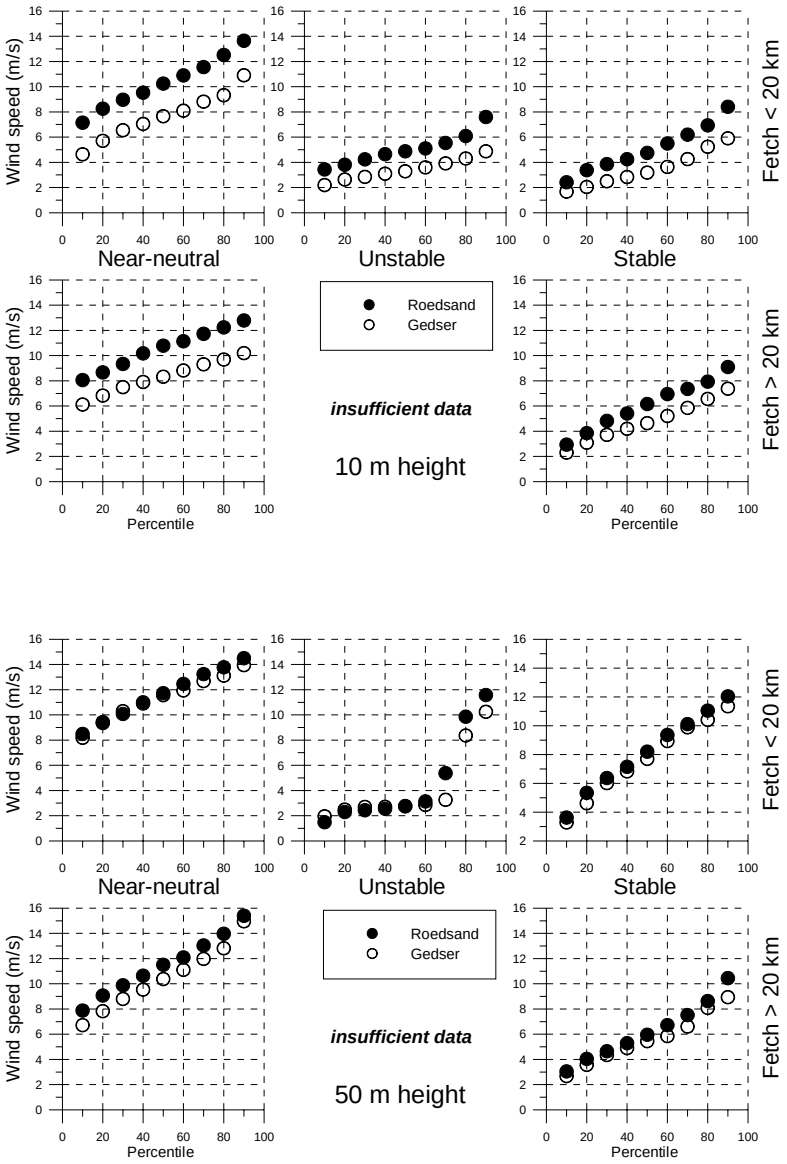

Figure 5-11. Wind speed distributions from Gedser land mast and Rødsand sea mast at 10 m and 50 m for flow over land to the Gedser mast and over sea (with varying fetch) at the Rødsand mast under different stability conditions. Fetch refers to the oversea fetch distance to the Rødsand mast.

5.3 Integrating the CDM and WAsP for the POWER project

5.3.1 Comparison of predictions based on geostrophic wind speeds

In this section both WAsP and the CDM are initialised with geostrophic wind speeds for the period 1985-97. Results from these models are denoted here as GEO-WAsP and GEO-CDM, respectively. Predicted near-surface wind speeds are compared to evaluate the differences produced by the different algorithms as discussed in section 5.2.1.

5.3.1.1 Comparing the neutral GEO-CDM with GEO-WAsP

Major differences are observed between the GEO-WAsP and neutral GEO-CDM predictions which are unexpected in far offshore areas. Differences in wind speed predictions are expected close to the coast where topography, stability and the IBL height are important. However, in near-neutral conditions, it is anticipated that these differences are negligible beyond 10 km from the coast line. The most likely cause of differences in the wind speeds shown in Figure 5-12 is the stable correction to the wind speed profile above the sea which WAsP applies. A further possibility which should be investigated is that the iteration procedure using the Charnock relationship in the GEO-CDM is producing a friction velocity which is too low.

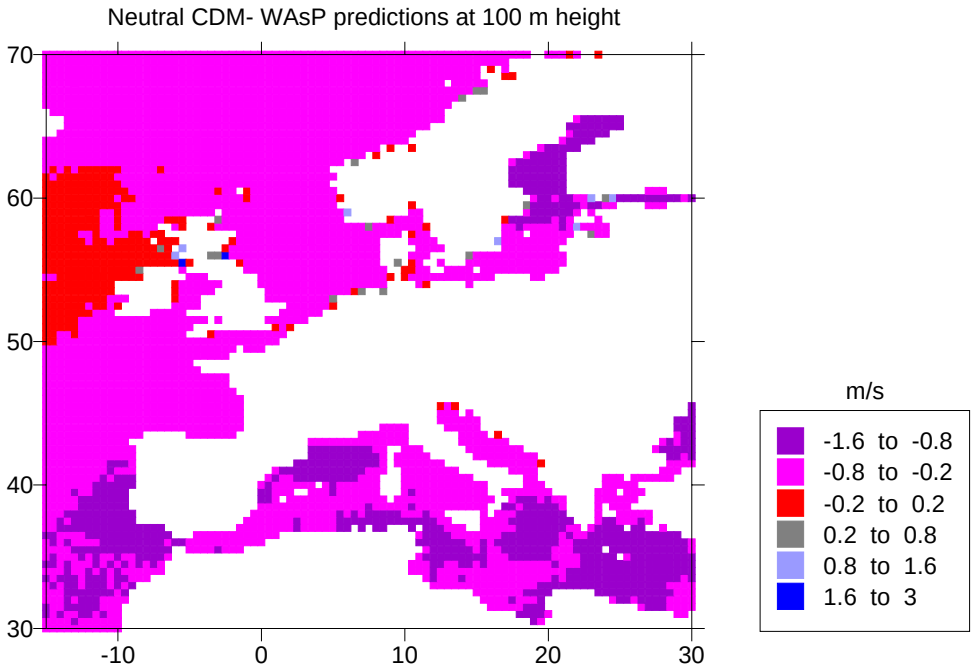

Figure 5-12. Differences in wind speed predicted at 100 m height between the neutral GEO-CDM and GEO-WAsP models (mean for the period 1985-97)

5.3.1.2 Comparing the stability corrected GEO-CDM with GEO-WAsP

Figure 5-13 shows GEO-WAsP predicted wind speeds at 10 m height, GEO-CDM predicted wind speeds at 10 m height, the difference in each grid square and the air-sea temperature difference. As illustrated differences in the wind speed prediction do not appear to be related to the pattern of air-sea temperature differences. Figure 5-14 shows the GEO-CDM stability correction at 10 m. The stability correction is likely to be most important in areas with relatively low wind speeds since higher wind speeds will tend to increase the value of the Monin-Obukhov length. Hence the stability correction is mainly large in Mediterranean. Relatively large stability corrections driven by large air-sea temperature differences are also present along the north Norwegian coast and in the north Baltic. The atmosphere over the Baltic is known to be slightly stable on average (implying that air temperatures are typically higher than sea surface temperatures). However, differences in the north Norwegian Sea were not expected.

Figure 5-15 shows the difference in wind speeds at 100m between the wind speeds predicted from the stability corrected GEO-CDM and GEO-WAsP models. Biggest differences are found in the Mediterranean region. As shown in Figure 5-16 at 10m height, stability corrections predicted by in the GEO-CDM are only important in coastal regions.

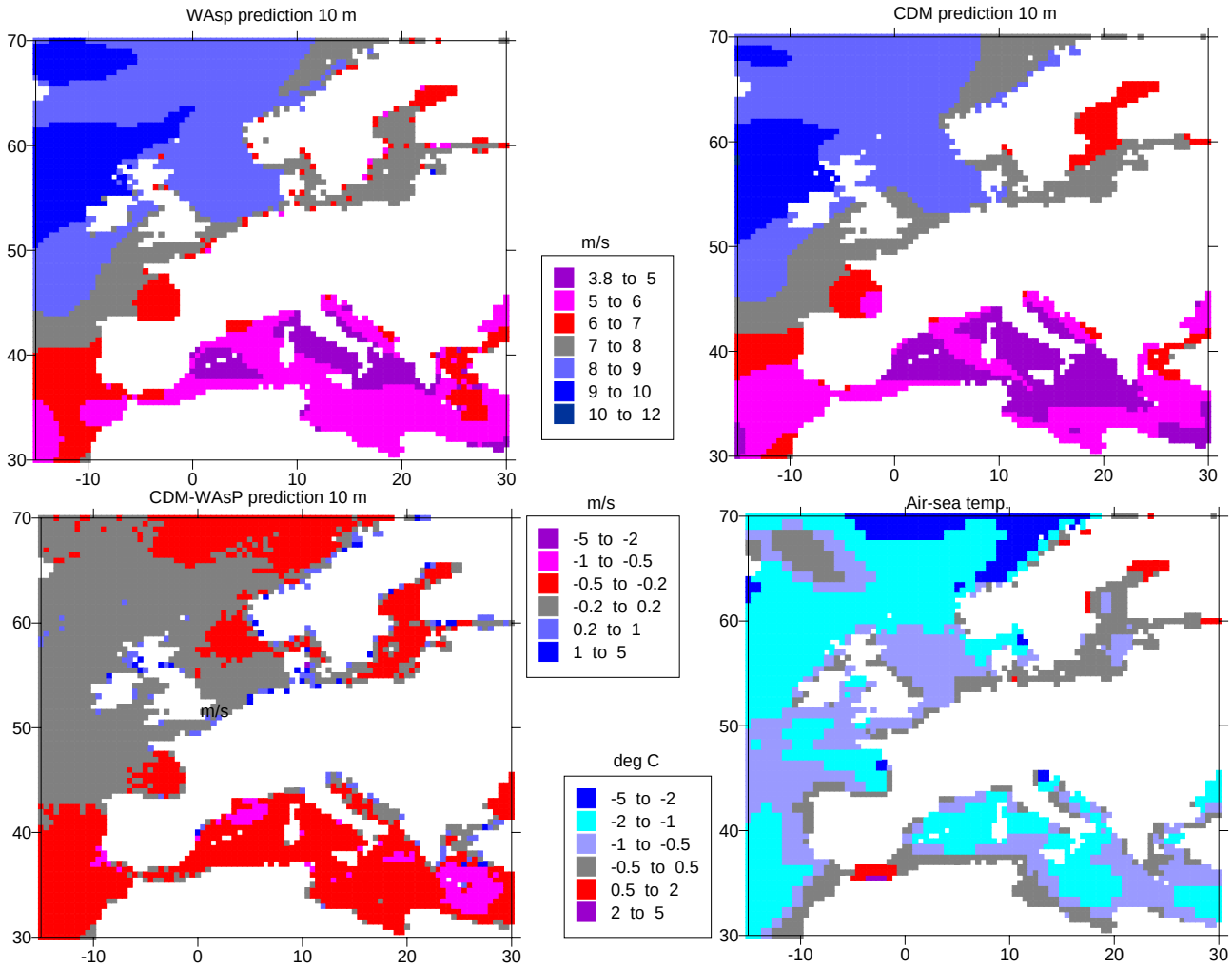

Figure 5-13. GEO-WAsP predicted wind speeds at 10 m height, GEO-CDM predicted wind speeds at 10 m height, the difference in each grid square and the air-sea temperature difference (mean for the period 1985-97).

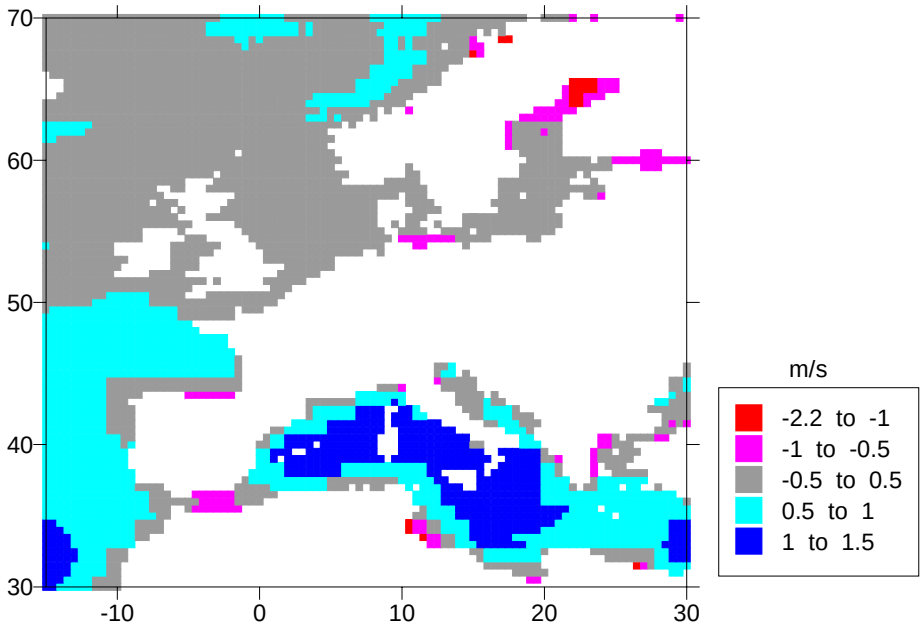

Figure 5-14. GEO-CDM calculated stability correction at 10 m (mean for the period 1985-97).

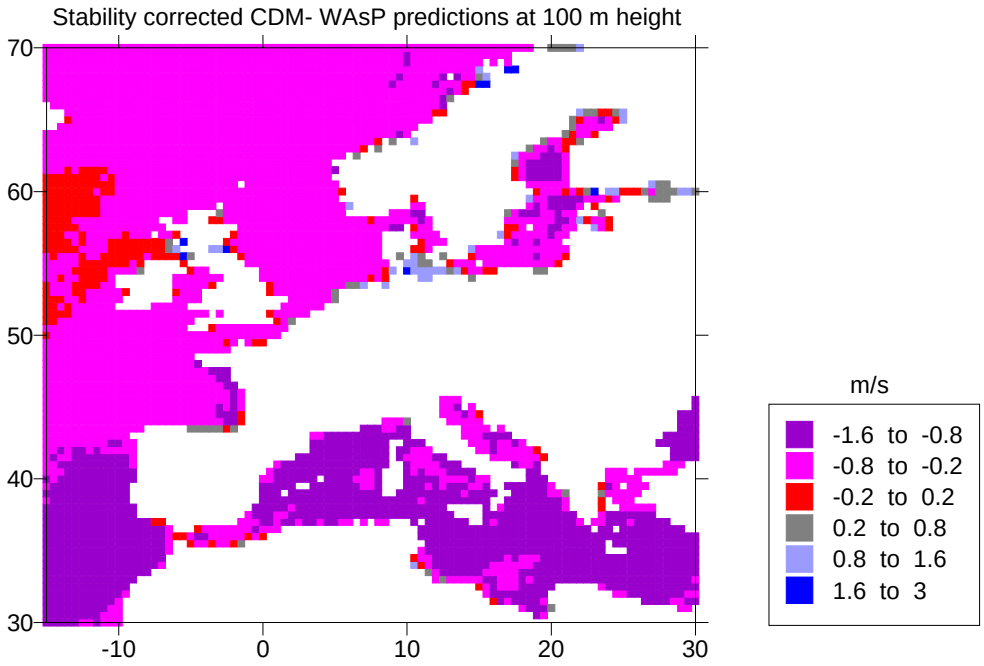

Figure 5-15. Differences in wind speed predicted at 100 m height between the stability corrected GEO-CDM and GEO-WAsP models (mean for the period 1985-97)

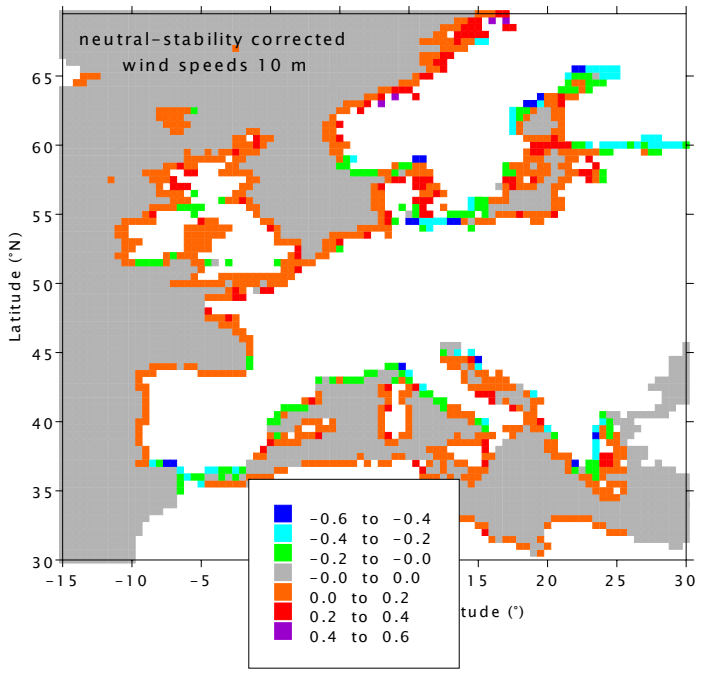

Figure 5-16. Differences in wind speed predicted at 10 m height between the stability corrected GEO-CDM and neutral GEO-CDM formulations (mean for the period 1985-97).

5.3.2 Applying the CDM to WAsP predicted wind speeds

5.3.2.1 General approach

In order to correct WAsP wind speeds for observation-specific stability (rather than the general stability correction applied in the typical application of WAsP) the general stability correction has to be removed from the WAsP predictions. Following this, the stability correction is calculated as in Barthelmie (1999) (based on the Monin-Obukhov length determined from grid-specific wind speeds and air and sea temperatures) and applied to each observation. It should be noted that neither the CDM nor WAsP account for large scale thermal flows such as the sea breeze and low level jets.

Both the Coastal Discontinuity Model (CDM) and the Wind Analysis and Application Programme (WAsP) (Mortensen *et al.*, 1993) can be initialised with geostrophic wind speeds and used to predict near-surface winds as described above. The main differences in the predicted wind fields stem from:

- *The transformation from geostrophic to near-surface winds.*

  In both models the geostrophic drag lag is used to estimate the friction velocity from the geostrophic wind speed U_g which can be used to predict near-surface winds. The same values for the constants A and B are used where A=1.8 and B=4.5.

$$U_g = \frac{u_*}{k}\sqrt{\left(\left(\ln\left(\frac{u_*}{fz_0}\right) - A\right)^2 + B^2\right)}$$

  Here the CDM uses an iterative procedure since the value of the roughness length z_0 over sea is determined according to the Charnock equation (Charnock, 1955) (i.e. varies with wind speed) rather than the fixed value of 0.0002 m used in WAsP.

- *The calculation of the internal boundary layer height*

  Within WAsP the calculation of the internal boundary layer height, *h*, (IBL) is dependent on both the roughness and the fetch based on (Panofsky, 1973):

$$\frac{h}{z_0'}\left(\ln\frac{h}{z_0'} - 1\right) = 0.9\frac{x}{z_0'}$$

  where

  z_0' is the highest value of the two roughnesses at the discontinuity

  x is the distance to the discontinuity

  Additionally, a weighting factor is used to account for the approach to equilibrium at large distances from the discontinuity (Troen and Petersen, 1989). This decay length is 10000 m (Mortensen *et al.*, 1993).

  In practice the roughness change model is more complicated. A three layer IBL model is employed as described in (Troen and Petersen, 1989) to ensure a smooth transition of the wind speed profile over roughness changes. Here the defaults for the heights of the layers are:

  inner (lowest) layer : 0.09 *h*
  outer layer : 0.3 *h*

  An example of the WAsP predicted wind speed profiles moving away from the coast is given below (Figure 5-17). This is a prediction for a site in North Lolland moving away from the coast at distance 0 km to 9 km. As is illustrated, the majority of the wind speed adjustment close to the

surface occurs in the first 2-3 km, while the shape of the wind speed profile occurs in the first 2km. Figure 5-18 shows the same data plotted as a contour plot. The IBL height (dashed line) is estimated to reach about 100 km at 2 km from the coast. Equation (1) with $z_0^{'}$=0.1 m suggests that an IBL of 100 m at about 650 m from the coast and of 150 m at 1050 m.

Within the CDM the IBL height is calculated using:

$$h = 0.2x^{(0.78-0.33z/L)}$$

When conditions are near-neutral z/L is close to zero. Thus for comparison with WAsP an IBL of 100 m is reached after about 2500 m and of 150 m after about 4000 m. This is expected to have a significant impact on wind speed profiles in coastal areas. The reason for this difference is that WAsP uses a 'generic' roughness change formula which determines the roughness change according to the highest roughness (land) which is several orders of magnitude higher than the roughness over the sea surface.

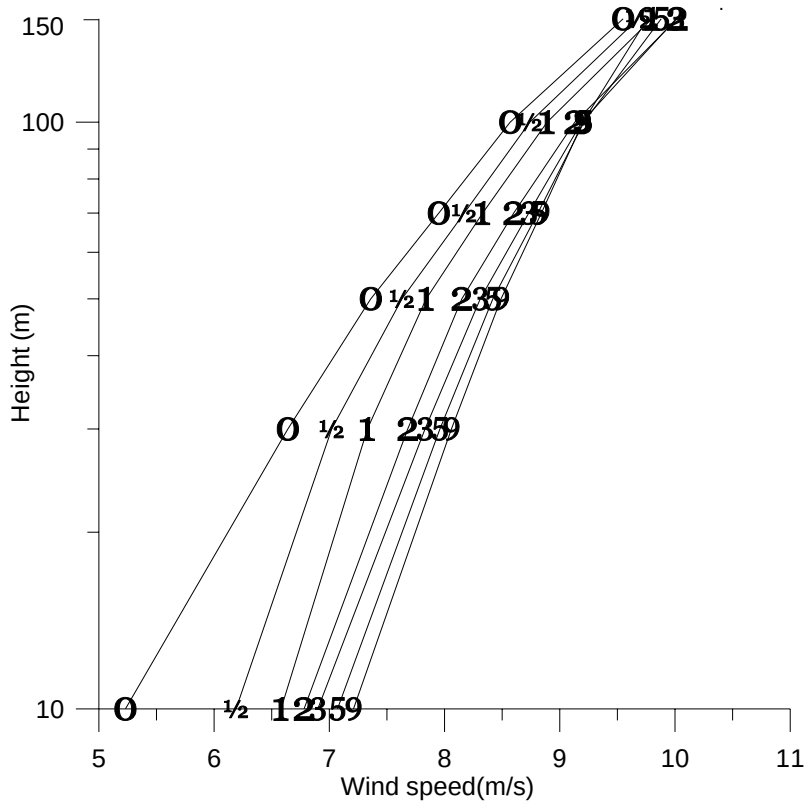

Figure 5-17. Variation of WAsP-predicted wind speed profiles moving away from the coast. Labels on the profiles indicate the distance from the coast from 0 km (coastline) to 9 km.

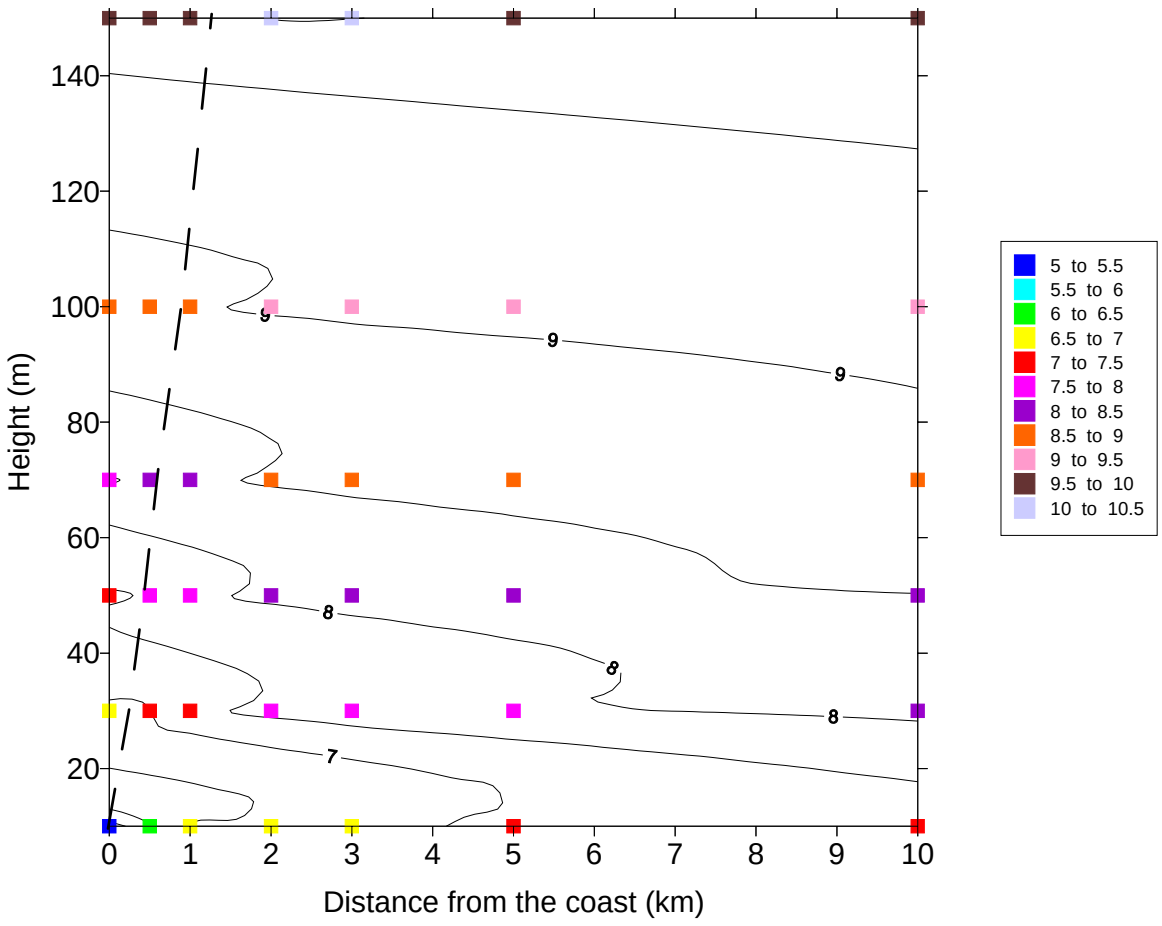

Figure 5-18. Change of wind speed profile with distance from the coast (moving offshore). The dashed line is the IBL height.

- *WAsP utilises a topographic correction*
  This maybe important in some coastal areas e.g. parts of the Mediterranean but only in the first few kilometres of the coastal zone.

- *The applied stability correction*
  WAsP applies a stability correction to the wind speed profile which reflects the underlying surface (land or sea). The difference between the correction to the profile depends on a parameter for the heat flux, its root mean square and the height to which the correction is applied (Troen and Petersen, 1989).

  Default parameters are (Mortensen *et al.*, 1993):

  1) Height of minimum correction over land 100 m (default=not used)
  2) r.m.s. of stability induced variation in wind speed over land 0.12 (default=not used)
  3) Relative increase of wind speed at height set by 1) 0.11(default=not used)
  4) Height of minimum correction sea 50 m (default=not used)
  5) r.m.s. of stability induced variation in wind speed 0.0 (default=not used)
  6) Relative increase of wind speed at height set by 4) 0.0 (default=not used)

  Thus in the general application of WAsP the stability variation is determined by the heat flux where:

  r.m.s. heat flux over land 100 Wm^{-2}
  r.m.s. heat flux over sea 30 Wm^{-2}
  Offset heat flux over land -40 Wm^{-2}
  Offset heat flux over sea 15 Wm^{-2}

Additional factors are used:

Factor in heat flux induced perturbation of u* 1.65
Form factor in heat flux distribution over land 0.6
Form factor in heat flux distribution over sea 0.6

Then corrected wind speed *u* at height *z* is:

$$u(z) = u_0(z)\left(1 + \frac{\Delta u(z_m)}{u(z_m)}\right)\left(1 - f(z)\right) + \frac{\Delta u_{*off}}{u_{*0}}$$

where:

z_m is the height of the minimum variance in wind speed
and

$$f(z) = 1 - \frac{z}{z_m}\frac{\ln(z_m / z_0)}{\ln(z / z_0)}$$

Stability correction within the CDM is carried out on an observation by observation basis. For each grid cell, a time and location specific geostrophic wind speed and direction, air temperature and sea surface temperature are used as input to the model. The friction velocity is determined assuming near-neutral conditions using the drag law and used within an iterative procedure with the temperature profile to estimate the Monin-Obukhov length (using an amended version of the methodology of (Beljaars *et al.*, 1989). This is used to correct the wind speed profile based on the Businger-Dyer flux profile relationships (see e.g. (Stull, 1988)). Then for each grid square the corrected profile is averaged for the required period.

Thus the major difference between WAsP and the CDM is that the CDM accounts for both temporal and spatial variability in stability (as reflected by the temperature profile above the sea and the wind speed) whereas WAsP applies a mean stability correction to all sea areas which is dependent on distance to the coast.

The procedure for Integrating CDM and WAsP is as follows:

1) Read WAsP output for Weibull A and k factors at each height and percentage occurrence in each sector.
2) Mean wind speed in each sector is calculated from Weibull factors:

$$U = A\Gamma\left(1 + \frac{1}{k}\right)$$

3) Mean wind speed calculated by this procedure is higher than the mean given by WAsP where:

   SUM U (SEC)=1.01*U (MEAN)

   At this point the frequency distribution of direction is available.

4) Calculate factors to correct wind speed profiles with land roughness of 0.03 m according to distance offshore and height. Two sets are required - one corrects profiles to give equilibrium on-shore wind speed profile and one gives equilibrium offshore wind speed profiles. This is done using WAsP.

5) Read in air and sea temperatures for each 1 by 1 degree grid cell. Calculate average air and sea temperatures for each grid.

6) Read in fetch distances by direction for each grid cell.

7) Merge the data sets so that each grid point has associated with it a mean wind speed profile by direction, frequency distribution by grid cell, mean air and sea temperature and a fetch distance by grid cell.

8) Use the WAsP generated wind speed profile and the air and sea temperatures to calculate an average Monin-Obukhov length by grid cell.

9) For each grid cell and each direction, use the fetch distance to interpolate between factors to correct WAsP profiles to equilibrium offshore and onshore profiles.

10) Calculate the internal boundary layer height according to fetch and stability

11) Calculate the new grid square wind speed based on the IBL height and the equilibrium offshore and onshore profiles. If the height of the wind speed to be predicted is above the IBL then the land wind speed at that height is used. If the height is below the IBL then the sea wind speed at that height is used. There is also an adjustment zone which is 10% above the IBL height and 10% below. If the height is in this region then the wind speed is extrapolated between the land and sea wind speeds, according to the log of the height. This gives a smooth transition in wind speeds over the IBL.

12) Removing the stability correction from WAsP. According to the WAsP manual there are a number of stability parameters (such as the height above ground at which the differences between stable and unstable profiles are smallest, relative increase at this height due to stability effects etc) but the default is that these are not set. However, more detailed discussion in the European Wind Atlas indicates that the treatment of stability corrections as perturbations to the neutral profile is complex. The corrections are based on average values of the heat flux where:

    rms heat flux over land=100 Wm^{-2}
    rms heat flux over sea=30 Wm^{-2}
    Offset heat flux over land=-40 Wm^{-2}
    Offset heat flux over sea=15 Wm^{-2}

The height above ground where the heat flux variations are minimum is defined by:

$$\frac{z_m}{z_0} \cong 0.002\left(\frac{G}{fz_0}\right)^{0.9}$$

where $f=2\Omega\sin\phi$ and Ω *is* $7.292 \times 10^{-5}\ s^{-1}$

13) The direction is corrected as a linear function of the on- and offshore wind directions according to the distance from the coast

Table 5-2. Height of minimum variance for z_0=0.03m

UG/LAT	30.00	40.00	50.00	60.00	70.00
1.00	7.45	5.94	5.07	4.54	4.22
2.00	13.90	11.09	9.47	8.48	7.88
3.00	20.03	15.97	13.64	12.21	11.35
4.00	25.94	20.69	17.67	15.82	14.70
5.00	31.71	25.30	21.60	19.34	17.97
6.00	37.37	29.81	25.45	22.79	21.18
7.00	42.93	34.24	29.24	26.19	24.33
8.00	48.41	38.62	32.98	29.53	27.44
9.00	53.83	42.93	36.66	32.83	30.51
10.00	59.18	47.21	40.31	36.10	33.54
11.00	64.48	51.43	43.92	39.33	36.54
12.00	69.73	55.62	47.50	42.53	39.52
13.00	74.94	59.78	51.05	45.71	42.47
14.00	80.11	63.90	54.57	48.86	45.40
15.00	85.24	67.99	58.06	51.99	48.31
16.00	90.34	72.06	61.54	55.10	51.20
17.00	95.41	76.10	64.99	58.19	54.07
18.00	100.44	80.12	68.42	61.27	56.93
19.00	105.45	84.11	71.83	64.32	59.76
20.00	110.44	88.09	75.22	67.36	62.59
21.00	115.39	92.04	78.60	70.38	65.40
22.00	120.33	95.98	81.96	73.39	68.19
23.00	125.24	99.90	85.31	76.39	70.98
24.00	130.13	103.80	88.64	79.37	73.75
25.00	135.00	107.68	91.95	82.34	76.51

Table 5-3. Height of minimum variance for z_0=0.0002 m

UG/LAT	30.00	40.00	50.00	60.00	70.00
1.00	4.51	3.60	3.07	2.75	2.56
2.00	8.42	6.72	5.74	5.14	4.77
3.00	12.13	9.68	8.26	7.40	6.88
4.00	15.72	12.54	10.71	9.59	8.91
5.00	19.22	15.33	13.09	11.72	10.89
6.00	22.64	18.06	15.42	13.81	12.83
7.00	26.01	20.75	17.72	15.87	14.74
8.00	29.33	23.40	19.98	17.89	16.62
9.00	32.61	26.01	22.21	19.89	18.48
10.00	35.86	28.60	24.42	21.87	20.32
11.00	39.07	31.16	26.61	23.83	22.14
12.00	42.25	33.70	28.78	25.77	23.95
13.00	45.41	36.22	30.93	27.70	25.73
14.00	48.54	38.72	33.06	29.61	27.51
15.00	51.65	41.20	35.18	31.50	29.27
16.00	54.74	43.66	37.28	33.39	31.02
17.00	57.81	46.11	39.37	35.26	32.76
18.00	60.86	48.54	41.45	37.12	34.49
19.00	63.89	50.96	43.52	38.97	36.21
20.00	66.91	53.37	45.58	40.81	37.92
21.00	69.91	55.77	47.62	42.64	39.62
22.00	72.90	58.15	49.66	44.47	41.32
23.00	75.88	60.53	51.69	46.28	43.00
24.00	78.84	62.89	53.70	48.09	44.68
25.00	81.79	65.24	55.71	49.89	46.36

5.3.2.2 Results

Figure 5-19 shows results of applying the CDM to WAsP predicted wind speed profiles. Results from this model combination are denoted as WAsP-CDM in order to distinguish then from results generated using WAsP and geostrophic wind speeds (GEO-WAsP) and from results using the CDM to modify the wind speed profile from individual observations using stability correction and IBL calculations (WAsP-CDM). The WAsP-CDM gives slightly lower wind speeds in the North Atlantic due to a mean unstable correction in the CDM replacing a mean stable correction within WAsP. As shown in Figure 5-20, GEO-WAsP wind speeds are almost always higher than WASP-CDM predicted wind speeds. This is because the mean stability correction applied in offshore areas in WAsP is always positive (stable) whereas the mean stability correction calculated from the mean air-sea temperature difference is always small and sometimes negative (unstable).

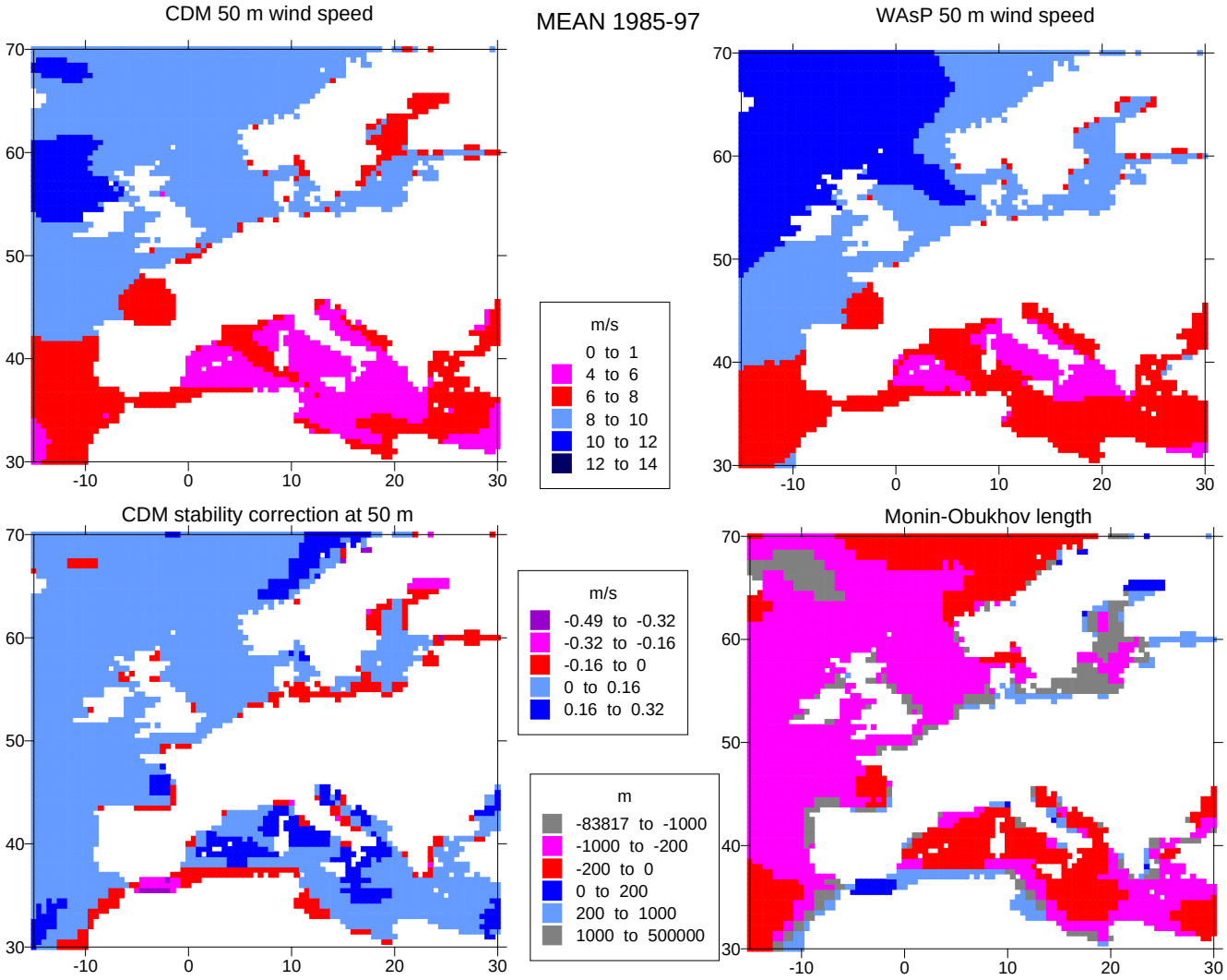

Figure 5-19. WAsP-CDM and GEO-WAsP predicted wind speeds at 50 m height for 1985-97.

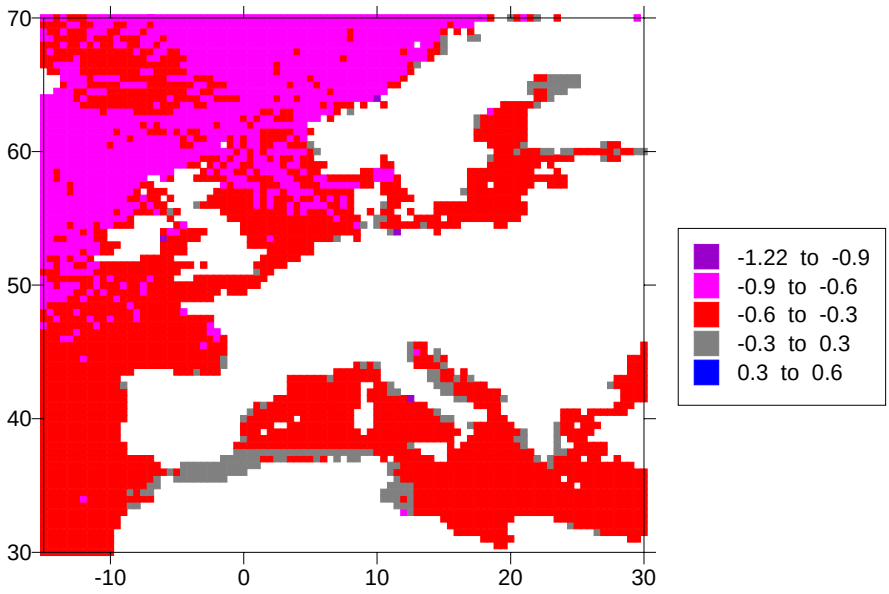

Figure 5-20 WASP-CDM minus GEO-WASP predicted wind speeds at 50 m for 1985-97 (m/s).

5.4 Validation

5.4.1 Validation of stability routines

Evaluation has been conducted as part of the POWER project using the Risø Air-Sea EXperiment (RASEX) measurements (Mahrt *et al.*, 1996) from Vindeby Sea Mast West. For details regarding site locations etc. see (Barthelmie *et al.*, 1994). The RASEX data set and the routine measurements conducted at SMW overlap for two periods: 28th April to 30th June 1994 and 17th August to 31st December 1994 giving 3645 observations for comparison. The Monin-Obukhov length calculated from direct flux measurements at 6m was compared with values based on routine measurements using a model based on flux estimation codes from Beljaars et al. (1989) which are called here Monin-Obukhov Length derived stabiLitY(MOLLY). For each half-hourly observation the Monin-Obukhov length was calculated for data from based on the corrected sea surface temperature and the absolute air temperature and wind speed at 7m height. Results of the comparison are shown in Table 5-4. There is good agreement between the frequency of different stability classes using the values of the Monin-Obukhov length calculated from fluxes measured directly and modelled using MOLLY.

Table 5-4. Comparison of frequency of stability classes at SMW based on Monin-Obukhov lengths 1) calculated using fluxes determined from data from a sonic anemometer at 6m at SMW and 2) calculated using MOLLY. Stability classes are defined according to (Van Wijk et al., 1990a) based on the Monin-Obukhov length (m).

Stability class	Monin-Obukhov length (m)	Percentage of observations	
		Direct	MOLLY
Very stable	0 < L < 200	19.5	21.1
Stable	200 < L < 1000	14.2	14.8
Near-neutral	1000 < L < -1000	9.3	9.6
Unstable	-1000 < L < -200	12.2	12.5
Very unstable	200 < L < 0	44.7	42

Since most observations offshore do not include flux measurements from which the stability parameter the Monin-Obukhov length can be calculated, this parameter is estimated using routine measurements and MOLLY. In total MOLLY has been applied at 10 sites ranging from routine synoptic coastal sites to purpose built offshore monitoring locations. MOLLY gives good results at all sites except one. At this site, (Horns Rev Fyrskib), temperature profiles were not available and a further parameterization was introduced using cloud cover to estimate radiation. This routine did not give reasonable results for this site and probably requires further modification for use in offshore areas.

The most detailed work to date has been conducted on data from the Vindeby masts (Barthelmie *et al.*, 1996a), (Barthelmie *et al.*, 1996b). (Pryor and Barthelmie, 1998) and showed that wind speed distributions at 38 m height and above are not in equilibrium with the sea surface (suggesting that they are frequently at or above the IBL). The median IBL height (two layer model) was estimated as 48 and 57 m at the two sea masts at Vindeby which are 1.2 and 1.7 km from the coast. However at heights of 20 m and below there are statistically significant differences in the wind speed distribution for on- and off-shore flow (Pryor and Barthelmie, 1998).

Using MOLLY, all sites had a mean slightly positive Monin-Obukhov length with small corrections to the logarithmic wind speed profile of between 0.1 and 0.2 m/s at heights of about 50m. This is expected since, over the course of a year, large stable corrections are typically balanced by more frequent but smaller unstable corrections to wind profiles (see also (Van Wijk *et al.*, 1990b). There was also a fetch dependence to the stability correction with the largest corrections to the wind speed profile found when offshore fetches are between 1 and 20 km from the coast and the smallest corrections (tending towards zero) when fetches exceeded about 40 km.

This suggests that for stability effects are important to about 40 km from the coast. This work is continuing to evaluate the effects of stability at seasonal and finer temporal resolution and close to the coast where the IBL is an important influence on the shape of the vertical wind speed profile and the acceleration of winds moving away from the coastline.

5.4.2 CDM modelling of SODAR derived wind speeds

As part of the POWER project, meteorological observations were made at Measurement Platform Noordvik approximately 10 km from the Dutch coast in the period January - June 2000 (see Chapter 6). A major advantage of operating a SODAR is that the SODAR observes wind speeds at greater heights than are typically monitored using a meteorological mast. Offshore masts are typically in the range 10-60 m above mean sea level whereas a SODAR should recover wind speed profiles to 100-150 m above sea level. Hub-heights of wind turbines currently being installed are in the range 60-70 m with blades of 30-40 m. Hence detailed observations of offshore wind speed profiles to 150 m are of great utility for planning offshore wind farms. However, the main objective of operating of SODAR was to provide a data set for comparison with predictions from the Coastal Discontinuity Model (CDM).

The CDM was developed to use gridded geostrophic wind speeds as input together with air and sea-surface temperatures on a 0.5 by 0.5 grid over European Seas (Barthelmie, 1999a). Since geostrophic wind speeds are not available as input to the CDM for the period of SODAR measurements, an alternative approach was required. The model uses each land-based observation to estimate geostrophic wind speed and then estimates the offshore wind profile according to fetch, estimated roughness and stability. The procedure is:

1) Use wind speed and direction from a coastal location to estimate geostrophic winds assuming that conditions are near-neutral and that the roughness length onshore is 0.03 m and offshore is 0.0002 m. Wind directions are also corrected, first transforming wind directions to geostrophic and then back at the offshore site using:

$$\sin\alpha = -Bu_* / kG$$

where α is the angle
B is a constant 4.5
u_* is the friction velocity
G is the geostrophic wind speed
k is the von Karman constant

2) Estimate friction velocity offshore based on the geostrophic wind speed using the drag law.
3) Determine the Monin-Obukhov length from observed air and water temperatures and estimated friction velocity using routines from KNMI (Beljaars *et al.*, 1989).
4) Estimate the equilibrium land and offshore wind speed profiles according to the friction velocity and roughness (either set for land or calculated using the Charnock equation (Charnock, 1955))
5) In each sector, calculate the internal boundary layer height according to fetch and stability and correct the wind speed profile.

Because wind speed profiles are not uniformly near-neutral the initial step of estimating geostrophic wind speed from land-based observations introduces a relatively large uncertainty in the estimation of geostrophic wind speeds which is propagated through the analysis. In some measurement periods the predicted wind speed at 150 m exceeded the geostrophic wind speed. In this situation, an error in the initial determination of the geostrophic wind speed was assumed and the friction velocity was reduced through an iterative procedure until all near-surface wind speeds were below that of the estimated friction velocity.

A number of assumptions have to be made. These include:

- The fetch distances to the measurement locations: Hoek van Holland (HVH), Measurement Platform Noordvik (MPN) and Ijmuiden (IJM). Site locations are given in Table 5-7. Fetch distances were estimated using WAsP (see Table 5-8 and Figure 5-21).
- Roughness of the land surface (here estimated as 0.03 m). Sector specific roughness lengths are given in Table 5-9. These were estimated using the gustiness method (Wieringa, 1976), (Wieringa, 1986).

Figure 5-21. Location of the measurement sites.

SODAR data and recovery procedure are not described in detail here since these have been reported separately (Coelingh *et al.*, 1999),(Coelingh *et al.*, 2000) – see also Chapter 6. The remaining observations required are from two sites Hoek Van Holland and IJmuiden wind speed) and the air and sea temperatures measured at MPN.

Table 5-5. Locations of the measurement sites

	Latitude	Longitude	UTM (Zone 31)		Measurement height (m)
			E (m)	N (m)	
Measurement platform Noordvik (MPN)	52°16’26” N	4°17’46”E	588299	5792090	27.6
Hoek Van Holland (HVH)	51º59’06” N	04º03’00” E	572111	5759899	15
Ijmuiden (IJM)	52º27’47” N	04º33’22” E	605593	5813215	18.5

Table 5-6. ***Fetch distances to the sites used in m. Here fetch is defined as the minimum distance to the coast.***

		HVH	MPN	IJM
1	0	>50000	>50000	17000
2	30	>50000	31800	1645
3	60	5300	12820	land
4	90	land	9730	land
5	120	land	9450	land
6	150	land	9880	land
7	180	land	13590	land
8	210	land	28480	land
9	240	>50000	>50000	19380
10	270	>50000	>50000	>50000
11	300	>50000	>50000	>50000
12	330	>50000	>50000	>50000

Table 5-7. Roughness length at IJM and HVH (m)

Sector	IJM	HVH
1	0.000193	6.18E-05
2	0.001394	7.86E-06
3	0.000908	0.000224
4	0.00066	0.001284
5	0.003108	0.000151
6	0.000538	0.000305
7	2.21E-05	0.000379
8	1.28E-06	0.001632
9	1.12E-06	0.003098
10	5.1E-06	0.000188
11	4.9E-05	7.67E-05
12	0.000108	9.62E-05

The CDM is implemented using observations from HVH to estimate geostrophic wind speeds. Using all observations during the period 24 February -16 June 2000 the observed wind speed at 15 m height is 6.62 m/s and the direction is predominately south-westerly (Figure 5-22).

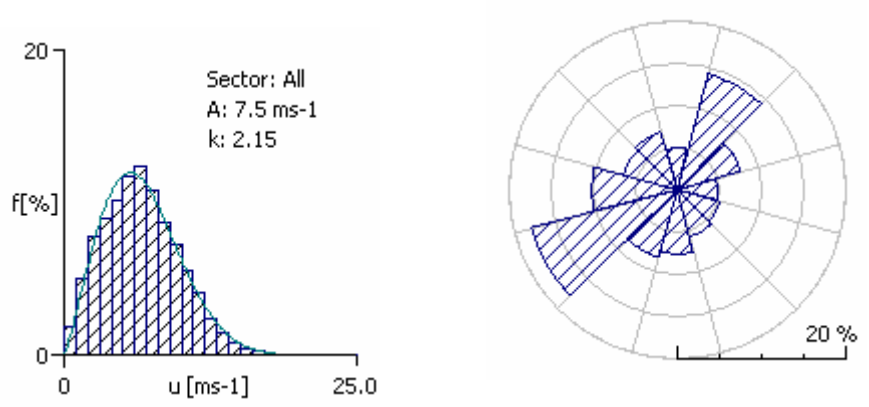

Figure 5-22. Wind speed distribution and wind rose from HVH.

Geostrophic wind speed is calculated as 9.71 m/s over the same period with a stronger westerly component in the direction (Figure 5-23).

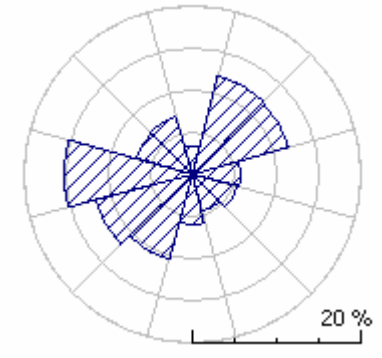

Figure 5-23. Wind rose of calculated geostrophic wind speeds.

Mean sea surface temperature (from MPN) over the same period is 9.6°C and mean air temperature is 10.1°C indicating that conditions should be slightly stable on average. Figure 5-24 shows the variation of air and sea temperature and the calculated Monin-Obukhov length over the whole period. At the

beginning of the measurement period, conditions are mainly stable whereas at the end of the period more unstable conditions are indicated.

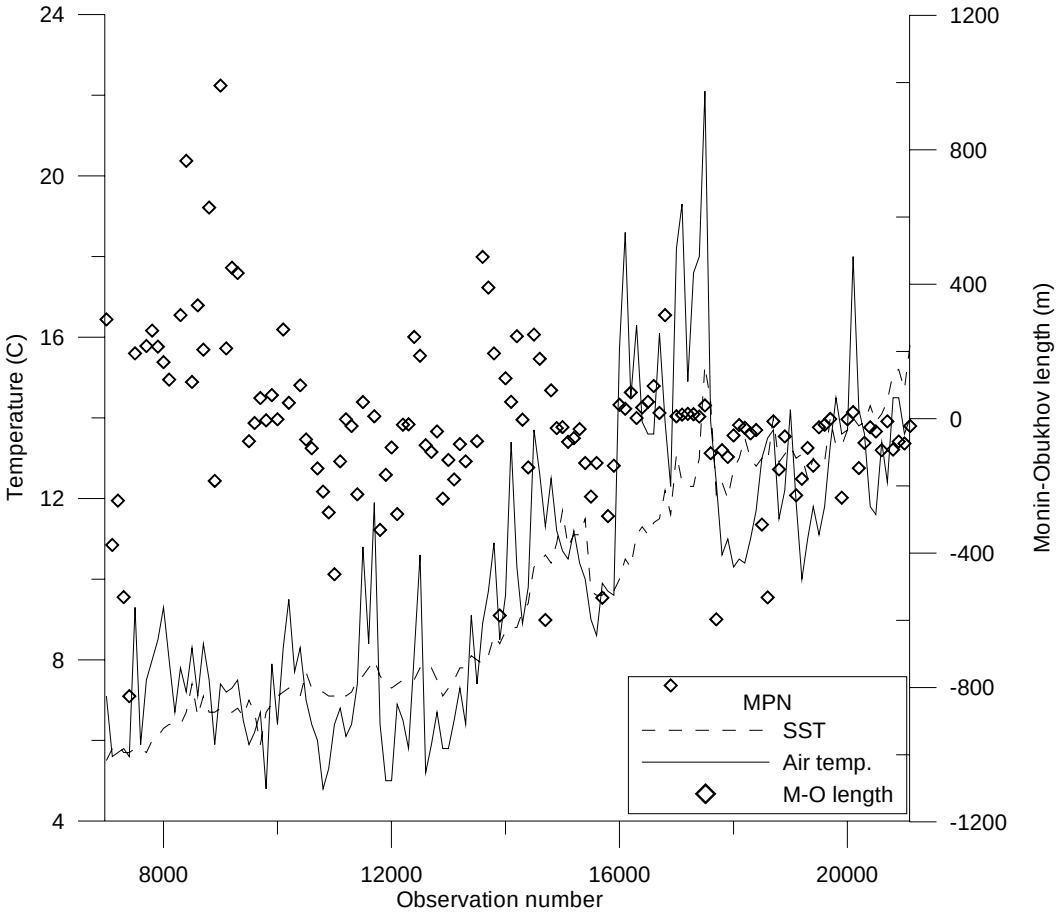

Figure 5-24. Observed air and sea surface temperature (degrees c) at MPN and estimated Monin-Obukhov length from 24 February to June 15 2000.

Figure 5-25 shows the mean wind speed profile observed by the SODAR and the predicted wind speed profile from the CDM. The observations are limited to those periods in which the SODAR collected data at all heights between 20 and 90 m. In the Figures shown below 15 m is added to the SODAR wind speed height to account for the height of the platform. Wind speeds below 55 m are excluded to the distortion of the profile by the measurement platform itself. Predictions were then made for coincident data observations excluding periods with rain. Over-prediction of wind speeds is to be expected due to the procedure used to estimate geostrophic wind speeds. However, the CDM indicates a near-neutral wind speed profile unaffected by the internal boundary layer while the SODAR observations suggest greater wind shear due either to higher roughness or to stability. Note that mean wind speeds above 90m (115 m above sea level) are included although there may be relatively few observations. Under-prediction of wind speed may be a result of predicting wind speeds for the grid square in which MPN lies rather than using actual fetch distances in each sector. In order to examine the impact of fetch, further calculations were conducted by sector (Figure 5-26), again restricting both observed and predicted wind speeds to periods of coincident observations. This reduces the number of observations in each sector. Comparing CDM predicted and SODAR observed wind speed profiles between 55 and 115 m there is considerable variability by sector. The CDM gives good predictions in Sector 1, over-predicts wind speeds in Sectors 3, 4, 5,6 and 7, under-predicts in Sectors 9,10, 11 and 12. In Sectors 2 and 8, the SODAR indicates a profile which is disrupted by thermal structures - possibly a low internal boundary layer. This distribution of over - and under- prediction by sector may indicate a problem with using HVH observations to estimate the geostrophic wind speed. Geostrophic wind speeds from HVH observations with land fetch may be overestimated due to the relatively high friction velocity while those from the sea fetch maybe underestimated due to the low friction velocity over sea. However, one feature which is not solely determined by the geostrophic wind speed is the

wind shear. The observed SODAR wind shear is greater than the CDM predictions in all sectors except 1,3 and 4. This indicates either a much higher roughness than is predicted by the CDM using the Charnock equation, or a greater thermal contribution. This is also suggested by over-prediction of the mast wind speed in these sectors. The second factor is investigated by comparing observed and predicted wind speed profiles in different stability groups.

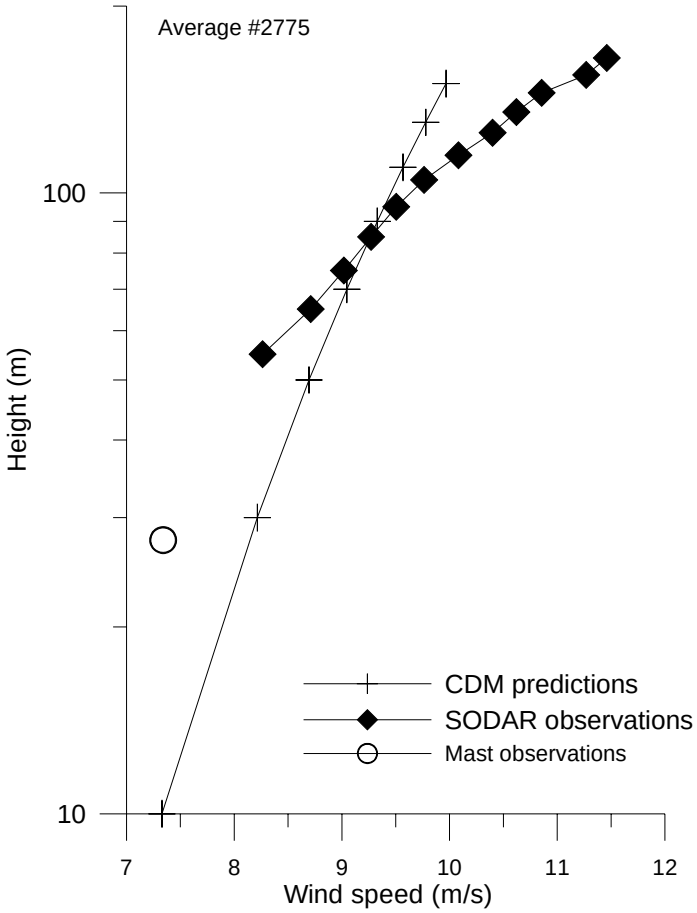

Figure 5-25. Mean wind speed profiles at MPN from the SODAR and predicted by the CDM.

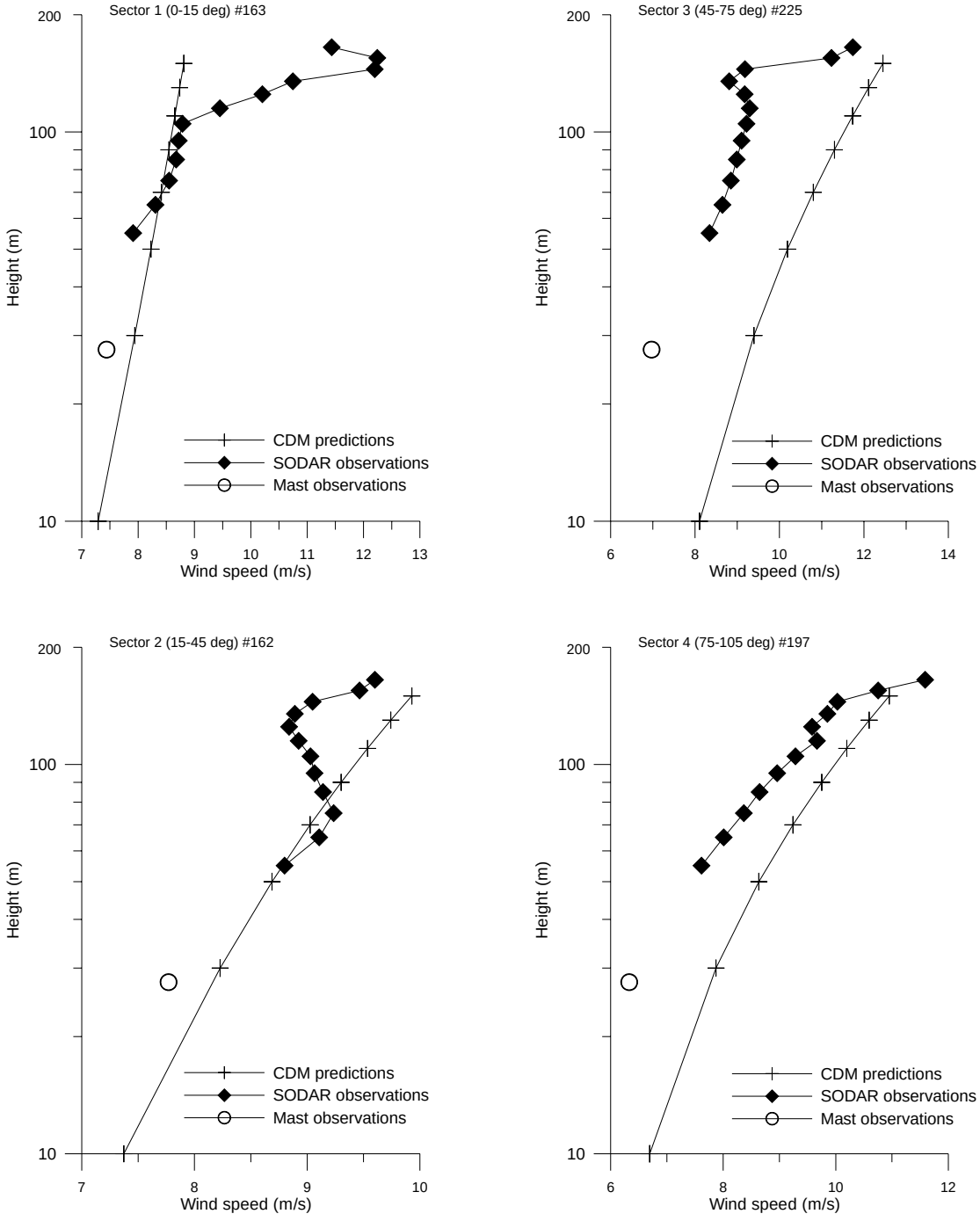

Figure 5-26. ***SODAR observed wind profiles and CDM predictions by sector. Also shown are mean wind speeds from the mast at MPN.***

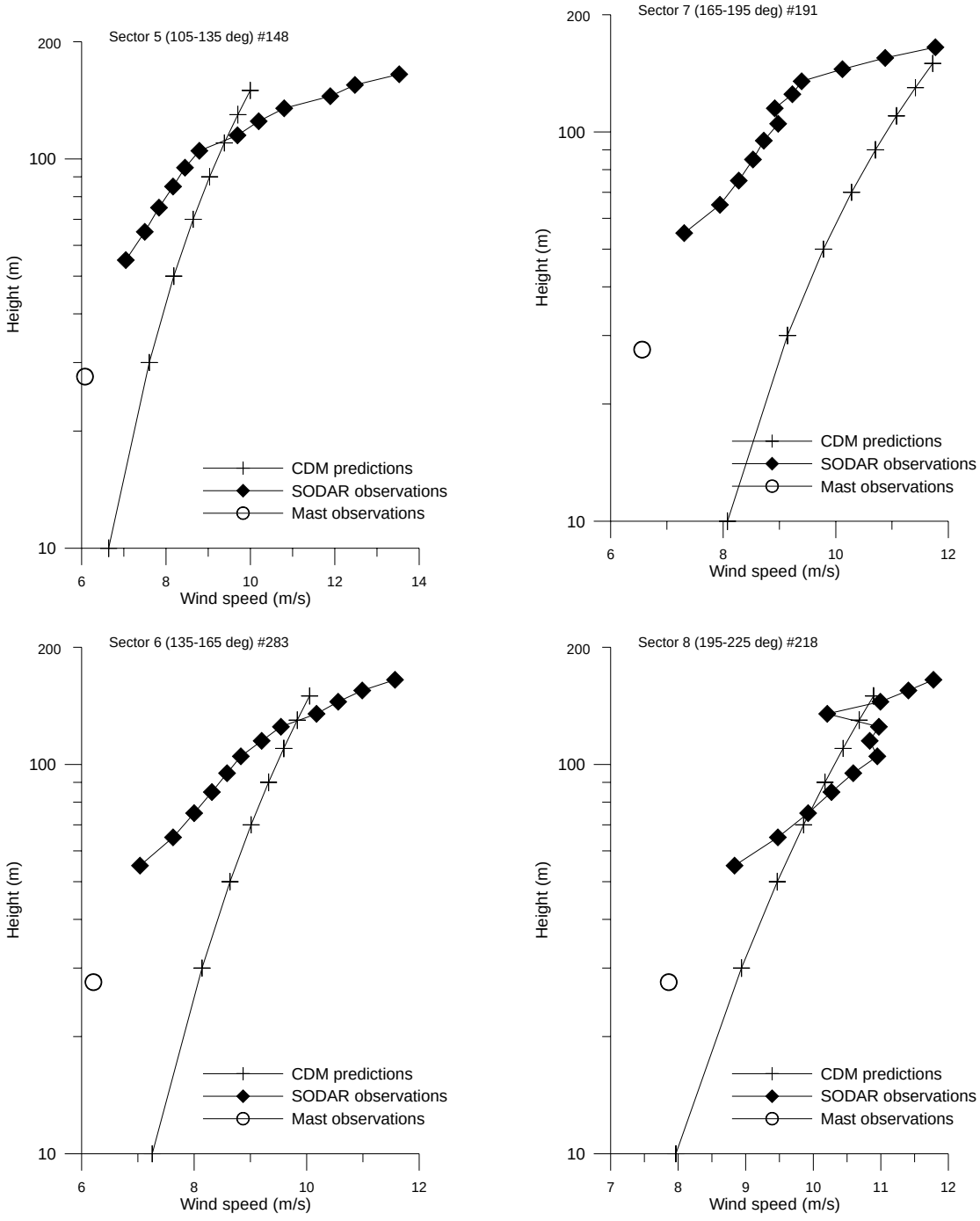

Figure 5-26. ***SODAR observed wind profiles and CDM predictions by sector. Also shown are mean wind speeds from the mast at MPN (continued).***

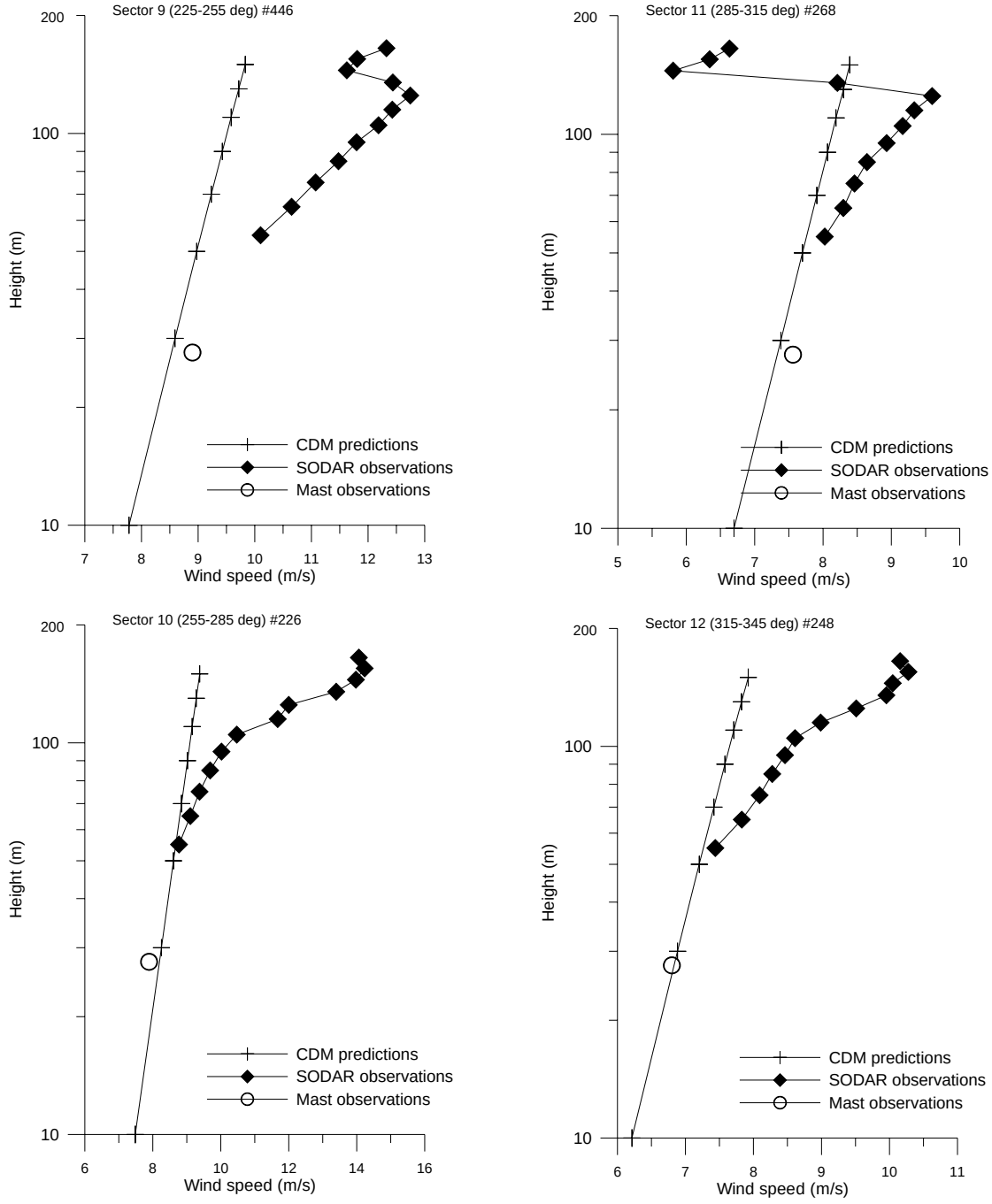

Figure 5-26. SODAR observed wind profiles and CDM predictions by sector. Also shown are mean wind speeds from the mast at MPN (continued).

In terms of stability Table 5-10 shows that the near-neutral class is not very frequent. Observations are divided between stable and unstable classes. Unusually both very stable and very unstable classes have relatively high mean wind speeds indicating a strong temperature profile at MPN.

Table 5-10-. Frequency of different stability classes

Stability class	L	Mean mast wind speed (m/s)	# Obs.	%
Very stable	0-200	6.6	726	26
Stable	200-1000	7.9	509	18
Near-neutral	±1000	7.1	213	8
Unstable	-200- -1000	7.2	326	12
Very unstable	0- -200	5.5	1001	36
Total			2775	100

Figure 5-27 shows the predicted and observed wind speeds in different stability classes. In the stable and very stable classes, the CDM predicts the shape of the profile well in comparison with the observed although the wind speeds are over-predicted in the very stable class. In the neutral and unstable classes the shape of the profile is not well predicted with the SODAR observed wind shear being higher than that predicted. In the Unstable classes the wind speeds are under-predicted in comparison with the observations.

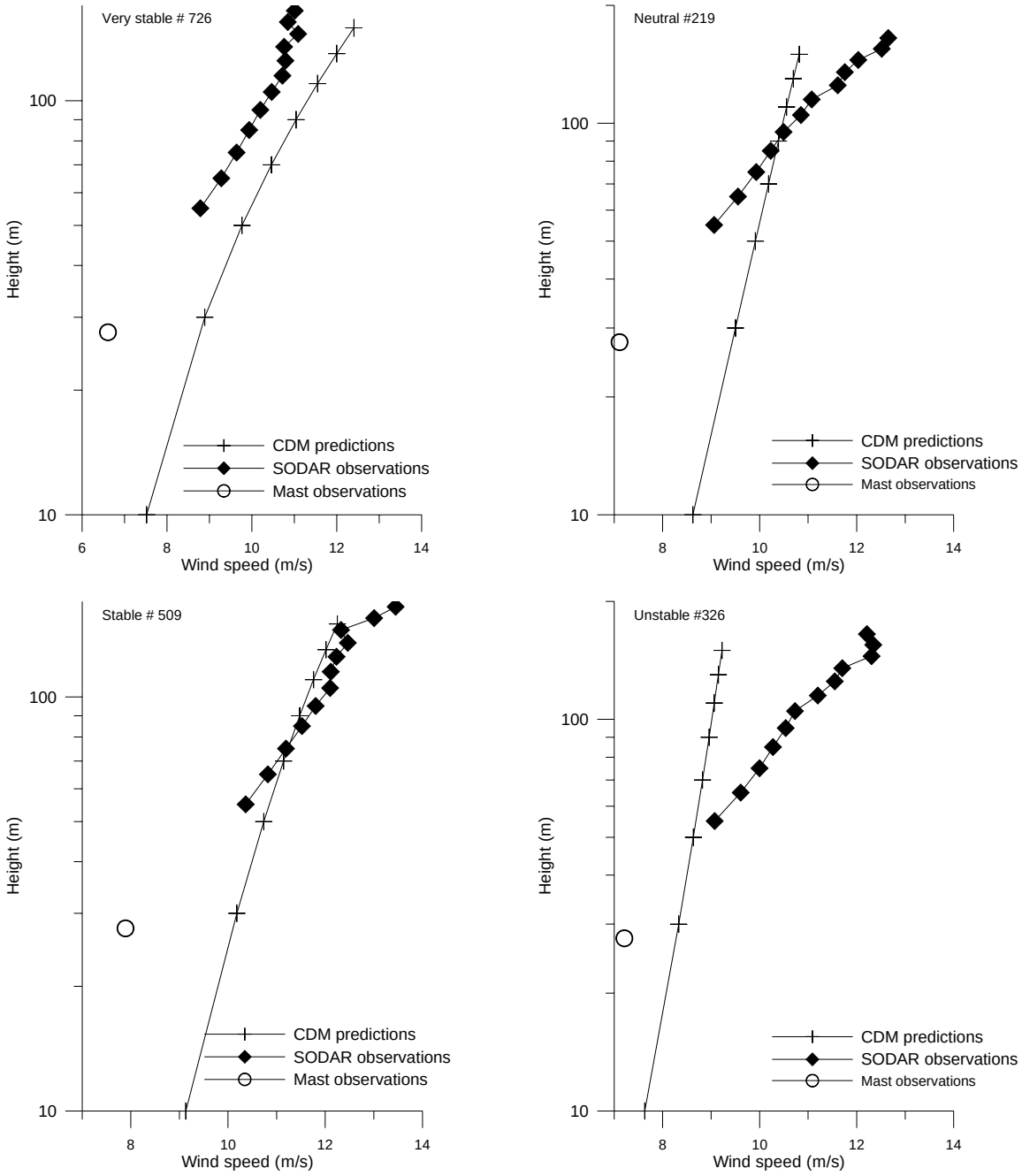

Figure 5-27. SODAR observed wind profiles and CDM predictions by stability class. Also shown are mean wind speeds from the mast at MPN.

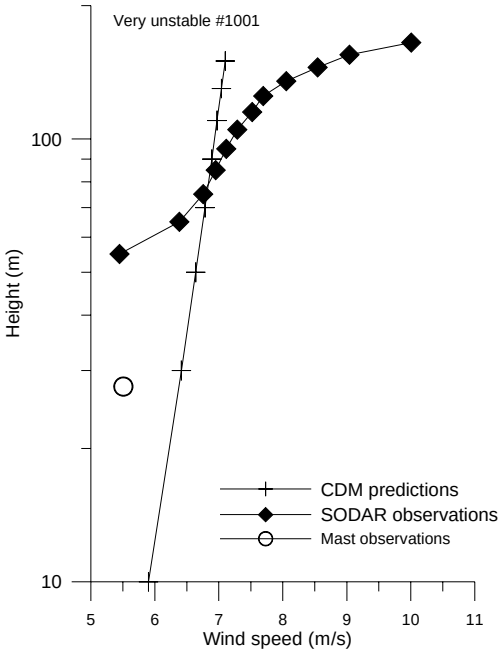

Figure 5-28. SODAR observed wind profiles and CDM predictions by stability class. Also shown are mean wind speeds from the mast at MPN.

Predictions can also be made based on observed wind speeds at Ijmuiden. For the period 24 Feb to 15 June 2001 the mean wind speed at IJmuiden is 6.41 m/s. The wind speed distribution and wind rose are shown in Figure 5-29. The wind direction is predominantly south westerly with components from the east and north east.

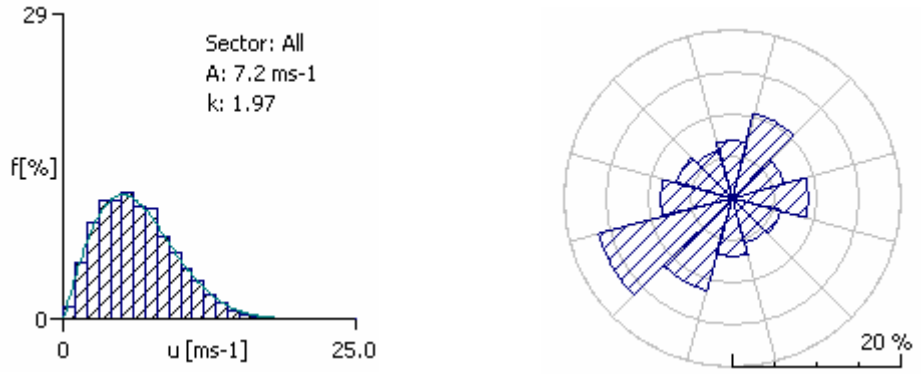

Figure 5-29. Wind speed distribution and wind rose from data at IJmuiden.

Predictions of wind speed at MPN were made using the CDM and data from IJM as outlined above for the period 24 February to 15 June 2000. As shown in Figure 5-30 this gives very similar results to predictions using data from HVH.

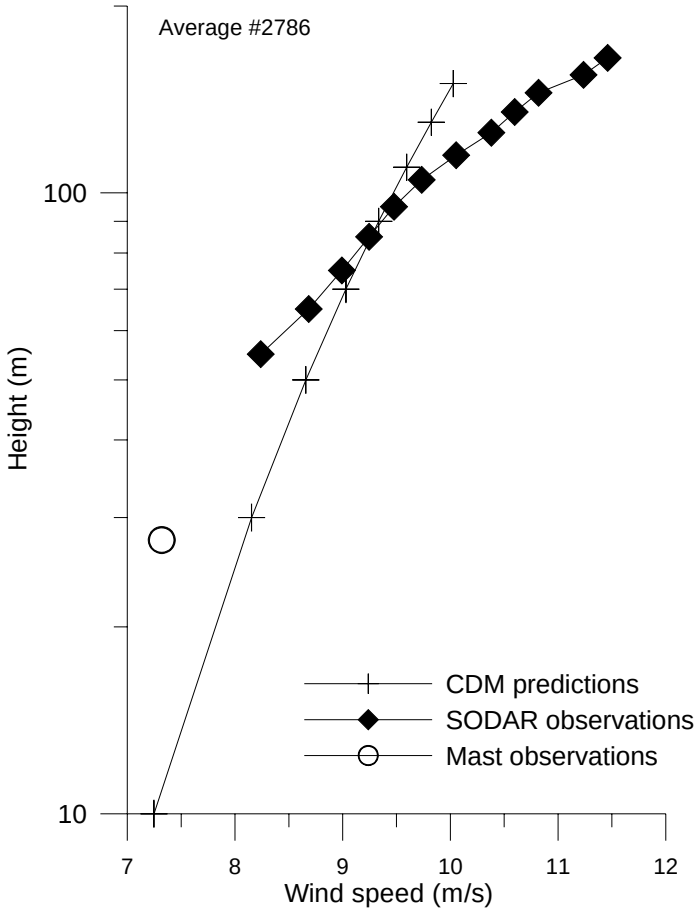

Figure 5-30. CDM predicted wind speeds and SODAR observed wind speeds at MPN.

As the problems in the predictions appear to be associated with the geostrophic predictions from the land sites a new approach was adopted for predictions from IJM, assuming that the site is surrounded by sea except in Sector 5 where the roughness length exceeds 0.002 m (Table 5-9). Predictions using this approach are shown in Figure 5-31. Although the predicted wind speeds are low compared with the SODAR there is good agreement with the mast wind speed. The wind speed profile predicted using the mast wind speeds (using the stability correction) shows the same general form as the CDM predictions. CDM predictions are higher because of the correction from IJM to geostrophic wind speeds. The form of the profile compared with the SODAR observations indicates that it is the thermal correction to the profile which is not correctly estimated using the temperature difference between land and sea. This can arise for a number of reasons - the estimated stability correction is highly sensitive to the temperature profile, here assumed to be the difference between two relatively small numbers. If this difference between two temperature sensors which are not calibrated together is slightly incorrect the stability profile at the site will be distorted. The large frequency of both stable and unstable classes rather than a dominance of one or the other would tend to indicate that this is not a problem so much as the relatively large temperature gradients. Further illustration of the stability classification at the site is given in Figure 5-32. Typically the number of observations in the near-neutral class increase with increasing wind speed. At this site, although the number of observations in the very stable or very unstable classes decrease with increasing wind speed, the number of observations in the near-neutral class does not increase. Figure 5-32 also shows the frequency of different stability classes by direction. Directions associated with a relatively short sea fetch have very few observations classified as neutral, with observations divided into the very unstable or very stable classes. This seems to reflect the influence of land at the site, giving large temperature gradients which are classified into the ‘extreme’ classes.

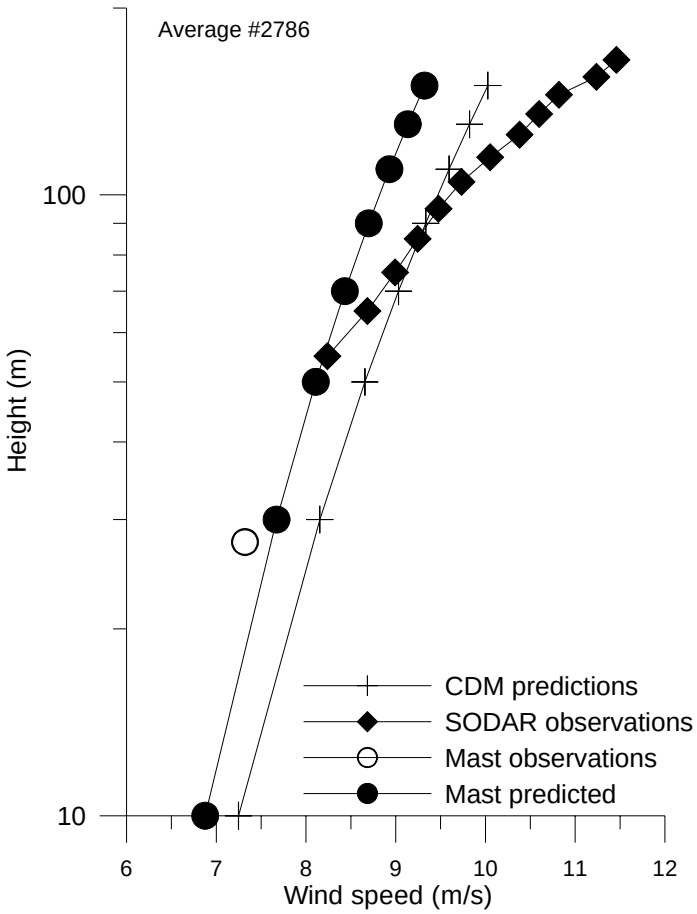

Figure 5-31. CDM predictions assuming IJM is an offshore site with only one land sector (sector 5).

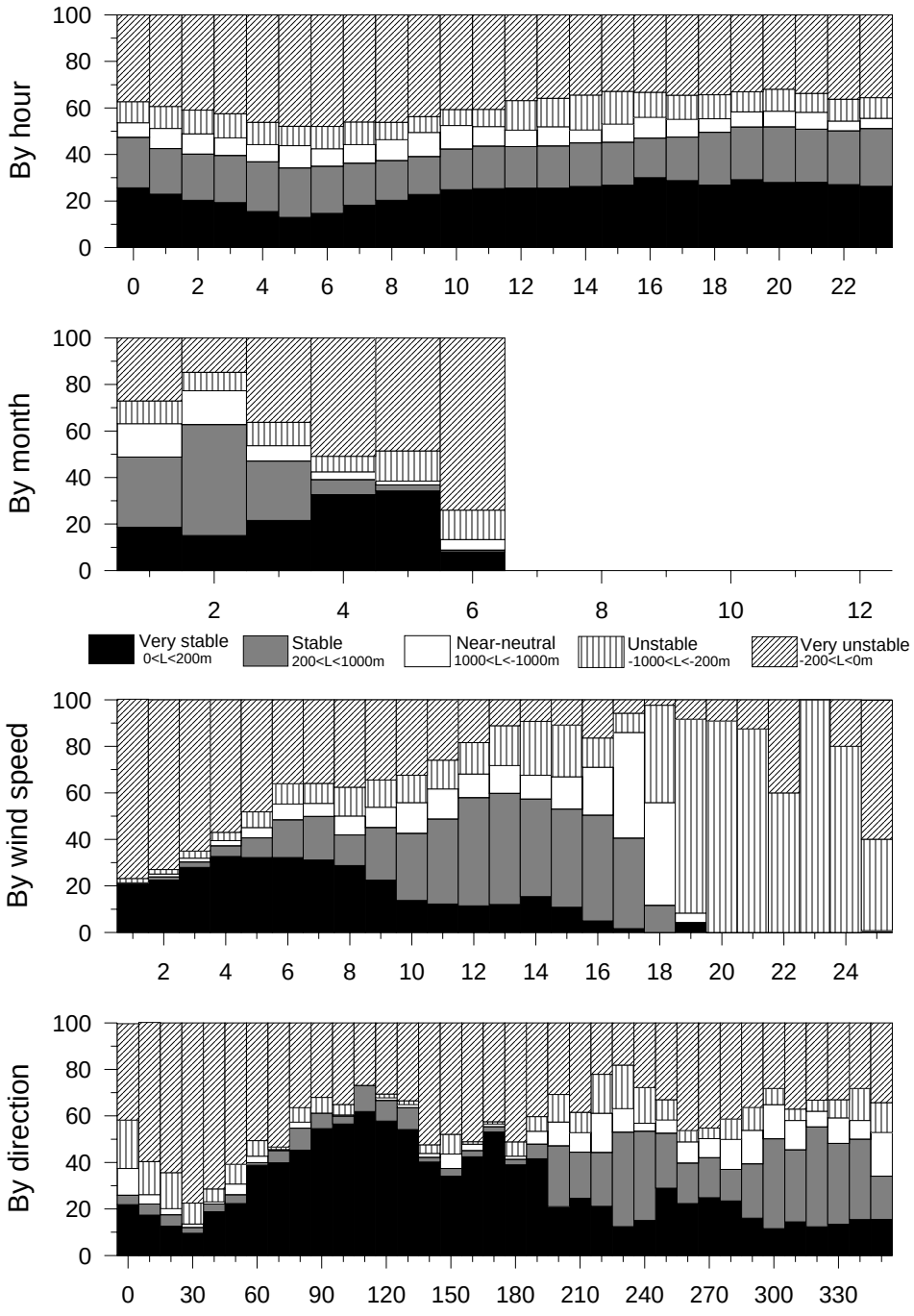

Figure 5-32. Classification of stability by hour, by month, by wind speed and by direction at MPN.

A comparison has been made between wind speed profiles observed by SODAR at MPN off the coast of the Netherlands and predictions using a coastal model (CDM) which accounts for stability variations in each observation. The CDM gives a good prediction of mean wind speeds at about 100 m height but over-predicts wind speeds below this height and under-predicts wind speeds at greater heights. Differences between the predictions and the observations are ascribed to two factors. Over-prediction of geostrophic wind speeds from land-based observations in sectors which have land fetch and greater wind shear than expected assuming a sea surface roughness of about 0.0002 m. Under-prediction of wind shear is ascribed to the stability definitions at the site which suggest that near-neutral conditions are comparatively infrequent while very stable and very unstable conditions dominate the observations.

5.4.3 Comparison of modelled and measured offshore wind speed profiles

Evaluation and comparison of the GEO-WASP, GEO-CDM and WASP-CDM focuses on offshore data collected at sites in Denmark (Figure 5-33). The data are collected on purpose-built meteorological masts offshore and are high quality wind speed profile data from a period of at least two years (except at Horns Rev and Læsø when one years data are available). The data record at Vindeby is the longest and most complete (over 91,000 observations) while that at Middelgrunden is the shortest (just over 21,000 records).

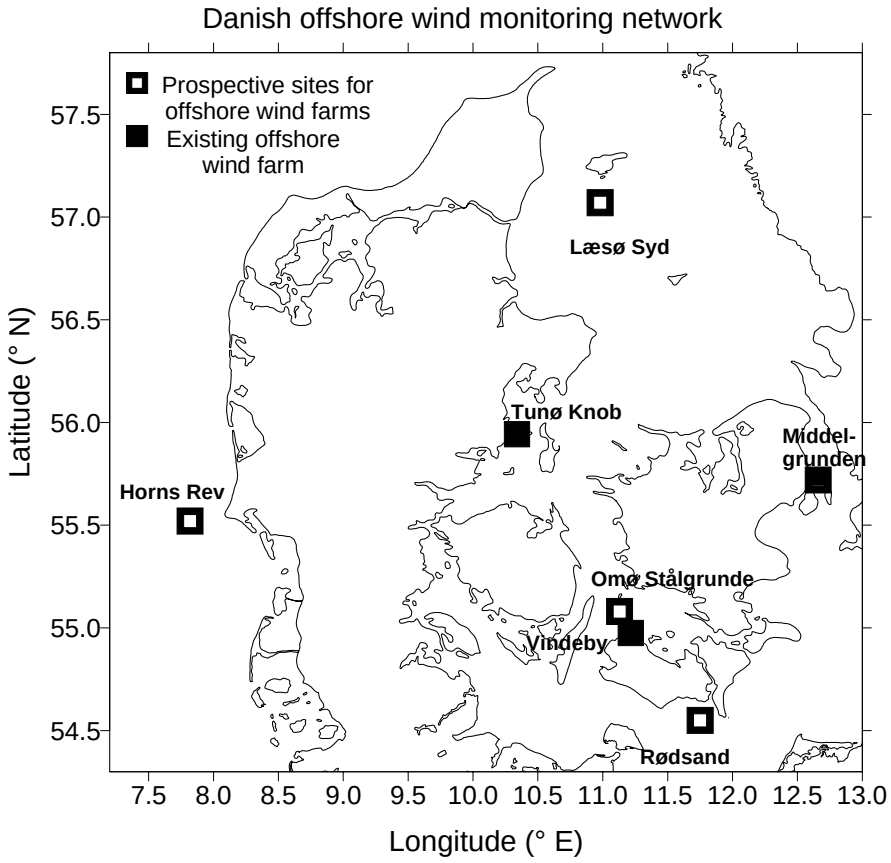

Figure 5.33. Danish Offshore Wind Monitoring Network

Editorial note : Unfortunately the analysis reported in the following section can not be published as the data was obtained under a non-disclosure agreement. The section and its associated figures 5.34-5.40 has been deleted from this PDF version.

5.5 Conclusions

The CDM and WAsP have been applied to the waters of the European Union based on geostrophic wind speeds and have been found to give reasonable predictions in comparison with mast and platform data. Typically all three methods evaluated (GEO-WASP, GEO-CDM and WASP-CDM) overpredict wind speeds in comparison with those observed.

Applying the CDM to WASP predicted wind speeds does not improve the predictions at all sites. The main reason for this is that a mean stability correction has to be applied to the wind speed distribution predicted by WAsP and this is not sufficiently accurate. Instead a time series of corrections should be calculated and applied prior to summarising the wind statistics.

The major problem with applying all three models appears to be with the spatial resolution and the calculation of the stability correction. The initial data sets are supplied on 0.5 by 0.5 ° grid whereas it is known that mean offshore wind speeds vary on scales of about 0.5 km in coastal regions. The CDM and WAsP applied at the 0.5 by 0.5 ° grid scale are unable to resolve complex coastlines (such as those around Denmark). Applying the same techniques with an improved coastline resolution would improve the predictions. In addition the use of air temperatures from mixed land/sea grid cells may not provide an accurate determination of stability, particularly when combined with a sea surface temperature data base from different sources. As noted above errors in the databases are of the same order as the temperature difference which is used to calculate the stability parameter. However to improve the stability correction is more difficult since a) currently sea surface and air temperatures are not available at better than 0.5 by 0.5° grid resolution and b) a more precise estimate of stability requires either direct flux measurements or a measured temperature difference.

5.6 References for Chapter 5

Barthelmie, R.J., 1999a: *Development of the Coastal Discontinuity Model*, Risoe National Laboratory, Roskilde.

Barthelmie, R.J., 1999b: The effects of atmospheric stability on coastal wind climates. *Meteorological Applications*, **6(1)**, 39-48.

Barthelmie, R.J. 2002: Evaluating the impact of wind induced roughness change and tidal range on extrapolation of offshore vertical wind speed profiles. *Wind Energy* (in press).

Barthelmie, R.J., Courtney, M.S., Højstrup, J. and Larsen, S.E., 1996a: Meteorological aspects of offshore wind energy - observations from the Vindeby wind farm. *Journal of Wind Engineering and Industrial Aerodynamics*, **62(2-3)**, 191-211.

Barthelmie, R.J., Courtney, M.S., Højstrup, J. and Sanderhoff, P., 1994: *The Vindeby Project: a description*. Risø-R-741(EN), Risø National Laboratory, Denmark.

Barthelmie, R.J., Grisogono, B. and Pryor, S.C., 1996b: Observations and simulations of diurnal cycles of near-surface wind speeds over land and sea. *Journal of Geophysical Research (Atmospheres)*, **101(D16)**, 21,327-21,337.

Barthelmie, R.J., Lange, B. and Nielsen, M., 1999*: Wind resources at Rødsand and Omø Stålgrunde.* Risø-I-1456(EN), Risø National Laboratory, Roskilde.

Barthelmie, R.J. and Palutikof, J.P., 1996: Predicting offshore wind speeds in coastal regions suitable for wind energy. *Journal of Wind Engineering and Industrial Aerodynamics*, **62(2-3)**, 213-236.

Beljaars, A.C.M., Holtslag, A.A.M. and van Westrhenen, R.M., 1989: Description of a software library for the calculation of surface fluxes. Technical report TR-112, KNMI, De Bilt, Netherlands.

Bergstrom, H., Johansson, P.-E. and Smedman, A.-S., 1988: A study of wind speed modification and internal boundary-layer heights in a coastal region. Boundary-Layer Meteorology, 42(4), 313-335.

Charnock, H., 1955: Wind stress on a water surface. *Quarterly Journal of the Royal Meteorological Society*, **81**, 639-640.

Coelingh, J., Folkerts, L., Wiegerinck, G. and van Zuylen, E., 2000: Study of the offshore wind climate using a SODAR, Offshore Wind Energy in Mediterranean and other European Seas. ATENA, Rome, Sicily, April 2000, pp. 61-70.

Coelingh, J.P., van Wijk, A.J.M. and Holtslag, A.A.M., 1996: Analysis of wind speed observations over the North Sea. *Journal of Wind Engineering and Industrial Aerodynamics*, **61**, 51.

Coelingh, J.P., van Wijk, A.J.M. and Holtslag, A.A.M., 1998: Analysis of wind speed observations over the North Sea coast. *Journal of Wind Engineering and Industrial Aerodynamics*, **73**, 125-144.

Donelan, M.A., Dobson, F.W., Smith, S.D. and Anderson, R.J., 1993: On the dependence of sea surface roughness on wave development. *Journal of Physical Oceanography*, **23(9)**, 2143-2149.

Garratt, J., 1977: Review of drag coefficients over oceans and continents. *Monthly Weather Review*, **105**, 915-929.

Garratt, J.R. and Ryan, B.F., 1989: The structure of the stably stratified internal boundary layer in offshore flow over the sea. *Boundary-Layer Meteorology*, **47(1-4)**, 17-40.

Geernaert, G., Katsaros, K. and Richter, K., 1986: Variation of the drag coefficient and its dependence on sea state. *Journal of Geophysical Research*, **91(C6)**, 7667-7679.

Johnson, H.K., Højstrup, J., Vested, J. and Larsen, S.E., 1997: On the dependence of sea surface roughness on wind waves. *Journal of Physical Oceanography*, **28**, 1702-1716.

Kitaigorodsky, S.A. and Zislavsky, M.M., 1974: A dynamical analysis of the drag coefficients at the sea surface. *Boundary-Layer Meteorology*, **6**, 53-61.

Mahrt, L., Vickers, D., Howell, J., Hojstrup, J., Wilczak, J., Edson, J. and Hare, J., 1996: Sea surface drag coefficients in RASEX. *Journal of Geophysical Research*, **101**, 14,327-14,335.

Mortensen, N.G., Landberg, L., Troen, I. and Petersen, E.L., 1993*: Wind Analysis and Application Program (WASP)*. Risø-I-666 (EN)., Risø National Laboratory, Roskilde, Denmark.

Nordeng, T.E., 1991: On the wave age dependent drag coefficient and roughness length at sea. *Journal of Geophysical Research*, **96**, 7167-7174.

Panofsky, H.A., 1973: Tower micrometeorology. In: D.A. Haugen (Editor), Workshop on micrometerology. American Meteorological Society, Boston, MA, pp. 151-176.

Pryor, S.C. and Barthelmie, R.J., 1998: Analysis of the effect of the coastal discontinuity on near-surface flow. *Annales Geophysicae*, **16**, 882-888.

Smedman, A.-S., Bergstrom, H. and Grisogono, B., 1997: Evolution of stable internal boundary layers over a cold sea. *Journal of Geophysical Research*, **102(C1)**, 1091-1099.

Smedman, A.S., Hogstrom, U. and Bergstrom, H., 1996: Low level jets - a decisive factor for off-shore wind energy siting in the Baltic Sea. *Wind Engineering*, **20(3)**, 137-147.

Smith, S.D., 1988: Coefficients for sea surface wind stress, heat flux, and wind profiles as a function of wind speed and temperature. *Journal of Geophysical Research*, **93(C12)**, 15467-15472.

Stull, R.B., 1988: *An introduction to boundary layer meteorology*. Kluwer Publications Ltd, Dordrecht, 666 pp.

Troen, I. and Petersen, E.L., 1989: *European Wind Atlas*. Risø National Laboratory, Roskilde, Denmark, 656 pp.

Van Wijk, A.J.M., Beljaars, A.C.M., Holtslag, A.A.M. and Turkenburg, W.C., 1990a: Diabatic wind speed profiles in coastal regions: comparison of an internal boundary layer (IBL) model with observations. *Boundary-Layer Meteorology*, **51**, 49-75.

Van Wijk, A.J.M., Beljaars, A.C.M., Holtslag, A.A.M. and Turkenburg, W.C., 1990b: Evaluation of stability corrections in wind speed profiles over the North Sea. *Journal of Wind Engineering and Industrial Aerodynamics*, **33**, 551-566.

Wieringa, J., 1986: Roughness-dependent geographical interpolation of surface wind speed averages. *Quarterly Journal of the Royal Meteorological Society*, **112(473)**, 867-889

CHAPTER 6 : SODAR Measurements

Chapter authors:

Sections 6.1-6.6 : Drs. J.P. Coelingh, Dr. L. Folkerts, Dr. E.J. van Zuylen, Ir. G.F.M. Wiegerinck (Ecofys)
Sections 6.7 : Dr T Holt and Dr J P Palutikof (University of East Anglia)

6.1 Introduction to SODAR

Wind turbine technology has developed very rapidly over the past 20 years. One of the eye-catching consequences is the enormous increase in size of wind turbines. E.g., in Germany the *average* rated power per wind turbine installed in the year 2000 is nearly 1 MW. The hub height of MW-size wind turbines ranges from 70 to over 100 m, with rotor diameters ranging from about 65 m to 80 m. For design specifications there is a need to know the wind characteristics over the whole rotor diameter. Upscaling the wind turbines this corresponds to the layer between 60 m and 140 m. However, the costs of erecting a wind measurement mast of sizes over 30–40 m increase progressively with height, so the need for cheaper measurement techniques starts to arise. A very promising alternative for mast measurements is by making use of a (mini–)SODAR. This has been explored within the POWER-project to study the wind characteristics of the coastal zone. Some of the preliminary results have been reported [Coelingh et al. (1999)] and [Coelingh et al. (2000)]. The basic measurement principle of the SODAR will be explained in the next paragraph (for an overview also see [Crescenti, G.H.(1997)]).

6.2 Basic description of SODAR measurement principle

The acronym SODAR means **SO**und **D**etecting **A**nd **R**anging. In the case of the Aerovironment 4000, the basic principle is as follows (although. slightly different techniques are sometimes being used by other manufacturers) : A sound beam is emitted in an upward direction. Part of the signal is reflected off temperature inhomogeneities in the air. The reflected signal is then detected again by a microphone. The duration between emission and detection is indicative for the vertical distance (height) the reflected signal represents (as we know the speed of sound). The Doppler shift of the signal is a measure for the wind speed. Because one cycle consists of three beams under angles of 16° a three dimensional vector is being measured. The signal is then decomposed into the two horizontal directions and the vertical. The working frequency of the signal can be set by the user, but is usually 4500 Hz. The sampling frequency is about 1 Hz, so one cycle of three beams takes about a period of 3 s.

6.3 Features of SODAR measurements

SODAR can be used to measure the component of the wind speed in the direction of the sound beam, and thus is a wind measurement device with several distinctive advantages over conventional cup anemometry. First, it is easy to install and does not require any permits. Apart from the sound produced by the outgoing pulse no hindrance is being posed by a SODAR. The only requirements are a flat and stable surface, power supply (either by connection to the grid or a stand alone system with batteries), and (optional) a telephone connection for remote operation (either by a cable or by GSM).

Depending on the specifications of the different models from several manufacturers (mini-)SODARs can measure wind speeds up to several hundreds of meters, with a vertical resolution of 5 to 20 m and a minimum height of 10 to 30 m. The distinction between a mini-SODAR and a SODAR is the working range: a SODAR works up to the region of a km, with a resolution of hundreds of meters. They have been in use for a long period near air fields and nuclear plants. Their main function is to monitor the wind characteristics in the upper air (compared to near the surface) for either ascending and descending aeroplanes or the dispersion of plumes of nuclear material in case of accidents.

In recent years the specifications have been adapted to suit e.g. the wind energy industry with higher vertical resolutions and a lower maximum height (higher than 200 m is hardly of interest for wind energy purposes anymore). Experiences with mini-SODARs, particularly for wind energy purposes, are scarce, but increasing fast. Generally, two types of applications are of interest: one is for wind turbine manufacturers, the other is for wind project developers. The first group needs to make measurements on operating wind turbines, the second group also as part of site assessment.

The costs of operating a SODAR are mainly capital costs and labour costs for installation and removal, and also for data analysis. In contrast, costs for anemometer mast are also costs for equipment to install and remove (high) masts from a site.

Depending on the manufacturer and the model, SODARs may weigh in the order of 100 kg, and can easily be transported in a van and installed by hand by a few people within hours.

The disadvantages of a SODAR are that it is not possible to calibrate them as cup anemometers. It is not possible to put a SODAR in a wind tunnel and thus obtain a calibration curve. However, as experience is being gained with this relatively new technique more and more evidence from field experiments become available with which the results increase in quality.

6.4 Description of Aerovironment 4000

The Aerovironment 4000 mini-SODAR as used in this project is a phased-array type system. Its default operating frequency is 4500 Hz, corresponding to a wave length of about 8 cm. Several parameters can be adjusted by the user, and need to be optimised for the specific experimental conditions. E.g., the averaging time was set to 10 minutes, the vertical resolution to 5 m and the maximum height range to 200 m. The minimum height is 15 m.
The system consists of an acoustic antenna, an Acoustic Signal Processor (ASP), and a computer for data storage. By using a (GSM-)modem data can be transferred to enable remote control operation.
To shield the signals from ambient noise and to increase the signal-to-noise-ratio the an encasing is present, which extends to over 2 m by the hinging cuffs.

6.5 SODAR measurement campaigns

Within the POWER project three sets of SODAR measurements were performed:

- *SODAR trials at Petten (The Netherlands).*
  Equipment trials were carried out by staff from Ecofys in collaboration with ECN and gave the project staff valuable experience in setting up the SODAR system and performing the mesaurements as well as enabling them to set up quality control and analysis systems for the observations. Full details are available in a separate report [Dam, J.J.D. van and E.J. van Werkhoven (1999)].
- *Measuring Post Noordwijk (9km off the coast of The Netherlands)*
  These are the measurements used to help validate the Coastal Discontinuity Model (see Chapter 5). This work was performed by Ecofys staff and is described in Section 6.6.
- *Weybourne (UK)*
  SODAR data was measured at a coastal site in eastern England by staff from UEA. This work is reported in Section 6.7

6.6 SODAR measurements at Measuring Post Noordwijk (MPN)

6.6.1 Introduction

The location MPN is an offshore platform located 9 km off the Dutch coast (see Figure 6-1). The platform is owned and operated by the Public Works Department (Rijkwaterstaat), Directie Noordzee. Permission was obtained to set up the SODAR at MPN, which was installed in January 2000.

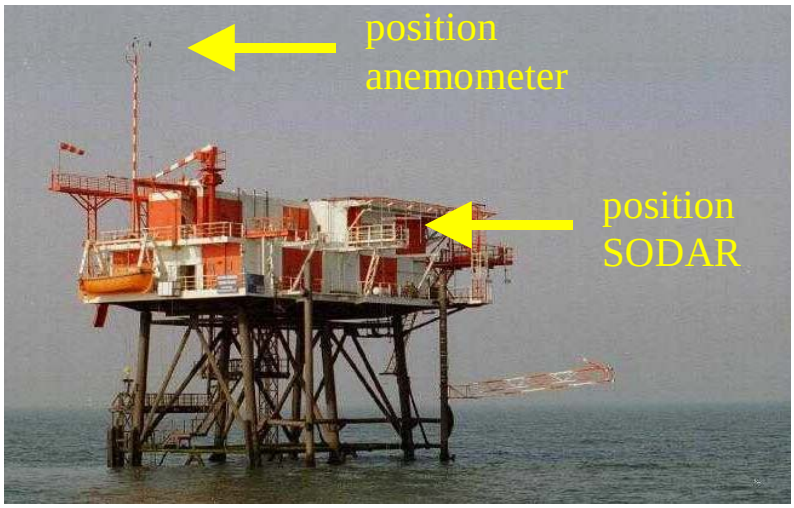

Figure 6-1: MPN platform located in the North Sea 9 km off the coast; the positions of the anemometer and of the SODAR (not installed yet) have been indicated (photograph courtesy of OCN, Delft, The Netherlands).

.

After initial measurements without the cuffs (see Figure 6-2), on February 23 2000 the measurements were started that were of suitable quality. The end date was June 15 2000, so about 4 months of observed data have been gathered for the validation of the CDM.

Figure 6-2: SODAR located at MPN as seen from below (without cuffs).

Figure 6-3: SODAR located at MPN as seen from above (with cuffs).

The SODAR is situated at a small platform about 15 m above MSL, which is at the level 3 m below the helicopter platform (for illustration see Figure 6-3and Figure 6-4). This is not ideal due to possible acoustic reflections, and flow distortion by the build-up of the platform itself. However, suitable locations are restricted at the platform so there was no alternative available.

Figure 6-4: SODAR located at MPN as seen from the side (with cuffs).

6.6.2 Data processing and software

For each averaging period, the SODAR software (Doplmain) produces a so-called wind table. This is a standard output file that forms the basis for further analysis and will be explained further.. For data analysis purposes, a vector with (wind speed) data is far more desirable than the wind table format. The supplier of the SODAR provides a computer programme called PADS that is able to convert wind tables to time series to be described in further detail. As this software tool did not fulfil our requirements, we decided to build a conversion software tool ourselves. Before building such a tool, the output has to be understood completely. In the final section , the features of the developed software package are described.

Wind tables

An example of a wind table produced by the SODAR software is shown in Figure 6-5. The header of the wind table contains information on date and time of the observation period and it shows the actual parameter settings of the SODAR. The meaning of each setting is given in the Doplmain manual [Aeronvironment (1998)].. Below the header, a matrix is printed. Each line gives information about one specific height including the horizontal wind speed and direction, the wind speeds split in three orthogonal directions (*u* and *v* in the horizontal plane, *w* the vertical direction), the number of measurements per component, the intensity of the returned signal, the signal-to-noise ratio per component and the observed gust wind speed and direction. After each day all wind tables are written to a text file (*yymmdd*dv.dat) on the PC connected to the ASP.

```
MPN      06/13/2000 17:30:04 TO 06/13/2000 17:40:03 VR4.56  4500   800   100    50    10     0     0
600 5 10 7 -120 0 10 1 64 960 6 5 3 -1200 1200 -1200 1200 -600 600 1 10 0 500 68 1 40 0 -1 2 0 10 2
3 COMPONENT 39HTS ZENITH 16-16 ARA 000 SEPANG 090 MXHT    40 UNOISE   127 VNOISE   220 WNOISE   143 ANTENNA STATUS:   OK AC
STATUS:   OFF
  HT    SPD  DIR      W    SDW   IW   GSPD GDIR      U    SDU   NU   IU SNRU      V    SDV   NV   IV SNRV   NW SNRW
 200  99.99 9999  99.99  99.99   15  99.99 9999  99.99  99.99    0   13    2  99.99  99.99    0   23    3    0    2
 195  99.99 9999  99.99  99.99   15  99.99 9999  99.99  99.99    0   12    2  99.99  99.99    0   23    3    0    2
 190  99.99 9999  99.99  99.99   14  99.99 9999  99.99  99.99    0   12    3  99.99  99.99    0   22    3    0    2
 185  99.99 9999  99.99  99.99   14  99.99 9999  99.99  99.99    0   12    3  99.99  99.99    0   22    3    0    2
 180  99.99 9999  99.99  99.99   14  99.99 9999  99.99  99.99    0   12    3  99.99  99.99    0   21    3    0    2
 175  99.99 9999  99.99  99.99   13  99.99 9999  99.99  99.99    0   11    3  99.99  99.99    0   21    3    0    2
 170  99.99 9999  99.99  99.99   13  99.99 9999  99.99  99.99    0   11    3  99.99  99.99    0   20    3    0    2
 165  99.99 9999  99.99  99.99   13  99.99 9999  99.99  99.99    0   11    3  99.99  99.99    0   19    3    0    2
 160  99.99 9999  99.99  99.99   12  99.99 9999  99.99  99.99    0   10    3  99.99  99.99    0   19    3    0    2
 155  99.99 9999  99.99  99.99   12  99.99 9999  99.99  99.99    0   10    2  99.99  99.99    0   18    3    0    2
 150  99.99 9999  99.99  99.99   11  99.99 9999  99.99  99.99    0   10    3  99.99  99.99    0   18    3    0    2
 145  99.99 9999  99.99  99.99   11  99.99 9999  99.99  99.99    0    9    2  99.99  99.99    0   17    3    0    2
 140  99.99 9999  99.99  99.99   11  99.99 9999  99.99  99.99    0    9    3  99.99  99.99    0   17    3    1    2
 135  99.99 9999  99.99  99.99   11  99.99 9999  99.99  99.99    2   10    3   5.57   0.25    4   17    3    1    2
 130  12.79  247  99.99  99.99   13  13.04  246  11.74   0.47    6   11    3   5.08   0.40    8   19    3    3    3
 125  12.14  246   0.04   0.37   19  14.62  239  11.09   0.45   25   15    4   4.95   0.56   23   24    4   25    4
 120  12.50  248  -0.16   0.32   28  15.80  244  11.55   0.45   58   22    6   4.78   0.37   37   28    5   54    6
 115  11.75  248  -0.08   0.36   38  15.24  242  10.88   0.45   74   30    8   4.45   0.33   61   37    7   82    8
 110  11.53  246  -0.07   0.39   49  17.92  232  10.53   0.37  113   40   10   4.69   0.35   83   44    8  113   10
 105  11.06  245  -0.06   0.37   54  14.58  238  10.04   0.38  123   45   12   4.64   0.38   97   47    8  121   11
 100  10.90  246  -0.10   0.36   53  14.96  246   9.96   0.37  136   45   12   4.42   0.39  100   46    9  120   11
  95  10.72  245  -0.09   0.35   47  14.17  228   9.75   0.39  137   41   12   4.45   0.36   95   42    8  125   11
  90  10.30  245  -0.10   0.36   41  14.53  249   9.36   0.37  134   38   12   4.31   0.33   91   36    8  130   11
  85   9.92  245  -0.12   0.36   37  14.41  236   9.00   0.36  132   34   12   4.17   0.33   79   30    7  128   10
  80   9.63  248  -0.11   0.31   31  14.12  236   8.93   0.35  127   30   11   3.61   0.31   74   27    7  114   10
  75   9.78  245  -0.11   0.30   30  13.55  235   8.85   0.34  129   28   11   4.16   0.36   87   27    8  115   10
  70   9.45  246  -0.06   0.35   28  14.25  243   8.61   0.35  124   25   11   3.89   0.35   79   25    7  119   10
  65   9.28  245  -0.07   0.34   25  14.28  243   8.43   0.35  116   23   11   3.87   0.36   80   23    7  119   10
  60   9.09  246  -0.04   0.33   22  12.75  246   8.29   0.35  125   21   11   3.74   0.32   73   21    7  110    9
  55   8.88  245  -0.05   0.34   20  12.78  233   8.04   0.31  128   19   11   3.76   0.38   72   20    8  105    9
  50   8.82  245  -0.07   0.35   19  13.11  248   8.03   0.35  125   17   10   3.66   0.34   71   18    7  105    9
  45   8.67  246  -0.05   0.37   17  12.31  233   7.92   0.37  125   16   11   3.53   0.35   76   15    7  113   10
  40   8.35  248   0.00   0.32   16  11.80  264   7.77   0.38  131   15   11   3.07   0.35   83   15    8  117   10
  35   7.92  254   0.00   0.32   16  16.47  220   7.62   0.36  141   13   12   2.17   0.46  119   17    9  136   11
  30   7.40  262   0.03   0.27   18  10.83  254   7.33   0.39  140   13   12   1.04   0.32  144   23   13  146   14
  25   7.45  261  -0.17   0.23   22  10.62  249   7.35   0.41  139   13   13   1.20   0.41  149   27   13  149   15
  20   7.67  260  -0.42   0.31   33  10.49  254   7.56   0.44  145   14   13   1.29   0.29  145   37   12  150   14
  15   5.54  274  -0.23   0.29   52  10.77  270   5.53   0.50  120   20   11  -0.40   0.55  133   45   11  143   15
  10  99.99 9999  99.99  99.99  128  99.99 9999  99.99  99.99    2  110    4  -2.83   0.13  151  200   10    0    3
```

Figure 6-5: Example of a wind table as produced by the Doplmain SODAR software.

PADS

The Profiler Analysis and Display Software tool PADS is a custom made computer programme provided by the manufacturer Aerovironment that is able to convert wind tables to time series and perform some offline processing. Ecofys obtained a version of PADS in order to evaluate its performance regarding capabilities, user-friendliness. All of PADS' exporting features provide a time series of wind speeds and some user defined other quantities (like vertical wind speed, standard deviation per beam etc.). The programme can also display some typical output like

time series, wind profiles, histograms and wind roses graphically**.** Unfortunately, no clear description of the method of conversion is given in the manual of the software [Aeronvironment (1998a)]. Therefore it is unclear for which criteria data points were (in)validated and it was not possible to reproduce all of PADS calculated mean wind speeds. Apart from this, the version of the programme as made available to us was not very user friendly, rather slow and unstable. For these reasons, it was decided not to use PADS but to develop a specific software tool for our purposes. In this way, there is exact control over the offline processing method and adaptations can be made to preference. Besides, it is possible to define the format of the output (time series) and make it flexible. Such a flexible output file enables adding other relevant time series like rain, other wind speeds (from a nearby mast), air and water temperature to the SODAR data file. This makes further analysis of the data and adding model output results possible.

Input and output file formats

Before a conversion programme can be developed, relevant input and outputs have to be determined. In this case the input files consist of the wind tables as they are produced by the SODAR software Doplmain. The output files are being produced by the conversion programme and consist of files with time series of SODAR observations. Therefore a standard output file format was developed to store the SODAR data but also other (meteorological) data. This format enables the development of standard software to analyse the data. The requirements the format file had to fulfil were:

- flexibility in the number of quantities for which time series can be stored, including SODAR data and other quantities.
- date and time stamp referring to the observation period.
- listing of SODAR parameter settings, conversion settings and other relevant information with respect to the data during the specified observation period.
- file compatibility for easy use of Matlab and Excel.
- simple file manipulation.
- chronological file structure: all data referring to one interval have to be written to one line.
- fixed format: it has to be possible to derive the complete format (length, number of rows and columns, number of characters per quantity) from the information in the header.
- All information in one file has to refer to one location.

Based on these requirements it was decided to produce two text files for each data set: a data file with extension .wta (wind table array) and a log file with extension .log. The exact definition and an example of both data and log file are described in [Wiegerinck, G.F.M. and J.P. Coelingh (2000)].

The data file comprises the actual data: it consists of a header followed by a matrix with the data. In the header, the time of first and last interval written to the data file are shown, the averaging interval, the minimum and maximum height of which SODAR data are available, the SODAR height interval and the location the data refer to. A vector with ones and zeros indicates the quantities that are stored to the file. Above each column, an abbreviation indicating the contents of that column is also given.

The log file contains a header with the same information as the data file. In this file also the data source is stored (e.g. SODAR type) and the relevant measurement settings per period. In case of SODAR measurements, also the parameters used for offline processing are mentioned. In such a way, it is always clear in what way the original SODAR data has been processed.

MatLab routines

Several possible software environments exist suitable for programming the conversion programme like MatLab, Excel/Visual Basic and general environments like Turbo Pascal and C. Each environment was judged on relevant issues: the maximum number of measuring points, possibility to run the software under future operating systems, complexity of use, possibilities to extend the programme and the possibilities to import data from and to other applications.

Excel is generally known and is easy to use. It is very easy to import data from other applications. Major drawbacks are that Excel becomes extremely slow and unstable when a spreadsheet becomes large and the length of the time series is limited to 65536 intervals. MatLab does not have these drawbacks. It is less well known than Excel but detailed MatLab knowledge is not required once the tool is developed. The software is easy to extend. Importing other data is possible and can be standardised but is somewhat more difficult then importing data in Excel. (Note : Other environments like C and Pascal would be as suitable for this purpose as MatLab). As the analysis of the time series

will be performed by MatLab as MatLab is especially developed for working with matrices. Therefore, we have chosen to use MatLab for the conversion programme. The developed conversion programme will be discussed here in a global way. For detailed information the reader is referred to the manual [Wiegerinck, G.F.M (2001)] .

The Wind Table to Standardised AVerages file (WT2STAV) is able to convert wind tables to the standard file format from the previous section. At the start of the programme, the user can enter the desired start and stop date, averaging period and minimum and maximum height of the SODAR. The user can also set requirements on the percentage of data that has to be valid in order to produce a valid mean, the signal intensity, the signal-to-noise ratio, the standard deviation and the magnitude of horizontal and vertical wind speed. After that, the programme request the user to enter which quantities have to be written to the output file.

The software checks which wind tables are available within the entered period and checks whether the requested time and height resolution are possible. After that, per averaging interval the corresponding wind table(s) are determined. For each wind table, the data are (in)validated according to the user selected settings and if the set requirements are met, the average wind speed is calculated. For each interval, the mean values are written to a data file and a log file is composed from the input and observed problems. The programme turns out to be very stable but somewhat slow.

To analyse the SODAR data, also rain information and other meteorological quantities are of importance like wind speed and direction measured at a mast, water temperature and air temperature. Algorithms have been developed to convert these data to the standard format and add it to the file with SODAR data.

In MatLab, also standardised procedures were developed to analyse the data in a data file. This included procedures to read data from and write data to a file, select a specific period or quantity, add stability data . and procedures to make graphs and calculated mean wind speeds for the analysis as described in the next section.

6.6.3 Data analysis

According to the manufacturer's specifications the working range of the Aerovironment 4000 is between the heights of 15 m to 200 m, with a vertical resolution of 5m. An example of a time series measured by the SODAR at MPN is shown in Figure 6-6 over a period of just over 2 days. In this figure, the wind speeds at 15 m, 35 m, 55 m and 75 m with respect to the SODAR level are shown and for comparison also the wind speeds of the anemometer at 27.6 m (above MSL) sea level.

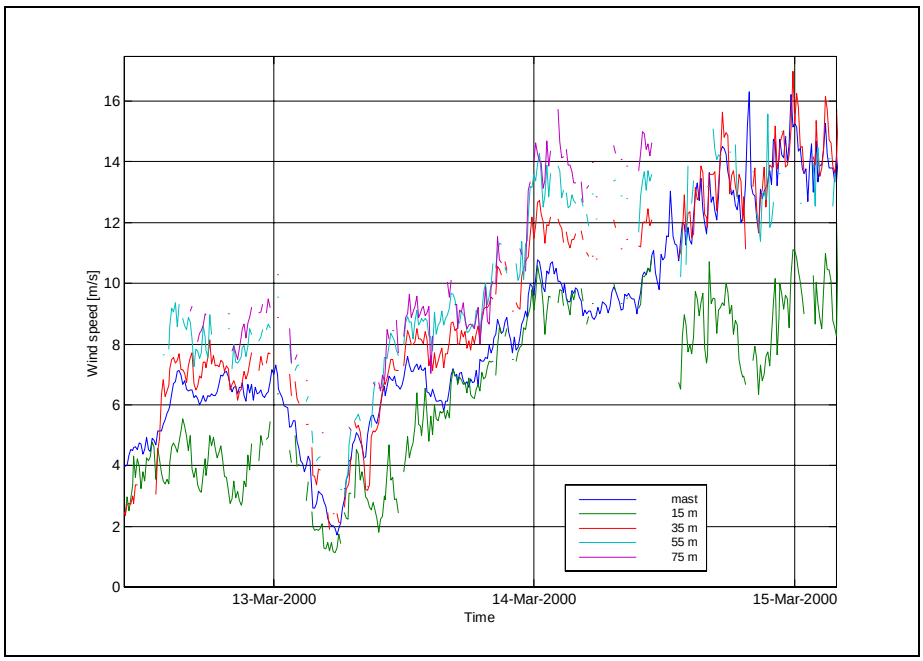

Figure 6-6: Time series SODAR measured wind speed, 15 m, 35 m, 55 m and 75 m above SODAR level.

It turns out from that for some periods, the wind speed measured by the SODAR is lower than the wind speed measured by the anemometer despite the higher height. Besides, the higher the height the lower the amount of data that is recovered. This is an intrinsic problem of SODAR: the intensity of the emitted pulse decreases with height because of absorption, scatter and increase of the area over which the beam propagates. Hence, the higher the

height, the larger the chance that the back scattered signal drowns in the back ground noise and the Doppler shift can not be determined. Figure 6-7 shows the percentage of recovered data as a function of the height relative to mean sea level.

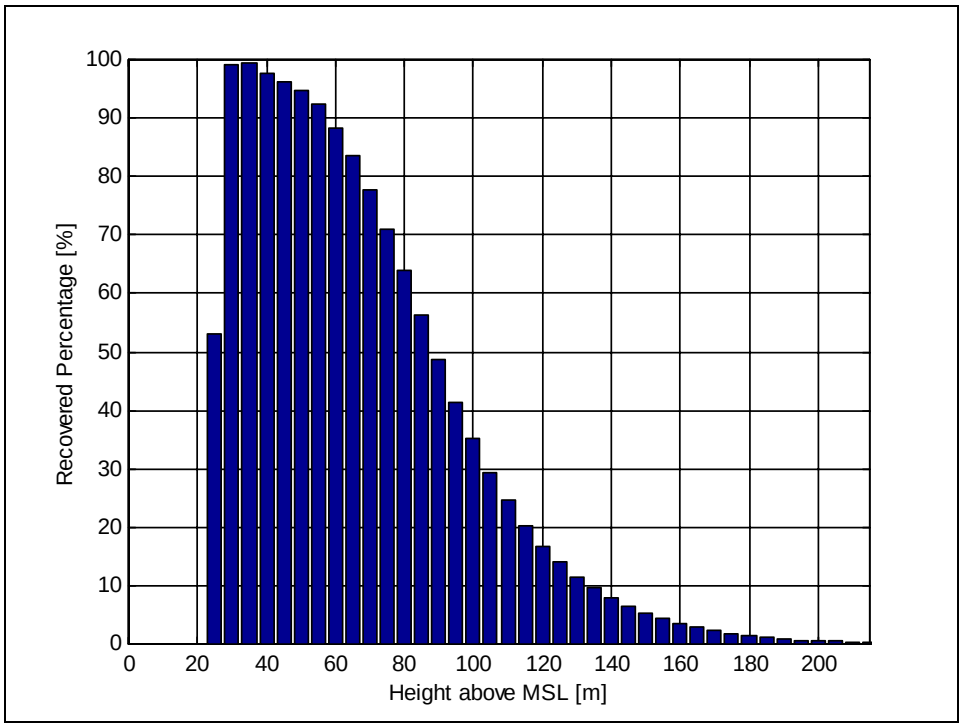

Figure 6-7: Recovered percentage of wind speed data as a function the height relative to mean sea level for the measurements at MPN from February 23 to June 16, 2000.

The height range of the SODAR at MPN is generally less than the height range the SODAR obtained at the ECN-terrain [Dam, J.J.D. van and E.J. van Werkhoven, (1999)]. Above 60 m, the availability falls more rapidly than at ECN. Low availability of data at larger heights may limit the usefulness of a SODAR because it deteriorates the quality of statistical analysis of the data. The best solution is of course to analysis the reasons for the worse performance and try to alleviate these in order to get better results. In addition, if it is understood under which circumstances results are poor theoretical modelling may help to add modelled wind speeds to replace missing or erroneous values. However, this last step may prove to be too complicated.

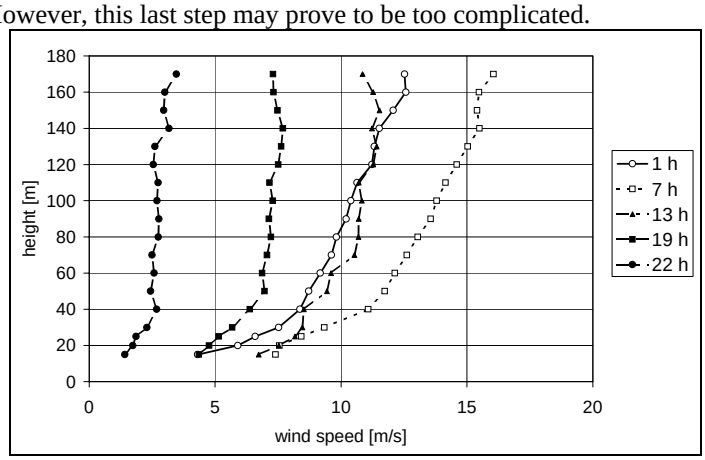

Figure 6-8: Wind speed profiles as measured with a SODAR on one day. The profiles shown are hourly averages.

One of the most powerful features of the SODAR is that wind profiles over a specific period can be determined. This gives detailed insight in phenomena that play a role in the boundary layer. Some examples of profiles averaged over one hour on one day are shown in Figure 6-8. The increase of the wind speed with height depends on stability of the atmosphere and roughness of the sea. At the moment, several theories exist, but until now it was not possible to *measure* complete profiles. Apart from the efforts to understand SODAR operation, in this chapter the SODAR measurements will also be compared to wind speeds calculated with the help of Monin-Obukhov similarity theory. The SODAR does not only measure wind speeds, but also produces quantities per height indicating the reliability of the measurement. This includes signal-to-noise-ratio, signal intensity and number of measurements within the aver-

aging period. It is a task for the user to select the criteria to (in)validate data. The requirements data had to fulful in order to be valid for the measurement series at MPN are given in Table 6-1. These are the settings as advised by the supplier of the SODAR. The exact meaning of the requirements is explained in the manual of the conversion programme WT2STAV [Wiegerinck, G.F.M. and J.P. Coelingh, (2000)].

Table 6-1: Overview settings for offline processing SODAR data measured at MPN.

Description	Requirement
Number of accepted returns	≥ 50 %
Intensity	> 4
Standard deviation	≥ 0.02 & ≤ 10 m/s
Magnitude horizontal wind speed	≤ 35 m/s
Magnitude vertical wind speed	≤ 15 m/s
Signal-to-Noise ratio	≥ 2

Reliability and quality of SODAR data

The reliability and quality of the SODAR data is of importance. First, the problem of rain is discussed. After that, we try to identify the causes for the poor height range With this knowledge in mind, measurements of SODAR and mast are compared with each other. The section concludes with a discussion on the reliability of the current SODAR set and recommendations for future measurements will be given. For the analysis, we will only focus on the measurements at MPN from February 23, 2000 until June 15, 2000.

Influence of rain

During the preliminary SODAR measurements at the ECN-terrain, it was found out that the SODAR does not always function well during rain. This is shown with the help of Figure 6-9 and Figure 6-10.In Figure 6-9, the 10-minute averages of the anemometer are plotted against the SODAR measured wind speed at 50 m height. The sector 110°–230° is excluded as in this sector mast and SODAR are situated in the wake of a wind turbine. Quite some points occur where the SODAR wind speed is too high. When periods with rain are also filtered from the data set (Figure 6-10) these points disappear and all points are more or less on a straight line.

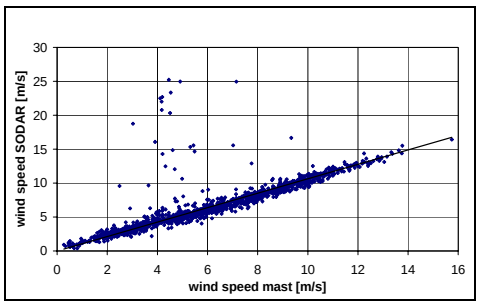

Figure 6-9: Mast wind speed versus SODAR wind speed at ECN, both at 50 m AGL including periods with rain. Wind directions from 110°–230° excluded.

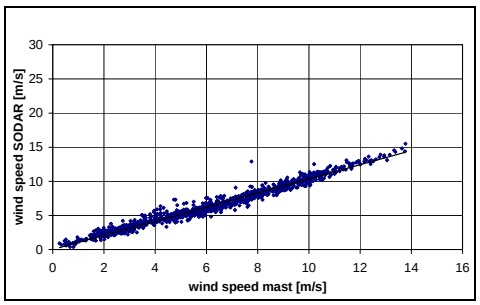

Figure 6-10: Mast wind speed versus SODAR wind speed at ECN, both at 50 m AGL. Points measured during rain and wind directions from 110°–230° excluded.

According to the supplier, the rain causes an additional (false) peak in the spectrum per height. The SODAR software searches the highest peak in the spectrum. From the corresponding frequency, the Doppler shift is determined and from that the wind speed at the specific height. So, in case the 'rain peak' is higher than the real signal peak, the wrong peak is taken to calculate the wind speed. The shape of the rain peak is more or less similar to that of the signal peak and hence the data is not invalidated by the SODAR software. The rain problem is more or less intrinsic to the SODAR principle of operation, probably depending on the frequency of operation. The supplier is currently looking for a software solution.

When looking to time series, it turns out that the SODAR performance is not disturbed during all rain showers. This probably depends on the fall down intensity of the rain: the higher this intensity, the larger the noise caused by rain. To overcome the rain problem, a rain detector was installed near the SODAR at MPN. For our further analysis periods of rain are excluded from the data set. The disadvantage of this is that also periods with good data are excluded.

Height range

A SODAR gives valuable wind profile information that can be used for a number of purposes. Unfortunately, for the measurements at MPN the recovered percentage of data decreases rapidly with height. This is a serious limitation in order to statistically analyse the data at the higher heights. Therefore, it is important to find out under what circumstances the SODAR performs well. Possible causes for the poor height range are back ground noise, the state of the weather and the magnitude of the wind speed.

First we will discuss the influence of back ground noise on the height range. After that, the influence of stability and wind speed is investigated even as other possible quantities that may play a role with respect to the SODAR height range.

Influence of background noise

A SODAR emits a pulse in a specific direction. Directly after that the SODAR records the returned signals. As explained in section 6.2, the time between emitting and receiving of the returned signal is a measure for the height. A fast Fourier transform algorithm is applied to the measured signal. In the obtained spectrum the band width with the largest signal intensity is determined and the corresponding frequency is used to determine the Doppler shift.

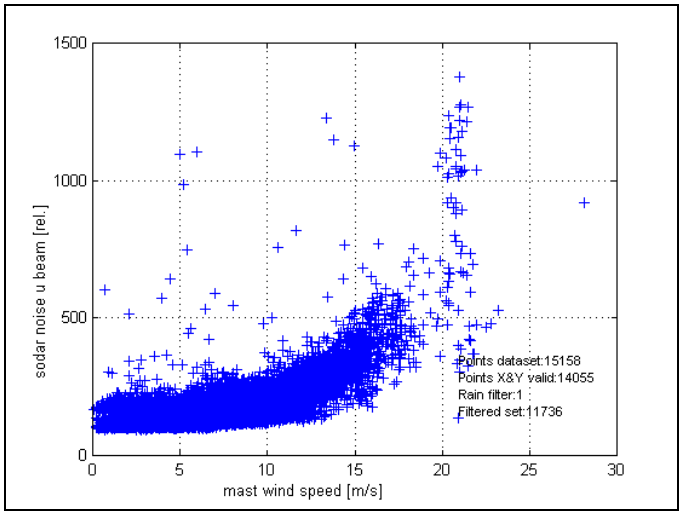

Figure 6-11: Scatter plot of wind speed versus observed back ground noise in the *u*-beam.

The signal intensity of the sent beam decreases with height because of scattering, absorption and spreading of the total signal intensity over an increasing surface. Hence, the signal reflected from high heights easily 'drowns' in the background noise, depending on the nature and frequency of that noise.

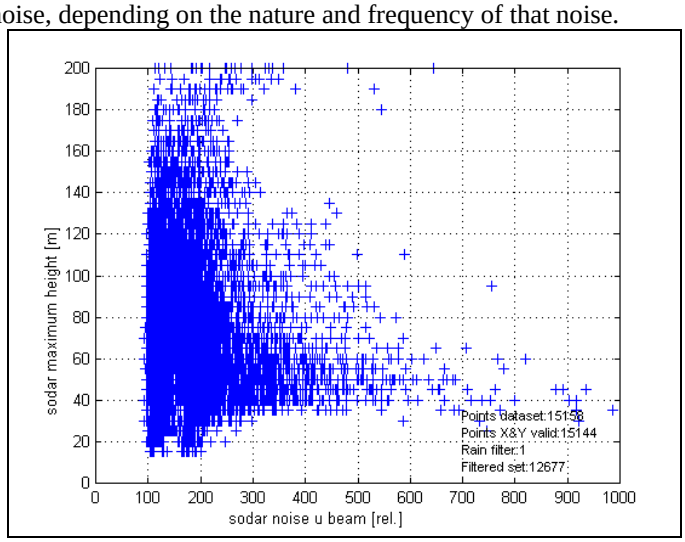

Figure 6-12: Scatter plot of noise level u beam versus the maximum height reached by the SODAR.

Sources of back ground noise are the noise produced by the diesel generator needed for electricity supply, noise of the waves and whistling of the wind around the superstructure of the platform. The noise produced by the diesel

generators is independent of the wind speed. The noise generated by the waves and whistling of the wind increases with the wind speed. In Figure 6-11, the noise observed by the SODAR u beam is plotted versus the mast wind speed. At low wind speeds, the noise of the beam does not go below a lower limit, most probably the noise produced by the diesel generators. Above roughly 7 m/s, the noise starts to increase with wind speed: the noise produced by waves and wind whistling around the superstructure of the platform drowns out the noise of the diesel generators. Similar patterns are observed for the *v*- and *w*-beam. The only difference is that the lower limit of the noise for the *v*-beam is significantly higher than for the other two beams. An explanation is that this is the beam that is sent along the diesel generators.

From the above described operation of the SODAR, one would expect that a higher back ground noise level results in a lower signal-to-noise ratio and hence the maximum height reached decreases. In Figure 6-12, a scatter plot of the noise of a beam versus the maximum height reached by the SODAR is shown. As expected, the maximum height decreases with increasing back ground noise level. When averaging the mean maximum height per noise 'bin', Figure 6-13 results. A clear decrease is observed. Similar plots are obtained for the other two beams.

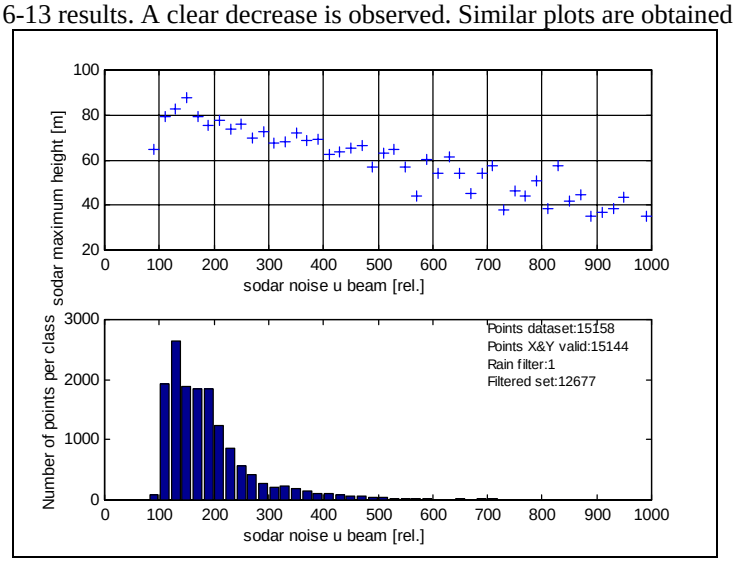

Figure 6-13: Noise of the u beam versus the maximum height of the SODAR

Hence, the back ground noise is a clear cause for the poor height range. However, because of the broad scatter in Figure 6-13 it appears that also other effects play a role.

To increase the height range, it is important to reduce the back ground noise as far as possible. A recommendation for future measurements is to position the SODAR on top of the platform. This would have the following effects:

- Less disturbance from diesel generators. On top of the platform, no sound from the diesel generators can be heard. Near the current position of the SODAR, one can clearly observe this noise. Hence, repositioning the SODAR to the top of the platform reduces the back ground noise level due to the diesel generators.
- No disturbance from reflections of the platform. At the moment , part of the sent beams is reflected by the superstructure of the platform. Positioning the SODAR on top will reduce this.
- The SODAR is positioned further away from the waves. A lower noise level may result.
- The SODAR is placed on a higher position with respect to mean sea level. This can be positive with respect to the availability of data at e.g. 100 m MSL but the wind speeds at low heights (until 30 m MSL) are not observed.
- In case the back ground noise only occurs in a limited frequency band, a shift in the frequency of operation may be helpful. It would be wise to analyse the frequency of the waves, diesels and floating of wind along the superstructure. When changing the frequency also other effects play a role. A lower frequency will result in a higher absorption rate and hence the signal intensity that returns to the SODAR decreases. Another frequency also implies another wave length and this may also affect the performance.

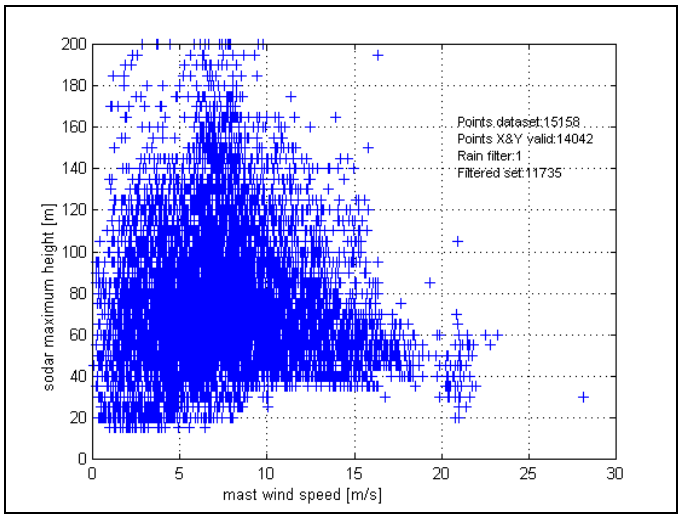

Figure 6-14: Maximum height reached by the SODAR relative to the SODAR level as a function of the mast wind speed at measuring height.

Influence of wind speed

From the previous section we know that there is at least an indirect relation between wind speed and SODAR height range: a larger wind speed causes a higher back ground noise level and hence a poorer height range. It is possible that wind speed also directly affects the height range. To investigate this, we made a plot of the mast wind speed versus the maximum height of the SODAR reached (Figure 6-14) Averaging this scatter plot per wind speed 'bin' of 1 m/s, Figure 6-15 results.

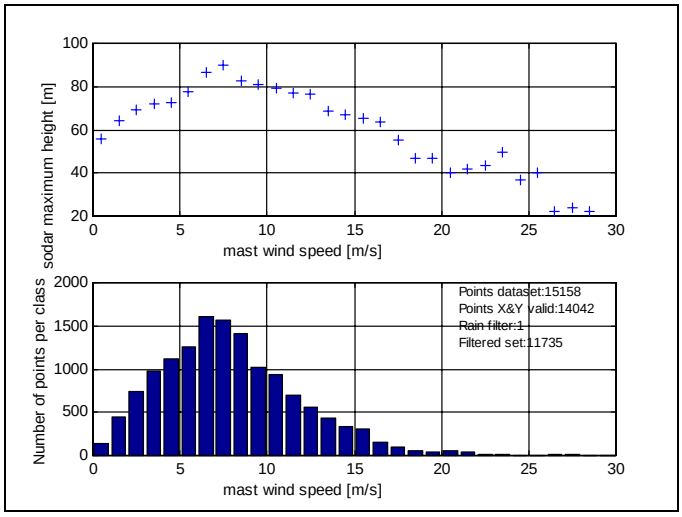

Figure 6-15: Average height reached by the SODAR per wind speed 'bin'of the mast.

For low wind speeds (< 7 m/s) the height reached increases with wind speed. For wind speeds higher than 7 m/s, the influence of noise as described above is clearly observed. The cause of the increase of the SODAR height range with wind speed is not clear. An option is that the stability of the atmosphere plays a role. The stability becomes in general important at low wind speeds which is an indication that both effects may be related.

Influence of stability

The stability of the atmosphere plays a major role for understanding the wind and temperature profile and may affect the height range of the SODAR. First of all, we will describe the several stability classes that occur and a way to parameterise the stability of the atmosphere. After that, the possible influence on the SODAR height range is discussed.

Calculation of the stability parameter:

A parameterisation of the stability does exist: the Monin-Obukhov length or stability parameter *L*. This parameter describes the ratio between mechanical vertical turbulence and thermal vertical turbulence. Mechanical turbulence occurs when in a rough terrain (e.g. a rough sea) the wind speed is high. By means of gust of wind, the air in the bottom tens of metres of the atmosphere is stirred intensively by movements on a very small and on a very large scale. This is caused by friction at ground level. Another cause for vertical air movements are air density differences. In case the air flowing over sea has a temperature lower than that of the sea water, the air density at the lower levels of the atmosphere will be smaller than that at higher level. Vertical mixing will occur. This is called convection or thermal turbulence. The scale of thermal turbulence is somewhat larger than that of mechanical turbulence.

Several stability classes occur: neutral, stable and unstable. In a neutral atmosphere, the mechanical turbulence is dominant. This occurs under relatively high wind speeds at ground level and under heavy cloud. The wind speed at a specific height depends solely on the roughness of the terrain and the geostrophic wind speed and can be described by a logarithmic profile:

$$u(z) = \frac{u_*}{\kappa} \ln\left(\frac{z}{z_0}\right) \qquad (6.1)$$

Here, u (m/s) is the wind speed, u_* (m/s) the friction velocity, κ the dimensionless Von Karman constant, z (m) the height and z_0 (m) the roughness length.
For table and unstable conditions, equation (6.1) does not hold anymore as also thermal aspects start playing a role. In an unstable atmosphere, the density of air does not decrease with height and vertical mixing results. By the vertical exchange of air also the horizontal wind speed of the air is exchanged. The exchange of wind speed downwards is very effectively and as a result, the wind speed near ground level is only slightly smaller than the wind speed at large heights.

Under stable conditions, the air density decreases with increasing height and hardly any vertical exchange of air occurs. In this case, a strong wind at higher heights can coexist with calm in the bottom tens of metres of the atmosphere.

In case of a stable or unstable atmosphere, the influence of thermal effects has to be included in equation (6.1), then

$$u(z) = \frac{u_*}{\kappa}\left[\ln\left(\frac{z}{z_0}\right) - \Psi\left(\frac{z}{L}\right)\right] \qquad (6.2)$$

with ψ the stability function and L (m) the Monin-Obukhov length. For a more detailed discussion on stability, the reader is referred to literature (e.g. [Garratt, J.R.(1994)]).

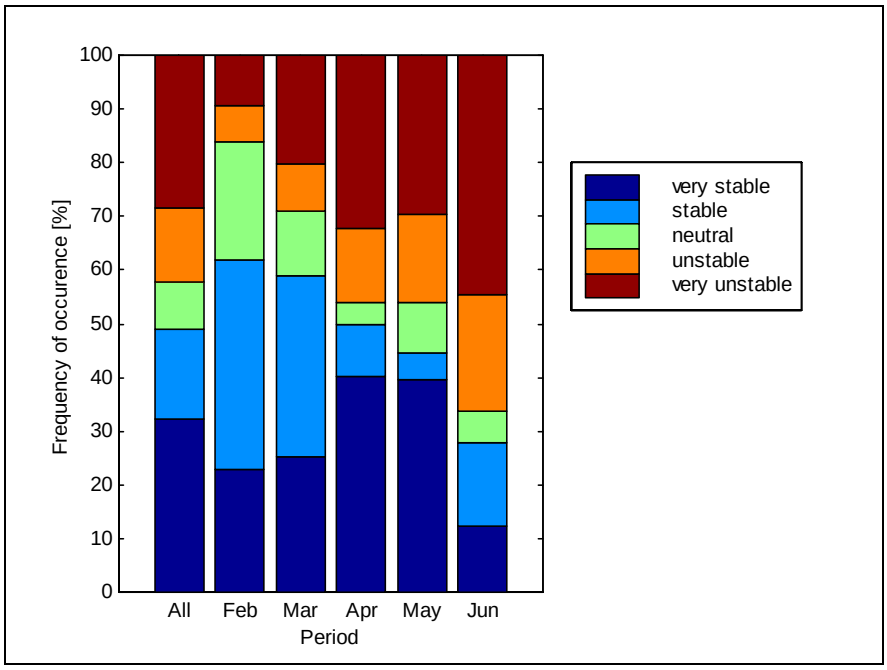

Figure 6-16: Distribution of stability conditions at the MPN platform from February 23 to June 16 2000 from very stable (bottom) to very unstable (top). The number of points for which the stability length could be determined is also given per period.

It is possible to determine the stability parameter from a single wind speed, one air temperature and the water temperature using Monin-Obukhove similarity theory. At Measuring Post Noordwijk, these quantities are measured on a routine basis. Hence, for every 10 minute mean, one can calculate the stability parameter. For the period of useful measurements (February 23 to June 15), the stability was determined per month and for the whole period. The result is shown in Figure 6-16. We have used the Monin-Obukhov length to define the five stability classes: very stable ($0 \le L < 200$), stable ($200 \le L < 1000$), very unstable ($-200 \le L < 0$), unstable ($-1000 \le L < -200$) and neutral ($|L|>1000$). We compared the calculated distribution of stability classes with the long term mean [Coelingh et al. (1996)]. For the Spring months (March–May), very stable occurs 35% of the time, stable 14%, neutral 8%, unstable 11% and very unstable 32%. This compares well to our distribution. Because of the small number of points, the outcome for February is not representative.

Stability and SODAR height range:

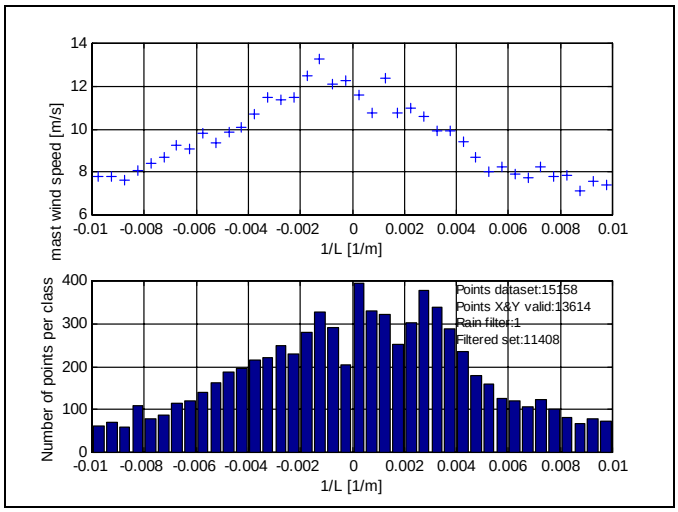

Total: 13753 points
Feb: 610 points
Mar: 3743 points
Apr: 3535 points
May: 4461 point
June: 1404 points

Figure 6-17: Relation between stability and mast wind speed, averaged per 'stability bin'.

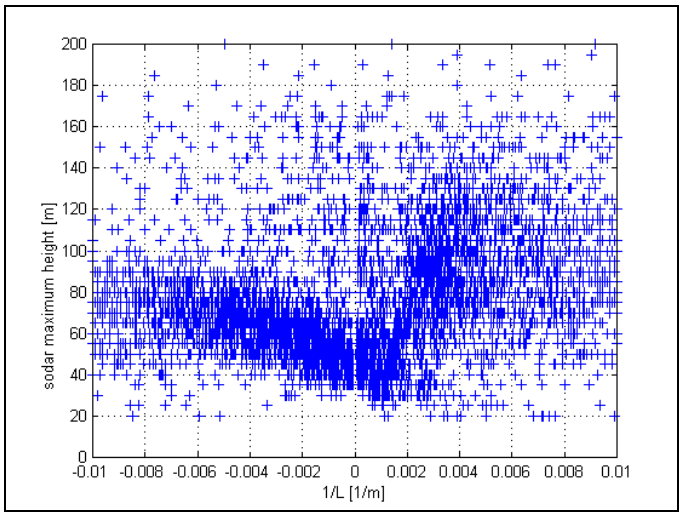

Figure 6-18: Influence of stability of the height reached by the SODAR (relative to the SODAR level).

As indicated in the description of the stability classes, stability and wind speed are related. For the considered period, we plotted the wind speed of the mast versus a measure for the stability (Figure 6-17). The highest wind speeds occur under neutral circumstances. Under very stable circumstances, there is hardly any horizontal movement of air and also hardly any vertical movement. When the wind speed increases for some reason, the influence of mechanical turbulence will increase and the atmosphere becomes somewhat less stable. This explains the increase in wind speed when the atmosphere becomes less stable. For very unstable conditions, the influence of frictional forces is limited and the wind speed near ground level is only slightly smaller than the wind speed at high heights. An increase in this wind speed implies that the influence of frictional forces becomes more important and the atmosphere will become less unstable.

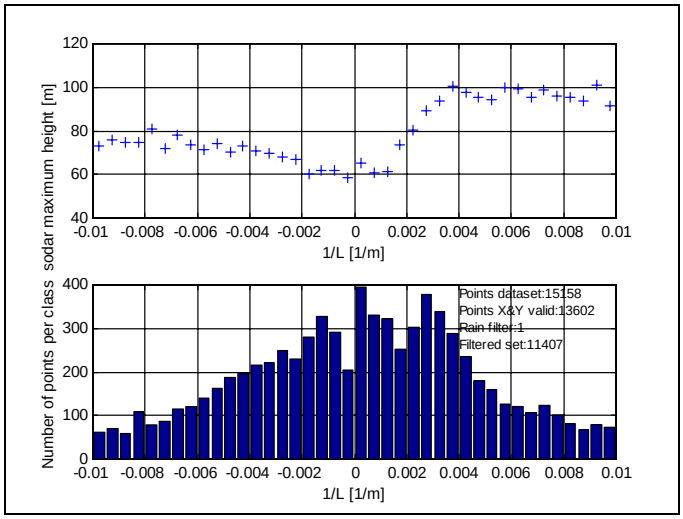

Figure 6-19: Mean maximum SODAR height per stability bin.

This relation between wind speed and stability complicates the analysis of the influence of stability on the height range. First, we will look to the overall influence of stability on the height reached by the SODAR. A scatter plot is shown in Figure 6-18, the average height reached per bin is shown in Figure 6-19. The height range is worst under neutral conditions. An obvious reason is that the wind speeds and hence the back ground noise levels are the highest under these circumstances. The more unstable the atmosphere, the higher the height reached. This also holds for stable conditions, although here there tends to be a "maximum" height range.

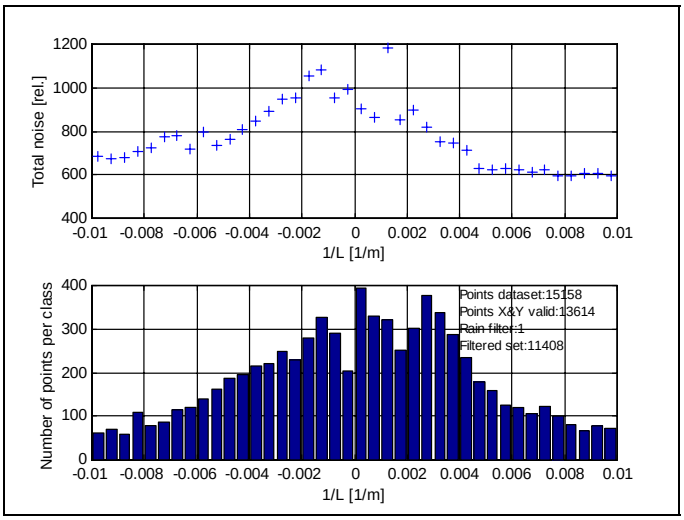

Figure 6-20: Scatter plot total noise observed versus stability.

A difference between the latter two is that under unstable circumstances the SODAR hardly ever exceeds 100 m height. Under stable circumstances, much higher heights are reached but in this case there is a broad 'scatter band' between approximately 50 m and 150 m height. From Figure 6-17 it appears that for very stable and very unstable conditions, the average wind speed is approximately 7.5 - 8.0 m/s. For stable circumstances the average height range is roughly 100m while for unstable circumstances this is only 75m. As the average wind speeds in these areas are the same, one would also expect a comparable height range for both stability classes but this does not seem to be the case. An interesting question is the noise level as a function of stability (Figure 6-20). It turns out that under stable conditions the total noise is somewhat lower (600) than under unstable conditions (650) but the difference is not very significant. It appears that apart from the wind speed related effect, the SODAR works somewhat better under stable conditions than under unstable conditions. Further analysis of the data set is needed to confirm this idea but is beyond the scope of this report.

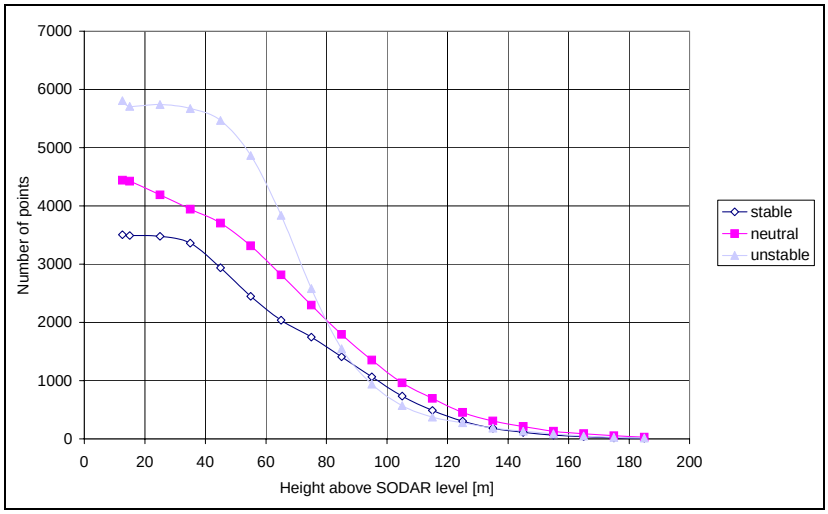

Figure 6-21: Absolute number of points of a certain stability class.

Another way to look to this is shown inFigure 6-21. For each SODAR height, the time steps for which valid data are measured were determined and the subsequent stability was looked up and summed per stability class. The number of points decreases for all stability classes with increasing height. However, the decrease is much stronger for an unstable atmosphere than for stable and neutral conditions. One explanation might be that in near neutral conditions, there are smaller (or even non-existent) temperature inhomoegeneities for the SODAR beam to reflect off.

Is it now possible to explain the better height range with increasing wind speed (for low wind speeds) and/or why stability seems to improve the height range? No, a guess is the best we can do for now.

A SODAR measures wind speeds at three points. The angle between the vertical beam and the non-horizontal beams is 16 degrees. The higher the height a measurement refers to, the larger the distance between the measuring points. The vertical wind speed is used to derive the horizontal wind speed components from the two non-vertical beams. For non-laminar flows, the three measured values may not correspond to each other with an invalid outcome as result. The higher the height the measurement refers to, the larger the chance that the wind speeds measured do not correspond with each other. For very low wind speeds, the variability is high. This is also the cause under unstable circumstances. This might explain the better height performance with wind speed and the better performance under stable circumstances. A way to investigate this would be to look to the average height related to the turbulence-intensity. As no standard deviations are determined by the mast, this is not possible.

Other influences

In the above, we derived the influence of noise, wind speed and stability on each other and on the height range of the SODAR. Also other effects may play a role. The most obvious quantities that may affect the performance are the absolute air and water temperature. A scatter plot for both quantities is shown in Figure 6-22and Figure 6-23 respectively.

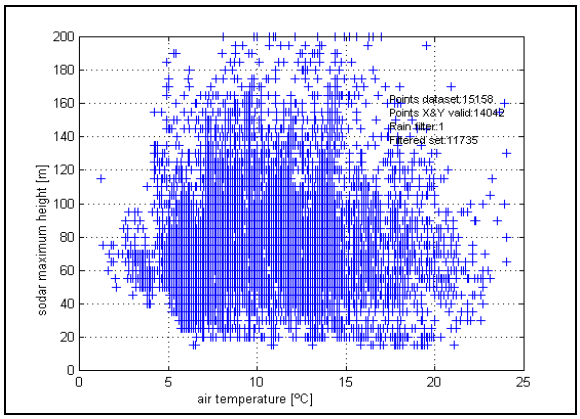

Figure 6-22: Scatter plot of SODAR height range versus air temperature.

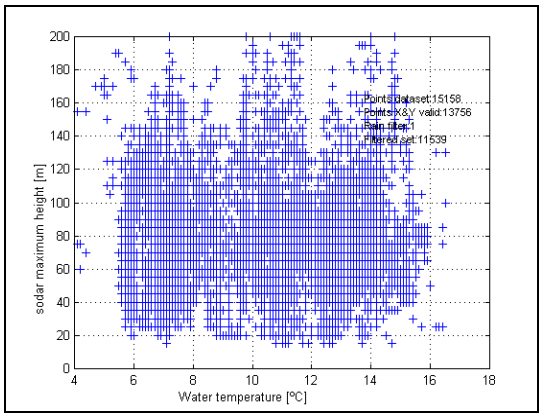

Figure 6-23: Scatter plot of SODAR height range versus water temperature.

It is clear that these quantities on its own are not related to the SODAR height range. Another important quantities are the influence of humidity and turbulence-intensity. Unfortunately both quantities are not available.

6.6.4 Conclusions

From the analysis described in this section, we can conclude the following:

- The height range of the SODAR at MPN is less than during earlier onshore measurements at ECN and should be improved.
- The back ground noise level is quite high and increases with wind speed. The base noise source are the diesel generators for the electricity supply which sets a lower limit for the back ground noise. When the wind speed increases, additional noise sources arise: the sound of the wave grows and the wind whistles along the superstructure of the platform.

- The height range of the SODAR decreases with an increase in back ground noise level; the returned signal 'drowns' in the noise.
- For wind speeds smaller than 7 m/s (measured at the mast) the SODAR height range improves with increasing wind speed. The reason may be the more laminar flow, but this is just a guess.
- For wind speeds larger than 7 m/s the height range decreases with wind speed. This is caused by the increase of back ground noise with wind speed above 7 m/s.
- Wind speed and stability are related. The wind speed is largest under neutral conditions and decreases for stable and for unstable atmosphere.
- The SODAR height performance is worst under neutral conditions. The more unstable the atmosphere, the better the height performance. This also holds for stable conditions. This is to a large extent caused by the larger noise level at higher wind speed but there may be a relation that the more stable the atmosphere, the better the SODAR height range.

6.6.5 Comparison of SODAR data with MPN measuring mast data

In the previous section the height performance of the SODAR was discussed. Of course, the produced wind speeds and directions should also be correct. In this section we use the wind speeds and directions from the mast anemometer and vane and Monin-Obukhov similarity theory to check the SODAR measurements. When comparing mast and SODAR data with each other, one has to take in mind that the platform disturbs the wind flow pattern. Hence, mast and SODAR may (under specific circumstances) measure the disturbed flow instead of the undisturbed flow which complicates the analysis.

We shall first compare the wind directions measured with the mast and the SODAR with each other. This will give some first insight into the influence of the platform. After that, the wind speed measurements will be compared.

Wind direction

InFigure 6-24, the frequency of occurrence per sector is plotted for the mast (27.6 m MSL) and for the SODAR at several heights. In order to make a fair comparison, only intervals are used for which the direction of the wind speed at the mast and at the SODAR from 30 to 120 m MSL are available ('equal statistics'). The distribution of the wind direction of the mast and that of the SODAR above 60 m MSL are roughly the same. Between 30 m and 60 m, the distribution differs considerably from that of the mast. The measure of deviation differs per sector.

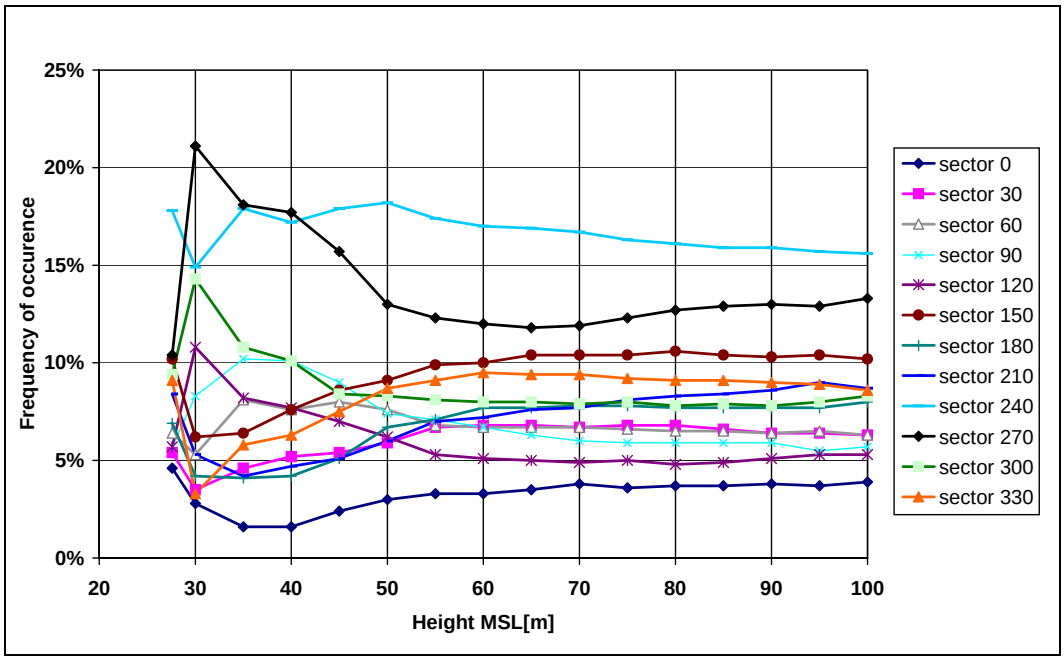

Figure 6-24: Frequency of occurrence per sector for mast and SODAR from 30–100 m above MSL with equal statistics (4472 points).

Another way to look at this is shown in Figure 6-25. In this figure, the wind direction distribution of mast and of the SODAR at 30 m, 35 m and 60 m is plotted for equal statistics from 30 m- 60 m MSL. Again the distribution of mast and SODAR at 60 m MSL compare well, while the lower heights have a different distribution compared to the mast, the wind for the lower SODAR heights has shifted from the west-south-west sector to the west sector. The North-north-east sector has shifted to the east and east-north-east sector.

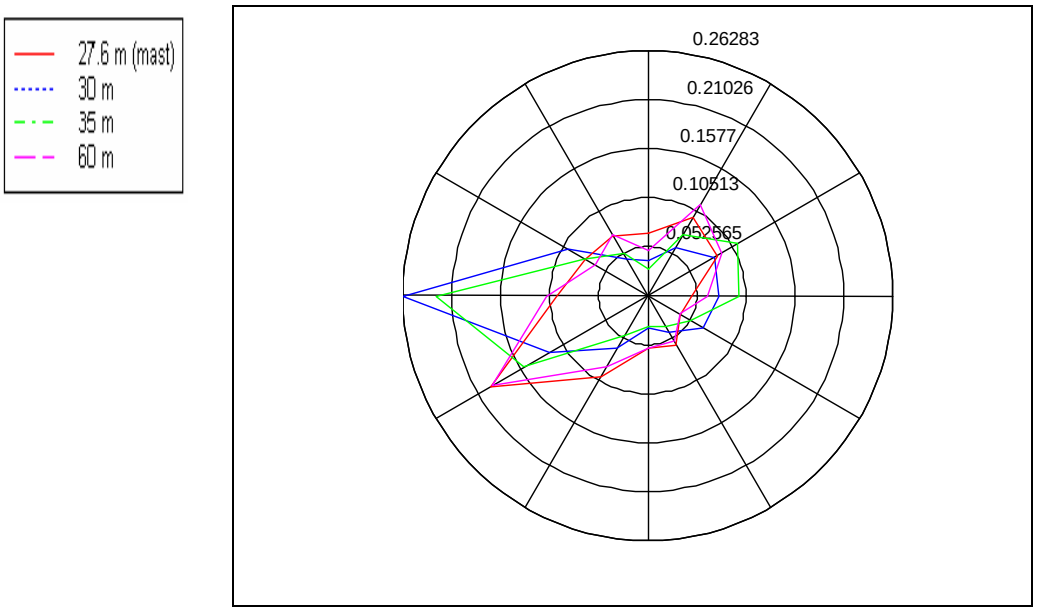

Figure 6-25: Wind rose for the mast and SODAR at 30m, 35m and 60 m MSL. Equal statistics for 30 m–60 m of the SODAR and the mast (11753 points)

A possible explanation for the observed behaviour is that the wind at the lower SODAR heights is disturbed by the platform: wind from the WSW flows along the helicopter deck and appears to flow from the west. Similar effects may occur at the east side of the platform. It is remarkable that the mast wind direction is hardly disturbed while a clear disturbance is seen at the lower SODAR heights.

We will return to this issue in the next section where the mast wind speed and SODAR wind speed are compared.

Wind speed

Wind speed profiles

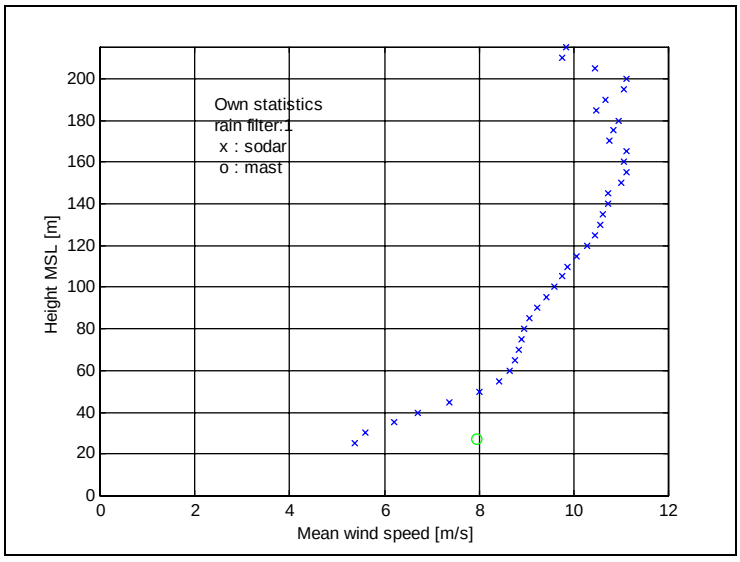

Figure 6-26: Wind speed profile based on SODAR and mast. Each mean is calculated based on own statistics. A rain filter (threshold value 1) was applied, 14055 points remain.

Figure 6-26 shows the mean wind speed for the mast and for each SODAR height. Per height, all available measurements are used to calculated the mean wind speed. For the SODAR, a rain filter with threshold value 1 is applied. The magnitude of the measured wind speeds seems fair. The mean mast wind speed is larger than that of the

SODAR measurements at the lowest heights but the difference in statistics may be the cause. A better way to compare mast and SODAR wind speed is by comparing a set for which each height has the same statistics.

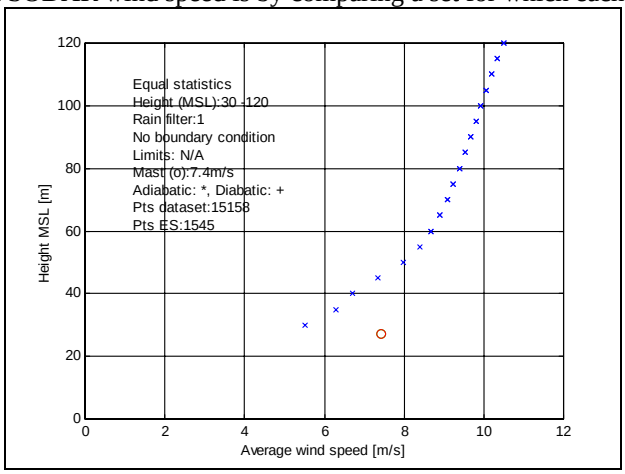

Figure 6-27: Wind speed profile with equal statistics for SODAR heights from 60–120m MSL and mast wind speed. Rain filter (threshold value 1) applied.

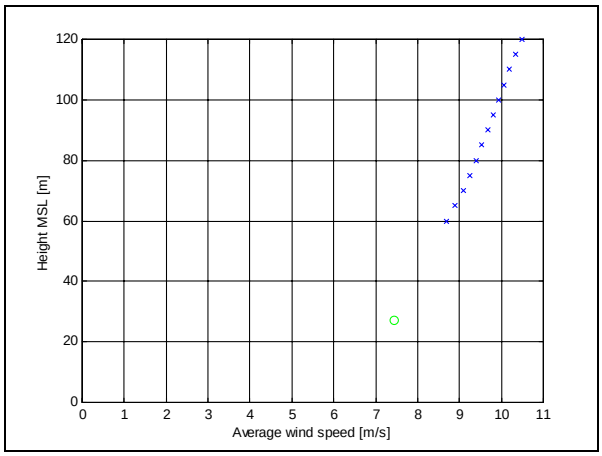

Figure 6-28: Wind speed profile with equal statistics for SODAR heights from 60– 120m MSL and mast wind speed. Rain filter (threshold value 1) applied.

In Figure 6-27 such a wind speed profile is shown. An interval is only included in the calculation of the mean when for 30m to 120m MSL at *all* heights and for the mast a valid wind speed is measured. Besides, a rain filter with threshold value 1 is applied. In total 1513 of the 15158 intervals of 10minutes available are used to calculate the mean wind speed which is rather limited. Despite the fact that now the same set is used, the mast mean does not correspond to the SODAR measurements at the lower heights. When we ignore the SODAR measurements below 60 m MSL, the mean mast wind speed does correspond to the SODAR measurements at heights above 60 m MSL. The same holds for other sets. Compared to the mast, the SODAR measured wind speeds below 60 m are too low. Above 60 m, the measured wind speeds may be correct but there is no way to validate this.

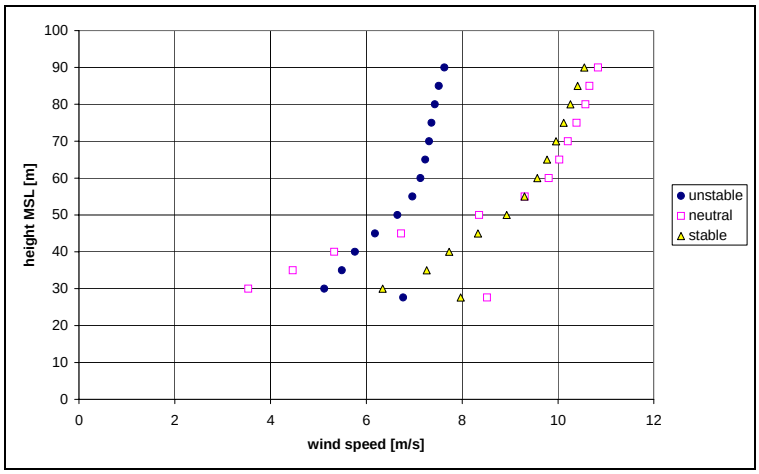

Figure 6-29: Wind speed profile for 30 – 90 m MSL (equal statistics) for several stability conditions. Neutral: 184 pts, stable: 2831 pts, unstable: 2003 pts.

We investigated whether this phenomenon does occur under all circumstances or not. First of all, we made a subdivision to stability class: stable, neutral and unstable. The resulting profiles are shown in Figure 6-29. It turns out that under all stability circumstances, the SODAR measured wind speeds below 60 m are too low compared to the mast. Under neutral conditions the underestimation is considerably larger than under stable and unstable conditions. Remarkable is the clear 'discontinuity' in the unstable and neutral profile at 60 m MSL.
Similar profiles were made for several wind speed and noise classes. The too low wind speeds below 60 m was observed for all wind speeds and noise levels. Besides, it appears that for all circumstances, 60 m MSL is the lowest height with a not too low wind speed compared to the mast.

Conclusion: Above 60 m MSL, the mean wind speed of the mast and the SODAR fit in a neat profile. When the mast measurements are correct, the SODAR measured wind speeds below 60 m MSL are too low. under all circumstances. Above 60 m, it appears that the SODAR produces valid means, but there is no way to validate this. It also appears that the height from which onwards mast and SODAR profile corresponds is fixed at 60 m MSL.

Scatter plots

Until now, we have only considered mean wind speeds. Another approach is to compare the time series of the mast and SODAR in scatter plots. In Figure 6-30 to Figure 6-32 the mast wind speed is plotted against the wind speed at the SODAR from 30 m MSL to 60 m MSL. Only points are plotted for which both mast and SODAR measurements are available. A rain filter was applied.

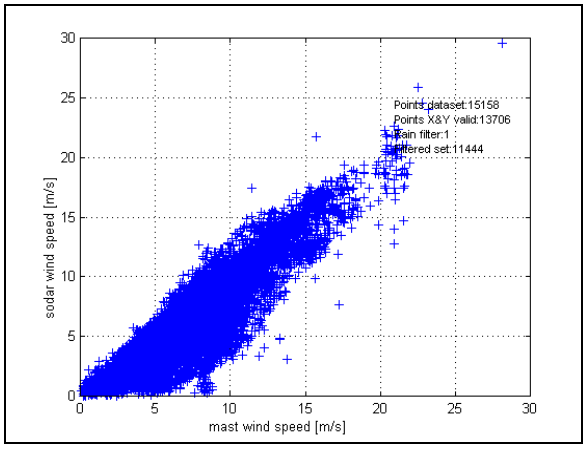

Figure 6-30: Mast versus SODAR wind speed at 40 m MSL. Rain filter (1) applied.

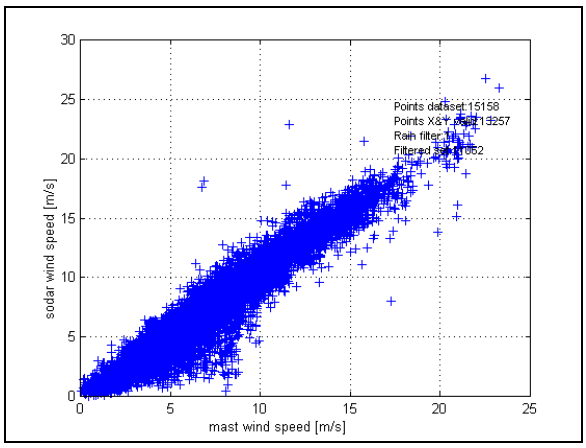

Figure 6-31: Mast versus SODAR wind speed at 50 m MSL. Rain filter (1) applied.

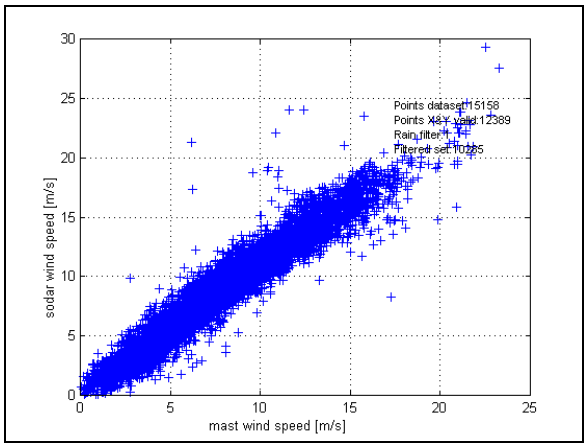

Figure 6-32: Mast versus SODAR wind speed at 60 m MSL. Rain filter(1) applied.

The scatter plot of mast wind speed and SODAR wind speed at 40 m MSL shows that below a mast wind speed of 10 m/s the SODAR wind speed varies between 0 m/s and the mast wind speed. For larger wind speeds, the underestimation by the SODAR is at maximum 5 m/s. this underestimation disappears for larger SODAR heights. At 60 m, the underestimation has disappeared but the scatter band is quite broad. the cause is most probably the variation in stability and roughness length. In Figure 6-32 still some points are situated outside the scatter band. More stringent requirements for data validation and rain filter will probably prevent from this.

From the scatter plots, we can conclude the following. At heights below 60 m MSL, the SODAR sometimes gives too low wind speeds compared to the mast wind speeds, but sometimes also the correct wind speed is measured. At larger heights, underestimation does not occur anymore. More stringent requirements for data validation will probably reduce the number of points outside the scatter band.

Monin-Obukhov similarity theory

With the help of Monin-Obukhov similarity theory, it is possible to calculate the wind speed at an arbitrary height based on one measured wind speed, the roughness length and the stability. For each time interval, we have calculated the wind speed at 60 m and 120 m MSL from the mast wind speed with the help of this theory and by applying the logarithmic profile. A scatter plot of SODAR wind speed at these heights versus the transformed wind speed is a means to validate the performance of the SODAR. A scatter plot for 60 m MSL of the SODAR and the wind speed calculated with Monin-Obukhov similarity theory is plotted in.Figure 6-33 A similar plot for the logarithmic method is shown in Figure 6-34. Both plots are more or less a straight line. On average the Monin-Obukhov calculated wind speeds at 60 m MSL are somewhat lower than the SODAR measurements. The underestimation is somewhat larger when the adiabatic profile is used. Note that the scatter bands are quite broad.

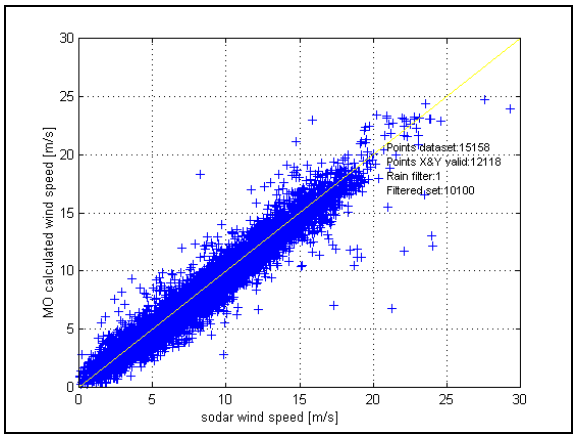

Figure 6-33: Wind speed SODAR versus diabatic wind speed at 60 m MSL. A rain filter with threshold value 1 is applied.

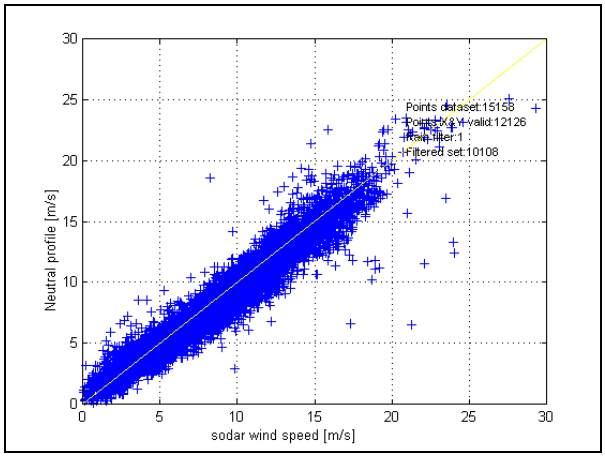

Figure 6-34: Wind speed SODAR versus adiabatic wind speed at 60 m MSL. A rain filter with threshold value 1 is applied.

For 120 m MSL (Figure 6-35 and Figure 6-36) the same is observed although the underestimation of the theory is larger, especially at higher wind speeds. This corresponds to earlier observations that the accuracy of the model decreases for increasing heights.

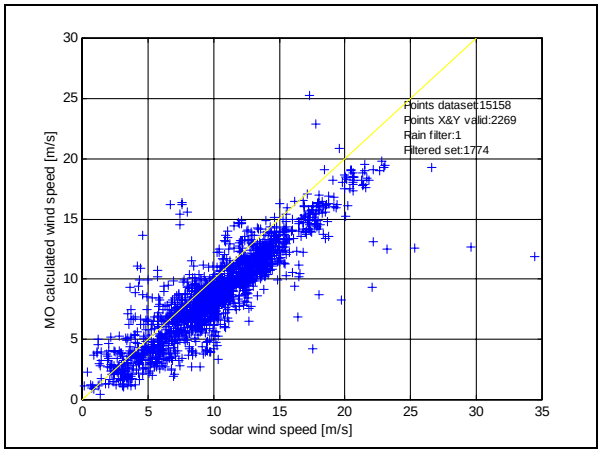

Figure 6-35: Wind speed SODAR versus diabatic wind speed at 120 m MSL.

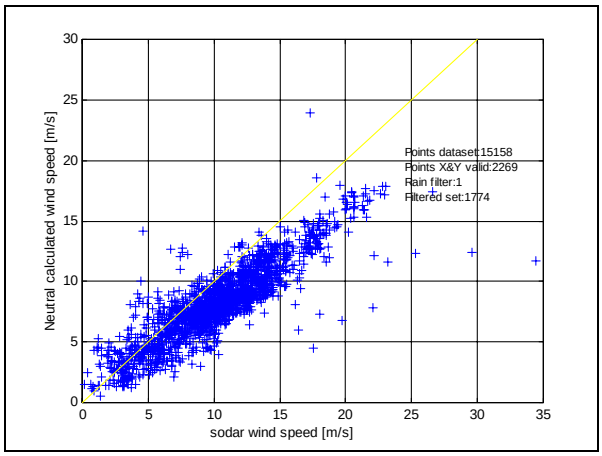

Figure 6-36: Wind speed SODAR versus adiabatic wind speed at 120 m MSL.

6.6.6 Summary of results

In summary, the following conclusions can be drawn.

Wind direction
Above 60 m MSL the wind direction distribution of the SODAR and that of the mast compare well. Below 60 m, the distribution measured by the SODAR deviates significantly from that of the mast. The measure of the deviation varies per sector.

Wind speed profiles
The mean wind speed of the mast and the SODAR observation above 60 m MSL form a neat profile. When we assume that the mast measurements are correct and undisturbed, the SODAR wind speeds below 60 m MSL are too low compared to the mast. It appears that above 60 m, the SODAR produces valid means, but there is no data available to validate this. The 60 m border seems fixed and is observed under all circumstances.

Scatter plots
From the scatter plots, it turns out that below 60 m the SODAR measured wind speeds vary between 0 m/s and the mast wind speed for wind speeds below 10 m/s. For larger wind speeds, the maximum observed underestimation is roughly 5 m/s. At larger heights, no extreme underestimation occurs. More stringent requirements for data validation will probably reduce the number of points outside the scatter band.

Comparison SODAR with Monin-Obukhov similarity theory
At 60 m MSL, the SODAR measurements correspond well with the wind speed calculated from the mast wind speed and Monin-Obukhov theory, although on average the Monin-Obukhov calculated values are somewhat lower than the SODAR measurements. At 120 m, the MO theory based calculated give larger deviations especially at the higher wind speeds.

How can these observations be explained? In case the mast gives correct and not disturbed measurements, the SODAR underestimates the undisturbed wind speed below 60 m MSL. The cause should be a mechanism that only affects the SODAR. A mechanism that may affect the SODAR measurements are reflections of the emitted SODAR pulse against waves and water. The SODAR is positioned on the platforms superstructure 15 m above the water surface. Part of the emitted pulses will reflect against the waves and the water. The speed of the waves and the water may determine the Doppler shift for this part of the beam. It is not sure whether the Dop-lmain software filters this data or not. This effect cannot explain all of the observed phenomena: the SODAR is positioned 15 m above MSL. Therefore this effect can only play a role until roughly 30 m MSL.
Disturbance of the wind by the platform appears a more probable explanation. Then, the mast and SODAR function correctly and the deviation is caused by the disturbance of the wind flow by the platform. In general, disturbance of wind speed by an object causes a larger turbulence intensity and a lower mean wind speed. The latter is indeed observed by the SODAR. Besides, the wind speed distribution at the lower SODAR height is shifted which can be a result from the shape of the platform. From the scatter plots it turns out that at 30 m height the SODAR measured wind speeds vary between 0 and the mast wind speed. This is also an indication that the platform disturbs the wind speed. In case the platform is the cause for the low observed wind speed by the SODAR below 60 m MSL, it is remarkable that the SODAR observes a significant disturbance as a result of the platform while this is

absent in the mast measurements. Possible explanations are the difference in measuring principle (plane versus point), the difference in position with respect to the platform or the higher level of the turbulence intensity.

The alternative is that the SODAR measures the undisturbed wind speed and the mast is not correct. This option seems not very likely. The mast directions compare well with SODAR observations above 60 m. Besides, some SODAR profiles show clear discontinuities below 60 m that are an contra-indication for the above assumption. The mast wind speed compares well with mast wind speeds from other stations [Coelingh et al. (1996)]. Further evidence is that the 60 m Monin-Obukhov calculated wind speed compares well with the SODAR at 60 m MSL. When we assume that the theory is correct, this implies that mast measurements and SODAR measurements at 60 m correspond with each other. This is further evidence for the correctness of the mast measurements.

It seems likely that the SODAR measures wind speed correctly and that the platform disturbs the wind flow. As a consequence, the SODAR measures the disturbed wind speed. Unfortunately, there is not enough data at present to validate this preliminary conclusion more thoroughly. First of all, longer data sets can give more insight. It is then possible to analyse data per sector. An alternative is to place anemometers at higher heights (preferably measuring the undisturbed wind speed) or one close to the SODAR. As we are interested in undisturbed wind profiles, it is for the given platform advisable to position the SODAR where disturbance by the platform is the least.

At 60 m MSL, the SODAR measurements are on average somewhat higher than the mast measured wind speeds transformed by Monin-Obukhov theory. The width of the scatter band is quite broad. Partly this may result from the measuring error of the SODAR but also the theory may not be suitable for small time intervals. The higher the height referred to, the larger the difference between theory and SODAR measurements. With the current information it is not possible to determine which of the two compares best with the actual wind speed.

6.6.7 Discussion

A SODAR is a very useful device to measure wind speed profiles and can help to describe boundary layer phenomena. In this section the performance of the SODAR in the period from February 23 to June 16 200 at Measuring Post Noordwijk was investigated. It turned out that the SODAR does not produce correct wind speeds during some periods of rain. For this reason, periods with rain are excluded from the data set.

The percentage of data recovered by the SODAR decreases with height. The height range of the SODAR at MPN is poor and worse than earlier onshore measurements at ECN. We tried to identify the causes.

The back ground noise level is quite high and increases with wind speed. The base noise source are the diesel generators for the electricity supply which sets a lower limit for the back ground noise. When the wind speed increases, additional noise sources arise: the sound of the wave grows and the wind whistles along the superstructure of the platform. The height range of the SODAR decreases with an increase in back ground noise level; the returned signal 'drowns' in the noise.

For wind speeds smaller than 7 m/s (measured at the mast) the SODAR height range improves with increasing wind speed. The reason may be the more laminar flow, but this is just a guess. For wind speeds larger than 7 m/s the height range decreases with wind speed. This is caused by the increase of back ground noise with wind speed above 7 m/s.

Stability and height range are also related. There is a indirect effect because wind speed and stability are related. The wind speed is largest under neutral conditions and decreases for stable and for unstable atmosphere. There is small evidence that there is also a direct effect between stability and SODAR height range. The SODAR height performance is worst under neutral conditions. The more unstable the atmosphere, the better the height performance. This also holds for stable conditions. This is to a large extent caused by the larger noise level at higher wind speed but there may be a relation that the more stable the atmosphere, the better the SODAR height range.

We also compared the SODAR measurements to the wind speed mast at MPN-platform.

Above 60 m MSL the wind direction distribution of the SODAR and that of the mast compare well. Below 60 m, the distribution measured by the SODAR deviates significantly from that of the mast. The measure of the deviation varies per sector. The mean wind speed of the mast and the SODAR observation above 60 m MSL form a neat profile. When we assume that the mast measurements are correct and undisturbed, the SODAR wind speeds below 60 m MSL are too low compared to the mast. It appears that above 60 m, the SODAR produces valid means, but there is no data available to validate this. The 60 m border seems fixed and is observed under all circumstances.

It seems likely that the SODAR measures wind speed correctly and that the platform disturbs the wind flow. As a consequence, the SODAR measures the disturbed wind speed. Unfortunately, there is not enough data at present to validate this preliminary conclusion more thoroughly. First of all, longer data sets can give more insight. It is then possible to analyse data per sector. An alternative is to place anemometers at higher heights or close to the SODAR. As we are interested in undisturbed wind profiles, it is for the given platform advisable to position the SODAR where disturbance by the platform is the least.

With the help of Monin-Obukhov theory it is possible to transform measured mast wind speeds to other heights, taking into account the stability of the atmosphere. The mast wind speed was transformed to 60 m and 120 m MSL and compared to the SODAR measurements.

At 60 m MSL, the SODAR measurements are on average somewhat higher than the mast measured wind speeds transformed by Monin-Obukhov theory. The width of the scatter band is quite broad. Partly this may result from the measuring error of the SODAR but also the theory may not be suitable for small time intervals. The higher the height referred to, the larger the difference between theory and SODAR measurements. With the current information it is not possible to determine which of the two compares best with the actual wind speed.

The SODAR functions well but because of the large back ground noise level, the height range is poor. This makes the SODAR data less valuable for statistical purposes but does not affect the usefulness for validation of the CDM-model: only the amount of available data points at the higher heights reduces. At the lower heights, enough data is present for statistical purposes. Unfortunately, it seems that below 60 m MSL, the SODAR measurements are disturbed by the platform. Therefore, below 60 m the SODAR measurements do not reflect the undisturbed wind flow and can not be used for validation of the CDM. Above 60 m MSL, the SODAR measurements seem correct and correspond with the mast measurements. These data can be used to validate the CDM.

The only identified cause for the poor height range that can be influenced is the back ground noise. Positioning the SODAR further away from the diesel generators will enormously reduce the back ground noise level. When repositioning the SODAR, it is also of importance to look for a position where the noise from waves and whistling of the wind is as low as possible. Another position of the SODAR may also reduce the disturbance of the platform on the heights lower than 60 m.

In order to further analyse the performance and correct functioning of the SODAR a longer data set is desirable. The positioning of an anemometer at a low level near the SODAR or at a larger height (> 60 m) can also give valuable information.

6.7 Analysis of SODAR data collected in the UK

6.7.1 The Weybourne site

A mini-SODAR was installed at Weybourne in August 2000 and remained on site until the end of October 2000. Weybourne is a village located on the north coast of Norfolk. The SODAR site is within the grounds of an outstation belonging to the University of East Anglia School of Environmental Sciences, where laboratory facilities are available for atmospheric chemistry measurements. The site position is 52.95^{o}N by 1.13^{o}W. It has the advantage of having no-one living nearby, which is a consideration with a mini-SODAR which makes a persistent ‘pinging’ noise. Ambient noise levels are low, which allowed high quality measurements to be taken, with few missing data. The site is well exposed to the open sea to the north (see Figure 6-37)

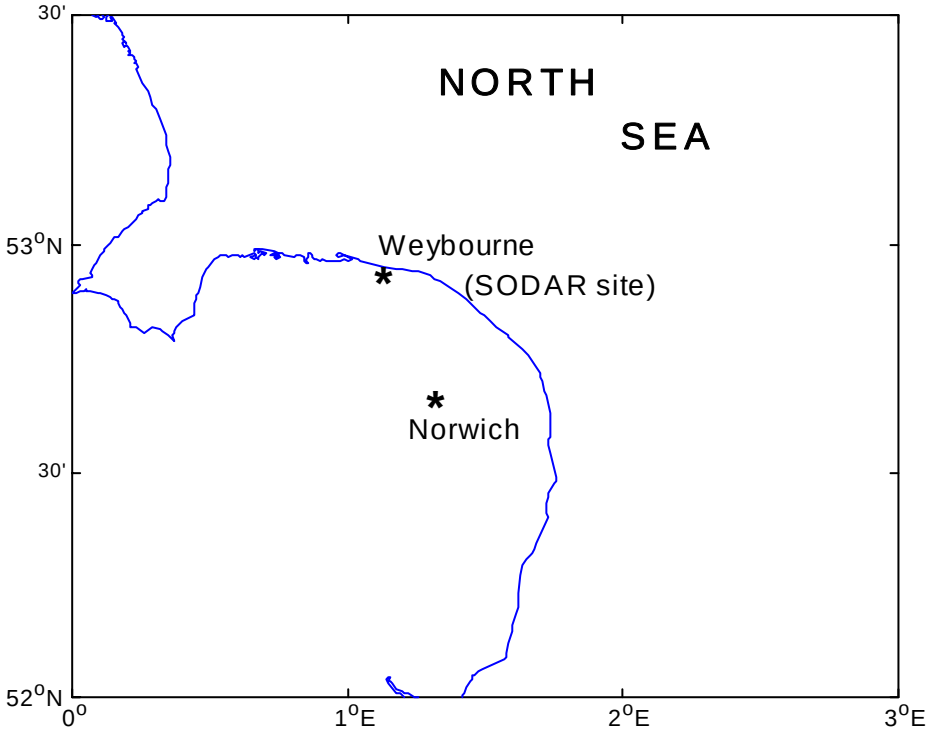

Figure 6-37: Location of the SODAR installation at Weybourne

These factors made it an ideal location for looking at the vertical profile of winds moving onshore from the open sea.

6.7.2 Data processing

High quality data for 80 days were collected, from 26th August 2000 to 22nd October 2000. The mini-SODAR was on site for a longer period, but some data were lost due to the activities of rabbits (see Figure 6-38), problems with a disk drive, and occasional erratic behaviour of the system. The rabbit problem was solved by encasing the cables in rigid plastic piping. Data were collected every 5 minutes at 5 m intervals from 10 to 200 m and the variables of main interest include wind speed and direction, gust speed and direction, vertical wind speed, and the u and v components of the horizontal wind field.

Figure 6-38: Damage to SODAR cabling by rabbits

Before analysis the SODAR data required extensive filtering to rationalise missing values and to adjust obviously incorrect estimates. In addition to the degrading of data due to destruction of the cable by rabbits, the data quality is affected by random fluctuations and systematic bias during rainfall. Error-correction software was developed using the last 57 days of measurements, where the only errors in the data were due to rainfall and apparently random "spikes". The methodology was then applied to the less reliable part of the record. The error-correction procedure is as follows:

- Pass 1: sets all data in the current record to missing if wind speed, u, or v component is missing. The lack of any of these elements on a 5-minute time step makes it impossible to validate the remaining data and to create time-averaged wind speeds and direction.
- Pass 2: sets all data in the current record to missing if the previous and subsequent values of wind speed, u, or v are missing. This circumstance makes reliable interpolation impossible.
- Pass 3: interpolates up to three consecutive missing 5 minute timesteps, if the adjacent values form a series of smooth estimators with no spikes. It was considered that interpolation of more than three successive 5 minute timesteps could lead to unreliable estimates of hourly mean wind. Prior to interpolation, adjacent data were checked for abnormally high or low values.
- Pass 4: this stage is a subjective assessment of the time series. The data are visually "tuned" using a graphical display by interactively adjusting isolated peaks, interpolating isolated missing values, and inserting missing values when the series appears dubious.

Following error-correction, hourly and daily mean vertical wind speed and horizontal wind speed and direction, were calculated, and output to files at each 5 m level along with maximum gust and maximum gust direction.

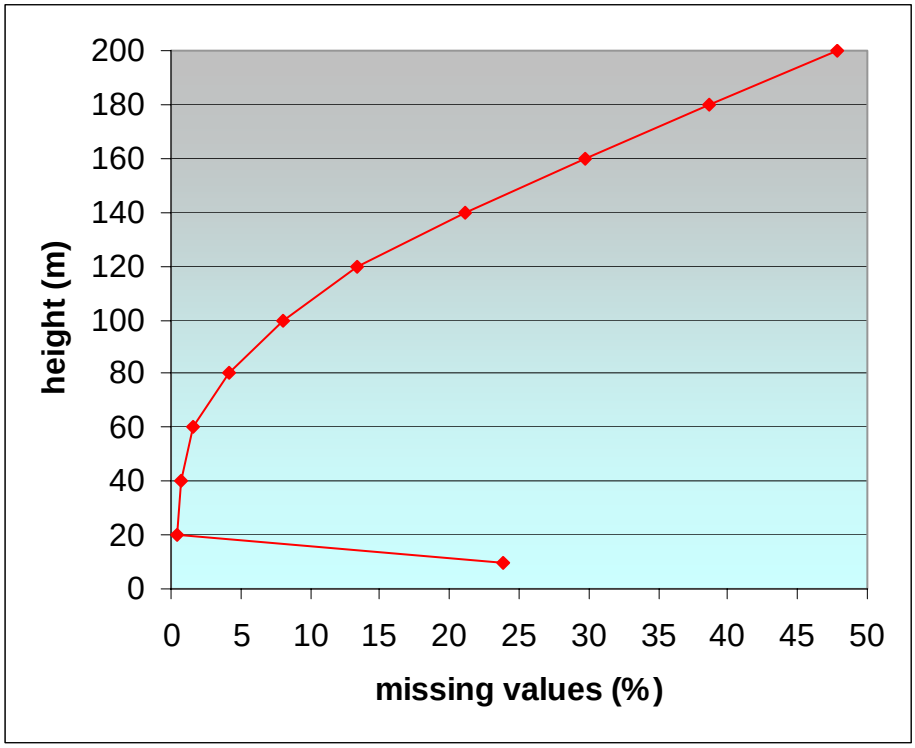

Figure 6-39 : Percentage of missing values with height

Figure 6-39 shows that, because of missing values, it would not be possible to estimate a reliable diurnal cycle above about 120 m and below 20 m. The missing values at height are not caused by a failure of the SODAR but indicate that the effective measuring height of the instrument varies with atmospheric conditions.

6.7.3 Analysis of the data

Mean wind speed profile

Figure 6-40 shows how the mean wind speed profile varies with height according to the SODAR data. An exponential curve fits the data better than a logarithmic curve, with r^2 of 0.9954. The curve is calculated from hourly mean wind speeds, averaged over a day, and then averaged over the last 57 days of recorded data.

Diurnal cycle of wind speeds

Figure 6-41 shows the diurnal cycle in wind speed, averaged over all values at each hour from 0000 to 2300, at heights from 20 to 120 m at 20 m intervals. The averaging to calculate the diurnal cycle only uses data from the last 57 days of the record, to avoid problems related to missing values in the first few days of instrumentation. Heights above 120 m are not shown because they contain increasing numbers of missing values. The diurnal cycle at all heights has a trough centred on 1800 hours. At 20 m, there is a gradual decline in wind speeds from a maximum at 1200 hours. This peak at 20 m at 1200 hours is not found aloft, where the maximum is at about 2300 hours.

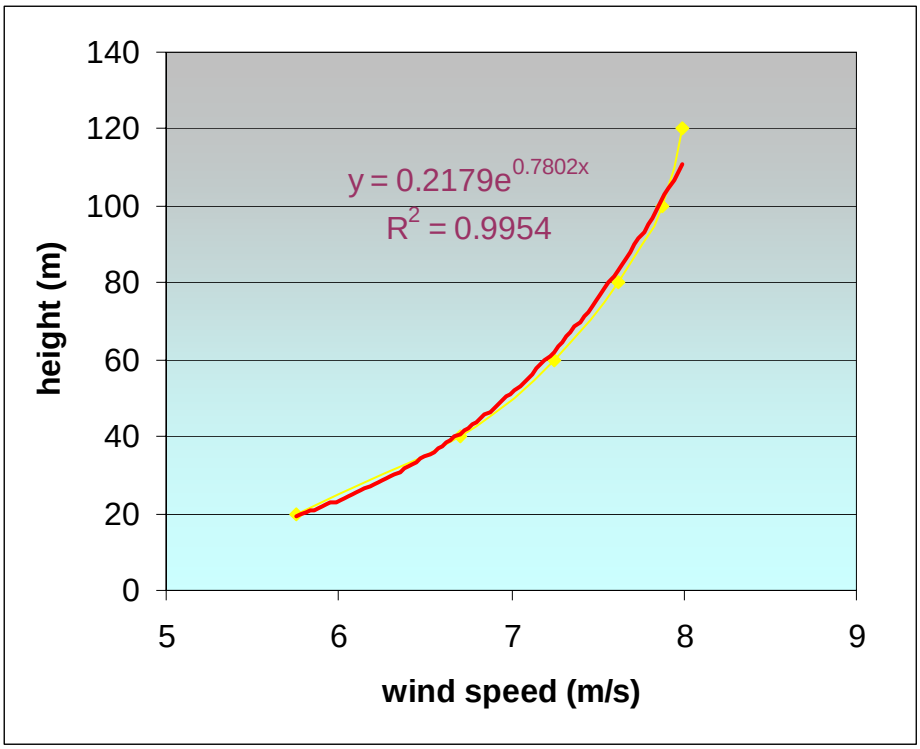

Figure 6-40 Mean daily wind speed profile

Figure 6-42 shows the daily mean wind speed over the whole 80 days. The charts are organised to display wind speeds at two heights on each plot. The dashed rectangle indicates the period when the record was disrupted by rabbits chewing through the cable. In the daily mean data, this appears to have had little effect, apart from the period when the instruments cut out entirely. Wind speeds at height above 100 m are shown in smaller plots since the vertical wind shear is much less at these heights.

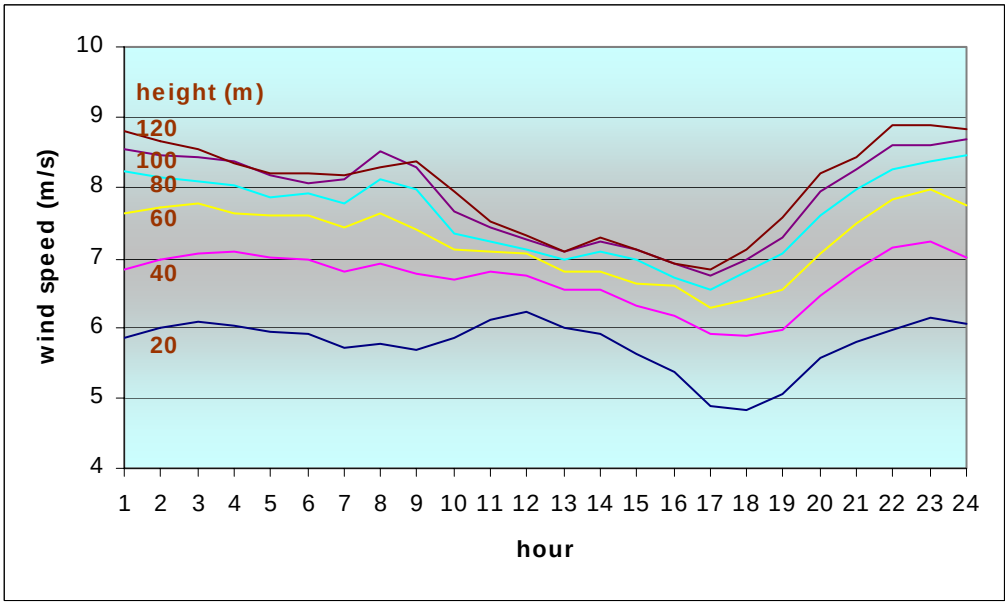

Figure 6-41 Diurnal cycle of wind speed at Weybourne

Partitioning the data into land and sea fetches

The Weybourne site is well exposed to the open sea from the north, but has a land fetch to the south. In order to understand the differences between land- and sea-fetch winds with respect to:

- the diurnal cycle of wind speeds and
- the vertical wind speed profile,

the data set of wind speeds was partitioned into land and sea subsets:

- land fetch: defined as wind directions 130^o-270^o
- sea fetch: defined as wind directions 310^o-70^o

and analysed further. The partitioning was carried out conservatively, to ensure the purity of the two subsets. Winds from the west-north-west and from the east, blowing along the coast, were rejected at this stage. Note that when the data are partitioned in this manner, there are many more land-fetch observations than sea-fetch observations. Analyses of the land-fetch wind speeds can be carried out up to 200 m above the ground, whereas for the sea-fetch wind speeds there are insufficient observations above 100 m for meaningful results to be obtained.

As shown clearly in Figure 6-39, there are many missing data from the mini-SODAR at the 10 m height (and in fact it turns out that mini-SODAR data are not reliable this close to the ground). We therefore obtained data from a standard anemometer mast located very close to the mini-SODAR. This is the Weybourne SAWS anemometer, at a standard 10m above the ground, located some 200 m south of the mini-SODAR. The data for the period during which the mini-SODAR took measurements were obtained from the British Atmospheric Data Centre (BADC). In the analyses which follow, the 10 m data is always from Weybourne SAWS.

First, we used the partitioned data to look at differences in the diurnal cycle Figure 6-43 shows the mean wind speed at each hour in the day, at heights up to 200 m for the land fetch and 100 m for the sea fetch. The diurnal cycles are quite different, as is their evolution with height.

For the land fetch, at the lower heights there is a clear peak in the middle of the day. However, by 60m the amplitude of the cycle has reduced to close to zero. As the height increases still further, wind speeds become higher at night, and reach their minimum in the early afternoon hours. This is according to theory, and has been observed by, for example, [Emeis (2001)]. At night, a low-level inversion forms as the land surface cools. The surface layer decouples from the rest of the boundary layer, giving very low wind speeds close to the ground and higher wind speeds above the surface layer. In the daytime, as the land surface warms, vertical mixing leads to small vertical gradients in wind speed.

Over the sea at the lower observation heights, wind speeds are lower in the afternoon, and higher at night, with the transitions occurring in the late morning and late evening. [Barthelmie et al. (1996)] noted that the temperature of the sea surface will tend to be lower than that of the overlying air during the day, leading to stable conditions and lower windspeeds, whereas at night the sea surface will tend to be warmer than the overlying air, leading to less stable conditions and higher wind speeds. Therefore, the diurnal cycle over the sea may be the inverse of that observed over the land. Here, we see that this pattern is not only preserved with height, but there is some indication that it becomes more intense. There are important implications here for wind turbines located in the near-shore zone, whose hub heights are expected to be of the order of 100 m above the surface.

Figure 6-44 shows the vertical wind speed profiles in the sea- and land-fetch data subsets. Sea profiles are very similar through the day. There is little variation in speed with height, suggesting well-mixed unstable conditions. Over the land, there is a diurnal cycle in these profiles. In the early hours of the morning, there is a substantial increase in speed with height, indicating stable conditions. After dawn, the profile gradually steepens until by midday there is little variation in speed with height. As evening progresses, the profiles move once more towards increasing wind speed with height. These clear differences in land-fetch and sea-fetch wind speed profiles are potentially important for developers attempting to predict hub-height windspeeds from near surface observations.

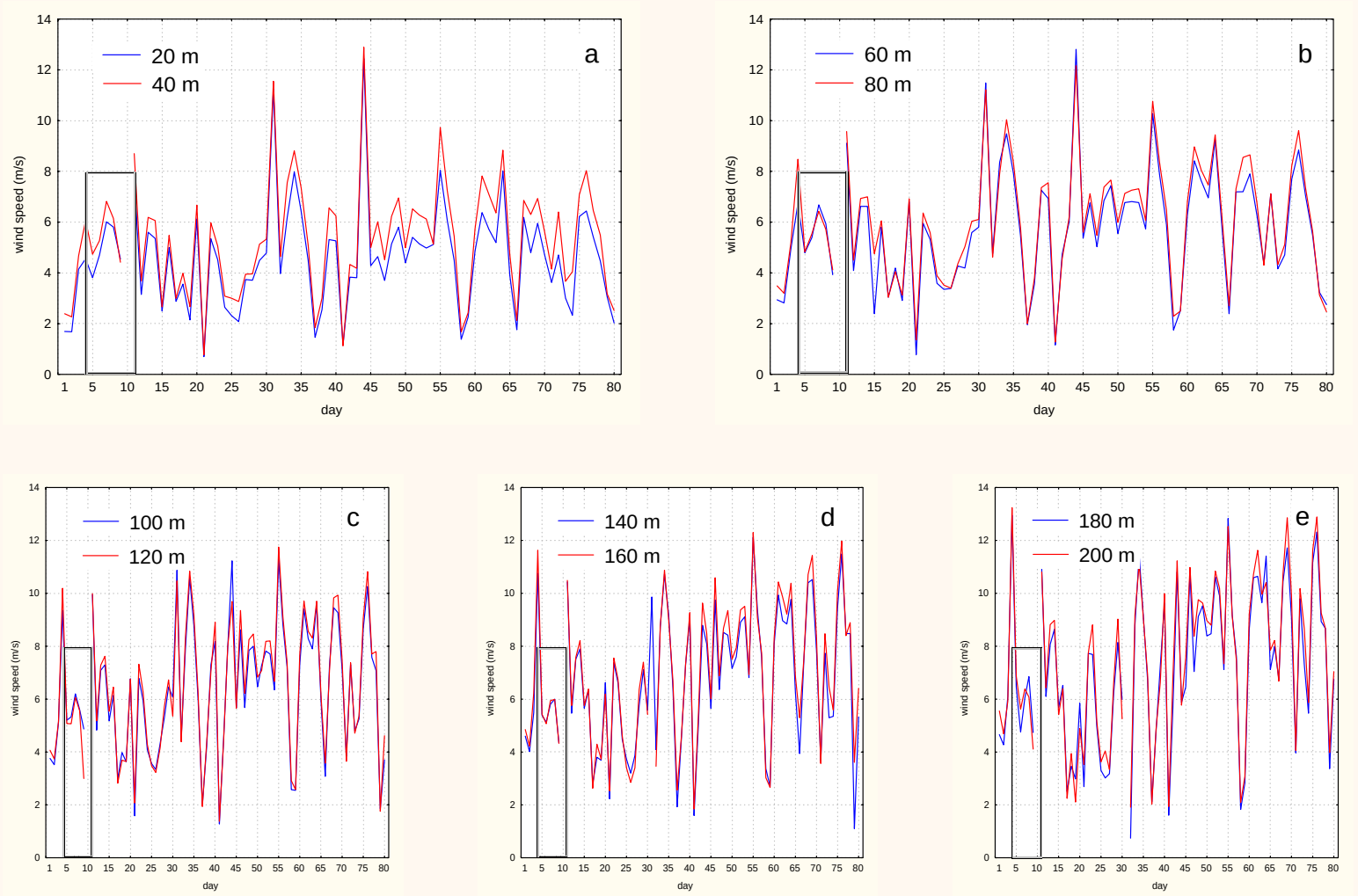

Figure 6-42 Daily mean wind speed (dashed rectangle encloses suspect data)

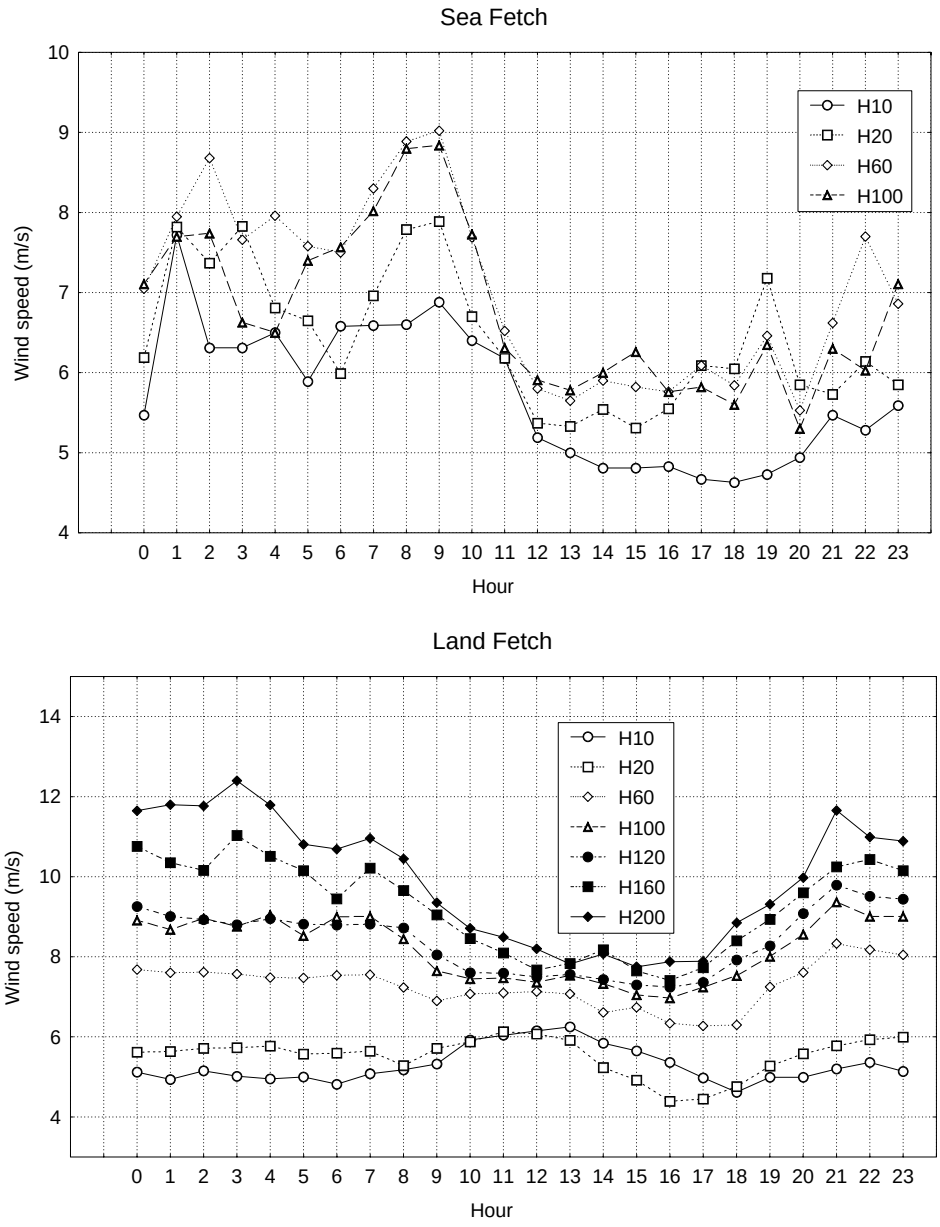

Figure 6-43 Diurnal cycles of sea-fetch and land-fetch wind speeds

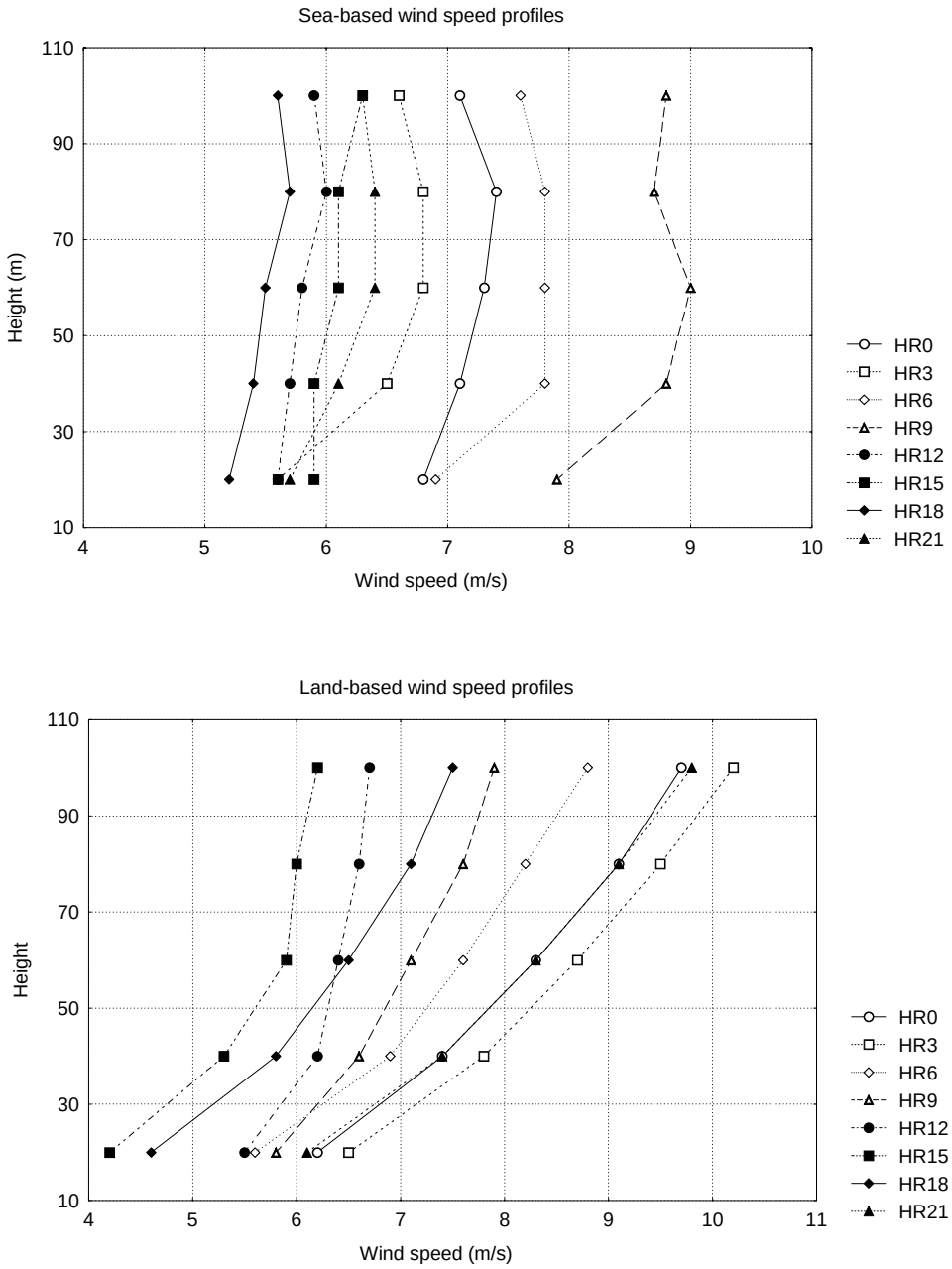

Figure 6-44 Vertical profiles of sea-fetch and land-fetch wind speeds

6.8 References for Chapter 6

Aeronvironment, Doplmain, software description, Monrovia, USA, 1998

Aeronvironment, PADS (Profiler Analysis and Display Software), software description, Monrovia, USA, 1998a.

Coelingh, J.P., A.J.M. van Wijk and A.A.M. Holtslag, Analysis of wind speed observations over the North Sea, Journal of Wind Engineering and Industrial Aerodynamics, Vol, 61, pp 51 – 69, 1996.

Coelingh, J.P., L. Folkerts, E.. van Zuylen and G.F.M. Wiegerinck, Using SODAR measurements in the POWER project, Proceedings BWEA21, Cambridge, UK, Professional Engineering Publishing, 1999

Coelingh, J.P., L. Folkerts, G.F.M. Wiegerinck and E.J. van Zuylen, Study of the offshore wind climate using a SODAR, Proceedings OWEMES, Siracuse, Italy, 2000

Crescenti, G.H., A look back on two decades of Doppler SODAR comparison studies, Bulletin of the American Meteorological Society, Vol. 78, No. 4, pp 651 – 673, April 1997.

Dam, J.J.D. van and E.J. van Werkhoven, Mini-SODAR for wind energy application – exploring experiments, ECN – C99-034, Petten, The Netherlands, 1999

Garratt, J.R., The atmospheric boundary layer, Cambridge University Press, Cambridge, UK, 1994.

Wiegerinck, G.F.M. and J.P. Coelingh, WT2STAV Manual version 1.2, Ecofys, Utrecht, The Netherlands, September 2000.

Wiegerinck, G.F.M., Manual SODARTOOL, Ecofys, Utrecht, The Netherlands, January 2001.

Barthelmie, R.J., B. Grisogono and S.C. Pryor (1996) Observations and simulations of diurnal cycles of near-surface wind speeds over land and sea. Journal of Geophysical Research, 101 (D16), 21327-21337.

Emeis, S (2001) Vertical wind variation observed by SODAR. Meteorologische Zeitschrift, 10, 141-149.

CHAPTER 7 : Variability of offshore winds

Chapter authors: : Dr T Holt and Dr J P Palutikof (University of East Anglia)

7.1 Introduction

Offshore wind speeds are known to vary over a wide range of time scales:

long-term – inter-annual, decadal and other long-term trends such as global warming
medium-term - seasonal cycles
short-term – e.g. gusts and the diurnal cycle

Within POWER, staff from UEA sought to extend the current understanding of three types of variability in the offshore wind regime, namely, long-term trends, the diurnal cycle and gusts. This work is reported in the following sections.

7.2 The long-term characteristics of the wind field over Western Europe

7.2.1 Introduction

As part of the POWER project, The Climatic Research Unit constructed and validated a data set of the geostrophic wind field over Western Europe, using sea level pressure data on a 0.5° by 0.5° latitude/longitude grid at 6-hourly intervals from 1985 to present (see Section 3.1 of this report). Using data over this relatively short period it is not possible to say anything about the long-term time series characteristics of the wind field. It would be extremely useful to know, for example, if the wind regime is subject to periodic changes or is part of some long-term trend. Furthermore, it may be possible to identify regional patterns of windiness and to search for evidence of climate change.

In order to pursue these objectives it was necessary to create a new data set. The geostrophic winds in Section 3.1 were calculated from the NCEP Reanalysis pressure data, but these are not really suitable for long-term analysis since the record is only 50 years long. The UK Meteorological Office (UKMO) provides a Northern Hemisphere mean sea level pressure data set that is available from 1871 to present as mean monthly data and from 1881 to present as daily data [Jones (1987)]. Prior to about 1900, the daily data set has large numbers of missing values in the more northerly latitudes. Since we are considering the long-term variability of the wind field, the daily geostrophic wind has been calculated from the daily pressure data from 1900 to 1997, and averaged to give the monthly mean wind. Missing pressure values in this period were replaced with estimates using the method of [Holt (2001)].

7.2.2 Data and methodology

As with the POWER studies using the NCEP data (Section 3.1), the geostrophic wind is calculated from pressure data, this time on the 10° longitude by 5° latitude grid of the UKMO pressures, at daily intervals from 1900 to 1997, over the European domain defined by POWER and shown in Figure 7.1. The monthly mean geostrophic wind was calculated by averaging the daily values.

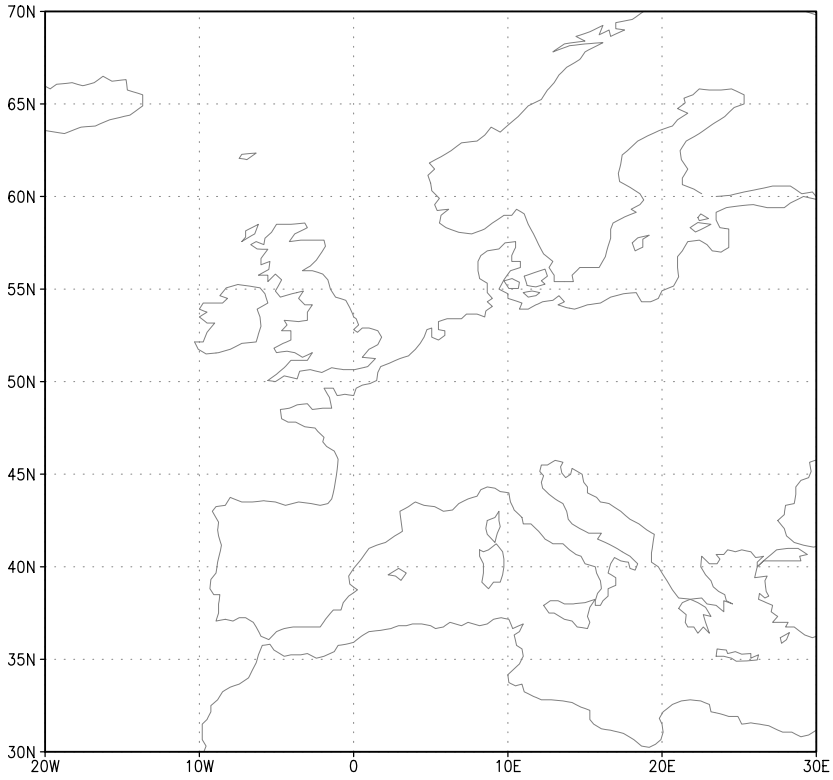

Figure 7.1 The domain of the geostrophic wind calculated from the UKMO pressures

7.2.3 Principal Components Analysis of the geostrophic wind data

With nearly 100 years of monthly wind data covering the area shown in Figure 7.1, we need a method of organising the data in space before performing any time series analysis. Principal Components Analysis (PCA) offers an objective and efficient method of identifying spatially coherent patterns (factors) that are mutually uncorrelated. That is, the patterns produced by the factors are statistically independent of each other. PCA also has the added bonus of providing new time series of data (factor scores) associated with the factors. It is not necessary to explain all the detailed aspects of PCA here, there are many excellent references to the application of the technique to climate data that do this (for example, [Preisendorfer (1988)]. Instead we concentrate on interpreting the results of our particular experiment, introducing technical discussion only where clarification is necessary.

An important consideration with PCA carried out on a long time series is that the statistical properties of the data may change markedly with time. This could invalidate the PCA since the factors may be unstable, that is, the factor loadings may be significantly different if the PCA were repeated using the first 50% of observations and then the second 50%. The results of such a stability test are described in Section 7.2.6.

In a previous study, [Holt (1999)] demonstrated that pressure fields can be reduced to extremely simple patterns using the varimax orthogonal rotation of factor loadings. The rotation also removes the tendency for spurious edge patterns from the factor loadings when a spatial subset of the data is used [Richman(1986)], as is the case in this analysis. For these reasons, we perform our PCA using varimax rotation of significant factors. The significant factors are chosen according to the Kaiser criterion of eigenvalues less than 1.0 representing only statistical noise [Jackson (1993)]. The PCA is performed with the wind speeds at the grid nodes in Figure 7.1 as the variables to be grouped by the analysis. The initial 54 variables are reduced by the PCA to just seven significant factors explaining 83.46% of the variance in the original data, as shown in Table 7.1. Table 7.1 also demonstrates the effect of orthogonal factor rotation. Prior to rotation, the factors explained reducing amounts of variance. The variance explained by the rotated factors is much more evenly distributed and not in magnitude order.

Factor	Eigenvalue	% of variance explained (before rotation)	% of variance explained (after rotation)
1	30.51	56.49	26.37
2	4.47	8.28	17.19
3	3.58	6.64	5.01
4	2.26	4.19	8.89
5	1.60	2.97	17.47
6	1.38	2.56	4.17
7	1.26	2.33	4.35
	Total	83.46	83.46

Table 7.1 Eigenvalues from the PCA of geostrophic wind.

7.2.4 Patterns of Factor Loadings

The wind regimes associated with the rotated factors will now be examined. Each plot contours the loadings of a particular factor against each of the original variables. The rotation has yielded very simple plots, with a single dominant wind regime associated with each factor. Low absolute values indicate areas not associated with the dominant pattern of windiness.

Factor 1

Figure 7.2 shows the pattern of loadings associated with Factor 1 of the PCA. This represents a region of high (or low) wind speeds centred over the Baltic and southern Scandinavia. This pattern influences sea areas over the Baltic, Scandinavia, the UK, Ireland, the North Sea, and northern France.

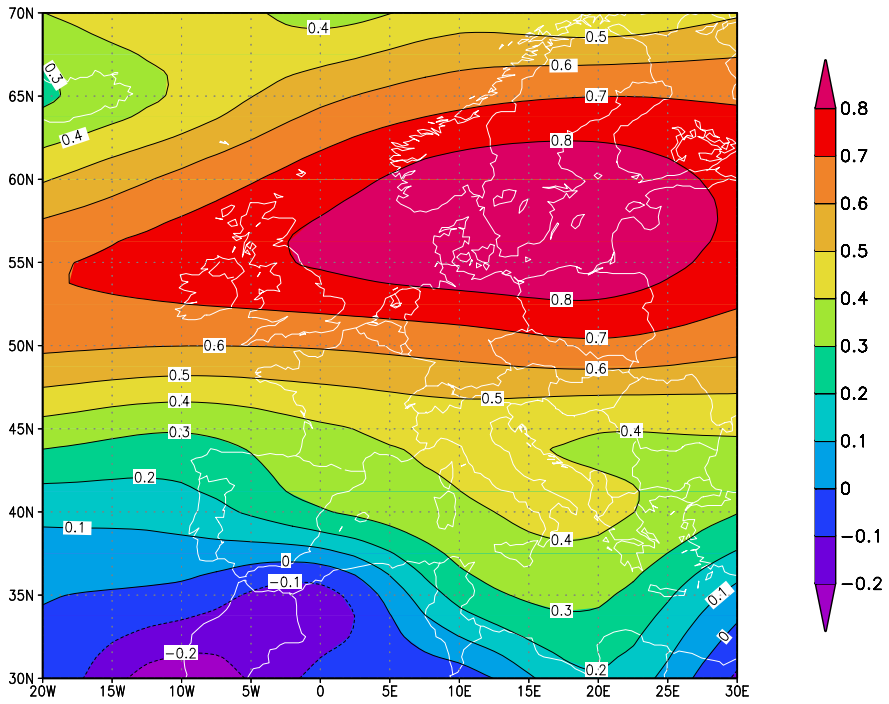

Figure 7.2 Factor 1, explaining 26.37% of the variance

Factor 2

The wind regime associated with Factor 2 (Figure 7.3) is centred over the western Mediterranean and affects the Mediterranean, Spain, Portugal, and western France.

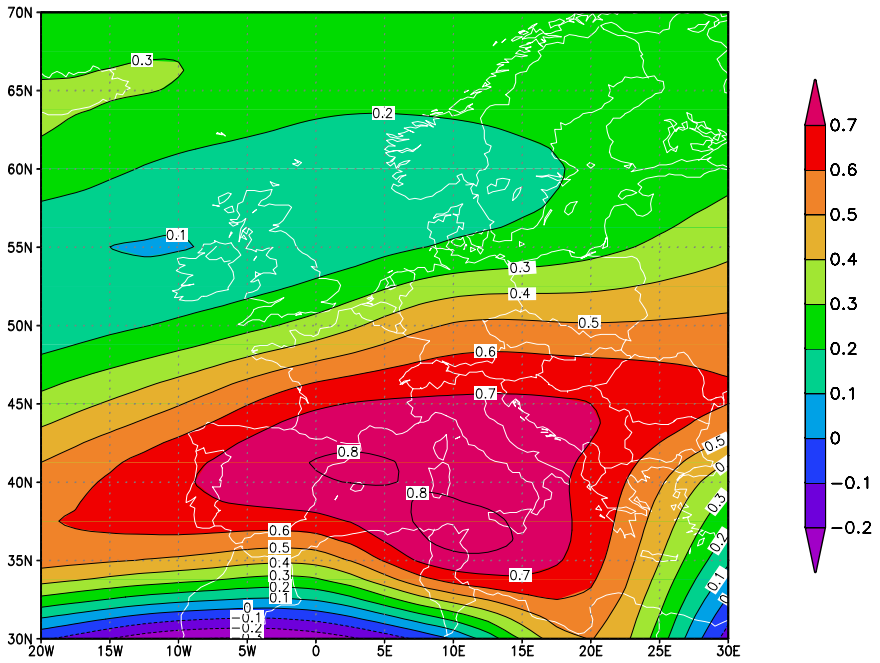

Figure 7.3 Factor 2, explaining 17.19% of the variance

Factor 3

The wind regime represented by Factor 3 (Figure 7.4) affects the Sahara and northern Africa.

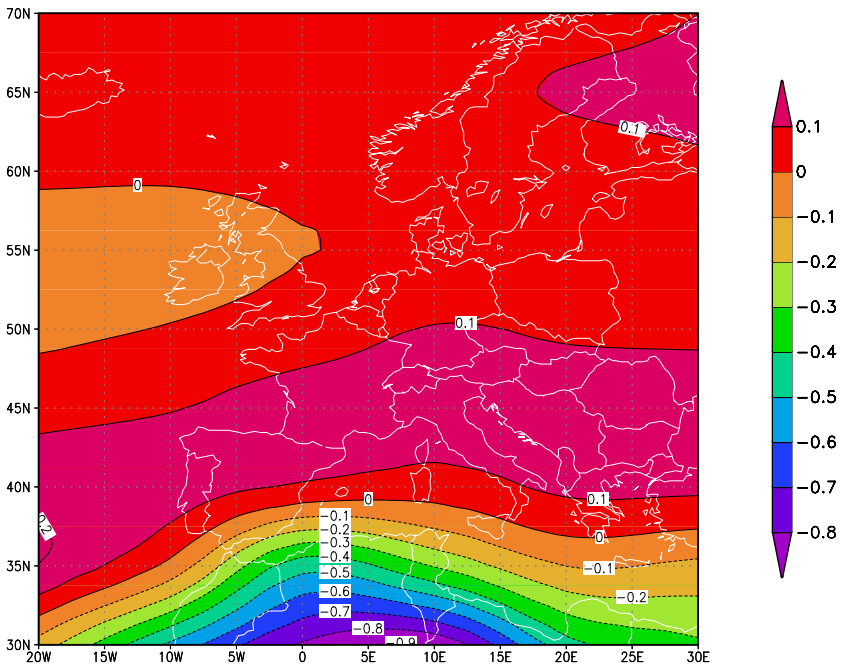

Figure 7.4 Factor 3, explaining 5.01% of the variance

Factor 4

Figure 7.5 shows the wind regime associated with Factor 4 to be centred over the Azores, affecting northern Portugal and Spain, northern and western France, Ireland, Wales, and England.

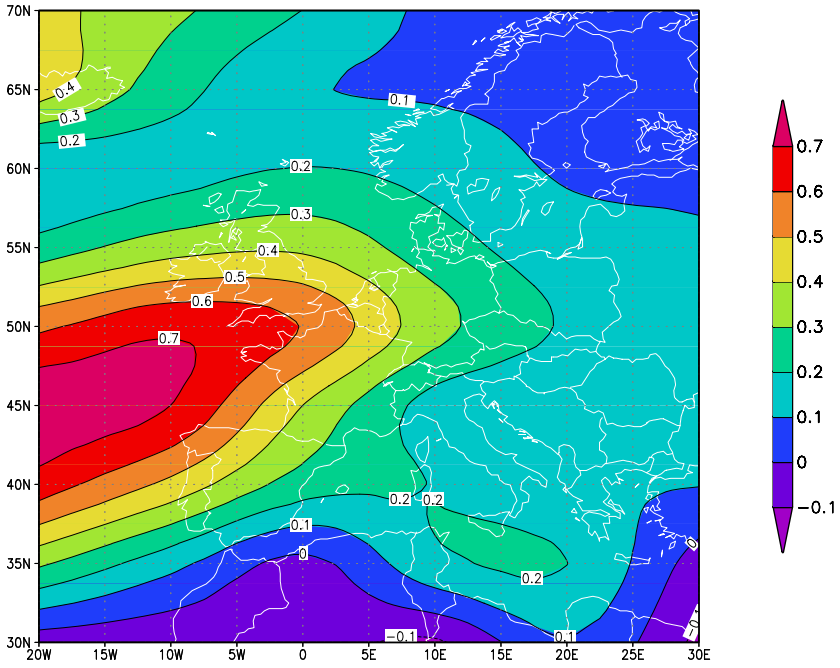

Figure 7.5 Factor 4, explaining 8.89% of the variance

Factor 5

Factor 5 (Figure 7.6) is centred north east of Iceland. Regions affected include Iceland, Scotland, northern Norway, Sweden, and Finland.

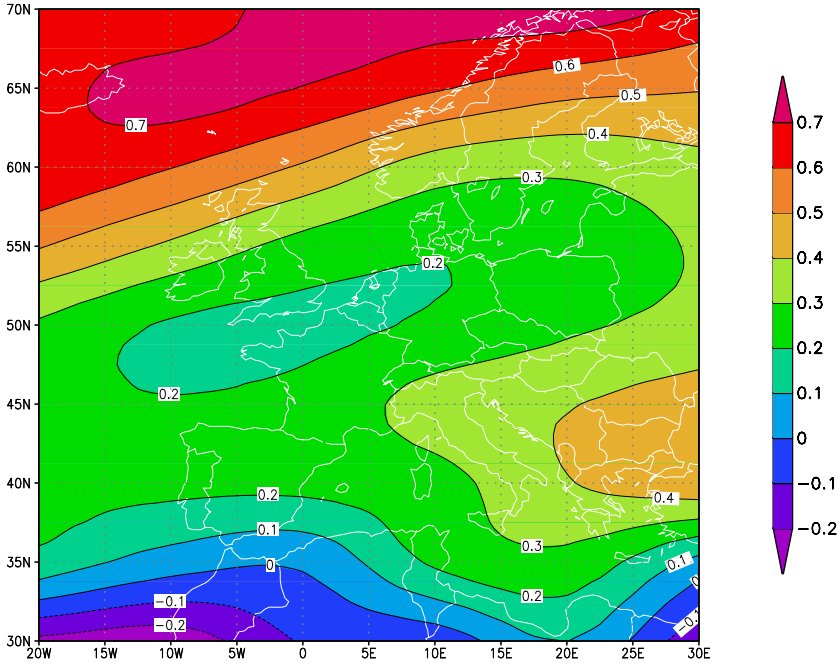

Figure 7.6 Factor 5, explaining 17.47% of the variance

Factor 6

Factor 6 (Figure 7.7) represents the dominant mode of the wind field centred south west of Spain, influencing northwest Africa and southern Spain and Portugal.

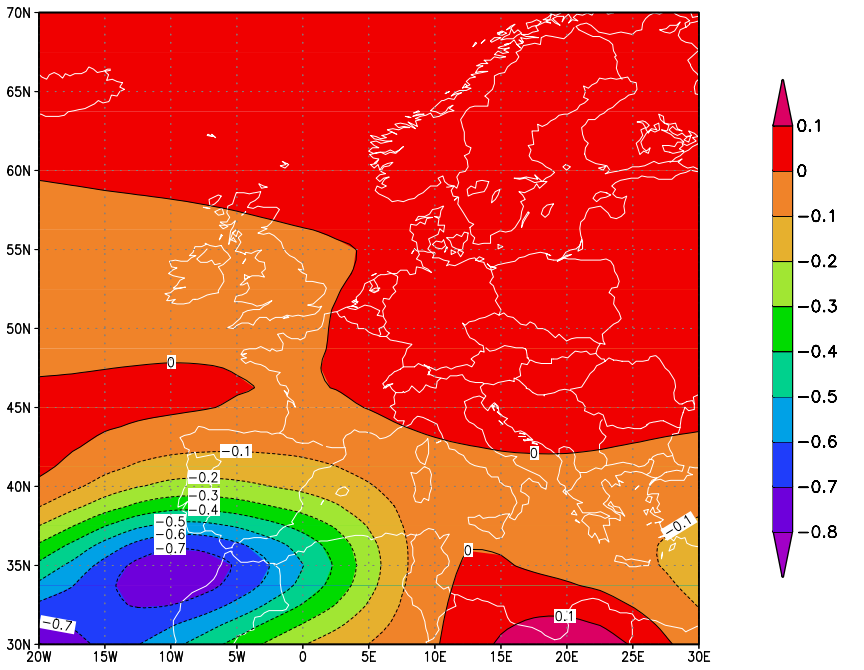

Figure 7.7 Factor 6, explaining 4.17% of the variance

Factor 7

Figure 7.8 shows the loading pattern from Factor 7, centred over the Middle East. The affected regions include Egypt, southern Turkey, south-eastern Greece, Israel, and Lebanon.

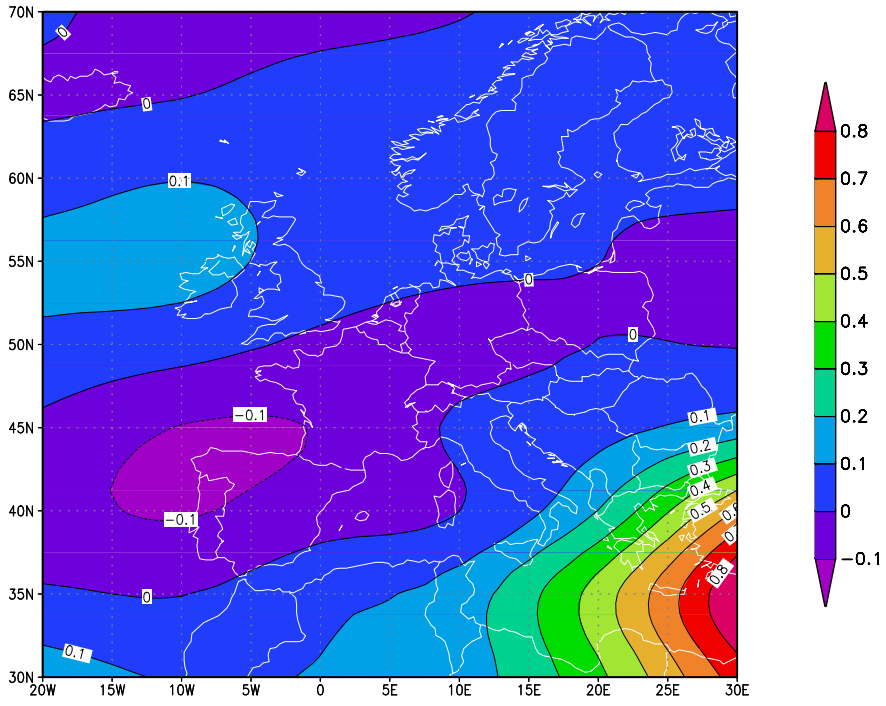

Figure 7.8 Factor 7, explaining 4.35% of the variance

7.2.5 Summary

Table 7.2 summarises the patterns of factor loadings (Figures 7.2 to 7.8) relevant to the POWER project. It is important to note that the lists of coasts affected only includes members of the European Union and the identification of locations may be misleading. Moreover, an arbitrary cut-off of the highest four absolute contour intervals was used to define the effective limits of a particular wind regime. For precise geographical location of the wind regime and for non-EU countries, the reader should refer to the plot of the relevant factor. The factors in Table 7.2 are sorted in order of percentage of variance explained. This can be interpreted as order of overall "importance". Factor 3, centred on northern Africa, does not influence the offshore wind regime of any EU member state and will not be considered further.

Factor number	% variance	Centre	*EU Coasts affected
1	26.37	Baltic, S. Scandinavia	Ireland, UK, W. France, Holland, Belgium, Denmark, Germany, Sweden, Finland
5	17.47	Northeast of Iceland	Scotland, Sweden, Finland
2	17.19	W. Mediterranean	Portugal, Spain, W. and S. France, Italy, Greece
4	8.89	Azores	N. Portugal, N. Spain, N. and W. France, Ireland, Wales, England, Belgium, S. Holland
7	4.35	Middle East	S. Greece
6	4.17	Off S.W. Spain	S. Spain, S. Portugal

Table 7.2 Summary of factor loading patterns from the wind data PCA

In Table 7.3, the information in Table 7.2 is reorganised to facilitate identifying the wind regimes associated with offshore conditions for each country. The same country can appear in different regions, for example Spain has Atlantic and Mediterranean coasts. Similarly, the same factor can appear twice in the table if it affects more than one region (for example, Factor 1). The factors affecting any part of the coast of each country, within a particular region, are presented in order of percentage of variance explained. Cross-referencing Table 7.3 with Figures 7.2 to 7.8 will enable an assessment of the wind regimes associated with particular countries.

Region	Country	Factors
Atlantic	Belgium	1, 4
	Denmark	1
	France	1, 2, 4
	Germany	1
	Holland	1, 4
	Ireland	1, 4
	Portugal	2, 4, 6
	Spain	2, 4, 6
	United Kingdom	1, 5, 4
Baltic	Denmark	1
	Finland	1, 5
	Germany	1
	Sweden	1, 5
Mediterranean	France	2
	Greece	2, 7
	Italy	2
	Spain	2, 6

Table 7.3 Factors affecting particular countries

The patterns of factor loadings provide an objective assessment of the main wind regimes affecting the coasts of Europe. However, they only describe the main modes of the organisation of the wind field in space. There is no information on the intensity of the wind fields, or how this changes in time. We

now consider time-dependent changes in the wind regimes, first assessing how representative the factor loading patterns are of the general wind field.

7.2.6 Testing the stability of the factor loadings

It is possible that over the length of the record, patterns of windiness have changed fundamentally so that the wind regimes identified by our PCA are simply artefacts that do not represent typical wind fields at all. To test the stability of the factor loadings in time the PCA is repeated using data from 1900 to 1939 and from 1940 to 1997. If the patterns of factor loadings are essentially the same, one can conclude that the patterns for the whole series in Figures 7.2 to 7.8 represent genuine wind regimes and the analysis can proceed.

Table 7.4 shows that although the factor identifiers are sometimes different, the PCA for 1900 to 1939 gives essentially the same patterns as for the 1940 to 1997 analysis and the factors explain roughly the same amount of the overall variance in the data. The failure of the PCA to always give the same identifier to similar patterns of variance is not important. When we compare the results of the early and late period analyses to the analysis of the full data set (Table 7.4), there are some strange anomalies. There is some switching of identifiers but generally good agreement on the amount of variance explained. The patterns for Factors 5 and 1 of the full analysis bear only a passing resemblence to their nearest equivalents in the partial analyses, and explain dramatically different amounts of variance. Factor 6 of the 1900-1939 analysis (and Factor 7 of the 1940-1997 analysis) present a pattern with two centres of equal magnitude and opposite sign. Factor 1 of these analyses represents the wind field for more or less the whole of the domain north of 50 N. The full analysis performs a more effective rotation, with a single centre for Factor 1 (the equivalent of Factor 6, and a large part of the variance from Factor 1, in the 1900-1939 analysis) and allocates the remaining variance from Factor 1 of the 1900-1939 analysis to a new Factor 5. In spite of this reallocation of variance in the full analysis to create a more efficient set of rotated factors, there is no evidence that the PCA gives different results when applied to different parts of the record. That is, the PCA is stable in time.

The factor scores from the full analysis are now examined for evidence of changes in the strength of the patterns through time. The results from the short period analyses will not be considered further.

1900-1939 Factor	**1940-1997 Factor**	**1900-1939 Variance (%)**	**1940-1997 Variance (%)**	**Full Factor**	**Full Variance (%)**
1	1	39.83	37.68	5*	17.47
2	5	5.21	4.52	7	4.35
3	2	14.83	18.84	2	17.19
4	3	5.39	5.22	3	5.01
5	4	12.21	9.91	4	8.89
6	7	3.67	3.32	1*	26.37
7	6	3.54	4.32	6	4.17
	Total	84.68	84.81		83.46

Table 7.4 Test parameters

7.2.7 Factor Scores

The factor scores from a PCA are the original time series weighted by the loadings against each factor. So, in the case of the above PCA of monthly mean wind speeds, we have seven new, uncorrelated, time series to analyse. The factor scores are usually normalised to enable valid comparison between them. Since the scores are derived from the factors, and the sign of the factors is assigned arbitrarily, a score of a given sign can indicate high wind speeds for one factor and low wind speeds for a different factor. The only way to determine what the scores are showing is to compare them with the wind speed data. For example, Figure 7.9 shows the scores for Factor 1, representing the wind field centred over southern Scandinavia. There is evidence of declining wind speeds but, even though the seasonal component has been removed and a smoother applied to simplify the residuals, it is extremely difficult to say anything else about the series from simple visual inspection.

Although the factor scores provide objective time series, related to a spatially consistent wind regime, the presentation of the data is hampered by the inclusion of all months, irrespective of windiness, the absence of units, and the arbitrary sign of the scores.

Time series more suitable for the purposes of this study are now presented, derived using the properties of the factors from the PCA.

7.2.8 Wind speed time series

Grid squares with wind speeds closely matching the patterns shown in Figures 7.2 to 7.8 can be identified from the factor loading matrix. The higher the loading, the more the wind speed matches the pattern for a particular factor. Unfortunately, there is no way of readily determining the significance of factor loadings. Therefore, the threshold of important factor loadings has to be identified subjectively. Here, an absolute loading of 0.6 was used as the threshold on the basis that only very high loadings can be guaranteed to fit the pattern well. Lower values reflect a combination of lower wind speeds and deviation from the pattern that is difficult to assess other than in the context of the PCA. The wind speeds for each of the grid squares chosen by this method were averaged for each timestep, to give a representative monthly wind speed time series for each factor.

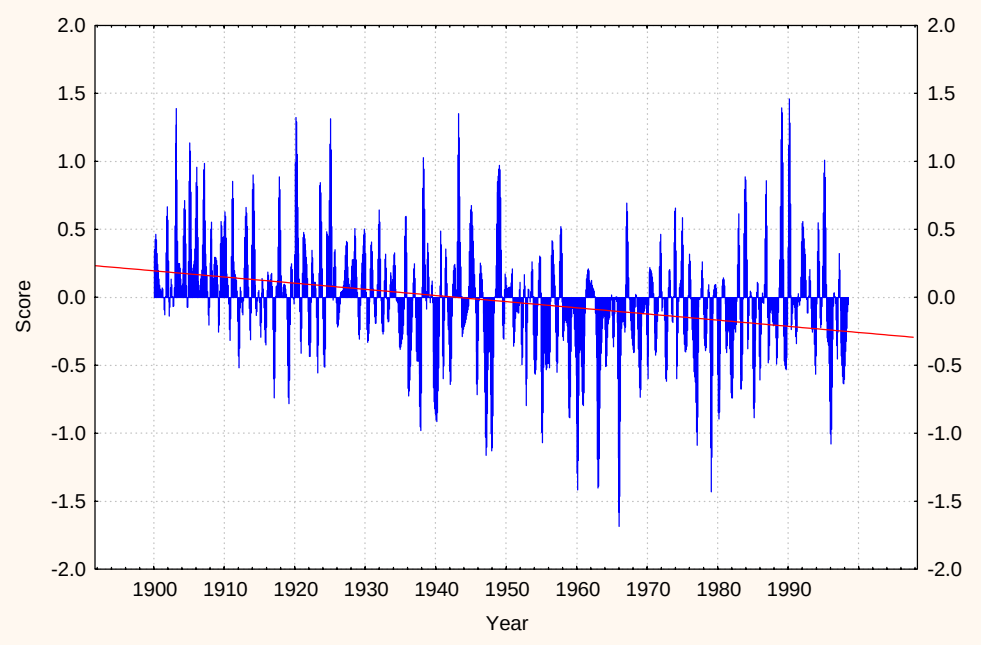

Figure 7.9 Scores from component 1 of the wind PCA

Construction of seasonal series

The seasonal cycle in the monthly wind speeds for each factor was identified using a 12-month moving average on the factor scores. Table 7.5 lists the months with above average wind speeds for each factor.

Factors representing more northern regions (Factors 1 and 5) have the highest wind speeds in an extended Northern Hemisphere winter, defined by the data as lasting from October to April. Shorter winters are found in more southern regions. Factors 6 and 7 (the entrance to the Mediterranean and Middle East, respectively) have both winter and summer maxima.

Factor	**1**	**2**	**4**	**5**	**6**	**7**
High wind-speed months	Oct. to Feb.	Nov. to April	Dec. to Mar.	Oct. to April	May, Sep. to Oct.	Dec. to Feb., July to Sep.

Table 7.5 High wind speed seasons for each factor of the PCA

Having identified the seasons, annual wind speed indices were created for each factor by averaging the monthly data over the seasons identified in Table 7.5. Figures 7.10 to 7.15 show, for each factor, the annual series together with a smoothed line, to reveal the overall time series features of the data, and the linear trend line over the whole period of record.

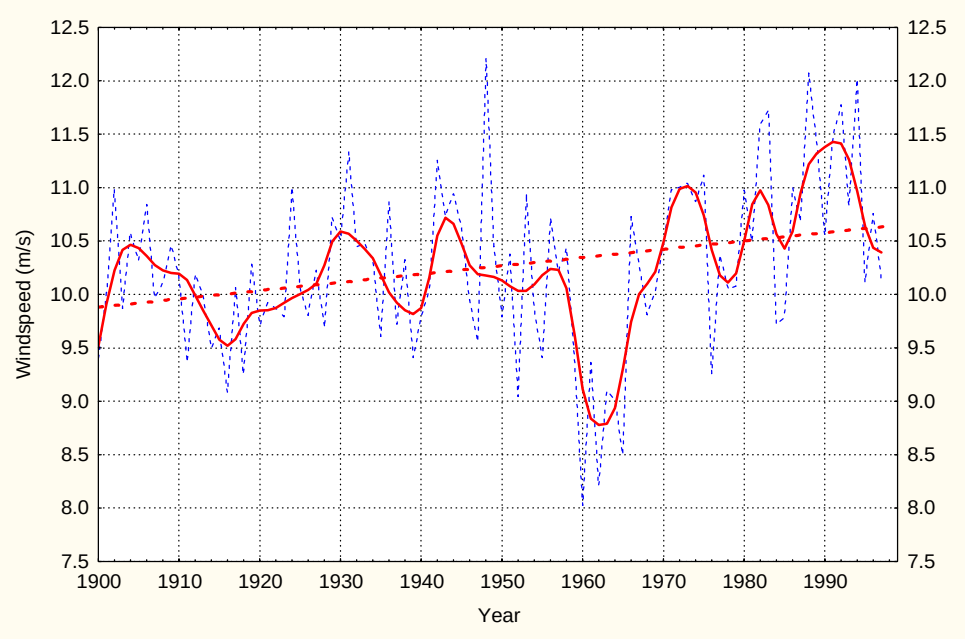

Figure 7.10 Winter (Oct. to Feb.) wind speeds associated with Factor 1

Figure 7.10 shows that winter wind speeds over north western Europe have long-term rising trend that is largely a function of increasing wind speeds since the 1960s. Prior to this, the record shows no trend. The period of anomalously low wind speeds in the 1960s is almost certainly partly an artefact of excessive smoothing of the pressure data during a change in gridding method [Jenkinson (1977)]. There is no evidence of regular periodicity in these data.

The wind field associated with winter in the Mediterranean (Figure 7.11, Factor 2 in Table 7.5) shows minimal falling trend. Again, wind speeds appear to be anomalously low during the early 1960s. There is no evidence of periodic behaviour.

Figure 7.12 shows the winter wind field to the southwest of Ireland (Factor 4) to have slight rising trend over the period of record. The trend is particularly marked over the last four decades with mean winter wind speeds rising by about 2 m/s since 1950. However, 1950 was a low point in the record. Wind speeds were more variable prior to 1950, show no trend, and sometimes equalled recent levels. There is no evidence of persistent periodic behaviour.

The time series for the northeast Atlantic (Factor 5, Figure 7.13) shows that the winter wind field exhibits rising trend over the full period of record. Apart from the anomalously low wind speeds in the 1960s, associated with errors in the data, the trend is remarkably persistent and indicates that wind speeds in the region increased by about 20% over 100 years. There is no evidence of periodicity in these data.

Factor 6, representing the Atlantic just west of the Mediterranean, has winter and summer wind speed maxima (Figures 7.14a and 7.14b, respectively). The winter time series (Figure 7.14a) shows falling trend of about 0.5 m/s over the period of record. Summer wind speeds in this region (Figure 7.14b) show no notable trend and are about 9% higher than winter wind speeds. There is no evidence of persistent periodic behaviour.

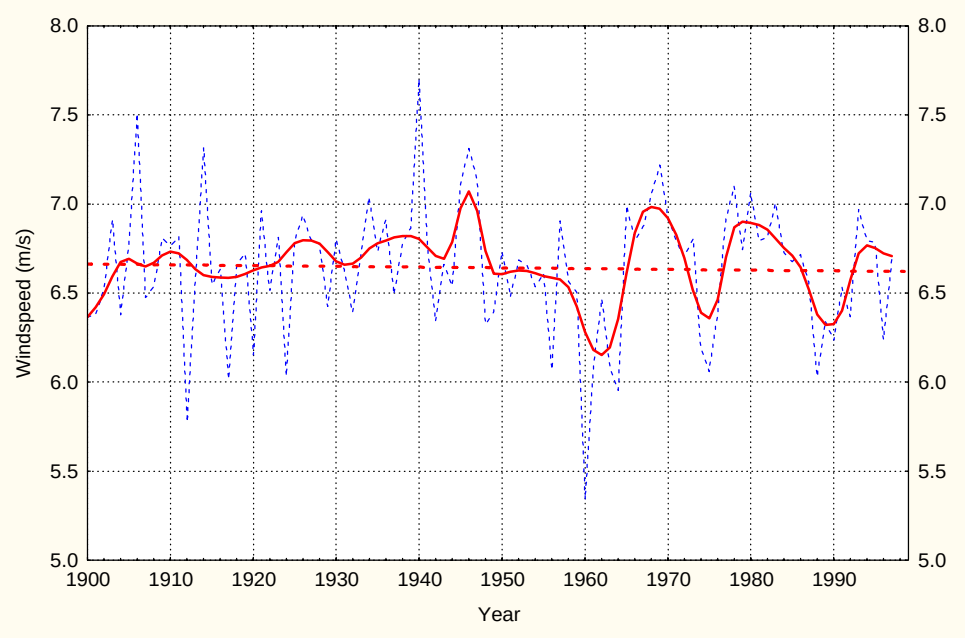

Figure 7.11 Winter (Nov. to April) wind speeds associated with Factor 2

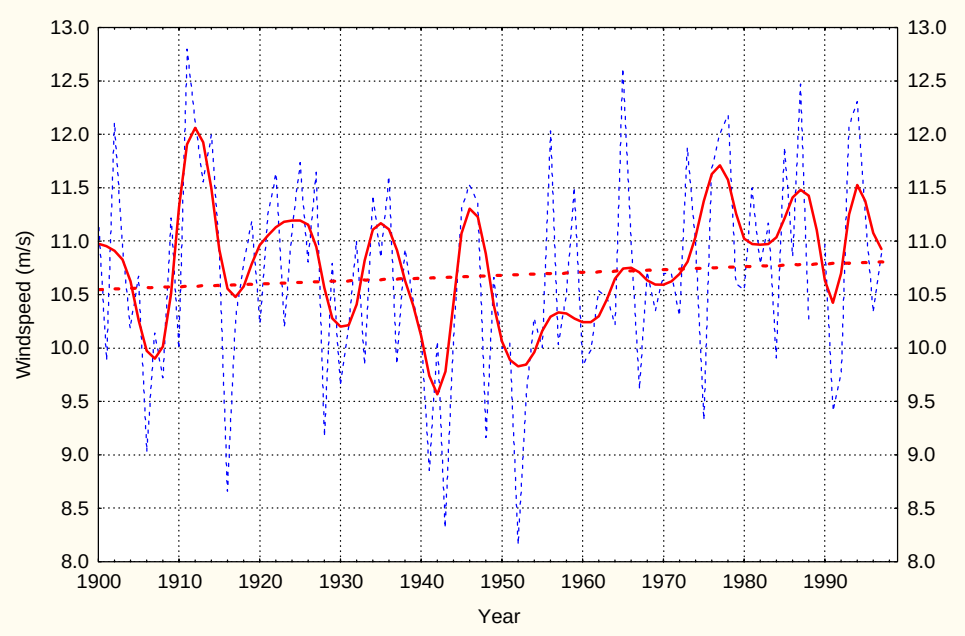

Figure 7.12 Winter (Dec. to March) wind speeds associated with Factor 4

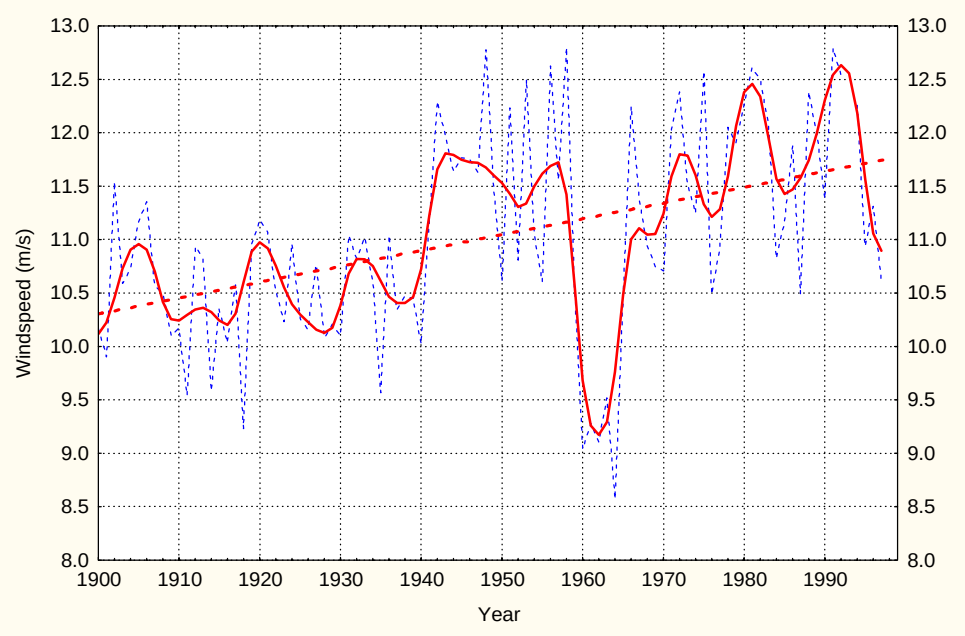

Figure 7.13 Winter (Oct. to April) wind speeds associated with Factor 5

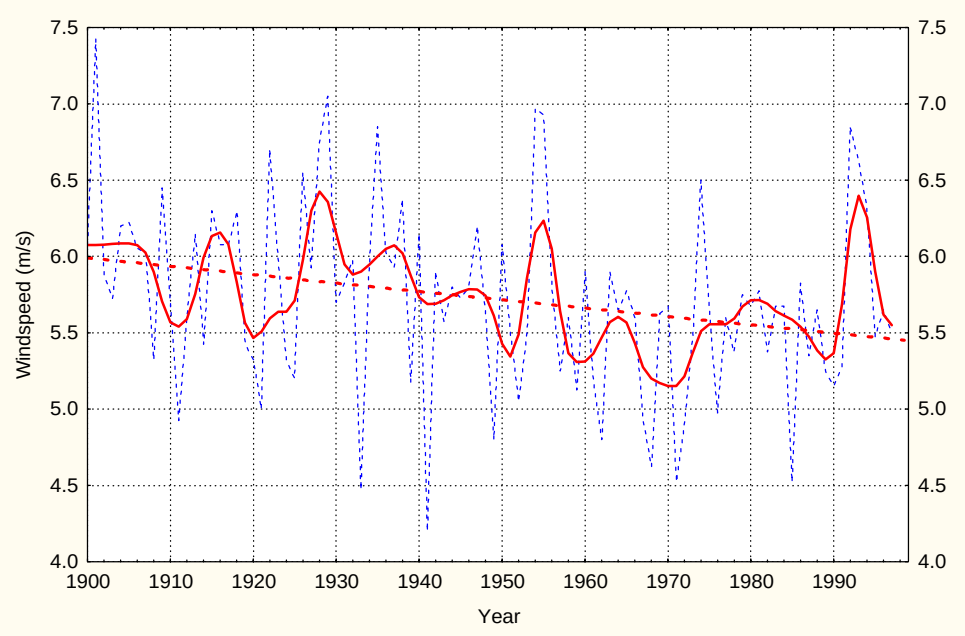

Figure 7.14a Winter (Sep. to Oct.) wind speeds associated with Factor 6

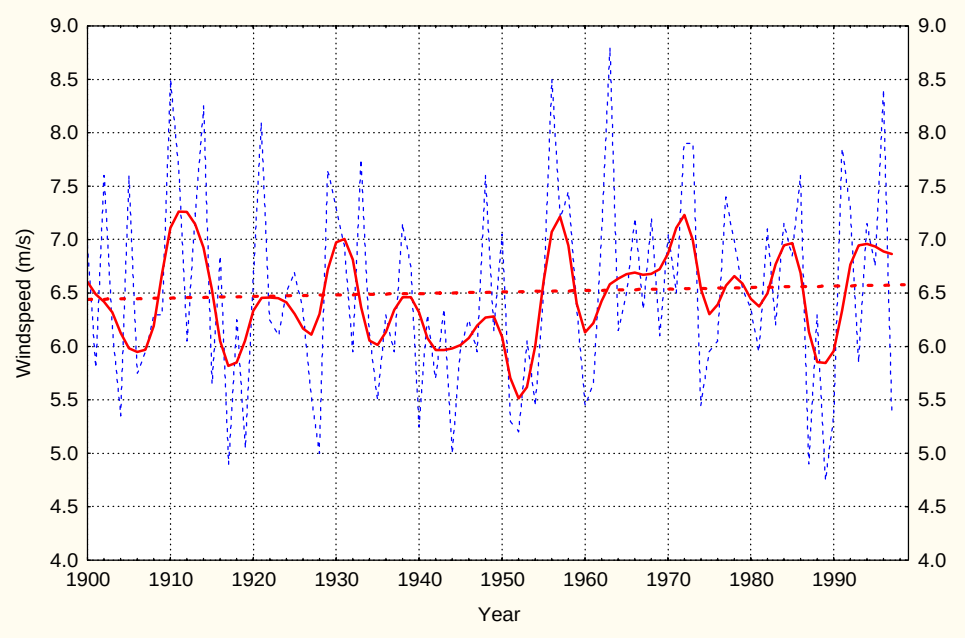

Figure 7.14b Summer (May) wind speeds associated with Factor 6

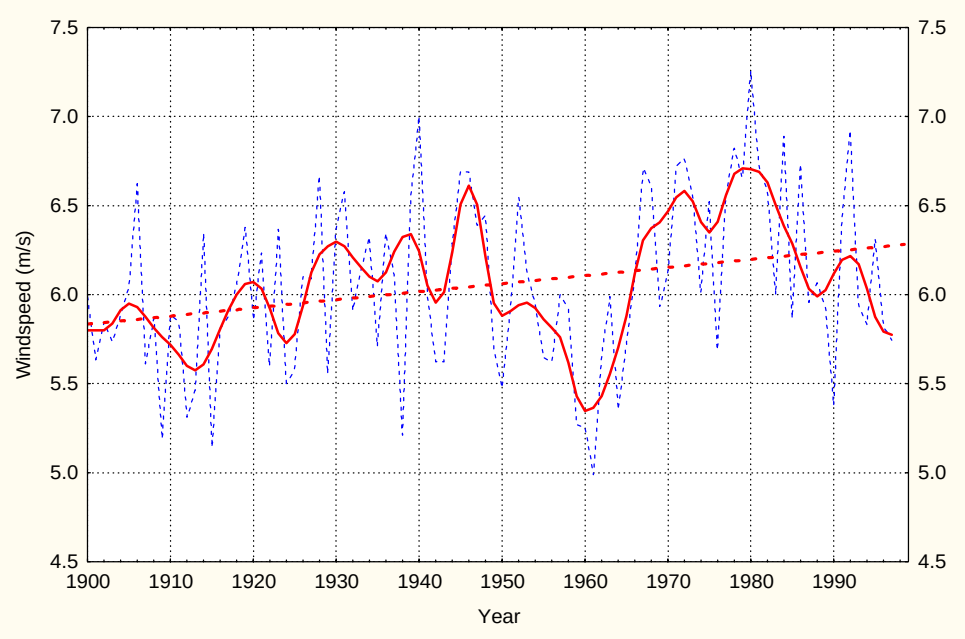

Figure 7.15a Winter (Dec. to Feb.) wind speeds associated with Factor 7

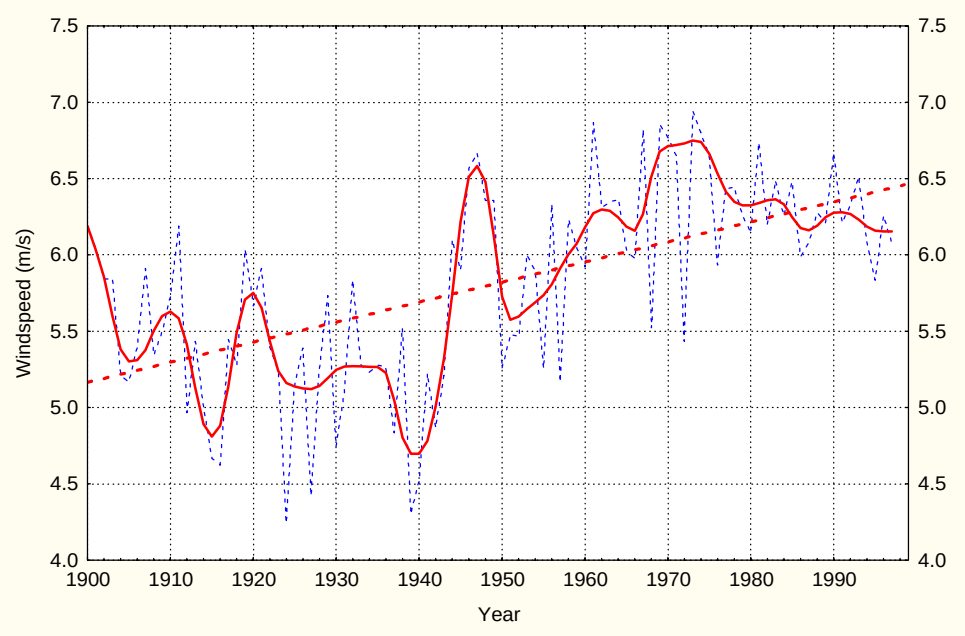

Figure 7.15b Summer (July to Sep.) wind speeds associated with Factor 7

Factor 7, centred over the Middle East, has winter and summer wind speed maxima (Figures 7.15a and 7.15b, respectively). Both series exhibit rising trend with no evidence of periodicity. Summer wind speeds are slightly higher than winter and have more pronounced trend (Figure 7.15b) with wind speeds increasing by about 30% over the period of record. Once more, wind speeds in winter in the 1960s appear to be anomalously low.

Summary

The seasonal wind speed time series for each region identified by the factors from the PCA show no periodic behaviour but do display some important long-term trend. In terms of offshore wind potential, the regions affected by trend can be readily determined from Table 7.6, which is an extension of Table 7.3. The final column in Table 7.6 gives the percentage change in wind speed over the period of trend described in the previous two columns.

The way to use Table 7.6 for the POWER project is to identify the ocean basin in which there is an interest in offshore wind resources, find the relevant country, then look at the trend and duration columns. Rising trend indicates that variations in the wind field are taking place about a rising mean, the duration indicates the stability of the trend expressed as years before present. Where the trend duration is relatively short, it is essential to examine the plots of the full time series to estimate the likelihood of the trend reversing in the near future. The final column in Table 7.6 indicates the percentage change in wind speed over the period of trend. For example, if we were interested in exploiting the offshore wind resources of Greece we can see from Table 7.6 that Greece is experiencing trivial falling trend associated with Factor 2. However, the wind field associated with Factor 7 has rising trend over southern Greece with an increase in wind speeds of 30% over 60 years in summer and of 10% over 100 years in winter. Given that wind speeds off Greece are relatively low, the rising trend is encouraging for the development of offshore wind energy, assuming that it persists.

Basin	Country	Factors	Season	Trend	Duration (yrs)	Amount (%)
Atlantic	Belgium	1, 4	winter	rising	40	+15
	Denmark	1	winter	rising	40	+15
	France	1, 4	winter	rising	40	+15
		2	winter	falling	100	trivial
	Germany	1	winter	rising	40	+15
	Holland	1, 4	winter	rising	40	+15
	Ireland	1, 4	winter	rising	40	+15
	Portugal	2	winter	falling	100	trivial
		4	winter	rising	40	+15
		6	summer/winter	none/falling	0/100	0/-8
	Spain	2	winter	falling	100	trivial
		4	winter	rising	40	+15
		6	summer/winter	none/falling	0/100	0/-8
	United Kingdom	1, 5, 4	winter	rising	40, 80, 40	+15, +20, +15
Baltic	Denmark	1	winter	rising	40	+15
	Finland	1, 5	winter	rising	40, 80	+15, +20
	Germany	1	winter	rising	40	+15
	Sweden	1, 5	winter	rising	40, 80	+15, +20
Mediterranean	France	2	winter	falling	100	trivial
	Greece	2	winter	falling	100	trivial
		7	summer/winter	rising	60/100	+30/trivial
	Italy	2	winter	falling	100	trivial
	Spain	2	winter	falling	100	trivial
		6	summer/winter	none/falling	0/100	0/-8

Table 7.6 Countries affected by trend in seasonal wind speeds

7.2.9 Summary and Conclusions

Rotated Principal Component Analysis (PCA) has been used to identify regional wind regimes over Europe using monthly mean geostrophic wind speeds from 1900 to 1997. The method identified seven factors explaining 83.71% of the total variance in the original data. The rotational strategy ensured that each factor was associated with a single homogenous wind regime, greatly simplifying interpretation and enhancing the value of time series associated with the factors. For the convenience of offshore wind energy exploitation, the factors have been associated with the coastlines of individual member states of the European Union.

Although the factor scores from the PCA proved too detailed to directly indicate long-term features of the time series associated with each factor, they would be of great value in an analysis of, for example, extremes on a monthly basis. The factor loadings were used to determine grid squares with wind speeds most closely matching the wind regimes identified by the PCA. The wind speeds at these grid squares were then averaged to give representative monthly time series for each factor. Seasonal wind speed indices were created by identifying the seasons associated with each factor, and averaging the relevant monthly values. The resulting seasonal time series were examined for trend and periodic behaviour.

There is no indication in the data of any significant periodic activity. There is considerable evidence of stable long-term trend associated with particular factors. This is important since a background of rising trend, for example, in the more northern high wind speed regions, may mean more downtime as turbines cut-out more frequently. Conversely, rising trend in relatively low wind speed regions may mean that a currently inadequate resource may eventually become economically viable.

7.3 The diurnal cycle of the coastal wind field of the UK

7.3.1 Introduction

The offshore wind resource may be highly variable, particularly when the prevailing wind has a fetch over land. Wind speed variations related to the diurnal cycle have implications for the sustained productive capacity of a wind farm. The diurnal cycle of coastal wind has been examined using example stations around the United Kingdom. Ten coastal stations were selected on the basis of geographical coverage, suitable site exposure, and length of record.

7.3.2 Data

The location and length of record of the stations are shown in Figure 7.16. The data are hourly wind speed and direction and were extracted from the British Atmospheric Data Centre (BADC) archives.

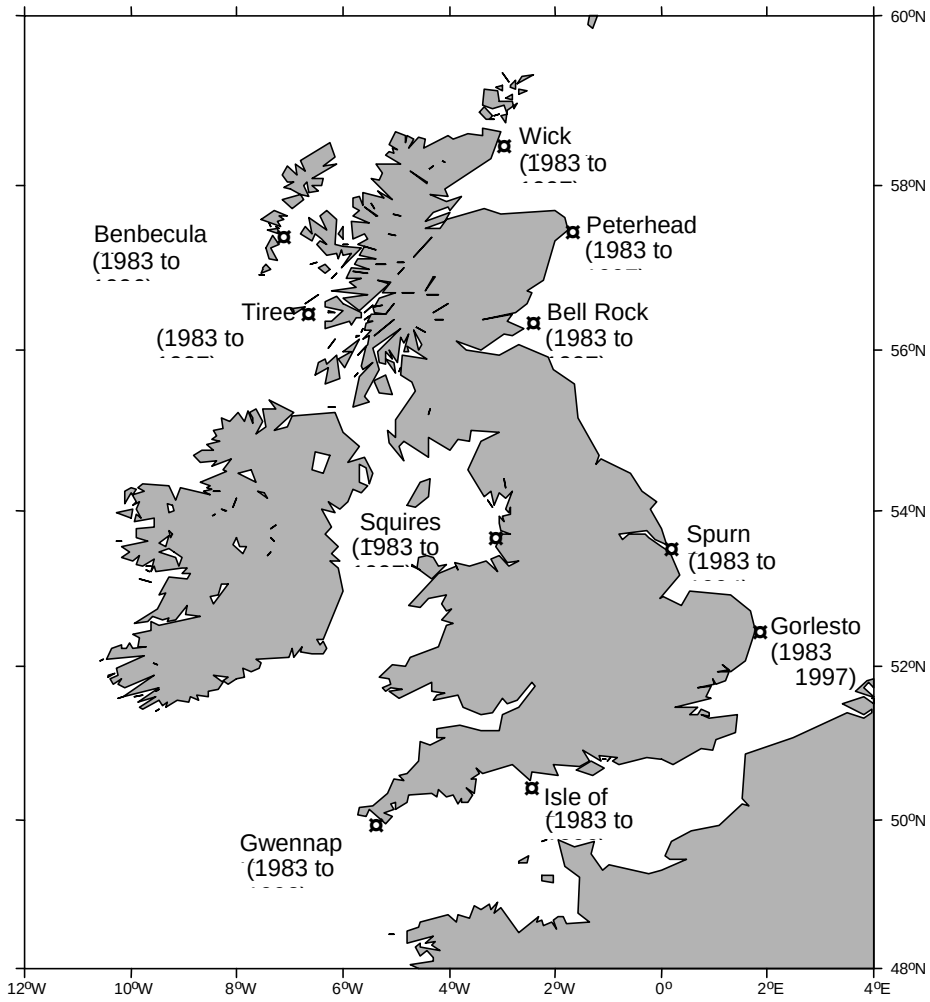

Figure 7.16 Station locations and length of record

7.3.3 Method

The diurnal cycle of UK coastal wind was examined using seasonal averages for each hour of the day. The averages were calculated over the length of the available record (see Figure 7.16) and seasons were defined as follows:

Winter – December, January, February

Spring – March, April, May
Summer – June, July, August
Autumn – September, October, November

For the purposes of this discussion, wind may be seen as the result of thermal contrasts between air masses. In winter, wind regimes over the UK are dominated by large-scale flow associated with mid-latitude depressions. In summer, local circulations become more important. Summer winds over land typically have a strong diurnal cycle associated with warming of the surface by solar radiation, and transfer of this heat to the overlying air by conduction and convection. Hence, wind speeds peak in the early afternoon, reaching a minimum early in the morning. In winter this diurnal cycle is weaker because there is less solar radiation, and may be obscured by the large-scale flow. But when conditions are right, for example under an anticyclone, a diurnal cycle should appear, again with highest wind speeds in the afternoon.

Usually, in summer the ocean is cooler than the land during the day and warmer than the land during the night. In winter, the ocean tends to be warmer than the land throughout the day and night, but the maximum temperature differences between land and ocean are lower than on summer days.

Over the sea, the diurnal cycle of warming is largely smoothed-out by vertical and horizontal mixing of the surface ocean layer. The surface water tends to remain cooler, and the transfer of heat to the overlying air during daylight hours by conduction and convection is less.

There are few anemometers located at sea. In order to study the diurnal cycle over land and over sea we use wind data from coastal stations. Winds with an ocean fetch can be expected to show little evidence of a diurnal cycle, even in summer. Conversely, winds with a land fetch should exhibit a strong diurnal cycle in summer, and a weak diurnal cycle in winter when temperature contrasts are lower and regional winds are stronger. Because the large-scale westerly circulation is strongest in winter and weakest in summer, the highest wind speeds will normally be found in winter and the lowest in summer. By choosing sites from all around the coast of the UK, it is possible to explore contrasts imposed by geographical position.

To determine the appropriate directions for land and sea fetches at each of our stations, it is necessary to know the location accurately and examine a large-scale map of the vicinity. Table 7.7 shows the station locations and the directional bins associated with land and sea fetches. Land and sea fetches are determined conservatively, with no possibility of a land fetch including an element of sea winds and *vice versa*. No land fetch could be defined for four stations either surrounded by water or with a land fetch too short or too narrow for the wind to recover fully to the land state.

Station	Latitude	Longitude	Land fetch	Sea fetch
Bell Rock	56.433	-2.383	n/a	0 – 180
Benbecula Airport	57.467	-7.367	120 – 210	290 – 330
Gorleston	52.567	1.733	240 – 330	50 – 120
Gwennap Head	50.036	-5.68	0 – 60	190 – 280
Isle of Portland	50.521	-2.455	n/a	200 – 280
Peterhead Harbour	57.502	-1.773	240 – 310	50 – 150
Spurn Point	53.567	0.117	n/a	70 – 130
Squires Gate	53.767	-3.033	40 – 140	210 – 270
Tiree	56.499	-6.879	n/a	150 – 180
Wick Airport	58.450	-3.083	220 – 310	40 – 130

Table 7.7 Station locations and directional bins for land and sea fetches

7.3.4 Results

For each coastal station, the mean hourly winds for each season were binned according to the directions defining land and sea fetches. For each layer, the seasonal means were calculated and plotted. Figures 7.17 to 7.20 show the diurnal cycle in wind speeds with a sea fetch for Bell Rock, Isle of Portland, Spurn Point, and Tiree stations, respectively. There is no land fetch for this group of stations. As expected with a sea fetch, there is no clear evidence of a diurnal cycle in wind speed. Summer winds

are weakest and winter winds are strongest, with the transition seasons falling somewhere in between. A feature of the Bell Rock sea fetch data is the considerable overlap between the autumn and spring wind speeds between 0800 and 1200 h, and the peak in the autumn data at 0900 h. This is not found elsewhere.

Figures 7.21a and 7.21b show the diurnal cycle in wind speed for Benbecula Airport for sea and land fetches, respectively. The pattern of wind speed for the sea fetch (Figure 7.21a), as with Figures 7.17 to 7.20, shows either no diurnal cycle, or shows a wind speed peak at night between midnight and 0400 h. This peak is clear in spring, summer, and autumn, but not in winter. [Barthelmie et al. (1996)] explained this as due to quasi-constant sea surface temperature throughout the day, such that at night the air-sea temperature difference will be negative, giving more unstable conditions. Presumably, in winter, this effect is masked by the large-scale circulation. In contrast, the wind speeds associated with a land fetch (Figure 7.21b) exhibit a pronounced diurnal cycle in spring and summer, a slightly weaker diurnal cycle in autumn, and a trivial diurnal cycle in winter, always with the maximum in the early afternoon. This is entirely consistent with the theoretical expectations outlined in Section 7.3.3. The spring and summer diurnal cycles peak at 1400-1500 hours and the maximum wind speeds are about 40% higher than during the night. It can be seen that the strength of the land fetch diurnal cycle is such that the spring diurnal maximum wind speed (Figure 7.21b) is higher than the concurrent mean winter wind speed. This emphasises the importance of examining the diurnal cycle of winds with a land fetch.

The sea and land fetch diurnal cycles for the remaining stations are shown in Figures 7.22a to 7.26b. These follow the expected patterns described for Benbecula Airport (Figures 7.21a and 7.21b). For Gwennap Head (Figure 7.23b), early morning wind speeds with a land fetch are very similar irrespective of season, with mean hourly wind speeds at the peak of the diurnal cycle in spring and summer being considerably higher than the concurrent winter hourly means. Even where there is considerable disparity between winter and summer early morning wind speeds, the diurnal peak hourly mean wind speeds in spring and summer can exceed the winter hourly means (Figures 7.24b, 7.25b, and 7.26b).

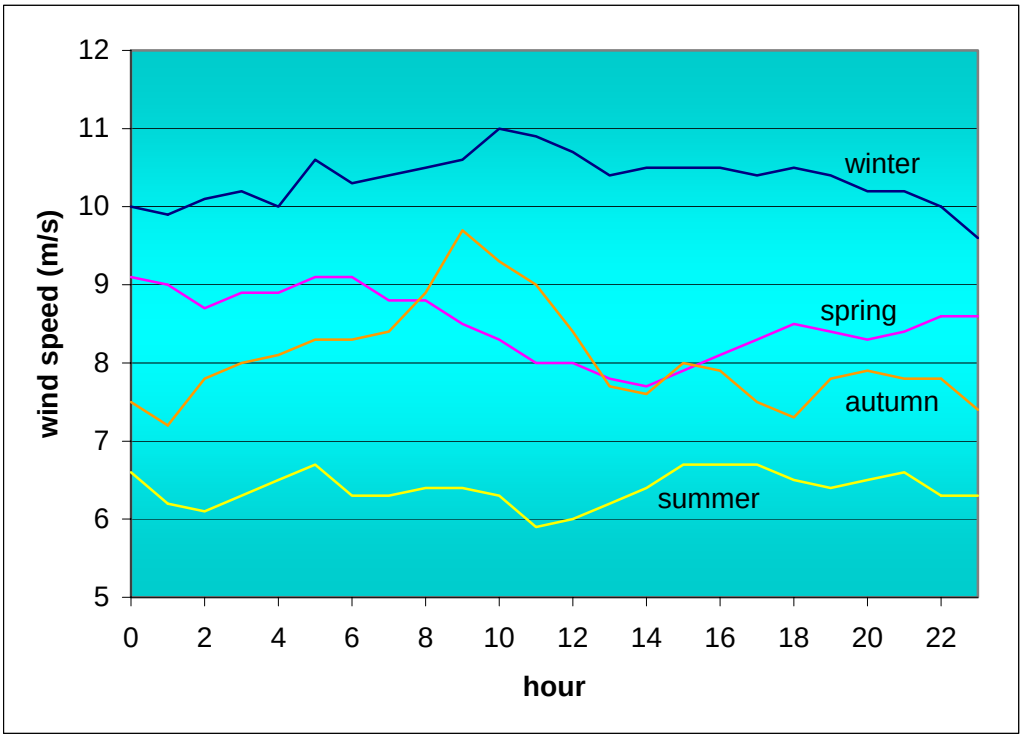

Figure 7.17 Bell Rock: sea fetch diurnal cycle by season (no land fetch)

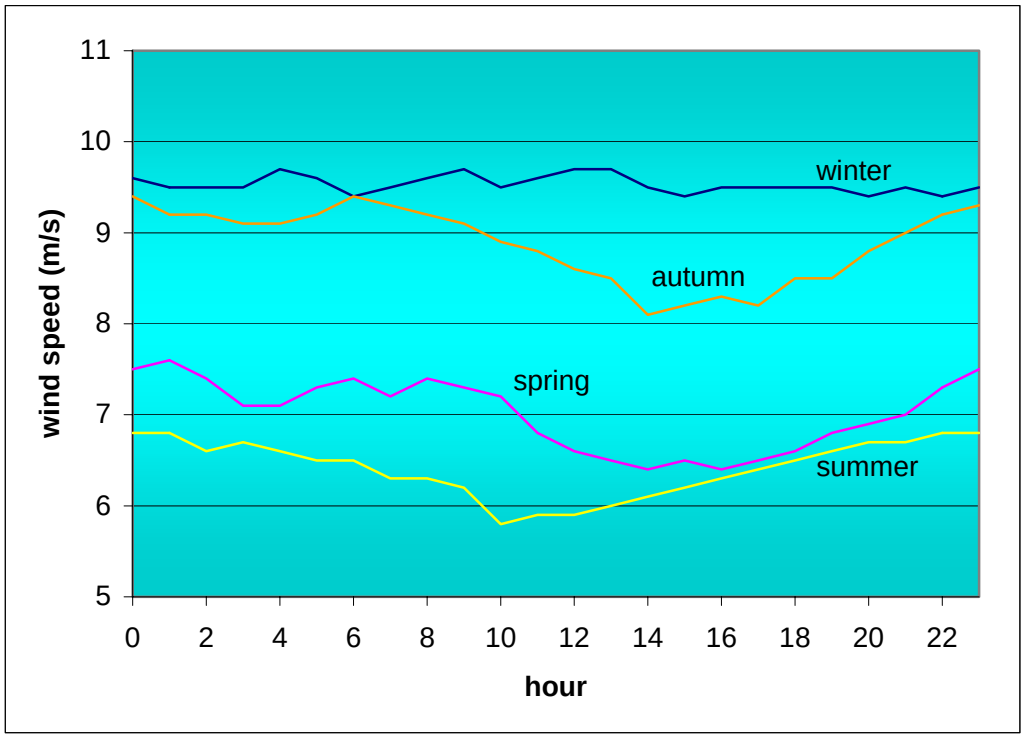

Figure 7.18 Isle of Portland: sea fetch diurnal cycle by season (no land fetch)

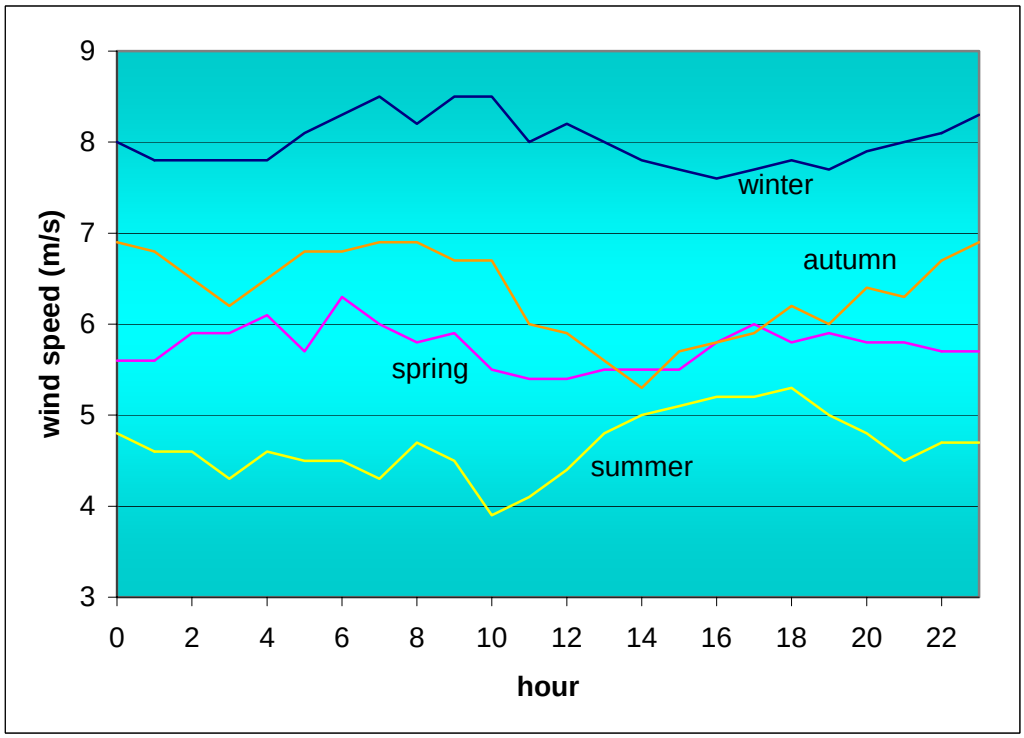

Figure 7.19 Spurn Point: sea fetch diurnal cycle by season (no land fetch)

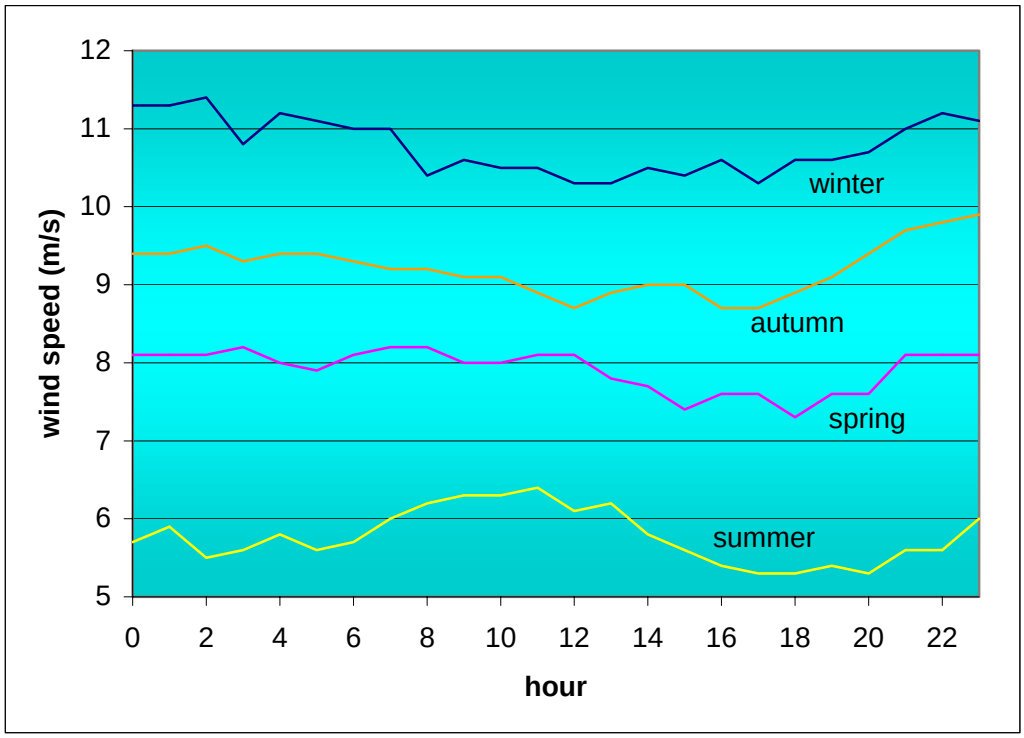

Figure 7.20 Tiree: sea fetch diurnal cycle by season (no land fetch)

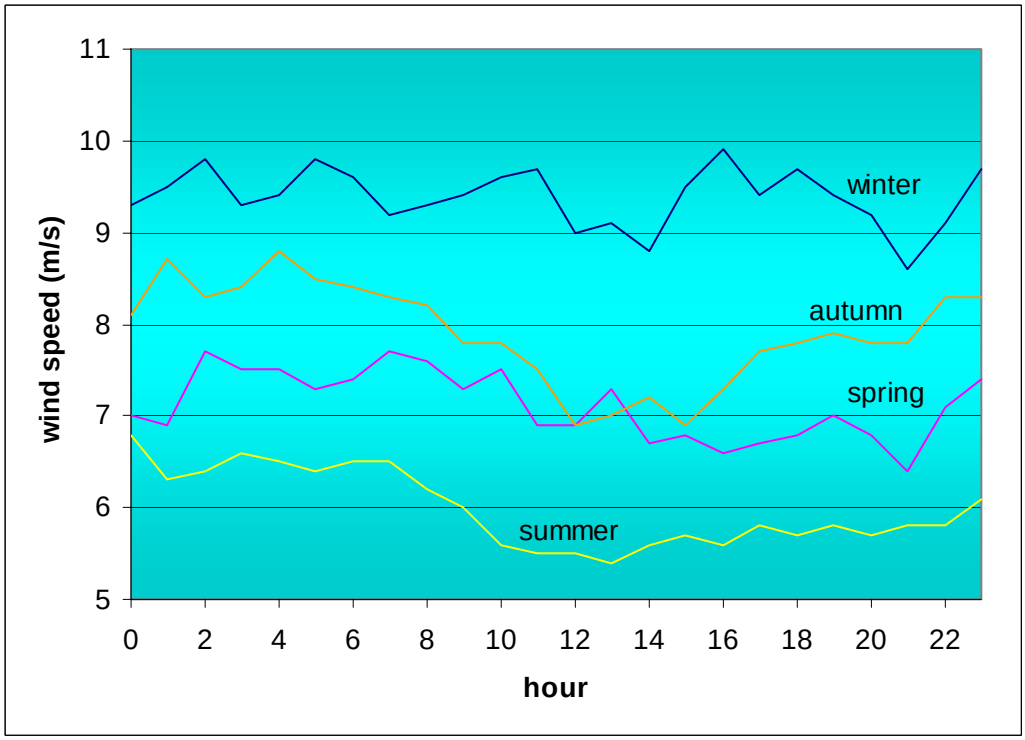

Figure 7.21a Benbecula Airport: sea fetch diurnal cycle by season

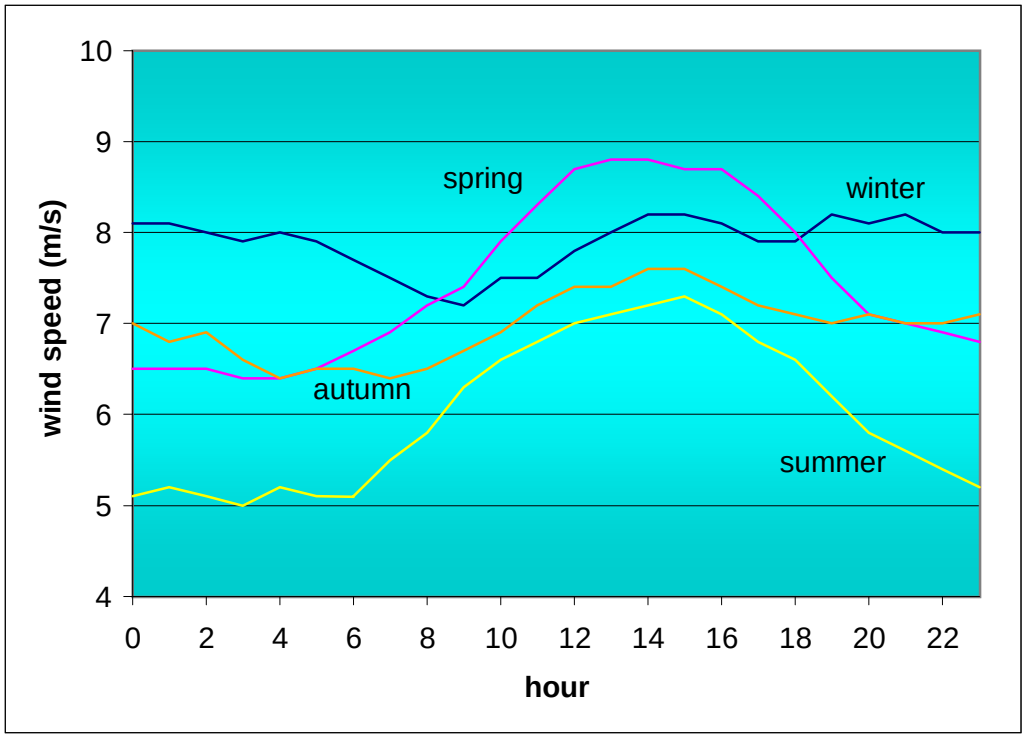

Figure 7.21b Benbecula Airport: land fetch diurnal cycle by season

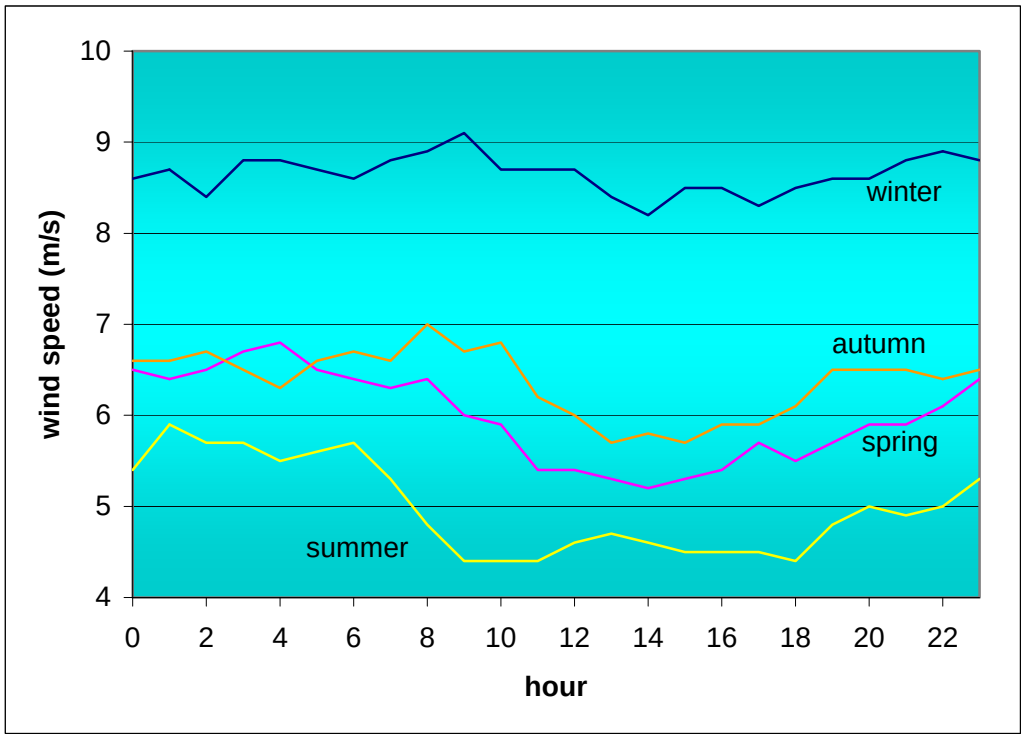

Figure 7.22a Gorleston: sea fetch diurnal cycle by season

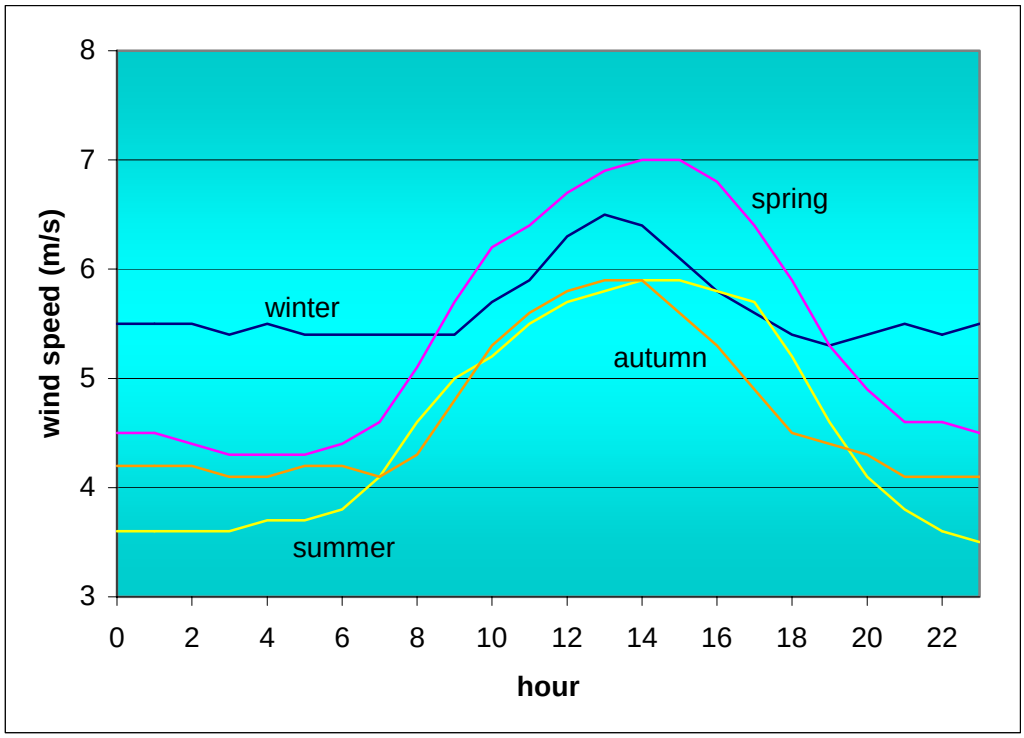

Figure 7.22b Gorleston: land fetch diurnal cycle by season

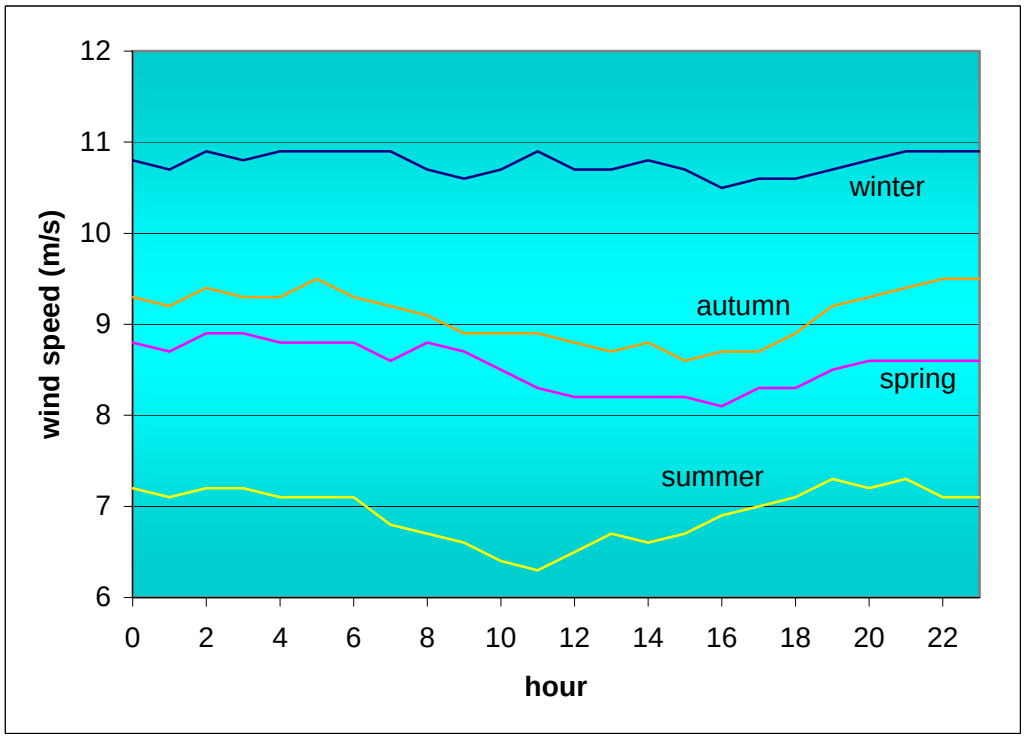

Figure 7.23a Gwennap Head: sea fetch diurnal cycle by season

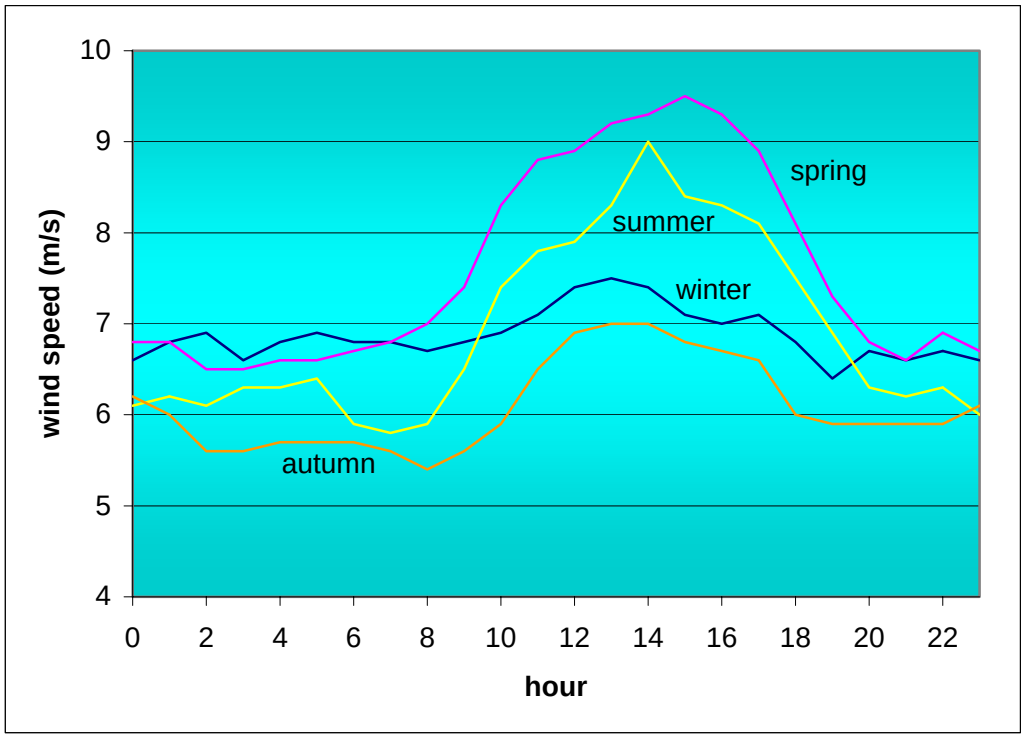

Figure 7.23b Gwennap Head: land fetch diurnal cycle by season

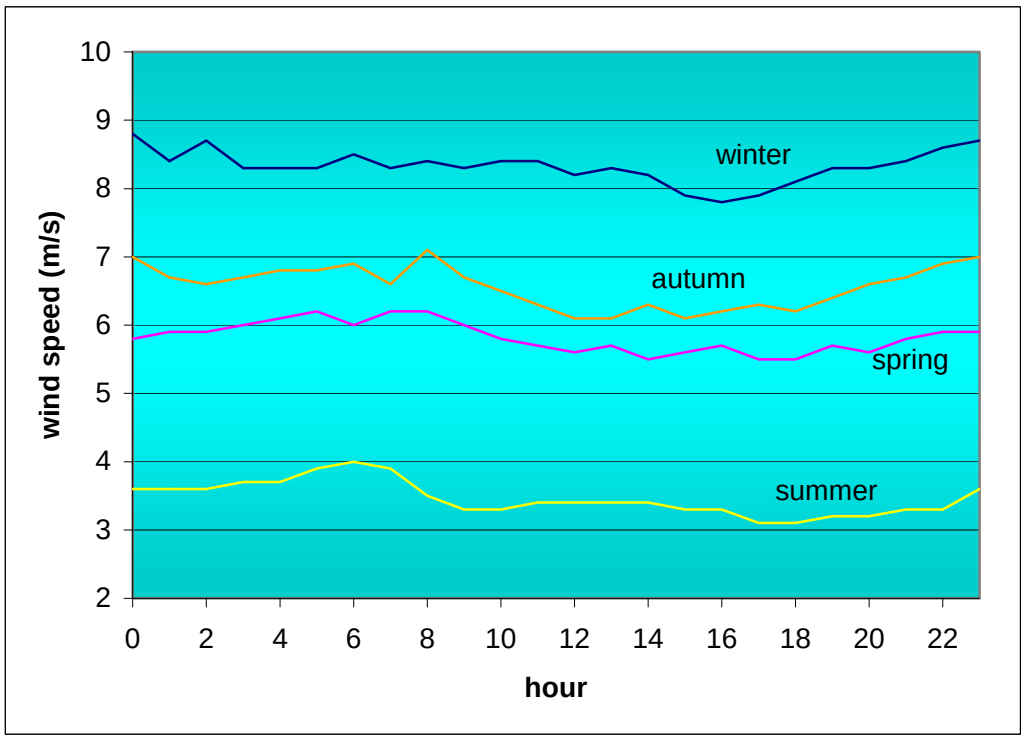

Figure 7.24a Peterhead Harbour: sea fetch diurnal cycle by season

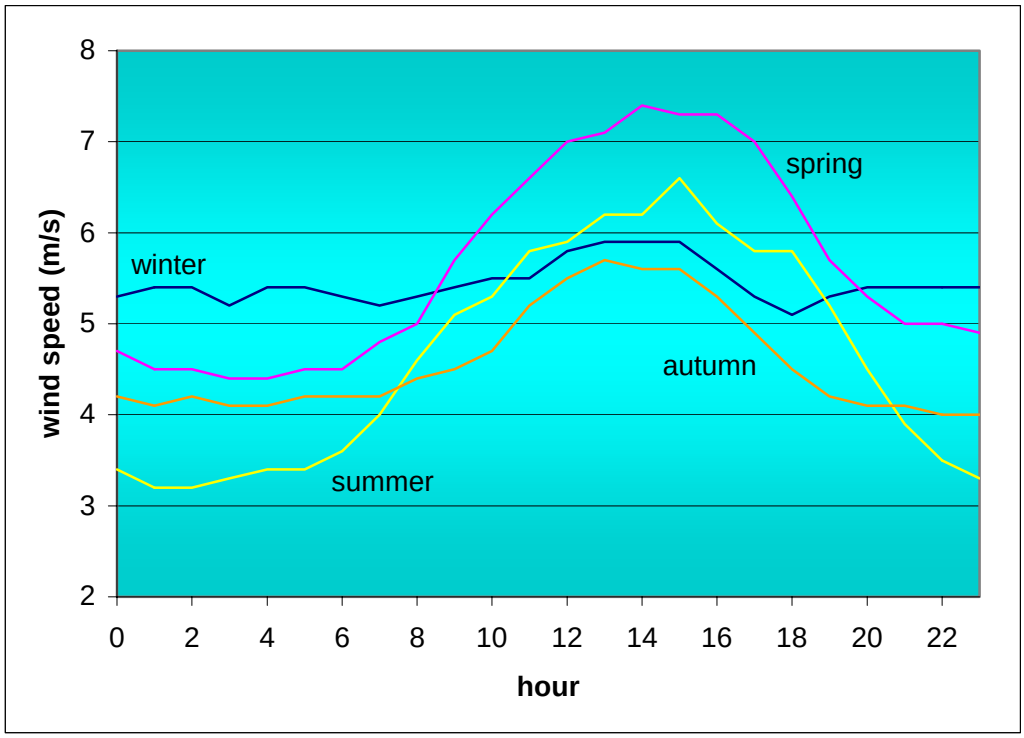

Figure 7.24b Peterhead Harbour: land fetch diurnal cycle by season

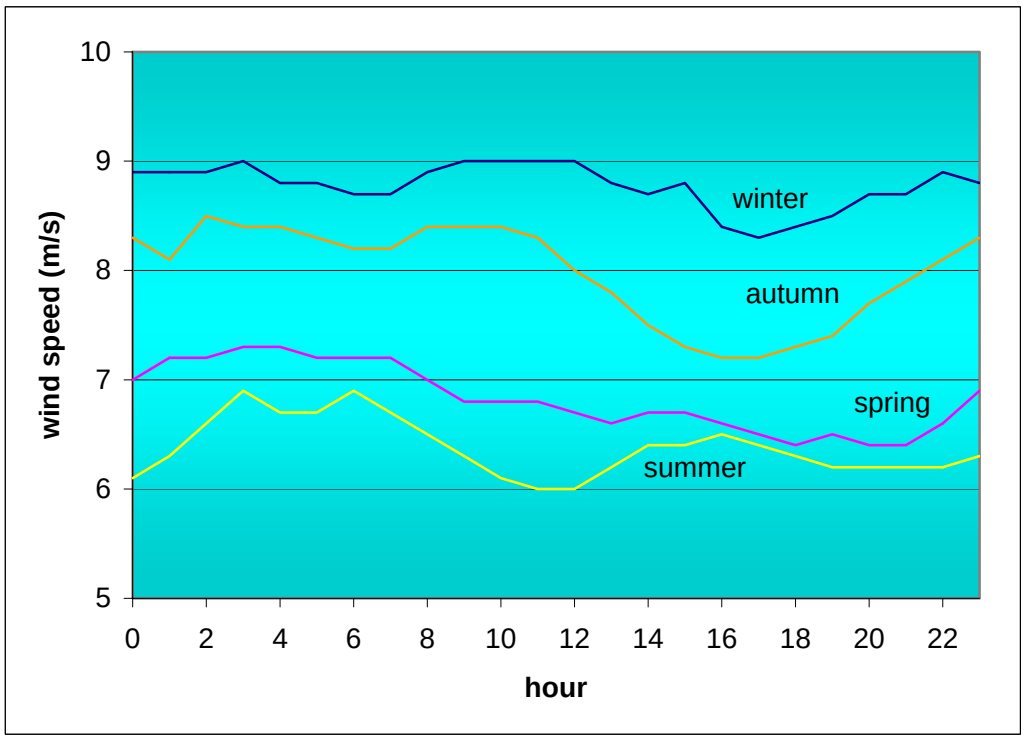

Figure 7.25a Squires Gate: sea fetch diurnal cycle by season

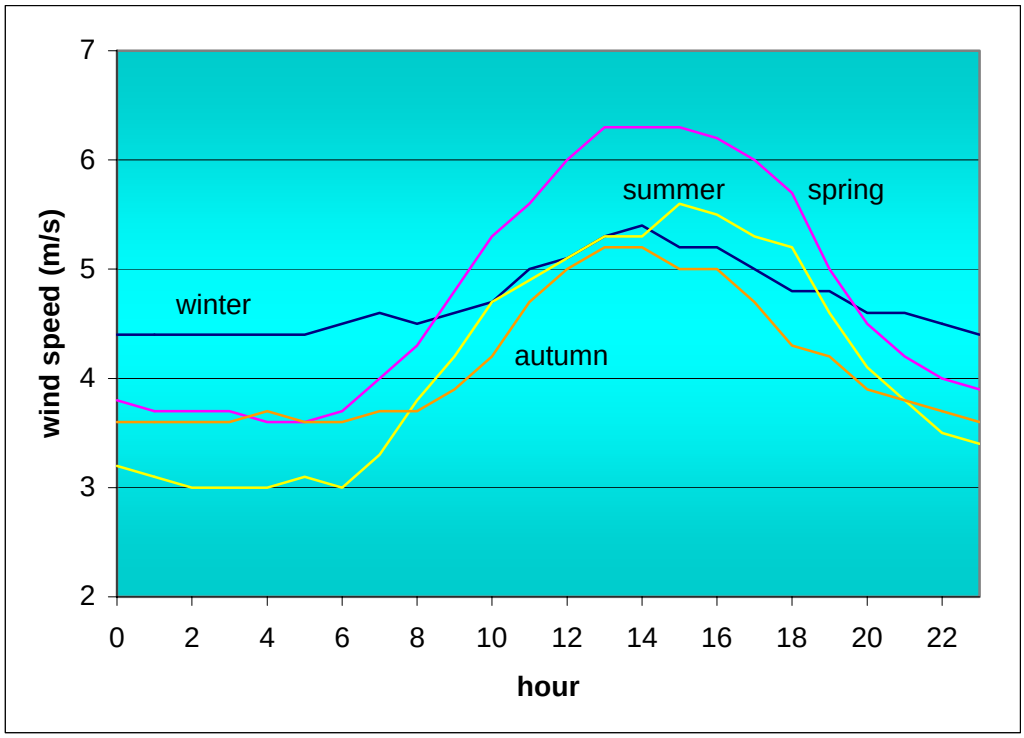

Figure 7.25b Squires Gate: land fetch diurnal cycle by season

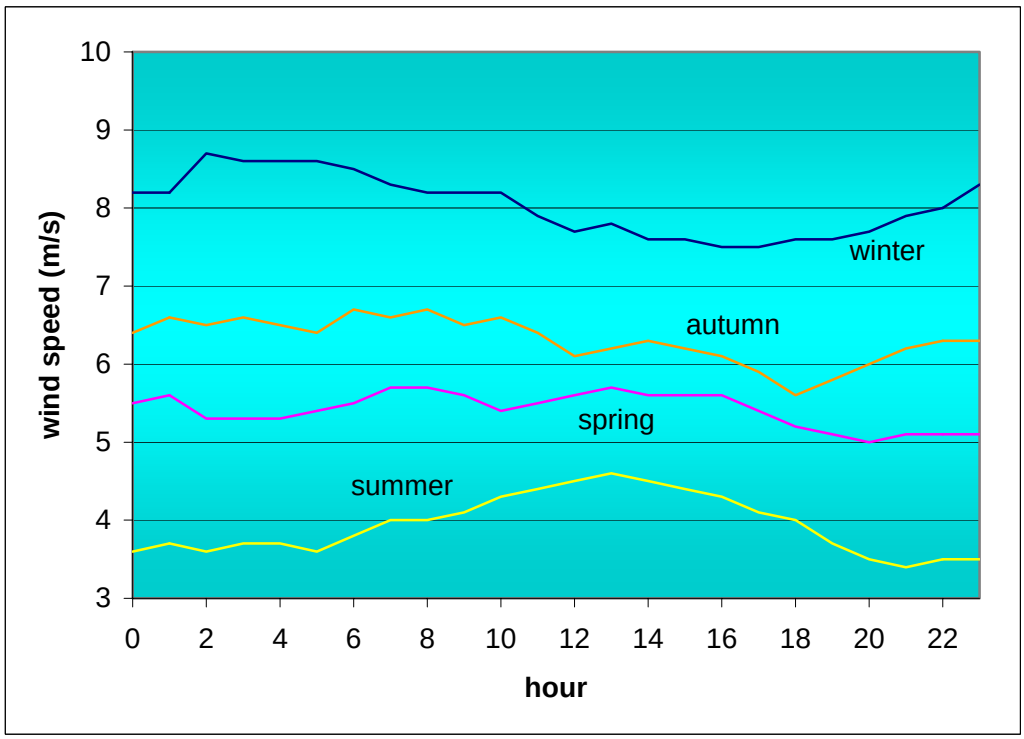

Figure 7.26a Wick Airport: sea fetch diurnal cycle by season

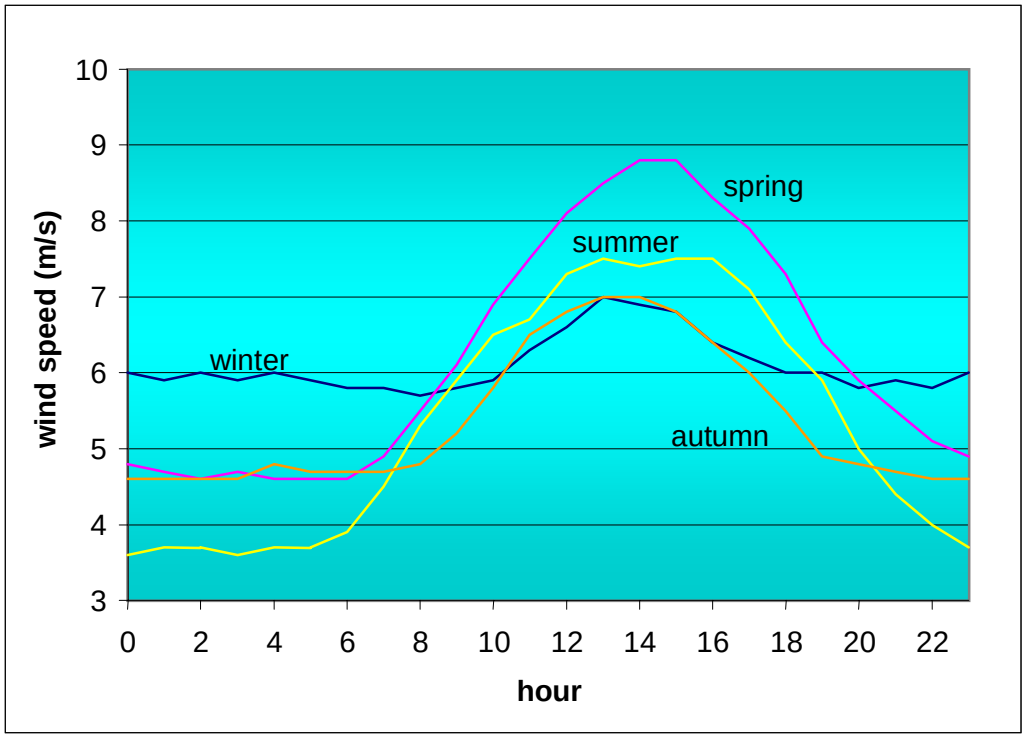

Figure 7.26b Wick Airport: land fetch diurnal cycle by season

7.3.5 Conclusions

Data from coastal stations around the UK demonstrate that consideration of the diurnal cycle of wind speed is essential in any assessment of offshore wind potential, especially for the near offshore where early wind farm developments are most likely to be located. For winds with a land fetch there is a pronounced diurnal cycle, peaking in the early afternoon, in spring, summer, and autumn. The peak of the cycle can give higher mean hourly wind speeds in summer than in winter. No diurnal cycle, or a weak cycle peaking in the early hours of the morning, is associated with winds having a sea fetch. In winter, wind speeds have no diurnal cycle irrespective of fetch. The diurnal cycle appears not to have any relation to the direction of the wind, being purely a function of land fetch. Moreover, any relation with the geographical location of the recording station appears to be weak. Benbecula in the northwest of Scotland has the most poorly developed land-fetch diurnal cycle. But this may be simply a function of choice of directions. Overall, the suggestion is that the results should apply equally to other European coasts at similar latitudes, including the whole of the North Sea, the Baltic Sea, central and southern Norway, western France and, probably, the Atlantic coasts of Spain and Portugal. The Mediterranean behaves essentially as an inland sea, with little mixing between warm surface water and cool water advected from polar latitudes. Thus, it is likely that the surface waters have more of a diurnal cycle of temperature than the open ocean and that the difference in wind speeds between land and sea fetches is less pronounced than on the coasts of the North Atlantic. Station data from the Mediterranean would be required to test this hypothesis.

7.4 Analysis of Wind Gusts

7.4.1 Introduction

The station datasets used in the analysis of the diurnal cycle of wind speed, and listed in Table 7.7, also contain information on the maximum gust speed in each hour. Damaging high wind speeds are of concern to wind farm developers. It was decided to analyse these gust speeds with a view to exploring techniques for obtaining information on extreme events.

We selected from Table 7.7 the four stations with no land fetch to represent patterns of gust behaviour over the open sea. These four are:

- Bell Rock
- Isle of Portland
- Spurn Point
- Tiree

Their locations are shown in Figure 7.16. A preliminary examination of maximum daily gust for each station (Figures 7.27 to 7.30) reveals that, with the exception of Tiree (Figure 7.30), all stations have discontinuities in the time series because of missing values. Fortunately, as well as having virtually no missing values, Tiree is also the longest record (15 years). It is therefore possible to carry out a full analysis of extreme values for this site, therefore, whilst for the other three stations the record is too short.

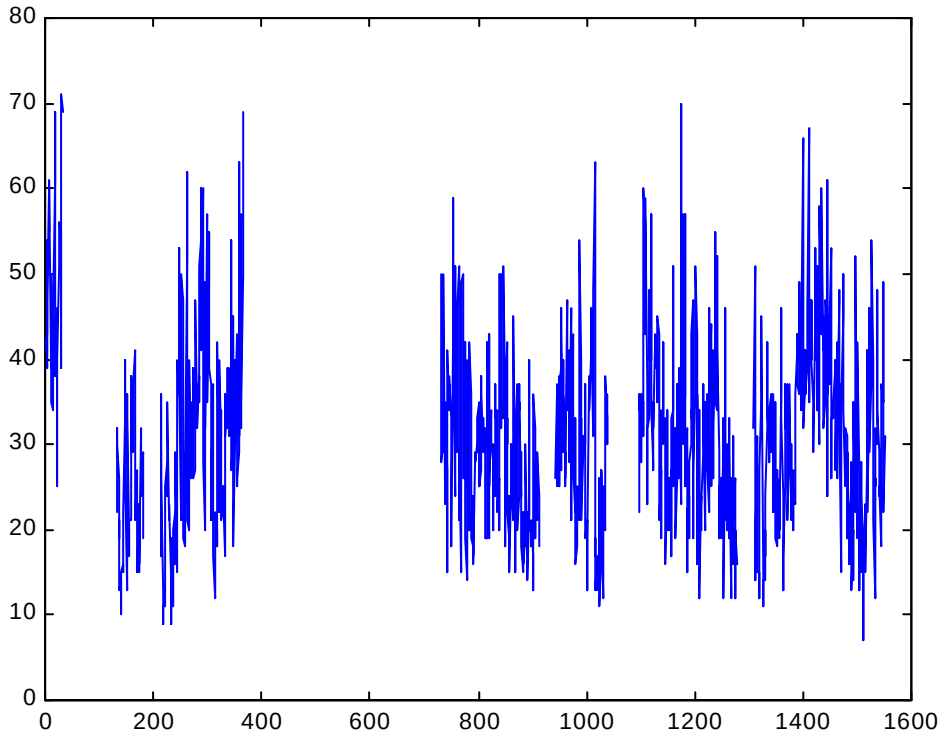

Figure 7.27 Maximum daily gust at Bell Rock: January 1983 to March 1987

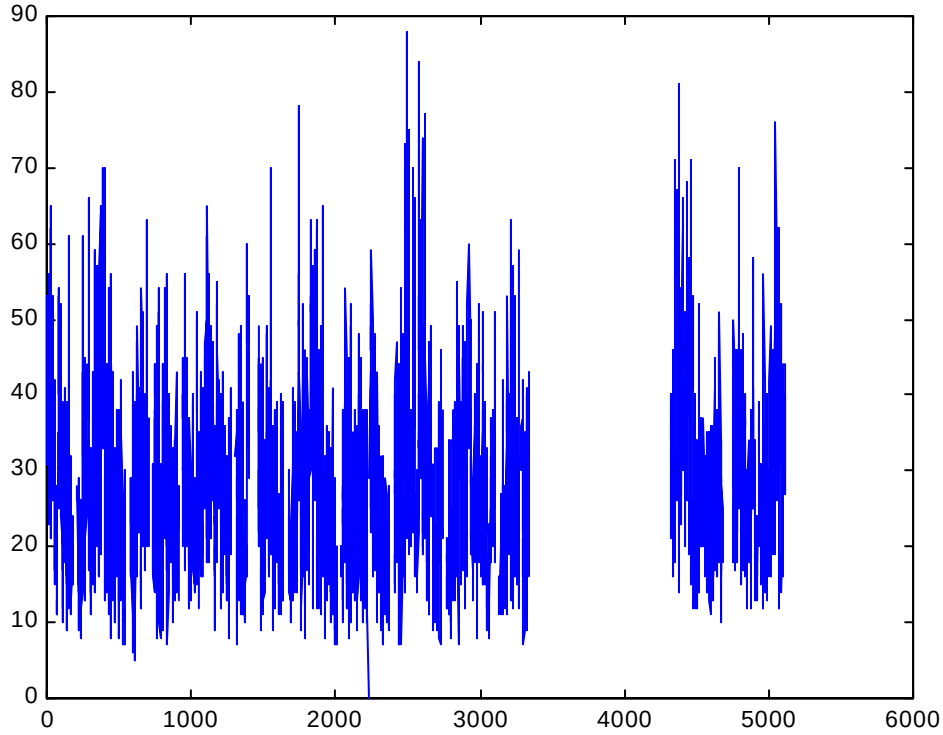

Figure 7.28 Maximum daily gust at Isle of Portland: January 1983 to December 1996

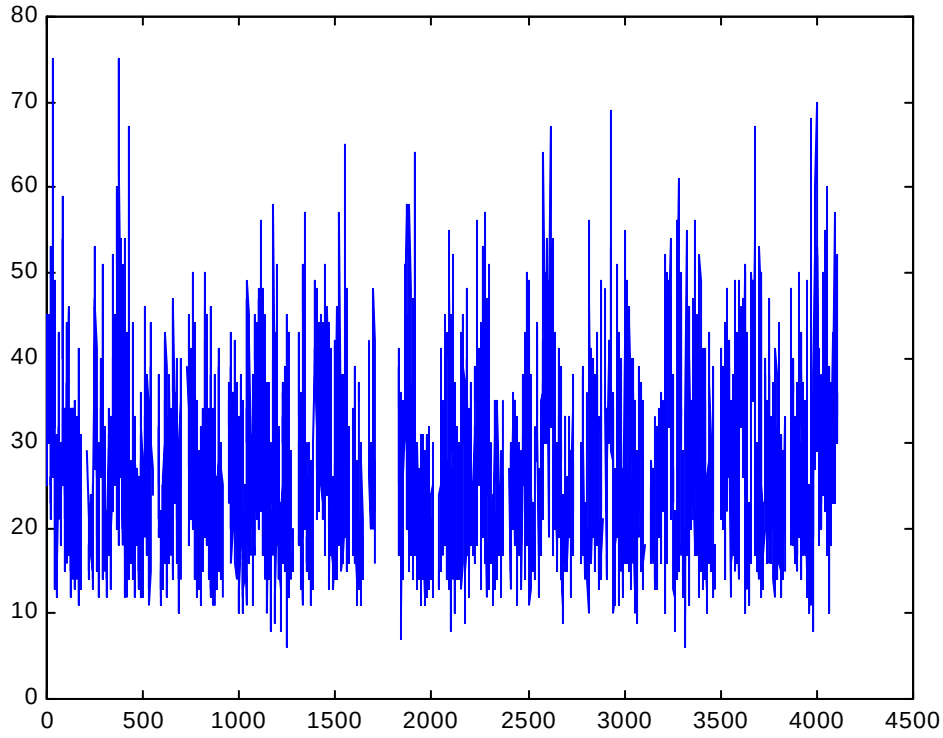

Figure 7.29 Maximum daily gust at Spurn Point: January 1983 to March 1994

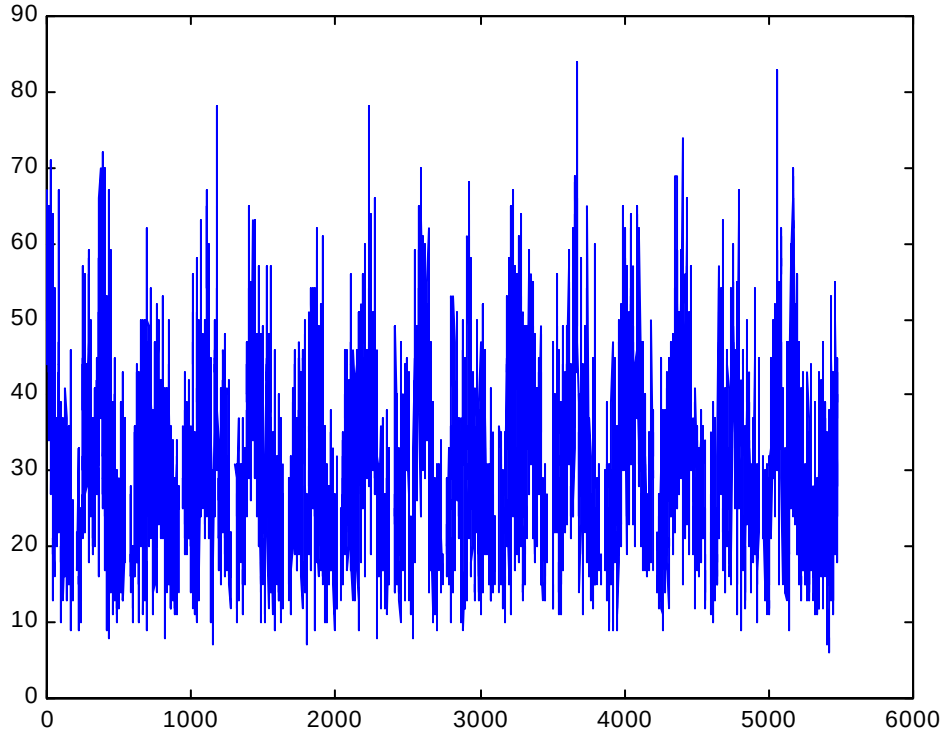

Figure 7.30 Maximum daily gust at Tiree: January 1983 to December 1997

7.4.2 Extreme value analysis of maximum daily gust speed

A simple but elegant method of examining the long-term behaviour of maxima involves fitting the Generalised Extreme Value (GEV) Distribution to the data. If a reasonable fit is obtained, various statistics about the return period of maximum gusts over many years can be deduced. We tested three methods of fitting the GEV to the annual maximum gust:

- maximum likelihood,
- method of moments, and
- probability weighted moments (PWM)

(see [Palutikof et al. (1998)]). In order to carry out an extreme value analysis based on the Tiree data, it is first necessary to extract the annual maximum gust speed value in each year, because the GEV distribution describes the distribution of a set of annual maxima.

Figure 7.31 shows the time series of the 15 annual maxima for Tiree. Figure 7.32 shows the cumulative density functions (CDF) derived empirically from this maximum gust time series together with the CDF from the GEV, calculated using PWM, that best fits this time series. The match appears to be very good. Figure 7.33 plots the same functions using normal probability scaling. We can test for a goodness of fit between the empirical function and the GEV model using the chi-squared test, giving X^2 of 0.5 and associated p-value of 0.97. This indicates that we can be 97% certain that the underlying distribution of the gust annual maxima is the GEV.

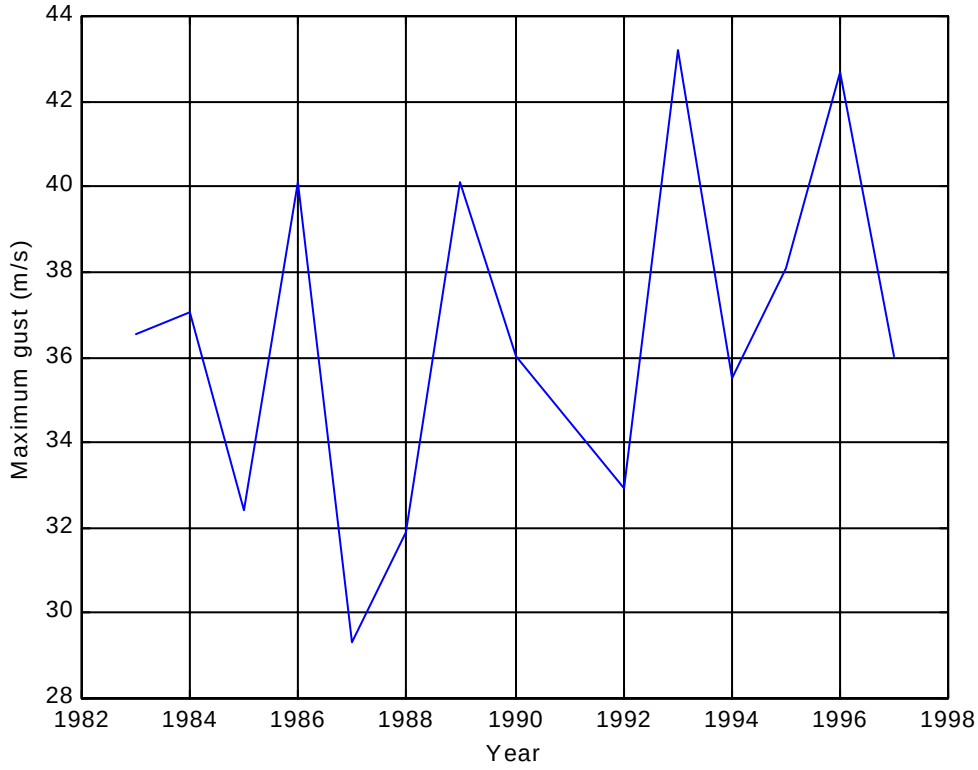

Figure 7.31 Annual gust maxima for Tiree

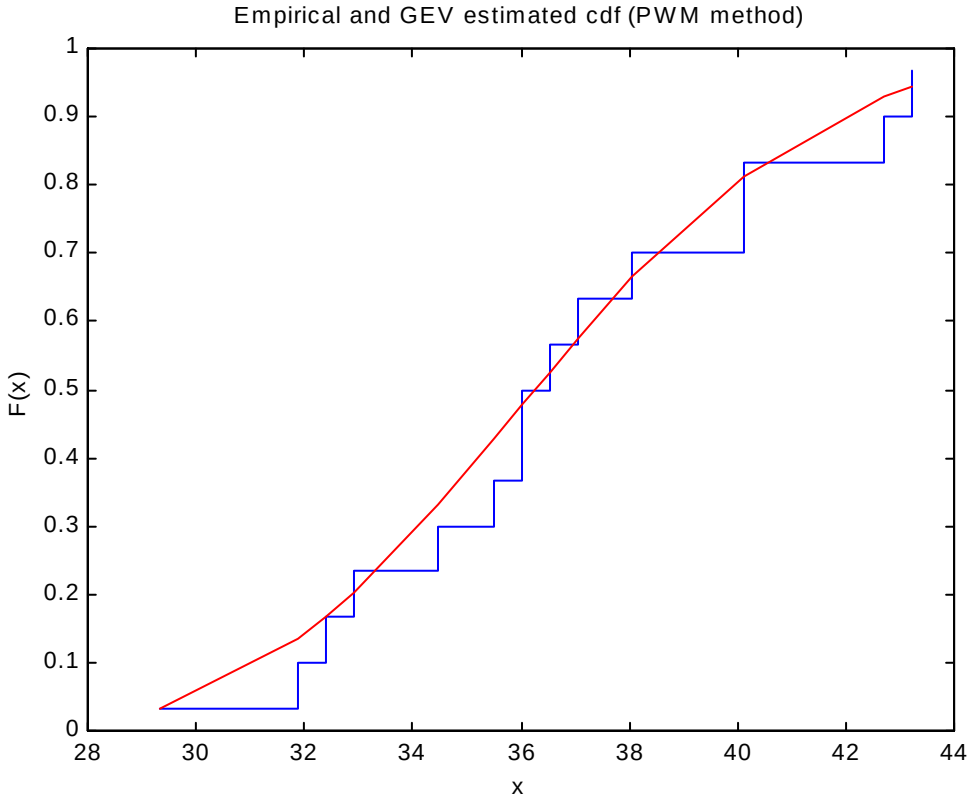

Figure 7.32 Empirical CDF (solid blue line) and GEV CDF (dashed red line) of annual gust maxima for Tiree

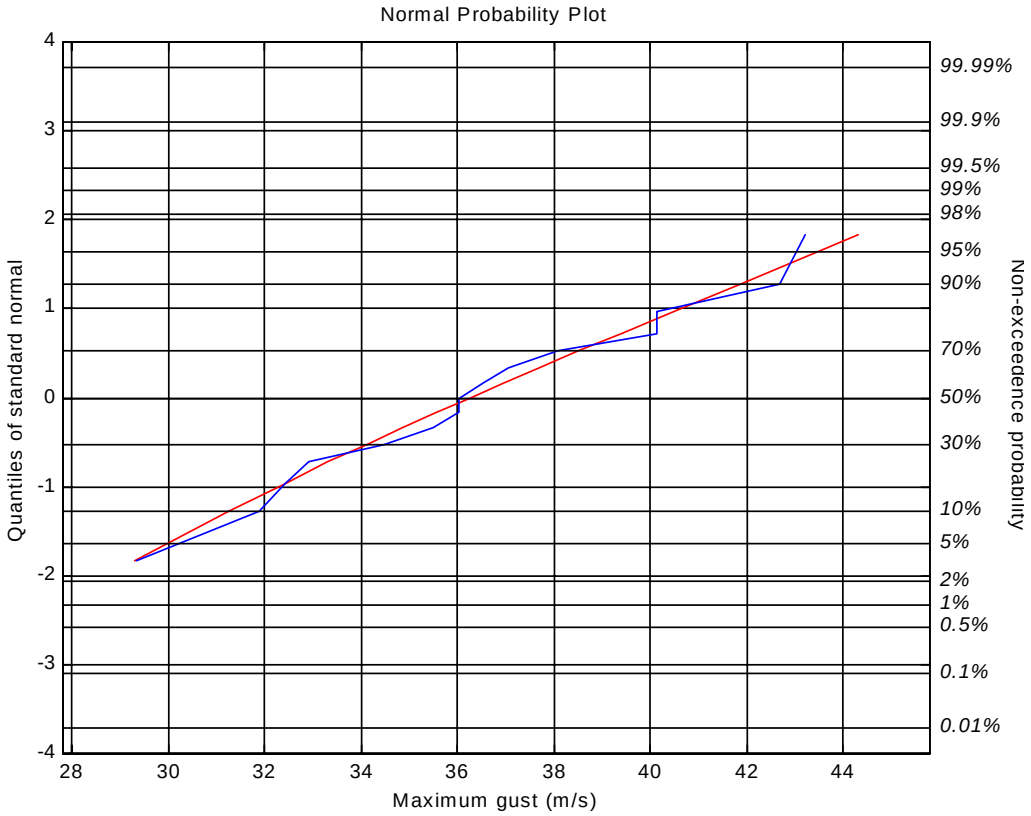

Figure 7.33 Normal probability plot of empirical (blue line) and GEV (red straight line) functions for Tiree annual maximum gust speeds

The right hand y-axis in Figure 7.33 enables us to read off the probability that a particular gust speed will not be exceeded. For example, there is an approximately 90% probability that a gust speed of about 42 m/s will not be exceeded. This can also be interpreted as a 10% probability that gust speeds will exceed 42 m/s.

The comparative statistics in Table 7.8 show in more detail the good match between the GEV model and the gust maxima. In the table:

- coefficient of variation = standard measure of variability (stand. dev./average)
- skewness = deviation of a distribution from symmetry (0 for normal)
- kurtosis = peakedness of a distribution (0 for normal)

	Population (GEV model)	**Sample (gust maxima)**
Mean	36.4	36.4
Standard deviation	4.1	4.0
Median	36.3	36.0
Coefficient of variation	0.11	0.11
Skewness	0.19	0.13
Kurtosis	2.8	2.0

Table 7.8 Model fitting statistics for the series of annual maximum gust speeds for Tiree

It is important to note that, because of the good fit of the gust maxima to the GEV model, the validity of these probability conclusions is not necessarily limited to the period of gust observations. Assuming that the time series of maximum gust speeds remains stable over time, such that the shape of the GEV distribution also remains constant, conclusions can be drawn regarding return periods of particular gust maxima over very long periods.

Table 7.9 shows the annual gust maxima to be expected from our GEV model for particular return periods. For example, on average, every 50 years we would expect a maximum gust of 45.2 m/s. The column of confidence limits for this example shows that we are 95% confident that the annual maximum gust speed with a return period of 50 years will lie between 40.1 and 50.4 m/s. Generally speaking, it is considered inadvisable to predict for return periods more that 3-4 times the duration of the empirical time series on which the calculations are based. Here, there are 15 years of observations and we have restricted the maximum return period in Table 7.9 to 50 years..

Return period (years)	Gust speed (m/s)	95% Confidence limits (m/s)
50	45.2	40.1 to 50.4
20	43.5	39.7 to 47.3
10	41.9	38.8 to 44.9
5	39.9	37.3 to 42.5
3	38.1	35.6 to 40.6
2	36.3	33.9 to 38.6

Table 7.9 Expected annual gust maxima for particular return periods at Tiree

7.4.3 Conclusions

Extreme value analysis offers a valuable technique for the evaluation of damaging high wind occurrence at offshore wind speed sites. From a relatively short run of data, here 15 years, it is possible to explore the behaviour of severe winds over much longer time periods.

7.5 References for Chapter 7

1. Barthelmie, R.J., B. Grisogono and S.C. Pryor (1996) Observations and simulations of diurnal cycles of near-surface wind speeds over land and sea. *Journal of Geophysical Research*, **101 (D16)**, 21327-21337.

2. Holt, T. (1999) A classification of ambient climatic conditions during extreme surge events off Western Europe. *International Journal of Climatology*, **19**, 725-744.

3. Holt, T. (2001) One hundred years of gales over the Northern UK: an analysis using enhanced pressure data. To be submitted to International Journal of Climatology.

4. Jackson, D.A. (1993) Stopping rules in Principal Components Analysis - a comparison of heuristic and statistical approaches. *Ecology*, **vol 74**, 8, pp 2204-2214.

5. Jenkinson, A.F. (1977) Analysis of maximum significant wave height data for selected North Sea storms. London Meteorological Office, Synoptic Climatology Branch Memorandum No. 55.

6. Jones, P.D. (1987) The early twentieth century Arctic High – fact or fiction? *Climate Dynamics*, **1**, 63-75.

7. Palutikof, J.P., B.B. Brabson, D.H. Lister and S.T. Adcock (1998) A review of methods to calculate extreme wind speeds. *Meteorological Applications*, **6**, 119-132.

8. Preisendorfer, R.W. (1988) Principle Component Analysis in meteorology and oceanography. Elsevier, Amsterdam.

9. Richman, M.B. (1986) Rotation of Principal Components. *Journal of Climatology*, **vol 6**, pp 293-335.

CHAPTER 8 : WIND AND WAVE LOADING

Chapter authors: : Dr H Cleijne (KEMA Sustainable)

8.1 Introduction

In their lifetime of about 20 years, OWECs have to withstand several environmental forces. Traditionally, for wind turbines the only factor to account for has been the wind. In the offshore industry, structures much more solid than wind turbines show a limited dynamic response to hydrodynamic loading because of their high structural stiffness. Now with the realisation of offshore wind farms with slender wind turbines, both aerodynamic and hydrodynamic forces inducing dynamic responses have to be accounted for, requiring a merging of the offshore and the wind turbine design technology. Wind and water each have their own distinctive contribution to the overall environmental loading of an OWEC. The loading comprises extreme loading by large loads with a certain probability of occurrence and fatigue loading due to loads with a cyclic nature.

Standards for determining the extreme and fatigue loading by aerodynamic and hydrodynamic forces separately have been developed, but it is the combination of the two latter that needs to be focussed on. Recent studies have shown that taking into account the combined wind and wave loading in the design codes may lead to less conservative designs [Kuhn(2001)]. In order to take advantage of this design method, it is necessary that relevant data for wind and wave loading become available.

Experimental data on the combination of wind and wave loading is scarce. For the determination of combined loads, therefore, use is often made of a hind-cast data set. Starting from known meteorological conditions on e.g. a 3 hourly time scale, the sea wave state is calculated by means of a wave model. An example of such a data set is the North European Storm Study (NESS) data base. This is proprietary information and the owners are not willing to disclose the underlying data to third parties. Fortunately, the project team has been able to get access to a comparable data set, which has been compiled by the UK Meteorological Office, which is very well suited for making the aforementioned cross-correlation analysis.

In this section the following topics are touched upon:
- Loading of wind turbines under offshore conditions
- Background
- Description of the UKMO data set

In the past, a number of projects have reported results for wind and wave loading of offshore wind turbines [Hendriks et al. (2000) and Kuhn (1998)]. This is the first study in which a complete set of hind cast data is reported.

8.1.1 Environmental conditions for offshore wind turbines

An Offshore Wind Energy Converter (OWEC) must be designed to withstand:
- fatigue loads caused by the turbulence in the wind and the cyclic loading of the incoming waves, sometimes combined with sea currents.
- extreme loads caused by heavy storms and extreme wave conditions. This may include breaking waves slamming on the construction.

A number of design codes have been developed for the certification of OWECS (e.g. [Germanischer Lloyd (2000)]). These design codes give a list of load cases, which must fall within the design envelope of the OWECS. These load cases are defined by the sea state.

The sea state is a statistical description of the wind and wave conditions at the sea surface during a 3-hour time interval. It is assumed that the wind and wave conditions remain constant during this 3-hour interval and that the same holds for all statistical parameters. Examples of statistical parameters are windspeed, turbulence intensity, significant wave height, wave period, wave direction, wave spectrum, etc.

The sea state is a description of the properties of the wind sea and swell in a 3 hour period. It is considered as a stationary stochastic process, defined by the average zero-crossing wave period and the significant wave height. Within a given sea state the wave height varies at random; the wave height distribution can be described by the wave energy spectrum and the wave direction spectrum.

Thus when describing waves we can distinguish between:
1. The wave climate. The wave climate describes the long term likelihood of sea states at a given location.
2. The wave energy spectrum: distribution of period and height within a sea state.

These items will be discussed next.

It is common to classify surface waves according to their periods as in the table below.

Period	Wave length	Name
0 – 0,2 s	centimetres	ripples
0,2 – 9 s	to about 130 m	wind sea
9 – 15 s	hundreds of meters	swell
15 – 30 s	many hundreds of meters	long swell
30 s – hours	to thousands of kilometres	long period waves
12.5 h, 25 h, etc.	thousands of kilometres	tides

In this overview, it is the wind sea and swell that are most important to the loading of OWECs. Wind sea includes all waves generated by local winds. They are generated by the wind blowing for some hours duration over a certain length of sea called fetch. Waves receive their energy from the movement (turbulent stress) of wind on the ocean surface. During generation the disturbed sea surface is not regular and contains many different oscillatory motions at different frequencies. The directional distribution and the height of wind sea corresponds with the wind speed.
As wind sea grows the sea surface becomes more regular, and wind sea turns into swell that is able to leave the area of generation (figure 8.1).

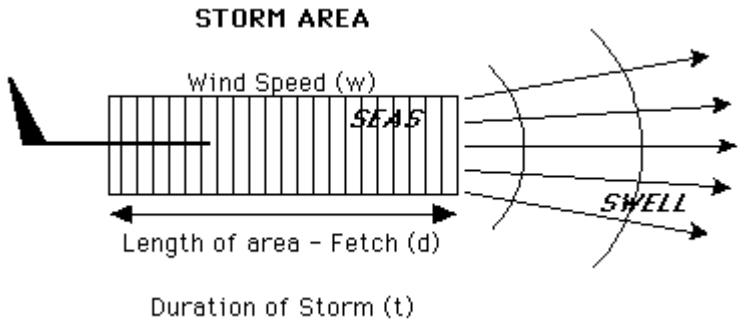

Figure 8.1 Development of wind sea and swell

Thus swell refers to waves generated by distant wind fields. Swell travels in one direction and is much more regular than wind sea. Swell is mostly low frequent, wind sea is generally of a higher frequency.

The transition regime between wind sea and swell in the area close to but outside the immediate wind generation region, where the wind forcing has already decreased but the non-linear interactions are still important, plays a critical role in determining the ratio of wind sea to swell energy. Laboratory experiments have shown that wind sea achieves lower energy density, and hence amplitudes, in the presence of swell compared with their energy without swell.

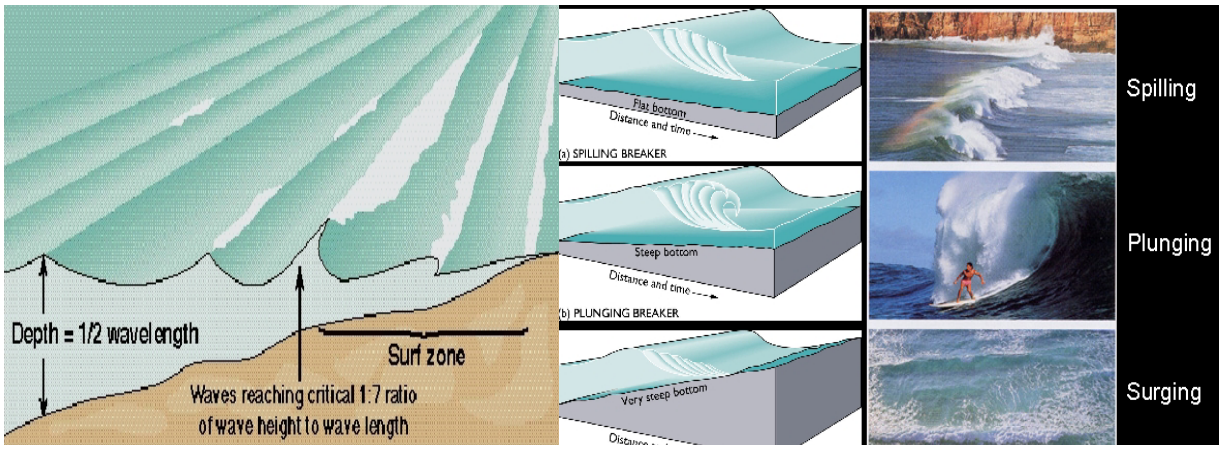

Figure 8.2 Criteria for and types of Breaking waves

In shallow water the waves start to “feel” the bottom and this leads to shoaling. The bottom becomes noticeable if the water depth is less than 0.5 the wave length. In the shoaling area two effects take place. The waves refract and they steepen. Since the waves travel slower in undeep water, they bend towards the coast and the wave crests and the coast line become more parallel. However the wind direction is not affected by this process, which can lead to a significant difference between wave and wind direction. The steepening of the waves can eventually lead to breaking or plunging waves. This can lead to severe loads on the wind turbine structure. Waves break when the wave height becomes more than 7 times the wave length. It depends on the bottom slope, which kind of breaking occurs (see figure 8.2).

1. Long term distribution; wave scatter

The probability distribution of sea states is presented in a wave scatter diagram, describing the long term distribution. A wave scatter diagram is a two dimensional histogram of the significant wave height and wave period for all sea states. A sea state is assumed to be stationary during three hours. Wave heights and periods can be ‘binned’ in scatter diagrams with for example 0.5 meter and 1 second width. Not being able to consider all sea states, a limited number of typical load cases are extracted, referred to as lumped sea states.
Like for wind, information about the distributions of wave heights and the frequency of the varying wave directions can be presented in a wave rose based on meteorological observations of wave heights and wave directions.

2. Short term distribution; wave spectrum

Statistical description assumes that waves of all frequencies and corresponding wavelengths are present. It does not attempt to describe the form of the sea surface but concentrates on wave energy.

The Pierson-Moskowitz spectrum is generally agreed to be representative for fully developed seas. When the waves are in the process of growing under strong winds, this spectrum is, however, too broad and the peak of maximum density is too low. It is based on the significant wave height and the zero crossing period. The PM spectrum is a special case of the Gamma spectrum.

$$S_{zz}(\omega) = \frac{4\pi^3 H_s^{\,2}}{T_z^{\,4}\omega^5}\exp\left[-\frac{1}{\pi}\left(\frac{\omega T_z}{2\pi}\right)^{-4}\right]$$

The JONSWAP spectrum, a peak enhanced version of the PM spectrum is usually considered to be appropriate when the fetch is limited, as is the case for wind sea. The model is based on significant wave height and the mean wave period.

$$S_{zz}(\omega) = \frac{5{,}23\pi^3 H_s^{\,2}}{T_1^{\,4}\omega^5}\exp\left[-32{,}29\frac{\pi^3}{T_1^{\,4}\omega^4}\right]\gamma^p$$

$$p = \exp\left(-\left(\frac{0.191\omega T_1 - 1}{\sqrt{2\sigma}}\right)^2\right)$$

$\gamma = 3.3$

$\sigma = 0.07$ for $\omega \le 5.24/T_1$

$\sigma = 0.09$ for $\omega > 5.24/T_1$

γ is a peak-enhancement factor, the effect of which is to increase the peak of the Pierson-Moskowitz spectrum. σ is a relative measure of the width of the peak The effect of the additional factors for the JONSWAP spectrum allowes narrower, more peaked spectra which are typical forms of growing wind seas in deep water.
Both spectra are characterised by the significant wave height H_s and the wave period T_1. The significant wave height is defined by the 33% exceedance level.

8.1.2 Design criteria

The difficulty in the specification of extreme load cases is further complicated by the presence of wave and current. In general it is assumed that the wind and wave loads are not correlated during a sea state (3 hours). Furthermore, extreme loads are not always result of extreme environmental conditions. Operating conditions, control system and dynamics of the structure etc. have also influence on the extreme loads.

Extreme conditions are characterised by the return period. An extreme wind speed with a return period of 50 years refers to a wind speed that, on average, occurs once in 50 years. This concept also applies to the wave height. The problem arises in the combination of extreme values. One can calculate the extreme wind load and extreme wave load separately and adds them together. This approach would be too conservative, as mentioned before, the correlation between the wind speed and wave in small time scale is non existent.

8.1.3 The UKMO-data set

The UKMO data covers 10 years: 1987 to 1996. The data has been retrieved from the European Wave Model archive data covering the area 30.5ºN to 66.75ºN and 14.0ºW to 35.5ºE at grid point intervals of 0.4º in longitude and 0.25 º latitude. This comprises the Baltic Sea, the North Sea, the Atlantic, the Mediterranean and the Black Sea.
The number of grid points in the European waters considered is 8467. The data is 3-hourly (6-hourly prior to mid 1988) and provides the following:

1. Wind speed and wind direction (at 19.5 m ASL)
2. Wind sea height and wind sea period
3. Swell height, swell period and swell direction
4. Resultant wave height, resultant wave period and resultant wave direction.

The wind data is taken from the UKMO Unified model, at 19.5m above sea level for neutral atmospheric stability conditions. The wind speed and wind direction are the input for the wave model. The UKMO European Wave Model is a fine resolution model nested within a coarser global wave model, taking its boundary conditions directly from the global model. In shallow regions, bathymetry is taken into account by means of the following phenomena:

– bottom friction
– refraction
– shoaling
– depth dependent group velocity

Processes that are not included are:

– gustiness of surface wind
– wave induced motion of muddy bottom
– percolation of water through porous sea floor
– resonant triad interaction near coastline
– wave breaking

Water is assumed to be deep beyond 200 meters depth. The global model assimilates significant wave heights from the ERS-2 satellite, but the European model does not assimilate any observed data.
The mean wave period and the significant wave height are calculated from the wind speed, determining the JONSWAP spectrum of that particular sea state. The wave energy of growing wind sea is then forced to match the JONSWAP spectrum. The wave model represents non-linear transfer of wave energy from high frequencies to lower frequencies, as wind seas grow to become swell. The fully developed sea fits a Pierson Moskowitz spectrum. The fully developed sea is described by the significant wave parameters.

The consistency of the data set has been checked by careful inspection of the data. Three periods showed missing data:
– 22 February 1988 to 2 May 1988, due to loss of archive tape by UKMO
– Several records in 1989
– January 1994 is lacking a large number of data

It showed that complete records are missing for each of the grid points in the spatial domain. Since the number of missing data records is limited, the analysis will be continued using the complete data set without further corrections. The impact on the accuracy of the analysis will estimated.

- model
- dataset (gridsize, parameters and timeperiod)
- quality
- credits

8.1.4 Wind and wave climate analysis

The UKMO data set has been analysed and has been presented in maps and graphs.

Figures 8.3-8.16 shows the spatial data, displayed in maps. Maps are presented for 4 categories of data. Resultant wave data, wind sea, swell data and wind speed data. For each of these categories is displayed: average value, i.e. average wave height and wind speed, wave period, direction and the estimated 50 year extreme.

More detailed footprint data is presented for 14 locations (table 8.1) selected to represent different areas in the European waters. These include data for mean conditions, direction, 50 year extremes, Weibull parameters, frequency distributions, annual variations, monthly variations. (Annex 1). Wind wave interaction has been analysed and is presented in Annex 2. This includes wind-wave diagrams, wave scatter diagrams and wave-period diagrams.

Table 8.1 Locations for the footprint data

Location	**Lattitude**	**Longitude**
Adriatic Sea	43.00	15.53
Aegean Sea	38.00	25.53
Atlantic (North)	60.00	-10.07
Atlantic (Central)	44.00	-12.87
Atlantic (South)	35.00	-10.07
Baltic Sea	58.00	20.33
Bay of Biscay	45.00	-2.87
Black Sea	42.00	29.93
Ionian Sea	36.00	19.13
Mediterranean (East)	33.50	27.93
Mediterranean (West)	39.00	5.93
North Sea	57.00	3.13
Norwegian Sea	65.00	2.33
Tyrrhenian Sea	40.00	12.33

Mean conditions
The mean values of the following parameters were calculated:

- Wind: wind speed, and wind direction
- Significant: wave height, wave direction and wave period
- Swell: wave height, wave direction and wave period
- Wind sea: wave height, wave direction (by definition equal to the wind direction) and wave period

Annual variation
The average wave height and wind speed are presented for each year and compared to the overall mean. This shows the interannual variation of the presented parameters.

Monthly variations
The average wave height and wind speed for each month, averaged over all the years in the data set are presented to show the monthly variation. This graph is relevant for planning maintenance periods.

Annual variation the maximum value
The maximum value of wave height and wind speed for each year is presented and compared with the extrapolated 50 year extreme level.

Extreme conditions
The once per 50-year exceedance level was calculated for the wind speed and wave height using Gumbel-theory. The yearly maximum value was stored and sorted. The sorted maximum values were then used to estimate the parameters *a* and and *y* in the Gumbel distribution.

$$P(x \le x_i) = \exp(-\exp(-a(x_i - y))$$

Using the distribution parameters, the 50 year extreme value was estimated by extrapolation.

Frequency distributions
Bin analyses were made of the wind and wave parameters. In the analysis, the following values were used:

Parameter	Bin size	Maximum value
Wave height	0.5 m	15 m
Wind speed	0.5 m/s	25 m/s
Direction	30	360
Wave period	0.5 s	25 s

Weibull parameters
The frequency distributions for wind speed and wave height were used to estimate the two parameter Weibull-distribution. The shape factor ‘k’ and the scale factor ‘a’ were estimated by a least square fit between exceedance levels of 10% and 90%.

Scatter diagram
The scatter diagram shows the distribution of wind sea wave height vs. the wave direction.

Wind wave diagram
The wind wave diagram shows the distriburion of wind speed vs. wind sea wave height. This diagram is a requirement for calculating integral wind wave loading on wind turbines

Wave period diagram
The wave period diagram presents the relation between the wind sea wave height and the wave period

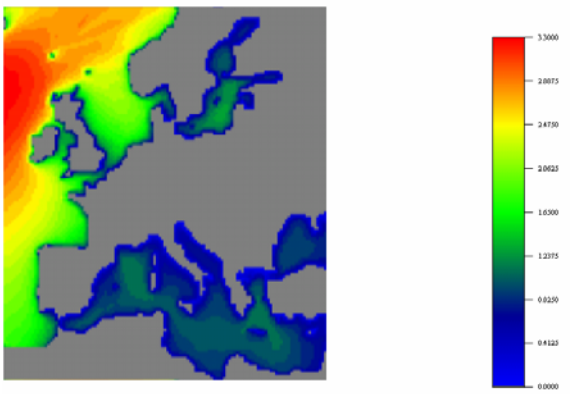

Fig 8.3 Resultant wave height

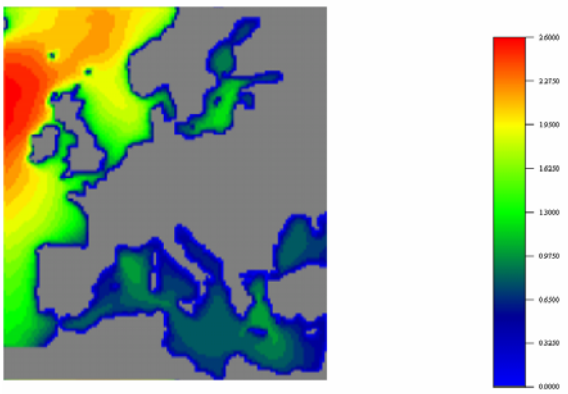

Fig 8.4 Windsea wave height

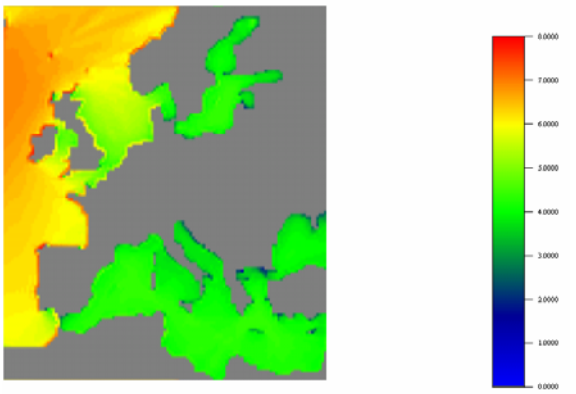

Fig 8.5 Resultant wave period

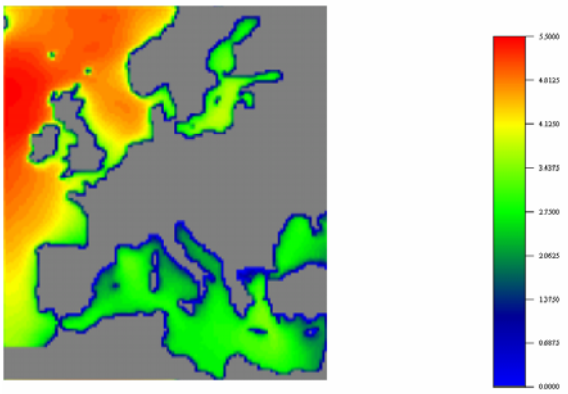

Fig 8.6 Windsea wave period

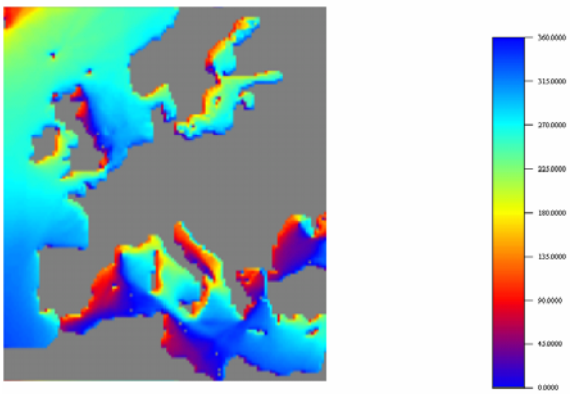

Fig 8.7 Resultant wave direction

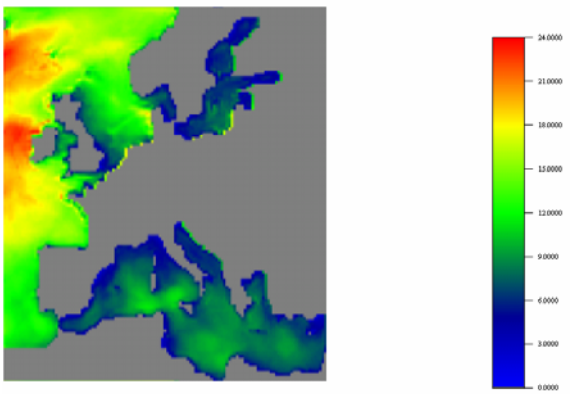

Fig 8.8 Resultant 50 year extreme wave height

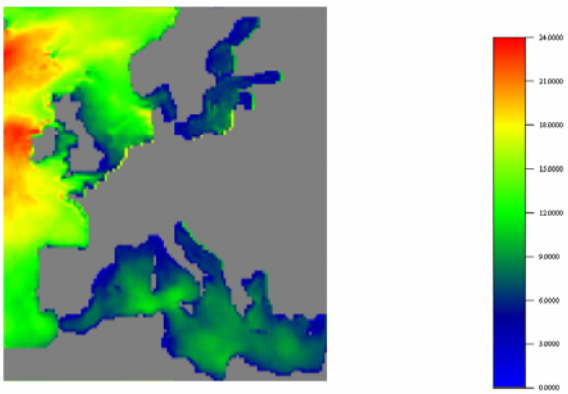

Fig 8.9 Wind sea 50 year extreme wave height

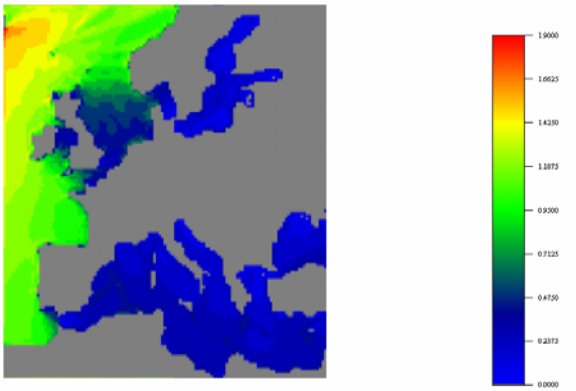

Fig 8.10 Swell Wave height

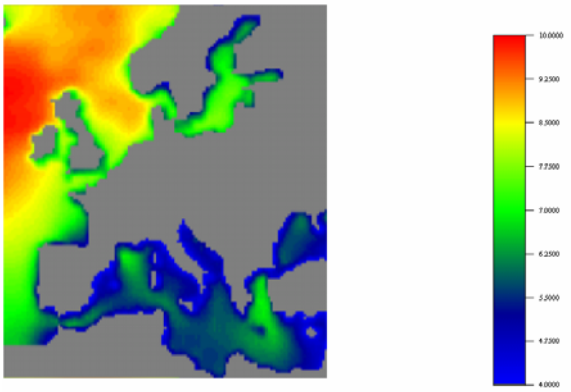

Fig 8.11 Average wind speed

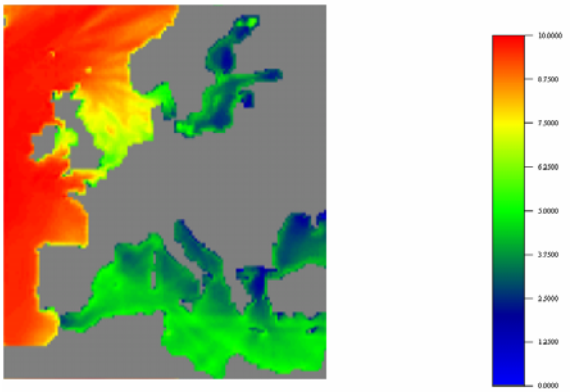

Fig 8.12 Swell wave period

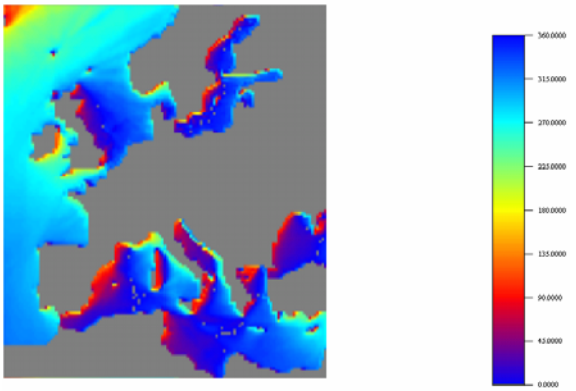

Fig 8.13 Swell wave direction

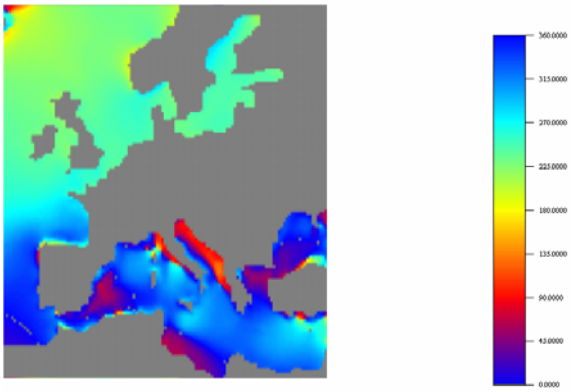

Fig 8.14 Wind direction

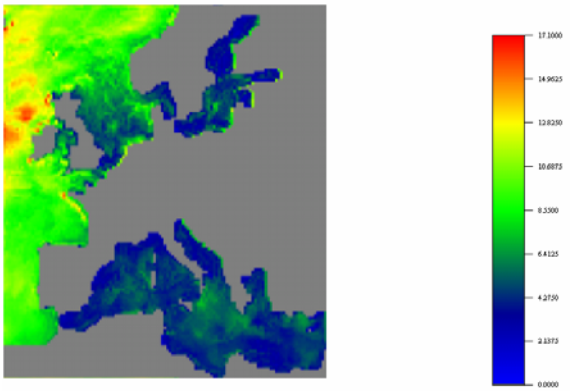

Fig 8.15 Swell 50 year extreme wave height

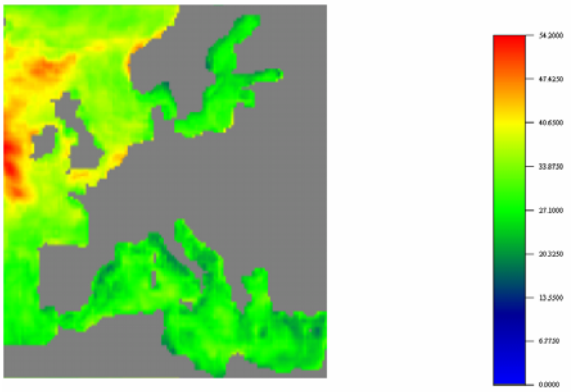

Fig 8.16 50 year extreme wind speed

8.1.5 Relevant conclusions

The UKMO wave data archive has shown to be very valuable for the calculation of the wave climate in the European waters.

The wave height can be well described by a Weibull-type distribution. The 50-year extremes were derived by fitting the annual extremes to a Gumbel distribution.

The wave climate in the Atlantic and the North Sea is more severe than in the Baltic, the Mediterranean and the Black Sea. The most severe wind conditions are in the West Coast of Ireland.

	Average (m/s)	**50-year extreme (m/s)**
Atlantic (N)	3.2	20.1
North Sea	2.1	12.9
Mediterranean Sea	1.1	9.9
Black Sea	0.9	6.2
Baltic Sea	1.2	6.7

The wave height varies considerably over the seasons. The winter seasons shown an average wave height, which is a factor of 2 - 2.5 higher than that in the summer season. This is an important factor for scheduling offshore installations and maintenance.

8.1.6 References

1. Coelingh J.P. et al. (2000). Wind and wave data compiled for the DOWEC concepts study, Delft university, Section wind energy, IW – 00162R, Delft, February 2000

2. Germanischer Lloyd Rules and guidelines 2000, Offshore wind energy converters.

3. Hendriks et al. (2000). DOWEC Concept study task 7, Standards and criteria for offshore wind turbines, , ECN-CX--00-039, October 2000.

4. Kühn M. et al (1998). Structural and economic optimisation of bottom-mounted offshore wind energy converters (OPTI-OWECS), Final reports (vol. 0-5), 1998.

5. Kühn, M (2001). Dynamics and Design Optimisation of Offshore Wind Energy Conversion Systems..; Delft University of Technology, 2001.

6. Matthies H.G. et al (1995). Study of offshore wind energy in the EC, Joule I (JOUR 0072),. Verlag Natürliche Energie, Brekendorf, 1995.

8.1.7 Annex 1 : Footprint data for 14 locations

Location	Adriatic Sea	Lattitude	43.00	Longitude	15.53

	Significant wave height
Average height	0.7 m
Average direction	9.1
Average Period	3.8 S
Maximum	5.1 m
50 yr return value	5.6 m
Weibull scale factor	0.7 m
Weibull shape factor	0.96

	Wind Sea wave height
Average height	0.6 m
Average direction	-
Average Period	2.2 S
Maximum	5.1 m
50 yr return value	5.6 m
Weibull scale factor	0.59 m
Weibull shape factor	0.84

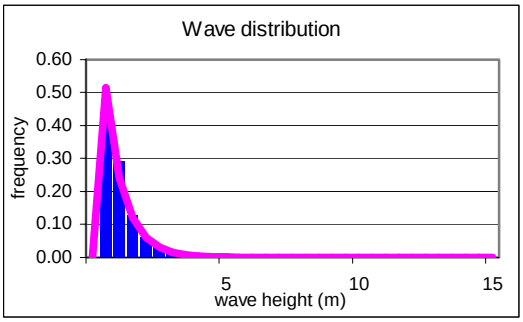

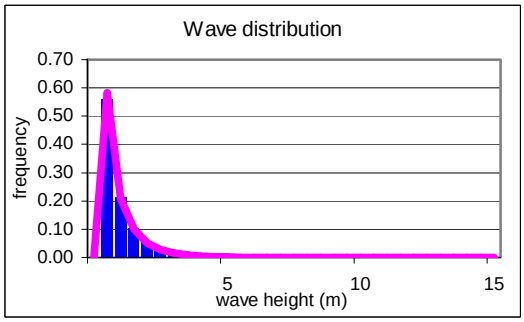

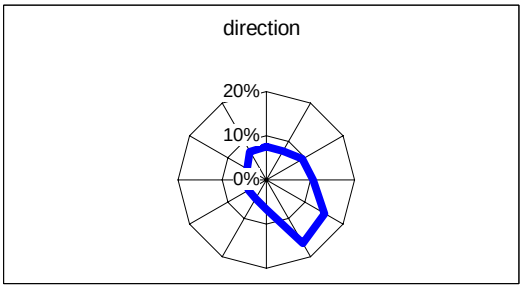

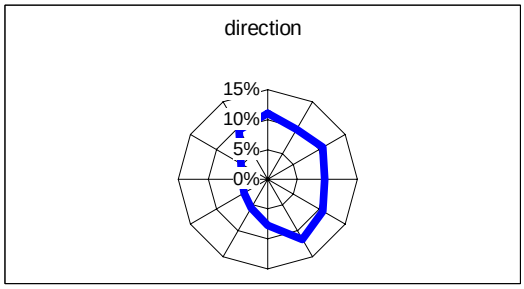

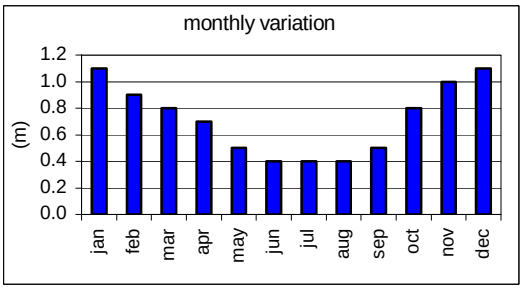

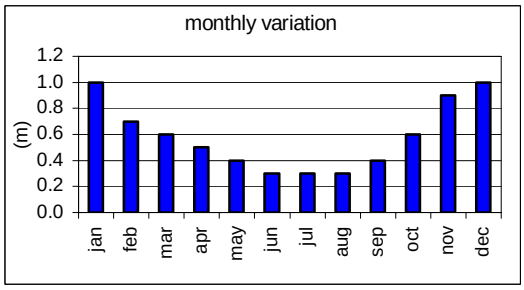

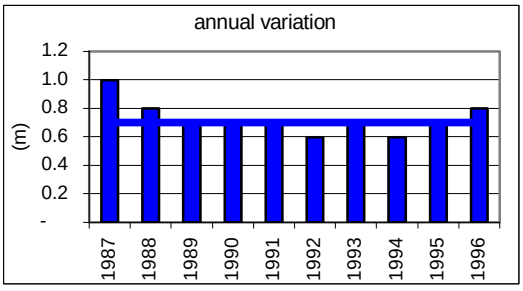

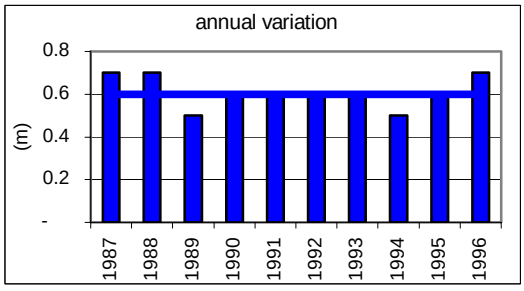

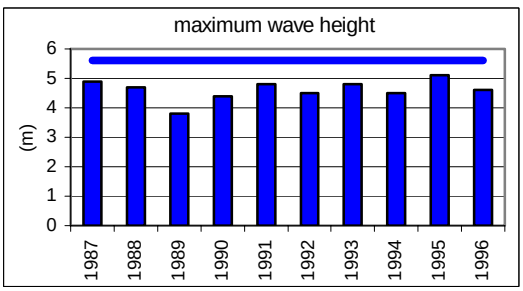

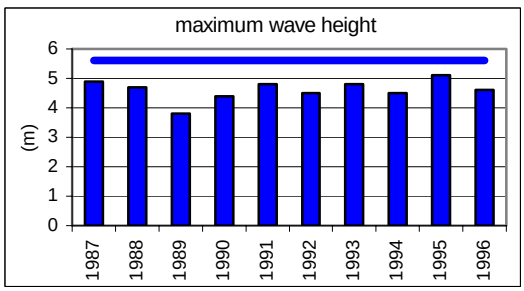

Location	Adriatic Sea	Lattitude	43.00	Longitude	15.53

	Swell wave height	
Average height	0.2	m
Average direction	3.2	
Average Period	2.9	S
Maximum	2.9	m
50 yr return value	3.3	m
Weibull scale factor	0.94	m
Weibull shape factor	90.4	

	Wind Speed	
Average height	5.1	m/s
Average direction	5.8	
Average Period	-	S
Maximum	22.5	m/s
50 yr return value	23.6	m/s
Weibull scale factor	5.73	m/s
Weibull shape factor	1.66	

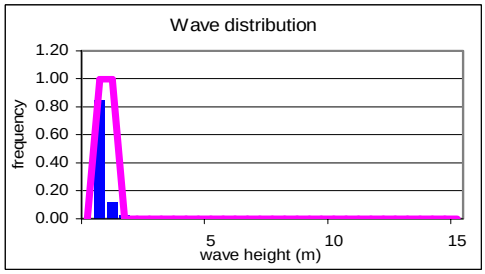

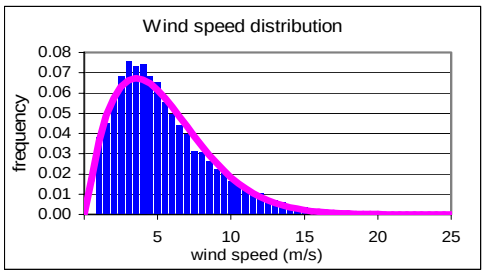

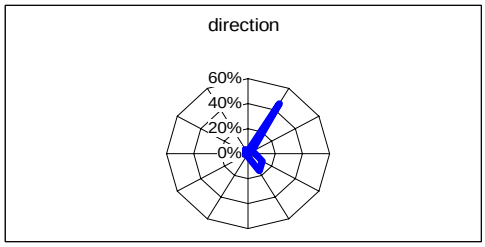

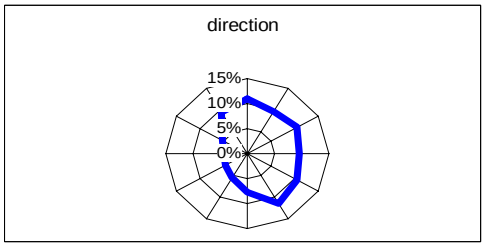

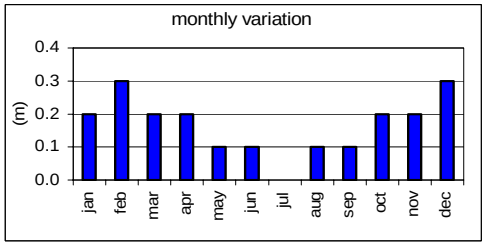

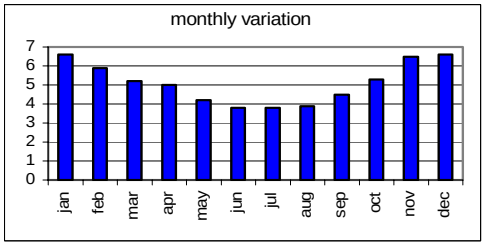

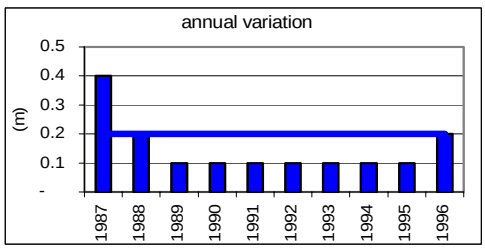

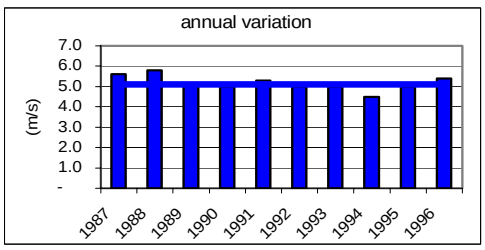

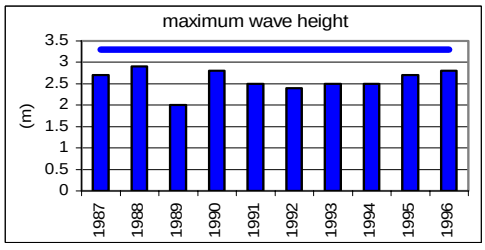

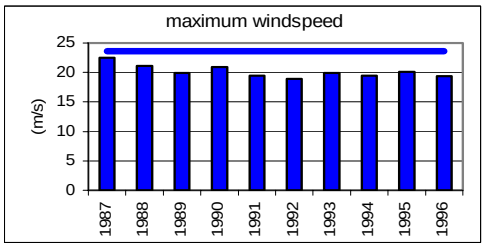

Location	Aegean Sea	Lattitude	38.00	Longitude	25.53

	Significant wave height	
Average height	1	m
Average direction	34.6	
Average Period	4.2	S
Maximum	6.1	m
50 yr return value	7.1	m
Weibull scale factor	1.15	m
Weibull shape factor	1.24	

	Wind Sea wave height	
Average height	0.9	m
Average direction	-	
Average Period	3.2	S
Maximum	6	m
50 yr return value	6.9	m
Weibull scale factor	1.08	m
Weibull shape factor	1.17	

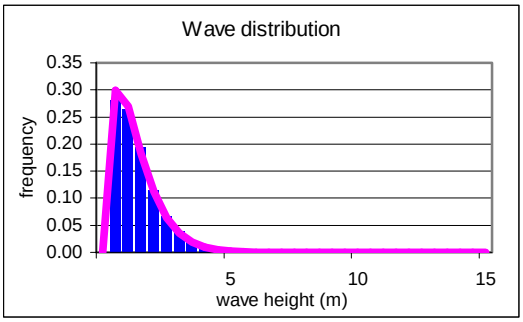

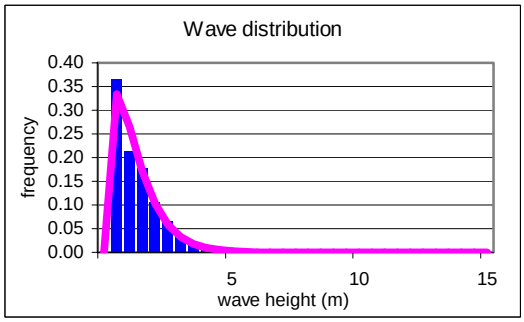

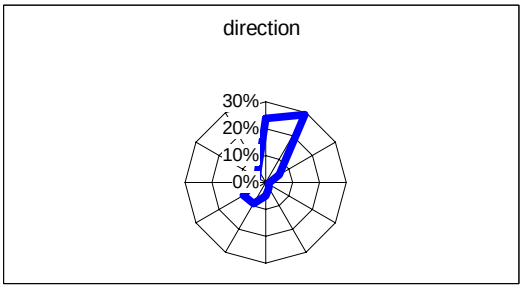

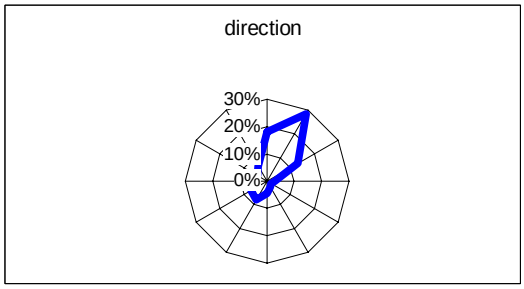

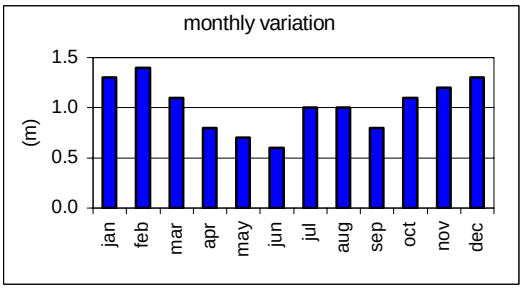

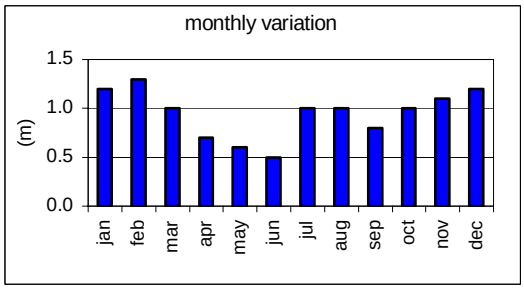

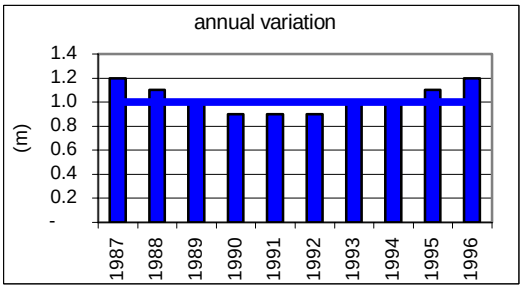

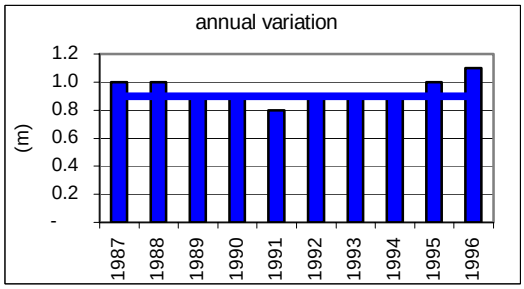

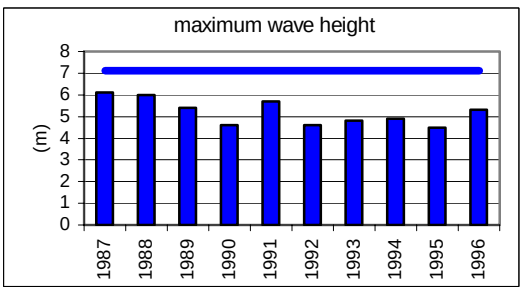

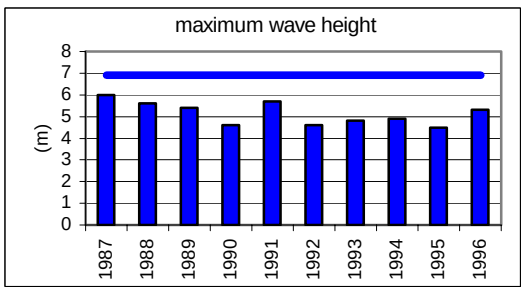

Location	Aegean Sea	Lattitude	38.00	Longitude	25.53

	Swell wave height	
Average height	0.2	m
Average direction	34.5	
Average Period	3	S
Maximum	4	m
50 yr return value	5	m
Weibull scale factor	0.18	m
Weibull shape factor	0.71	

	Wind Speed	
Average height	6.9	m/s
Average direction	35.9	
Average Period	-	S
Maximum	27.2	m/s
50 yr return value	31.4	m/s
Weibull scale factor	7.87	m/s
Weibull shape factor	1.85	

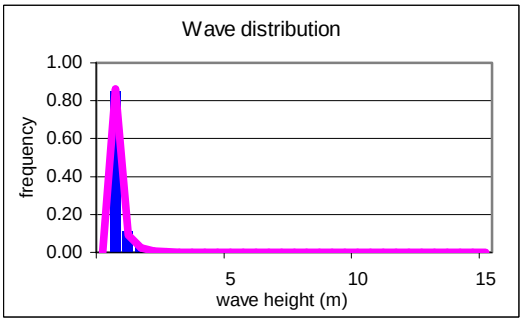

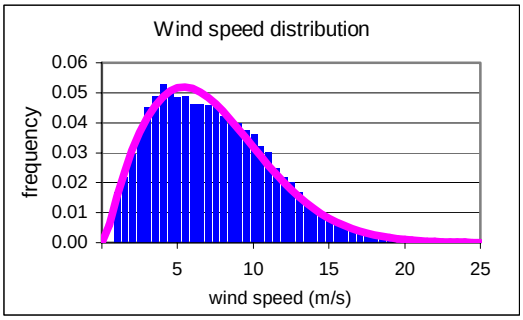

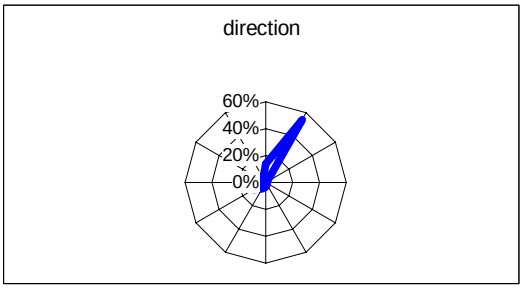

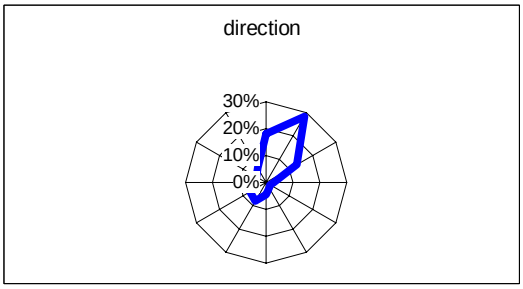

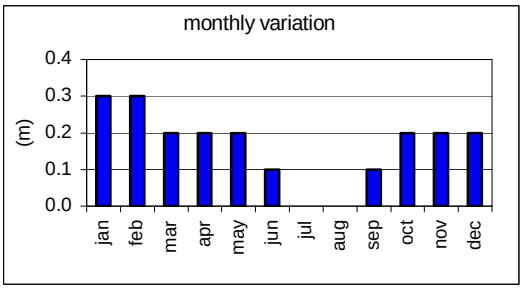

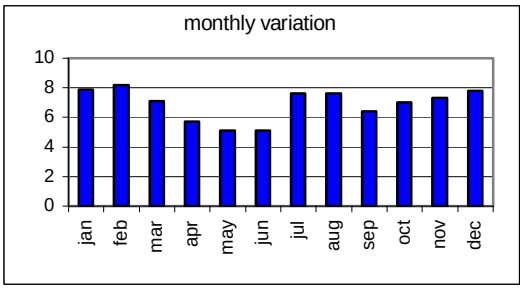

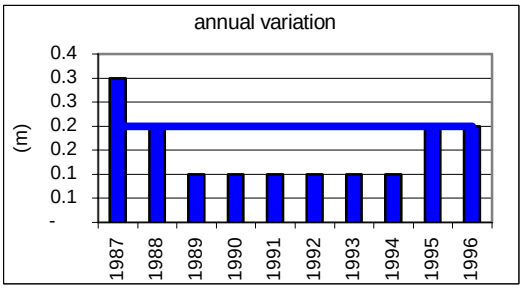

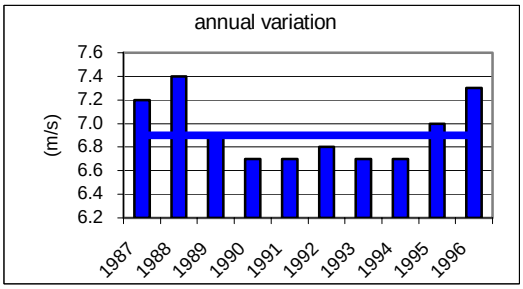

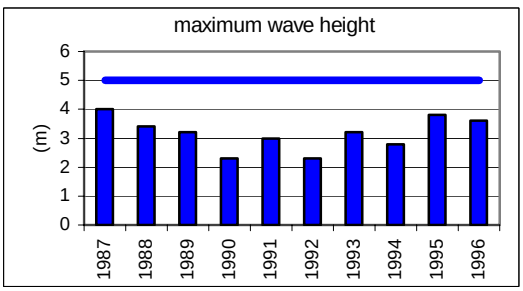

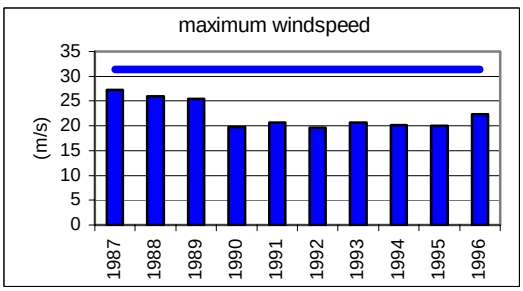

Location	Atlantic (Central)	Lattitude	44.00	Longitude	12.87-

	Significant wave height
Average height	2.4 m
Average direction	30.6
Average Period	6.3 S
Maximum	13.6 m
50 yr return value	16.9 m
Weibull scale factor	2.67 m
Weibull shape factor	1.86

	Wind Sea wave height
Average height	1.8 m
Average direction	-
Average Period	4.6 S
Maximum	13.6 m
50 yr return value	16.9 m
Weibull scale factor	1.98 m
Weibull shape factor	1.26

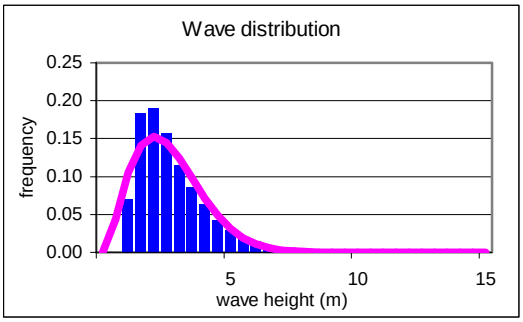

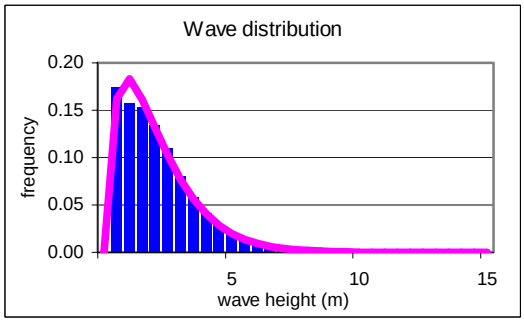

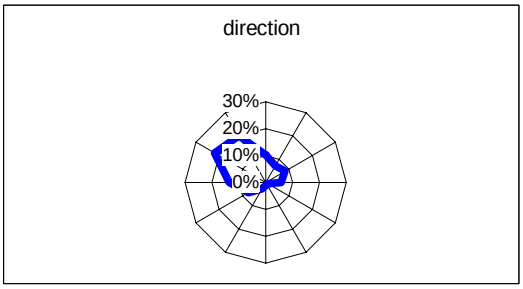

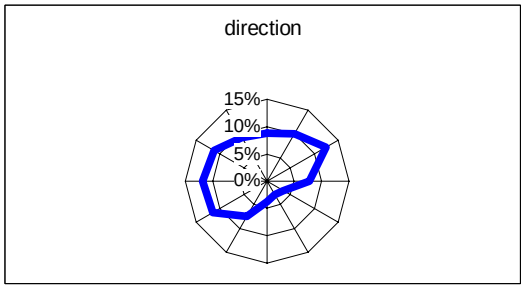

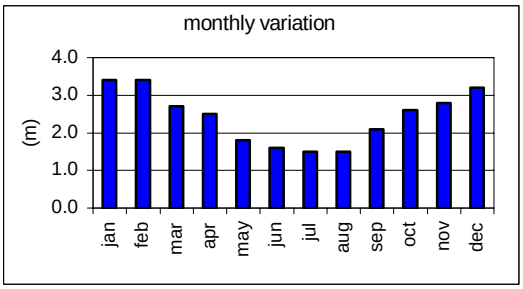

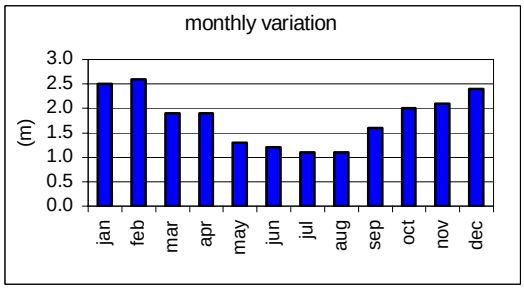

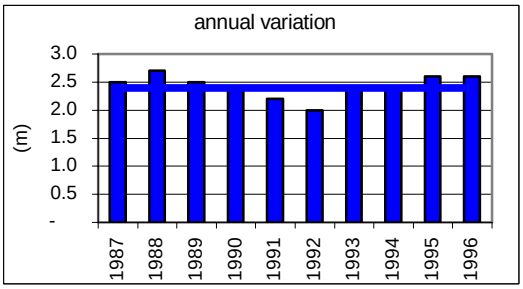

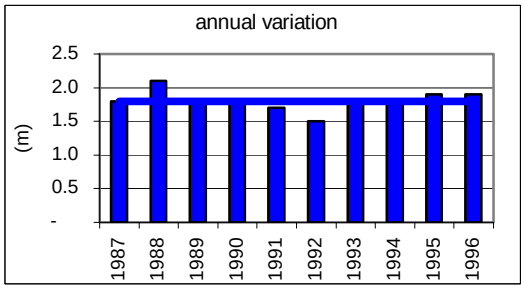

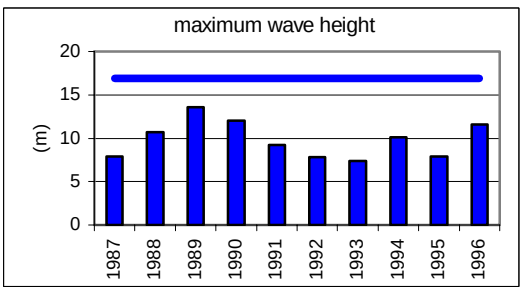

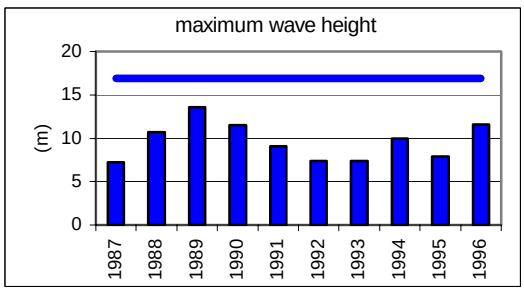

Location	Atlantic (Central)	Lattitude	44.00	Longitude	12.87-

	Swell wave height
Average height	1.2 m
Average direction	30.4
Average Period	9.7 S
Maximum	7.9 m
50 yr return value	9.5 m
Weibull scale factor	1.32 m
Weibull shape factor	1.34

	Wind Speed
Average height	8.3 m/s
Average direction	31
Average Period	- S
Maximum	29.8 m/s
50 yr return value	31.1 m/s
Weibull scale factor	9.35 m/s
Weibull shape factor	2.22

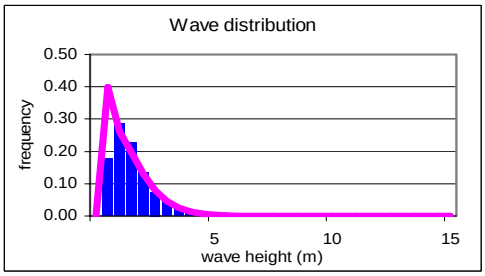

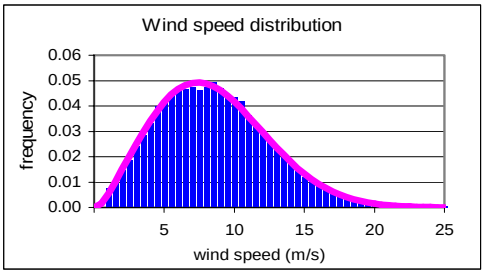

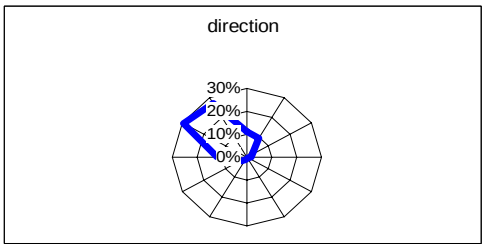

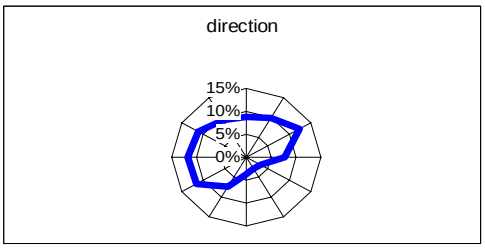

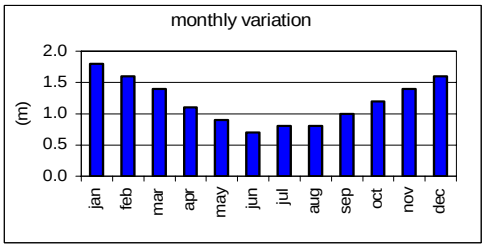

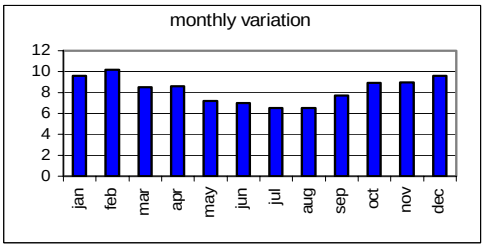

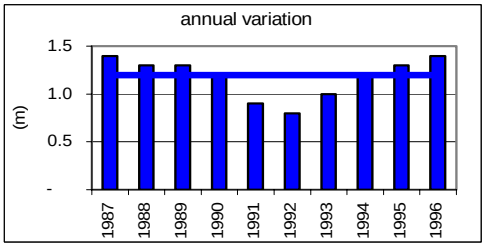

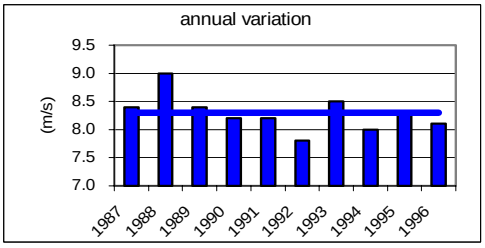

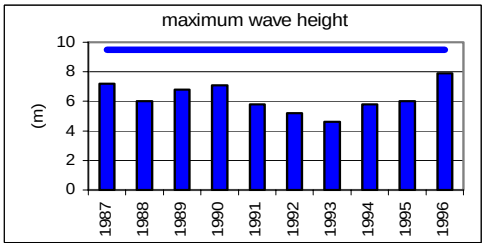

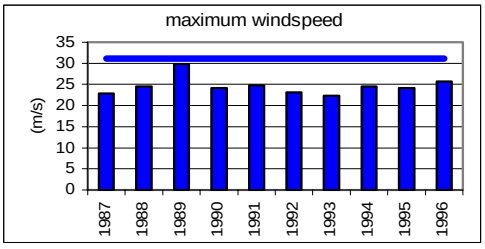

Location	Atlantic (North)	Lattitude	60.00	Longitude	10.07-

	Significant wave height	
Average height	3.2	m
Average direction	24.2	
Average Period	6.8	S
Maximum	16	m
50 yr return value	20.1	m
Weibull scale factor	3.53	m
Weibull shape factor	1.79	

	Wind Sea wave height	
Average height	2.5	m
Average direction	-	
Average Period	5.4	S
Maximum	16	m
50 yr return value	20.1	m
Weibull scale factor	2.7	m
Weibull shape factor	1.21	

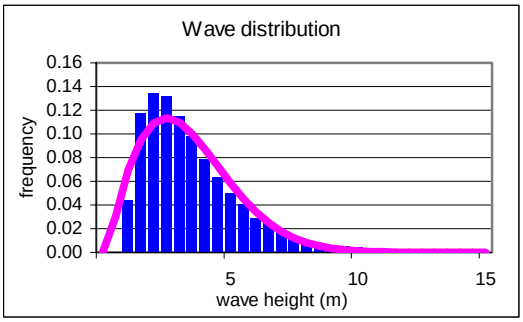

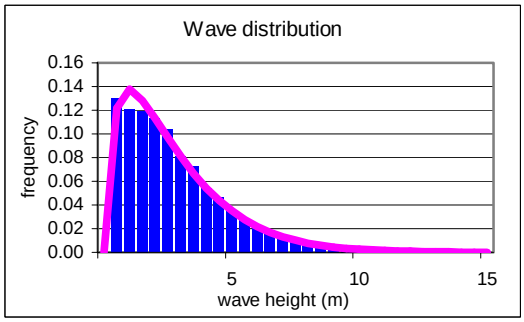

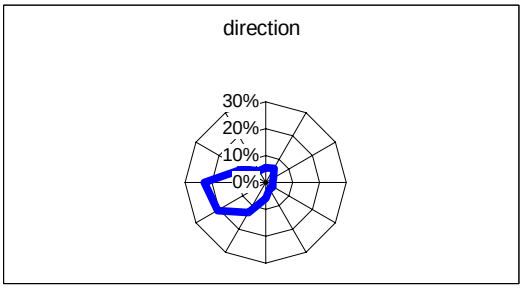

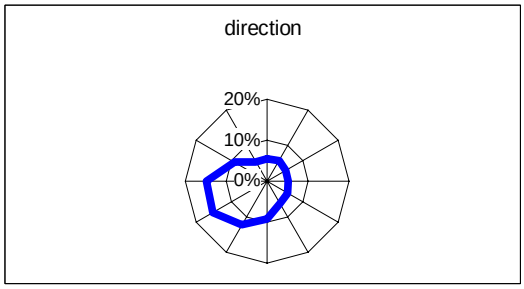

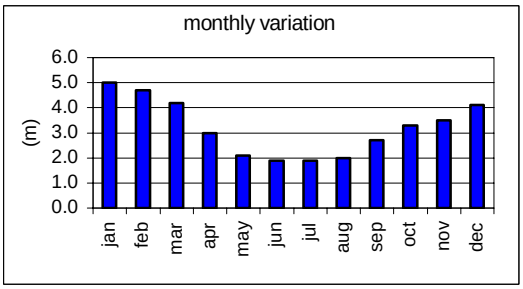

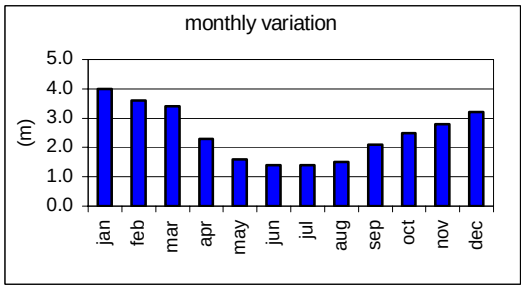

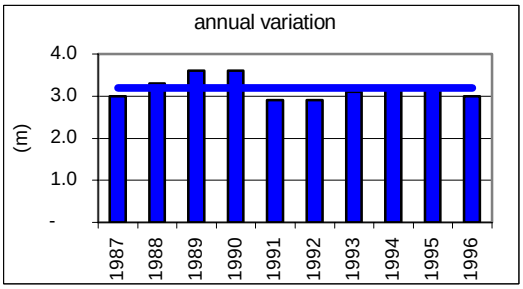

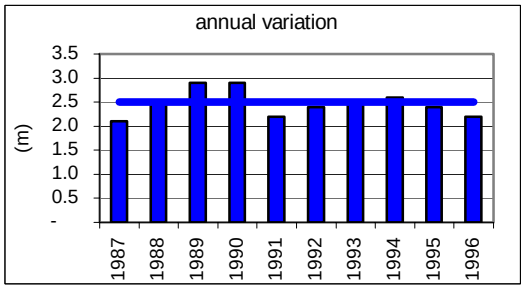

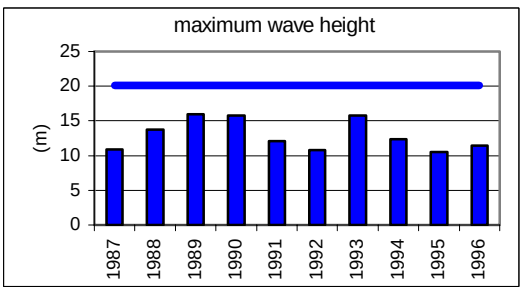

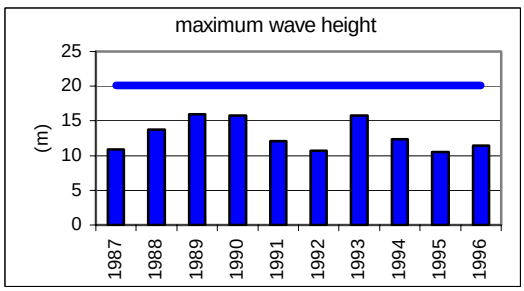

Location	Atlantic (North)	Lattitude	60.00	Longitude	10.07-

	Swell wave height
Average height	1.4 m
Average direction	26.3
Average Period	9.8 S
Maximum	10.9 m
50 yr return value	13.2 m
Weibull scale factor	1.52 m
Weibull shape factor	1.21

	Wind Speed
Average height	9.7 m/s
Average direction	22.6
Average Period	- S
Maximum	36.2 m/s
50 yr return value	43.8 m/s
Weibull scale factor	10.97 m/s
Weibull shape factor	2.18

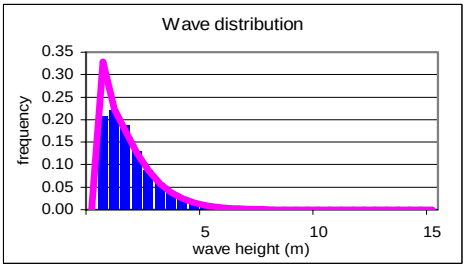

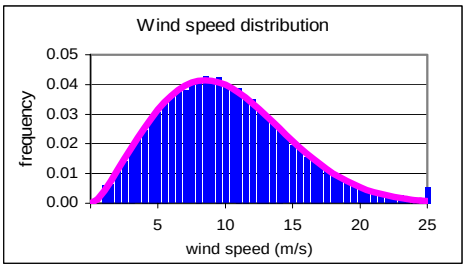

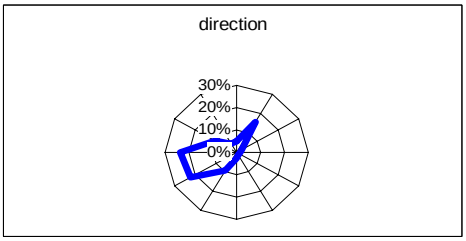

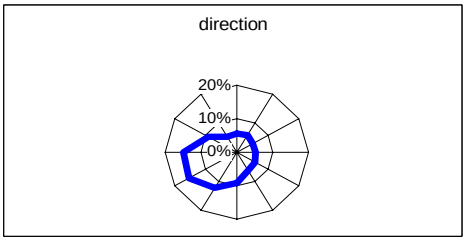

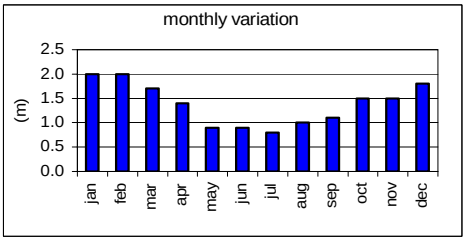

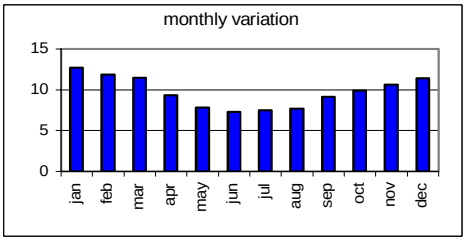

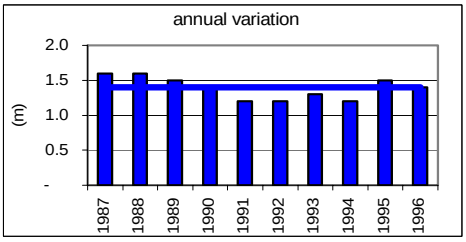

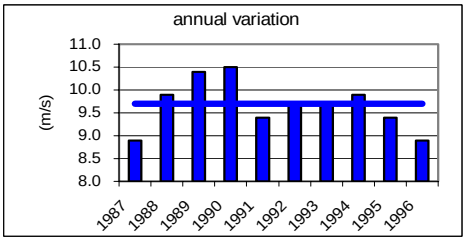

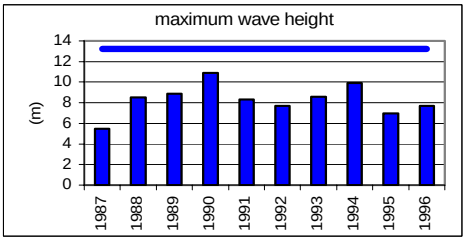

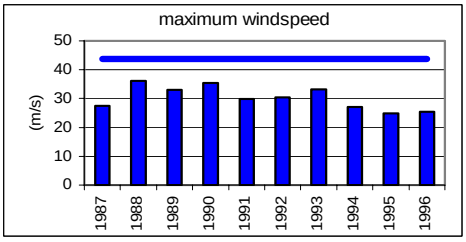

Location	Atlantic (South)	Lattitude	35.00	Longitude	10.07-

	Significant wave height
Average height	1.7 m
Average direction	32.4
Average Period	5.9 S
Maximum	8.9 m
50 yr return value	11.3 m
Weibull scale factor	1.93 m
Weibull shape factor	2.41

	Wind Sea wave height
Average height	1.1 m
Average direction	-
Average Period	3.4 S
Maximum	8.7 m
50 yr return value	11.3 m
Weibull scale factor	1.22 m
Weibull shape factor	1.31

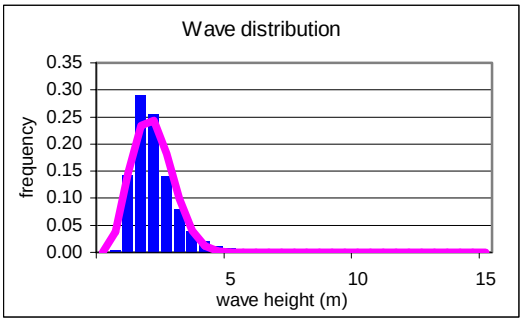

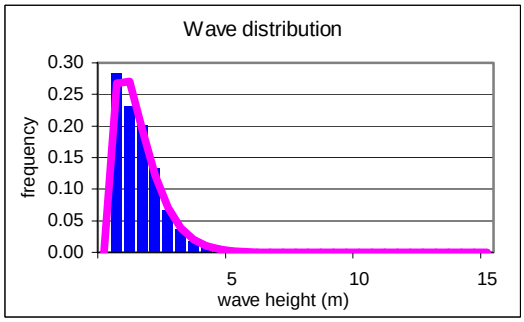

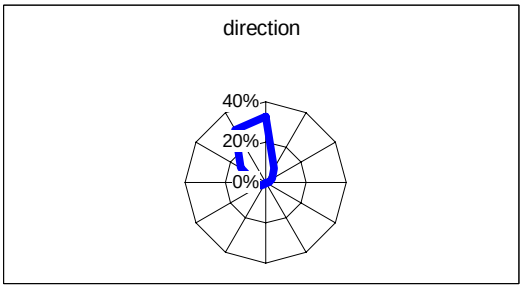

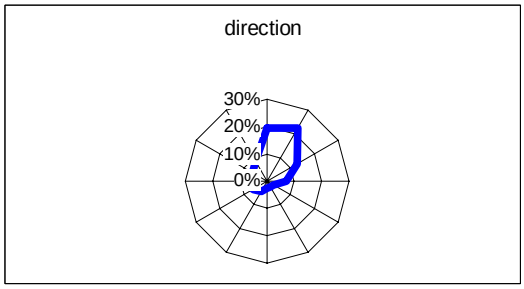

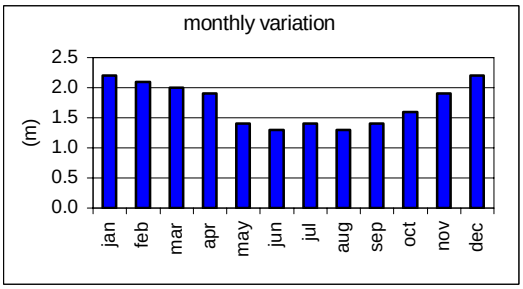

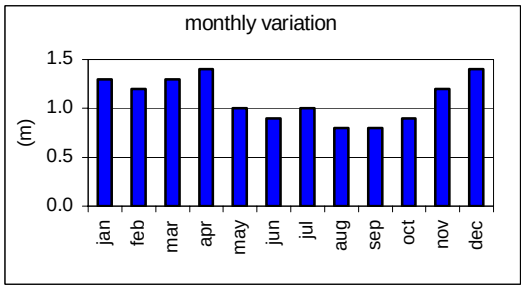

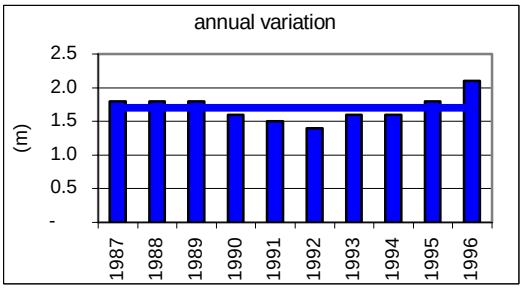

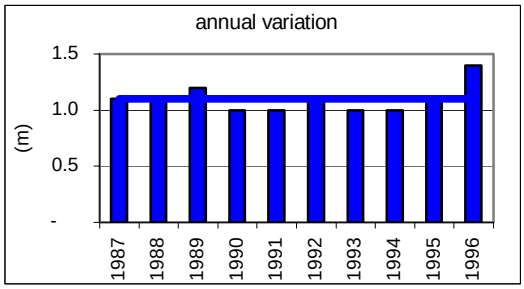

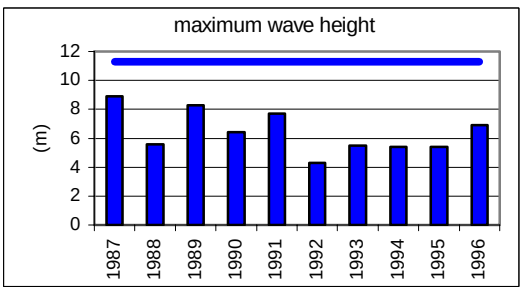

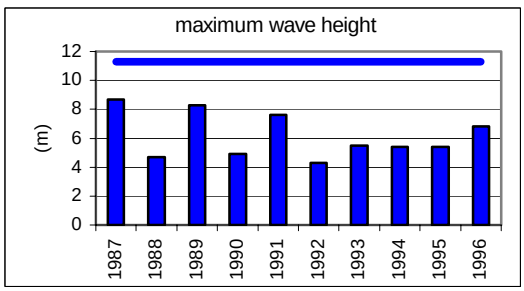

Location	Atlantic (South)	Lattitude	35.00	Longitude	10.07-

	Swell wave height	
Average height	1.1	m
Average direction	31.3	
Average Period	9.2	S
Maximum	6.5	m
50 yr return value	8.6	m
Weibull scale factor	1.19	m
Weibull shape factor	1.59	

	Wind Speed	
Average height	6.4	m/s
Average direction	35.8	
Average Period	-	S
Maximum	22.7	m/s
50 yr return value	27.5	m/s
Weibull scale factor	7.2	m/s
Weibull shape factor	2.23	

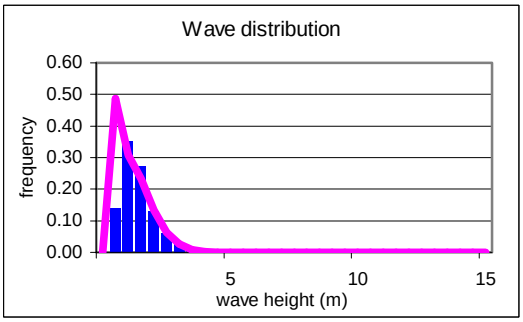

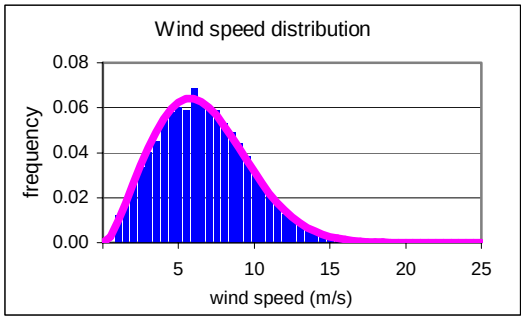

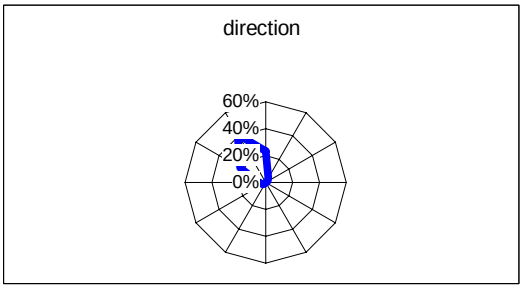

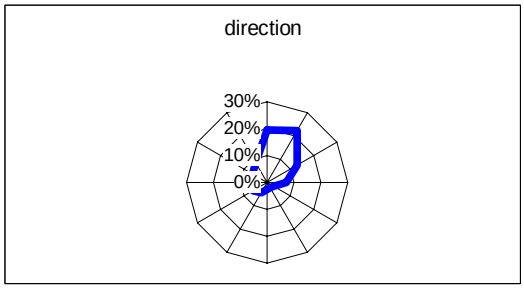

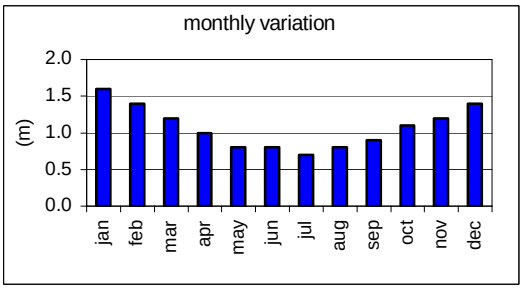

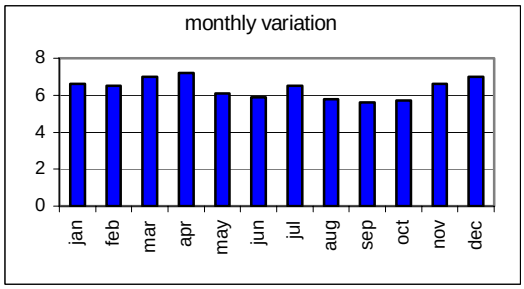

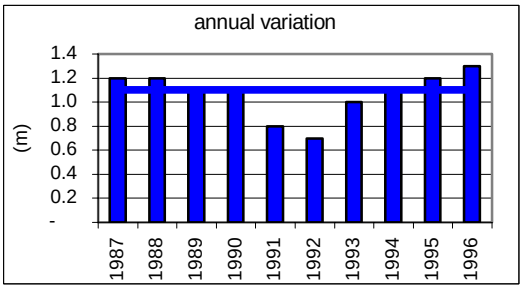

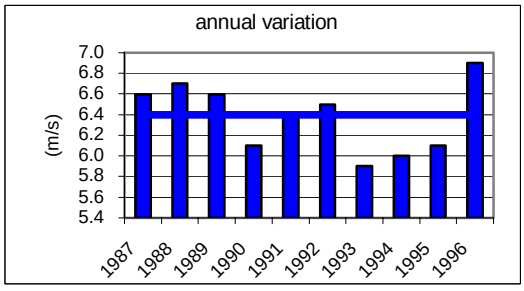

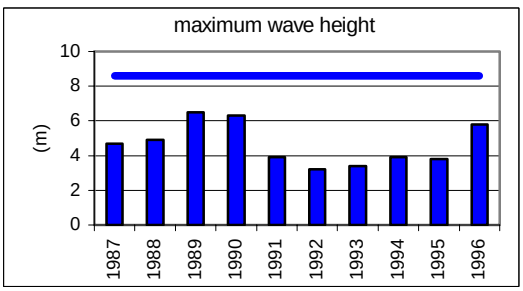

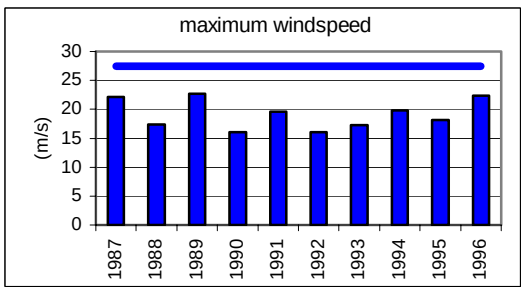

Location	Baltic Sea	Lattitude	58.00	Longitude	20.33

	Significant wave height
Average height	1.2 m
Average direction	24.5
Average Period	4.4 S
Maximum	6.3 m
50 yr return value	6.7 m
Weibull scale factor	1.38 m
Weibull shape factor	1.24

	Wind Sea wave height
Average height	1.2 m
Average direction	-
Average Period	3.7 S
Maximum	6.3 m
50 yr return value	6.8 m
Weibull scale factor	1.3 m
Weibull shape factor	1.17

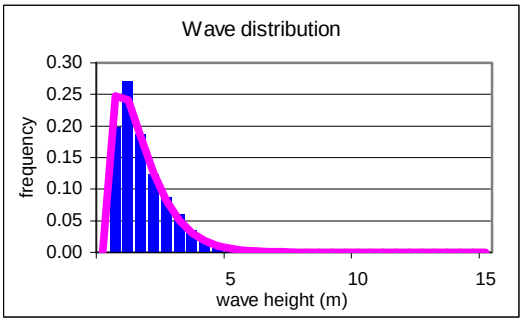

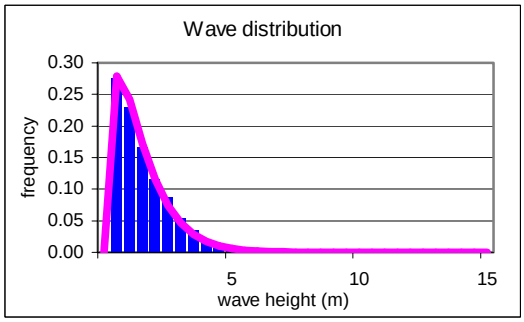

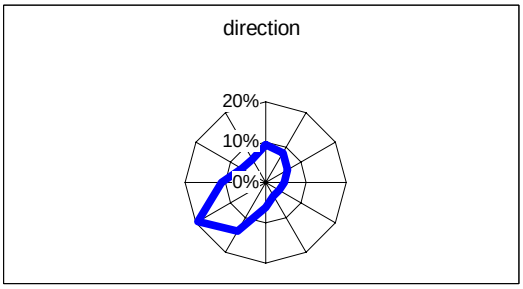

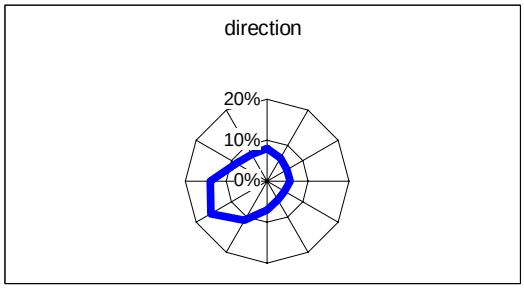

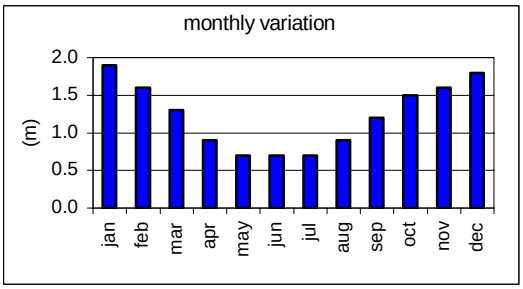

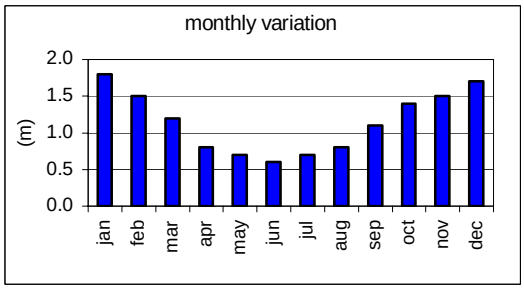

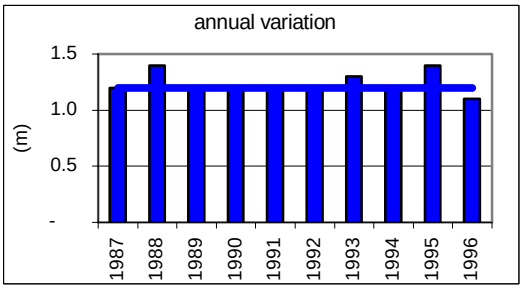

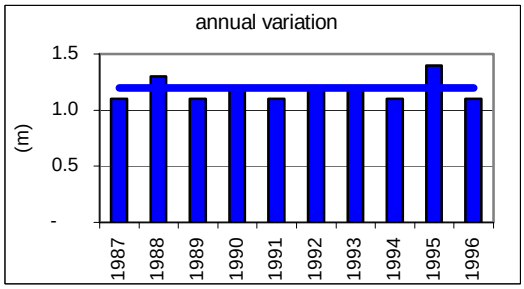

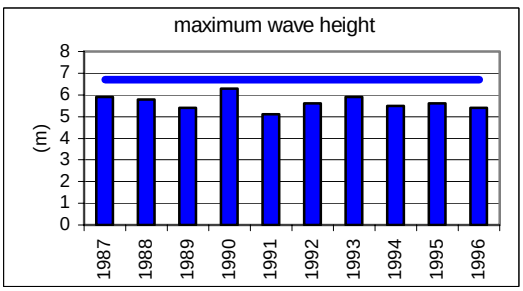

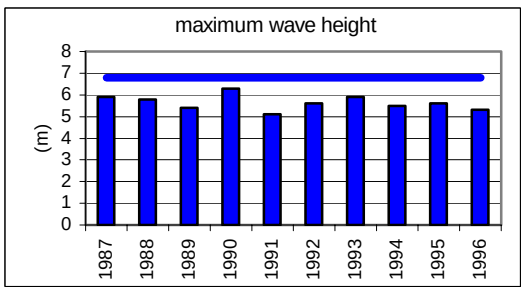

Location	Baltic Sea	Lattitude	58.00	Longitude	20.33

	Swell wave height	
Average height	0.2	m
Average direction	34.9	
Average Period	3	S
Maximum	4.2	m
50 yr return value	5.1	m
Weibull scale factor	0.93	m
Weibull shape factor	47.21	

	Wind Speed	
Average height	7.6	m/s
Average direction	24.5	
Average Period	-	S
Maximum	24.9	m/s
50 yr return value	27.1	m/s
Weibull scale factor	8.57	m/s
Weibull shape factor	2.06	

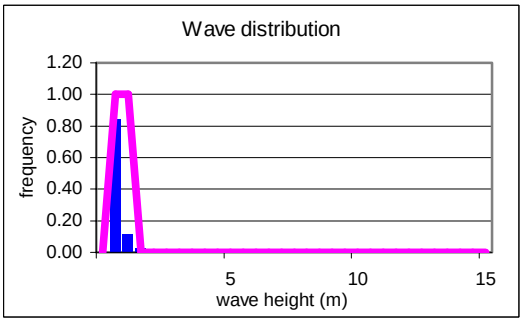

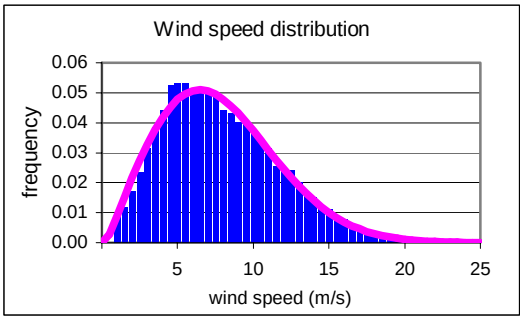

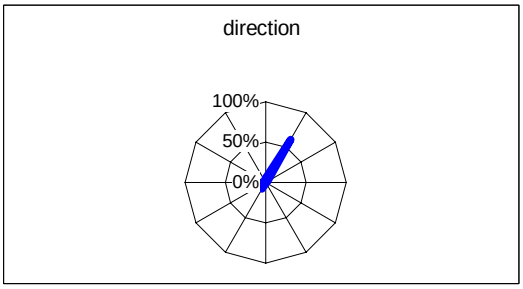

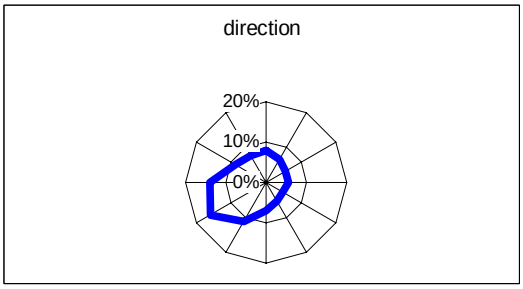

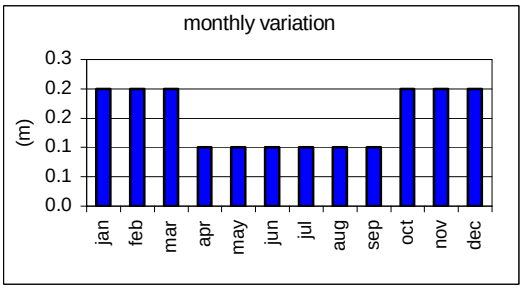

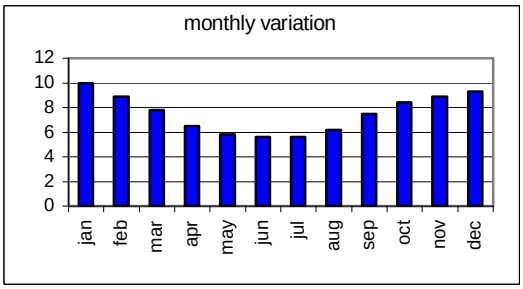

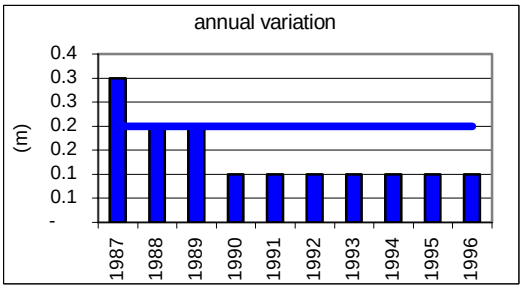

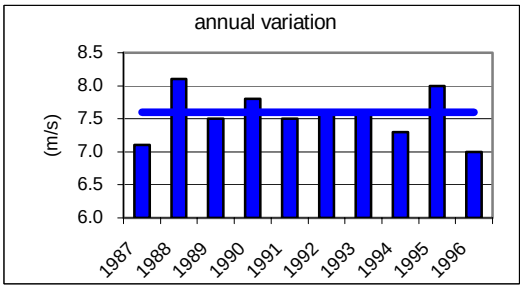

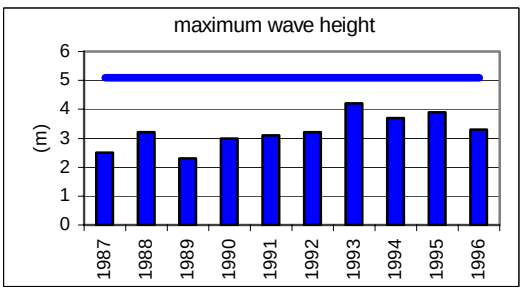

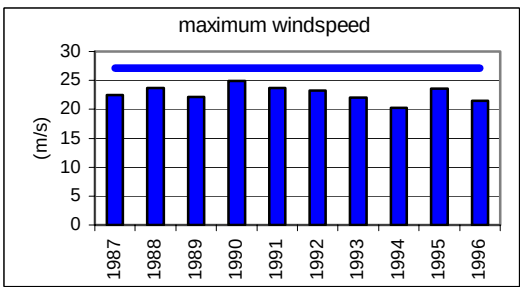

Location	Bay of Biscay	Lattitude	45.00	Longitude	2.87-

	Significant wave height
Average height	1.7 m
Average direction	29.9
Average Period	5.9 S
Maximum	12.1 m
50 yr return value	15 m
Weibull scale factor	1.84 m
Weibull shape factor	1.52

	Wind Sea wave height
Average height	1.1 m
Average direction	-
Average Period	3.3 S
Maximum	12.1 m
50 yr return value	15 m
Weibull scale factor	1.05 m
Weibull shape factor	0.88

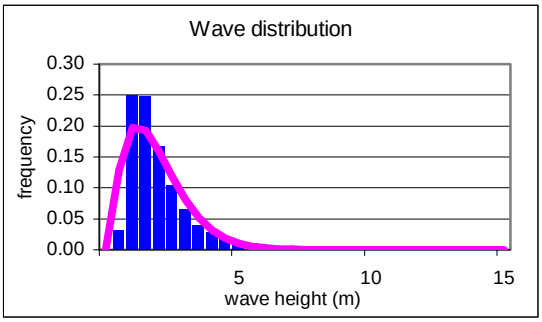

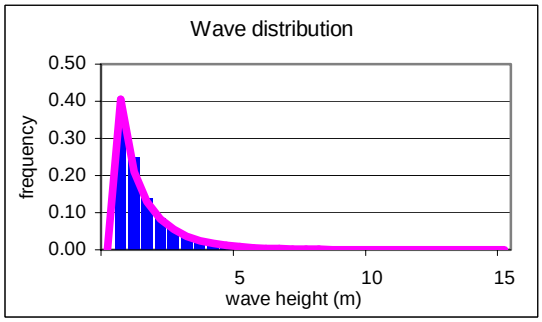

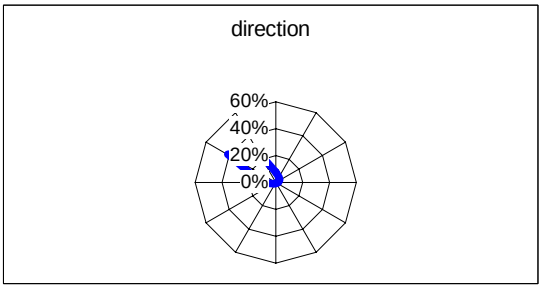

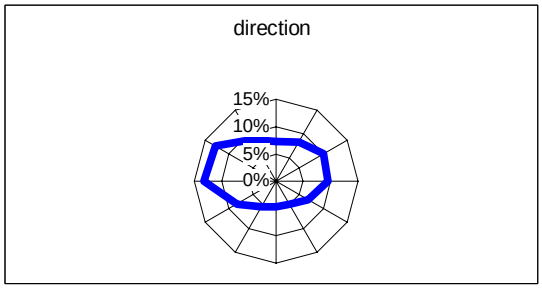

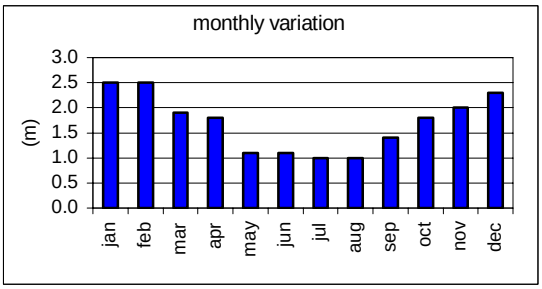

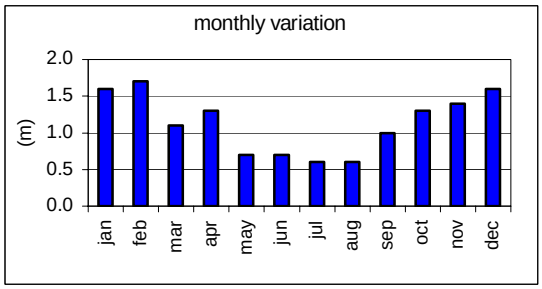

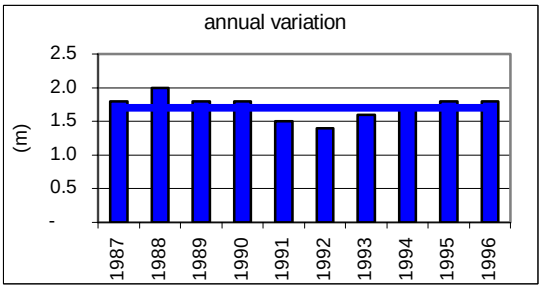

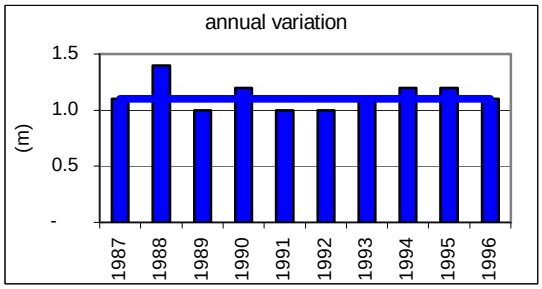

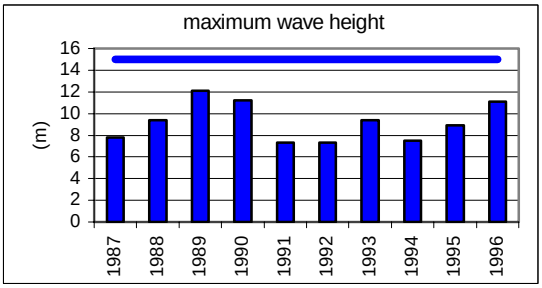

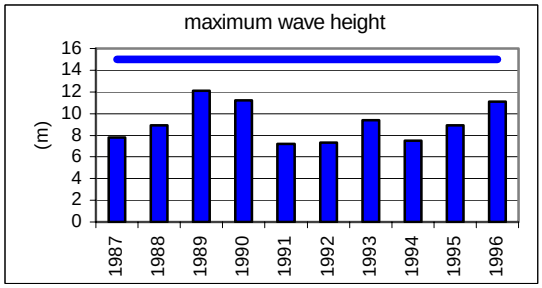

Location	Bay of Biscay	Lattitude	45.00	Longitude	2.87-

	Swell wave height
Average height	1 m
Average direction	29.8
Average Period	8.9 S
Maximum	6.8 m
50 yr return value	8.3 m
Weibull scale factor	1.08 m
Weibull shape factor	1.29

	Wind Speed
Average height	6.4 m/s
Average direction	31.2
Average Period	- S
Maximum	26 m/s
50 yr return value	29.8 m/s
Weibull scale factor	7.19 m/s
Weibull shape factor	2.01

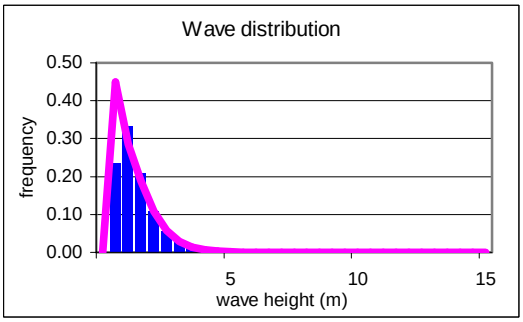

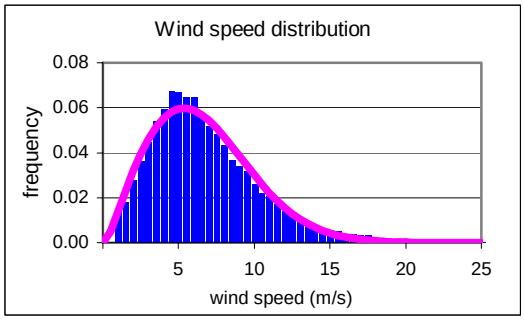

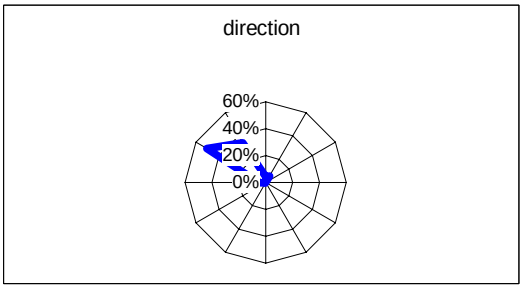

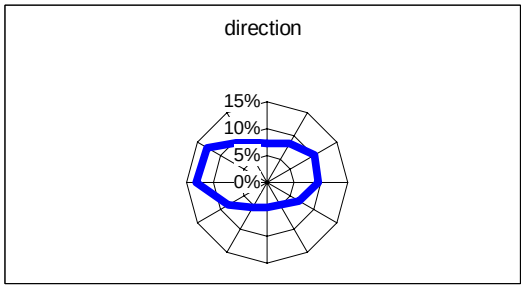

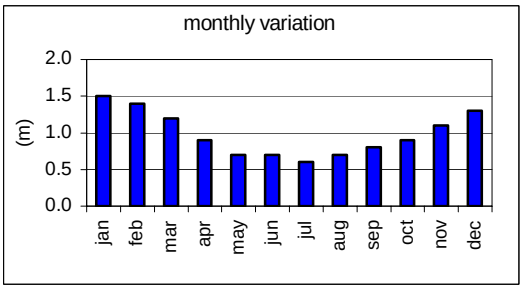

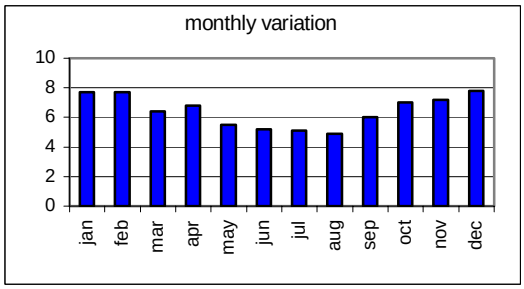

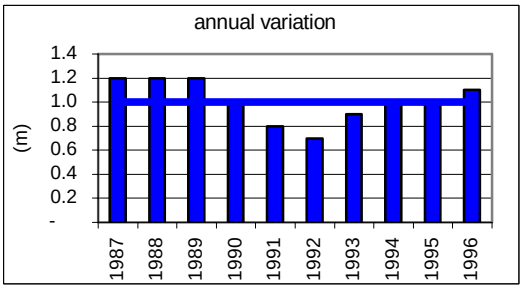

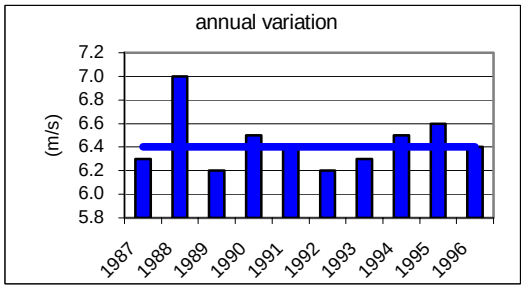

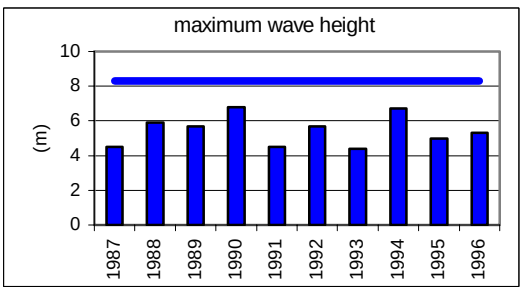

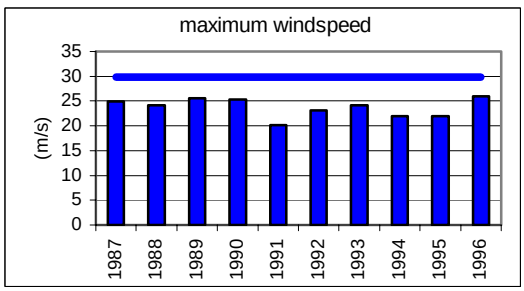

Location	Black Sea	Lattitude	42.00	Longitude	29.93

	Significant wave height	
Average height	0.9	m
Average direction	2.9	
Average Period	4	S
Maximum	6.2	m
50 yr return value		m
Weibull scale factor	0.95	m
Weibull shape factor	1.19	

	Wind Sea wave height	
Average height	0.8	m
Average direction	-	
Average Period	2.8	S
Maximum	6.2	m
50 yr return value		m
Weibull scale factor	0.84	m
Weibull shape factor	1.06	

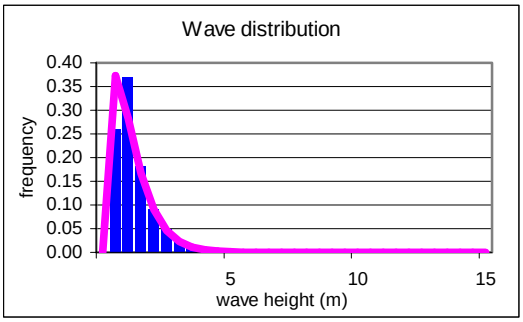

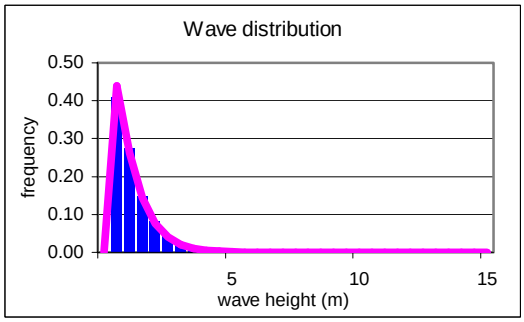

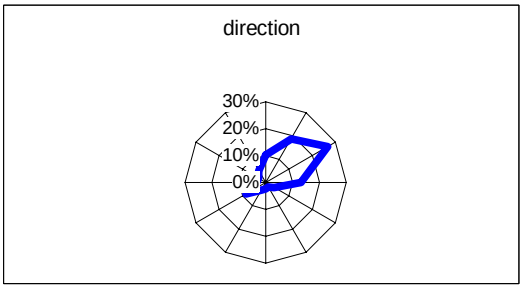

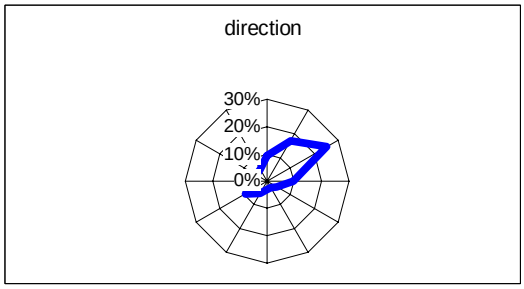

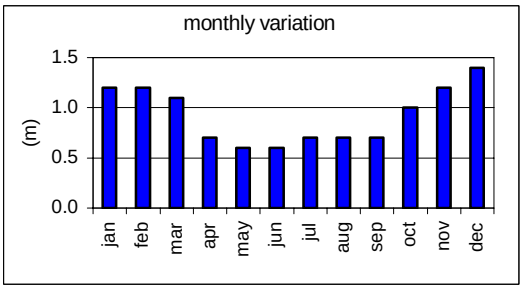

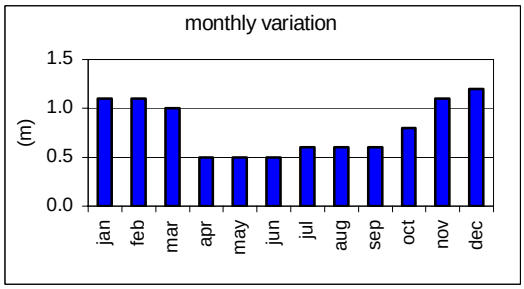

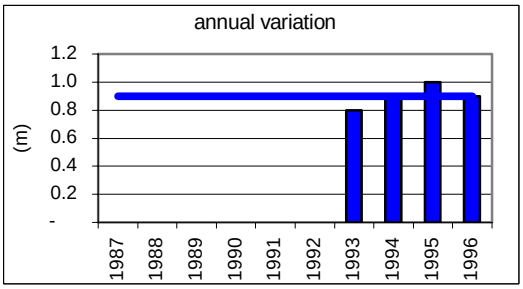

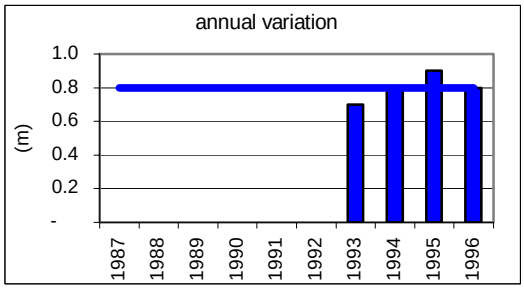

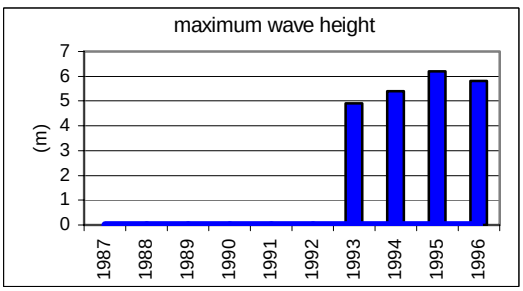

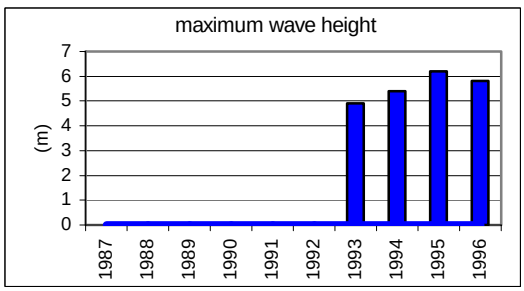

Location	Black Sea	Lattitude	42.00	Longitude	29.93

	Swell wave height	
Average height	0.2	m
Average direction	1.7	
Average Period	3	S
Maximum	3.2	m
50 yr return value		m
Weibull scale factor	0.62	m
Weibull shape factor	2.74	

	Wind Speed	
Average height	5.7	m/s
Average direction	2.5	
Average Period	-	S
Maximum	18.4	m/s
50 yr return value		m/s
Weibull scale factor	6.41	m/s
Weibull shape factor	1.96	

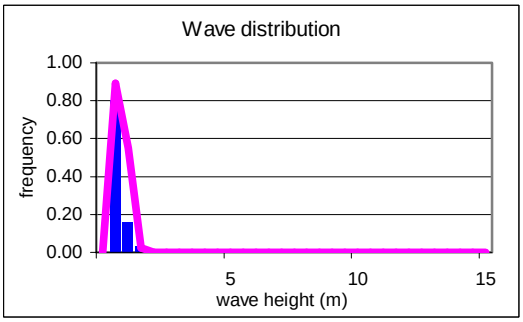

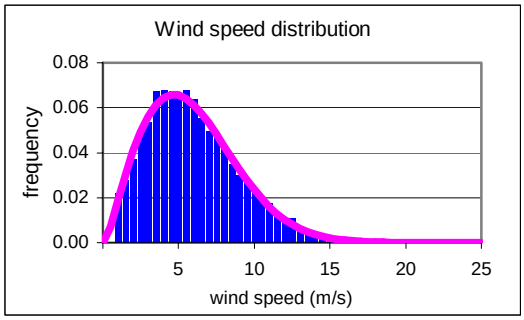

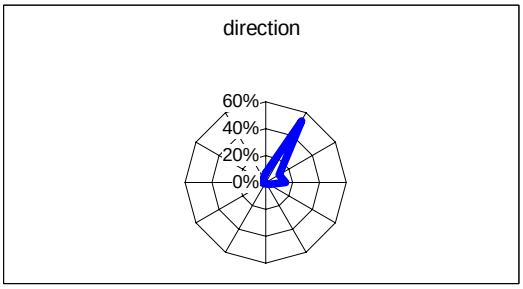

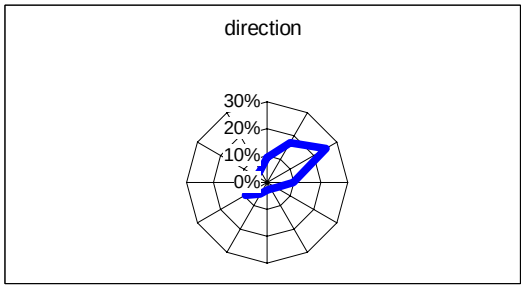

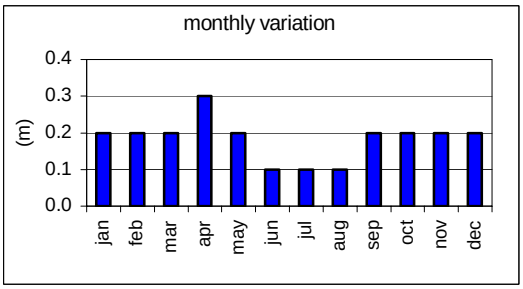

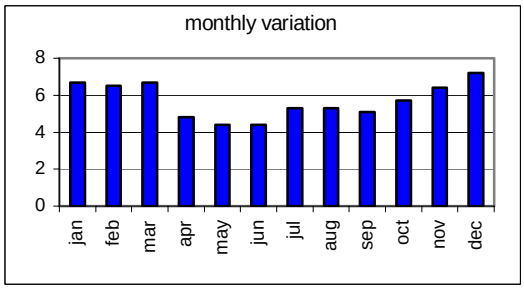

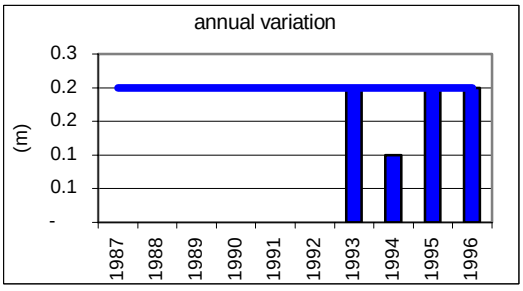

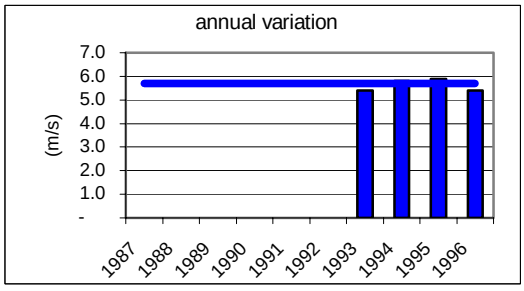

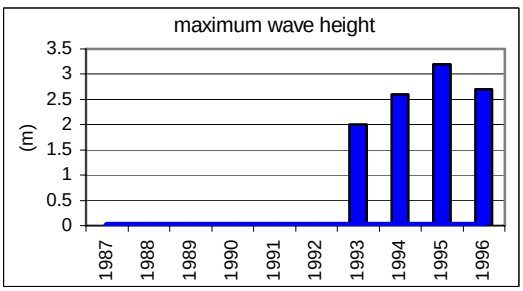

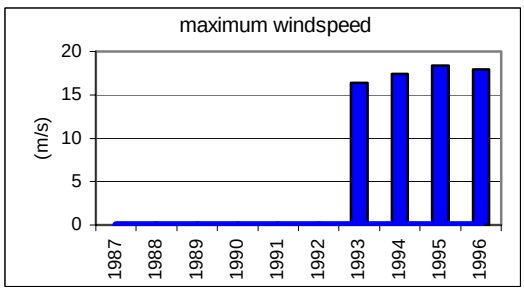

Location	Ionian Sea	Lattitude	36.00	Longitude	19.13

	Significant wave height
Average height	1 m
Average direction	32.8
Average Period	4.2 S
Maximum	7.4 m
50 yr return value	8.7 m
Weibull scale factor	1.01 m
Weibull shape factor	1.12

	Wind Sea wave height
Average height	0.8 m
Average direction	-
Average Period	2.8 S
Maximum	7.4 m
50 yr return value	8.6 m
Weibull scale factor	0.84 m
Weibull shape factor	0.95

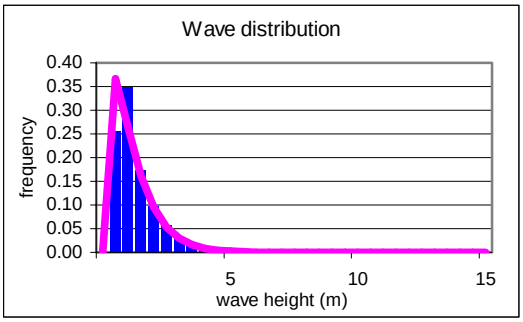

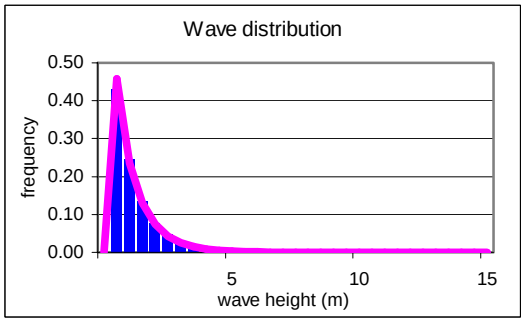

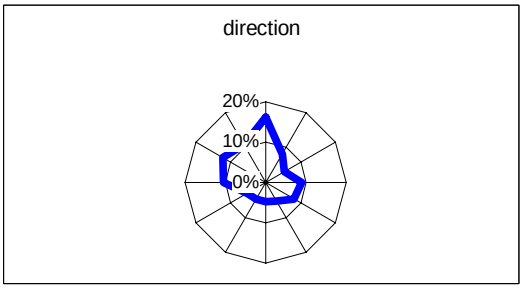

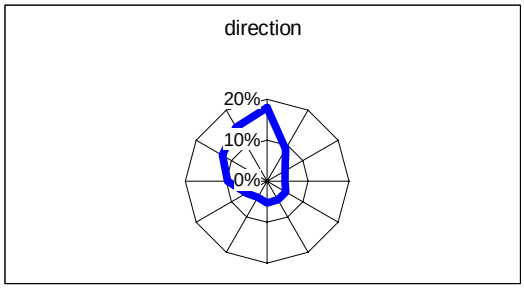

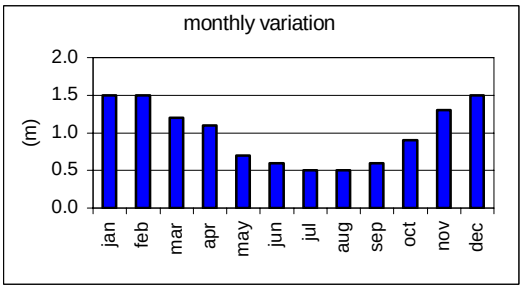

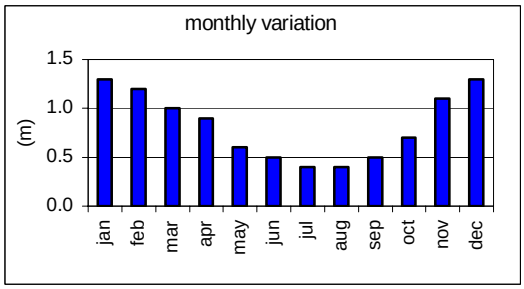

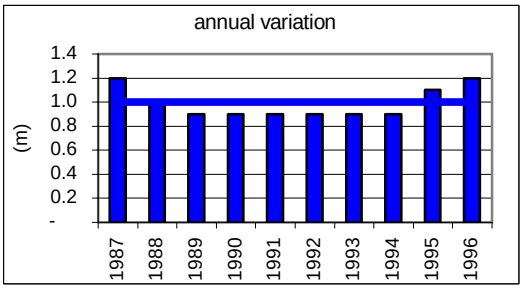

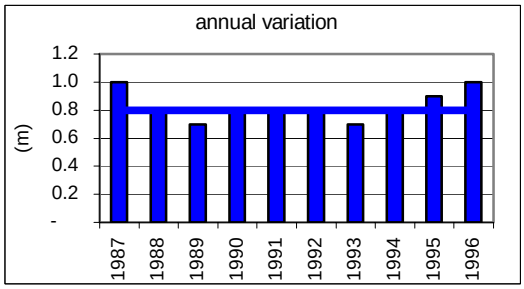

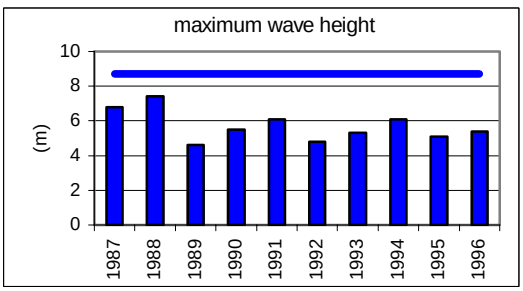

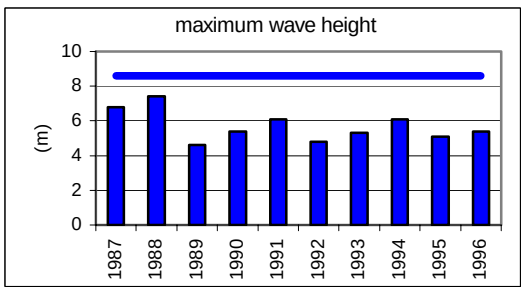

Location	Ionian Sea	Lattitude	36.00	Longitude	19.13

	Swell wave height	
Average height	0.3	m
Average direction	0.6	
Average Period	4.4	S
Maximum	4.1	m
50 yr return value	5.2	m
Weibull scale factor		m
Weibull shape factor	1	

	Wind Speed	
Average height	5.8	m/s
Average direction	31.7	
Average Period	-	S
Maximum	25.1	m/s
50 yr return value	29	m/s
Weibull scale factor	6.57	m/s
Weibull shape factor	2.01	

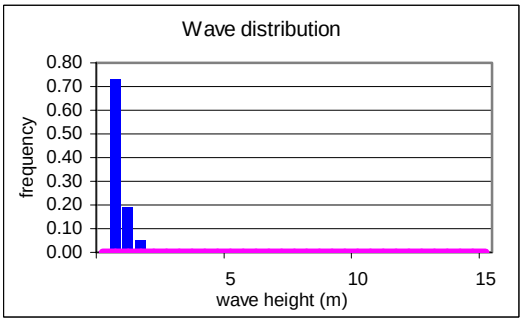

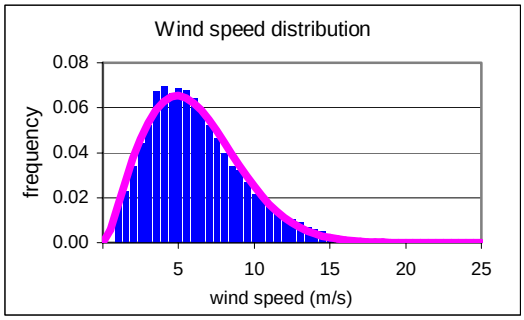

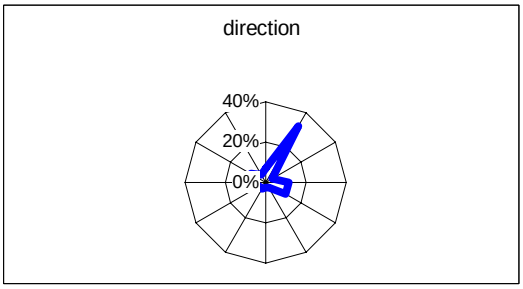

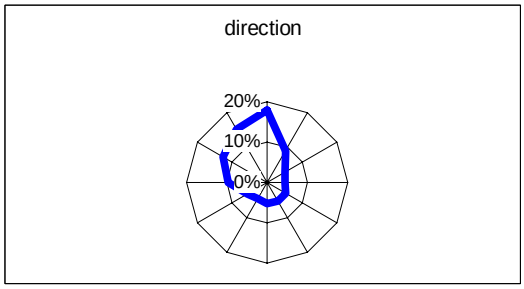

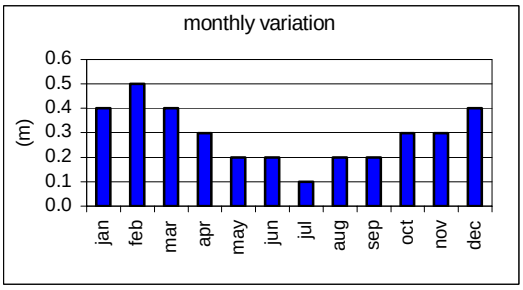

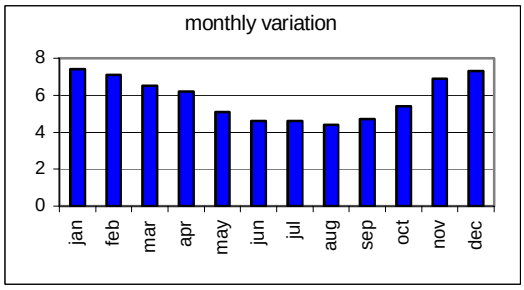

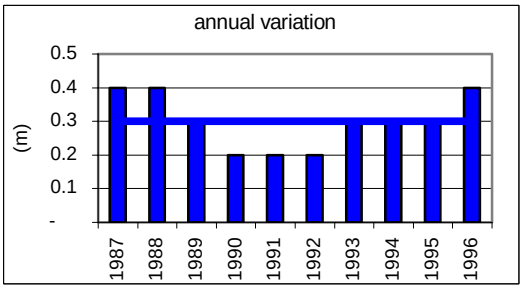

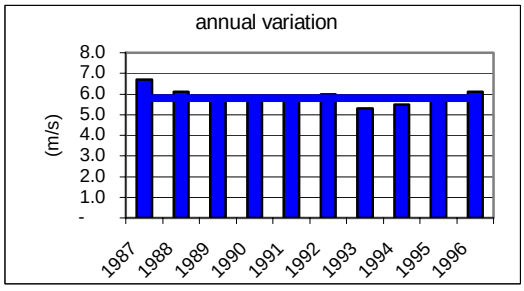

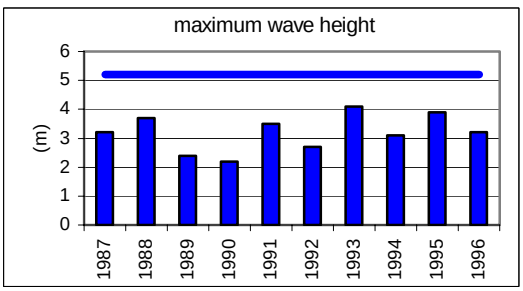

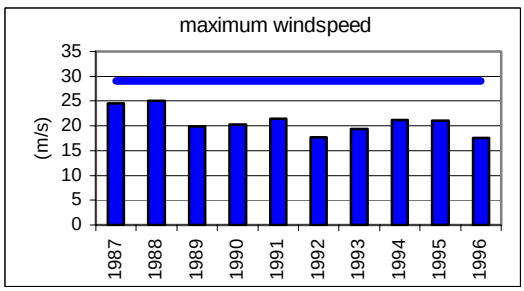

Location	Mediterranean (East)	Lattitude	33.50	Longitude	27.93

	Significant wave height
Average height	1.1 m
Average direction	30.9
Average Period	4.3 S
Maximum	6.8 m
50 yr return value	8.6 m
Weibull scale factor	1.16 m
Weibull shape factor	1.41

	Wind Sea wave height
Average height	0.9 m
Average direction	-
Average Period	3.2 S
Maximum	6.8 m
50 yr return value	8.6 m
Weibull scale factor	1.02 m
Weibull shape factor	1.21

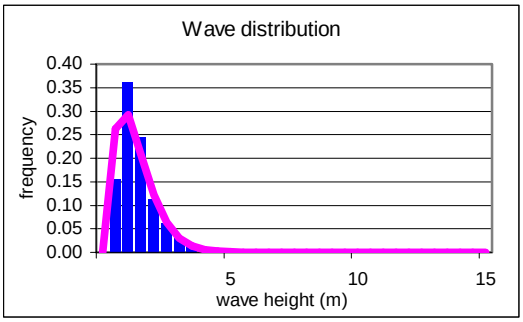

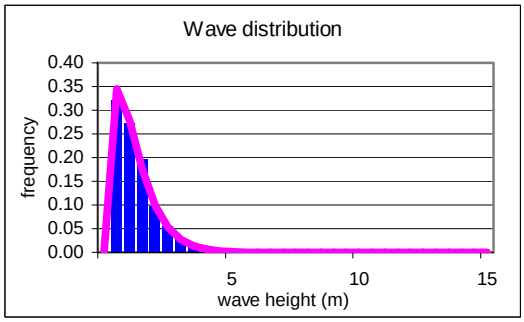

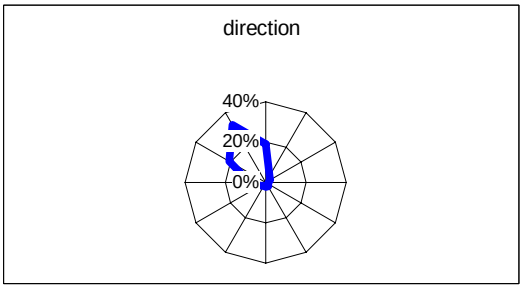

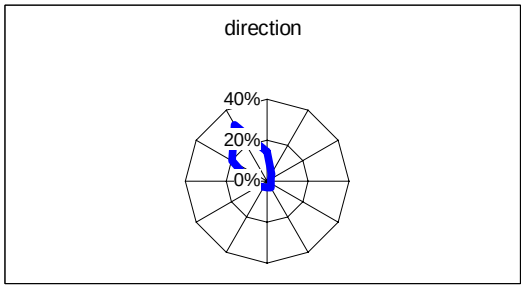

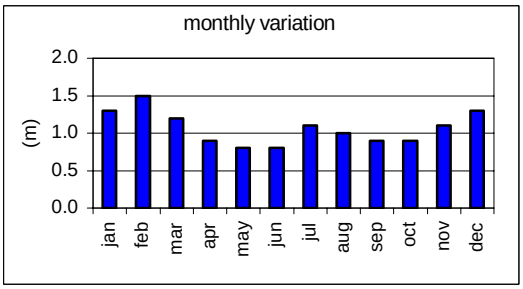

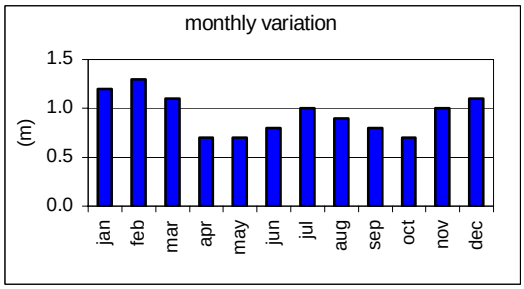

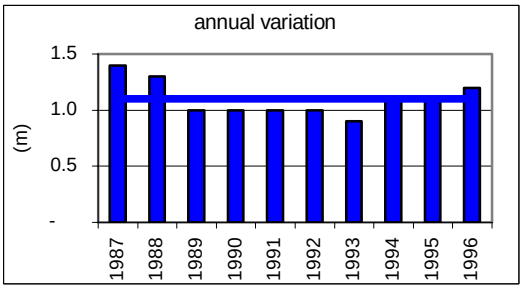

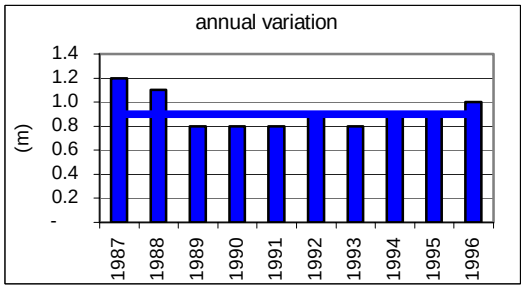

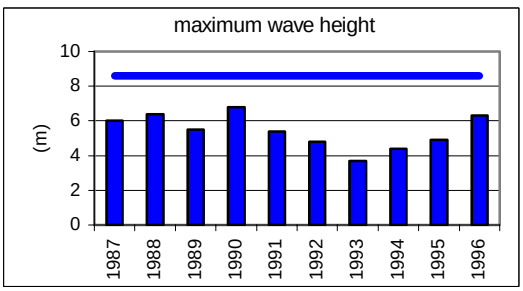

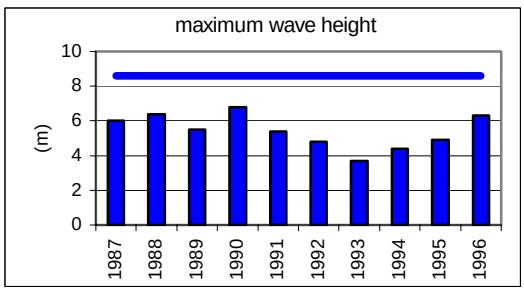

Location	Mediterranean (East)	Lattitude	33.50	Longitude	27.93

	Swell wave height	
Average height	0.3	m
Average direction	33.2	
Average Period	4.5	S
Maximum	2.8	m
50 yr return value	3.5	m
Weibull scale factor		m
Weibull shape factor		

	Wind Speed	
Average height	6.3	m/s
Average direction	30.4	
Average Period	-	S
Maximum	24.8	m/s
50 yr return value	28.9	m/s
Weibull scale factor	7.11	m/s
Weibull shape factor	2.36	

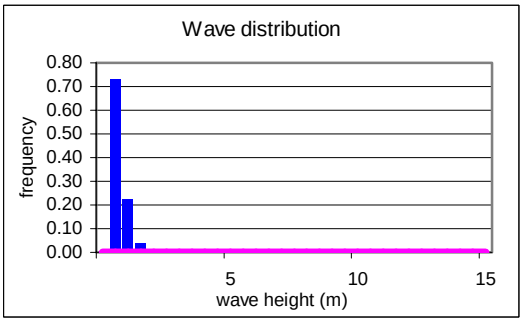

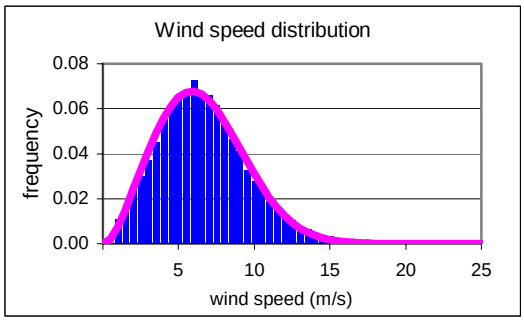

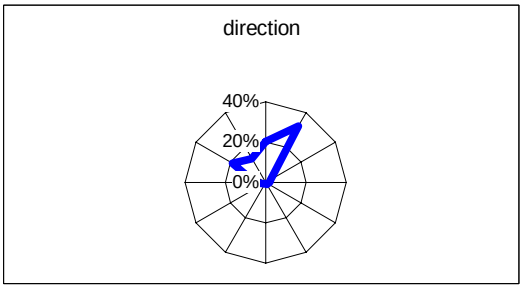

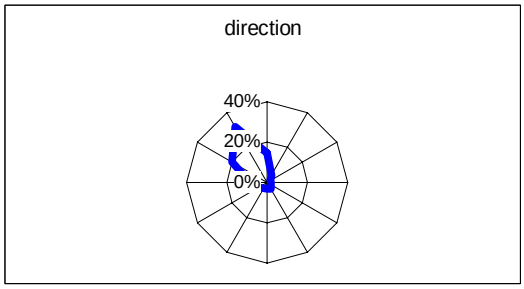

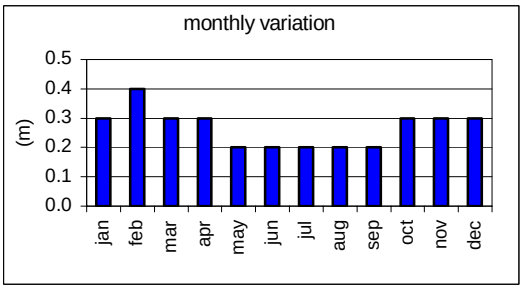

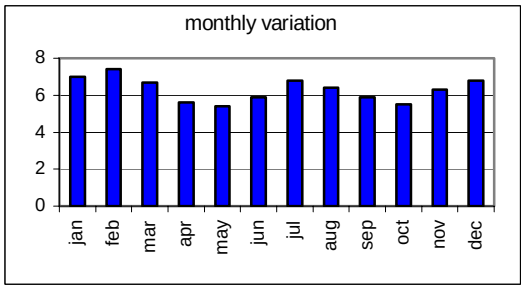

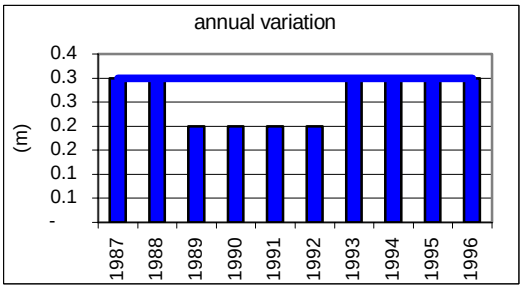

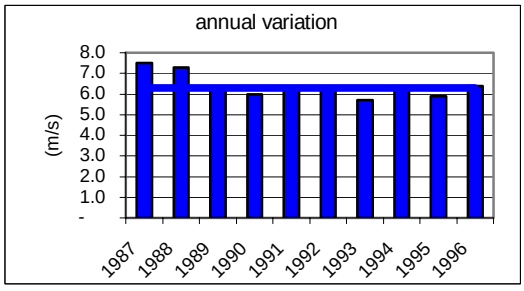

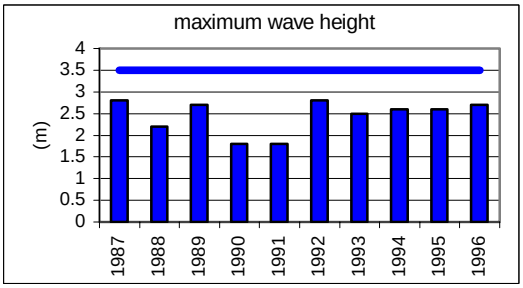

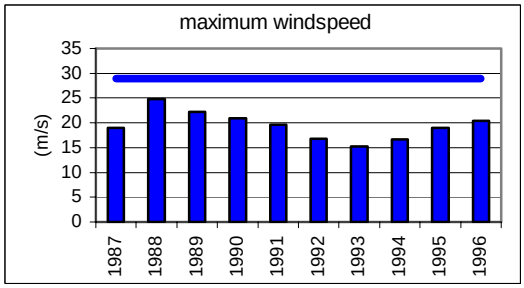

Location	Mediterranean (West)	Lattitude	39.00	Longitude	5.93

	Significant wave height
Average height	1.1 m
Average direction	35.3
Average Period	4.4 S
Maximum	8.7 m
50 yr return value	9.9 m
Weibull scale factor	1.13 m
Weibull shape factor	1.14

	Wind Sea wave height
Average height	0.9 m
Average direction	-
Average Period	2.9 S
Maximum	8.7 m
50 yr return value	9.9 m
Weibull scale factor	m
Weibull shape factor	

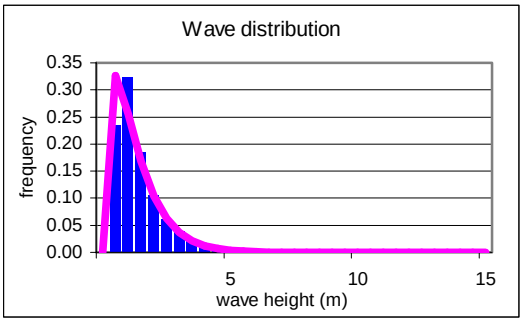

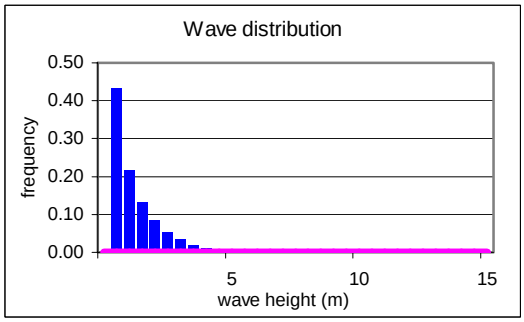

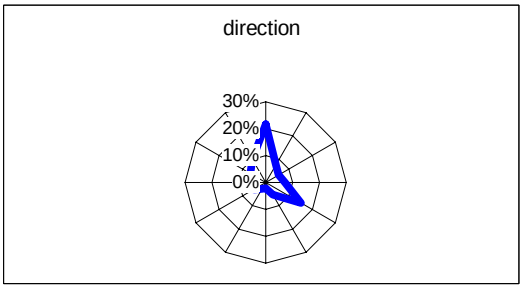

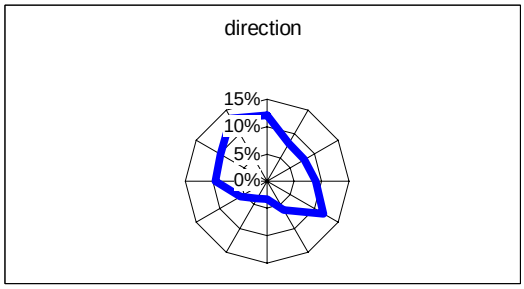

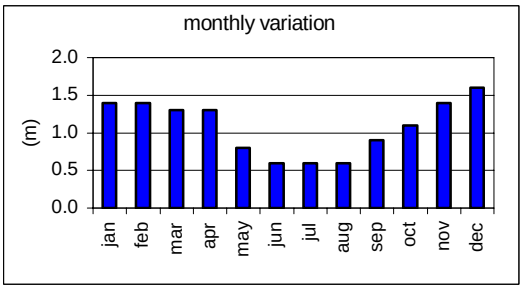

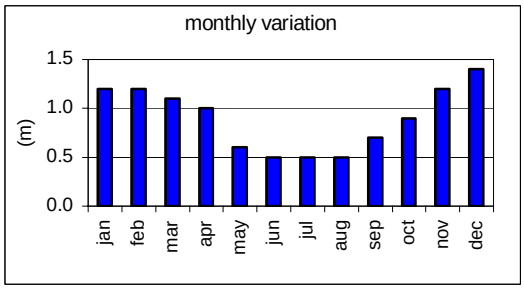

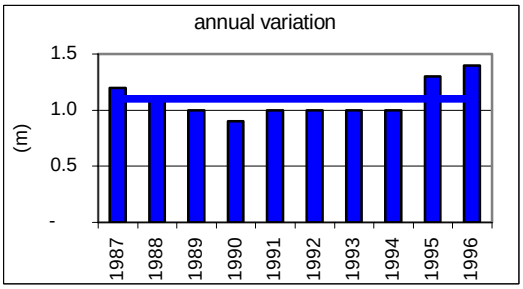

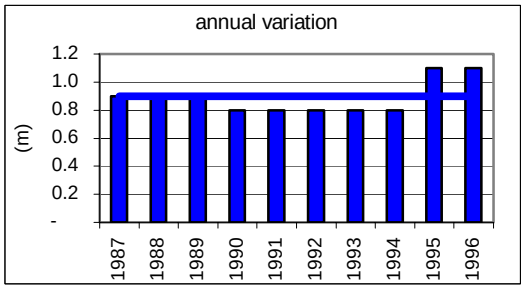

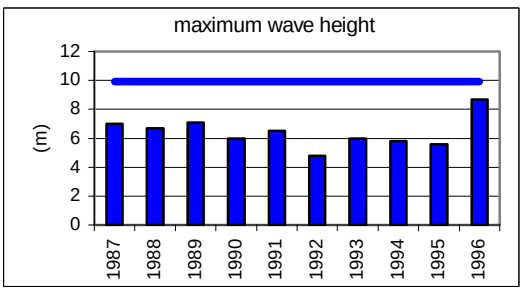

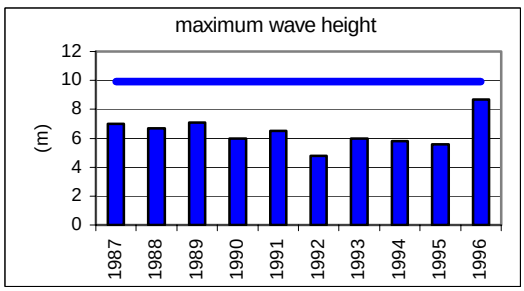

Location	Mediterranean (West)	Lattitude	39.00	Longitude	5.93

	Swell wave height	
Average height	0.3	m
Average direction		
Average Period	4.4	S
Maximum	4.7	m
50 yr return value	5.7	m
Weibull scale factor		m
Weibull shape factor		

	Wind Speed	
Average height	6	m/s
Average direction	35	
Average Period	-	S
Maximum	24.8	m/s
50 yr return value	28.6	m/s
Weibull scale factor	6.75	m/s
Weibull shape factor	1.85	

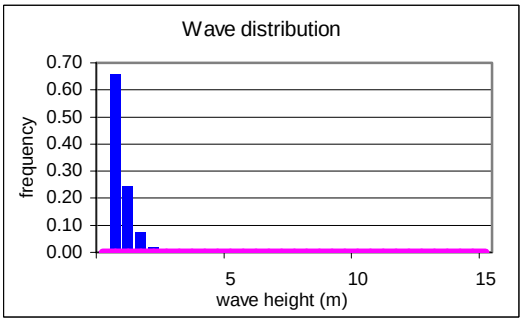

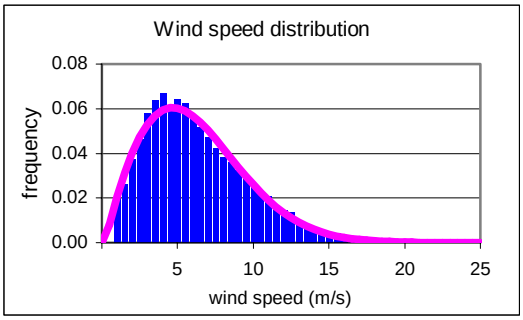

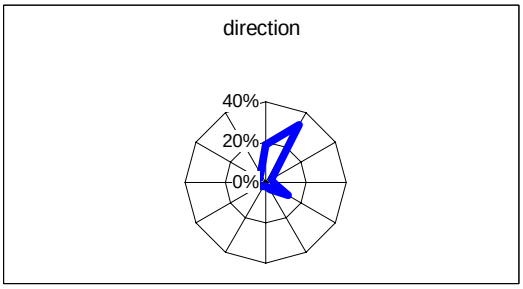

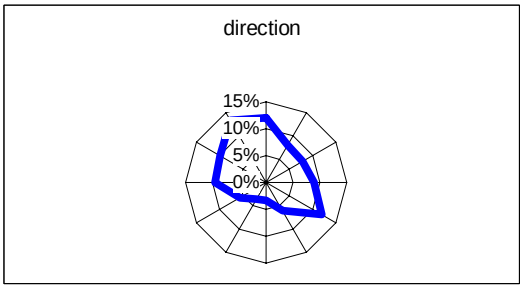

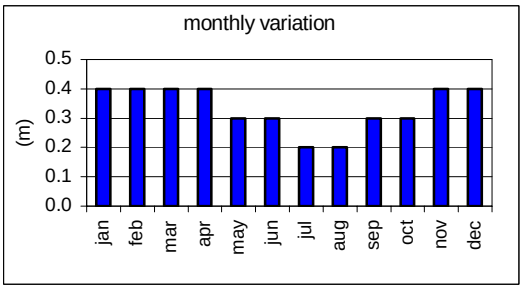

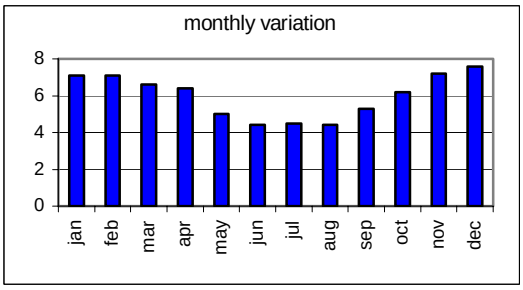

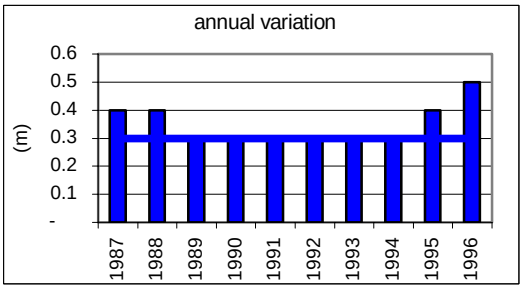

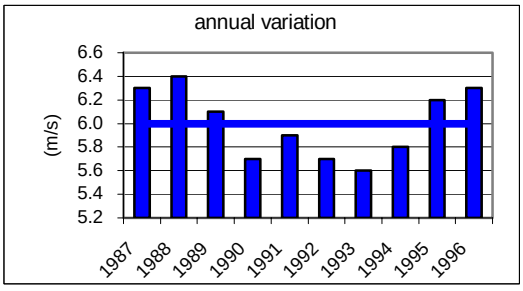

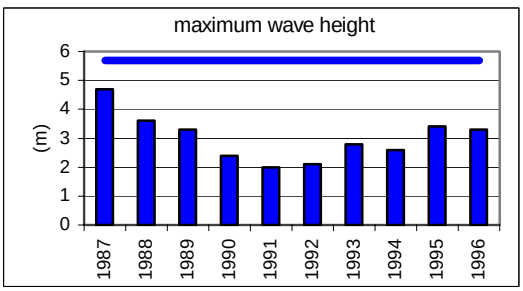

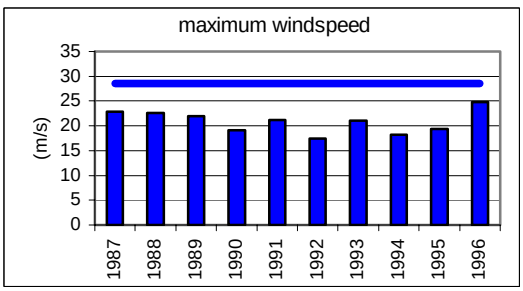

Location	North Sea	Lattitude	57.00	Longitude	3.13

	Significant wave height	
Average height	2.1	m
Average direction	28.8	
Average Period	5.6	S
Maximum	11.7	m
50 yr return value	12.9	m
Weibull scale factor	2.37	m
Weibull shape factor	1.58	

	Wind Sea wave height	
Average height	1.8	m
Average direction	-	
Average Period	4.7	S
Maximum	11.7	m
50 yr return value	12.9	m
Weibull scale factor	2.05	m
Weibull shape factor	1.24	

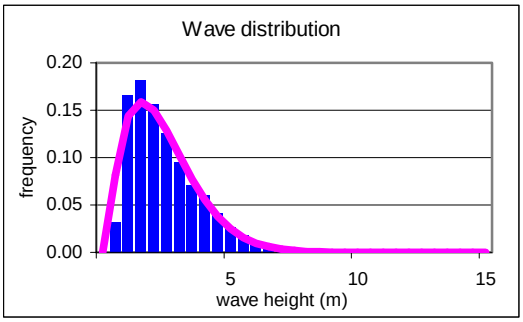

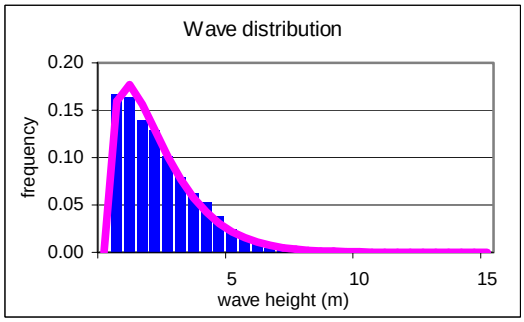

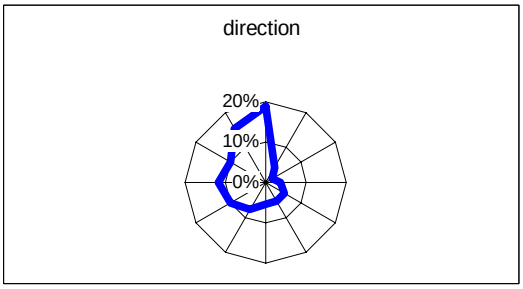

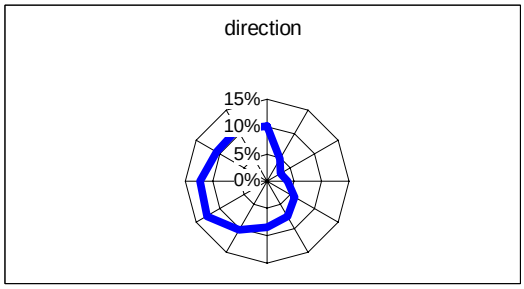

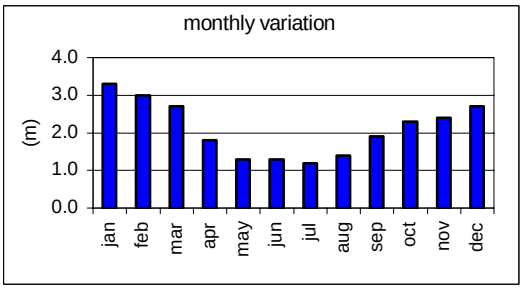

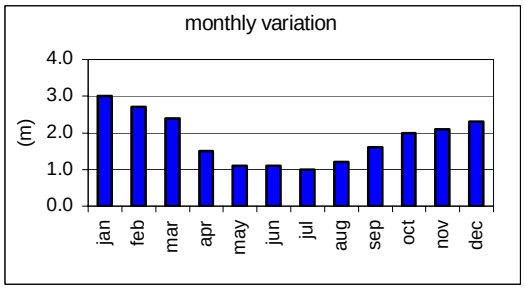

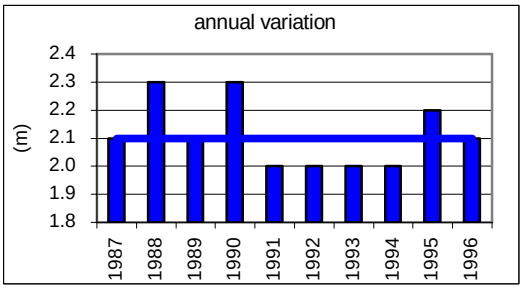

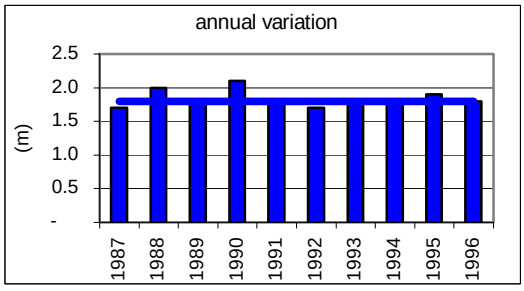

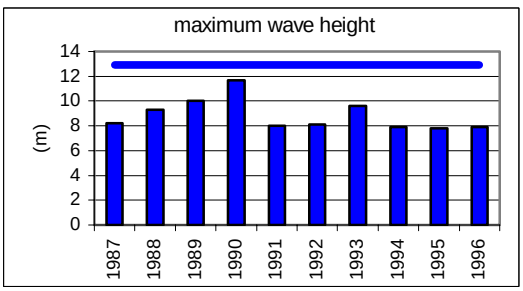

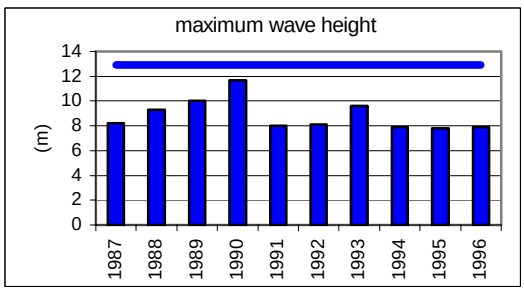

Location	North Sea	Lattitude	57.00	Longitude	3.13

	Swell wave height	
Average height	0.6	m
Average direction	33.6	
Average Period	7.9	S
Maximum	5	m
50 yr return value	5.5	m
Weibull scale factor	0.64	m
Weibull shape factor	1.05	

	Wind Speed	
Average height	8.9	m/s
Average direction	24.8	
Average Period	-	S
Maximum	29.9	m/s
50 yr return value	34.3	m/s
Weibull scale factor	10.12	m/s
Weibull shape factor	2.12	

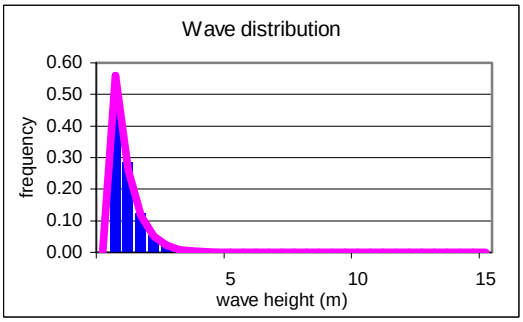

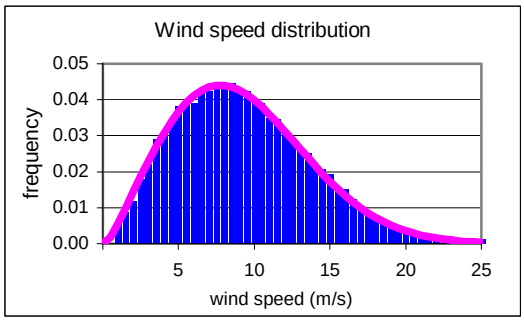

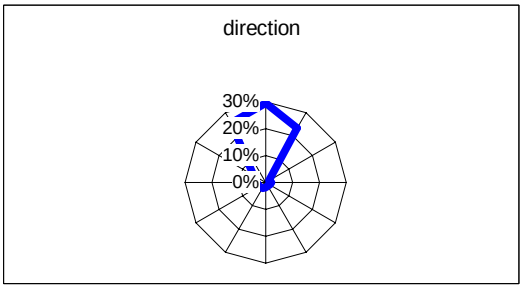

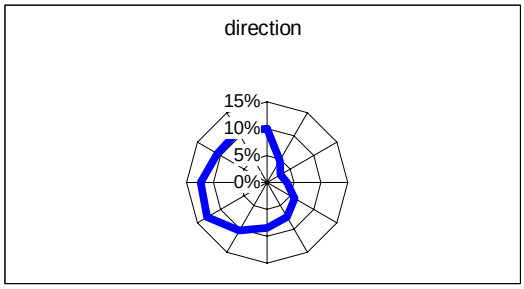

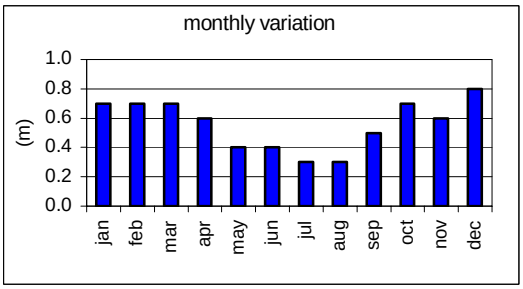

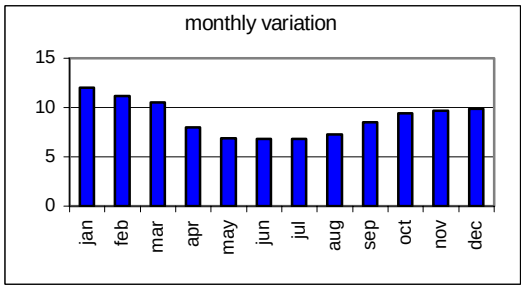

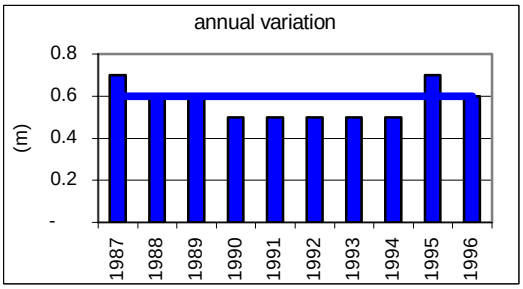

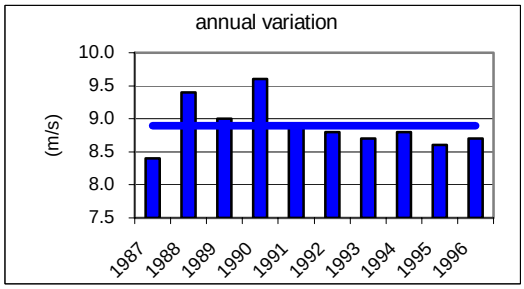

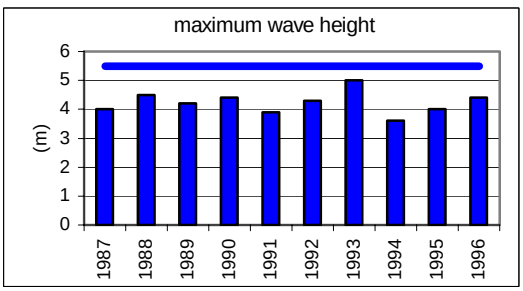

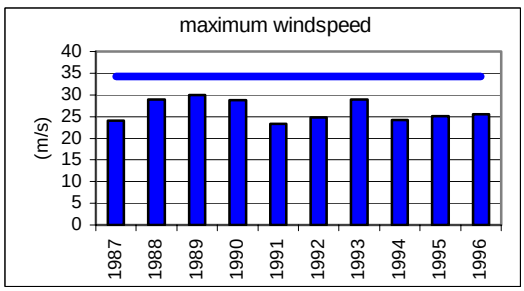

Location	Norwegian Sea	Lattitude	65.00	Longitude	2.33

	Significant wave height
Average height	2.8 m
Average direction	24.8
Average Period	6.5 S
Maximum	13.1 m
50 yr return value	15.2 m
Weibull scale factor	3.1 m
Weibull shape factor	1.73

	Wind Sea wave height
Average height	2.2 m
Average direction	-
Average Period	5 S
Maximum	13.1 m
50 yr return value	15 m
Weibull scale factor	2.37 m
Weibull shape factor	1.2

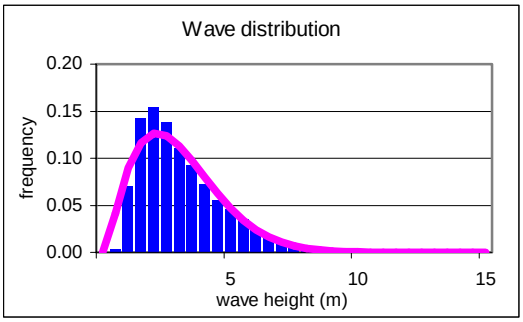

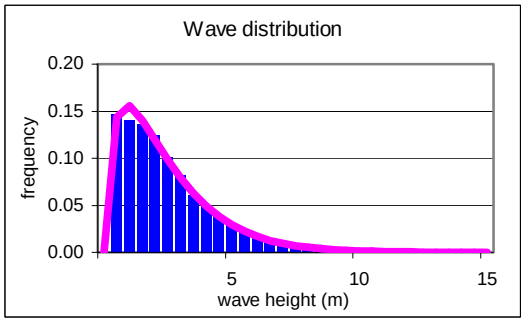

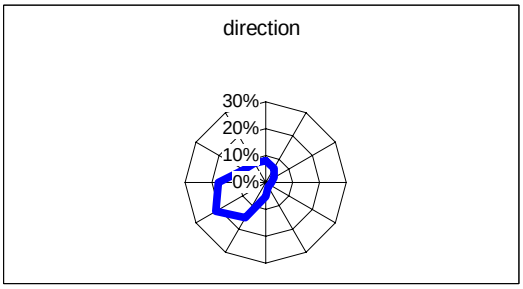

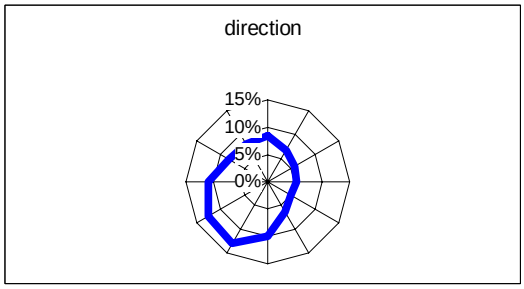

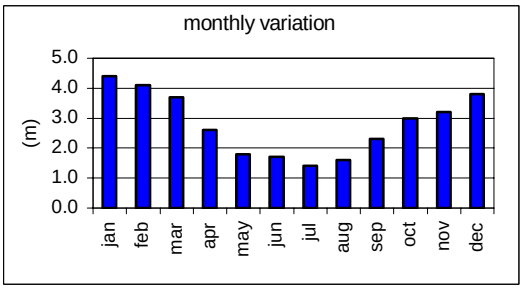

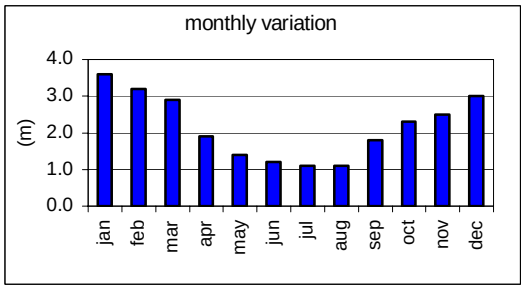

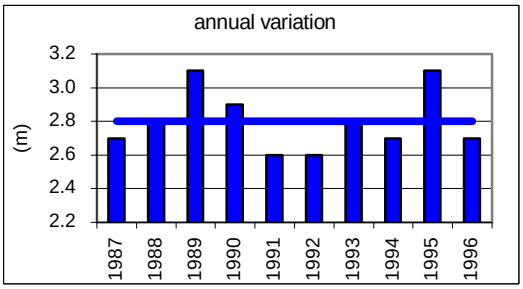

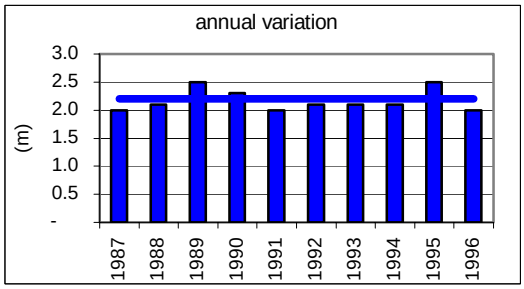

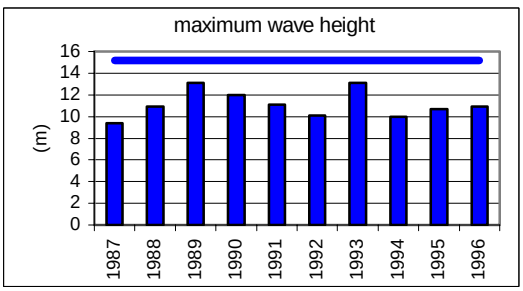

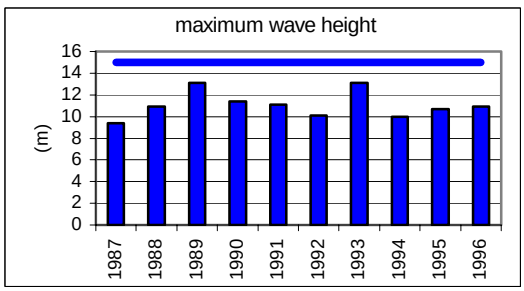

Location	Norwegian Sea	Lattitude	65.00	Longitude	2.33

	Swell wave height	
Average height	1.2	m
Average direction	26.3	
Average Period	9.6	S
Maximum	9.2	m
50 yr return value	10.7	m
Weibull scale factor	1.37	m
Weibull shape factor	1.23	

	Wind Speed	
Average height	9.1	m/s
Average direction	23.2	
Average Period	-	S
Maximum	29.2	m/s
50 yr return value	32.2	m/s
Weibull scale factor	10.34	m/s
Weibull shape factor	2.17	

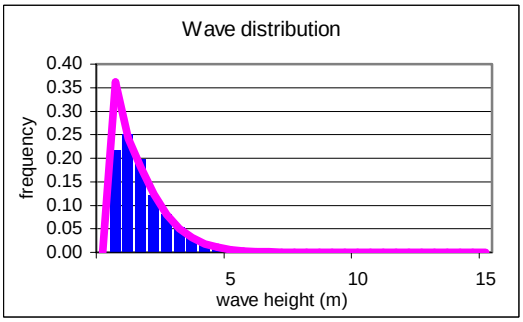

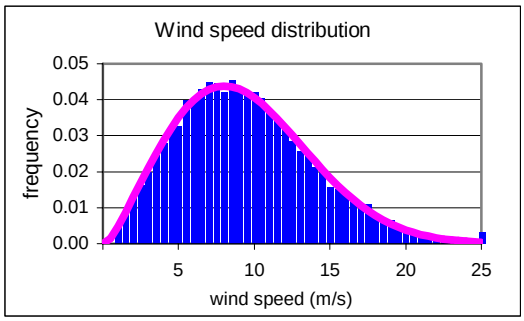

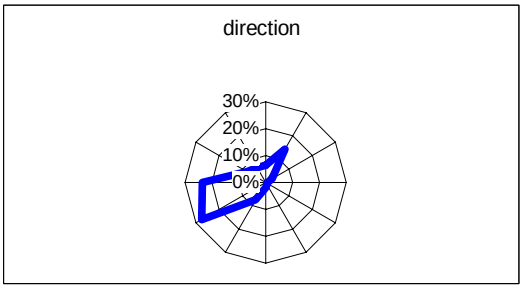

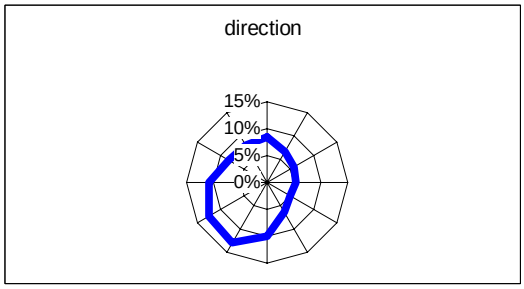

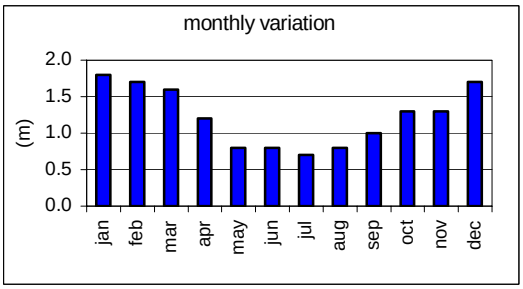

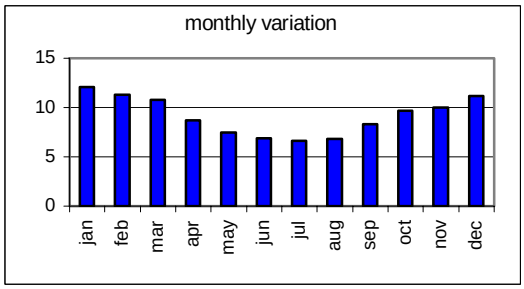

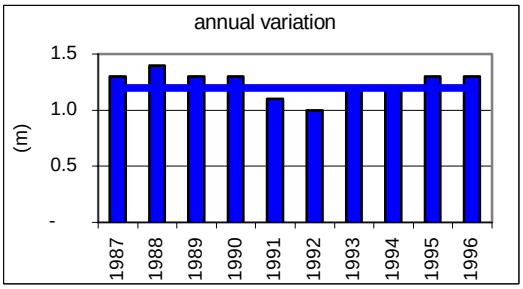

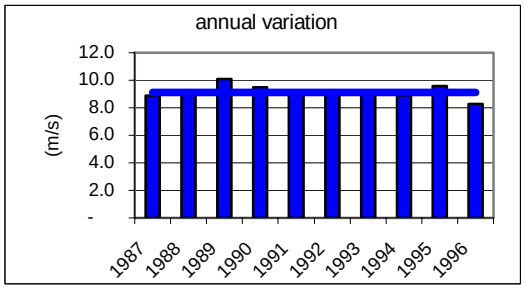

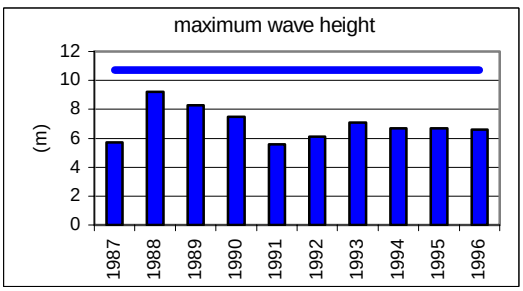

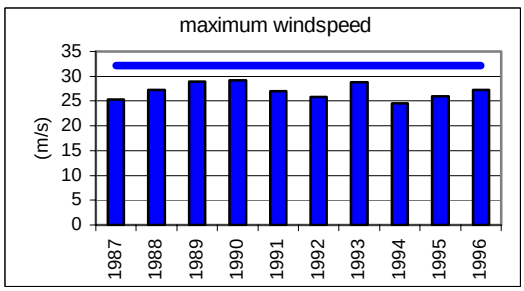

Location	Tyrrhenian Sea	Lattitude	40.00	Longitude	12.33

	Significant wave height
Average height	0.8 m
Average direction	25.3
Average Period	4 S
Maximum	7.1 m
50 yr return value	7.7 m
Weibull scale factor	0.82 m
Weibull shape factor	

	Wind Sea wave height
Average height	0.7 m
Average direction	-
Average Period	2.4 S
Maximum	6.9 m
50 yr return value	7.5 m
Weibull scale factor	0.67 m
Weibull shape factor	1

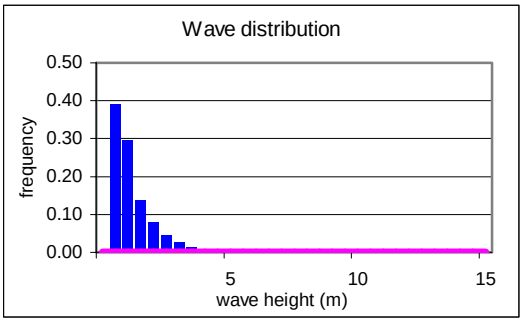

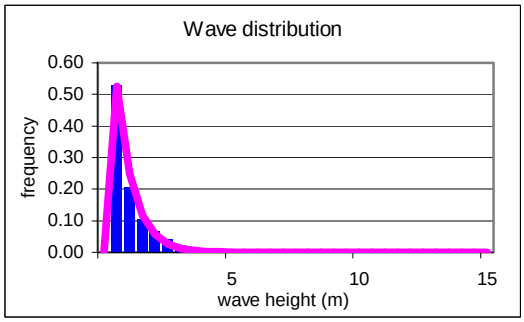

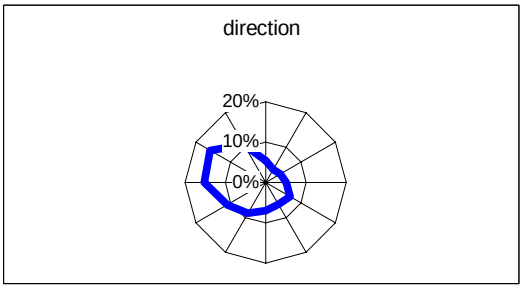

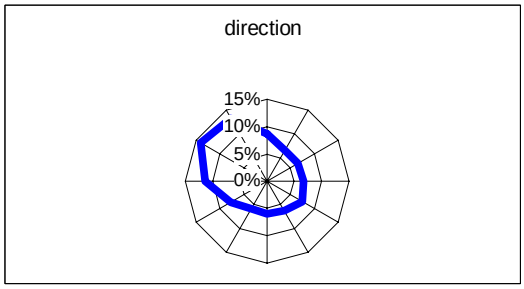

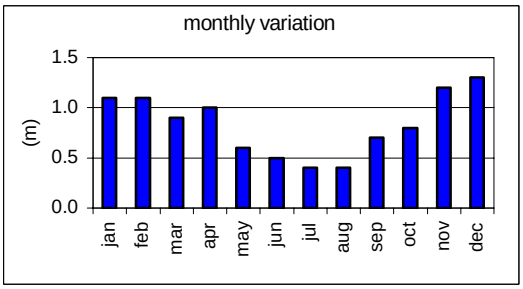

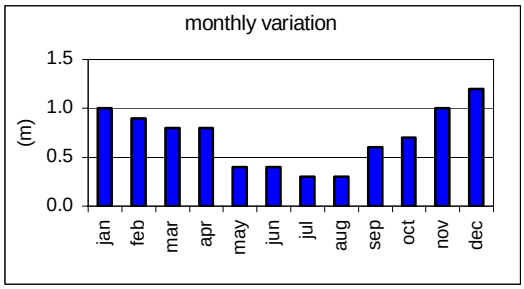

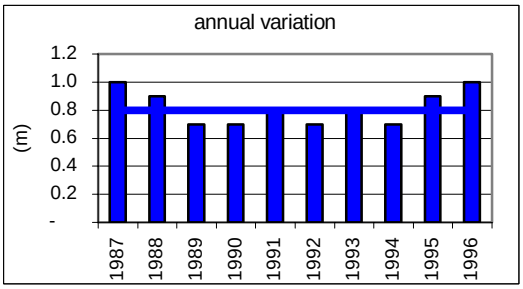

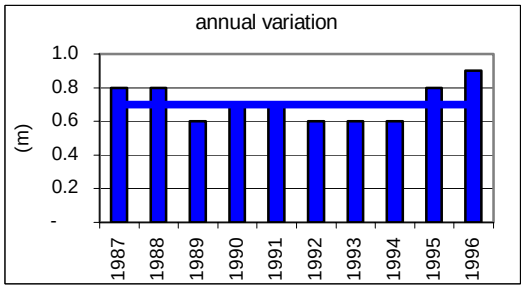

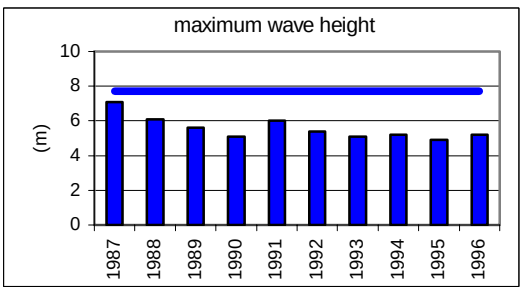

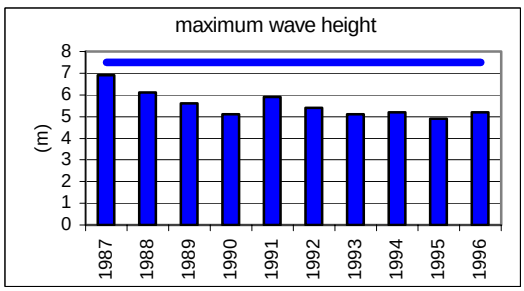

Location	Tyrrhenian Sea	Lattitude	40.00	Longitude	12.33

	Swell wave height
Average height	0.2 m
Average direction	29.8
Average Period	3.7 S
Maximum	3.9 m
50 yr return value	4.7 m
Weibull scale factor	0.4 m
Weibull shape factor	1

	Wind Speed
Average height	5.4 m/s
Average direction	29.4
Average Period	- S
Maximum	25 m/s
50 yr return value	28.5 m/s
Weibull scale factor	6.05 m/s
Weibull shape factor	1.68

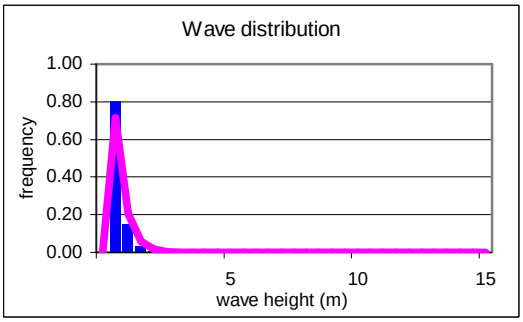

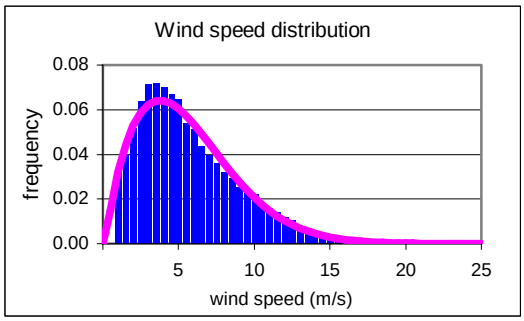

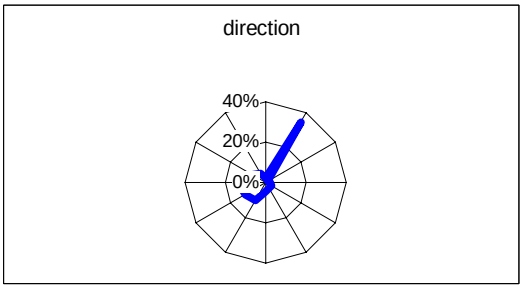

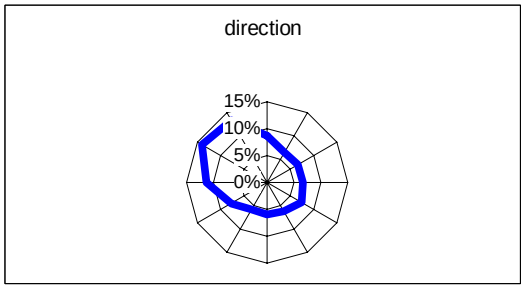

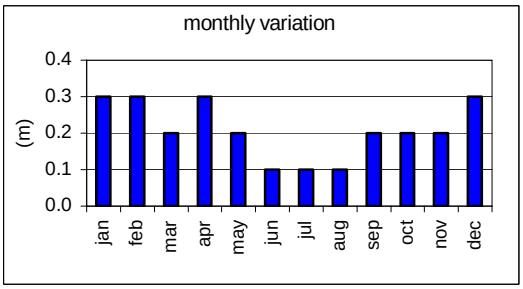

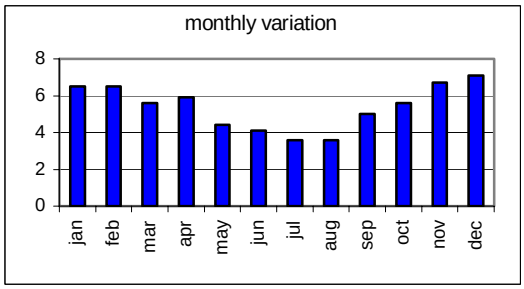

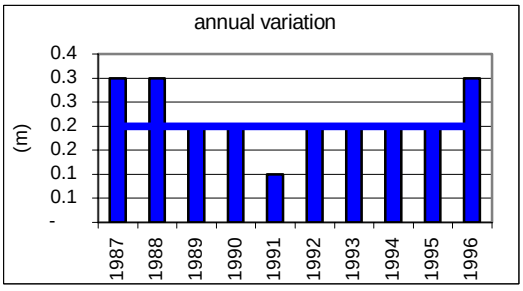

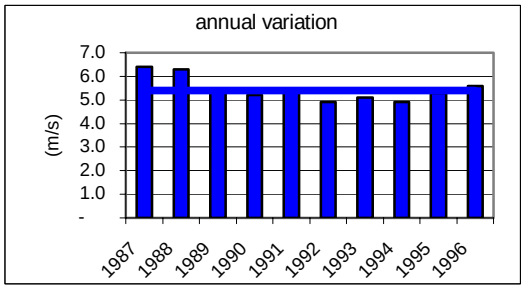

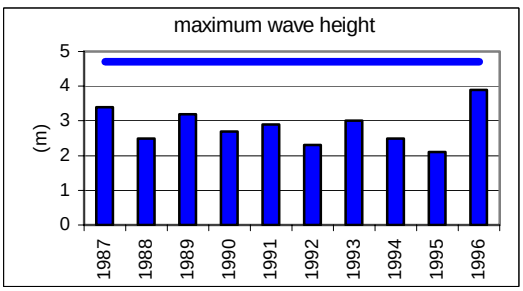

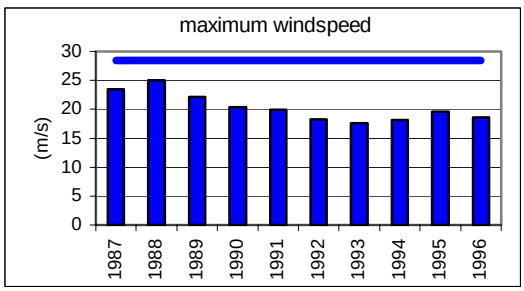

Annex 2 Wind wave diagrams

Location	Adriatic Sea	Lattitude	43.00	Longitude	15.53

Wind sea waves

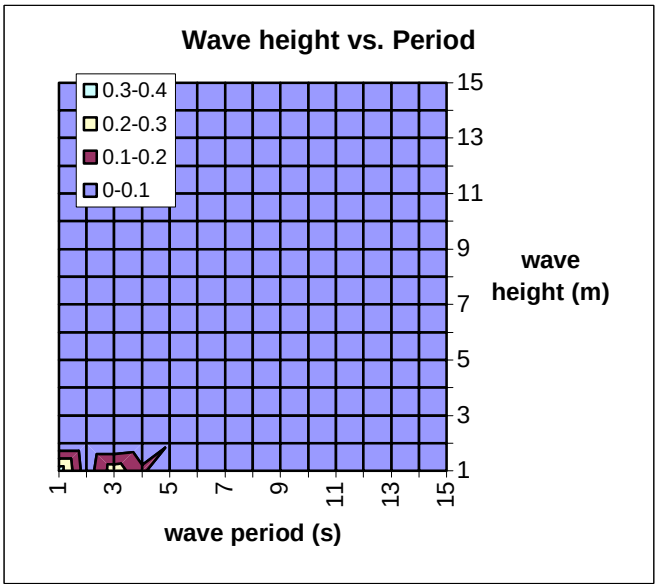

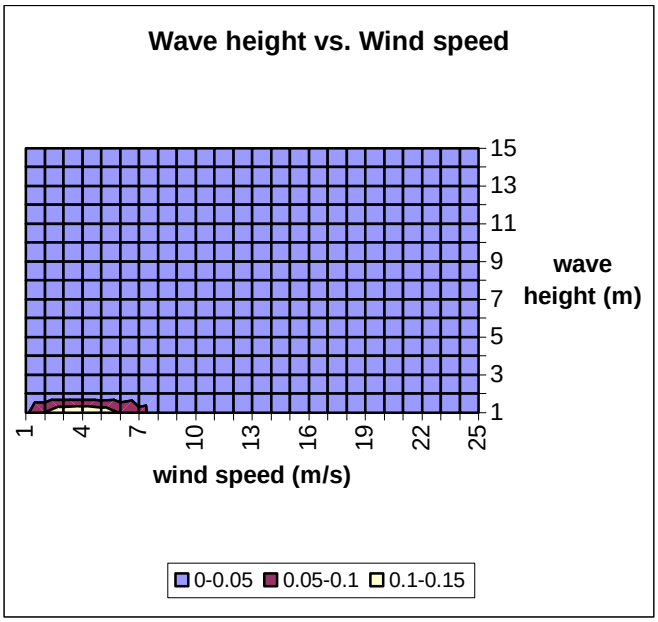

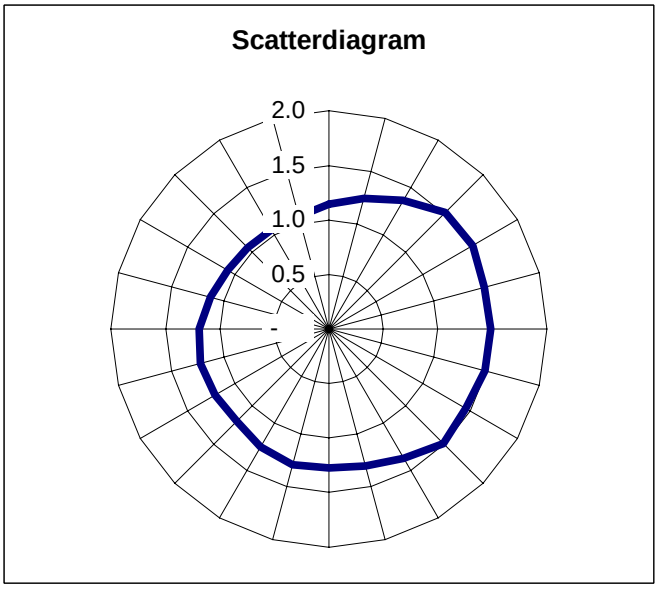

Location	Aegean Sea	Lattitude	38.00	Longitude	25.53

Wind sea waves

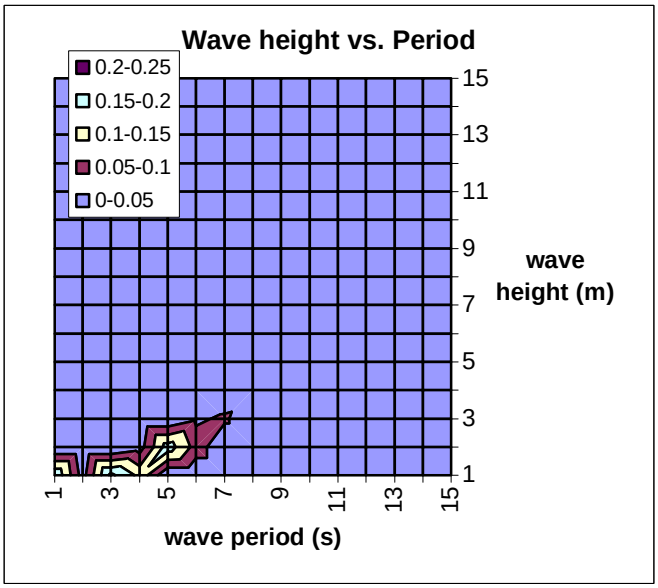

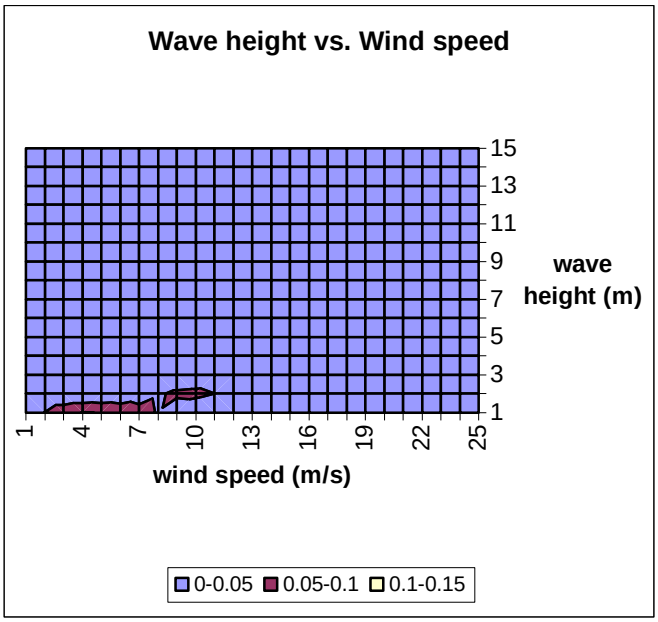

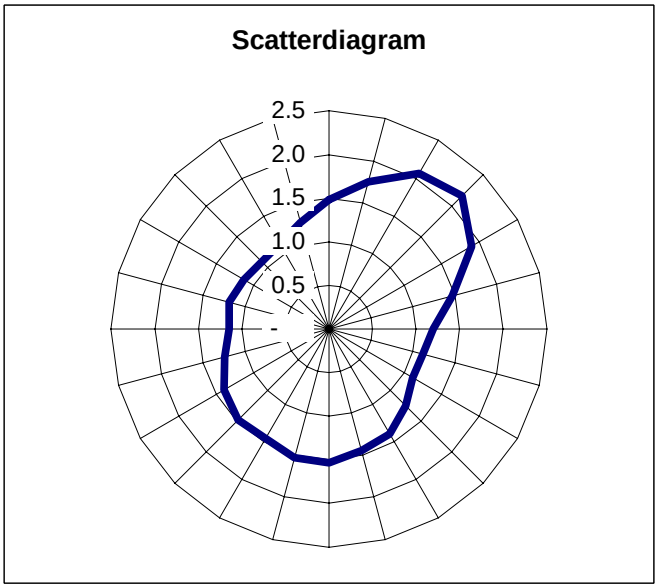

Location	Atlantic (Central)	Lattitude	44.00	Longitude	12.87-

Wind sea waves

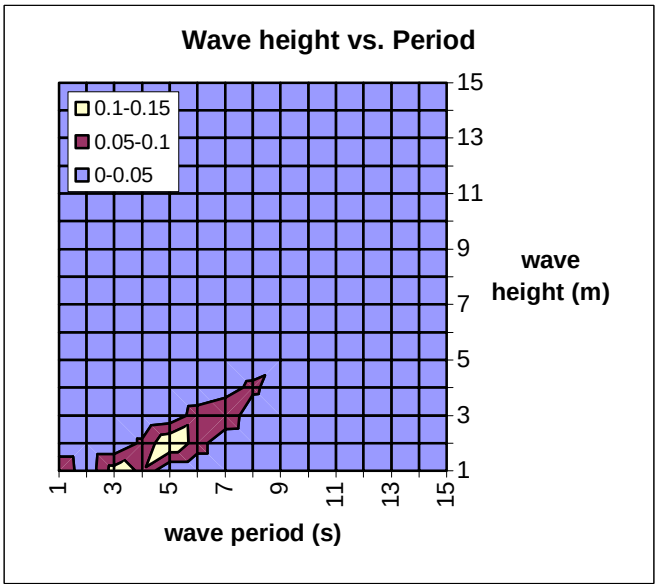

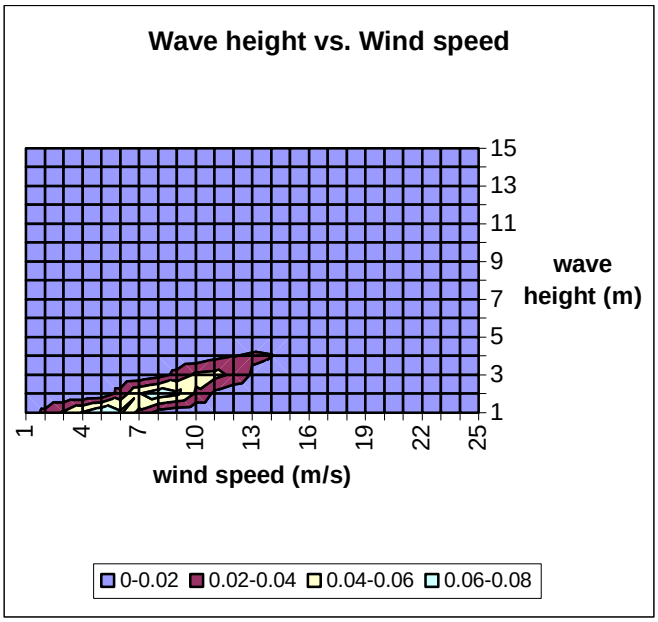

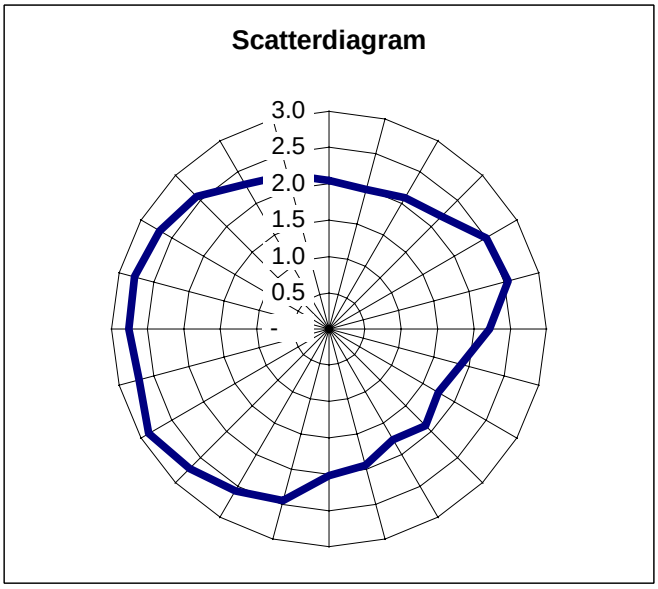

Location	Atlantic (North)	Lattitude	60.00	Longitude	10.07-

Wind sea waves

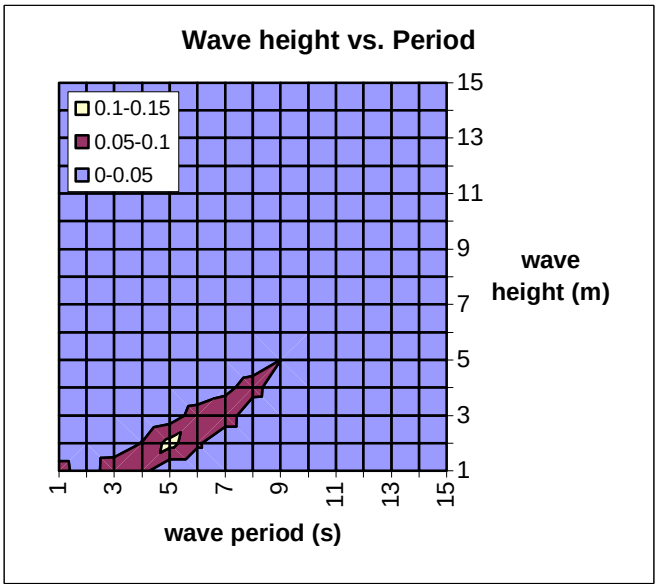

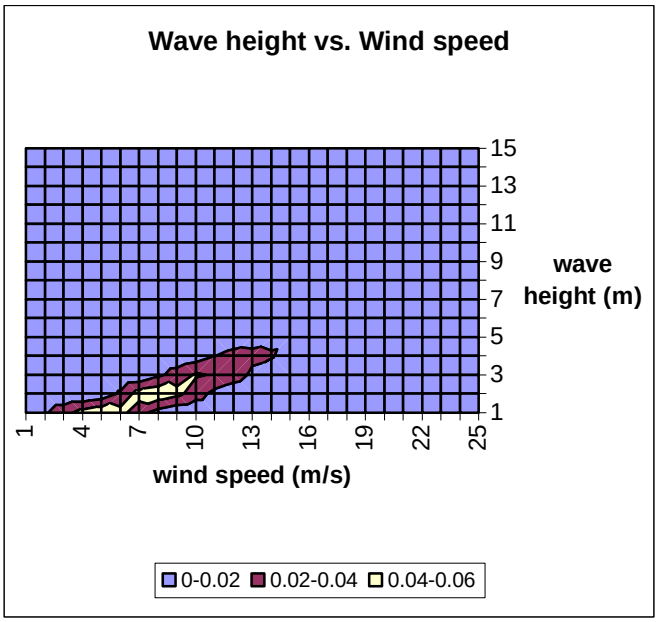

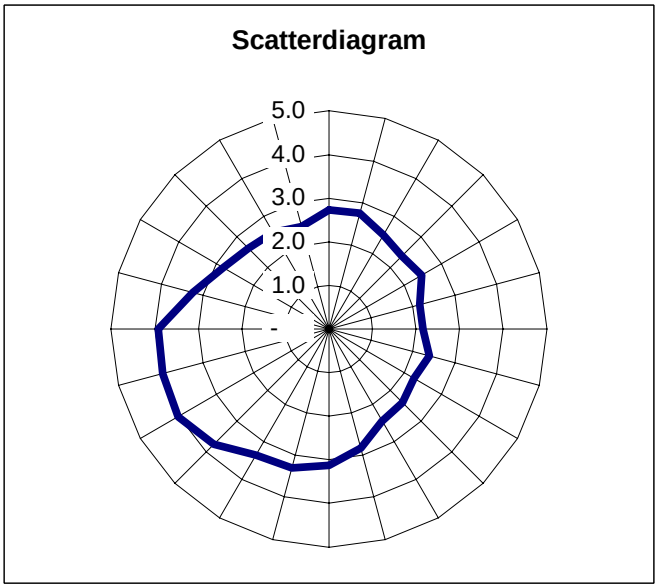

Location	Atlantic (South)	Lattitude	35.00	Longitude	10.07-

Wind sea waves

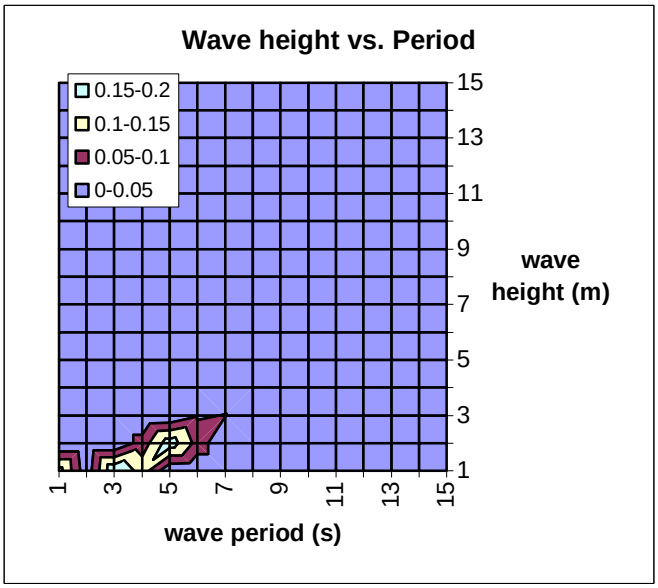

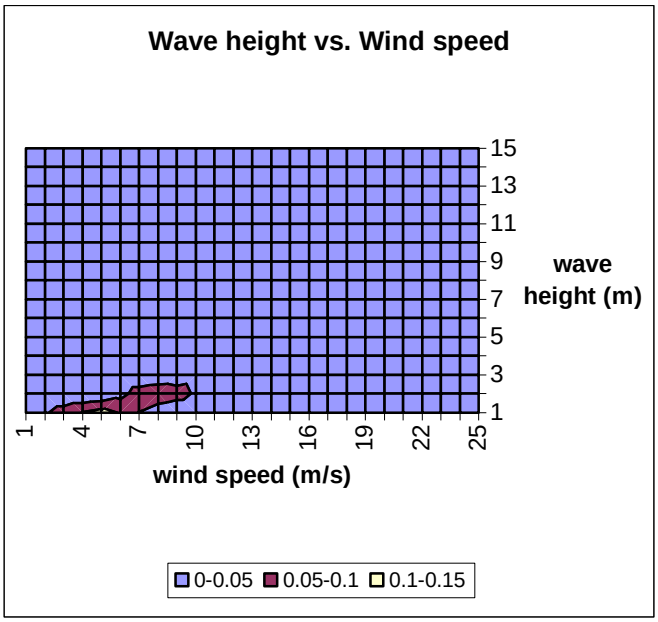

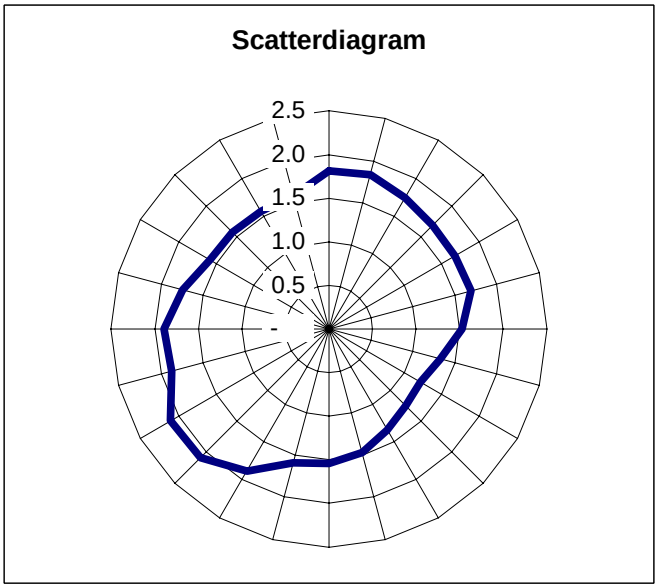

Location	Baltic Sea	Lattitude	58.00	Longitude	20.33

Wind sea waves

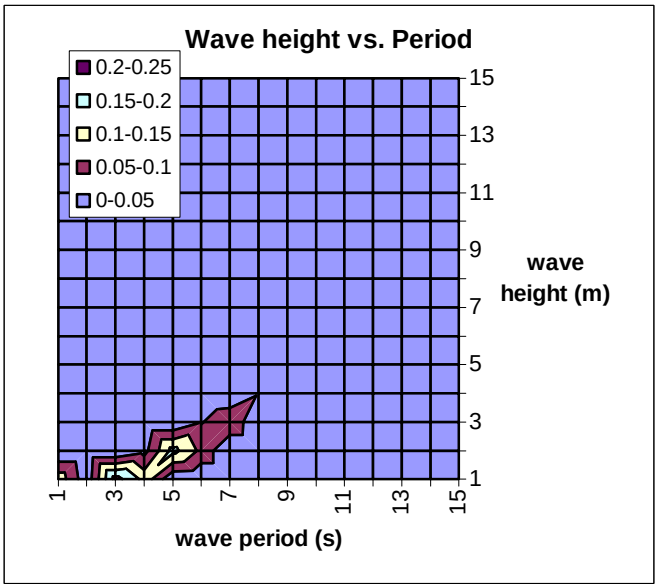

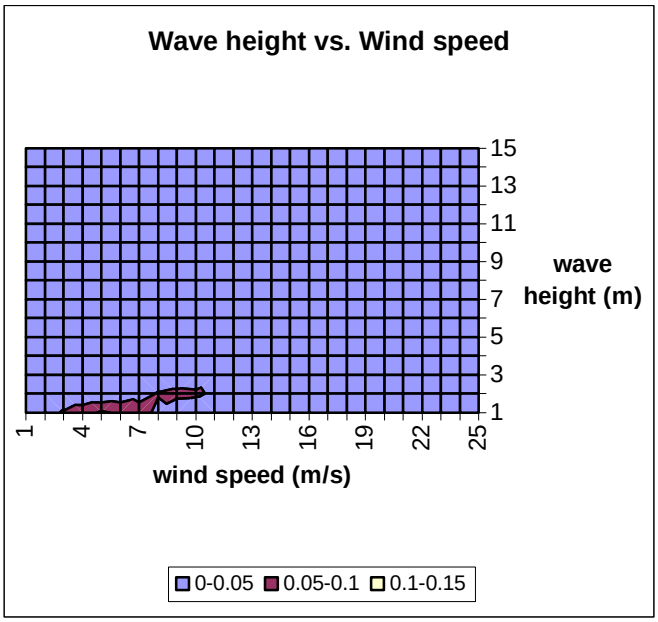

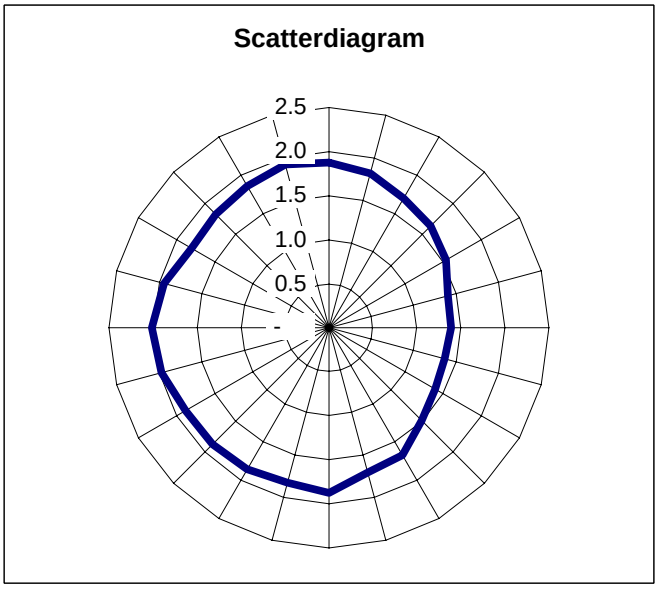

Location	Bay of Biscay	Lattitude	45.00	Longitude	2.87-

Wind sea waves

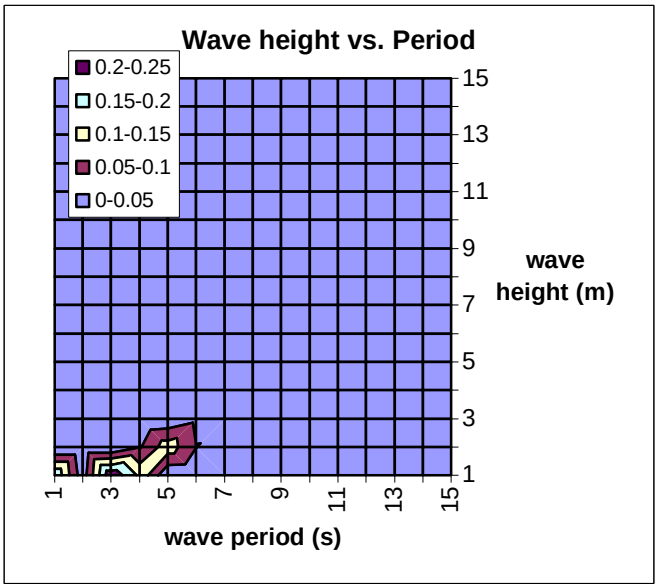

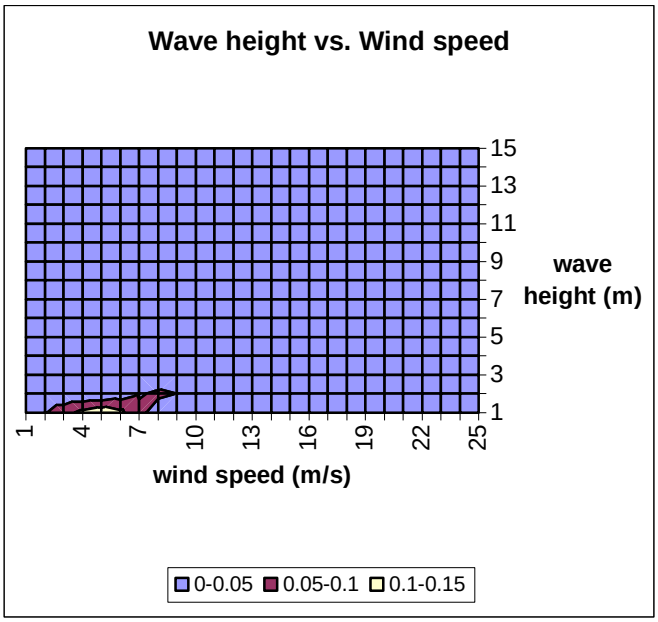

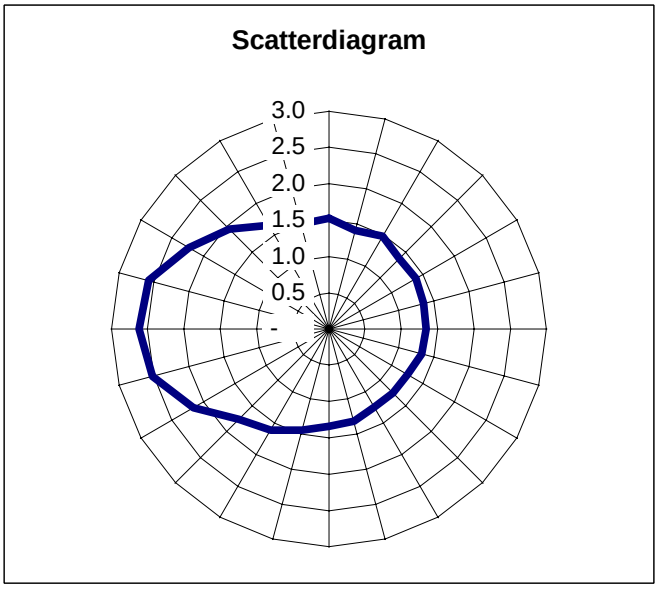

Location	Black Sea	Lattitude	42.00	Longitude	29.93

Wind sea waves

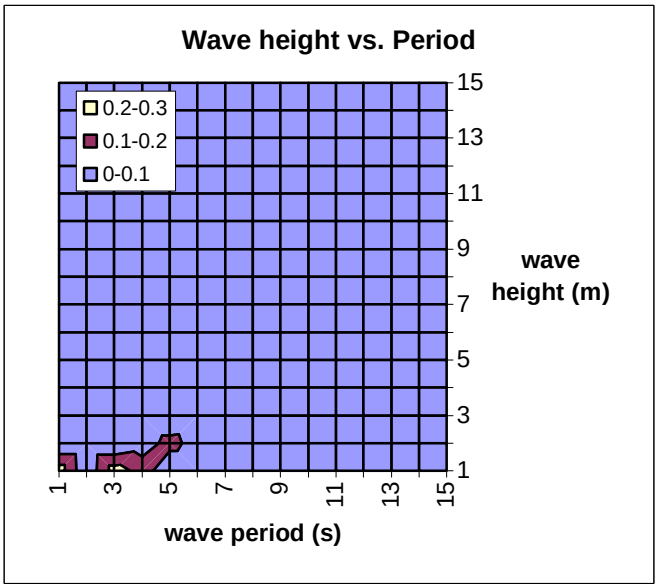

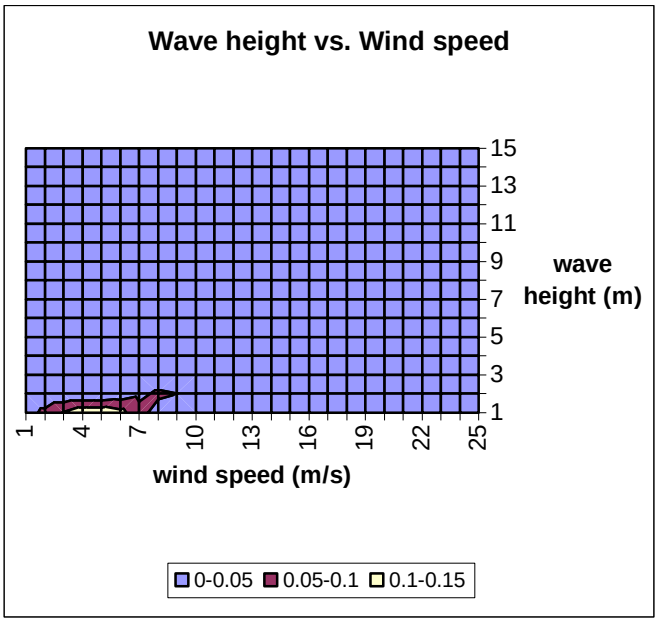

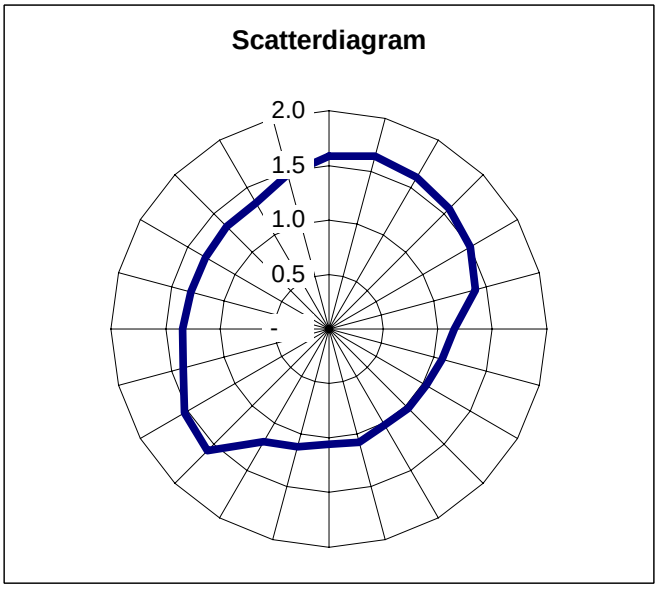

Location	Ionian Sea	Lattitude	36.00	Longitude	19.13

Wind sea waves

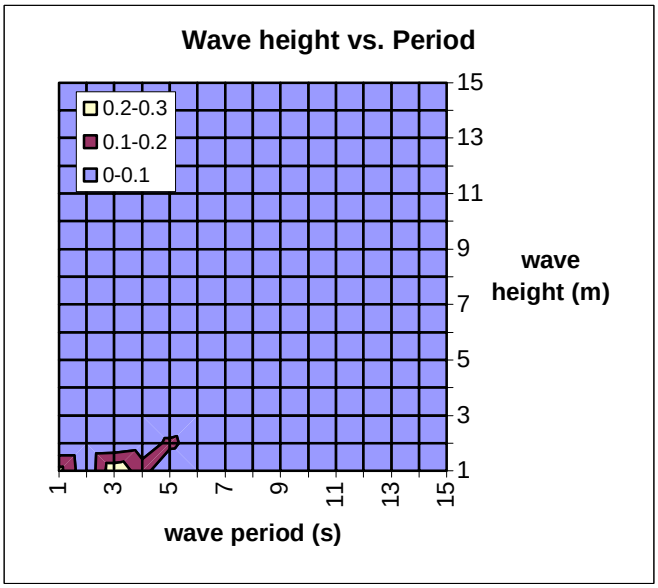

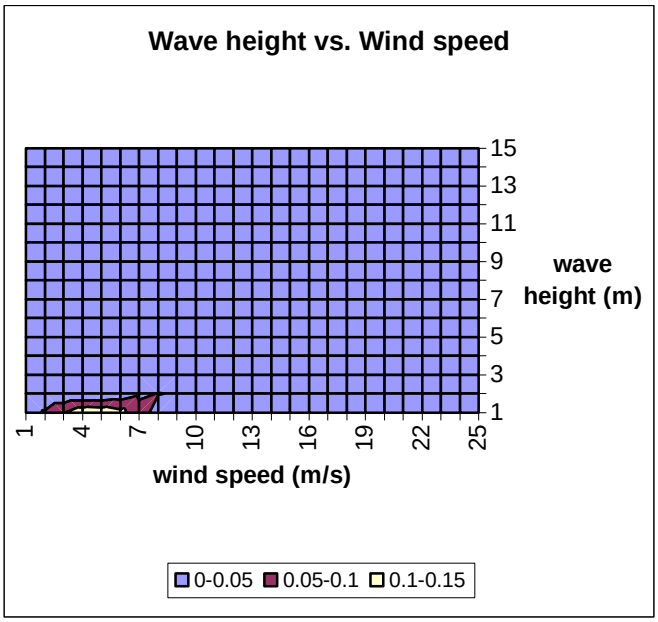

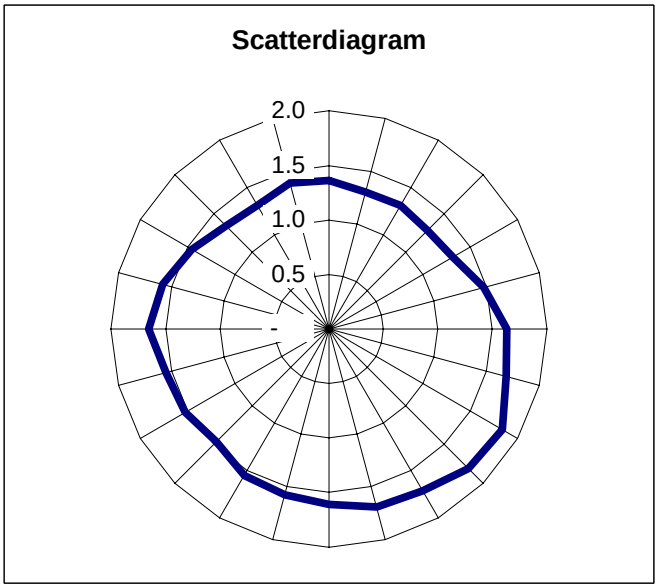

Location	Mediterranean (East)	Lattitude	33.50	Longitude	27.93

Wind sea waves

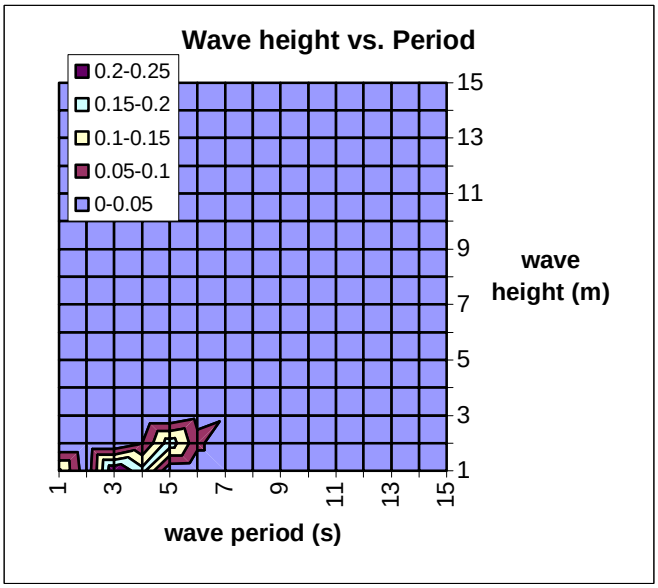

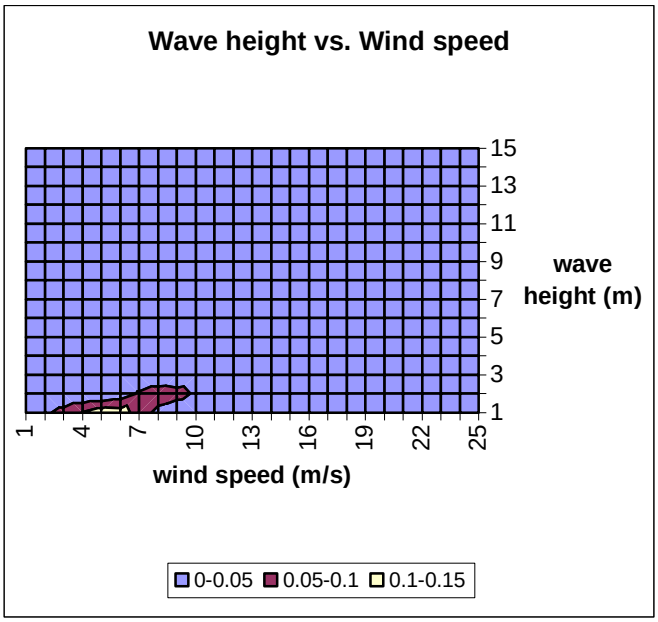

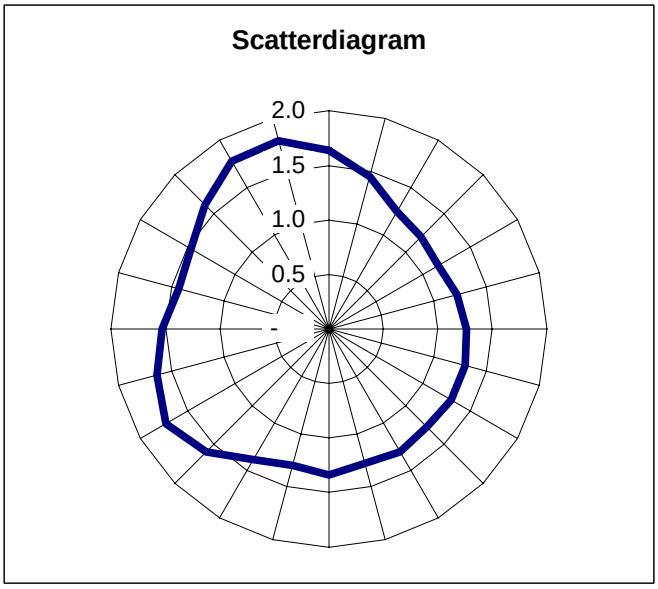

Location	Mediterranean (West)	Lattitude	39.00	Longitude	5.93

Wind sea waves

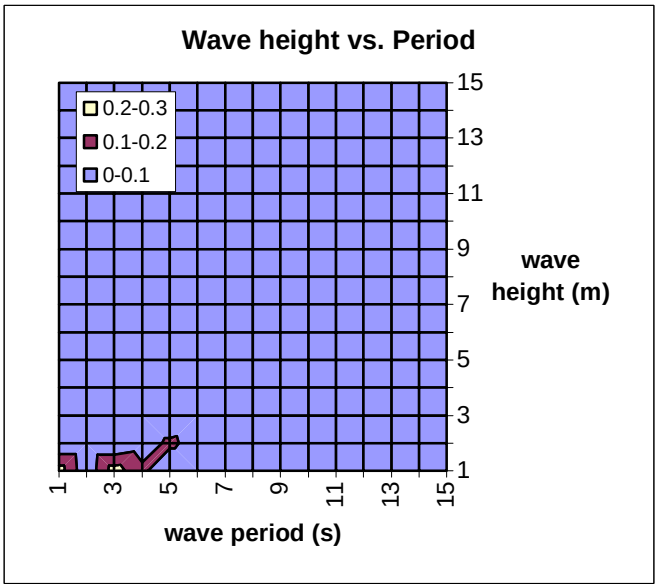

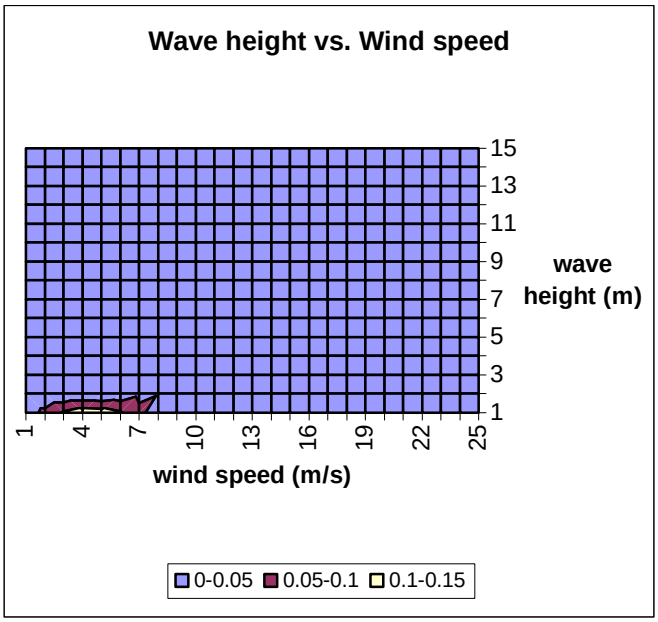

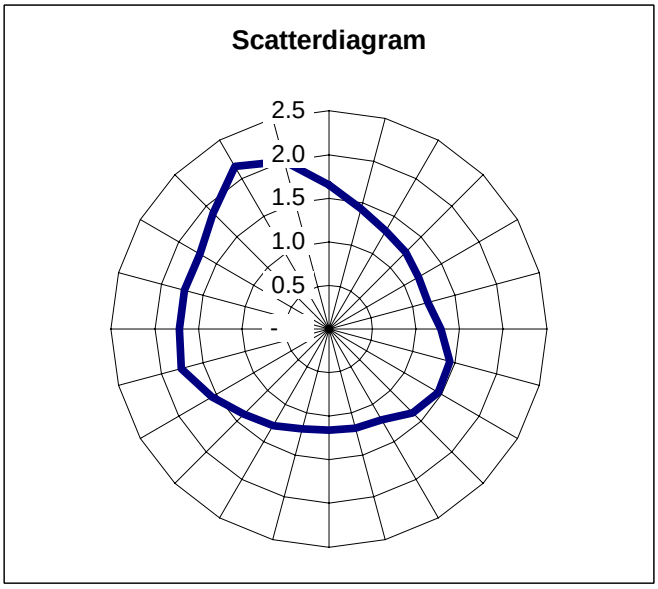

Location	North Sea	Lattitude	57.00	Longitude	3.13

Wind sea waves

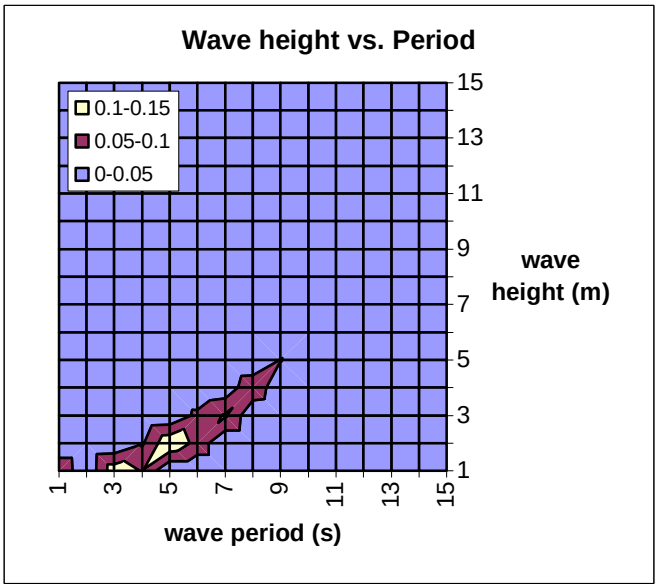

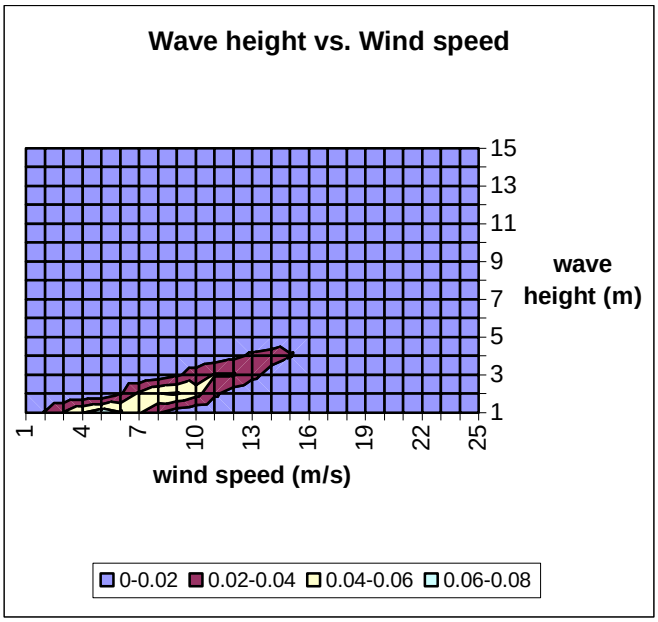

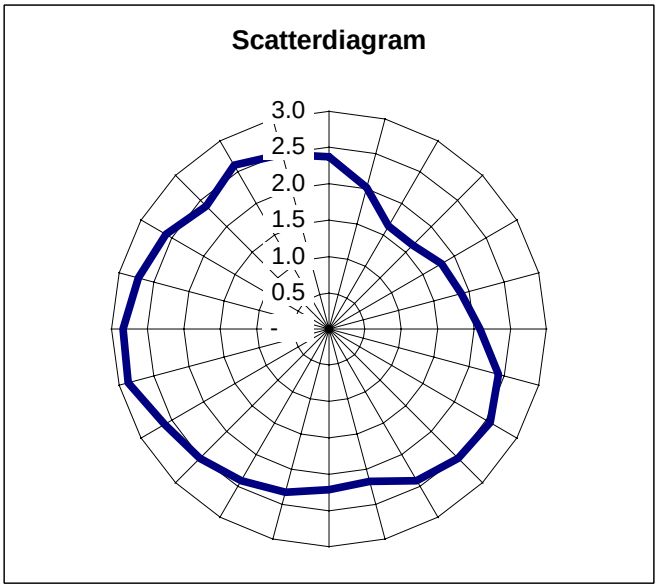

Location	Norwegian Sea	Lattitude	65.00	Longitude	2.33

Wind sea waves

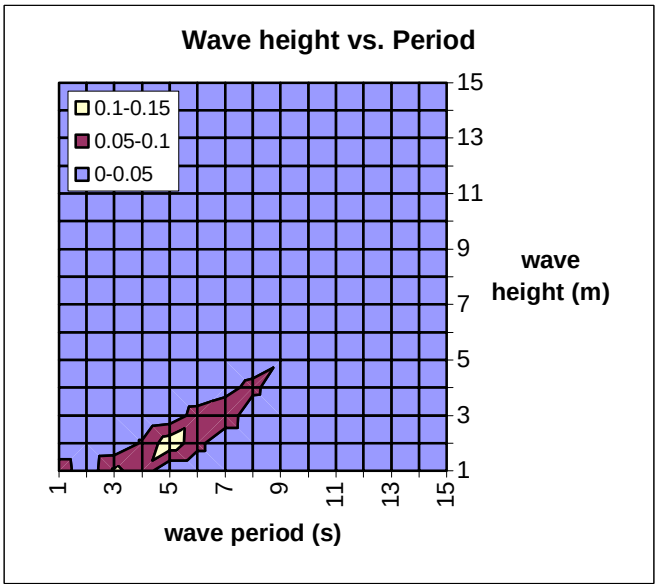

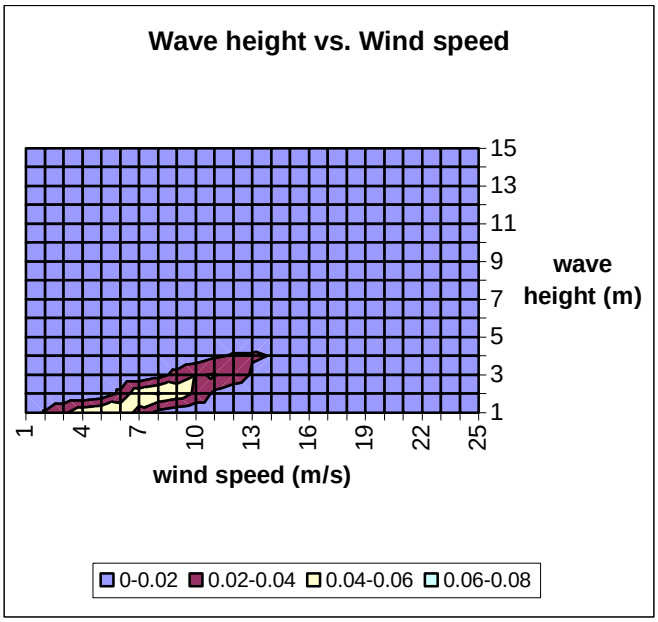

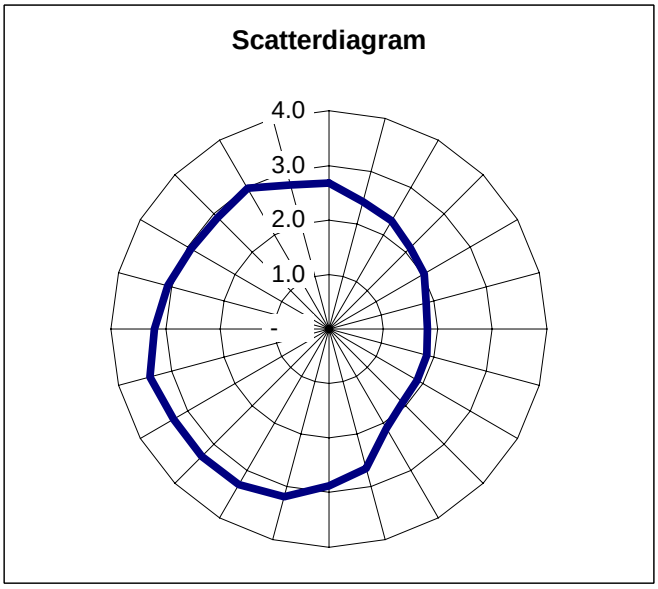

Location	Tyrrhenian Sea	Lattitude	40.00	Longitude	12.33

Wind sea waves

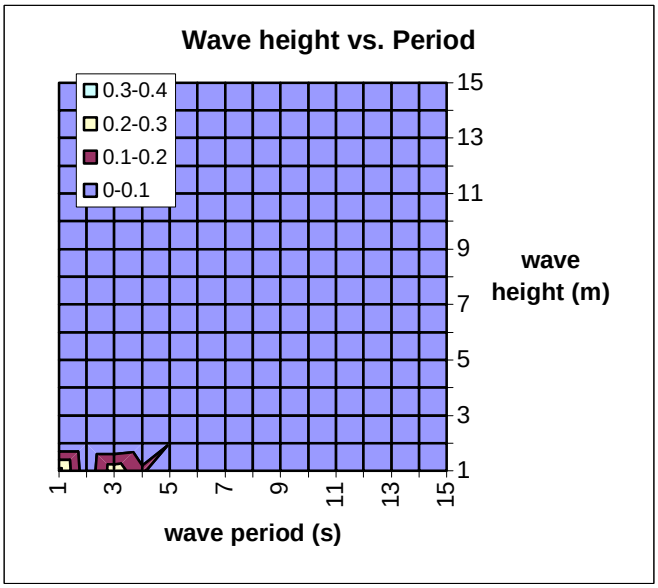

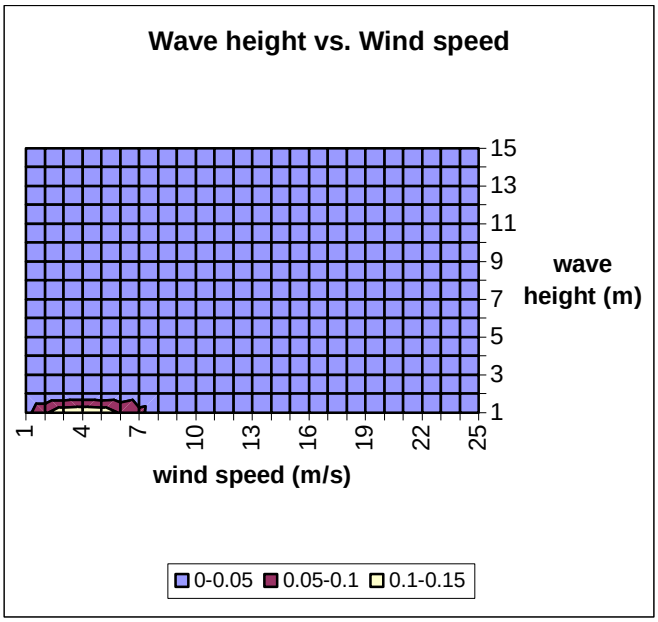

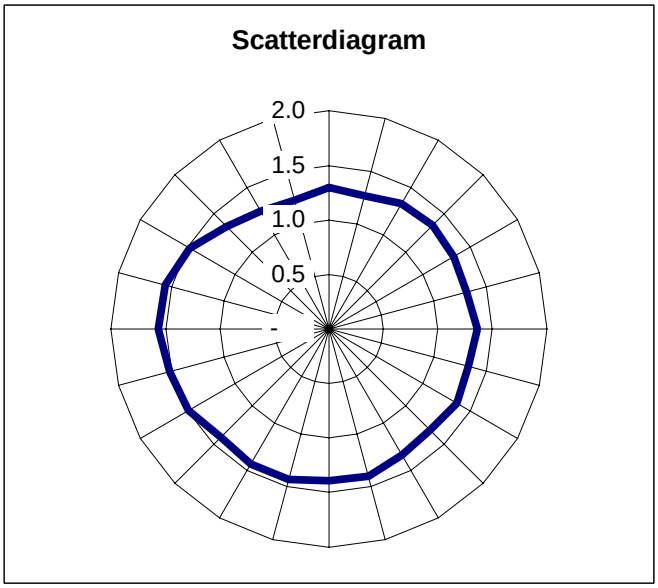

CHAPTER 9 : Confidence limits for mean monthly wind speeds

Chapter authors: : Dr T Holt and Dr J P Palutikof (University of East Anglia)

9.1 Introduction

The WAsP model has been used in POWER to predict the parameters of the wind field at various heights (see Chapter 4 and [Watson et al. (2000)]) from the geostrophic winds (see Chapter 3 and [Palutikof and Holt [2000)]). Here, we summarize the methodology for gauging the reliability of the estimated wind speeds by calculating confidence limits. It is not practical to present results for each height and grid point. Therefore, we concentrate on regions identified as important in the analysis of the long-term wind field (see Section 7.2, Table 7.2) and provide results for a single height, selected to be a typical hub height for offshore wind turbines.

9.2 Data

The WAsP output described in Chapter 4 gives the monthly mean parameters shown in Table 9.1 for each grid square at heights from 10 to 150m at 20 m intervals. The columns are: wind direction in 30 degree bins, the scale (A) and shape (k) parameters of the Weibull distribution, the frequency of the wind in each directional bin, and the proportion of the wind energy associated with a direction.

Direction	A (scale)	k (shape)	Wind%	Energy%
0	10.0	2.13	3.0	1.5
30	10.6	2.56	2.9	1.5
60	10.5	2.17	3.5	1.9
90	12.1	2.35	5.5	4.4
120	11.8	2.36	7.1	5.2
150	12.0	2.40	8.3	6.3
180	12.4	2.29	9.4	8.2
210	13.9	2.64	11.4	12.8
240	15.3	2.82	18.6	27.0
270	13.2	2.51	15.0	14.8
300	13.4	2.15	9.9	11.6
330	11.3	1.74	5.4	4.8

Table 9.1 Example monthly mean wind parameters from WAsP

Principal Component Analysis of the long term wind field (Section 7.2) identifies six areas of spatially coherent wind variability relevant to offshore wind energy development. For this demonstration analysis, we selected a grid square to represent these areas (Table 9.2) and extracted the relevant data from the WAsP output. To provide a concise example, we only analysed data for 90 m, this being the closest the WAsP output comes to the expected hub height of large offshore turbines. The methodology can be readily applied to data for any height at any location.

The columns in Table 9.2 represent: the factor identified by the PCA in the analysis of the long term wind field, the region identifier used in here (to avoid confusion because PCA factor 3 is not relevant), the latitude and longitude of the grid square chosen to represent the region, and the area identified as having a spatially coherent wind field. It is important to note that the results presented for each sample grid square are not intended to give reliable estimates of confidence limits for the whole of the region defined in Table 9.2. The confidence limits apply just to the grid square, and need to be reworked for every required grid square.

Factor	Region	Latitude	Longitude	Area identified
1	1	55 N	10 E	Baltic, Scandinavia, UK, Ireland, North Sea, and northern France
2	2	40 N	5 E	Mediterranean, Spain, Portugal, and western France
4	3	40 N	10 W	northern Portugal and Spain, northern and western France, Ireland, Wales, and England
5	4	60 N	5 W	Iceland, Scotland, northern Norway, Sweden, and Finland
6	5	35 N	10 W	northwest Africa and southern Spain and Portugal
7	6	35 N	25.5 E	Egypt, southern Turkey, south-eastern Greece, Israel and Lebanon

Table 9.2 Areas represented in the determination of confidence limits (taken from the Principal Components Analysis performed in Section 7.2)

9.3 Methodology

The methodology is applied to data similar to that in Table 9.1 for each month in each of the six regions identified in Table 9.2. This gives 72 sets of results.

Using the Weibull parameters for each directional bin, twelve sets of simulated wind speeds are created, one for each directional bin, with 100 simulated wind speeds per bin. It is important that the number of simulated wind speeds is of the same order as the observed wind speeds. Here, the calculation of the Weibull parameters is based on 10 years of 6-hourly data, that is, 1200 values in total, and hence of the order of 100 per directional bin. If, for example, 1000 simulated wind speeds were used this could give a possibly spurious precision to the estimated confidence limits.

The simulated wind speed data for each directional bin are then resampled with replacement (see for example, [Efron (1983)]) 1000 times and confidence limits estimated using the bias-adjusted percentile method as described by [Davison and Hinkley (1997)]. This method of determining confidence limits is described as bootstrapping. The simulated data are then used to calculate the monthly mean wind speed for that grid square for each bin. To arrive at an overall mean, the bin means are weighted according to the frequency of wind speeds associated with each direction, and then summed. The 95% confidence limits for the overall mean are derived by applying the frequency weighting procedure to the confidence limits for each directional bin. The methodology is summarised below. A detailed review is beyond the scope of this report.

The creation of simulated data fitting a known distribution is fairly straightforward and the facility is available in many commercial statistics packages. The whole of this analysis was performed in MatLab, a widely-used graphical/mathematical analysis utility. The advantage of using an analytical tool of this type, over a conventional statistics package, is that the development of the analysis is completely flexible since MatLab is essentially a specialised high-level programming language. The formula to create a random number x from a Weibull distribution with parameters A and k is:

```
x = A*(-log(1-p))^(1/k)
```

p in the equation is a probability generated by a uniform random number routine giving values between 0 to 1. The expression is evaluated once for each required item in the simulated data series, with a new random value for p being chosen each time.

Bootstrap estimation of confidence limits eliminates many of the theoretical restrictions limiting the application of “classical” statistical methods to the problem. A further advantage of bootstrapping is that it is relatively easy to understand and the methodology seems intuitively sensible. Essentially, bootstrapping uses the available data to create a large number of extra data sets using resampling with replacement. The original data is resampled, using a random number generator, with the proviso that the new data set must have the same number of items as the original and can contain only the numbers present in the original series. The “with replacement” condition allows any of the original numbers to be repeated in the new data set on a random basis. The assumption is that, in the absence of further information, if the original sample data set is resampled a sufficient number of times, the resulting suite

of data series will give a fairly reliable representation of the population statistics of the variable. The number of resamples required will vary with the analysis but, generally, 1000 should be adequate.

In this analysis, we first generate confidence limits for the monthly mean wind speed of each directional bin, at the 95% confidence level. That is, we wish to say that we are confident that 95% of the time the monthly mean wind speed for a directional bin will be between the specified upper and lower limits. Following the resampling with replacement, we can calculate 1000 mean wind speeds for each directional bin. The 95% confidence level could then be determined by sorting the means and simply taking the 25^{th} value as the lower limit and the 975^{th} value as the upper limit. A problem with this approach is that it assumes the 1000 wind speeds are symmetrically distributed. This is often not the case and various adjustments can be applied to compensate for asymmetry. The method used here, bias-adjusted percentiles, was tested and found to give consistent estimates of confidence limits using a range of iterations from 500 to 20000.

The monthly mean wind speed as a weighted average over all directional bins is obtained from:

```
weight(i) = meanwind(i)*windfrequency(i)/100
```

where i ranges from 1 to 12 (for each directional bin). To obtain the monthly mean wind speed averaged over all directional bins, we sum the 12 weights. To obtain the 95% confidence limits for the overall average wind speeds, the weighting procedure is applied to the 95% confidence limits for each directional bin.

9.4 Results

The estimated monthly mean wind speed over all wind directions and the 95% confidence limits, for each month and the grid squares identified in Table 9.2, are shown in Table 9.3. The 95% confidence limits for the mean wind speed for each directional bin can be found in the next Section.

Month	Region	Lower (m/s)	Mean (est.) (m/s)	Upper (m/s)
January	1	10.6	11.6	12.6
	2	7.6	8.4	9.2
	3	7.8	8.6	9.6
	4	12.3	13.7	15.1
	5	7.3	8.1	8.8
	6	6.9	7.7	8.4
February	1	10.2	11.2	12.2
	2	7.5	8.3	9.3
	3	8.0	9.0	10.0
	4	11.8	13.0	14.3
	5	6.5	7.3	8.1
	6	7.5	8.4	9.2
March	1	9.4	10.3	11.1
	2	7.4	8.3	9.1
	3	7.5	8.4	9.3
	4	12.2	13.3	14.5
	5	7.1	7.9	8.6
	6	6.5	7.3	8.1
April	1	7.7	8.6	9.5
	2	7.5	8.3	9.1
	3	7.9	8.8	9.7
	4	10.0	11.0	12.0
	5	7.0	7.7	8.5
	6	5.7	6.3	7.0

Table 9.3 95% Confidence limits for monthly mean wind speed averaged over all directional bins

Month	Region	Lower (m/s)	Mean (est.) (m/s)	Upper (m/s)
May	1	7.1	7.8	8.5
	2	5.2	5.9	6.6
	3	7.1	7.8	8.6
	4	8.6	9.4	10.3
	5	6.4	7.0	7.6
	6	5.5	6.1	6.6
June	1	6.7	7.4	8.2
	2	4.5	5.1	5.7
	3	7.8	8.5	9.2
	4	7.8	8.7	9.5
	5	6.4	7.0	7.5
	6	6.2	6.6	7.1
July	1	7.0	7.6	8.4
	2	4.1	4.6	5.1
	3	8.1	8.8	9.5
	4	7.9	8.6	9.4
	5	7.4	8.0	8.6
	6	8.1	8.5	9.0
August	1	7.0	7.7	8.5
	2	4.0	4.4	4.9
	3	7.0	7.6	8.3
	4	8.2	9.1	10.0
	5	6.3	6.8	7.3
	6	7.4	7.8	8.2
September	1	8.0	8.8	9.7
	2	4.7	5.3	5.9
	3	6.6	7.3	8.1
	4	10.0	11.0	12.1
	5	5.9	6.4	6.9
	6	6.1	6.6	7.0
October	1	8.5	9.4	10.3
	2	6.0	6.6	7.3
	3	7.2	8.1	8.9
	4	10.7	11.8	13.0
	5	5.6	6.3	6.9
	6	5.2	5.7	6.3
November	1	9.7	10.5	11.4
	2	6.9	7.6	8.4
	3	7.8	8.6	9.5
	4	11.0	12.0	13.2
	5	6.8	7.5	8.3
	6	6.2	6.9	7.6
December	1	9.8	10.8	11.8
	2	7.4	8.3	9.1
	3	8.3	9.2	10.2
	4	11.1	12.3	13.6
	5	7.2	8.0	8.8
	6	6.9	7.6	8.4

Table 9.3 (continued) 95% Confidence limits for monthly mean wind speed averaged over all directional bins

9.5 Comments

Bootstrapping gives apparently reasonable estimates of the limits of the 95% confidence level in monthly mean wind speed data defined by Weibull parameters. Confidence limits can also be estimated

using Monte Carlo simulation, a method similar to bootstrapping but requiring many more iterations. We tested Monte Carlo simulation on the 12 directional bins for Region 1 in January. The confidence limits were similar to those from bootstrapping but the analysis took 100 times longer, making the use of this method prohibitively slow.

The bias adjusted percentile method of estimating confidence limits used here transforms the data by fitting to a normal distribution. The method will give erroneous results in the presence of outliers. This is not an issue here since our data are simulated from the Weibull distribution.

The following tables contain the 95% confidence limits of the mean monthly wind speed for each directional bin.

Confidence limits for Region 1 Coasts of Northern Europe

Direction	lower Jan	mean Jan	upper Jan	Lower Feb	mean Feb	upper Feb	Lower Mar	mean Mar	upper Mar
0	7.84	8.56	9.33	7.74	8.64	9.56	6.52	7.25	7.98
30	7.97	8.62	9.30	7.52	8.36	9.34	5.93	6.58	7.32
60	8.09	8.90	9.70	7.18	8.01	8.92	7.06	7.79	8.62
90	8.74	9.70	10.62	9.68	10.57	11.42	8.35	9.20	10.01
120	9.18	10.04	10.88	11.15	11.99	12.98	9.57	10.33	11.01
150	10.09	11.01	12.00	10.94	11.91	12.91	9.76	10.63	11.54
180	9.87	10.90	11.98	9.93	10.91	11.85	7.97	8.82	9.75
210	11.61	12.69	13.76	10.93	11.88	12.80	8.91	9.98	10.98
240	12.63	13.64	14.69	13.14	14.21	15.24	9.47	10.32	11.13
270	11.31	12.14	13.07	9.42	10.49	11.50	10.28	11.12	12.00
300	11.14	12.23	13.16	9.97	11.00	12.20	12.20	13.33	14.42
330	9.62	10.68	11.97	7.62	8.73	9.78	9.91	11.04	12.23

Table 9.4 Region 1: 95% confidence limits for mean monthly wind speed by direction, January to March

Direction	lower Apr	mean Apr	upper Apr	Lower May	mean May	upper May	lower Jun	mean Jun	upper Jun
0	6.75	7.55	8.44	5.66	6.30	7.00	4.79	5.33	6.00
30	6.84	7.77	8.73	5.76	6.39	6.99	4.82	5.40	5.99
60	7.19	8.08	8.95	6.87	7.56	8.26	5.84	6.63	7.33
90	9.07	9.82	10.66	8.21	8.84	9.50	6.02	6.65	7.42
120	8.63	9.54	10.47	7.87	8.53	9.17	6.72	7.41	8.14
150	7.59	8.52	9.58	7.71	8.37	9.03	7.18	7.88	8.62
180	6.86	7.60	8.49	5.59	6.27	6.91	6.19	7.05	7.98
210	7.11	7.83	8.70	6.93	7.52	8.20	6.69	7.25	7.88
240	7.24	8.16	9.08	7.11	7.91	8.79	7.70	8.45	9.22
270	7.04	7.74	8.61	6.14	6.82	7.51	6.65	7.29	8.05
300	9.11	10.19	11.24	7.68	8.59	9.52	7.86	8.71	9.56
330	8.37	9.51	10.74	7.52	8.33	9.22	6.83	7.61	8.50

Table 9.5 Region 1: 95% confidence limits for mean monthly wind speed by direction, April to June

Direction	lower Jul	mean Jul	upper Jul	Lower Aug	mean Aug	upper Aug	lower Sep	mean Sep	upper Sep
0	5.26	5.88	6.58	5.21	5.81	6.55	7.00	7.55	8.13
30	4.45	5.06	5.67	4.83	5.72	6.67	6.65	7.21	7.75
60	4.55	5.03	5.56	4.97	5.82	6.60	8.73	9.39	10.17
90	5.82	6.54	7.21	5.41	6.09	6.81	7.98	8.73	9.41
120	6.67	7.36	8.06	6.80	7.61	8.34	8.08	8.90	9.86
150	6.28	6.89	7.56	7.21	8.00	8.84	7.65	8.37	9.11
180	5.16	5.68	6.22	6.21	6.91	7.82	5.72	6.46	7.27
210	5.67	6.25	6.86	7.02	7.79	8.59	8.26	9.20	10.02
240	7.01	7.69	8.40	7.68	8.35	9.19	9.00	9.73	10.57
270	7.78	8.45	9.25	7.05	7.66	8.30	8.05	9.11	10.14
300	9.34	10.17	11.01	8.55	9.37	10.26	8.37	9.39	10.39
330	7.50	8.33	9.16	6.97	7.83	8.68	7.40	8.19	9.06

Table 9.6 Region 1: 95% confidence limits for mean monthly wind speed by direction, July to September

Direction	lower Oct	mean Oct	upper Oct	Lower Nov	mean Nov	upper Nov	lower Dec	mean Dec	upper Dec
0	6.71	7.45	8.32	8.49	9.62	10.90	7.78	8.70	9.56
30	6.78	7.65	8.61	7.14	7.96	8.78	7.92	8.82	9.78
60	7.08	8.07	9.13	8.35	9.19	10.18	7.80	8.67	9.67
90	8.92	9.92	10.89	9.03	9.76	10.59	9.35	10.33	11.41
120	10.39	11.27	12.14	9.47	10.28	11.05	8.45	9.54	10.48
150	8.67	9.62	10.60	9.07	10.02	11.00	8.77	9.81	10.87
180	8.12	9.00	9.93	9.54	10.28	11.15	8.53	9.50	10.46
210	8.71	9.54	10.45	10.89	11.78	12.71	9.57	10.54	11.56
240	9.16	9.91	10.88	10.87	11.77	12.62	11.52	12.44	13.47
270	7.66	8.44	9.13	9.62	10.45	11.22	10.34	11.13	11.88
300	8.59	9.57	10.66	10.08	10.98	12.07	11.58	12.70	13.78
330	7.72	8.66	9.69	8.21	9.17	10.21	9.85	10.86	11.96

Table 9.7 Region 1: 95% confidence limits for mean monthly wind speed by direction, October to December

Confidence limits for Region 2 Coasts of Western Mediterranean

Direction	lower Jan	mean Jan	upper Jan	Lower Feb	mean Feb	upper Feb	lower Mar	mean Mar	upper Mar
0	6.60	7.33	8.06	6.86	7.94	8.98	7.51	8.56	9.58
30	6.03	6.79	7.58	6.56	7.33	8.18	7.46	8.43	9.47
60	5.78	6.57	7.47	5.68	6.36	7.05	8.45	9.26	10.02
90	7.21	7.95	8.76	6.87	7.71	8.53	7.52	8.48	9.43
120	6.17	6.82	7.49	7.07	7.86	8.69	6.40	7.17	7.91
150	6.38	7.10	7.85	4.75	5.23	5.78	5.33	5.92	6.47
180	6.96	7.66	8.38	5.09	5.77	6.56	4.94	5.60	6.35
210	8.34	9.20	9.88	7.32	8.12	9.09	5.57	6.26	6.97
240	7.59	8.35	9.19	7.12	7.88	8.74	6.40	7.14	7.89
270	8.80	9.89	10.83	7.84	8.60	9.58	7.54	8.32	9.18
300	8.67	9.51	10.40	8.94	9.88	11.13	8.32	9.15	10.09
330	7.87	8.77	9.70	9.01	9.99	11.02	8.69	9.57	10.53

Table 9.8 Region 2: 95% confidence limits for mean monthly wind speed by direction, January to March

Direction	lower Apr	mean Apr	upper Apr	Lower May	mean May	upper May	lower Jun	mean Jun	upper Jun
0	6.63	7.65	8.59	4.74	5.24	5.77	3.58	4.00	4.48
30	5.03	5.92	7.01	3.91	4.44	4.98	2.41	2.77	3.25
60	5.35	6.20	6.99	4.72	5.22	5.68	3.70	4.22	4.90
90	7.14	8.04	9.06	5.35	5.93	6.64	4.64	5.39	6.18
120	6.39	7.10	7.85	4.59	5.17	5.77	4.13	4.65	5.35
150	4.95	5.52	6.14	3.36	3.79	4.24	3.30	3.65	4.05
180	4.71	5.27	5.91	3.18	3.64	4.08	3.33	3.75	4.22
210	5.57	6.29	6.99	4.76	5.41	6.15	4.06	4.58	5.04
240	7.11	7.79	8.56	4.56	5.22	5.90	4.91	5.37	5.85
270	8.80	9.61	10.39	5.85	6.67	7.60	4.60	5.17	5.75
300	9.27	10.17	10.99	7.35	8.15	8.91	5.59	6.24	6.96
330	9.49	10.42	11.40	6.09	6.88	7.61	5.05	5.59	6.23

Table 9.9 Region 2: 95% confidence limits for mean monthly wind speed by direction, April to June

Direction	lower Jul	mean Jul	upper Jul	Lower Aug	mean Aug	upper Aug	lower Sep	mean Sep	upper Sep
0	3.24	3.74	4.30	2.90	3.32	3.78	3.98	4.35	4.77
30	2.72	3.02	3.42	3.16	3.48	3.77	4.06	4.54	4.98
60	3.49	3.94	4.37	3.65	3.95	4.25	4.66	5.24	6.01
90	4.45	4.98	5.57	3.84	4.26	4.76	5.52	6.11	6.71
120	3.70	4.15	4.65	3.51	3.90	4.28	4.77	5.26	5.75
150	3.66	4.00	4.39	3.52	3.85	4.19	4.58	5.00	5.43
180	3.49	3.87	4.30	3.22	3.59	3.96	4.49	5.04	5.62
210	3.27	3.73	4.32	3.22	3.67	4.14	3.98	4.64	5.40
240	4.06	4.54	4.99	3.84	4.31	4.75	4.88	5.47	6.12
270	4.45	4.92	5.35	4.33	4.81	5.27	4.54	5.08	5.71
300	5.15	5.63	6.12	5.08	5.57	6.17	4.80	5.43	6.19
330	4.45	4.93	5.43	4.65	5.16	5.71	5.07	5.58	6.14

Table 9.10 Region 2: 95% confidence limits for mean monthly wind speed by direction, July to September

Direction	lower Oct	mean Oct	upper Oct	Lower Nov	mean Nov	upper Nov	lower Dec	mean Dec	upper Dec
0	5.56	6.55	7.64	6.83	7.77	8.75	8.90	9.91	10.78
30	3.58	4.45	5.53	4.39	4.99	5.71	6.20	7.10	8.21
60	5.00	5.63	6.26	6.18	6.69	7.29	5.77	6.54	7.30
90	6.24	6.75	7.33	6.13	6.74	7.43	7.11	7.78	8.49
120	6.05	6.58	7.23	6.04	6.76	7.54	7.07	7.71	8.34
150	5.28	5.88	6.44	6.18	6.78	7.43	5.67	6.28	6.94
180	5.02	5.58	6.12	6.05	6.78	7.66	5.67	6.37	7.09
210	5.39	5.98	6.57	6.21	6.99	7.83	7.50	8.30	9.14
240	6.35	6.96	7.51	6.87	7.57	8.22	7.65	8.46	9.31
270	6.28	6.93	7.58	7.03	7.86	8.59	7.12	7.89	8.69
300	6.59	7.25	7.99	7.92	8.66	9.42	7.96	8.97	10.02
330	7.45	8.24	9.13	8.44	9.26	10.22	8.94	9.84	10.81

Table 7.11 Region 2: 95% confidence limits for mean monthly wind speed by direction, October to December

Confidence limits for Region 3 Coasts of Southern UK to Northern Iberia

Direction	lower Jan	mean Jan	upper Jan	lower Feb	mean Feb	upper Feb	lower Mar	mean Mar	upper Mar
0	6.93	7.85	8.77	8.68	9.76	10.85	8.35	9.13	10.02
30	7.73	8.48	9.32	8.34	9.31	10.32	8.68	9.47	10.29
60	6.11	6.88	7.72	5.32	6.29	7.37	7.06	8.00	8.90
90	5.01	5.71	6.43	4.20	4.96	5.79	6.64	7.65	8.82
120	5.87	6.54	7.34	4.76	5.53	6.43	5.98	6.84	7.93
150	6.41	7.26	8.19	5.36	6.19	7.05	6.94	7.82	8.69
180	9.11	10.11	11.24	8.55	9.51	10.58	6.38	7.24	8.10
210	9.61	10.57	11.66	9.56	10.56	11.65	8.22	9.21	10.53
240	9.85	10.75	11.86	10.01	11.13	12.38	8.09	9.02	9.97
270	8.63	9.82	11.13	9.07	10.19	11.29	6.70	7.48	8.33
300	7.90	8.68	9.50	7.89	8.91	9.95	6.56	7.34	8.14
330	5.75	6.67	7.61	8.04	8.92	9.84	6.80	7.60	8.52

Table 9.12 Region 3: 95% confidence limits for mean monthly wind speed by direction, January to March

Direction	lower Apr	mean Apr	upper Apr	lower May	mean May	upper May	lower Jun	mean Jun	upper Jun
0	8.88	9.79	10.64	7.98	8.70	9.53	8.97	9.75	10.57
30	9.27	10.05	10.85	9.64	10.41	11.23	9.97	10.66	11.43
60	6.88	7.51	8.21	5.24	5.93	6.71	8.98	9.55	10.20
90	5.94	6.68	7.39	3.55	4.06	4.59	4.82	5.42	6.06
120	5.21	5.89	6.74	4.72	5.31	5.94	3.92	4.44	4.97
150	6.53	7.72	9.01	6.82	7.64	8.38	4.52	5.27	6.03
180	9.00	10.00	11.08	8.06	8.92	9.74	5.91	6.71	7.60
210	8.06	9.09	10.16	6.75	7.57	8.51	7.05	7.99	8.91
240	7.41	8.61	9.70	6.36	7.24	8.14	6.38	7.18	7.94
270	7.11	7.99	9.01	5.90	6.62	7.46	5.45	6.07	6.56
300	6.92	7.67	8.57	5.61	6.27	6.98	5.62	6.03	6.48
330	8.06	8.82	9.74	6.38	7.04	7.75	6.75	7.41	8.02

Table 9.13 Region 3: 95% confidence limits for mean monthly wind speed by direction, April to June

Direction	lower Jul	mean Jul	upper Jul	Lower Aug	mean Aug	upper Aug	lower Sep	mean Sep	upper Sep
0	9.07	9.85	10.58	8.50	9.17	9.89	7.53	8.24	8.92
30	9.80	10.48	11.20	8.38	9.08	9.78	7.75	8.53	9.33
60	7.17	7.87	8.52	6.86	7.44	8.05	6.48	7.13	7.81
90	4.66	5.07	5.57	3.35	3.84	4.38	3.77	4.26	4.77
120	3.64	3.97	4.25	2.23	2.51	2.77	3.37	3.80	4.33
150	3.43	3.75	4.08	3.44	3.87	4.28	4.46	5.22	5.97
180	2.50	2.74	3.00	3.96	4.39	4.88	5.46	6.36	7.15
210	4.26	4.50	4.75	4.36	5.05	5.73	6.24	7.25	8.33
240	5.12	5.55	6.01	4.25	4.89	5.55	6.58	7.52	8.65
270	5.08	5.65	6.26	4.37	4.84	5.35	5.20	5.97	6.73
300	5.19	5.65	6.09	4.68	5.15	5.62	5.15	5.73	6.38
330	7.46	8.08	8.74	6.92	7.62	8.30	6.70	7.42	8.11

Table 9.14 Region 3: 95% confidence limits for mean monthly wind speed by direction, July to September

Direction	lower Oct	mean Oct	upper Oct	lower Nov	mean Nov	upper Nov	lower Dec	mean Dec	upper Dec
0	7.30	8.12	8.96	7.29	8.06	8.80	7.39	8.15	8.89
30	6.70	7.34	8.11	7.28	8.09	8.88	7.50	8.45	9.43
60	6.68	7.31	7.93	6.44	7.17	7.89	5.82	6.58	7.46
90	5.11	5.84	6.68	4.92	5.49	6.28	6.21	7.06	8.00
120	5.25	6.01	6.69	7.33	8.19	9.16	7.34	8.18	9.04
150	7.47	8.22	9.02	6.91	7.80	8.82	8.32	9.17	10.22
180	8.74	9.67	10.56	8.72	9.68	10.87	8.86	9.95	11.05
210	8.67	9.72	10.99	9.27	10.21	11.21	10.45	11.60	12.75
240	8.71	9.91	11.20	9.72	10.51	11.44	11.63	12.75	13.91
270	6.90	7.65	8.34	8.32	9.11	9.83	7.79	8.75	9.71
300	6.02	6.79	7.66	6.83	7.41	8.06	6.73	7.44	8.16
330	6.44	7.11	7.82	7.90	8.61	9.29	6.27	6.98	7.75

Table 9.15 Region 3: 95% confidence limits for mean monthly wind speed by direction, October to December

Confidence limits for Region 4 Coasts of Iceland to Scotland

Direction	lower Jan	mean Jan	upper Jan	lower Feb	mean Feb	upper Feb	lower Mar	mean Mar	upper Mar
0	9.19	10.37	11.76	7.46	8.41	9.44	10.07	11.17	12.65
30	8.08	9.30	10.63	7.13	8.24	9.32	8.94	10.25	11.67
60	9.66	10.84	12.04	6.62	7.63	8.71	7.64	8.75	9.85
90	10.19	11.33	12.66	9.11	10.28	11.44	8.87	9.76	10.69
120	11.42	12.62	13.74	13.36	14.81	16.32	9.69	10.67	11.57
150	11.96	13.06	14.20	12.71	13.88	15.23	11.94	13.03	14.20
180	14.20	15.64	17.20	13.66	14.83	16.05	13.08	14.32	15.69
210	15.49	17.02	18.48	13.51	14.80	16.01	12.51	13.48	14.51
240	13.22	14.57	15.98	14.33	15.69	16.89	14.57	15.67	16.89
270	13.08	14.42	15.71	11.93	13.04	14.30	13.87	15.02	16.46
300	9.39	10.94	12.58	10.27	11.58	12.98	10.74	11.85	12.80
330	8.72	10.04	11.35	9.50	10.60	11.89	10.97	11.94	13.26

Table 9.16 Region 4: 95% confidence limits for mean monthly wind speed by direction, January to March

Direction	lower Apr	mean Apr	upper Apr	lower May	mean May	upper May	lower Jun	mean Jun	upper Jun
0	10.34	11.41	12.50	7.89	8.69	9.41	7.98	8.67	9.48
30	9.20	10.18	11.11	7.45	8.20	9.09	6.57	7.55	8.81
60	9.23	10.04	10.89	7.08	7.90	8.81	6.45	7.37	8.31
90	8.97	10.01	11.13	8.69	9.59	10.55	7.18	7.98	8.88
120	9.43	10.68	12.09	9.82	10.69	11.61	6.93	7.58	8.25
150	10.95	11.81	12.81	9.69	10.48	11.18	8.07	8.92	9.76
180	10.58	11.49	12.52	9.94	10.82	11.75	8.18	8.89	9.77
210	10.98	11.83	12.70	9.77	10.71	11.74	9.10	9.86	10.56
240	10.49	11.34	12.32	8.32	9.27	10.35	8.92	9.85	10.76
270	10.14	11.23	12.34	8.14	9.05	10.03	8.14	9.00	10.03
300	9.13	10.18	11.17	7.69	8.58	9.47	7.14	8.03	9.16
330	8.71	9.60	10.61	8.22	8.98	9.77	7.41	8.25	8.99

Table 9.17 Region 4: 95% confidence limits for mean monthly wind speed by direction, April to June

Direction	lower Jul	mean Jul	upper Jul	lower Aug	mean Aug	upper Aug	lower Sep	mean Sep	upper Sep
0	7.12	8.15	9.17	9.02	10.07	11.39	9.23	10.24	11.28
30	8.19	9.15	10.09	8.69	9.75	10.92	8.58	9.49	10.42
60	8.88	9.72	10.59	6.13	6.82	7.64	6.92	7.66	8.48
90	8.52	9.14	9.75	8.28	9.11	9.91	7.84	8.83	9.71
120	7.83	8.56	9.29	8.55	9.46	10.44	7.63	8.56	9.50
150	6.69	7.45	8.23	7.76	8.55	9.45	9.88	11.05	12.24
180	7.70	8.54	9.27	8.58	9.53	10.50	11.80	12.85	13.95
210	9.02	9.63	10.32	8.60	9.46	10.39	11.89	12.88	14.06
240	7.96	8.66	9.37	9.25	10.18	11.15	10.29	11.20	12.21
270	7.79	8.60	9.48	7.59	8.34	9.20	11.36	12.36	13.55
300	7.31	8.15	8.98	6.74	7.49	8.28	8.62	9.66	10.85
330	6.98	7.80	8.63	7.34	8.35	9.41	8.33	9.35	10.50

Table 9.18 Region 4: 95% confidence limits for mean monthly wind speed by direction, July to September

Direction	lower Oct	mean Oct	upper Oct	Lower Nov	mean Nov	upper Nov	lower Dec	mean Dec	upper Dec
0	10.60	11.79	13.07	10.11	11.34	12.62	9.25	10.39	11.82
30	12.16	13.30	14.72	9.57	10.81	12.27	7.51	8.93	10.25
60	9.71	11.03	12.40	9.00	10.19	11.43	9.24	10.50	12.01
90	10.16	11.21	12.25	9.76	10.77	11.82	8.89	10.14	11.56
120	10.90	11.86	12.87	10.80	11.78	12.79	9.75	11.10	12.42
150	10.81	11.84	12.89	12.59	13.92	15.02	11.60	13.07	14.45
180	10.34	11.61	12.70	13.05	14.12	15.40	11.84	13.02	14.18
210	11.21	12.52	13.73	10.95	12.11	13.27	12.16	13.24	14.35
240	11.20	12.24	13.35	11.70	12.68	13.75	12.00	13.12	14.29
270	10.24	11.24	12.36	10.25	11.02	11.95	11.46	12.70	13.94
300	9.85	11.19	12.56	10.18	11.12	12.08	10.88	11.93	13.19
330	10.02	11.35	12.66	9.65	10.79	11.88	11.25	12.38	13.56

Table 9.19 Region 4: 95% confidence limits for mean monthly wind speed by direction, October to December

Confidence limits for Region 5 Coasts of Northwest Africa & Southern Iberia

Direction	lower Jan	mean Jan	upper Jan	lower Feb	mean Feb	upper Feb	lower Mar	mean Mar	upper Mar
0	5.22	5.83	6.36	5.82	6.55	7.34	6.71	7.26	7.87
30	6.67	7.29	7.86	6.41	7.06	7.71	7.88	8.52	9.17
60	7.36	8.00	8.71	6.37	7.08	7.87	7.38	8.09	8.80
90	6.00	6.64	7.35	6.41	7.22	8.22	7.48	8.41	9.43
120	5.19	5.91	6.67	5.04	5.60	6.22	5.35	6.08	6.93
150	6.69	7.43	8.17	3.78	4.24	4.75	5.69	6.41	7.23
180	7.84	8.56	9.51	5.03	5.70	6.44	6.38	7.18	8.04
210	8.74	9.58	10.47	7.55	8.39	9.40	5.96	6.98	8.08
240	10.31	11.25	12.21	7.56	8.47	9.31	7.18	8.20	9.22
270	9.75	10.92	12.33	7.85	8.99	10.06	7.07	7.84	8.75
300	7.62	8.56	9.46	7.60	8.47	9.46	7.25	7.88	8.64
330	3.86	4.55	5.33	6.63	7.61	8.57	6.92	7.63	8.31

Table 9.20 Region 5: 95% confidence limits for mean monthly wind speed by direction, January to March

Direction	lower Apr	mean Apr	upper Apr	lower May	mean May	upper May	lower Jun	mean Jun	upper Jun
0	7.22	7.83	8.43	6.61	7.12	7.73	6.98	7.54	8.14
30	7.60	8.27	8.98	8.19	8.80	9.36	7.78	8.34	8.89
60	7.83	8.63	9.39	8.40	9.03	9.73	7.58	8.22	8.86
90	6.42	7.36	8.17	4.12	4.97	5.82	2.72	3.19	3.78
120	3.43	4.00	4.59	3.01	3.39	3.81	1.91	2.14	2.37
150	3.08	3.45	3.77	3.47	3.90	4.33	3.08	3.41	3.82
180	5.36	6.04	6.78	6.16	6.87	7.64	2.64	2.92	3.23
210	8.18	9.24	10.32	6.25	6.88	7.54	3.90	4.50	5.14
240	7.94	8.94	9.86	5.19	5.83	6.49	4.43	4.98	5.61
270	6.73	7.56	8.40	4.66	5.22	5.73	4.21	4.66	5.08
300	5.80	6.51	7.28	4.27	4.82	5.34	4.84	5.30	5.74
330	5.95	6.58	7.22	5.12	5.65	6.28	6.00	6.62	7.19

Table 9.21 Region 5: 95% confidence limits for mean monthly wind speed by direction, April to June

Direction	lower Jul	mean Jul	upper Jul	Lower Aug	mean Aug	upper Aug	lower Sep	mean Sep	upper Sep
0	7.75	8.36	9.00	7.25	7.81	8.39	6.18	6.66	7.13
30	8.48	9.06	9.65	6.91	7.45	7.93	6.97	7.53	8.08
60	9.07	9.61	10.14	7.02	7.48	7.99	6.80	7.41	8.00
90	8.82	9.26	9.66	5.27	5.83	6.39	4.13	4.71	5.38
120	0.08	0.09	0.10	2.63	2.93	3.24	3.59	4.06	4.53
150	0.09	0.09	0.10	3.30	3.60	3.93	4.53	5.10	5.61
180	1.37	1.55	1.76	2.91	3.19	3.49	4.72	5.28	5.84
210	2.21	2.37	2.52	3.43	3.73	4.05	4.93	5.54	6.09
240	4.82	5.37	6.07	3.18	3.54	3.86	4.65	5.19	5.81
270	4.20	4.66	5.10	3.83	4.18	4.49	3.94	4.42	4.97
300	4.87	5.31	5.66	4.22	4.53	4.82	4.37	4.92	5.42
330	6.00	6.59	7.19	5.36	5.83	6.28	4.92	5.37	5.86

Table 9.22 Region 5: 95% confidence limits for mean monthly wind speed by direction, July to September

Direction	lower Oct	mean Oct	upper Oct	lower Nov	mean Nov	upper Nov	lower Dec	mean Dec	upper Dec
0	5.30	5.77	6.22	5.26	5.84	6.43	5.20	5.75	6.32
30	5.89	6.45	7.03	6.59	7.16	7.71	6.59	7.34	7.99
60	5.85	6.48	7.04	6.87	7.37	7.88	6.21	6.86	7.57
90	4.71	5.20	5.77	6.38	7.03	7.58	5.33	5.87	6.45
120	3.90	4.57	5.29	4.89	5.52	6.25	5.37	6.33	7.26
150	4.73	5.49	6.30	6.41	7.17	8.02	6.96	7.75	8.53
180	6.06	6.82	7.69	7.10	7.89	8.76	9.46	10.42	11.51
210	8.01	9.01	9.99	8.32	9.18	10.21	10.00	11.06	12.19
240	6.99	7.79	8.64	9.25	10.36	11.48	9.23	10.26	11.38
270	5.14	5.96	6.70	7.96	8.95	10.17	7.22	8.14	9.30
300	4.06	4.46	4.93	6.19	7.01	7.96	6.60	7.54	8.55
330	4.46	4.91	5.40	4.43	4.94	5.51	5.67	6.39	7.13

Table 9.23 Region 5: 95% confidence limits for mean monthly wind speed by direction, October to December

Confidence limits for Region 6 Coasts of Eastern Mediterranean

Direction	lower Jan	mean Jan	upper Jan	lower Feb	mean Feb	upper Feb	lower Mar	mean Mar	upper Mar
0	7.98	8.68	9.40	8.04	8.87	9.72	6.15	6.97	7.89
30	6.96	7.60	8.30	7.32	8.12	8.97	5.08	5.69	6.33
60	5.15	5.77	6.39	4.58	5.28	5.99	4.38	4.85	5.34
90	5.36	5.81	6.37	5.15	5.58	6.13	5.07	5.72	6.29
120	6.61	7.39	8.14	6.15	6.99	7.95	6.29	7.09	8.02
150	6.21	6.90	7.68	8.61	9.66	10.67	6.91	7.77	8.47
180	6.50	7.39	8.23	9.11	9.94	10.90	7.66	8.47	9.28
210	8.45	9.40	10.40	8.36	9.41	10.45	7.33	8.15	9.10
240	8.79	9.75	10.71	8.01	8.86	9.78	7.60	8.69	9.69
270	5.66	6.33	7.10	5.39	5.88	6.43	6.24	6.92	7.61
300	5.37	6.06	6.75	6.51	7.22	7.95	6.19	6.77	7.49
330	6.66	7.21	7.83	8.19	9.05	10.00	6.79	7.54	8.38

Table 9.24 Region 6 95% confidence limits for mean monthly wind speed by direction, January to March

Direction	lower Apr	mean Apr	upper Apr	lower May	mean May	upper May	lower Jun	mean Jun	upper Jun
0	5.19	5.81	6.52	5.38	5.93	6.58	7.35	7.86	8.32
30	4.76	5.29	5.86	3.23	3.75	4.32	4.17	4.84	5.54
60	3.56	4.04	4.60	3.15	3.76	4.51	3.20	3.57	3.99
90	4.89	5.39	5.95	3.92	4.54	5.38	3.21	3.50	3.81
120	6.47	7.25	8.04	4.99	5.62	6.22	4.26	4.70	5.21
150	7.86	8.70	9.66	6.24	6.92	7.62	5.07	5.56	6.11
180	6.47	7.20	7.85	6.06	6.85	7.69	4.01	4.48	5.01
210	5.46	6.18	7.02	4.40	5.02	5.69	3.23	3.64	4.10
240	5.76	6.56	7.35	4.46	4.99	5.58	4.17	4.68	5.27
270	5.41	5.91	6.47	4.93	5.45	6.06	5.52	5.95	6.42
300	5.65	6.19	6.84	6.21	6.68	7.13	6.31	6.71	7.17
330	5.58	6.12	6.68	6.16	6.65	7.12	7.19	7.62	8.08

Table 9.25 Region 6 95% confidence limits for mean monthly wind speed by direction, April to June

Direction	lower Jul	mean Jul	upper Jul	lower Aug	mean Aug	upper Aug	lower Sep	mean Sep	upper Sep
0	8.92	9.40	9.86	8.54	8.93	9.31	7.42	7.92	8.52
30	8.39	8.84	9.27	8.43	8.87	9.29	6.34	7.02	7.73
60	3.77	3.99	4.21	0.07	0.08	0.08	3.54	4.10	4.66
90	0.75	0.77	0.79	0.09	0.10	0.11	3.85	4.38	4.89
120	0.67	0.69	0.70	0.09	0.10	0.11	3.73	4.05	4.38
150	2.21	2.37	2.54	0.07	0.08	0.09	3.69	4.01	4.33
180	2.15	2.33	2.49	4.92	5.08	5.24	4.11	4.60	5.13
210	6.93	7.08	7.23	4.57	4.75	4.94	4.11	4.73	5.42
240	6.11	6.53	7.00	6.18	6.59	6.96	4.44	4.99	5.61
270	5.82	6.17	6.50	5.82	6.12	6.45	5.01	5.44	5.83
300	7.47	7.91	8.30	6.83	7.20	7.65	5.53	5.91	6.23
330	8.78	9.26	9.71	7.96	8.37	8.77	7.03	7.50	7.98

Table 9.26 Region 6 95% confidence limits for mean monthly wind speed by direction, July to September

Direction	lower Oct	mean Oct	upper Oct	lower Nov	mean Nov	upper Nov	lower Dec	mean Dec	upper Dec
0	5.52	6.18	6.80	7.18	7.96	8.73	7.76	8.53	9.35
30	4.68	5.28	5.81	5.85	6.65	7.54	5.72	6.35	6.96
60	3.37	3.81	4.18	4.09	4.54	5.14	4.28	4.70	5.14
90	3.63	3.96	4.31	3.28	3.73	4.25	4.02	4.46	4.83
120	3.74	4.21	4.66	4.53	5.18	5.89	4.35	4.74	5.22
150	4.95	5.56	6.24	6.02	6.61	7.14	6.55	7.27	8.04
180	4.94	5.49	6.17	6.52	7.18	7.81	8.48	9.50	10.52
210	4.80	5.44	6.11	7.75	8.59	9.47	8.40	9.16	9.96
240	4.41	4.93	5.47	7.10	7.72	8.48	7.47	8.37	9.30
270	4.32	4.69	5.09	4.68	5.13	5.65	5.14	5.77	6.38
300	4.84	5.30	5.80	5.05	5.55	6.08	6.23	6.90	7.59
330	6.12	6.79	7.41	6.50	7.22	7.95	6.68	7.53	8.50

Table 9.27 Region 6 95% confidence limits for mean monthly wind speed by direction, October to December

9.6 References

1. Davison, A C and D V Hinkley (1997) Bootstrap Methods and Their Application. Cambridge Series in Statistical and Probabilistic Mathematics, No 1, Cambridge University Press.

2. Efron, B (1983) Bootstrap methods: another look at the Jack-knife. Annals of Statistics, 7, 1-26

3. Palutikof, J P and T Holt (2000) Synoptic-scale wind data suitable for the preliminary assessment of the offshore wind resource, Proceedings of the OWEMES 2000 Conference, Siracuse, Sicily 13-15 April 2000, ENEA.

4. Watson, G M, J A Halliday, J P Palutikof, T Holt and others (2000) POWER – a methodology for predicting offshore wind energy resources, Proceedings of the OWEMES 2000 Conference, Siracuse, Sicily 13-15 April 2000, ENEA.

CHAPTER 10 : Comparisons with measured data

Chapter authors:

Sections 10.1-10.2 : Drs. J.P. Coelingh, Dr. L. Folkerts, Dr. E.J. van Zuylen, Ir. G.F.M. Wiegerinck (Ecofys)
Sections 10.3 : G M Watson and Dr R A Brownsword (CLRC Rutherford Appleton Laboratory)
Sections 10.4 : Dr R J Barthelmie (Risø National Laboratory) and other named authors
Sections 10.5 : Dr R A Brownsword (CLRC Rutherford Appleton Laboratory)

10.1 Introduction

Clearly it is important to establish the accurate of predictions of offshore wind conditions made within POWER. This has been achieved by comparing POWER's model results with measured data from sites off the coasts of The Netherlands (Measuring Network Zeeland (ZEGE) and Measuring Network North Sea (MNZ)), Denmark (Horns Rev and Læsø Syd) and the Mediterranean. Comparison of the POWER model results with those of an earlier EU study, JOUR0072 (Study of offshore wind Energy in the European community), carried out by Germanischer Lloyd AG and partners has also been made .

10.2 The Netherlands

10.2.1 Introduction

This section deals with three main subjects. First an analysis is presented of the wind speed observations of the ZEGE network. It is claimed these have not been processed, and therefore should provide a suitable reference. Then an analysis is made of the MNZ data. Here the situation is different: it is known that the data have been processed, and also that the processing method has not been consistent over the years. Therefore it has to be investigated how the processing has changed over the years, because it is necessary to have a consistent data set. The ZEGE data are invaluable as reference in this respect.

Finally, the reconstructed observed data are being used to compare against calculated results using the method developed in the POWER project. The scarce data that are available should match the results of the calculations. After that some generally conclusions will be drawn.

10.2.2 Data sources

An overview of all offshore locations where observations are being made is given in Figure 10.1 as taken from the SeaNet internet site [Internet SeaNet Workshop]. The locations are a combination of existing oil or gas platforms, a light-isle and coastal meteorological masts. On the internetsite it is also shown on which of the offshore locations wind speeds and/or temperatures and/or wave parameters are being collected. The main differences between ZEGE and MNZ are summarised in Table 10.1.

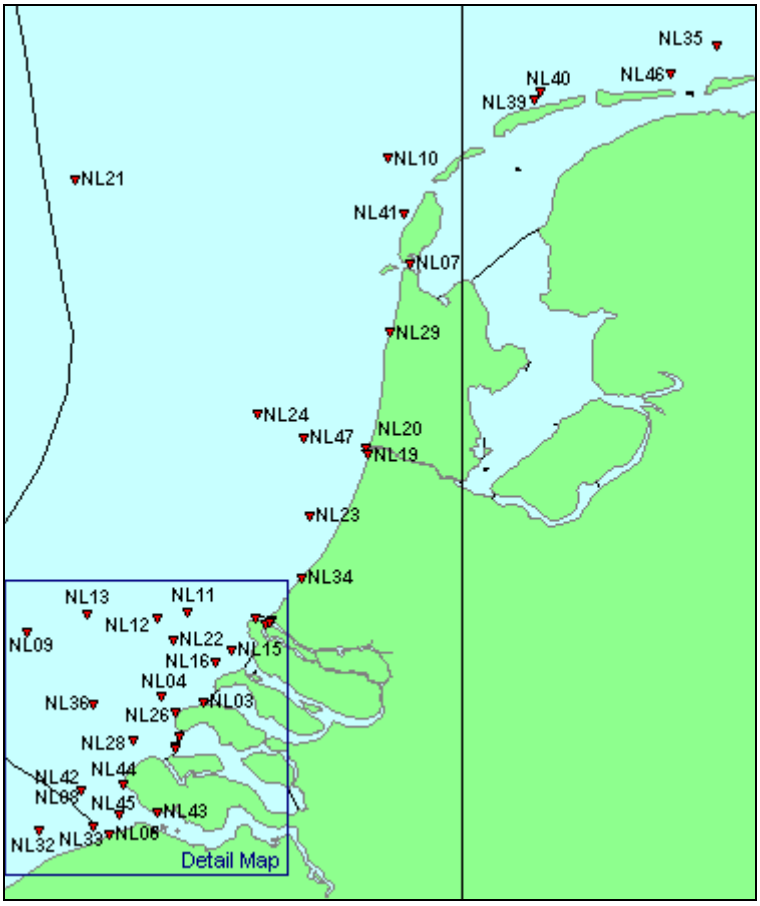

Figure 10.1: Overview of offshore locations with meteorological observations [Internet SeaNet Workshop].

The Measuring Network North Sea makes use of various types of existing offshore structures. Therefore observation heights for wind speeds also vary, which made it necessary to convert the wind speeds to other, standard, heights. In the course of the years however, the data processing has changed considerably leading to inconsistent time series that have to be studied scrutinously to meet the standards required.

The wind speeds observed at these various locations have recently become available for research purposes, and have been subject of thorough investigation to establish their use for climatological study as necessary for our goals. It must be kept in mind that these data were not primarily collected for use in this type of study. The care and attention given to the gathering, processing and storing of the observations may not have been up to the standard required for wind energy purposes. Therefore the quality and consistency of the data must be checked before drawing any conclusions.

Table 10.1: Comparison of Measuring Network North Sea and Measuring Network ZEGE.

Data source	**MNZ**	**ZEGE**
Location	North Sea and Dutch coast; mainly Dutch territorial waters	Limited to province of Zeeland, inland waters and a few kilometers of the coast
Observation	Existing offshore structures like light isles, oil and gas platforms	Especially equipped mast with standard anemometer height
Observation height	varying from 15.0 to 103 m above MSL	16.5 m above MSL
Data interval	1 hour	10 minutes

Responsibility	RWS – dir. North Sea & KNMI	RWS – dir. Zeeland

This has to do with the degree of accuracy and detail that is required for offshore wind energy purposes. For most uses of wind speed observations (weather forecasts, shipping, offshore activities, dike protection) an accuracy of 10% or 20% is quite acceptable. In wind energy projects such margins in average wind speeds may well determine whether or not an investment of many millions is profitable or not.

The character of the data sources as mentioned here led us to using the ZEGE data as a reference for the MNZ data. Whenever the information was either inconsistent, non-existent or unreliable a comparison between the two sources could sometimes be conclusive.

The results here are given for the period of 1985–1997, which is the selected reference period within the POWER-project. Although usually the wind speeds have been converted to a standard height of 10 m and are sometimes recalculated in knots, here all wind speeds have been recalculated for the original observation height (if necessary). There are three main reasons for that: the first is that the height conversion factors have changed throughout the period 1985–1997, making recalculation necessary anyway. The second is that a fixed conversion factor (if deduced properly) may well be valid on average, but the effects of stability and roughness are indeed topics of research. The third is that a particular aspect interesting in describing the wind climate is the calculation of the Weibull parameters. For this an unperturbed frequency distribution is needed (or as much as possible).

10.2.3 Measuring Network ZEGE

10.2.3.1 Description

Within the Measuring Network ZEGE wind data are gathered at 10 locations as shown in Figure 10.2. Some further specifications are given in Table 10.2.

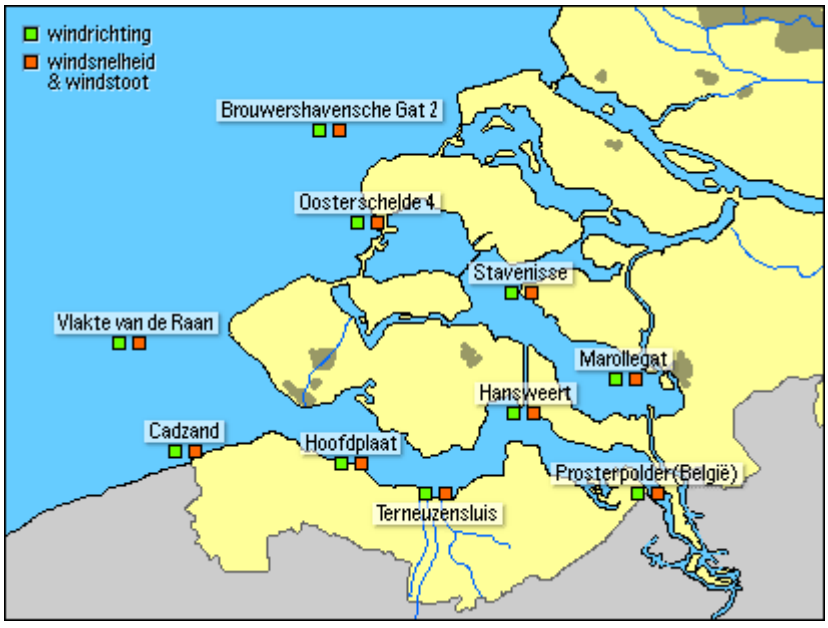

Figure 10.2: Overview of measuring locations for wind data within the Measuring Network ZEGE.

Table 10.2: Description of offshore locations with wind speed observations.

ID[1]	Name	Code	Northing[2]	Easting[2]	Height (m)[3]	Period
NL27	Oosterschelde	OS4	51º39'24"	03º41'43"	16.5 m	1982–1998
NL04	Brouwershavensche Gat	BG2	51º46'06"	03º37'06"	16.5 m	1982–1998
NL42	Vlakte van de Raan	VLR	51º30'16"	03º14'37"	16.5 m	1988–1998
NL14	Prosperpolder	PRO	n.a.	n.a.	16.5 m	1989–1997
NL18	Stavenisse	STA	n.a.	n.a.	16.5 m	1990–1997
NL05	Cadzand	CAD	51º22'48"	03º22'39"	17.0 m	1991–1998
n.a.	Hoofdplaat	HPL	n.a.	n.a.	16.5 m	1991–1998
n.a.	Hansweert	HNW	n.a.	n.a.	16.5 m	1987–1997
n.a.	Terneuzen	TER	n.a.	n.a.	26.5 m	1990–1998
n.a.	Marollegat	MAR	n.a.	n.a.	16.5 m	1982–1997

[1]ID as given in the documentation of SeaNet (if available)
[2]position given if available; otherwise the reader is referred to Figure 10.2
[3]above Mean Sea Level (MSL)

10.2.3.2 Statistical analysis

Rijkswaterstaat that provided the data stated they had not been processed. To check this, some standard statistical analysis was performed. This includes annual mean wind speeds, monthly and hourly variations, distribution of the wind speed per sector and the determination of histograms and the derivation of the Weibull parameters.

10.2.3.3 Annual mean wind speeds

An important indication for the consistency of the wind speed time series is a comparison of the interannual variability of the wind speed for the different stations. Figure 10.3 shows a similar pattern for all stations. Roughly speaking, the mean wind speed decreases for locations situated more inland, except for MAR. The deviation is probably caused by the large water area around MAR. The most deviating behaviour is observed for HPL: from 1995 to 1997, the annual mean wind speeds appear to be considerably higher than expected compared to the other stations.

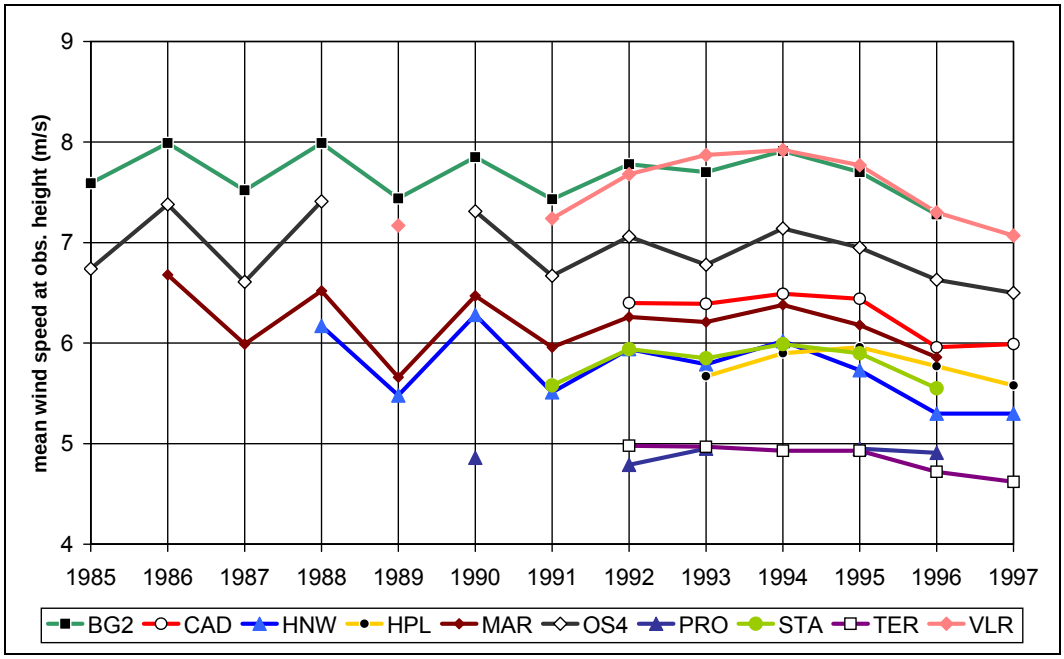

Figure 10.3: Annual mean wind speeds for the stations of ZEGE.

The mean wind speeds in Figure 10.3 at observation height are shown only in case the availability of data exceeds 90%.

To compare the locations more quantitatively we define a measure for the interannual variability ($\Delta_{interannual}$) as follows:

$$\Delta_{\mathrm{int}\,erannual} = \frac{U_{annual,\max} - U_{annual,\min}}{U_{annual,mean}} \times 100\%$$

The results for the calculations are shown in Table 10.3.

Table 10.3: Interannual variability for the stations of ZEGE.

Station	PRO	HPL	TER	CAD	STA	VLR	BG2	OS4	HNW	MAR
$\Delta_{interannual}$	3%	7%	7%	8%	8%	11%	13%	15%	17%	20%

Calculation of $\Delta_{interannual}$ shows values between 3% and 20%. The variability tends to be somewhat larger for the coastal stations than for the ‘inland’ stations, with the exception of MAR as explained before.

10.2.3.4 Monthly variations

Figure 10.4 shows the annual course of the wind speeds for the ZEGE locations at observation height for the period from 1990–1997 . The lines for VLR and BG2 are almost identical. The patterns of OS4 and MAR are similar, but the absolute wind speeds are somewhat lower. The courses of STA, HPL, PRO and TER are roughly similar to each other but differ somewhat more from the course of the 'offshore' stations. The pattern of HNW and CAD deviates significantly from the patterns of the other stations. The most probable explanation is the strong dependence on the wind direction for these stations as they are located on the coast line and are subject to the land/sea transition the most.

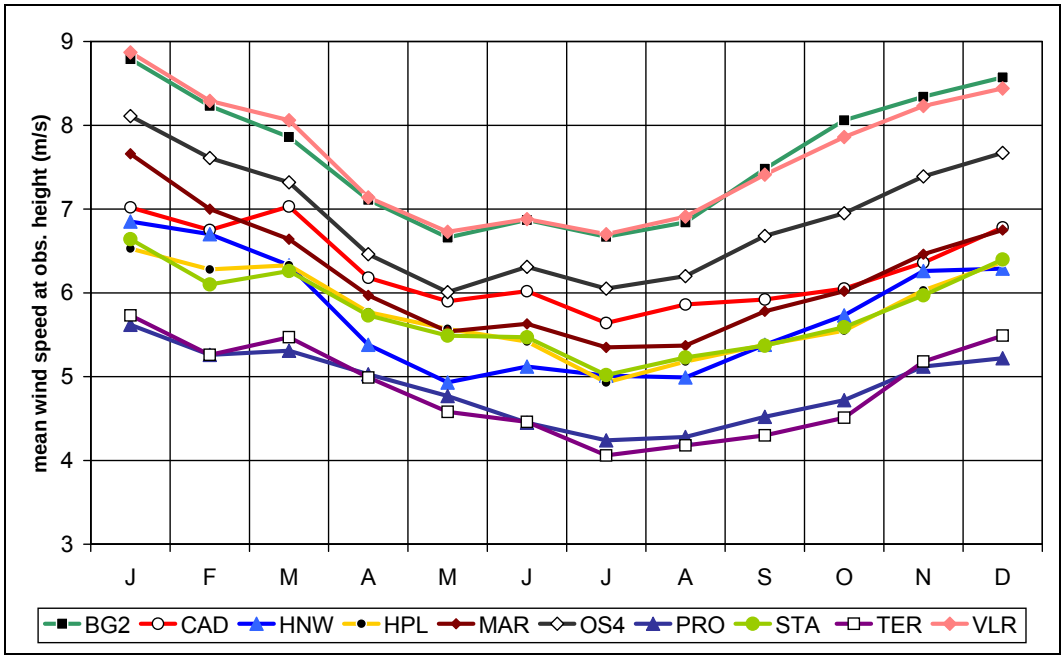

Figure 10.4: Monthly variations of the wind speed for the stations of ZEGE.

As expected the winter months show far higher wind speeds than the summer months. To quantify this a measure called continentality (C_{month}) was calculated, defined as:

$$C_{month} = \frac{U_{month,\max} - U_{month,\min}}{U_{month,mean}} \times 100\%$$

Table 10.4 gives an overview of the values calculated for all locations.

Table 10.4: Continentality (monthly) for the stations of ZEGE.

Station	CAD	BG2	HPL	PRO	STA	VLR	OS4	HNW	TER	MAR
C_{month}	22%	28%	28%	28%	28%	28%	30%	33%	34%	37%

The calculated values of C_{month} range from 22% (CAD) to 37% (MAR). No clear correlation between location and C_{month} could be derived based on these data.

10.2.3.5 Hourly variations

The hourly variations for the stations is shown in Figure 10.5. Most stations exhibit a day time maximum resulting from the heating of the earth surface. Only VLR and BG2 which are located 'offshore' do not show this, and even tend to have a slight day time minimum. The cause for this is not clear at this moment and requires more detailed analysis.

The ratio of the maximum versus minimum wind speed decreases when getting closer to open sea. An exception to this is MAR that is relatively far inland, but is situated within a large water mass.

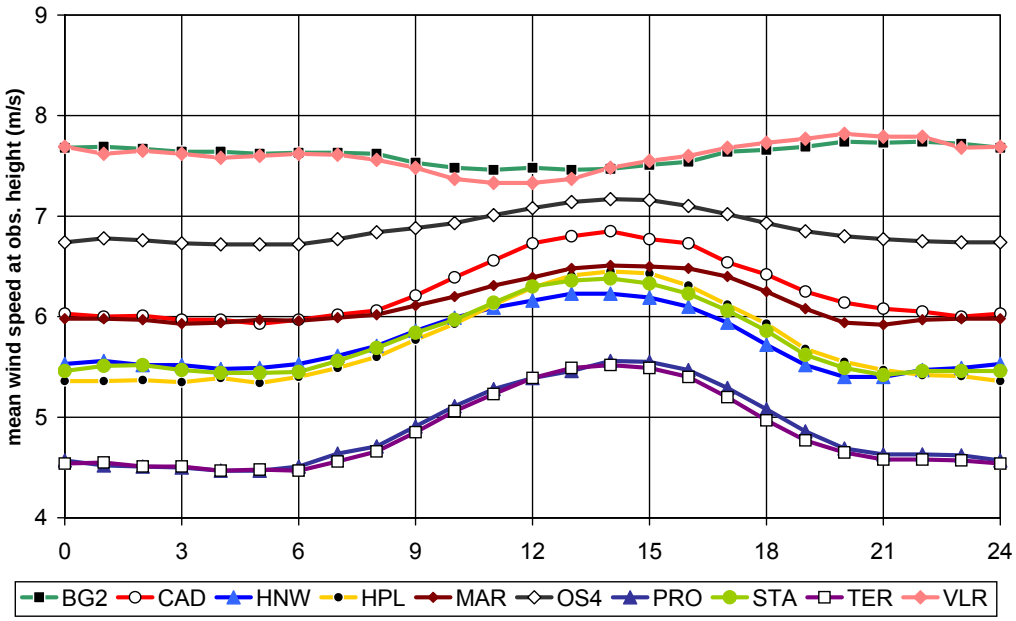

Figure 10.5: Hourly variations of the wind speed for the stations of ZEGE.

As a measure for the influence of the land mass on the behaviour of the hourly variations the measure C_{hour} (analogously to previous calculations) has been defined as follows:

$$C_{hour} = \frac{u_{hour,\max} - u_{hour,\min}}{u_{hour,mean}} \times 100\%$$

The results have been calculated for all stations and are shown in Table 10.5.

Table 10.5: Continentality (hourly) for the stations of ZEGE.

Station	BG2	VLR	OS4	MAR	HNW	CAD	STA	HPL	TER	PRO
C_{hour}	4%	6%	7%	10%	14%	15%	17%	19%	22%	22%

The calculated values of C_{hour} range from 4% (BG2) to 22% (TER and PRO). This shows that the further the location is located offshore the smaller the day time maximum in the diurnal course, as would be expected, but even resulting (slightly) in the inverse behaviour as shown for VLR and BG2 which cannot be explained and would need further investigation.

10.2.3.6 Variations by wind direction

Finally, the wind speeds by sector have been depicted in Figure 10.6. The wind sectors are defined as is customary: they are 30º each, numbered in clockwise order while sector 1 is centred around the north (345º–15º).

The lines for BG2 and VLR nearly coincide. The wind speed at OS4 is somewhat lower: with fetch over land (North-East) the wind speed is considerably lower, with fetch over sea (sector 9) the wind speeds are comparable. The importance of fetch of land or sea is also observed for the other stations.

The wind speed at CAD is larger than at OS4 for sectors 1 to 3 (CAD: fetch over sea while OS4 has a fetch over land), in sector 4 to 7 this is the other way round and so are the wind speeds. In sector 9 to 12 both stations have a fetch over sea and wind speeds are comparable. Similar behaviour is observed when comparing MAR with PRO, STA or HNW.

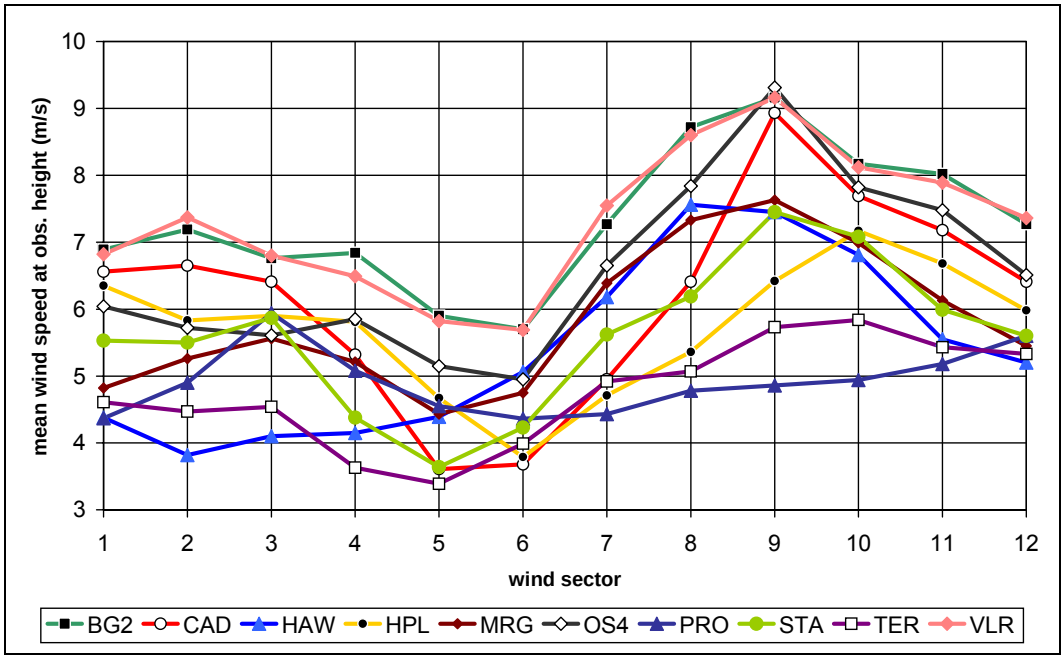

Figure 10.6: Mean wind speeds per sector for the stations of ZEGE.

Figure 10.7 shows the direction distribution for all stations. The course is more or less similar for all stations. Major exception is that for some stations sector 8 shows the highest frequency of occurrence, while sector 9 does for the other stations. This may be due to the way the original values of the wind direction have been grouped statistically into sectors.

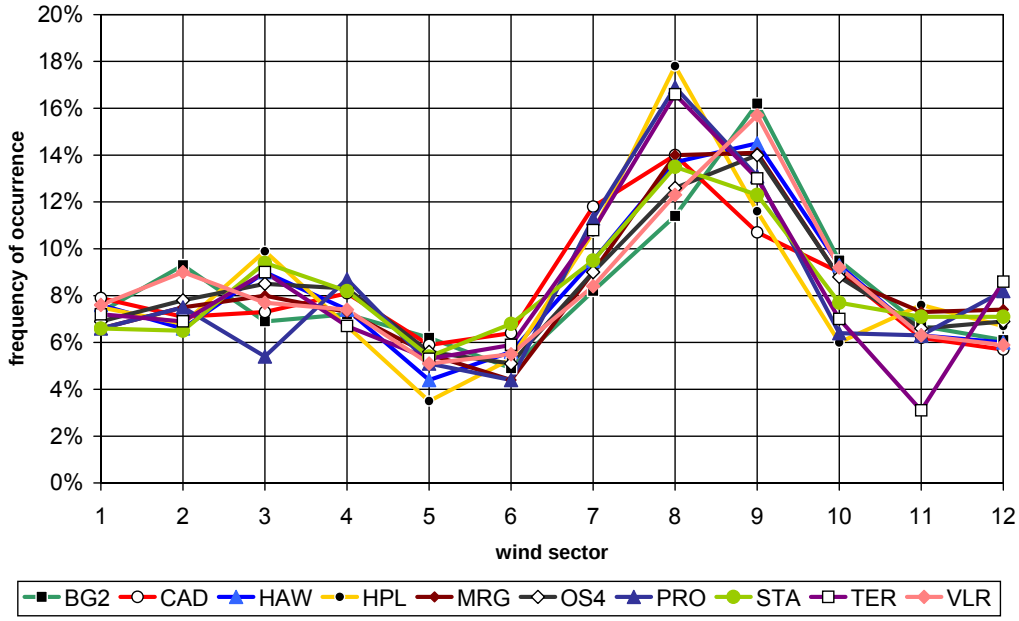

Figure 10.7: Frequency of occurrence per sector for the stations of ZEGE.

10.2.3.7 Histograms and Weibull parameters

The histograms were calculated for every year separately and for the complete period from 1985 to 1997. The resulting Weibull parameters are shown in Table 10.6. As an example the histogram for BG2 is shown in Figure 10.8.

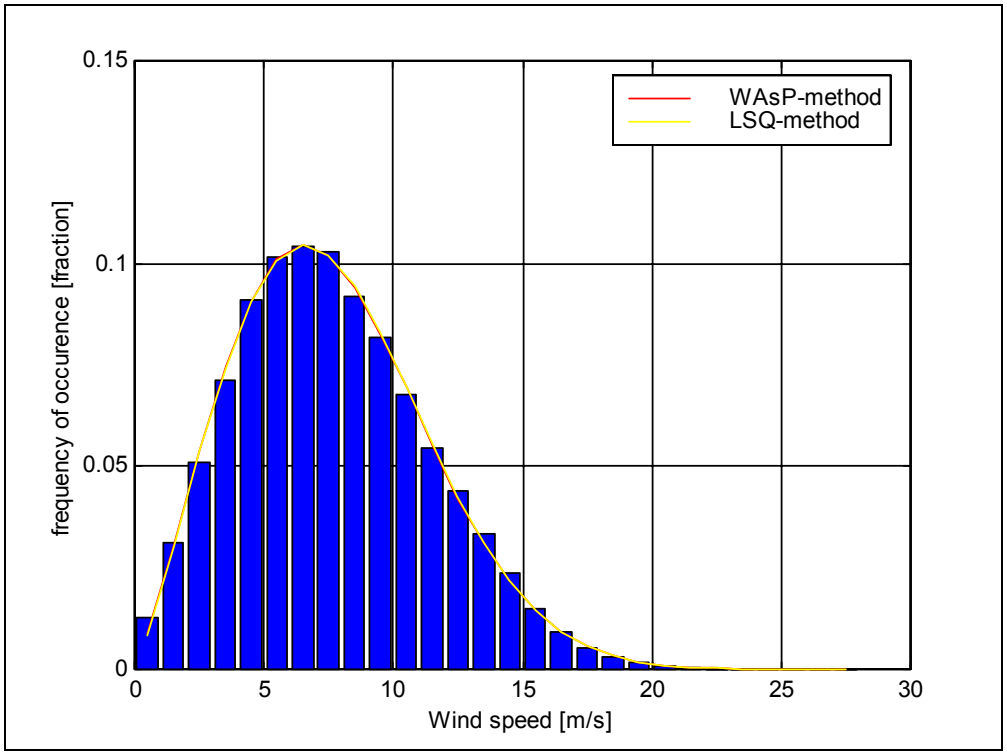

Figure 10.8: Histogram of wind speed for BG2 from 1985 to 1997 and the Weibull fit. Weibull parameters are determined according to the WAsP-method and the least squares method.

Table 10.6: Weibull factors, mean wind speed and percentage of available data for the stations of ZEGE.

Station	Period	Mean wind speed (m/s)	k	a (m/s)	Availability (%)
OS4	1985–1997	6.92	1.97	7.78	96
BG2	1985–1997	7.65	2.18	8.70	94
VLR	1988–1997	7.55	2.16	8.59	88
PRO	1989–1997	4.87	1.96	5.46	86
STA	1990–1997	5.77	1.80	6.38	87
CAD	1991–1997	6.27	1.77	6.91	97
HPL	1991–1997	5.75	1.89	6.40	94
HNW	1987–1997	5.76	1.76	6.42	92
TER	1990–1997	4.86	1.80	5.40	86
MAR	1985–1997	6.17	2.01	6.99	94

[1]mean wind speed and availability for wind speed and wind direction valid at the same time. The difference with only wind speed valid is negligible (at maximum 0.01 m/s).

The values of the Weibull k-parameter (shape factor) are between 1.77 and 2.18. The largest values are for the stations furthest offshore (BG2 and VLR). The relation between the mean wind speed and the Weibull a-parameter (scale factor) is rather insensitive for values of k between 1.5 and 4.0.

The availability of all stations is good: on average over 90% for all stations. An indication that data may have been processed is the rare occurrence of certain values in the time series. The number of zeros is compatible with the Weibull distributions for all years for nearly all stations. The exceptions are BG2 in 1986 (149 zeros) and PRO in 1990 and 1991 (roughly 80 zeros). Probably missing data are

replaced by zeros. There is at least not a long period of zeros and based on the neighbouring values, wind calm is not impossible at the times in the series.

According to the data sets for BG2, the north sector occurs very often in 1986 and 1987 for wind speeds between 0 and 1 m/s. Most probably, the wind direction of periods with varying wind speeds (occurring especially at low wind speeds) is set to 0, and subsequently interpreted as 0 , therefore grouped in sector 1. This is not observed at other years or for other stations. As these wind speeds are irrelevant for wind energy purposes (below cut-in wind speed of wind turbines), this does not disqualify the use of BG2 for wind energy purposes.

10.2.3.8 Conclusions

The data of ZEGE as obtained from Rijkswaterstaat have been analysed statistically. It was claimed no data processing had been performed other than some basic quality checks. In order to verify this claim, and also to learn about the wind climate several steps were undertaken. In summary, the following points are of interest.

- The annual mean wind speeds of the data sets from ZEGE exhibit a consistent behaviour. For HPL, the wind speeds are relatively high for 1995 to 1997.

- The annual course for the ZEGE stations is as expected. No irregularities were observed.

- The diurnal courses for VLR and BG2 show a small negative peak. We do not know an explanation for this. The other stations do show a slight positive peak. The relative magnitude of this peak decreases for stations further offshore.

- The dependence of the wind speed on the sector was calculated. The variations found can be explained by fetch over land and fetch over sea.

- No irregularities were observed within the histograms. The magnitude of the Weibull factors was as expected.

- No major irregularities were observed in the data set itself.

It indeed appears that the data have not been processed. Therefore, the conclusion is warranted that the data are of sufficient quality and consistency to use as reference to validate the MNZ data.

10.2.4 Measuring Network North Sea (MNZ)

10.2.4.1 Description

The locations of the Measuring Network North Sea (MNZ) are various offshore constructions, like gas and oil platforms, and also a light-isle. As an exception MPN is a platform solely in use for monitoring purposes and research projects. The various locations in use within MNZ have been summarised in Table 10.7. Also given are the observation heights (for wind speed) and the locations. In Figure 10.9 the locations closest to The Netherlands have been depicted, together with the locations of ZEGE located in the North Sea.

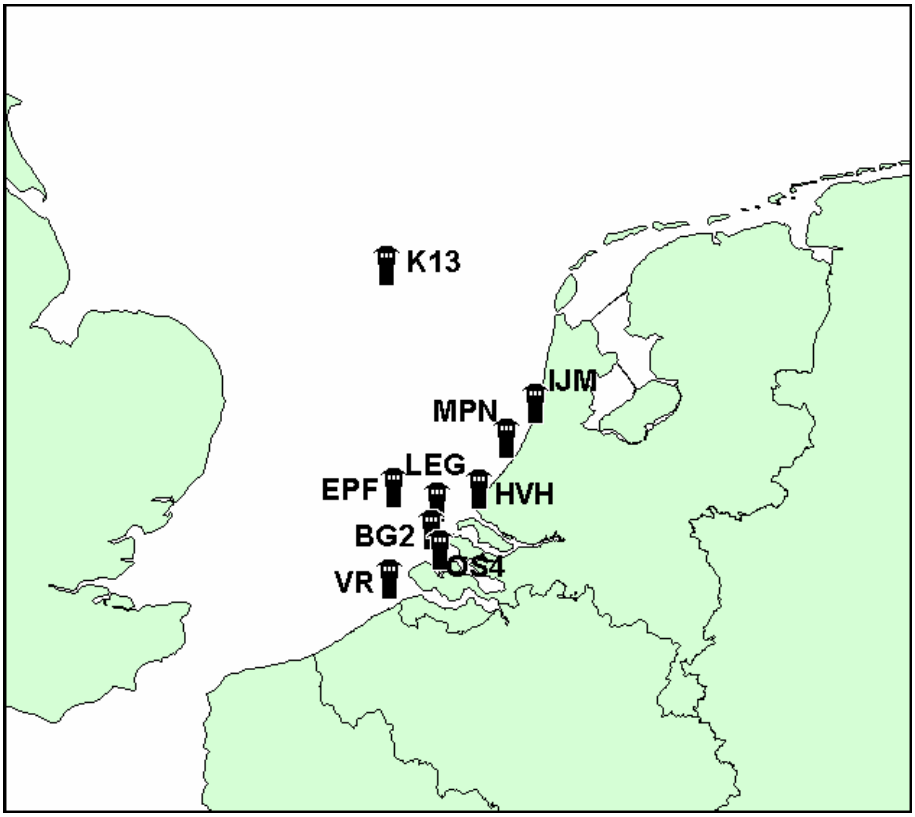

Figure 10.9: Overview of locations in the North Sea (some locations are outside the map).

Three institutes collaborate in running the MNZ. RWS (dir. North Sea) is principally responsible for the maintenance of the hardware and the data collection. KNMI is responsible for the validation of the data, and if necessary the filling of any gaps. Finally RIKZ maintains a central database called DONAR of all types of observations, meteorological, oceanographical, but also chemical and biological. From this database most observations were made available to us.

Table 10.7: Position and water depth of the locations within the Measuring Network North Sea (MNZ).

ID	Name	Code	Northing	Easting	Period	Water depth
NL20	IJmuiden-harbour	IJM	52º27'47"	04º33'22"	1989–1997	n.a.
NL24	IJmuiden depot	IJM	52º33'30"	04º03'30"	1989–1997	21 m
NL23	Measuring post Noordwijk	MPN	52º16'23"	04º17'50"	1987–1997	18 m
NL22	Light Isle Goeree	LEG	51º55'29"	03º40'06"	1991–1997[2]	22 m
NL13	Euro platform	EUR	51º59'55"	03º16'35"	1987–1997	32 m
NL14	F3-3B Platform	F3P	54º51'14	04º43'39	1995–1997	n.a.
NL18	Hoek van Holland	HVH	51º59'06"	04º03'00"	1985–1997	n.a.
NL21	K13 platform	K13	53º13'04"	03º13'13"	1985–1997	30 m
NL01	Auk platform	AUK	56º23'59"	02º03'56"	1987–1995	85 m

For the stations of MNZ the observation height differs per location. According to WMO guidelines, wind speeds have to be reported at 10 m above MSL. Therefore, the measured wind speeds are converted from observation height to 10 m by means of a fixed conversion factor. These factors were determined in 1977 by the North Sea Meteorological Panel. Eight different formulas for conversion to 10 m MSL were discussed. The roughness length z_0 of the sea varied within these formulae from

roughly $2x10^{-4}$ m to $18x10^{-3}$ m. As a compromise, the average of these options was taken for all stations. The result corresponds relatively well to the power law with a value of 0.13 for the exponent:

$$\frac{u(z)}{u(10)} = \left(\frac{z}{10}\right)^{0.13} \qquad (1)$$

with u the wind speed in m/s and z the height above MSL in m. This implies a roughness length of $12.3x10^{-3}$ m.

Later on, it was concluded that the resulting conversion factors were too large, resulting in a too low wind speeds at 10 m height. [Benschop (1996)] derived new conversion factors based on a more physical basis. The new conversion factors were used from July 12, 1995 onwards [Benschop (2000)]. An overview of both the old and revised conversion factors is given in Table 10.8.

Table 10.8: Characteristics of the offshore locations of MNZ.

Code	Observation height	Conversion factor	Revised conversion factor[1]
AUK	101.3 m	1.355	1.270
EPF	29.1 m	1.148	1.120
F3P	59.2 m	1.260	1.200
K13	73.8 m	1.298	1.230
LEG	22.5 m	1.120	1.150
	38.3 m	1.120[2]	
MPN	27.6 m	1.142	1.120

[1]as proposed by [Benschop (1996)] commencing date: July 12, 1995.

[2]in 1990 the mast at LEG was replaced by a higher mast at another position on the platform; the reason for this was that at the old position the wind flow was obstructed too much from certain directions; therefore the data from this earlier period were discarded; unjustly not adapted to new situation, at April 6, 1990, the observation height was changed from 22.5 m to 38.3 m.

NB:

Note that each year all wind speed data from the measuring Network North Sea are supplied to the KNMI for validation. After validation, the KNMI sends the data back to RIKZ. Unfortunately, not all measuring sets were complete. Therefore, it is possible that periods exist where the old conversion factors are used after July 1995. From the analysis of monthly average wind speeds, we could not deduce this and hence did not take this into account in our reprocessing and further analysis.

Since the early 80s when Measuring Network North Sea has been instituted then reliable and consistent wind speed observations have been made at various locations. Some of these observations were subject of earlier studies (see e.g. [Benschop (1996)], [Cleijne at al. (1991)] and [Coelingh et al. (1997)]). The same goes for the observations of ZEGE (see e.g. [Coelingh et al. (1998)]).

Data have been received from the DONAR database of the RIKZ (Rijksinstituut voor Kust en Zee) for Measuring Network North Sea. Data from the climatological database of the Royal Dutch Meteorological Institute KNMI, KEMA (obtained via RWS) and data of Voluntary Observing Ships have been used for reference to complete or validate data.

Basically, the source of all wind speed measurements is the same. However, the data have been distributed to several parties, and from there they have been processed and stored in different ways. Therefore it is not always exactly clear, particularly for periods in the (far) past, who has been responsible for each step. For the POWER project, the period of interest is from 1985–1997

A short summary of the availability for wind speed data is given in Table 10.9.

Table 10.9: Overview available data at RIKZ.

Station	Period
AUK	1981–7/95
EPF	1983–present
F3P	1995–1998
K13	1981–present
LEG	1981–present
MPN	1983–present

- all wind speeds are 10-minute means;
- all wind speeds are converted to 10 m height by division with the appropriate conversion factor;

10.2.4.2 Annual mean wind speeds

The annual mean wind speeds have been calculated the six offshore stations of MNZ. The annual mean wind speeds were converted to observation height by multiplying with the relevant conversion factor . Based on a comparison of RIKZ and RWS (dir. Zeeland) it appears that the conversion from m/s to knots was terminated as from 1/1/1991. The course of the annual means per station converted to observation height is plotted in Figure 10.10. In this figure, the conversion from knots to m/s is taken into account until 1/1/1991.

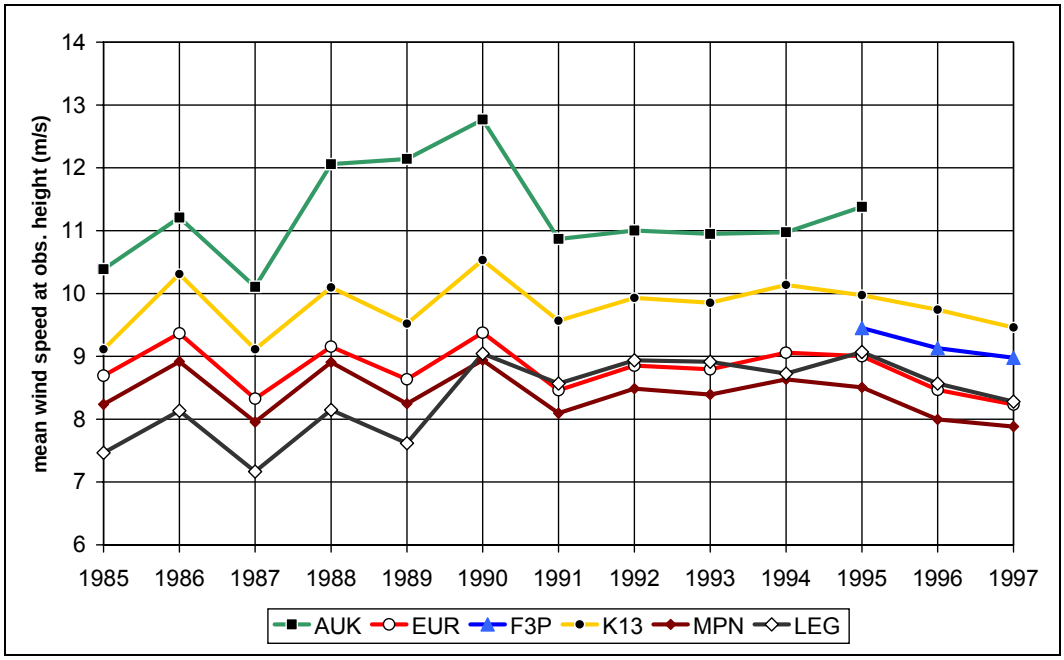

Figure 10.10: Annual mean wind speeds, converted to observation height, for the stations of MNZ.

On the other hand, a 3% deviation in the course of the annual mean is not impossible. Therefore, the performed graphical analysis is not a watertight proof. For the moment, we will however assume that the conversion to knots was terminated at this date.

From the above figure:

- The stations K13, MPN, EUR, F3P show consistent courses.

- The course of the annual mean of AUK is less consistent but is reasonable. Reasons for deviations can be the poor availability for 1989 and 1993 and possibly also the difference in the wind climate due to the large distance to the other stations.

- Originally, an increase in mean wind speed for LEG in 1990 was observed. The cause for this was an increase in anemometer height in April 1990 while the conversion factor had not been adapted. Data before April 11, 1990 has been excluded from the analysis.

For December 1994, no wind speed data are available for LEG. When looking to the monthly averages of LEG compared to MPN, it turns out that the mean wind speed from April to November is somewhat higher at LEG as would be expected from the annual mean. In the period from January to March, the wind speed roughly equals the mean wind speed at MPN. The data supplied by RIKZ for these three months were not reliable (mean wind speed of 2 m/s!) Therefore this period was replaced by the interpolated RWS data. For December 1994, no data are available at all. Effectively, data from before 11 April 1991 are ignored.

The annual mean of the valid wind speed data was already calculated and shown in Figure 10.10. For reference purposes, also some stations from Measuring Network ZEGE are included. The interannual variability is calculated for each station and is shown in Table 10.10.

Table 10.10: Interannual variability for stations of MNZ.

Station	LEG	MPN	EUR	K13	AUK
$\Delta_{interannual}$	8%	13%	13%	14%	23%

It appears from the table that the further offshore, the larger the interannual variability. This tendency was also recognised for Measuring Network ZEGE (Table 10.3).

10.2.4.3 Monthly variations

The annual courses at observation height have been determined for the period 1985–1997 as far as data were available within this period (Figure 10.11).

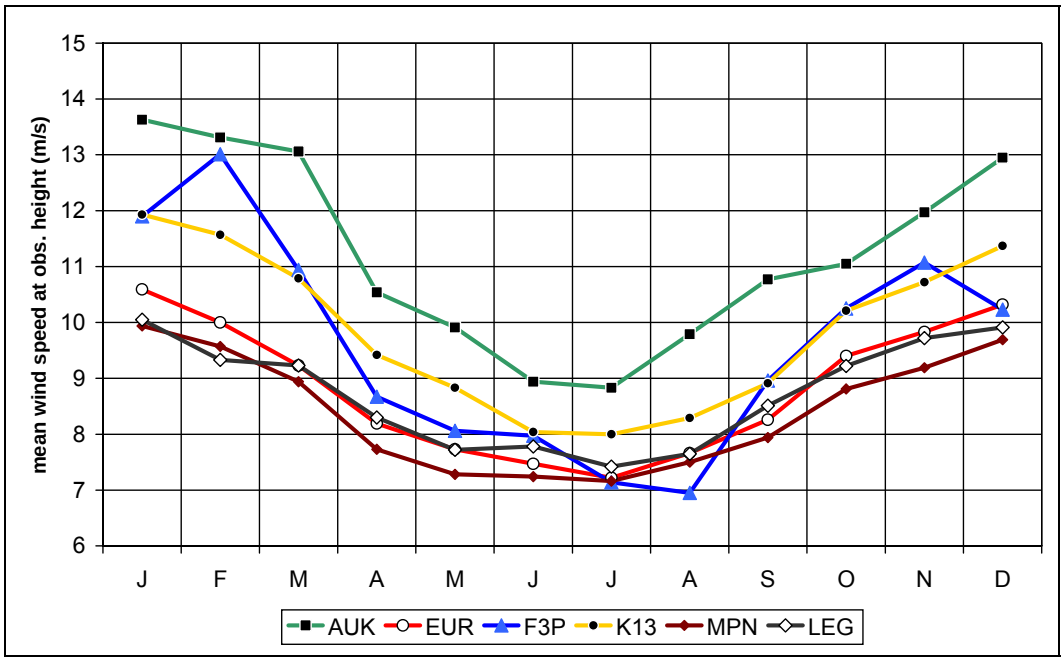

Figure 10.11: Monthly variations of the wind speed for location

The overall pattern seems good apart from the fact that the mean wind speed for February and October at F3P appear to be relatively high. However, for this station, only 3 years of data were available.

In this case the continentality is also calculated. The results are summarised in Table 10.11. The magnitude of the continentality for MNZ is the largest for the stations offshore and in general are higher than for ZEGE stations. Hence, the continentality appears a reasonable measure for the distance of the station to the coast.

Table 10.11: Continentality (monthly) for stations of MNZ.

Station	LEG	MPN	EUR	K13	AUK
Continentality	31%	33%	36%	40%	44%

10.2.4.4 Hourly variations

Figure 10.12 shows the diurnal course for the MNZ stations at observation height. AUK, F3P and K13 do not show a peak as to be expected from their location. LEG, EUR and MPN show a slight negative peak. The cause for this is unknown.

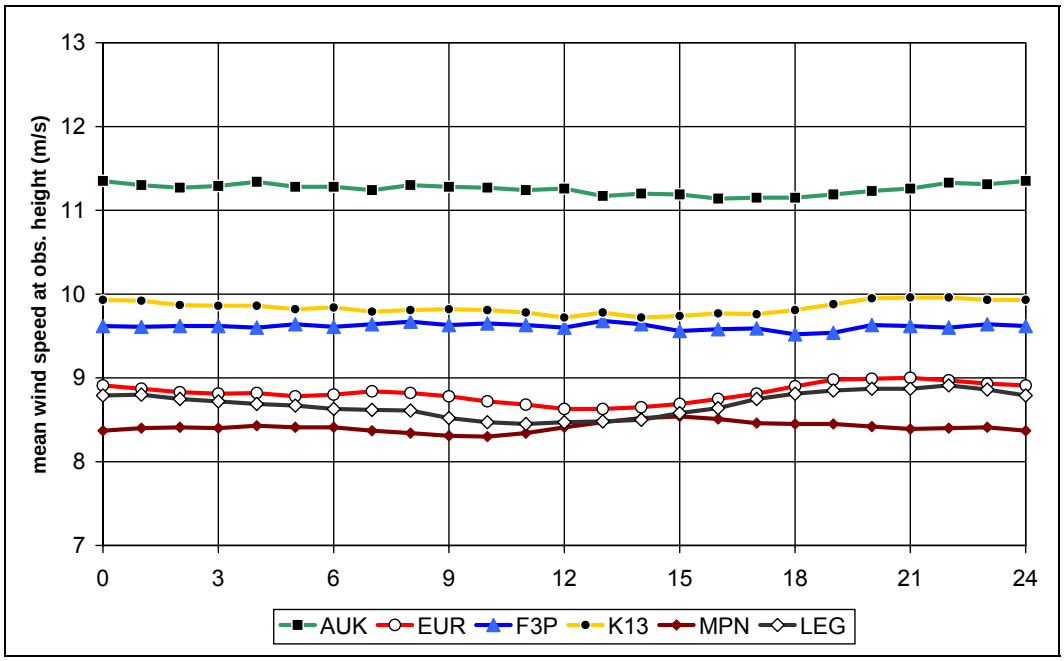

Figure 10.12: Hourly variations of the wind speed for the stations of MNZ.

The peaks of the diurnal course at observation height are again quantified by calculating Chour. The result is shown in Table 10.12.

Table 10.12: Continentality (hourly) for stations of MNZ.

Station	LEG	MPN	EUR	K13	AUK
C_{hour}	5%	3%	5%	2%	2%

As expected, the values are higher for the stations located closer to the shore showing increased influence of land .

10.2.4.5 Variations by wind direction

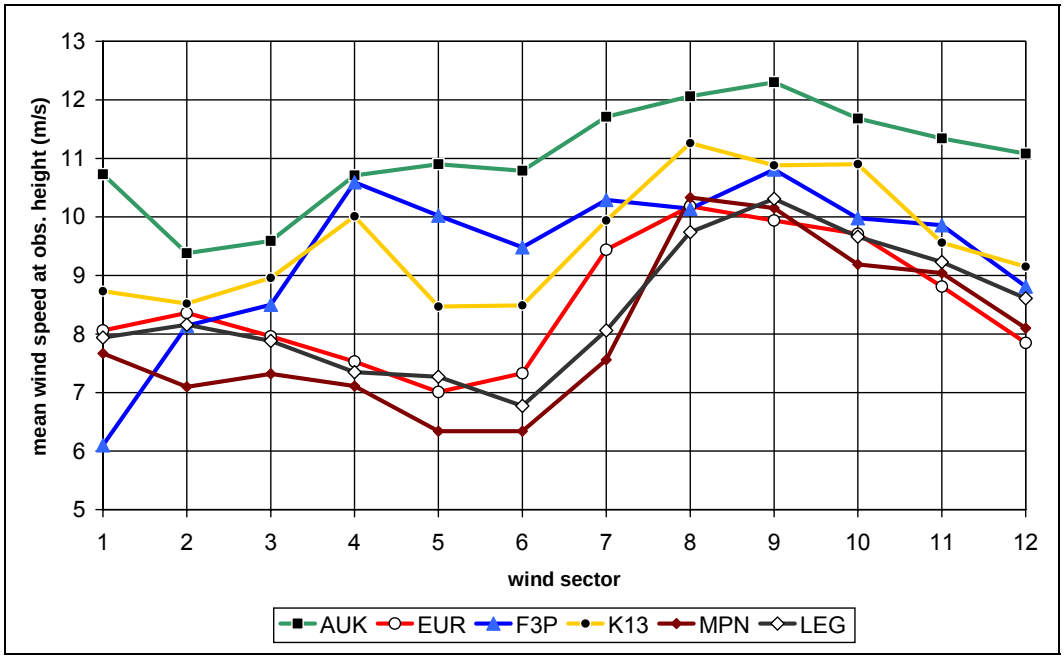

Figure 10.13: Mean wind speed by sector for the stations of MNZ.

The mean wind speed per sector was analysed and is shown in Figure 10.14.

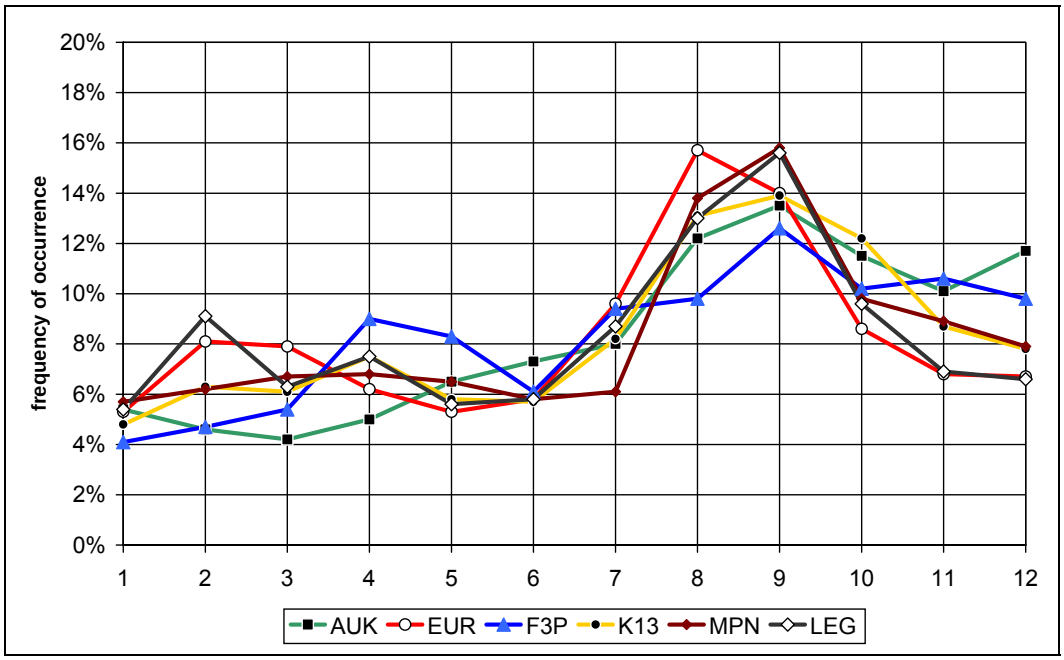

Figure 10.14: Frequency of occurrence by wind sector for the stations of MNZ.

10.2.4.6 Histograms and Weibull parameters

In order to obtain insight into the several processing methods used and to judge the reliability of the data sets, wind speed histograms were made for each year and station. An indication for a change in processing method is a change in shape of the histogram.

After reprocessing the mean wind speeds and Weibull factors have been calculated for all stations for each year and for the available period from 1985–1997. Table 10.13 shows the results.

Table 10.13: Overview availability, mean wind speed and Weibull parameters of offshore wind speed data sets.

Station	Period	Availability [%]	*k* [-]	*a* [m/s]	Mean wind speed [m/s]
MPN	1987-1997	99	2.02	9.37	8.42
EUR	1987-1997	98	2.10	9.83	8.81
K13	1985-1997	97	2.05	10.99	9.87
AUK	1987-1995	76	2.18	12.85	11.41
LEG	1991-1997[1]	94	2.19	9.86	8.71

The several processing methods have altered the shape of the histogram or the originally measured data set. The histograms have been fitted with the 'WAsP'-method and with the 'least squares'-method. Figure 10.15 shows the result for Measuring Post Noordwijk. The Weibull factors within the table are the ones derived with the WAsP-method. The mean wind speeds found correspond within 2% of an earlier study of (part of) the data from MPN, EUR and K13 [Coelingh et al. (1998)].

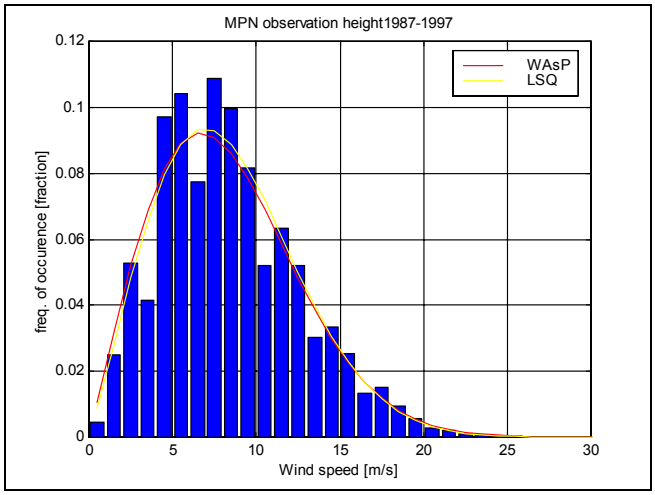

Figure 10.15: Histogram and Weibull fit for MPN.

10.2.5 Conclusions

The wind speed data from the measuring Network North Sea have been processed in several ways. Five different processing methods could be distinguished. Three of them affect the shape of the histogram considerably and possibly also affect the mean wind speed. The time series have been reconverted to observation height by applying the appropriate conversion factors. Also a correction for the conversion from knots to m/s has been applied.

The availability and consistency of the data sets were checked by means of data analysis and comparison with time series from other sources (KEMA, KNMI, voluntary observing ships) and stations from Measuring Network ZEGE. F3P shows good behaviour, but only a limited period (3 years) of data is available. Data of LEG until April 1990 were also not used as before that data the erroneous conversion factor was used in the past and because of the former shielding of the mast.

The time series have been reconverted to observation height by applying the appropriate conversion factors. The mean wind speed and Weibull parameters have been determined from these reconverted time series for the period 1985–1997 (as far as data were available).

[1] LEG: data interpreted as invalid until April 11, 1991 (due to change of mast)

10.2.6 Comparison with POWER results

10.2.6.1 Introduction

In order to validate the results as obtained from the WasP (see Chapter 4) a comparison was made to the observations as acquired and analysed from the Measuring Network North Sea and ZEGE. WasP was run to produce results for the exact location and observation height of the available locations. For a better insight this was done on different temporal scales: annual and monthly. Here we will only show the comparison on an annual basis for 6 locations: three of the Measuring Network North Sea (K13, Euro platform and Measuring Post Noordwijk) and for the three of ZEGE that are in the North Sea (Oosterschelde 4, Brouwershavensche gat 2 and Vlakte van de Raan).

10.2.6.2 Annual variations

Figure 10.16 shows the annual variations over the period 1985–1997 at the observation height for the three locations of Measuring Network North Sea. The solid lines are the results of the WAsP calculations, the dashed lines the averages of the (reconstructed) observations.

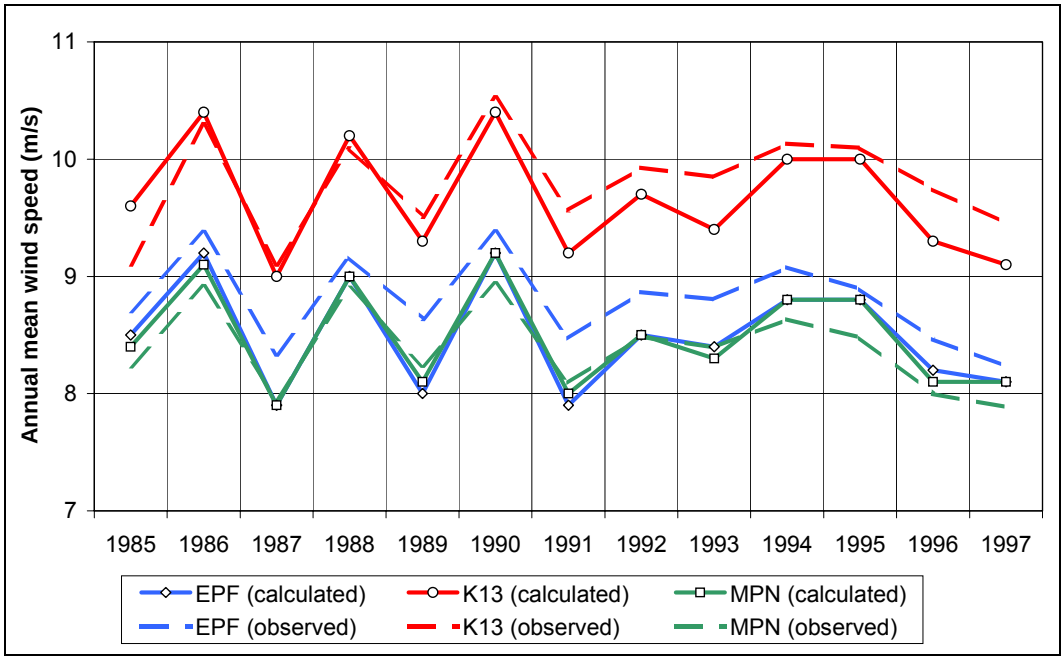

Figure 10.16: Comparison of observed and calculated annual mean wind speeds for three locations of the Measuring Network North Sea.

Looking at the figure the comparison over the years seems fairly good. The figure also shows that the calculated values for EPF and MPN are nearly equal, which is indication for the fact that the model the influence of the land is the same for these two locations.

Figure 10.17 shows the results for the three offshore locations of ZEGE. These are far closer to the shore than those in the previous figure. Furthermore it should be noted that the observations for Vlakte van de Raan are available as of the year 1989.

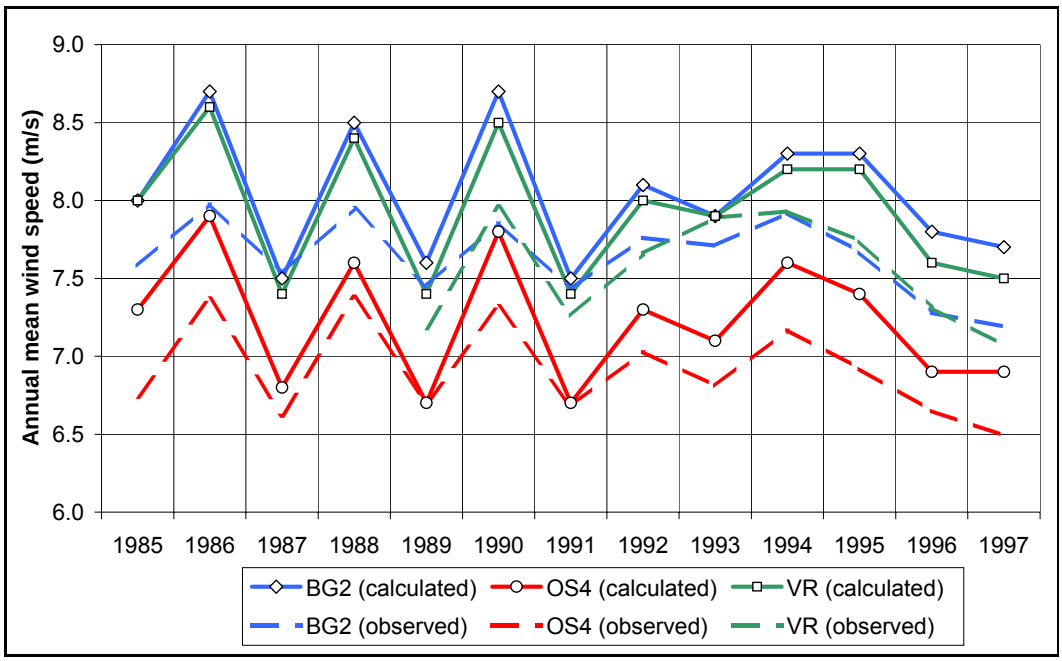

Figure 10.17: Comparison of observed and calculated annual mean wind speeds for three locations of ZEGE.

In this figure the comparison appears to be quite good over the years. In this case the model calculations for VR and BG2 are almost identical, showing the indifference of the model for these locations.

In Table 10.14 the average values over all years have been shown, as well as the ratio of observed vs. calculated mean wind speeds over the whole period. It is shown that the three locations of ZEGE are overestimated by 4-5%, while the three locations further offshore show less deviation. Overall the preliminary conclusion can be that these results are quite satisfactory although the validation will be finalised in the next few months, including a comparison on a monthly scale.

Table 10.14: Overview of observed versus calculated mean wind speeds.

location	EPF	K13	MPN	BG2	OS4	VR
observed mean wind speed (m/s)	8.80	9.80	8.40	7.64	6.91	7.56
calculated mean wind speed (m/s)	8.50	9.66	8.48	8.05	7.23	7.86
observed/calculated	104%	101%	99%	95%	96%	96%

10.2.7 Overall conclusions

In The Netherlands two separate data bases have been acquired containing offshore wind speed observations. The first one, called ZEGE, is a network of simple, relatively low masts specifically located in the province of Zeeland. Three of the masts are located in the North Sea. The advantage of these observations is that they have not been processed in any way, which has been verified. Therefore, the results can be used as reference.

The other data base is called MNZ. This network covers a large part of the North Sea making use of existing structures, like oil- and gas platforms and a light-isle. Therefore the circumstances for good measurements are not ideal, and the anemometer height varies from 20 to 100 m above MSL. Furthermore, the disadvantage of these data is that they have been processed over the years in different ways, making it difficult to reconstruct the original data in order to obtain a consistent time series. However, using the data of ZEGE as reference and with the information from some of the authorities involved a reasonable attempt could be undertaken to understand the different processing steps. In that way a consistent time series could be obtained for the locations of MNZ.

Calculations were made for the respective locations and at the respective anemometers height with the POWER method. Comparison with the observed wind speeds (as well as they could be derived from the originally obtained data) shows fairly good results. For all six points the deviations were less than 5%. Therefore the conclusion is that within the restrictions of this analysis the POWER results are within the range of the observed wind speeds at the 6 locations.

10.3 Denmark

10.3.1 Data source

The POWER WasP modelling results were compared against high quality wind speed profile data collected by ELSAM on purpose-built meteorological masts at two prospective offshore wind farms sites for in Danish waters – Horns Rev and Læsø Syd (see Figure 10.18). These data were gathered over the 12 month period between June 1999 and May 2000.

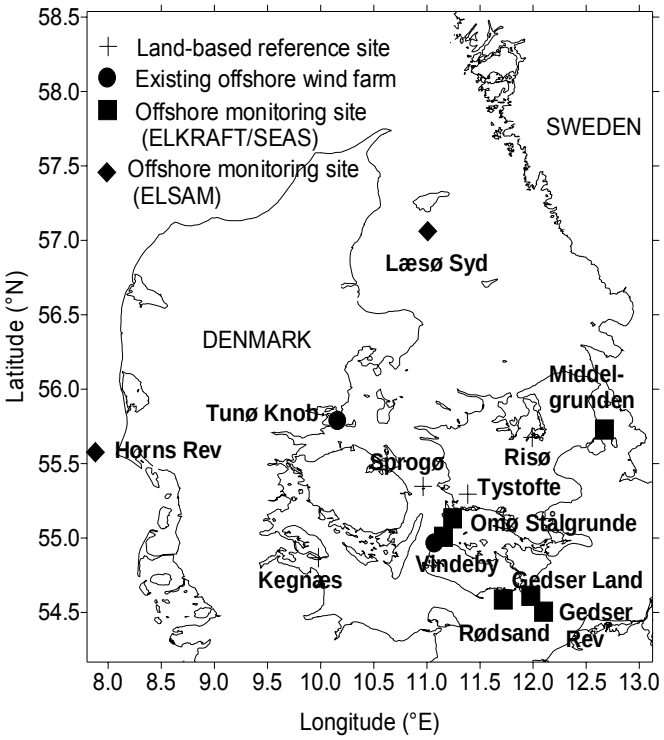

Figure 10.18 – Map showing locations of Horns Rev and Læsø Syd

The ELSAM Horns Rev and Læsø Syd data sets include hourly wind speed measurements at four heights (15m, 30m, 45m and 62m above mean sea level) and wind direction measurements at three heights (28m, 43m and 60m above mean sea level). Note that only one of the POWER prediction heights (30m ASL) coincides exactly with the instrument heights of the observed data.

10.3.2 Wind speeds

Figures 10.19 and 10.20 compare POWER WAsP model mean annual wind speed estimates with wind speeds observed at Horns Rev and Læsø Syd respectively.

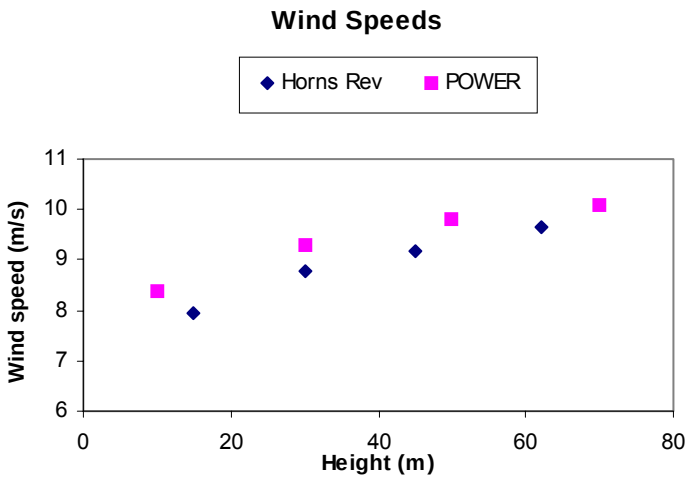

Figure 10.19 – Observed and calculated mean vertical wind speed profile for Horns Rev

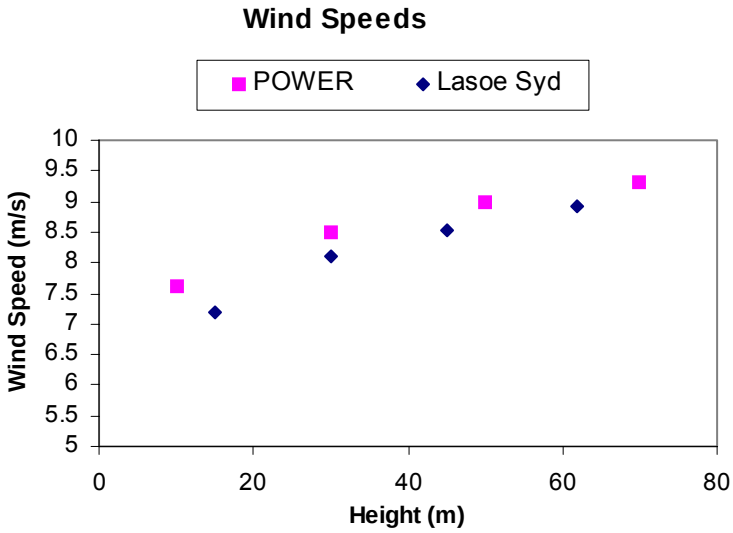

Figure 10.20 – Observed and calculated mean vertical wind speed profile for Læsø Syd

At first sight, these results suggest POWER has overestimated the mean wind speeds at these site by the order of 0.5m/s. However, it must be remembered that the ELSAM Horns Rev/ Læsø Syd observations represent the wind conditions that occurred at these locations during a single 12 month period (June 1999-May 2000), whereas the POWER results represent mean wind speeds over 13 year period (1985-1997). Figures 10.21 and 10.22 show POWER estimates of the inter-annual variation in mean wind speed over this 1985-1997 period at Horns Rev and Læsø Syd respectively. It is clear that from year to year there is significant variation in the mean wind speeds at the sites. Furthermore, the ELSAM Horns Rev/ Læsø Syd observed wind speed values lie within the overall range of mean wind speed values estimated for the sites.

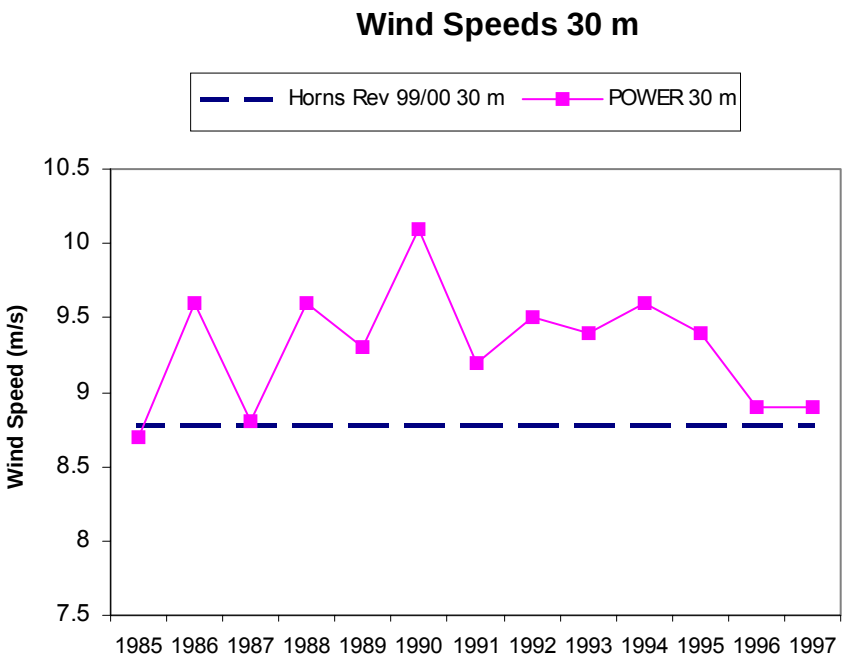

Figure 10.21 – Predicted variation in mean yearly wind speed at 30 m ASL for Horns Rev 1985-97

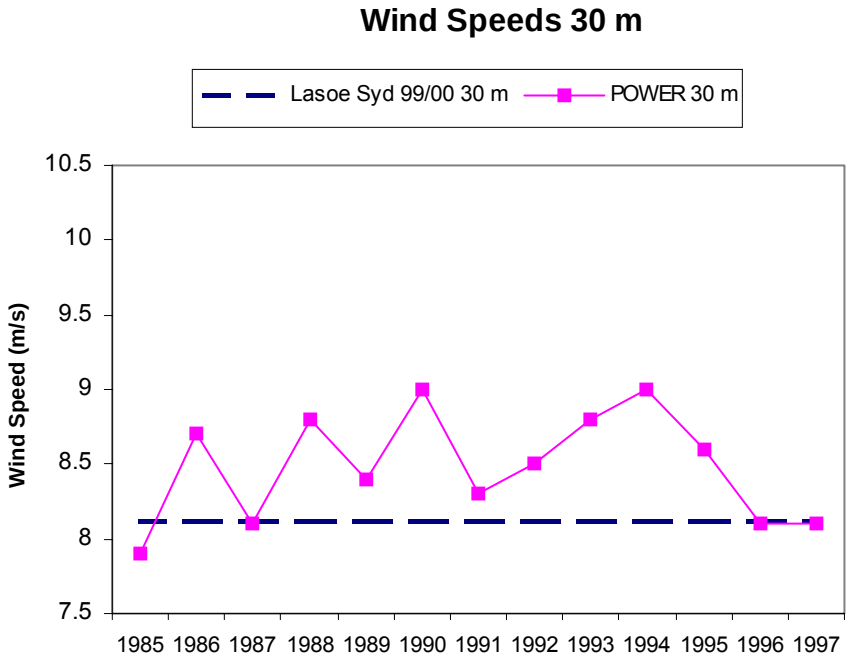

Figure 10.22 – Predicted variation in mean yearly wind speed at 30 m ASL for Læsø Syd 1985-97

10.3.3 Variation in wind speeds through the year

Figures 10.23 and 10.24 compare the observed variation in mean monthly wind speed (for June 1999 to May 2000) with the POWER model estimates for Horns Rev and Læsø Syd. The correlation between the observed and calculated values is good.

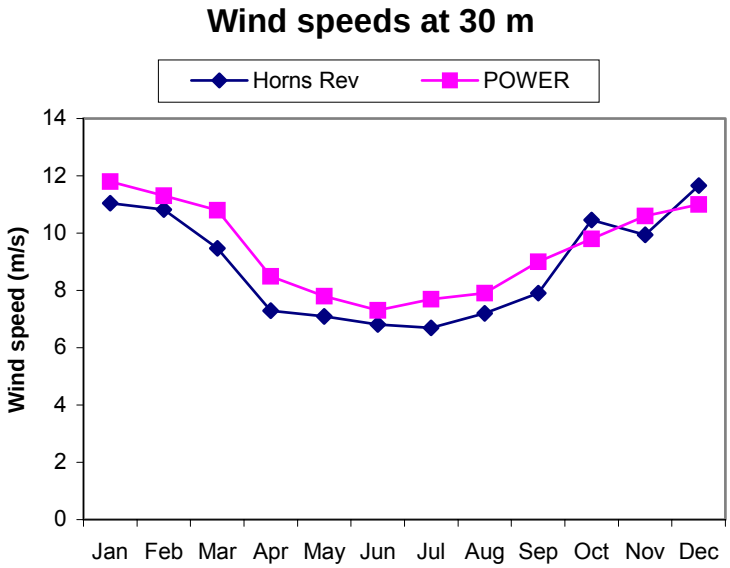

Figure 10.23 – Comparison of observed and calculated monthly variations in wind speed at Horns Rev

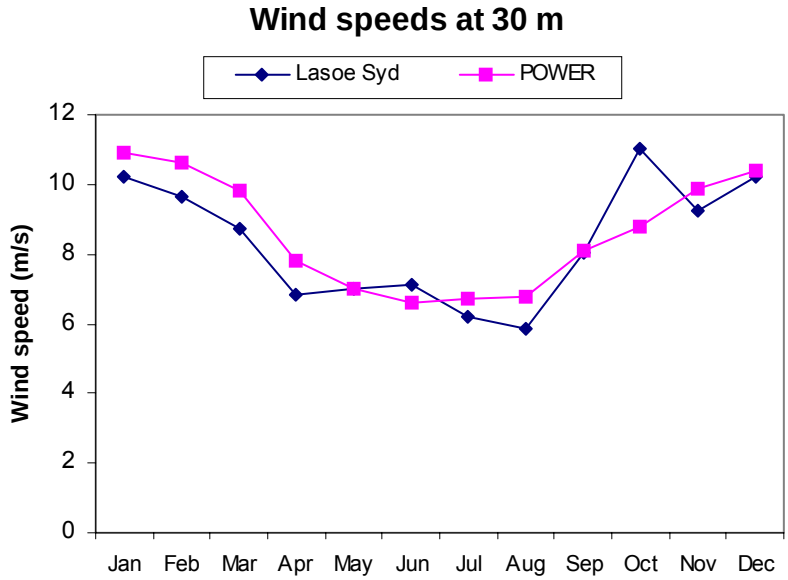

Figure 10.24 – Comparison of observed and calculated monthly variations in wind speed at Læsø Syd

10.3.4 Variation with direction

Figures 10.25 and 10.26 show the observed and calculated wind rose at Horns Rev and Læsø Syd respectively.

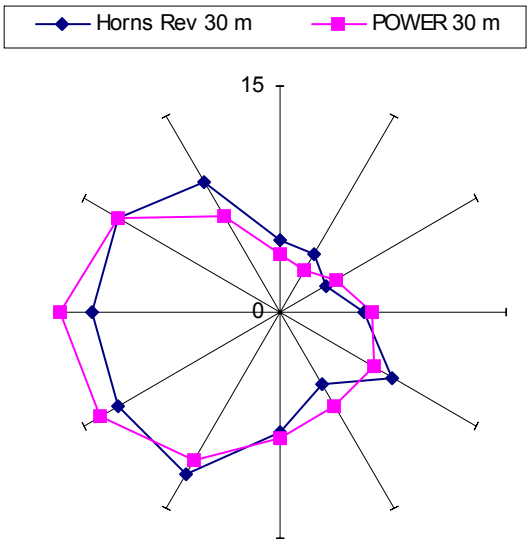

Figure 10.25 – Comparison of observed and calculated wind rose at Horns Rev

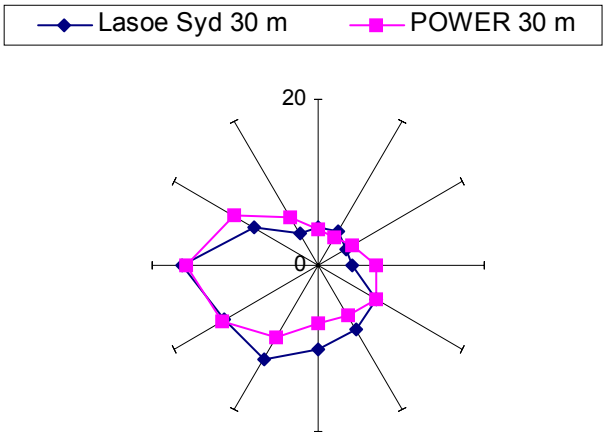

Figure 10.26 – Comparison of observed and calculated wind rose at Læsø Syd

10.3.5 Wind speed distributions

Figures 10.27 and 10.28 show the observed and calculated wind speed distributions at Horns Rev and Læsø Syd respectively.

In both cases, the POWER results seem to have under-estimated the frequency of medium- to low wind speeds, but over-estimated the frequency of high wind speeds

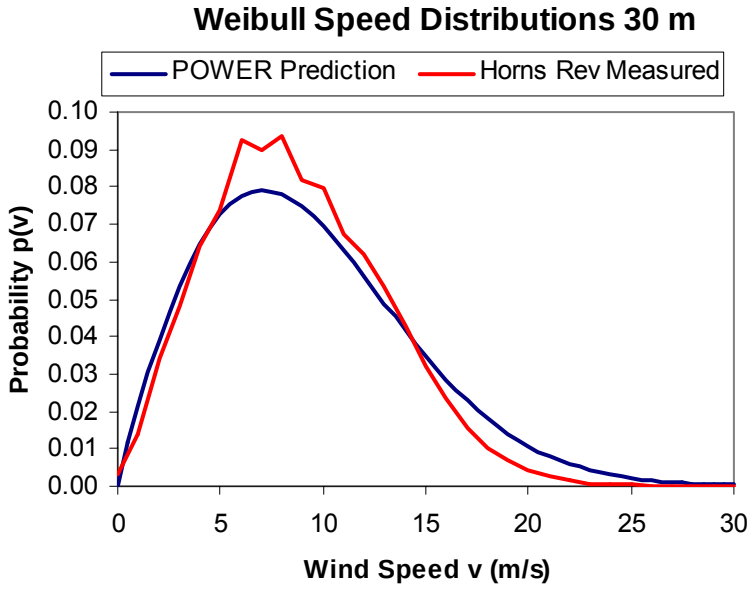

Figure 10.27 – Comparison of observed and calculated wind speed distribution at Horns Rev

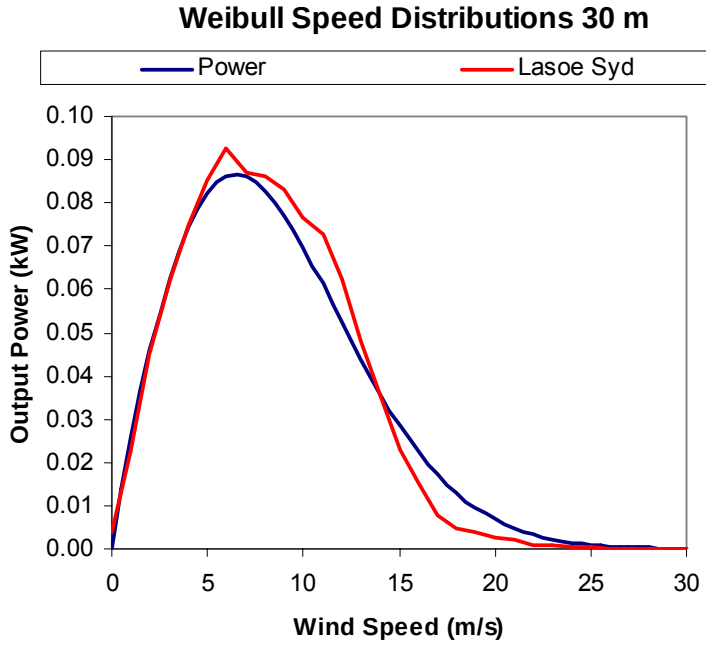

Figure 10.28 – Comparison of observed and calculated wind speed distribution at Læsø Syd

In both cases, the POWER results seem to have under-estimated the frequency of medium to low wind speeds, but over-estimated the frequency of high wind speeds compared to the observations.

10.3.6 Conclusions

Comparison of observed and calculated wind conditions at both of these proposed Danish offshore wind farm sites indicate that the POWER results are a good representation of the typical wind regime for these sites.

10.4 The Mediterranean.

The following paper was presented at the European Wind Energy Conference in Copenhagen in July 2001.

EVALUATION OF METHODS OF ESTIMATING OF WIND ENERGY POTENTIAL OFFSHORE IN MEDITERRANEAN AREAS.

A.Lavagnini [1], Anna M. Sempreviva [1], Luigi Cavaleri [2] and Rebecca J. Barthelmie [3]

[1] Istituto di Fisica dell'Atmosfera, CNR, via Fosso del Cavaliere 100, Rome, Italy,

[2] Istituto per lo Studio delle Grandi Masse, S.Polo 1364, 30125 Venice, Italy.

[3] Dept. of Wind Energy and Atmospheric Physics, Risø National Laboratory, Frederiksborgvej 399, 4000 Roskilde, Denmark.

ABSTRACT: Relatively few studies have been performed on the evaluation of offshore wind resources and mostly in North Europe. In Mediterranean areas the poorness of such studies is mainly linked to three reasons: 1) the difficulty of meteorological monitoring in the deeper waters 2) the complex orography, frequently extending down to the coasts; 3) the sea breezes wind regimes. In the North Adriatic Sea, a shallow basin of the Mediterranean, the first reason is missed, but the other two are challenging enough to make an the effort of evaluating those methods. In the present paper we have estimated estimate the wind climatology at a platform located 16 kilometres offshore of Venice based on 7 years of data and we have compared it with the wind climatology obtained using three different methods based on the long-term data of three coastal meteorological stations: Venezia Tessera, Venezia San Niccolò, Ronchi and Rimini. Furthermore, a Coastal Discontinuity Model (CMD) and a Geostrophic version of the WAsP model (Geo WasP) have been tested. We discuss the applicability of those methods and find that WAsP is still the best tool for wind climate estimates. The results of the CDM and Geo WasP are promising in view of computer power increase.
Keywords: Off-shore, Coastal sites, Statistical Analysis, Climatic conditions.

1 INTRODUCTION

Relatively few studies have been performed on the evaluation of offshore wind resources and these are mainly concentrated in North Europe. [1], [2], [3]. One reason for this is the additional difficulty of meteorological monitoring in the deeper waters of the Mediterranean. Various methods are available for predicting long-term wind speeds in offshore areas based on long-term data sets from nearby land sites. In this paper, we have chosen three methods that have been used in the evaluation of wind resources at Danish offshore sites and have shown to give promising results there. The used methods rely on long-term measurements at nearby land sites in comparison with short-terms records offshore. The performance of these methods will be evaluated in the North Adriatic area. Here 7 years of hourly data collected on an oceanographic platform 15 Km offshore of Venice and climatological data at four coastal stations (Venezia Tessera, Venezia S. Niccolò, Rimini and Ronchi) are available. Table1 and Figure.1.

Table 1. Location of the stations

Station	Lat. (deg.)	Long. (deg.)	H. asl (m)	H a. (m)	Period
1.Venezia Plat	45.31	12.51	0	15	76-82
2.Venezia Tess.	45.50	12.33	6	10	61-96
3.Venezia S.N.	45.43	12.38	5	10	51-77
4.Rimini	44.03	12.61	13	10	51-96
5.Ronchi	45.61	13.50	17	10	67-96

The main difference between wind climatology of North Europe and Mediterranean coastal areas is that, in the latter, stability conditions different than neutral and strong see breeze regimes are more frequent. If conditions offshore deviate significantly from near-neutral (either on average or by season), the effect of stability on the wind speed profile can be substantial. These methods are:

1) The standard measure-correlate-predict [3] (MCP) method, which assumes a linear relationship between wind speed at paired sites where one site with a long-term record acts as predictor and the wind speed at short-term measurement sites are the predictand. Once a regression equation has been conditioned based on the measurement overlap period, the regression parameters can then be used to derive an extended data record for the site of interest.

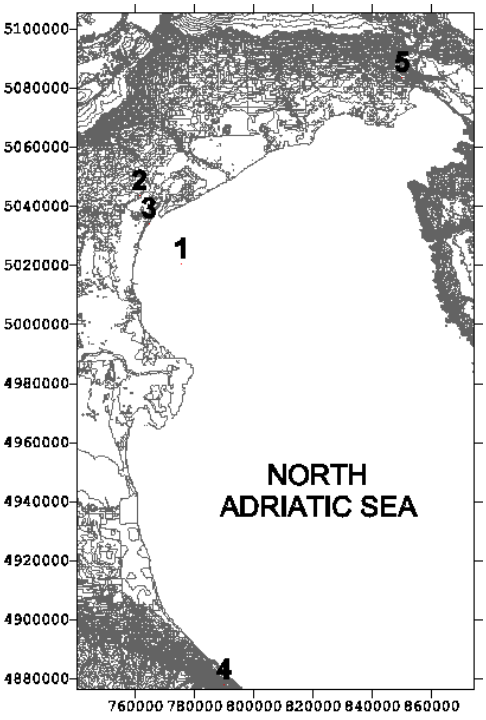

Figure.1. North Adriatic Sea, location of the stations.

This method generally used using one regression for each wind sector. 2) Risø's Wind Atlas Application and Analysis program (WasP7), which calculate the wind climatology in one site from wind climatology of long term representative stations. WAsP is a physically-based model and uses the change in heat flux between on- and off-shore to calculate a mean stability correction and the change in roughness to adjust the momentum flux. 3) The Weibull correction method [1] for extrapolating wind data series is based on the concept of modifying the Weibull parameters of the short term data series to characterise a longer data sampling period. It compares sector-based wind speed distributions at the on - and the off-shore site considering the on-shore long-term time series as representative of the area. The Weibull shape (A) and scale (k) factors are determined for 12 sectors at both sites for a common period and the ratio is used to modify the long term wind distribution to represent the off-shore station.

At the Danish sites, MCP tends to under-predict wind speeds in comparison with offshore data. WAsP typically gives good results except at sites that are less than five kilometres from the coast where wind speeds are predicted to be a few percent higher than those observed. The Weibull method gives good results provided sufficient data are available to accurately characterise the wind speed distribution in each sector and that the distribution conforms to a Weibull distribution.

Additionally we have used WasP applied to geostrophic wind distributions (Geo WasP) and the Coastal Discontinuity Model (CDM) developed as part of the EC POWER project. WAsP runs were conducted for each 0.5 by 0.5 grid of the waters of the European Union and Geostrophic wind speeds and directions are calculated from a sea level pressure data set. WAsP predictions were made using geostrophic wind speeds. The CDM works is a slightly different way to WasP. Instead of applying stability and land-sea corrections to the mean wind speed distribution as in WAsP, the CDM uses air and sea temperature, together with the geostrophic wind speed time series to calculate the stability the Monin-Obukhov length parameter for each grid point at each time step (input data are six-hourly). Air and sea temperatures were given for each 1x1° grid. Equilibrium land and sea wind speed profiles are corrected for stability. Finally the program uses the fetch distance to land to determine the internal boundary layer height and interpolates between equilibrium wind speed profiles over land and sea to the fetch distance accounting for the discontinuity caused in the profile by the IBL.

2 DATA AND CLIMATOLOGY

The four selected meteorological stations belong to the Italian Military Meteorological Service. The measurements are taken in integer knots at the synoptic hours (0, 3, 6, 9, 12, 15, 18, 21 GTM). The platform measurements are supplied by the Institute of the Dynamics of Large Masses of the Italian National Council of Research (CNR) in Venice. The platform measurements were hourly with a calm threshold of 2 ms^{-1}. In Table 1, the co-ordinates of the stations, altitude a.s.l (h), the altitude of the anemometers (Ha), and the period of measurements are shown. Data were analysed using WasP7® and WAsP Utilities® programmes.

2.1. Climatology of the North-Adriatic coastal areas.

In figure 2a and 2b the mean hourly velocity and the mean monthly velocity are shown respectively for 4 stations. From figure 2a we note that the sea breeze regime produce the effect to enhance the wind speed in the coastal areas and to reduce it at the platform distance in the central part of the day. From figure 2b we notice a maximum of wind speed during the spring and minimum during summer and winter time. The monthly climatology of Rimini is slightly different from the climatology of Venice and Ronchi that are in better agreement.

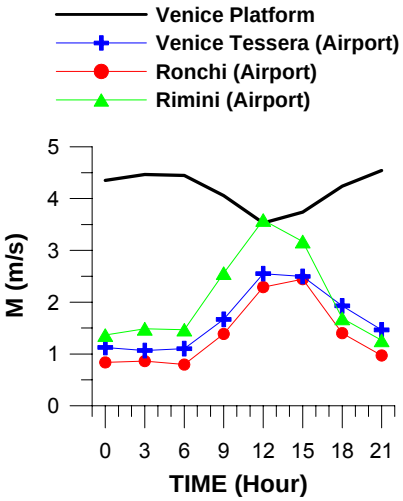

Figure 2a. Mean hourly wind speed.

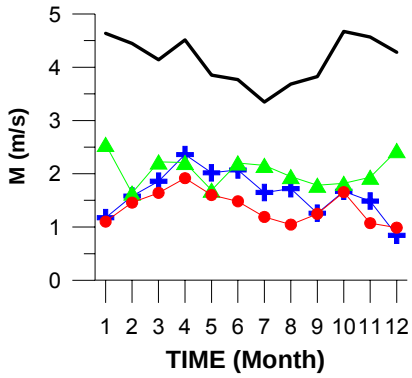

Figure 2b. Mean monthly wind speed. For the legend refer to figure 2a.

3 RESULTS.

We have applied the methodology [1], [2], [3] outlined above, which rely on long-term measurements at the nearby land sites in comparison with short-terms records offshore. The results of the application of the methods and two models are shown below:

1) MCP method. We could not find a satisfying correlation among stations (regression coefficients less than 0.4). This method is not applicable here.

2) WasP 7. Rimini and Ronchi stations are not able to reproduce the platform wind climatology then we focus on the results obtained using Venice Tessera (VT) (figure 3) and Venice San Niccolo' (VSN) (figure 4). There are not overlapping periods between the Platform and VSN. VT has seven years overlapping. Due to the large amounts of calms, (around 40%) in the two stations we have removed them in the estimate of the wind distribution. In WAsP the calms are uniformly distributed in the 12 sectors. In a region with large percentage of calms this procedure modify the sector wise frequency distribution especially in the sectors with low percentage. An alternative will be to distribute the calms accordingly to the frequency distribution of the wind speed without calms. Studies in this direction will be performed in stations where calm directions are based to the previous non calm record. In figure 3 and figure 4 the comparison amongst prediction and experimental mean wind speed **M** and frequency at the platform from VT for 7 years and for 35 years are shown respectively. Using 35 years long term wind distribution improve the prediction but WAsP overestimates the mean wind speed. Ratios among prediction and data are between 0.8 and 1.2.

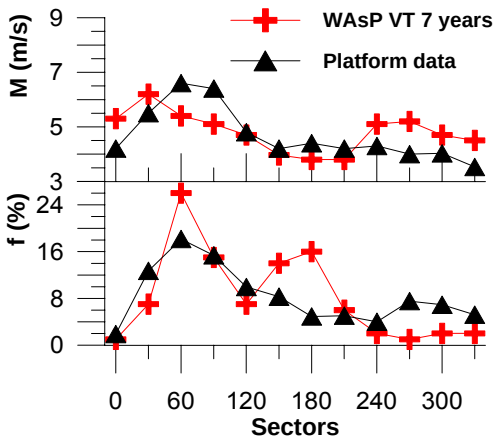

Figure 3. Predicted and experimental wind speed and frequency for each sector using seven years overlapping data from VT.

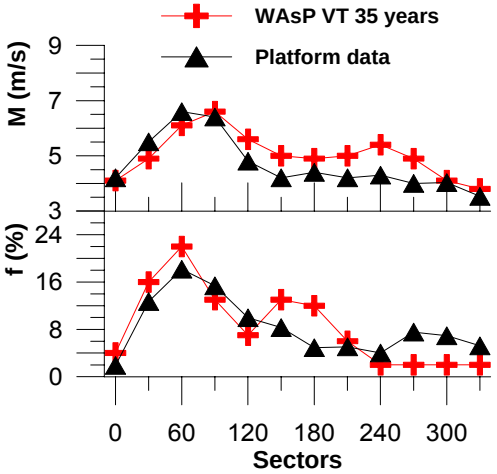

Figure 4. Predicted and experimental wind speed and frequency for each sector, using 35 years data from VT.

In figure 5 the prediction of mean wind speed and frequency at the platform from VSN are shown. Frequency are in better agreement than VT 35 years especially in the sea sectors. However, VSN underpredict the mean wind speed in the sea sector. Generally WAsP underestimates the wind at the platform in the sea sectors and overestimate in the land sectors.

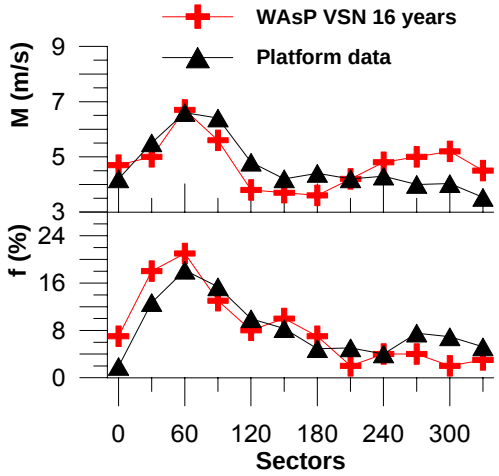

Figure 5. Predicted and experimental wind speed and frequency for each sectors using Venice S. N. 3)

The Weibull correction method. This method has been applied using the 7 years overlapping time series of VT and correcting the 35 years A and K wind distribution of VT. The results are shown in figure 6. The method reproduce well the frequency in all sectors except two. The reasons are under investigation.

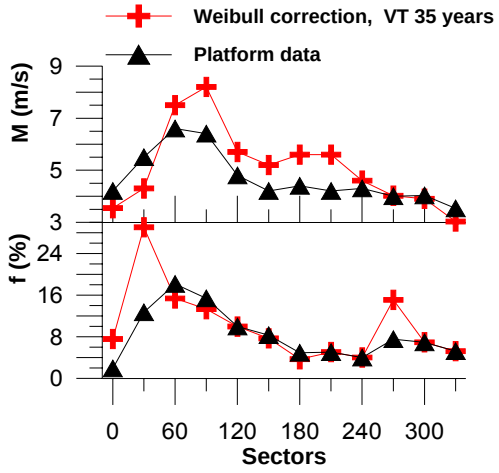

Figure 6. Predicted and experimental wind speed and frequency for each sector, using the Weibull method.

4) The CDM. The sector wise M and frequency obtained from the model, compared to the experimental one are shown in Figure 6. The model overestimate M but the results are promising. The frequency distribution is in agreement with the experimental one. In figure 6 the monthly average wind speed from the model is compared to the experimental averages at the platform. The two curves are in agreement showing a minimum in the summer months but the average wind speed from CDM is overestimated, especially in winter.

5) The Geo WAsP. Concerning the Geo WAsP model the results presented here are at 10 m height while the platform is at 15 m. The sector wise M and frequency obtained from the model, compared to the experimental one are shown in Figure 7. Both M and frequency distribution are in agreement with the experimental one.

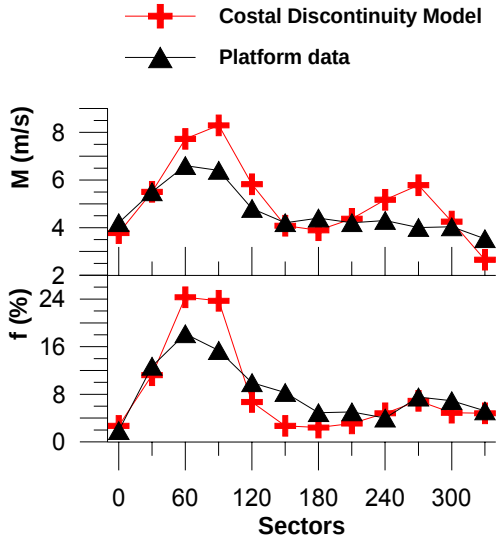

Figure 6. Predicted and experimental wind speed and frequency for each sector, using CDM model.

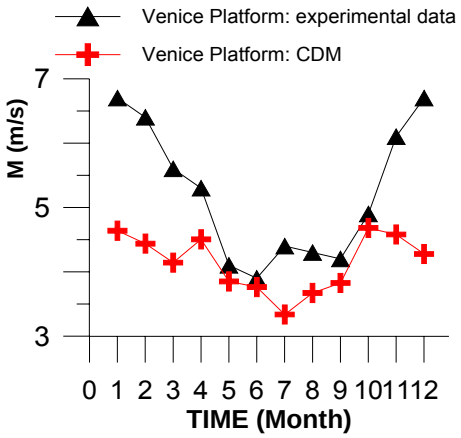

Figure 7. Comparison between Monthly mean wind speed from CDM and experimental values.

4 FINAL REMARKS.

We have applied three empirical methods used in North Europe to estimate climatology offshore by long-term data sets from nearby land sites. The major problems in our Mediterranean study area are: the large amount of calms whose distribution sector wise deserve a proper study and the local wind regimes as sea breeze that influence strongly the wind distribution. Because of the latter problem it is not possible to use long term time series located in a different sea breeze regime as Ronchi and Rimini. Furthermore although for $u > 4$ m^{-1}, a small correlation could be found, it is not possible to apply the CMP method as a whole. The methods based on WAsP (WAsP and Geo WAsP) are found to give the best results provided that the predictor station lay in an area with similar local circulations. Also the CDM shows promising results.

In table 2 the ratios between predicted and experimental mean wind speeds are reported for the CMD Model, the Geo WasP Model, the WasP model considering Venice Tessera 35 years (WAsP VT 35) and 7 years (WAsP VT 7) time series, the WasP model considering Venice SN, and finally the Weibull correction method applied to VT at 35 years.

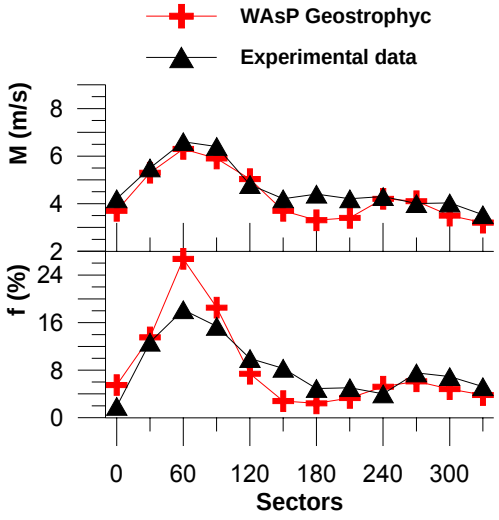

Figure 8. Predicted and experimental wind speed and frequency for each sector, using Geo WAsP.

Table 2. Ratios between mean wind speed M at the platform Mplat and predicted values from VT and VSN and applying the different methods Mpred.

Method	M(m/s)	A(m/s)	k	Mplat/Mpred
Platform	**4.6**	**5.5**	**1.28**	**1.00**
CDM	6.3			0.73
Geo WAsP	5.2	5.6	1.33	0.88
WAsP VT 35	5.4	6.1	1.69	0.85
WAsP VT 7	4.11	4.57	1.53	1.12
WAsP VSN	5.1	5.7	1.66	0.90
Weib corr VT35	5.1			0.90

5 ACKNOWLEDGEMENTS

The sea level pressure data set for the period 1985-1997 used for the CDM were supplied by Tom Holt of the Climatic Research Unit, UK. WAsP runs were conducted for each 0.5 by 0.5 grid of the waters of the European Union by Gillian Watson of the Rutherford Appleton Laboratory, UK. For the CDM we acknowledge funding from the European Union JOULE program project 'Predicting Offshore Wind Energy Resources' Contract # JOR3-CT98-0286. We would also thank Mr. Claudio Transerici from IFA-CNR for the data quality control of the Meteorological database.

6 BIBLIOGRAPHY

[1] Hoejstrup, J., M., Lange, B., Barthelmie,R.,J., Pedersen, A.,M.,J., Olsen, F. and Svenson, J., 96: Offshore Wind Resources at selected Danish sites. Risoe-I-1339 (EN), Risoe National Laboratory, Roskilde, Denmark.

[2] Barthelmie, R.J., Courtney, M., Lange, B., Nielsen, M., Sempreviva, A.M., Svenson, J., Olsen, F., and Christensen, T., 98: Offshore Wind Resources at Danish measurements sites. Risoe-I-1339 (EN), Risoe National Laboratory, Roskilde, Denmark.

[3] Barthelmie , R.J., M., Lange, B. and Nielsen, M., 99: Wind Resources at Roedsand and Omoe Staalgrunde. Risoe-I-1456(EN), Risoe National Laboratory, Roskilde, Denmark.

10.5 Comparison with a previous EU study

An earlier EU study (JOUR0072 : Study of offshore wind energy in the European Community, led by GERMANISCHER LLOYD AG and Garrad Hassan and Partners Ltd) had presented long term wind speed data (mean, Weibull parameters, shear profile) in an IDRISI database. Garrad Hassan and Partners Ltd kindly provided a copy of this database to enable a comparison with the POWER results to be made – hereafter the database will be referred to as the GLGH database. However, before such a comparison could be made two factors had to be taken into account : a) the heights at which wind speed was estimated was different in the two studies, therefore the 50m and 70m POWER wind speeds being interpolated (assuming a logarithmic drag law) to obtain 60m values which could be compared with the GLGH values; b) the GLGH and POWER databases had used different geographical grids – it was therefore decided to restrict the comparison to those points which were nearly co-incident (this was defined as those points whose maximum separation was 2.15 km). There were 1276 such grid points. The comparison was carried out by GLGH sea area with the following results :

Sea Area (GLGH dataset name)	No. of Points	Mean Absolute Error	Root Mean Square error	Correlation Coefficient
		(m/s)	(m/s)	
Belgium & Netherlands (be_nl)	45	0.513	0.968	0.395
Denmark & Germany (de_dk)	94	1.218	1.615	0.722
Spain & Portugal (es_pt)	195	-0.541	0.967	0.637
France, Atlantic (f_atl)	129	-0.034	0.689	0.475
France, Mediterranean (f_med)	72	-0.643	1.022	0.579
Great Britain, North (gb_n)	120	1.421	1.630	0.528
Great Britain, South (gb_s)	103	0.442	0.807	0.446
Greece (gr)	188	-0.055	1.365	0.129
Eire (ie)	75	0.984	1.205	0.391
Italy, North (it_n)	105	0.109	1.019	-0.109
Italy, South (it_s)	150	-0.279	0.813	0.11
Weighted average :		0.181	1.098	0.377
Total :	1276			

10.6 References for Chapter 10

1. Benschop, H., Windsnelheidsmetingen op zeestations en kuststations: herleiding waarden windsnelheid naar 10-meter niveau, KNMI, TR-188, 1996.

2. Benschop (2000). Personal communication with Henk Benschop, KNMI, De Bilt, 2000.

3. Børresen, J.A., Wind atlas for the North Sea and the Norwegian Sea, 1987, Norwegian University Press/The Norwegian Meteorological Institute

4. Cleijne, J.W., Coelingh, J.P., van Wijk, A.J.M., Description of the North Sea wind climate for offshore wind energy applications, TNO 91-327, 1991.

5. Coelingh, J.P., A.J.M. van Wijk, Analyse windsnelheidsdata meetpaal OS4, 1993, i.o.v. Energy-Connection (Delft), UU, Vakgroep NW&S, nr. 93048, Utrecht

6. Coelingh, J.P., A.J.M. van Wijk, Analyse windsnelheidsdata meetpaal Marollegat, 1994, i.o.v. Energy-Connection (Delft), UU, Vakgroep NW&S, nr. 94069, Utrecht

7. Coelingh, J.P., A.J.M. van Wijk, A.A.M. Holtslag, Comparing wind speeds on the North Sea coast and offshore, 1997, Proceedings OWEMES Sardinia

8. Coelingh, J.P., Near-Shore Windaanbod - Een verkennend onderzoek naar het windaanbod voor een near-shore windproject, 1997a, i.o.v. Haskoning/NOVEM, Adviesbureau E-Connection, Delft

9. Coelingh, J.P., A.J.M. van Wijk, A.A.M. Holtslag, Analysis of wind speed observations on the North Sea coast, 1998, J. Wind Engin. Industr. Aerodyn., 73, pp. 125-144

10. Doekes (2000). Personal communication with Koos Doekes, RIKZ, Rijswijk, 2000.

11. Internetsite SeaNet workshop, URL: www.minvenw.nl/rws/projects/seanet/

12. Verkaik, J.W., Documentatie windmetingen in Nederland, Royal Dutch Meteorological Institute (KNMI), De Bilt, Netherlands, December 1999.

CHAPTER 11 : The POWER Tool software

Chapter authors : Dr R A Brownsword and Dr J A Halliday (CLRC Rutherford Appleton Laboratory)

11.1 The POWER Tool

The data on wind and wave parameters for European waters produced by the POWER project has been compiled as a set of Microsoft Excel work books (hereafter referred to as 'the database', though note that the data are not strictly in database format). The POWER tool is a simple graphical user interface (GUI) allowing a user to display data, both in numerical and graphical form, from the database of wind and wave parameters.

The POWER tool presents four tabbed dialogue boxes (TDBs) to the user, entitled "Wind Details", "Wind Map", "Wave Map" and "Wave Details" respectively. Each TDB presents different aspects of the wind and wave database, and the user may switch freely between TDBs at any time. Each of the four tabbed dialogue boxes is now described in turn.

11.1.1 The Wind Details Box

The Wind Details TDB allows the user to view wind parameters associated with a selected offshore location. Data is available for offshore locations on a latitude-longitude grid ranging from 30° to 70° N and 15° W to 30° E, at a grid spacing of 0.5° in both latitude and longitude.

The available grid points are presented to the user in the "Latitude" and "Longitude" drop-down boxes at the top of the window. A negative value of longitude corresponds to a location west of the meridian.

Note that the longitude drop-down box remains empty until the user selects a latitude, and is cleared on selection of a new latitude value. The longitude values corresponding to offshore locations at the specified latitude are then selectable. The user next specifies a height above mean sea level from the range 10-150 m (selectable in 20 m increments) and clicks "OK". The following data for the selected location and height are now displayed :

In the five text boxes :

The mean annual wind speed, the Weibull A and k parameters of the annual wind speed probability distribution (see Section 11.3 for a description of the Weibull function), and the mean power density associated with the kinetic energy of the wind.

By choice of a suitable wind turbine power curve, the mean annual power output of a specific installation may be estimated from the Weibull parameters. The default power curve supplied is for a Vestas 1.65 MW machine. See Section 11.4 for details of the mean power calculation, and Section 11.5 for instructions on how to supply a power curve of your choice.

In the five polar or Cartesian plots :

The wind rose, showing the distribution (as a percentage) of wind direction at the selected height, over twelve 30° sectors. Due north is plotted in the upward direction.

The height profile, showing the variation of mean wind speed over the height range 10-150 m.

The wind speed probability distribution function p(v) as a Weibull function determined by the A and k parameters displayed above, for the selected height.

The mean monthly wind speed over the period 1985-1997 (see Section 11.6 for definition of terms)
the mean yearly wind speed.

11.1.2 The Wind Map Box

The Wind Map TDB can be used to inspect contour maps of :

- The mean annual wind speed at heights of 10-150 m in 20 m increments. Choice of the appropriate height in the upper drop-down box switches between contour maps of the different heights; or
- The mean monthly wind speeds at a pre-set height of 50 m. Selection of different months is possible through the lower drop-down box.

If a coordinate position and height has already been selected in the Wind Details TDB, the map for the relevant height is automatically displayed, with the coordinates of the selected location shown in the upper text box and a red circle marking the location on the map.

11.1.3 The Wave Map Box

The Wave Map TDB is analogous to the Wind Map TDB. The contour maps are available for three sea conditions :

- significant waves
- swell
- wind-sea waves

and for each of the above, for three wave parameters :

- mean wave height
- mean wave period
- a fifty-year extreme wave height

The means are taken over the 10-year period 1987-1996.

In addition, a map of the fifty-year extreme wind speed at 19.5 m is available.

11.1.4 The Wave Details Box

The Wave Details TDB can be used to extract data on sea conditions for fourteen “footprint” locations, each chosen to be representative of a sea area (for example, the North Atlantic or Aegean Sea). *Note that the data on sea state displayed in the Wave Details TDB does not necessarily bear any relation to a grid point selected in the Wind Details TDB.* Selection of different sea areas is made through the drop-down box at the top right of the TDB.

The following sea condition data are displayed :

In one polar and one Cartesian plots at the top of the GUI window :

- the wave rose, showing the distribution (as a percentage) of wave over twelve 30° sectors. Due north is plotted in the upward direction.

- the probability distribution p(H) of the significant wave height H.

In four Cartesian plots at the bottom of the GUI window :

- The mean yearly and mean monthly wave heights, for significant waves, swell and wind-sea waves.
- The mean yearly and mean monthly wave periods, for significant waves, swell and wind-sea waves.

In five text boxes at the right-hand side :

- The average and the maximum significant wave height over the period 1987-96
- The fifty-year extreme wave height
- The Weibull A and k parameters derived from a fit to the significant wave height probability distribution shown in the plot described above.

11.2 Installation of POWER Tool

It is recommended that installation of the POWER tool is performed by a user with Administrator rights on the relevant machine.

The following instructions have been used under MS Windows 98 (and on Windows 2000) to install the POWER tool :

1) Create a directory on your hard disk from which you want to run POWER. As an example, I created c:\Power.
2) Copy the first four files and all the directories from the CD to this directory. Do NOT copy the two files St6unst.log and St6unst.004.
3) In the example directory c:\Power, I now have 3 files and 6 sub-folders.
4) If I right-click on c:\Power in Windows Explorer, and select Properties, I find a total of 3828 files and 7 folders (the Package sub-folder has one sub-folder of its own).
5) Right-click on the file MainPath.txt, and select Properties. The Read-only box will be ticked. Click on it to clear the tick, and then click OK to close the Properties menu.
6) Edit the file MainPath.txt and replace the first line with the directory you copied the POWER files to. [In my example, it was c:\Power]. Now Save MainPath.txt.
7) Go to the sub-directory Package [in my case this is c:\Power\Package] and double click the setup.exe program.
8) The first message you have is about closing down other programs. It is important that, as a general rule, you don't have other programs running when installing new software. Attend to this and click OK.
9) If you don't want to use the suggested install directory [c:\Program Files\POWER\] click Change Directory and enter your choice. [I used c:\Power].
10) Make sure the correct directory is displayed and click the button with the picture of a computer on it.
11) Deal with the Program Group request. I used the default. Press Enter and install commences.
    {You may at this point receive various warning/error messages, particularly if you do not have administrator rights. In general either click 'OK' or 'ignore'. For more details see the next page of these notes}
12) If it is present, Click the Power Offshore Wind Resource Data icon to run the program; otherwise Run the application Power.exe in the C:\Power folder.

N.B. If you have had a failed install, use Settings-Control Panel-Add/Remove Programs to uninstall POWER. Then make sure that all traces of POWER files on your hard disk have gone (apart from those in the Windows directory and sub-directories of Windows). Then follow the above instructions.

Technical Notes :
The POWER CD supplied has following folder structure :
\Power
\Power\Curves
\Power\Data
\Power\Package
\Power\Package\Support
\Power\WaveData
\Power\WaveGIFs
\Power\WindGIFs

If you are installing POWER on a machine for which you do **not** have Administrator rights, you may receive the error message “Setup Error 168 : Setup has encountered a problem updating your system registry”. If so, click “OK”. You might also receive various messages about difficulties in installing various DLL files – ‘ignore’ these messages – the performance of POWER does not seem to be affected

If you are installing POWER on a machine for which you **do** have Administrator rights, you may receive the error message “Unable to configure ODBC driver Microsoft dBase driver (*.dbf) : Could not load the setup or translator library. If so, click “OK”. The performance of the POWER will not in either case be affected.

NOTE : It is strongly recommended that you do not store any files in the \Power\ sub-folders, other than those installed there by the Setup program.

11.3 Technical Appendix – The Weibull distribution

The "Wind Details" and "Wave Details" TDBs display the A and k parameters of the Weibull function used to fit wind speed and wave height distributions. The function is :

where the independent variable x is in this case either wave height (m) or wind speed (m/s).

$$p(x) = \left(\frac{k}{A}\right)\left(\frac{x}{A}\right)^{k-1} \exp\left[-\left(\frac{x}{A}\right)^{k}\right]$$

11.4 Technical Appendix – Calculation of wind turbine power

The "Wind Details" TDB gives the option of calculating the mean power output of a given model of wind turbine at the offshore location selected, using the turbine's power curve. Prediction of turbine power output from speed-to-power conversion must be done with care, and the facility offered by the POWER tool should be regarded as giving a first estimate only.

The calculation is performed by taking a power curve, consisting of a set of N wind speeds v_i and the corresponding observed power outputs $P(v_i)$, and calculating the Weibull probability $p(v_i)$of each v_i , using the relevant Weibull A and k parameters. The predicted mean power output P is then calculated as :

For an accurate power output estimate, the expression above implicitly assumes that the first data point

$$P = \sum_{i=2}^{N} \left[p(v_i)P(v_i) + p(v_{i-1})P(v_{i-1}) \right] \left[v_i - v_{i-1} \right] / 2$$

in the power curve defines the turbine's cut-in speed, and that the final data point defines the power output immediately prior to turbine stall To minimise the errors in this power output estimate, therefore, it is important that power curve supplied has data close to both the cut-in speed and stall speed of the turbine.

11.5 Technical Appendix – Defining a power curve

The POWER tool provides a power curve of a Vestas 1.65 MW turbine as a default. Users may supply an alternative power curve as follows : open an ASCII text file and enter the wind speed v_i and power output $P(v_i)$ values of each power curve data point as comma-delimited text, placing each pair of v_i, $P(v_i)$ values on a new line in the text file. The file \Power\Curves\Template.txt can be used as a template. Ensure that there are no trailing return characters at the end of the file. Save the new power curve as a text file in the \Power\Curves folder. The new file will appear in the power curves drop-down box the next time the POWER tool is run.

11.6 Technical Appendix - Definition of terms

The POWER tool makes reference to average wind and wave parameters as "mean annual", "mean monthly" or "mean yearly" values. The precise meaning of these terms is as follows :

"mean annual" refers to the average value over all months and all years in the period for which data was used (1985-1997 for wind data, 1987-1996 for wave data)

"mean monthly" refers to the average value for each individual month, over all years

"mean yearly" refers to the average value for each individual year, over all 12 months.

APPENDIX 1 : PUBLICATIONS

1. CONFERENCE PRESENTATIONS :

Watson S.J., Watson G.M., Palutikof J.P., Holt T., Bartelmie R.J., Coelingh J.P., van Zuylen E.J., Cleijne J.W., 1999 : *A methodology for the prediction of Offshore Wind Energy Resources*. Proc 1999 European Wind Energy Conference, 1-5 March 1999, Nice pp 1105-1108.

Barthelmie, R.J., 1999: *Developing a coastal discontinuity model for the POWER project*, Proceedings of the 21st British Wind Energy Association Conference – Wind Energy 1999 ed P. Hinson, Professional Engineering Publishing, Bury St Edmunds, UK. pp 403-404.

Barthelmie, R.J., 1999: *Monitoring offshore wind and turbulence characteristics in Denmark*, Proceedings of the 21st British Wind Energy Association Conference, Cambridge - Wind Energy 1999 ed P. Hinson, Professional Engineering Publishing, Bury St Edmunds, UK. pp 311-322.

Coelingh, J.P., Folkerts L., van Zuylen E.J., Wiegerinck G., 1999: *Using SODAR measurements in the POWER project.* Proceedings of the 21st British Wind Energy Association Conference, Cambridge - Wind Energy 1999 ed P. Hinson, Professional Engineering Publishing, Bury St Edmunds, UK. pp 283-288.

Watson G.M., Halliday J.A., Palutikof J.P., Holt T., Barthelmie R.J., Coelingh, J.P., Folkerts L., van Zuylen E.J, Cleijne J.W., 1999: *POWER – a methodology for predicting off-shore wind resources.* Proceedings of the 21st British Wind Energy Association Conference, Cambridge - Wind Energy 1999 ed P. Hinson, Professional Engineering Publishing, Bury St Edmunds, UK. Pp 357-362.

Pryor S.C. and Barthelmie R.J., 2000: *Flow characteristics in the coastal zone*. Proceedings of OWEMES 2000, Sicily, April 2000, ATENA, Rome. pp29-43.

Barthelmie R.J., 2000: *Measurements and modelling of coastal meteorology*. Proceedings of OWEMES 2000, Sicily, April 2000, ATENA, Rome. pp 45-59.

Coelingh J.P., Folerts L., Wiegerinck G.F.M., van Zuylen E.J., 2000: *Study of the offshore wind climate using a SODAR*. Proceedings of OWEMES 2000, Sicily, April 2000, ATENA, Rome. pp 61 – 70.

Palutikof J.P., Holt T., 2000: *Synoptic-scale wind data suitable for the preliminary assessment of offshore wind resources*. Proceedings of OWEMES 2000, Sicily, April 2000, ATENA, Rome. Pp 93-107.

Watson G.M., Halliday J.A., Palutikof J.P., Holt T., Barthelmie R.J., Coelingh, J.P., Folkerts L., van Zuylen E.J, Cleijne J.W., 2000: *POWER – a methodology for predicting off-shore wind resources.* Proceedings of OWEMES 2000, Sicily, April 2000, ATENA, Rome. Pp 109-120.

Halliday J.A., Watson G.M., Palutikof J.P., Holt T, Barthelmie R.J., Coelingh J.P., Folkerts L, van Zuylen E.J., Clejne J.W. (2001). POWER – A methodology for Predicting Offshore Wind Energy Rresources. Proceedings of the 2001 European Wind Energy Conference and Exhibition, Copenhagen, July 2001.

Pryor S.C., and Barthelmie R.J., 2001: Persistence of offshore wind speeds: implications for power quality offshore. Proceedings of the 2001 European Wind Energy Conference and Exhibition, Copenhagen, July 2001.

Lavagnini A., Sempreviva A.M., Calvalieri L, Barthelmie R.J., 2001: Evaluation of methods of estimating wind energy potential in Mediterranean areas. Proceedings of the 2001 European Wind Energy Conference and Exhibition, Copenhagen, July 2001.

2. PAPERS :

Barthelmie R.J. 2001: Practical guidelines for evaluating the significance of wind induced roughness change and tidal range on predicted offshore vertical wind speed profiles. Submitted to Wind Energy.

Pryor S.C. and Barthelmie R.J. 2001: statistical analysis of low characteristics in the coastal zone. Submitted to the Journal of Wind Engineering and Industrial Aerodynamics

3. BOOK CHAPTER :

Barthelmie R. J., 1999b, *Modelling and measurements of coastal wind speeds.* In: S.K. Majumdar, E.W. Miller and A.I. Panah (Editors), Renewable Energy: Trends and Prospects. Pennsylvania Academy of Science, Easton, PA.

4. OTHER :

J Halliday (CLRC-RAL) represented the POWER project at "Advances in Wind Energy RTD – From FP4 towards FP5" contractors meeting hosted by the European Commission in Athens from 3-5 May 2000.

5. INTERNAL PROJECT REPORTS :

Barthelmie, R.J., 1999a: *Development of the Coastal Discontinuity Model*, Risø National Laboratory, Roskilde. Report to the European Commission Contract JOR3-CT98-0286.

Barthelmie R. J., 1999a, *The wind resource at Middelgrunden*, Risoe-I-1334, Risø National Laboratory, Roskilde.

Barthelmie, R.J., 2001: *Integrating the CDM and WaSP for the POWER Project*, Risø National Laboratory, Roskilde. Report to the European Commission Contract JOR3-CT98-0286.

6. REPORTS SUBMITTED TO THE EUROPEAN COMMISSION :

Watson S. J., Watson, G. M., Palutikof, J. P., Holt, T., Barthelmie, R.J.,. Coelingh, J., van Zuylen, E., Cleijne, J. and Vesterdal J., 1999: Predicting offshore wind energy resources., Contract JOR3-CT98-0286, First periodic report (6-month) to the European Commission.

Halliday, J.A., Watson, G.M., Coelingh, J., van Zuylen, E., Folkerts, L., Wiegerink, G., Cleijne, J., Hommel, G., Barthelmie, R.J., Palutikof, J. and Holt, T., 1999: Predicting offshore wind energy resources., Contract JOR3-CT98-0286, Second periodic report (12-month) to the European Commission.

Halliday, J.A., Watson, G.M., Coelingh, J., van Zuylen, E., Folkerts, L., Wiegerink, G., Cleijne, J., Hommel, G., Barthelmie, R.J., Palutikof, J. and Holt, T., 2000(a): Predicting offshore wind energy resources., Contract JOR3-CT98-0286, Third periodic report (18-month) to the European Commission.

Halliday, J.A., Watson, G.M., Coelingh, J., van Zuylen, E., Folkerts, L., Wiegerink, G., Cleijne, J., Hommel, G., Barthelmie, R.J., Palutikof, J. and Holt, T., 2000(b): Predicting offshore wind energy resources., Contract JOR3-CT98-0286, Mid-Term Assessment (MTA) Report to the European Commission

Halliday, J.A., Watson, G.M., Coelingh, J., van Zuylen, E., Folkerts, L., Wiegerink, G., Cleijne, J., Hommel, G., Barthelmie, R.J., Palutikof, J. and Holt, T., 2000(c): Predicting offshore wind energy resources., Contract JOR3-CT98-0286, Fourth periodic report (24-month) to the European Commission.

Halliday, J.A., Watson, G.M., Coelingh, J., van Zuylen, E., Folkerts, L., Wiegerink, G., Cleijne, J., Hommel, G., Barthelmie, R.J., Palutikof, J. and Holt, T., 2001: Predicting offshore wind energy resources., Contract JOR3-CT98-0286, Fifth periodic report (30-month) to the European Commission.

In addition, there is a POWER project web page which hangs off the main CLRC-RAL Energy Research Unit web site at:
http://www.eru.rl.ac.uk/power_project/power_project.htm.

and a POWER Project web page which hangs off the main Climate Research Unit site at http://www.cru.uea.ac.uk/cru/projects/power/.